AD_____

Award Number: DAMD17-00-1-0386

TITLE: Molecular Biology of Breast Neoplasia

PRINCIPAL INVESTIGATOR: Virgil C. Jordan, Ph.D.

CONTRACTING ORGANIZATION: Northwestern University
Evanston, Illinois 60208-1110

REPORT DATE: September 2004

TYPE OF REPORT: Annual Summary

PREPARED FOR: U.S. Army Medical Research and Materiel Command
Fort Detrick, Maryland 21702-5012

DISTRIBUTION STATEMENT: Approved for Public Release;
Distribution Unlimited

The views, opinions and/or findings contained in this report are those of the author(s) and should not be construed as an official Department of the Army position, policy or decision unless so designated by other documentation.

REPORT DOCUMENTATION PAGE

Form Approved
OMB No. 074-0188

1. AGENCY USE ONLY (Leave blank)	2. REPORT DATE	3. REPORT TYPE AND DATES COVERED
	September 2004	Annual Summary (1 Sep 00 - 31 Aug 04)

4. TITLE AND SUBTITLE
Molecular Biology of Breast Neoplasia

5. FUNDING NUMBERS
DAMD17-00-1-0386

6. AUTHOR(S)
Virgil C. Jordan, Ph.D.

7. PERFORMING ORGANIZATION NAME(S) AND ADDRESS(ES)
Northwestern University
Evanston, Illinois 60208-1110

E-Mail: vcjordan@northwestern.edu

8. PERFORMING ORGANIZATION REPORT NUMBER

9. SPONSORING / MONITORING AGENCY NAME(S) AND ADDRESS(ES)
U.S. Army Medical Research and Materiel Command
Fort Detrick, Maryland 21702-5012

10. SPONSORING / MONITORING AGENCY REPORT NUMBER

11. SUPPLEMENTARY NOTES

12a. DISTRIBUTION / AVAILABILITY STATEMENT
Approved for Public Release; Distribution Unlimited

12b. DISTRIBUTION CODE

13. ABSTRACT (Maximum 200 Words)

The Northwestern University Robert H. Lurie Comprehensive Cancer Center is an NCI-funded comprehensive cancer center. One of the major accomplishments for the Cancer Center has been to establish a nationally recognized program in both laboratory and clinical based breast cancer research. The Cancer Center has received $14.2 million from the Avon Foundation and successfully competed for a SPORE in Breast Cancer from the National Cancer Institute. In September 2000 the Cancer Center received a four year award from the US Army for comprehensive training of graduate students and postdoctoral fellows conducting breast cancer relevant research entitled, "The Molecular Biology of Breast Neoplasia" (DAMD17-00-1-0386). In total, the Selection Committee reviewed applications and assisted in the selection of 10 graduate students and seven postdoctoral fellows for appointment to the Training Program. Trainees and mentors actively participated in the weekly meetings of the Breast Cancer Journal Club, as well as training program course entitled, Advanced Topics in Breast Cancer.

14. SUBJECT TERMS
Training Program, Molecular Biology, Hormones, Signal Transduction

15. NUMBER OF PAGES
208

16. PRICE CODE

17. SECURITY CLASSIFICATION OF REPORT	18. SECURITY CLASSIFICATION OF THIS PAGE	19. SECURITY CLASSIFICATION OF ABSTRACT	20. LIMITATION OF ABSTRACT
Unclassified	Unclassified	Unclassified	Unlimited

Table of Contents

INTRODUCTION

The Robert H. Lurie Comprehensive Cancer Center has a premier breast cancer program at Northwestern University, integrating basic laboratory research, clinical research and a program in cancer prevention and control. V. Craig Jordan, OBE, Ph.D., D.Sc. established the laboratory breast cancer research program and Seema Khan, M.D., directs the clinical breast cancer research program and the Lynn Sage Comprehensive Breast Center at Northwestern. Dr. Jordan is internationally recognized for his pioneering research on the antiestrogen tamoxifen, an important drug used in the treatment and prevention of breast cancer. In the last five years the Cancer Center has continued to successfully compete for national funding to support the breast cancer program. The Cancer Center received a $4.2 million dollar award from the Avon Foundation in March 2000 to expand the existing breast cancer research programs for medically underserved minority women. The Avon Foundation enhanced their commitment to breast cancer research at the Robert H. Lurie Comprehensive Cancer Center with an additional gift of $10 million to build an Avon Breast Cancer research floor in the new Robert H. Lurie Medical Sciences building that will open in March 2005. In September 2000 the Cancer Center received an award from the National Cancer Institute for a SPORE in Breast Cancer (P50 CA89018). The Program Director of the SPORE is V. Craig Jordan, Ph.D., D.Sc. The five-year award provides $13 million dollars in funding for six translational research projects investigating hormones and breast cancer, four core facilities, and career development and developmental research opportunities in breast cancer. A competitive renewal application will be submitted in October 2004. In September 2000 the Cancer Center also received a four year award from the US Army for training of graduate students and postdoctoral fellows, "The Molecular Biology of Breast Neoplasia". This program has enabled ten predoctoral students and seven postdoctoral fellows to receive in depth training in breast cancer research from laboratory investigators with research relevant to breast cancer and to clinical investigators who provide a translational link. Preceptors are nationally funded basic science faculty with a history of excellence in research with a focus on the cellular and molecular aspects of breast cancer. The goal of the Training Program has been to prepare scientists to function as independent investigators in the field of breast cancer research and to integrate their research with therapeutic advances made by clinicians.

BODY

In each year of the grant four graduate students and two postdoctoral fellows were appointed to The Molecular Biology of Breast Neoplasia. The Program's Administrative Director, Dr. Robin Leikin, sent out an email announcement requesting student nominations from faculty in the Breast Cancer Program. The Training Grant Selection Committee reviewed all applications. Committee members include: V. Craig Jordan, Ph.D., D.Sc., Program Director, Steven Rosen, M.D., Director, Cancer Center, Robin Leikin, Ph.D., Administrative Director; Kathleen Rundell, Ph.D., Professor, Microbiology-Immunology and Jonathan Jones, Ph.D., Professor, Cell and Molecular Biology. Students were selected based upon their academic credentials, the relevance of their research projects to breast cancer and their potential as future academicians in breast cancer research. The Training Grant Executive Committee provided final approval for the trainee selections. A total of 10 predoctoral students and 7 postdoctoral fellows received intense training in breast cancer biology under the auspices of this program.

All trainees participated in the Breast Cancer Journal Club that brings together the members of the Breast Cancer Program on a weekly basis to discuss journal articles relevant to the molecular biology of breast cancer. The Journal Club regularly attracts 15-25 graduate, postdoctoral and faculty participants in addition to the four predoctoral students and two postdoctoral fellows who are required to participate. Trainees were required to present one time per year at this meeting (see Appendix). In addition, trainees were required to attend the

course, "Advanced Topics in Breast Cancer" (see Appendix) that was developed as part of this Program. The monthly lectures given by established clinical faculty and translational researchers presented an integrated overview of clinical breast cancer for laboratory scientists. At the final meeting trainees presented their research projects for the Advisory Committee responsible for monitoring trainee progress (see Appendix).

The following predoctoral and postdoctoral students were allocated funds throughout the entire four years of the Grant:

Year 01:

Name	Preceptor	Department
Predocs:		
Lisa Salvador	Mary Hunzicker-Dunn	Cell and Molecular Biology
Hao Wang	Gerald Soff	Medicine
Michael Werner	Vince Cryns/Larry Jameson	Medicine
Yi Wu	Sharon Stack	Cell and Molecular Biology
Postdocs:		
Yongji Chung	Ann Thor	Pathology
Daisuka Tsuruta	Jonathan Jones	Cell and Molecular Biology

Year 02:

Name	Preceptor	Department
Predocs:		
Danijela Vignjevic	Gary Borisy	Cell and Molecular Biology
Hao Wang	Gerald Soff	Medicine
Michael Werner	Vince Cryns	Medicine
Yi Wu	Sharon Stack	Cell and Molecular Biology
Postdocs:		
Sudhakar Baluchamy	Bayar Thimmapaya	Microbiology-Immunology
Suresh Pillai	Larry Jameson	Medicine

Year 03:

Name	Preceptor	Department
Predocs:		
Joshua Bosman	Richard Morimoto	Biochemistry, Molecular Biology and Cell Biology
Anne Strohecker	Vincent Cryns	Medicine
Danijela Vignjevic	Gary Borisy	Cell and Molecular Biology
Yi Wu	Sharon Stack	Cell and Molecular Biology
Postdocs:		

Joan Lewis	V. Craig Jordan	Cancer Center
Suresh Pillai	Larry Jameson	Medicine

Year 04:

Name	Preceptor	Department
Predocs:		
Anne Strohecker	Vincent Cryns	Medicine
Kelly Kopp	Sui Huang	Cell & Molecular Biology
Christa Hestekin	Annelise Barron	Chemical and Biological Engineering
Anne Mongiu	Gary Borisy	Cell & Molecular Biology
Postdocs:		
Clodia Osipo	V. Craig Jordan	Cancer Center
Kristiana Kandere	Gary Borisy	Cell & Molecular Biology

Research Descriptions of Trainees:

Lisa Salvador

Ms. Salvador was a graduate student in the laboratory of Dr. Mary Hunzicker-Dunn. Her research project examined the pathway by which cAMP/PKA signals in concert with estrogen to promote cellular proliferation and differentiation and to inhibit apoptosis. The specific molecules studied are A kinase anchoring proteins (AKAPs). The AKAPs anchor PKAs to specific cellular sites, thereby promoting specific and efficient substrate phosphorylation in response to a specific stimulus. Ms. Salvador determined that PKA activates the mitogen activated protein kinase (MAPK) pathway. She also characterized an R1 AKAP that may be involved in breast cancer cell apoptosis.

Hao Wang

Hao Wang completed his Ph.D. in the laboratory of Dr. Gerald Soff. He studied the in vivo generation of angiostatin 4.5 (AS4.5) as an inhibitor of angiogenesis in breast cancer patients. Experiments have indicated that the "Angiostatic Cocktail" administered to cancer patients generated not only AS4.5, but also angiostatin related proteins and angiostatin-related complexes. Similar proteins and complexes are generated in human plasma given "Angiostatic cocktail" *in vitro*. The Soff data suggest that the complexes are plasmin-α2-antiplasmin complex and plasmin-α2-macroglobumin complex. Although these complexes do not show inhibiting effect in endothelial cell proliferation assay, their studies do suggest that α2-antiplasmin can protect AS4.5 from further degradation by plasmin and help to elevate AS4.5 concentration in the blood of cancer patients administered "Angiostatic cocktail." It is also suggested that α2-antiplasmin can influence the plasmin-angiostatin conversion through binding to plasmin. The purpose of Hao Wang's doctoral thesis is to determine the effect of α2-antiplasmin on plasmin-Angiostatin conversion and the structure and function of angiostatin-related proteins. These studies will improve our understanding of angiostatin and the effect of "Angiostatic cocktail" *in vivo*. This will be helpful to the clinical studies of "Angiostatic cocktail" in the treatment of cancer patients.

Michael Werner

Michael Werner studied caspases in the Cryns laboratory. Caspases are a conserved family of cysteine proteases that are universal effectors of programmed cell death. However, the molecular mechanisms by which

caspases induce breast cancer cell death are poorly understood. The Cryns laboratory developed a novel expression cloning strategy to identify cDNAs encoding caspase substrates. They identified integrin β4 as a new caspase-3 substrate that is cleaved in breast cancer cells undergoing chemotherapy-induced apoptosis. They have demonstrated that caspase cleavage of integrin β4 removes a large portion of its cytoplasmic tail. They hypothesize that caspase cleavage of integrin β4 promotes apoptosis by specifically disrupting integrin β4's ability to activate the PI3K/Akt cell survival pathway. Mike generated point mutations within the β4 integrin molecule to map the exact cleavage site and to analyze the effect on the signaling pathway. Identification of the exact cleavage site will provide novel insights into the mechanisms of breast cancer apoptosis, and they may lead to new breast cancer therapies specifically targeting integrin β4.

Daisuke Tsuruta, Ph.D.
Dr. Tsuruta's research in the Jones laboratory involved analyses of the regulation of breast cell behavior by extracellular matrix. Normal breast epithelial cells interact with the extracellular matrix, in part, via hemidesmosomes comprised of a complex of α6β4 integrin/laminin-5. This complex is the conduit for hemidesmosome-mediated cell signaling. Dr. Tsuruta focused on hemidesmosome protein dynamics using green fluorescent protein (GFP)-tagged β4 integrin in live confluent and subconfluent epithelial cells in order to learn more about their assembly. In confluent populations, rosette-like clusters of GFP-β4 remain stable over 1 hr. In subconfluent populations, clusters of GFP-β4 are not stable but assemble into and disassemble out of rosette-like arrays relatively rapidly in an energy-dependent fashion. Furthermore, Dr. Tsuruta monitored GFP-β4 in epithelial cells populating scrape wound sites. In these migratory cells, β4 integrin protein clusters progressively assemble and disassemble into primarily linear streaks located towards the periphery of the migrating cells. This data provided the first evidence that hemidesmosomes are dynamic in both migratory cells and non-motile cells. Dr. Tsuruta speculates that this allows them to respond rapidly and reversibly to external stimuli. This has important implications for normal and aberrant breast epithelial tissue morphogenesis since hemidesmosomes may play the role of sensitive mechano-signal tranducers.

Yongji Chung, Ph.D.
Transgenic mice bearing the rat wild-type erbB-2 gene were used to study the effects of short-term hormonal exposure [17beta-estradiol (E2) or tamoxifen] or a soy meal diet on mammary carcinogenesis. In mice fed a casein diet, mammary tumors developed at an earlier age after short-term E2 exposure during the early reproductive period. The median mammary tumor latency was shortest (29 weeks) for the high-dose estrogen as compared with the lowest dose of E2 treated or placebo control mice (33 and 37 weeks, respectively). The timing of short-term E2 exposure was also important, with the most significant changes observed in mice exposed to E2 between 8 and 18 weeks of age. Tumors from E2 treated mice appeared more aggressive as determined by histologic grade, multifocal tumor development, stromal invasion, and pulmonary metastasis. In contrast, short-term tamoxifen-exposed mice generally failed to develop mammary tumors by 60 weeks of age. Mice fed a soy meal diet developed mammary tumors at a later age than casein-fed animals treated with E2 or placebo, whereas no differences were observed by diet for the tamoxifen-treated mice. Preliminary analyses of differential gene expression by c-DNA array technology revealed greater than 8 fold differential expression of growth-related genes, such as MARK-1, MARK-3, cyclin A, and PCNA as well as several apoptosis related genes in the E_2 associated murine mammary breast cancer lines. Protein expression studies confirmed enhanced expression of several erbB-2 signaling pathway molecules.

Joshua Bosman
Transcriptional regulation of the heat shock response by heat shock factors (HSF) is a highly controlled process in cells exposed to stress conditions. In fact, many diseases such as cancer, Huntington's, Parkinson's and

Alzheimer's, have been associated with altered levels of heat shock proteins Hsp90, Hsp70 or Hsp27, which are under direct control of HSF. Mr. Bosman's research project involves a genome-wide approach to understand at the molecular level how the mammalian family of heat shock factors (HSF) function to regulate gene expression of heat shock proteins (ie Hsp90, Hsp27, Hsp70). His specific aims are:

-Genome-wide analysis of HSF target genes in humans using database searches and microarray data
-Validation of HSF target genes by Chip analysis
- To determine how HSE's and HSF regulate the heat shock response

These studies are critical, as understanding the regulation of molecular chaperones may have application to diseases that correlate with aberrant levels of heat shock proteins and these molecules may be applied in the future as potential novel therapies for cancer.

Danijela Vignjevic

The acquisition of a motile and invasive phenotype is an important step in the development of tumors and tumor metastasis. Electron microscopy analysis indicates that transformed breast cells differ from control cells by development of long filopodia, spike-like extensions of the cell. Actin bundling protein, fascin is present in filopodia and it is implicated with increased cell motility and malignancy. Increased levels of fascin are associated with overexpression of c-erbB2 in breast cancer cells, which correlates with poor prognosis in breast cancer patients. Whether fascin is required for filopodia formation, we addressed using two approaches: (1) expression of constitutively active or inactive fascin mutants tagged with GFP and (2) targeted depletion of fascin by hairpin siRNA expression with a GFP reporter. Both approaches demonstrated that fascin is required for filopodia formation. Expression of active fascin with serine39 mutated to alanine (S39A) dramatically increased number and length of filopodia. In contrast, inactive S39E fascin reduced the number of filopodia. We conclude that fascin is specifically required to tightly bundle actin filaments in filopodia, which may be important to provide stiffness for filopodial protrusion. Thus, fascin could be a novel target for treatment of tumor metastasis.

Selected by the DOD to receive a travel award to present at the Era of Hope Meeting in Orlando, 2002.

Yi Wu

The Stack laboratory is interested in membrane type 1-MMP (MT1-MMP) because of studies that correlate enhanced expression with breast cancer disease progression as well as with invasiveness of cultured breast cancer cell lines. This is further supported by in vitro studies showing MT-MMPs are the only subfamily of MMPs that mediates cellular invasion and transgenic mouse studies revealing MT1-MMP also plays a significant role in proliferation at the early stage of tumor development. The overall hypothesis of this research is that post-translational modifications, including proteolysis and glycosylation, regulates MT1-MMP activity, and thereby, controls invasive phenotype in tumor cells. In their studies, they demonstrated that MDA-MB-231 cells invade type I collagen matrix, the most important matrix barrier for tumor, in an MT1-MMP-dependent manner. Interestingly, they detected an inhibitory effect in invasion by overexpressing a truncation 44 kDa mutant, which is a naturally occurring cell surface autolytic product, suggesting MT1-MMP proteinase activity is tightly controlled in vivo. In addition, they identified MT1-MMP as a glycoprotein and found the glycosylation of MT1-MMP is crucial for its efficient activation of MMP-2, which is also extensively implicated in tumor progression. Currently the Stack group is vigorously investigating the significance of MT1-MMP glycosylation in different steps of breast cancer progression.

Sudhakar Baluchamy, Ph.D.

Jun B is a member of Jun- protooncogene family of transcription factors. The functions of c-Jun are well understood, while cellular functions of Jun B are poorly understood. Jun B functions are clearly different from

those of c-Jun. My goal is to study the role of Jun B in branching duct morphogenesis and mammary gland development. Northern blot analysis indicates that Jun B expression is induced about 3.5 fold during branching morphogenesis. To examine whether jun B is essential for invitro morphogenesis we constructed a recombinant adenovirus vector which express antisense Jun B sequences (As-Jun B). Growing MCF 10A cells were infected with Ad-Jun B or a vector express b-gal (control vector) and morphogenesis was recorded using light microscopy. This experiment shows that cells expressing antisense Jun B form duct like structure poorly when compared to cells infected with B-gal control vector. These results suggest that elevated levels of Jun B may play an important role on duct morphogenesis. Now we are attempting to identify downstream targets of Jun B while cells undergoing branching duct morphogenesis using antisense Jun B vector by DNA microarray. We are also interested in studying overexpression of Jun B in duct morphogenesis in vivo.

Suresh Pillai, Ph.D.
Estrogen Receptors (ERs) initiate gene transcription via numerous pathways. In the "classical" pathway, ERs bind to discrete response elements on DNA to activate transcription. In the "tethered" pathway, ERs initiate transcription via interaction with other transcriptional proteins. To examine the effects of selective estrogen receptor modulator (SERM) activation of ER-mediated transcription via the tethered pathway, we used a mutated ERalpha and microarray profiling. Amino acids within the DNA binding region of ERα were mutated to eliminate classical ER signaling, and an ER-negative breast cancer cell line (MDA-MB-231) was infected with adenoviral vectors containing these mutants. Cells were then treated with vehicle alone, estradiol, ICI 182 780 (a pure anti-estrogen), tamoxifen or raloxifene. RNA from these cells was then extracted, purified, and hybridized to Affymetrix U95A human gene arrays to compare gene expression profiles among the treatment groups. While few genes were regulated by estradiol, SERMS activated a much larger number of genes. This suggests that SERMS act, at least in part, through the tethered pathway. The consensus gene set was used in the generation of custom spotted microarrays containing the 253 targets from the high density screen. With standardization and verification of the microarrays now complete, hybridization of RNA from both cell culture and malignant breast tumors is currently underway. We hope to use these slides as a screening tool to generate gene expression profiles for different types of breast tumors.

Joan Lewis, Ph.D.
One of Dr. Lewis's goals in Dr. Jordan's lab is to determine the effects of estradiol (as well as structurally related estrogens) on the growth of long-term estrogen deprived breast cancer cells. Interestingly, she has found that treating long-term estrogen-deprived breast cancer cells with physiologic concentrations of estradiol (0.1-1 nM) reduces the growth of cancer cells. The growth-inhibitory effect of estradiol appears to be most dramatic in the MCF-7:5C cells and is highly dependent on the culture media. Further analysis indicates that the reduction in growth of MCF-7:5C cells is due to estradiol-induced cell death. Dr. Lewis is currently trying to elucidate the mechanism(s) for this paradoxical effect of estradiol (i.e. the ability to induce cell death rather than stimulate growth). Dr. Lewis is also interested in characterizing these cell lines in terms of their gene and protein expression profile to determine whether differences exist between MCF-7:WS8 versus MCF-7:5C, MCF-7:ED and MCF-7:2A. The information obtained from these studies using the different cell lines will further our understanding of the regulatory pathways involved in maintaining the critical balance between estrogen-induced cell death and cell proliferation and has important clinical application. Dr. Jordan is currently initiating clinical studies of estrogen therapy in breast cancer patients who have received exhaustive endocrine therapy.

Anne Strohecker
The Cryns laboratory has demonstrated that endogenous HER-2 is cleaved by caspases in response to multiple stimuli. They have identified four distinct cleavage sites within the carboxy terminus of HER-2 and used site

directed mutagenesis to create a cleavage resistant protein (4X HER-2). A retroviral system was used to create MDA-MB-231(which express low endogenous HER-2) breast cancer cell lines which stably express vector, wild type, caspase truncated (N terminal), or cleavage resistant (4X) HER-2. Control experiments confirmed that these constructs were expressed properly on the cell surface and responded to normal stimuli. Interestingly, dose response experiments demonstrate that cleavage of HER-2 has important consequences for cell death. Cells transfected with wild type HER-2 are protected at low doses of either TRAIL or the DNA damaging agent etoposide, but once cleaved, the cells readily undergo apoptosis. In contrast, cells expressing the cleavage resistant HER-2 are markedly protected throughout the entire dose range. Most interestingly, the truncated HER-2, containing the N terminal portion of HER-2 left after caspase cleavage, protects nearly as well as the cleavage resistant construct. Ongoing experiments will test the hypothesis that caspase cleavage of HER-2 converts it from a survival to a pro-apoptotic protein in breast cancer cells.

Christa Hestekin

Genetic mutation detection promises to revolutionize the diagnosis and treatment of cancer by enabling the correlation of prognosis with specific sequence alterations. Mutations in the p53 gene, in particular, are known to be important in the pathogenesis of a variety of human cancers including breast cancer. Single-strand conformational polymorphism (SSCP) and heteroduplex analysis (HA) are two excellent and complementary electrophoretic methods for genetic mutation detection, because of their simplicity, breadth of application, and low cost. We, and others, have shown that tandem SSCP/HA implemented on a capillary electrophoresis system offers a significantly higher sensitivity of mutation detection (~100%) than SSCP or HA alone in limited studies to date. However, several technical challenges remain before microchip electrophoresis-SSCP/HA can be used in a clinical setting. These challenges include determining the optimum polymer matrix, electric field strength, coating polymer, and sample purity. We show that single-base mutations in the p53 gene hotspot region (exons 5-9) can be detected by microchip electrophoresis-SSCP/HA, with analysis times of less than 5 minutes. Further studies will include analysis of breast cancer patient tumor samples by microchip electrophoresis-SSCP/HA.

Kelly Kopp

Ms. Kopp is studying transcriptional regulation within the nucleolus, the formation of the perinucleolar compartment (PNC) and associations with the malignant phenotype. This project will help us understand the coordination of events necessary for pol I transcription, thus increasing the efficiency of ribosome biosynthesis, a process which consumes a majority of the energy within a cell. Ribosome biosynthesis is highly regulated and often altered in malignantly transformed cells. We have described a novel interaction of pol I and rRNA, which is dependent upon nascent RNA, thus differing from the model of coordinated pol II transcription and pre-mRNA processing. Ms. Kopp is also investigating the PNC, a nuclear substructure which forms adjacent to the nucleus, the site of ribosome biosynthesis. The Huang laboratory has described the PNC as rarely forming in normal breast tissues, yet almost always present in malignant breast cells, increasing in prevalence with the progression of disease. Ms. Kopp is studying the role MRP RNA plays in the formation of the PNC. MRP RNA is one of four known RNAs found in the PNC and also part of an endoribonuclease involved with pre-rRNA processing in the nucleolus, a crucial part of ribosome biosynthesis. We believe MRP RNA forms a complex with proteins in the PNC that is functionally separate from the MRP RNAase complex found in the nucleolus and mitochondria. These studies are ongoing.

Anne Mongiu

In metastatic breast cancer, cell motility provides a mechanism for the cancer cell to escape the primary tumor and proliferate in distant spots throughout the body. Studies have shown that the Arp2/3 complex that regulates

and organizes the actin cytoskeleton are upregulated in metastatic cancers. This branched actin network comprises the underlying framework of the lamellipodia organelle involved in cell motility. The Arp2/3 complex consists of seven highly conserved subunits, consisting of two actin-related proteins Arp2 and Arp3, and five novel proteins, p16, p20, p21, p34, and p41. The p34 and p20 subunits form the core of the complex, while the Arp2 and 3 subunits mediate binding to the mother and daughter filaments. Depletion of p34 or Arp3 subunits was predicted to block formation of a functional Arp2/3 complex and would provide a direct way to evaluate the necessity of this complex for cellular morphology and motility. To test this, we performed individual targeted depletion of p34 or Arp3 subunits by RNAi in rat pheochromocytoma and mouse B16F1 melanoma cell lines. Cells depleted of p34 lacked the branched network found in the lamellipodia of normal cells. Knockdown cells contained a disorganized array of long unbranched actin filaments. We conclude that decreased levels of p34, and consequently Arp2/3 complex, lead to an inability to form a normal lamellipodia and initiate lamellipodial motility. Future studies hope to examine these knockdown cells in an animal model to determine clinical relevance of the Arp2/3 complex as a chemotherapeutic or genetic target.

Kristiana Kandere-Grybowska, Ph.D.

Dr. Kandere is trying to understand the relationship between crawling cell motility and breast cancer metastasis. Although metastasis is a multistep process involving altered cellular affinity for the extracellular matrix and secretion of matrix-degrading enzymes, a hallmark of the process is activation of the cell motility machinery, leading to cell movement and invasion. Directional cell migration requires morphological polarization in which a clear distinction between the leading edge and tail of the cell is established. Persistent motility consists of cycles of protrusion of the leading edge, adhesion formation in front, tail retraction and de-adhesion in the rear. The microtubule (MT) cytoskeleton is essential for the generation of polarized cell form and for establishing and maintaining the direction of movement. Recent evidence suggests that MTs coordinate the motility cycle by remodeling the pattern of cell adhesions to the substratum. Plus-end proteins, including adenomatous polyposis coli (APC) protein, EB-1, and cytoplasmic linker protein (CLIP)-170, due to their ability to regulate MT dynamic activity and also to interact with the target sites are ideal candidates to serve as molecular elements of MT-substrate adhesion control. Experiments involving gene silencing, evanescent wave microscopy and micropatterned surfaces are being conducted to understand these processes and to determine the contribution of specific MT plus-end proteins.

Clodia Osipo, Ph.D.

Dr. Osipo is investigating the mechanisms that contribute to tamoxifen resistant breast and endometrial cancers using *in vivo* tumor models. Tamoxifen-stimulated MCF-7 tumors developed by treating estradiol-stimulated MCF-7 tumors with tamoxifen for over 5 years paradoxically regress in response to post-menopausal levels of estradiol. Fulvestrant, a pure antiestrogen that initiates degradation of the ER, in combination with estradiol stimulates robust growth indicating that the ER is mediating both tumor growth regression by estradiol and stimulation by estradiol plus fulvestrant. More importantly, tumor regression by estradiol in tumors is caused by apoptosis of tumor cells possibly through the induction of the FAS/FASL death pathway and simultaneous down regulation of survival pathways, NF-kappaB and HER2/neu. Furthermore, the combination of estradiol plus fulvetsrant completely blocks induction of FAS/FASL and the decrease of NF-kappaB. Interestingly, HER2/neu and HER3 mRNAs are dramatically upregulated and the two receptors preferentially interact as determined by immunoprecipitation experiments in response to estradiol plus fulvestrant. These results suggest that the growth of TAM-stimulated breast cancer by estradiol + fulvestrant is in part mediated through enhanced signaling from the HER2/neu-HER3 signal transduction pathway.

KEY RESEARCH ACCOMPLISHMENTS

- Ten predoctoral students and seven postdoctoral fellows selected from a pool of candidates by Selection Committee received comprehensive training in breast cancer biology
- Journal Club held on Tuesdays at 11 am throughout the academic year (see attached schedule)
- Students attended Advanced Topics in Breast Cancer course (see attached schedule)
- Students exposed to translational relevance of their research through Breast SPORE meetings
- Trainees published their results in peer reviewed journal publications

REPORTABLE OUTCOMES

The success of the Training Program is exemplified by the publications by the trainees as a direct result of their funding through the Molecular Biology of Breast Neoplasia Training Grant. Publications include:

Salvador LM, Flynn MP, Avila J, Reierstad S, Maizels ET, Alam H, Park Y, Scott JD, Carr DW, Hunzicker-Dunn M. Neuronal microtubule-associated protein 2D is a dual a-kinase anchoring protein expressed in rat ovarian granulosa cells. (2004) J Biol Chem 279(26):27621-27632.

Cottom J, **Salvador LM**, Maizels ET, Reierstad S, Park Y, Carr DW, Davare MA, Hell JW, Palmer SS, Dent P, Kawakatsu H, Ogata M, Hunzicker-Dunn M. Follicle-stimulating hormone activates extracellular signal-regulated kinase but not extracellular signal-regulated kinase kinase through a 100-kDa phosphotyrosine phosphatase. (2003) J Biol Chem 278(9): 7167-7179.

Baluchamy S, Rajabi HN, Thimmapaya R, Navaraj A, Thimmapaya B.Repression of c-Myc and inhibition of G1 exit in cells conditionally overexpressing p300 that is not dependent on its histone acetyltransferase activity. Proc Natl Acad Sci U S A. 2003 Aug 5;100(16):9524-9.

Tsuruta D, Hopkinson SB, Lane KD, **Werner ME**, Cryns VL and Jones JCR. (2003). Crucial Role of the Specificity –determining Loop of the Integrin β4 Submunit in the Binding of Cells to Laminin-5 and Outside-in Signal Transduction. J Biol Chem 278:38707-38714.

Tam, E.M., Morrison, C., **Wu, Y.I.**, Stack, M.S., and Overall, C.M. (2004). Membrane Protease Proteomics: Isotope Coded Affinity Tags/Tandem Mass Spectrometry Identification of Novel MT1-MMP Substrates. Proceedings of the National Academy of Science, 101(18):6917-22.

Wu YI, Munshi HG, Sen R, Snipas SJ, Salvesen GS, Fridman R, Stack MS Glycosylation broadens the substrate profile of membrane type 1 matrix metalloproteinase.
J Biol Chem. 2004 Feb 27;279(9):8278-89.

Munshi, H.G., **Wu, Y.I.**, Mukhopadhyay, S., Platanias, L.C., and Stack, M.S. (2004). Differential regulation of membrane type 1-matrix metalloproteinase (MT1-MMP) activity by ERK 1/2 and p38 mitogen-activated protein kinase in oral squamous cell carcinoma cells. J Biol Chem, In Press.

Tam, E.M., **Wu, Y.I.**, Butler, G.S., Stack, M.S., and Overall, C.M. (2002). Collagen binding properties of the membrane type-1 matrix metalloproteinase (MT1-MMP) hemopexin C domain. The ectodomain of the 44-kDa autocatalytic product of MT1-MMP inhibits cell invasion by disrupting native type I collagen cleavage. *J Biol Chem.* 277:39005-14.

Munshi, H.G., **Wu, Y.I.**, Ariztia, E.V., and Stack, M.S. (2002). Calcium regulation of matrix metalloproteinase-mediated migration in oral squamous cell carcinoma cells. *J Biol Chem*. 277:41480-8.

Munshi, H.G., Ghosh, S., Mukhopadhyay, S., **Wu, Y.I.**, Sen, R., Green, K.J., and Stack, M.S. (2002). Proteinase suppression by E-cadherin-mediated cell-cell attachment in premalignant oral keratinocytes. *J Biol Chem*. 277:38159-67.

Vignjevic D, Danciu O, Kojima S, Svitkina TM, and Borisy GG. Fascin function in filopodia formation and tumor cell metastais. *J. Cell Biol.* Submitted for publication.

Kojima S, **Vignjevic D** and Borisy GG. An improved silencing vector co-expressing GFP and small hairpin RNA. J. Biotechniques. 2004. 36(1):74-79.

Vignjevic D, Yarar D, Welch MD, Peloquin J, Svitkina TM and Borisy GG. Formation of filopodial-like bundles *in vitro* from a dendritic network. *J. Cell Biol.* 2003. 160:951-962

Svitkina TM, Bulanova EA, Chaga OY, **Vignjevic D**, Kojima S, Vasiliev JM and Borisy GG. Mechanism of Filopodia Initiation by Reorganization of a Dendritic Network. 2003. *J. Cell Biol.* 160:409-21.

Joan S. Lewis and V. Craig Jordan. "Chemoprevention of Breast Cancer: Laboratory Principles". Submitted to: Diseases of the Breast, 3rd Edition Lippincott, Williams & Wilkins Editors: Drs. Jay R. Harris (Harvard University), Marc E. Lippman (University of Michigan), Monica Morrow (Northwestern University), C. Kent Osborne (Baylor University).

Joan S. Lewis, Dong Cheng, and V. Craig Jordan "Targeting Oestrogen to Kill the Cancer but not the Patient". Submitted to: British Journal of Cancer (Review Article)

I.V. Kourkine, **C.N. Hestekin**, B.A. Buchholz, and A.E. Barron (2002). High-throughput, high sensitivity genetic mutation detection by tandem single strand conformation polymorphism (SSCP) – heteroduplex analysis (HA) capillary array electrophoresis (CAE), *Anal.Chem.*, 74 2565-2572 (2002).

I.V. Kourkine, **C.N. Hestekin**, S. Magnusdottir, and A.E. Barron (2002). Optimized Sample Preparation for Tandem Capillary Electrophoresis Single-Strand Conformation Polymorphism/Heteroduplex Analysis (CE-SSCP/HA) *BioTechniques*, 33 318-325 (2002)

I.V. Kourkine, **C.N. Hestekin**, and A.E. Barron (2002) Technical Challenges in Applying Capillary Electrophoresis (CE)-Single Strand Conformation Polymorphism (SSCP) for Routine Genetic Analysis *Electrophoresis*, 23 1375-1385.

Liu, H., Lee, ES., Gajdos, C., Pearce, ST., Chen, B., **Osipo, C.,** Loweth, J., McKian, K., De Los Reyes, A., Wing, L., Jordan, VC. Apoptotic Action of 17β-Estradiol in Raloxifene Resistant MCF-7 Cells *in vitro* and *in vivo*. (2003). *J. Natl. Cancer Inst.* 95 (21); 1586-97.

Osipo, C., Gajdos, C., Liu, H., Chen, B, Jordan, V.C. (2003). Paradoxical Action of Fulvestrant in Estradiol-Induced Regression of Tamoxifen-Stimulated Breast Cancer. *J. Natl. Cancer Inst.* 95 (21); 1597-608.

Jordan VC, **Osipo C**, Schafer JM, Fox JE, Cheng D, Liu H. (2003). Changing role of the oestrogen receptor in the life and death of breast cancer cells. *The Breast.* Dec;12(6):432-41.

Jordan VC, **Osipo C**, Cheng D, **Lewis JS**. (2004). RESPONSE: Re: Playing the Old Piano: Another Tune for Endocrine Therapy. *J Natl Cancer Inst.* 96(7):556-7.

Clodia Osipo and V. Craig Jordan. (2004). SERMs (Selective Estrogen Receptor Modulators). (Elsevier Publishing). *Encylopedia of Endocrine Diseases.* 4:221-227.

Clodia Osipo, Hong Liu, Kathleen Meeke, V. Craig Jordan. (2004). The Consequences of Exhaustive Antiestrogen Therapy in Breast Cancer: Estrogen-induced Tumor Cell Death. *Experimental Biology and Medicine.* (In press).

Clodia Osipo, Csaba Gajdos, and V. Craig Jordan. (2004) Reversal of tamoxifen resistant breast cancer by low dose estrogen therapy . *J Steroid Biochem and Mol Biol* (Submitted).

Lewis, J.S., **Osipo, C.**, Meeke, K., and Jordan, VC. (2004). Estrogen induces apoptosis in a breast cancer model resistance to aromatase inhibitors. *J Steroid Biochem and Mol Biol* (Submitted).

O'Regan, R.M., **Osipo, C.,** Lee, E.S., Jorgenson, C., Ariazi, E., Meeke, K., and Jordan, V.C. (2004). Phase I resistant breast cancer to raloxifene is hypersensitive to 17β-estradiol and inhibited in part by herceptin, but not gefitinib. *Cancer Res.* (In preparation).

Osipo, C., Meeke, K., Cheng, D., Lim, S., Kidwau, N., Wing, L., and Jordan, V.C. (2004). Herceptin Blocks Tamoxifen-stimulated Endometrial Cancer in The Absence of Amplified HER2/neu. *J. Natl Cancer Inst.* (In preparation).

Osipo, C., Dardes, R.C. Liu, H., Gajdos, C., MacGregor-Schafer, J., Meeke, K., Cheng, D., Lim, S., and Jordan, V.C. (2004). Development of Phase III Raloxifene-stimulated Endometrial Cancer and the Use of Herceptin as a Therapeutic Strategy. *Clin Cancer Res.* (In preparation).

CONCLUSIONS:

The Molecular Biology of Breast Neoplasia Program provided state of the art laboratory and didactic training to 10 predoctoral students and seven postdoctoral fellows over the 4 year period. Dr. Jordan organized the Breast Cancer Journal Club to bring together the members of the Training Program on a weekly basis to discuss relevant journal articles and areas of research. Trainees on the Molecular Biology of Breast Neoplasia also attended the Advanced Topics in Breast Cancer course, where the monthly lectures present an integrated overview of clinical and translational breast cancer. Trainees also attended departmental seminars and journal clubs that have direct relevance to breast cancer. The Cancer Center's NCI funded SPORE in Breast Cancer Program provided further educational opportunities. In summary, this Program successfully enhanced the trainees' understanding of breast cancer so that the relevance of their laboratory research can be stimulated.

List of Personnel Receiving Support during the Grant Period

Name	Role	Current Position
V. Craig Jordan	Principal Investigator	Principal Investigator
Lisa Salvador	Predoctoral Trainee	Postdoctoral Fellow, Univ of Pennsylvania
Hao Wang	Predoctoral Trainee	Resident in Medicine, St. Louis University
Michael Werner	Predoctoral Trainee	Postdoctoral Fellow, Northwestern Univ
Yi Wu	Predoctoral Trainee	Postdoctoral Fellow, Univ of North Carolina
Danijela Vignjevic	Predoctoral Trainee	Postdoctoral Fellow, Paris, France
Joshua Bosman	Predoctoral Trainee	Still in training
Anne Strohecker	Predoctoral Trainee	Still in training
Kelly Kopp	Predoctoral Trainee	Still in training
Anne Mongiu	Predoctoral Trainee	Still in training
Christa Hestekin	Predoctoral Trainee	Still in training
Yongji Chung	Postdoctoral Fellow	Postdoctoral Fellow, China
Daisuke Tsuruta	Postdoctoral Fellow	Asst. Professor, Osaka Univ, Japan
Suresh Pillai	Postdoctoral Fellow	Senior Scientist, BioRad Corporation
Sudhakar Baluchamy	Postdoctoral Fellow	Still in training
Joan Lewis	Postdoctoral Fellow	Still in training
Clodia Osipo	Postdoctoral Fellow	Still in training
Kristiana Kandere	Postdoctoral Fellow	Still in training

APPENDIX I
TRAINEE ABSTRACTS

Abstracts:

In vitro system for filopodia formation. **Vignjevic D**, Svitkina T, Borisy GG. 41stAmerican Society for Cell Biology Meeting, Washington DC; 2001

Are Espins Mediators of Actin Polimerization in Parallel Actin Bundles? Changyaleket B, **Vignjevic D**, Eytan R, Zheng L, Borisy GG, Bartles JR. 41st American Society for Cell Biology Meeting, Washington DC; 2001

The role of alpha-actinin in actin based motility of Listeria. **Vignjevic D**, Peloquin J, Svitkina T, Borisy GG 40th American Society for Cell Biology Meeting, San Francisco; 2000

Estradiol and SERMS Differentially Regulate Tethered ERα-mediated Transcription. **Suresh Pillai**, Jeffrey Weiss, Monika Jakacka, Eun Jig Lee, and J. Larry Jameson. Presented at the Endocrine Society Meeting in San Francisco, 2002

The Molecular Biology of Breast Neoplasia. Robin Goldman Leikin, Ph.D. and V. Craig Jordan, Ph.D., D.Sc. Presented at the Era of Hope Meeting in Orlando, FL, 2002.

Fascin function in filopodia formation: Reconstruction in vitro and genetic analysis in vivo. **Danijela Vignjevic** and Gary Borisy. Northwestern University Medical School, Chicago, IL. Presented at meeting in Heidelberg, Germany.

In Vitro System for Filopodia Formation. **Danijela Vignjevic**, Tatyana Svitkina and Gary Borisy. Presented at the Era of Hope Meeting in Orlando, FL, 2002

Characterization of the Ovarian Phenotype of the Female ER^{AA} mouse: An in vivo model of the Tethered ERα Signaling Pathway. **Suresh Pillai**, Monika Jakacka, Lisa Hurley , Jeffrey Weiss and J. Larry Jameson. Northwestern University Feinberg School of Medicine, Chicago, IL. Presented at Endocrine Society National Meeting, June 18-22 2003; Philadelphia, PA

Biochemical and Biophysical Studies of Bag-1 and Hsp70 Chaperone Complexes. **Joshua Bosman** and Richard Morimoto. 8th Annual Midwest Stress Response and Chaperone Meeting in January 2003 in Evanston.

17β-Estradiol induces apoptosis in a long-term estrogen deprived variant clone of MCF-7 breast cancer cells. **Joan Lewis**, Vincent Cryns and VC Jordan. Presented at the 5th Annual Lunn Sage Breast Cancer Symposium, Chicago, IL 2003.

Dynamics of microtubule cytoskeleton and foacl adhesions in micropatterned cells. **Kristiana Kandere-Grzybowska**, Christopher Campbell, Yulia Komarova, Bartosz Grzybowski and Gary Borisy. Submitted to the 44th Annual ASCB Meeting Dec 4-8, 2004.

Osipo, C., Gajdos, C., Liu, H., and Jordan, VC. (2003). 17β-Estradiol causes rapid tumor regression of tamoxifen-stimulated breast cancer *in vivo* by induction of Fas and suppression of NF-κB. *Proc. AACR.* 44., Washington, D.C. (Poster Discussion Presentation of abstract #4911 at the Endocrinology 4 minisymposium).

Osipo, C., Chen, B., Meeke, K., and Jordan, V.C. (2004). 17β-Estradiol Plus Fulvestrant Stimulates Growth of Phase II Tamoxifen-Resistant Breast Cancer via HER2/neu and HER3 Interaction. *Proc. AACR.* 45., Orlando, FL (Oral Presentation of abstract #4062 at the Best Abstracts Plenary Session).

Lewis, J.S., Osipo, C., Meeke, K., and Jordan, VC. (2004). Estrogen induces apoptosis in a breast cancer model resistance to aromatase inhibitors. 16th International Symposium of the Journal of Steroid Biochemistry and Molecular Biology in Seefeld, Tyrol, Austria. Abstract # 102-P.

Osipo C, Liu H, Lim S, Meeke K, Cheng D, and Jordan VC. (2004). Herceptin blocks tamoxifen-stimulated endometrial cancer *in vivo* through inhibition of HER2/neu and estrogen receptorα activities. 2004 San Antonio Breast Cancer Conference (accepted for poster discussion presentation).

K Kopp, JZ Gasiorowski, D Chen, R Kamath, D Leary, C Wang, J Norton, E Chan, DA Dean and S Huang. Pol I Transcription Factors Complex with Pre-rRNA Processing Factors in a Transcription Dependent Manner in Vivo. (accepted for poster presentation at Cold Spring Harbor Meeting Sept 29 – Oct 3, 2004).

Nucleus

Oral
Kopp

POL I TRANSCRIPTION FACTORS COMPLEX WITH PRE-RRNA PROCESSING FACTORS IN A TRANSCRIPTION DEPENDENT MANNER *IN VIVO*.

K. Kopp[1†], J. Z. Gasiorowski[2†], D. Chen[1], R. Gilmore[1], R. Kamath[1], D. Leary[1], C. Wang[1], J. Norton[1], E. Chan[3], D. A. Dean[2] and S. Huang[1*]

[1] Department of Cell and Molecular Biology, and [2] Department of Medicine, Division of Pulmonary and Critical Care Medicine, Northwestern University Medical School, Chicago, IL 60611;[3] Department of Oral Biology, University of Florida College of Dentistry, Health Science Center, Gainesville, FL 32610

[†] Both authors contributed equally to this work.

We are interested in the relationship between polymerase I (pol I) transcription and pre-rRNA processing during ribosomal synthesis. To address this, we examined whether pol I transcription factors and the pre-rRNA processing factors are recruited to pol I promoters outside of nucleoli and if they are in the same complex *in vivo*. Plasmids containing rDNA promoter alone or promoter with transcribable sequences were injected into HeLa cell nuclei. The localization of the plasmids was examined simultaneously with those of pol I transcription and processing factors including UBF, RPA 39, fibrillarin, Nop 58, and U3 snoRNA. All of these factors are colocalized together with the plasmid containing transcribable sequences. However, only transcription factors are colocalized with the plasmid containing promoter alone, suggesting that the association of processing factors to the plasmid is dependent on rRNA synthesis. Co-immunoprecipitation with antibodies specific to either fibrillarin or UBF precipitated each protein reciprocally, demonstrating that fibrillarin and UBF can be in the same complex *in vivo*. In addition, this complex also contains Nop 58. The interaction is sensitive in tissue culture to treatment with actinomycin D and pre-treatment of cell lysates prior to immunoprecipitation with RNase, but not DNase, suggesting that the integrity of the complex is RNA dependent. These observations were further supported by the analyses of a series of fibrillarin deletion mutants that characterize the RNA binding domains as the domains essential for complex interaction. Altogether, our findings demonstrate that pol I transcription and pre-rRNA processing are closely associated and that processing factors are recruited to newly synthesized pre-rRNA before the release of the RNA from rDNA template in mammalian cells.

Poster Presentation
Cold Spring Harbor Sept 29 - Oct 3 2004

Fulvestrant Stimulates Growth of Phase II Tamoxifen-Resistant Breast Cancer in part through HER2/neu and HER3 Interaction.

Osipo, C., Chen, B., Meeke, K., and Jordan, V.C.

Robert H. Lurie Comprehensive Cancer Center of the Feinberg School of Medicine, Northwestern University, Chicago, IL

Five years of adjuvant tamoxifen is a standard of care for all stages of estrogen receptor α positive breast cancer. Inevitably, drug resistance to TAM does occur during therapy. Tumors that become resistant to TAM remain ERα positive and can be treated with other therapies which include aromatase inhibitors (letrozole, anastrozole, or exemestane) and the pure antiestrogen, fulvestrant. The use of these alternate therapies assume that the tumor cells continue to be stimulated to grow by 17β-estradiol (E_2). However, we have demonstrated previously [Yao *et al.*, Clin. Cancer Res. 2000., 6(5):2028-36, Osipo *et al.*, J Natl. Cancer Inst. 2003., 95(5), and Liu *et al.*, J Natl. Cancer Inst. 2003., 95(5)] that long-term treatment with TAM or raloxifene may produce phase II drug resistance whereby physiologic levels of E_2 induce tumor regression. More importantly, these tumors are robustly stimulated to grow by the combination of E_2 + fulvestrant suggesting that the ERα is mediating the growth of these breast tumors. Therefore, we investigated the function of the ERα in the mechanism of growth stimulation by the combination of E_2 + fulvestrant. The results demonstrate that the ERα protein is functional in TAM-stimulated MCF-7 breast tumors-grown in athymic mice by serial passage for than 5 years as evidenced by E_2-induced decrease of ERα protein and mRNA and simultaneous induction of the mRNA for estrogen responsive genes: *c-myc*, *igf-1*, *catd,* and *tgf-α*. Interestingly, while E_2 suppressed expression of *egfr* and *her2/neu* mRNAs in TAM-stimulated MCF-7 tumors, the combination of E_2 plus fulvestrant dramatically increased *egfr* (15 fold), *her2/neu* (50 fold), *her3* (70 fold), and *her4* (10 fold) mRNAs compared to untreated control. Western blot analyses revealed that phospho-EGFR, phospho-HER2/neu, HER3, HER4 and phospho-GSK3α and β proteins were increased by E_2 + fulvestrant compared to control. Furthermore, immunoprecipation of total HER2/neu protein followed by immunoblots for phospho-HER2/neu and HER3 showed that phosphorylated HER2/neu protein interacts with HER3 in tumors-treated with TAM or E_2 plus fulvestrant while E_2 alone almost completely abolished the interaction of phospho-HER2/neu with HER3. These results suggest the growth of TAM-stimulated breast cancer by E_2 + fulvestrant is in part mediated through enhanced signaling from the HER2/neu-HER3 signal transduction pathway.

Herceptin blocks tamoxifen-stimulated endometrial cancer *in vivo* through inhibition of HER2/neu and estrogen receptorα activities.

Osipo C, Liu H, Lim S, Meeke K, Cheng D, and Jordan VC. The Robert H. Lurie Comprehensive Cancer Center, Feinberg School of Medicine of Northwestern University, Chicago, IL. 60611

Background: Tamoxifen has been used for the last 25 years to treat estrogen receptor (ERα) positive breast cancer in post-menopausal women. One of the major side effects of adjuvant tamoxifen therapy is the increased risk of endometrial cancer. To date, there are currently no models *in vivo* that mimic the development of tamoxifen-stimulated endometrial cancer in order to elucidate the mechanism of action.

Materials and Methods: ERα-positive human endometrial cancer cells (ECC-1) were injected into athymic mice and supplemented with a 0.30cm 17β-estradiol (E_2) capsules. E_2-stimulated ECC-1 (ECC-1E_2) tumors were developed and treated with nothing (Control) or 1.5mg tamoxifen for up to 24 weeks. Tumors that survived in response to E_2 + tamoxifen treatment were subsequently transplanted into new athymic mice and treated with nothing, 0.30cm E_2, or 1.5mg tamoxifen alone. Tamoxifen-stimulated ECC-1 (ECC-1TAM) tumors were developed that were also stimulated by 1.5mg raloxifene. Both tamoxifen naïve and tamoxifen-stimulated ECC-1 tumors were grown to approximately 0.30 cm^2 in cross sectional area with E_2 or tamoxifen, respectively. Mice separated into five treatment groups of 10 mice per group: no treatment, 0.30cm E_2, E2 + 30mg/Kg Herceptin, 1.5mg tamoxifen, 1.5mg tamoxifen + 30mg/Kg Herceptin, or 10mg ICI 182,780 (fulvestrant). ERα transcriptional activity was determined by measuring expression of two estrogen-responsive genes, pS2 and c-myc. Western blot analyses for PY-HER2/neu, total HER2/neu, PS473-Akt, total Akt, P-ERK1/2, and β-actin were performed on total tumor protein extracts.

Results: Tamoxifen-stimulated endometrial tumors (ECC-1) were developed by treating ECC-1 tumors with 1.5mg tamoxifen for up to 6 months *in vivo*. Upon serial transplantation into new generations of athymic mice, the HER2/neu inhibitor Herceptin inhibited the growth of E_2-stimulated ECC-1E_2 tumors by about 50% while completely inhibiting the growth of tamoxifen-stimulated ECC-1TAM tumors. While E_2 induced expression of both pS2 and c-myc mRNA more than 20 fold in ECC-1E_2 and ECC-1TAM tumors, tamoxifen also induced pS2 and c-myc mRNA by 3 fold in ECC-1E_2 tumors and by 8-10 fold in ECC-TAM tumors. Herceptin blocked expression of both pS2 and c-myc mRNA in tamoxifen-stimulated ECC-1TAM tumors by 50% compared to tamoxifen alone. Western blot analyses showed that Herceptin almost completely inhibited tyrosine phosphorylation of HER2/neu by decreasing total levels in both ECC-1E2 and ECC-1TAM tumors. Interestingly, neither phospho-Akt nor phospho-ERK1/2 was altered with Herceptin treatment in ECC-1E2 tumors. However, phospho-Akt was induced by tamoxifen in ECC-1TAM tumors, but only phospho-ERK1/2 was decreased in response to Herceptin.

Discussion: Herceptin completely inhibits tamoxifen-stimulated ECC-1 tumors *in vivo* by blocking ERα transcriptional activity and downregulating HER2/neu protein. The results suggest that the combination of the HER2/neu signaling pathway through ERK1/2 and the genomic activity of ERα contribute to the development of tamoxifen-stimulated endometrial cancer *in vivo*. In addition, the results indicate that amplification of the HER2/neu oncogene is not necessary for Herceptin to be effective in tamoxifen-stimulated endometrial cancer.

Herceptin blocks tamoxifen-stimulated endometrial cancer *in vivo* through inhibition of HER2/neu and estrogen receptorα activities.

Osipo C, Liu H, Lim S, Meeke K, Cheng D, and Jordan VC. The Robert H. Lurie Comprehensive Cancer Center, Feinberg School of Medicine of Northwestern University, Chicago, IL. 60611

Background: Tamoxifen has been used for the last 25 years to treat estrogen receptor (ERα) positive breast cancer in post-menopausal women. One of the major side effects of adjuvant tamoxifen therapy is the increased risk of endometrial cancer. To date, there are currently no models *in vivo* that mimic the development of tamoxifen-stimulated endometrial cancer in order to elucidate the mechanism of action.

Materials and Methods: ERα-positive human endometrial cancer cells (ECC-1) were injected into athymic mice and supplemented with a 0.30cm 17β-estradiol (E_2) capsules. E_2-stimulated ECC-1 (ECC-1E_2) tumors were developed and treated with nothing (Control) or 1.5mg tamoxifen for up to 24 weeks. Tumors that survived in response to E_2 + tamoxifen treatment were subsequently transplanted into new athymic mice and treated with nothing, 0.30cm E_2, or 1.5mg tamoxifen alone. Tamoxifen-stimulated ECC-1 (ECC-1TAM) tumors were developed that were also stimulated by 1.5mg raloxifene. Both tamoxifen naïve and tamoxifen-stimulated ECC-1 tumors were grown to approximately 0.30 cm^2 in cross sectional area with E_2 or tamoxifen, respectively. Mice separated into five treatment groups of 10 mice per group: no treatment, 0.30cm E_2, E2 + 30mg/Kg Herceptin, 1.5mg tamoxifen, 1.5mg tamoxifen + 30mg/Kg Herceptin, or 10mg ICI 182,780 (fulvestrant). ERα transcriptional activity was determined by measuring expression of two estrogen-responsive genes, pS2 and c-myc. Western blot analyses for PY-HER2/neu, total HER2/neu, PS473-Akt, total Akt, P-ERK1/2, and β-actin were performed on total tumor protein extracts.

Results: Tamoxifen-stimulated endometrial tumors (ECC-1) were developed by treating ECC-1 tumors with 1.5mg tamoxifen for up to 6 months *in vivo*. Upon serial transplantation into new generations of athymic mice, the HER2/neu inhibitor Herceptin inhibited the growth of E_2-stimulated ECC-1E_2 tumors by about 50% while completely inhibiting the growth of tamoxifen-stimulated ECC-1TAM tumors. While E_2 induced expression of both pS2 and c-myc mRNA more than 20 fold in ECC-1E_2 and ECC-1TAM tumors, tamoxifen also induced pS2 and c-myc mRNA by 3 fold in ECC-1E_2 tumors and by 8-10 fold in ECC-TAM tumors. Herceptin blocked expression of both pS2 and c-myc mRNA in tamoxifen-stimulated ECC-1TAM tumors by 50% compared to tamoxifen alone. Western blot analyses showed that Herceptin almost completely inhibited tyrosine phosphorylation of HER2/neu by decreasing total levels in both ECC-1E2 and ECC-1TAM tumors. Interestingly, neither phospho-Akt nor phospho-ERK1/2 was altered with Herceptin treatment in ECC-1E2 tumors. However, phospho-Akt was induced by tamoxifen in ECC-1TAM tumors, but only phospho-ERK1/2 was decreased in response to Herceptin.

Discussion: Herceptin completely inhibits tamoxifen-stimulated ECC-1 tumors *in vivo* by blocking ERα transcriptional activity and downregulating HER2/neu protein. The results suggest that the combination of the HER2/neu signaling pathway through ERK1/2 and the genomic activity of ERα contribute to the development of tamoxifen-stimulated endometrial cancer *in vivo*. In addition, the results indicate that amplification of the HER2/neu oncogene is not necessary for Herceptin to be effective in tamoxifen-stimulated endometrial cancer.

Accepted for San Antonio Breast Cancer Conference (2004)

Dynamics of microtubule cytoskeleton and focal adhesions in micropatterned cells

Kristiana Kandere-Grzybowska[1], Christopher Campbell[2], Yulia Komarova[1], Bartosz Grzybowski[2] and Gary G. Borisy[1]

[1]Department of Cell and Molecular Biology, Northwestern University Medical School, 303 East Chicago Avenue, Chicago, IL 60611-3008

[2]Department of Chemical and Biological Engineering, Northwestern University, 2145 Sheridan Road, Evanston, IL 60208-3120

Heterogeneity of cell form complicates the investigation of the dynamics of supramolecular structural elements in animal cells. When experiments are carried out with such heterogeneous cell populations, it is difficult to discern whether the phenotype resulting from an experimental perturbation is due to the perturbation per se or a secondary effect due to change in cell shape. We have evaluated the feasibility of combining time-lapse fluorescence microscopy with surface microprinting technologies for the evaluation of the dynamics of adhesions and microtubule (MT) cytoskeleton. Cell-adhesive islands of uniform shape (circular, polygonal, polarized) and size (30 to 50 micron diameter) separated by cell-adhesion resistant regions were patterned by microcontact printing of alkanethiolates on gold. B16F1 mouse melanoma cells were transfected with complementary DNAs (cDNAs) for MT marker proteins (β-tubulin, EB-3) and adhesion components (α-actinin, paxillin) tagged with green-fluorescent protein (GFP) moieties and time-lapse series of MT and adhesion dynamics were obtained. Cells plated on islands of magnitude equal to average cell size (960 micron square) assumed the shape of the island. Focal adhesions localized exclusively around the circumference of circular cells. To circumvent fluorescence quenching by gold during live imaging, an alternative method of cell micropatterning by etching patterns in gold by wet stamping and protecting remaining areas with hydrophilic alkanethiolates was developed. The latter method simplifies experimental design, improves the resolution of fluorescence signal and allows manipulation, such as microinjection, to be carried out with patterned cells. The tools developed in this study will be useful in the design of assays for investigation of the MT-adhesion interaction in living cells. These assays provide an objective way of evaluating cytoskeletal perturbations under conditions where cell shape is maintained constant. Supported by Grant GM 25062 (GGB) and Camille and Henry Dreyfus New Faculty Award (BG). KKG is a DOD Breast Cancer Trainee.

APPENDIX II

BREAST CANCER JOURNAL CLUB

Breast Cancer Journal Club Schedule for 2003/2004

October 21: Eric Ariazi e-ariazi@northwestern.edu

October 28: **Clodia Osipo (trainee)** c-osipo@northwestern.edu

November 4: Joan Lewis j-lewis4@northwestern.edu

November 11: Hong Liu h-liu4@northwestern.edu

November 18: **Kristiana Kandere-Grzybowska (trainee)** k-kandere@northwestern.edu

December 2: (San Antonio Breast Cancer Symposium)

January 20: Carla Jorgensen carlacwalker@hotmail.com

January 27: Sue Gapstur sgapstur@northwestern.edu

February 3: **Anne Mongiu (trainee-winter).**

February 10: Noman Kidwai

February 17: **Anne Strohecker (trainee)** a-strohecker@northwestern.edu

February 24: Joan Lewis j-lewis4@northwestern.edu

March 2: Bin Chen bch075@northwestern.edu

March 9: AACR oral presentations

March 30: AACR Annual Meeting

April 6: Vince Cryns v-cryns@northwestern.edu

April 13: **Clodia Osipo (trainee)** c-osipo@northwestern.edu

April 20: Eric Ariazi e-ariazi@northwestern.edu

April 27: **Kelly Kopp (trainee-spring)** k-kopp@northwestern.edu

May 4: Hong Liu h-liu4@northwestern.edu

May 11: **Christa Hestekin (trainee)** c-hestekin@northwestern.edu

Journal Club meets from 11:00 am to noon on the Tuesdays listed above in the Vanderwicken library on the 8th floor (8260 Olson). A computer and projector will be available for PowerPoint presentations. If you are unable to give journal club on your scheduled date, please arrange to switch your date with one of the other journal club members.

APPENDIX III

ADVANCED TOPICS IN BREAST CANCER

ROBERT H. LURIE
COMPREHENSIVE CANCER CENTER
OF NORTHWESTERN UNIVERSITY

Advanced Topics in Breast Cancer Course

V. Craig Jordan, Ph.D., D.Sc.
Course Director

Advanced Topics in Breast Cancer will consist of eight classes taught be members of the Robert H. Lurie Comprehensive Cancer Center Breast Cancer Program. All sessions will be held on Thurdays in the Vanderwicken Library, Olson 8260, from 10 am to 11:30 am. The final class will be student presentations of their research in breast cancer.

DATE	FACULTY	TOPIC
January 8, 2004	Susan Gapstur , Ph.D.	Epidemiology of Breast Cancer
February 12, 2004	Monica Morrow, M..D.	Surgical Management of Breast Cancer
March 04, 2004	Elizabeth Wiley, M.D.	Pathology of Breast Cancer
April 8, 2004	Vince Cryns, M.D.	Cell Survival in Breast Cancer
May 6, 2004	V. Craig Jordan, Ph.D.	Endocrine Therapy of Breast Cancer
June 10, 2004	Eric Ariazi, Ph.D.	Signaling in Breast Cancer Cells
July 8, 2004	Boris Pasche, M.D., Ph.D.	Genetics of Breast Cancer
August 19, 2004	Robin Leikin, Ph.D.	Student Presentations

ROBERT H. LURIE
COMPREHENSIVE CANCER CENTER
OF NORTHWESTERN UNIVERSITY

Training Program
in
Molecular Biology of Breast Neoplasia

ANNUAL PRESENTATIONS

THURSDAY AUGUST 19
10:00 am Olson 8260 Vanderwicken Library

Kristiana Kandere, Ph.D.	**Borisy Laboratory**
Clodia Osipo, Ph.D.	**Jordan Laboratory**
Anne Strohecker	**Cryns Laboratory**
Kelly Kopp	**Huang Laboratory**
Christa Hestekin	**Barron Laboratory**
Anne Mongiu	**Borisy Laboratory**

APPENDIX IV

PUBLICATIONS

1: Exp Biol Med (Maywood). 2004 Sep;229(8):722-31.

The consequences of exhaustive antiestrogen therapy in breast cancer: estrogen-induced tumor cell death.

Osipo C, Liu H, Meeke K, Jordan VC.

Robert H. Lurie Comprehensive Cancer Center, Northwestern University, Feinberg School c Medicine, 303 East Chicago Avenue, Olson Pavilion, Room 8258, Chicago, IL 60611. vcjordan@northwestern.edu

Forty years ago, the endocrine treatment for breast cancer was a last resort at palliation befor the disease overwhelmed the patient (1). Ovarian ablation was the treatment of choice for th premenopausal patient, whereas either adrenalectomy or, paradoxically, high-dose synthetic estrogen therapy were used for treatment in postmenopausal patients. A reduction or an excess of estrogen provoked objective responses in one out of three women. Unfortunately, there was no way of predicting who would respond to endocrine ablation, and because so fe patients responded there was no enthusiasm for developing new endocrine agents. All hopes for a cure for breast cancer turned to appropriate combinations of cytotoxic chemotherapy.Today tamoxifen, a nonsteroidal antiestrogen (2), has proven to be effective i all stages of premenopausal and postmenopausal breast cancer, and several new endocrine strategies, including aromatase inhibitors, luteinizing-hormone releasing hormone (LHRH) superagonists, and a pure antiestrogen (fulvestrant), are now available for breast cancer treatment. Additionally, tamoxifen and raloxifene, a related compound, are used to reduce th risk of breast cancer and osteoporosis, respectively, in high-risk groups (3). Hormonal modulation and strategies to prevent the actions of estrogen in the breast are ubiquitous. However, with successful changes in treatment strategies comes the consequence of change.This minireview will describe the current strategies for the treatment and prevention of breast cancer and present emerging new concepts about the consequences of exhaustive antiestrogen treatment on therapeutic resistance.

PMID: 15337826 [PubMed - in process]

Paradoxical Action of Fulvestrant in Estradiol-Induced Regression of Tamoxifen-Stimulated Breast Cancer

Clodia Osipo, Csaba Gajdos, Hong Liu, Bin Chen, V. Craig Jordan

Background: **Long-term tamoxifen treatment of breast cancer can result in tamoxifen-stimulated breast cancer, in which estrogen inhibits tumor growth after tamoxifen withdrawal. We investigated the molecular mechanism(s) of estradiol-induced tumor regression by using an *in vivo* model of tamoxifen-stimulated human breast cancer.** ***Methods:*** **Growth of parental estradiol-stimulated MCF-$7E_2$ and long-term tamoxifen-stimulated MCF-7TAMLT xenografts in athymic mice was measured during treatment with vehicle, estradiol, estradiol plus tamoxifen, tamoxifen alone, estradiol plus fulvestrant, or fulvestrant alone. Apoptosis was detected by the terminal deoxynucleotidyltransferase–mediated deoxyuridine triphosphate nick-end labeling (TUNEL) assay. Protein expression was assessed by western blot analysis. mRNA expression was assessed by real-time reverse transcription–polymerase chain reaction. All statistical tests were two-sided.** ***Results:*** **MCF-$7E_2$ tumor growth was stimulated by estradiol (cross-sectional area at week 13 = 1.06 cm^2, 95% confidence interval [CI] = 0.82 to 1.30 cm^2; $P<.001$) compared with control (0.06 cm^2, 95%CI = −0.02 to 0.14 cm^2), but tumor growth was inhibited by tamoxifen or fulvestrant. MCF-7TAMLT tumor growth was stimulated by tamoxifen) cross-sectional area at week 10 = 0.60 cm^2, 95% CI = 0.50 to 0.70 cm^2; $P<.001$) compared with control (0.02 cm^2, 95% CI = 0.00 to 0.04 cm^2). For MCF-7TAMLT tumors that were initially 0.35 cm^2, estradiol-induced regression to 0.18 cm^2 (95% CI = 0.15 to 0.21 cm^2; $P<.001$), and tamoxifen or estradiol plus fulvestrant enhanced tumor growth to 1.00 cm^2 (95% CI = 0.88 to 1.22 cm^2). Estradiol increased the number of apoptotic cells in tumors by 23% (95% CI = 20% to 26%; $P<.001$) compared with all other treatments, decreased estrogen receptor α(ERα) protein expression, increased the expression of Fas mRNA and protein, decreased the expression of HER2/neu mRNA and protein and nuclear factor κB (NF-κB) protein but did not affect Fas ligand protein expression compared with control. Paradoxically, fulvestrant reversed this effect and stimulated MCF-7TAMLT tumor growth apparently through ERα-mediated regulation of Fas, HER2/neu, and NF-κB.** ***Conclusion:*** **Physiologic levels of estradiol induced regression of tamoxifen-stimulated breast cancer tumors, apparently by inducing the death receptor Fas and suppressing the antiapoptotic/prosurvival factors NF-κB and HER2/neu. [J Natl Cancer Inst 2003;95:1597–1608]**

Tamoxifen is currently used to treat all stages of estrogen receptor α (ERα)-positive breast cancer *(1)*. Tamoxifen is also used as a chemopreventive agent for pre- and postmenopausal women at high risk for breast cancer *(2,3)*. The benefits of tamoxifen as an adjuvant therapy continue for up to a decade after completion of 5 years of treatment *(4)*. However, resistance to tamoxifen does occur by clonal selection of breast cancer cells that, paradoxically, grow in response to

Affiliations of authors: Robert H. Lurie Comprehensive Cancer Center, Feinberg School of Medicine, Northwestern University, Chicago, IL (CO, HL, BC, VCJ); Department of Surgery, University of Alabama, Birmingham (CG).

Correspondence to: V. Craig Jordan, OBE, PhD, DSc, Robert H. Lurie Comprehensive Cancer Center, Feinberg School of Medicine, Northwestern University, 8258 Olson, 303 E. Chicago Ave., Chicago, IL 60611 (e-mail: vcjordan@northwestern.edu).

See "Notes" following "References."

DOI: 10.1093/jnci/djg079

Journal of the National Cancer Institute, Vol. 95, No. 21,

tamoxifen *(5,6)*. These tumors are ERα-positive, and their growth continues to be regulated by ERα. Consequently, new endocrine therapies have now been established to inhibit growth of breast tumors before or after tamoxifen therapy has failed. These therapies include the use of aromatase inhibitors to inhibit 17β-estradiol (hereafter estradiol) synthesis *(7–9)* and the pure antiestrogen fulvestrant (Faslodex or ICI 182,780) *(10,11)* to target the ERα for ubiquitin-mediated degradation *(12,13)*. The assumption made for using these second-line therapies is that if the formation of the estradiol–ERα complex is prevented, then breast tumors that have acquired resistance to tamoxifen will regress. These conclusions are based, in part, on laboratory models of early drug resistance to tamoxifen (1–2 years) that show that breast cancer cells *in vivo* grow in the presence of estrogen or tamoxifen *(14–16)*. However, a more complex situation with estradiol has been documented for tumors after 5 years of tamoxifen treatment, that is, postmenopausal levels of estradiol inhibit the growth of tamoxifen-stimulated MCF-7 breast tumors *in vivo (17,18)* and estrogen-deprived MCF-7 cells *in vitro (19)*. Thus, another hypothesis is emerging that the ERα mediates the dual actions of estradiol initially as a growth stimulator in breast cancer cells and then as a growth inhibitor in breast cancer cells after long-term therapy with tamoxifen or aromatase inhibitors. What is still unclear is the mechanism of estradiol-induced growth inhibition in breast cancer cells that are stimulated by tamoxifen or that grow spontaneously when deprived of estradiol.

Song et al. *(19)* showed that MCF-7 cells deprived of estrogen for up to 24 months *in vitro* (MCF-7LTED cells) express Fas, a member of the tumor necrosis factor α receptor family, in contrast to the parental MCF-7 cells, which do not express Fas. These authors also demonstrated that, although both parental and MCF-7LTED cells express Fas ligand (FasL), estradiol treatment increases the levels of FasL and induces apoptosis in Fas-expressing MCF-7LTED cells only.

The FasL/Fas death receptor pathway is activated by cross-linking Fas (CD95/APO-1), a type I transmembrane protein expressed by a variety of nucleated cells, to FasL, a type II transmembrane protein expressed by activated T cells and or various other non–T cells. The cross-linking of FasL to Fas results in trimerization of Fas, activation of downstream caspases, and induction of apoptosis *(20–24)*. The FasL gene promoter contains an estrogen response element and is regulated by estradiol *(25)*. From these results, Song et al. *(19)* concluded that estrogen-induced tumor regression might result from the estrogen-mediated overexpression of FasL, which would induce Fas-mediated apoptosis in MCF-7LTED cells.

The importance of the FasL/Fas death pathway as a mediator of apoptosis is clearly demonstrated in immune surveillance *(22)*. In breast cancer, tumor escape from immunologic surveillance results from the induction of apoptosis of Fas-bearing, activated lymphocytes by FasL-bearing breast cancer cells *(22)*. An earlier study *(24)* comparing normal human breast epithelium to breast carcinomas demonstrates that FasL mRNA and protein are overexpressed in carcinomas but that the expression of Fas mRNA and protein is almost completely undetected. Thus, by increasing the expression of FasL and simultaneously decreasing that of Fas, breast tumors evade the immune response and continue to grow.

In addition to dysregulation of apoptotic signals, such as those in the FasL/Fas pathway, breast carcinomas overexpress the prosurvival factor HER2/neu, a member of the epidermal growth factor receptor family of receptor tyrosine kinases *(26,27)*, and the antiapoptotic nuclear factor κB (NF-κB) *(28,29)*. In breast carcinomas, constitutively active HER2/neu and/or NF-κB appear to be critical for tumor survival and growth by blocking apoptotic signals from death receptors *(28,29)*.

The goal of this study was to investigate the mechanism of estradiol-induced tumor regression in tamoxifen-stimulated human MCF-7TAMLT breast cancers *in vivo*, a model generated by treating mice carrying tamoxifen-naive MCF-7E_2 tumors with tamoxifen for more than 5 years. This model is an example of breast tumors that are resistant to long-term tamoxifen therapy and is useful for examining the effects of various second-line treatments in tumors exposed to tamoxifen for 5 years. Thus, the model could mimic a clinical situation in which 5 years of adjuvant tamoxifen therapy may result in the evolution of a tamoxifen-sensitive breast cancer to a clinically undetected tamoxifen-stimulated micrometastatic breast cancer. We investigated whether estradiol causes tumor regression by inducing apoptosis. We examined ER function by measuring levels of transforming growth factor α (TGF-α) mRNA, an estrogen-responsive gene *(30,31)*. Expression of FasL protein, Fas mRNA and protein, HER2/neu mRNA and protein, and NF-κB and cyclooxygenase-2 proteins was measured to determine whether the FasL/Fas death pathway and/or the HER2/neu/NF-κB prosurvival/antiapoptotic pathways were modulated by estradiol in MCF-7TAMLT tumors.

Materials and Methods

Cell Culture

The human breast cancer cell line MCF-7 was purchased from the American Type Culture Collection (Manassas, VA) and maintained at 37 °C in a 95% humidified air/5% CO_2 atmosphere in phenol red–containing RPMI-1640 medium supplemented with 10% fetal bovine serum, insulin at 0.6 μg/mL, 1% L-glutamine, 1% nonessential amino acids, and a 1% solution of penicillin, streptomycin, and an antimycotic agent (Gibco-BRL, Life Technologies, Long Island, NY).

Drug Treatments

The following standard drug dosages were used throughout this study, unless otherwise stated. Estradiol was given subcutaneously in 0.30-cm silastic capsules (Baxter Healthcare, Mundelein, IL) to achieve postmenopausal serum levels of estradiol (83.8 pg/mL in serum) *(32)*. Tamoxifen (Sigma-Aldrich, St. Louis, MO) at 1.5 mg/day was given orally by gavage. Fulvestrant (AstraZeneca, Cheshire, U.K.) was dissolved in 100% ethanol and diluted in peanut oil; 5 mg was then injected subcutaneously twice a week.

Growth of MCF-7E_2 Tumors *In Vivo*

The mammary fat pads of 4- to 6-week-old ovariectomized BALB/c nu/nu athymic mice (Harlan Sprague Dawley, Madison, WI) were bilaterally inoculated with 0.10 mL containing 1×10^7 MCF-7 cells suspended in sterile phosphate-buffered saline. MCF-7 cells were inoculated into athymic mice, and

mice were treated with estradiol to achieve estradiol-stimulated tumor growth (MCF-7E_2 tumors) *(15,17,32–34)*. Tumors were maintained by serial passage of solid tumors into athymic mice as described previously *(17)*. Fifty mice were bi-transplanted with parental MCF-7E_2 tumors, and groups of 10 mice each were randomly assigned to the following treatments: vehicle, estradiol, estradiol plus tamoxifen, estradiol plus fulvestrant, or fulvestrant alone.

Growth of MCF-7TAMLT Tumors *In Vivo*

Long-term tamoxifen-stimulated tumors (MCF-7TAMLT) were developed by re-transplanting growing estradiol-dependent MCF-7 tumors into new athymic mice and treating the mice with tamoxifen *(17,33,35)*. Selected tamoxifen-stimulated MCF-7 tumors were then serially passaged into new athymic mice, and mice were treated with tamoxifen for more than 5 years, as described *(17)*. The mammary fat pads of 50 ovariectomized BALB/c nu/nu athymic mice, 4–6 weeks old, were bi-transplanted with tumors, and groups of 10 mice were randomly assigned to the following treatments: vehicle, tamoxifen alone, estradiol alone, fulvestrant alone, or estradiol plus fulvestrant. In another experiment, 40 mice were bi-transplanted with MCF-7TAMLT tumors and were treated with tamoxifen. Another 10 mice (controls) were bi-transplanted with MCF-7TAMLT tumors and were treated with vehicle alone. When the mean tumor cross-sectional area in tamoxifen-treated mice reached 0.35 cm^2, groups of 10 mice were randomly assigned to the following treatments: tamoxifen alone, estradiol alone, estradiol plus fulvestrant, or fulvestrant alone. The previous experiment was repeated as described above except this time 30 mice were bi-transplanted with MCF-7TAMLT tumors and treated with tamoxifen. When the mean tumor cross-sectional area in tamoxifen-treated mice reached 0.32 cm^2, mice were withdrawn from tamoxifen treatment, and groups of 10 mice were randomly assigned to the following treatments: continue tamoxifen alone, discontinue tamoxifen, or continue estradiol alone. Tumors were measured weekly with vernier calipers. The cross-sectional area was calculated by multiplying the length (l) by the width (w) and by π and dividing the product by 4 (i.e., $lw\pi/4$).

The Animal Care and Use Committee of Northwestern University approved all of the procedures involving animals.

Apoptosis Assay

The following two-step method was used to detect apoptosis: the terminal deoxynucleotidyltransferase–mediated deoxyuridine triphosphate nick-end labeling (TUNEL) assay followed by tetramethylrhodamine deoxyuridine 5′-triphosphate (TMR) staining. An *in situ* cell death assay with the TMR red detection kit (Roche Diagnostic, Indianapolis, IN) was performed on tumor sections from paraffin-embedded blocks, according to the manufacturer's instructions. The TUNEL assay was done in triplicate and repeated four times with independent tumors from each treatment group. The percentage of apoptosis was calculated by dividing the number of TMR-positive cells or TUNEL-positive cells by the total number of epithelial cells (identified by 4′,6-diamidino-2-phenylindole and hematoxylin–eosin staining) and multiplying the result by 100.

Western Blot Analysis

Tumors were pulverized in liquid nitrogen and resuspended in lysis buffer (1% Triton X-100, 1 m*M* EDTA, 150 m*M* NaCl, 50 m*M* Tris–HCl [pH 7.4], phenylmethylsulfonyl fluoride at 25 mg/mL, leupeptin at 10 mg/mL, aprotinin at 10 mg/mL, pepstatin at 10 mg/mL, *N*α-*p*-tosyl-L-chloromethyl ketone hydrochloride [i.e., TLCK] at 10 mg/mL, *N*-*p*-tosyl-L-phenylalanine chloromethyl ketone [i.e., TPCK] at 10 mg/mL, 100 m*M* NaF, 10 m*M* orthovanadate) (all supplied by Sigma-Aldrich). The extract was subsequently sonicated at level 1 three times at 1-second intervals with a Microson sonicator (Misonix, Farmington, NY) and then centrifuged for 5 minutes at 5000*g* at 4 °C. The supernatant was collected, and protein concentration was determined with the Bradford assay (Bio-Rad Laboratories, Hercules, CA). Equal amounts of protein (25–50 μg) were loaded into lanes of a 7% gel for sodium dodecyl sulfate–polyacrylamide gel electrophoresis. Proteins were transferred to a blot for western blot analysis of ERα (1 : 200 dilution of rabbit anti-human antibody; clone G20; Santa Cruz Biotechnology, Santa Cruz, CA), β-actin (1 : 20 000 dilution of mouse anti-human antibody; clone A15; Sigma-Aldrich), FasL (1 : 1000 dilution of mouse anti-human antibody; clone 33; BD Transduction Labs, San Diego, CA), Fas (1 : 500 dilution of rabbit anti-human antibody; clone C-20; Santa Cruz Biotechnology), phosphorylated HER2/neu (rabbit anti-human phosphorylated residue Y1248 antibody at 1 μg/mL; Upstate Biotechnology, Lake Placid, NY), HER2/neu (1 : 200 dilution of mouse anti-human HER2/neu antibody AB-11; Neomarkers, Fremont, CA), NF-κB p65 subunit (rabbit anti-human p65 antibody at 2 μg/mL; Upstate Biotechnology), and cyclooxygenase-2 (COX-2) (rabbit anti-human antibody at 1 μg/mL; Upstate Biotechnology). The appropriate secondary antibody conjugated to horseradish peroxidase was used to detect the primary antibody (either goat anti-rabbit or goat anti-mouse immunoglobulin G (Santa Cruz Biotechnology). The blot was developed with an enhanced chemiluminescence (ECL) kit (Amersham, Arlington Heights, IL). The membrane was exposed to Kodak X-Omat film for 10–30 seconds (Kodak, Rochester, NY).

Real-Time Reverse Transcription–Polymerase Chain Reaction for Human TGF-α, Fas, and HER2/neu mRNAs in Tumors

Total RNA, extracted from the tumors with the RNeasy mini kit (Qiagen, Valencia, CA) according to the manufacturer's instructions, was reverse transcribed with TaqMan reverse transcription reagents (Applied Biosystems, Hayward, CA) and random hexamers as the primers, according to the manufacturer's instructions. Primers and probes for human TGF-α and Fas were designed with Primer Express TM1.5 software (Applied Biosystems) set at default parameters to select the most optimized primer and probe sets for this system. The sequences for the forward and reverse primers for human TGF-α were 5′-GCCTGTAACACACATGCAGTGA-3′ and 5′-TTTCCAAAGGACTGACTTGGAAG-3′, respectively. The sequence for the TGF-α probe was 5′-AGGCCTCACATATACGCCTCCCTAGAAGTG-3′. Sequences for the forward and reverse primers for human Fas were 5′-TGGAAGGCCTGCATCATGA-3′ and 5′-CAGTCCCTAGCTTTCCTTTCACC-3′, respectively. The sequence for the human Fas probe was 5′-CCAATTCTGCCATAAGCCCTGTCCTCC-3′. Sequences for the forward and re-

verse primers for human HER2/neu were 5′-ACTGCAGAGGCTGCGGATT-3′ and 5′-ACGGCCAGGGCATAGTTGT-3′, respectively. The sequence for the human HER2/neu probe was 5′-TGCGAGGCACCCAGCTCTTTGA-3′. For all real-time reverse transcription–polymerase chain reactions (RT–PCRs), 6-carboxyfluorescein was the reporter, and QSY7 was the quencher (MegaBases, Chicago, IL). The quantity of human glyceraldehyde 3-phosphate dehydrogenase (GAPDH) mRNA was also measured in each total cDNA sample for normalization. The probe and primers for GAPDH were purchased from Applied Biosystems. The PCR portion of the reaction was performed with the TaqMan PCR core reagent kit (Applied Biosystems). The 25-mL PCR mixture contained 50 ng of total cDNA, 100 n*M* probe, and 200 n*M* primers. Real-time PCR was performed with the ABI-Prism 7700 sequence detection system (Applied Biosystems). PCR conditions were 50 °C for 2 minutes and 95 °C for 10 minutes followed by 40 cycles of 95 °C for 15 seconds and 60 °C for 1 minute.

Statistical Analysis

Tumor growth curves were analyzed longitudinally with a two-factor analysis of variance (ANOVA) to compare cross-sectional areas of all tumors for all treatment groups in a time-dependent manner. Tumors in athymic mice were assumed to be homogenous across individual mice. Tumors within and between mice were assumed to be independent of each other. Tumor growth curves represent means and 95% confidence intervals (CIs) of tumor cross-sectional areas. One-factor ANOVA was used to analyze differences in the percentage of apoptosis between the various treatment groups and the control group, as measured by the TUNEL assay. One-factor ANOVA was used to analyze differences in mRNA levels as detected by real-time PCR between the treatment groups and the control group. The error bars for the measurement of the percentage of apoptosis and mRNA copy number are 95% confidence intervals as calculated with StatMost 2.5 (DataMost, Salt Lake City, UT). All statistical tests were two-sided.

Results

Growth of MCF-7E_2 and MCF-7TAMLT Tumors *In Vivo*

The effects of estradiol, tamoxifen, and fulvestrant on the growth of tamoxifen-naive MCF-7E_2 and tamoxifen-stimulated MCF-7TAMLT tumors in athymic mice were investigated. The growth of parental MCF-7E_2 tumors was stimulated more by estradiol than by estradiol plus tamoxifen, estradiol plus fulvestrant, or control (Fig. 1, A). At 13 weeks, the cross-sectional area of estradiol-treated tumors was 1.06 cm^2 (95% CI = 0.82 to 1.30 cm^2) compared with that of control (0.06 cm^2, 95% CI = −0.02 to 0.14 cm^2), estradiol plus tamoxifen (0.30 cm^2, 95% CI = 0.26 to 0.34 cm^2), estradiol plus fulvestrant (0.01 cm^2, 95% CI = 0.00 to 0.02 cm^2), or fulvestrant alone (0.01 cm^2, 95% CI = 0.00 to 0.02 cm^2). In contrast, tamoxifen-stimulated MCF-7TAMLT tumors grew faster in mice treated with tamoxifen than in mice treated with estradiol, fulvestrant, or control vehicle ($P<.001$ for all) (Fig. 1, B). At 9 weeks, the cross-sectional area of MCF-7TAMLT tumors treated with tamoxifen (0.47 cm^2, 95% CI = 0.35 to 0.59 cm^2; $P<.001$) was greater than that of tumors treated with control (0.02 cm^2, 95% CI = 0.00 to 0.04 cm^2), fulvestrant alone, or estradiol alone. Surprisingly, the growth of MCF-7TAMLT tumors treated with a combination of estradiol plus fulvestrant was essentially the same as that of tumors treated with tamoxifen alone (Fig. 1, B). At 9 weeks, the cross-sectional area of tumors treated with estradiol plus fulvestrant was 0.47 cm^2 (95% CI = 0.32 to 0.62 cm^2). In addition, when we increased the weekly dose of fulvestrant to 20 mg in combination with estradiol, tumors continued to grow (data not shown). These results suggest that estradiol may act through the ERα pathway to inhibit the growth of MCF-7TAMLT tumors.

To investigate whether estradiol is acting as a tumoristatic or tumoricidal agent, mice bi-transplanted with MCF-7TAMLT tumors were treated with tamoxifen until the cross-sectional area of tumors reached approximately 0.35 cm^2. At this point, tamoxifen was withdrawn, and mice were randomly assigned to treatment groups as described above. In estradiol-treated mice, MCF-7TAMLT tumors continued to grow for 2 weeks and then regressed rapidly, in contrast to tumors in mice treated with tamoxifen, estradiol plus fulvestrant, or fulvestrant alone (all $P<.001$; Fig. 1, C). At 10 weeks, the mean cross-sectional area of tumors in mice treated with estradiol was 0.18 cm^2 (95% CI = 0.15 to 0.21 cm^2) compared with fulvestrant alone (0.44 cm^2, 95% CI = 0.37 to 0.51 cm^2), tamoxifen (0.60 cm^2, 95% CI = 0.50 to 0.70 cm^2), or estradiol plus fulvestrant (1.00 cm^2, 95% CI = 0.88 to 1.12 cm^2). Thus, at physiologic levels, estradiol appears to act as a potent tumoricidal agent for MCF-7TAMLT tumors. Remarkably, tumors treated with estradiol plus fulvestrant grew robustly (Fig. 1, C).

To determine whether the estradiol-induced tumor regression was a consequence of the tamoxifen withdrawal, mice bi-transplanted with MCF-7TAMLT tumors were treated with tamoxifen until tumors had a cross-sectional area of 0.32 cm^2. At this point, tamoxifen was withdrawn, and mice were randomly assigned to the following treatment groups: continue tamoxifen treatment, discontinue tamoxifen treatment, or discontinue tamoxifen treatment and begin estradiol treatment (Fig. 1, D). In the estradiol-treated group, MCF-7TAMLT tumors regressed, with a mean cross-sectional area at 10 weeks of 0.10 cm^2 (95% CI = 0.04 to 0.16 cm^2; $P = .001$), whereas tumors in the other groups continued to grow, with cross-sectional areas of 0.60 cm^2 (95% CI = 0.47 to 0.73 cm^2) in the tamoxifen-treated group and 0.40 cm^2 (95% CI = 0.33 to 0.70 cm^2) in the group for which tamoxifen was withdrawn. However, the growth rate was lower for tumors withdrawn from tamoxifen than for tumors treated with tamoxifen ($P = .038$).

Effects of Estradiol on Apoptosis

To determine whether apoptosis was involved in estradiol-induced regression of MCF-7TAMLT tumors, we used the TUNEL assay to quantitate apoptosis in tumor sections from all treatment groups at week 9 (Fig. 1, C) and week 10 (Fig. 1, D). MCF-7TAMLT tumors treated with estradiol had 23% (95% CI = 20% to 26%; $P<.001$) apoptotic cells compared with tumors treated with vehicle control (1.2%, 95% CI = 1.98% to 2.02%), tamoxifen (1.7%, 95% CI = 1.69% to 1.71%), fulvestrant (4.8%, 95% CI = 2.1% to 7.5%), or estradiol plus fulvestrant

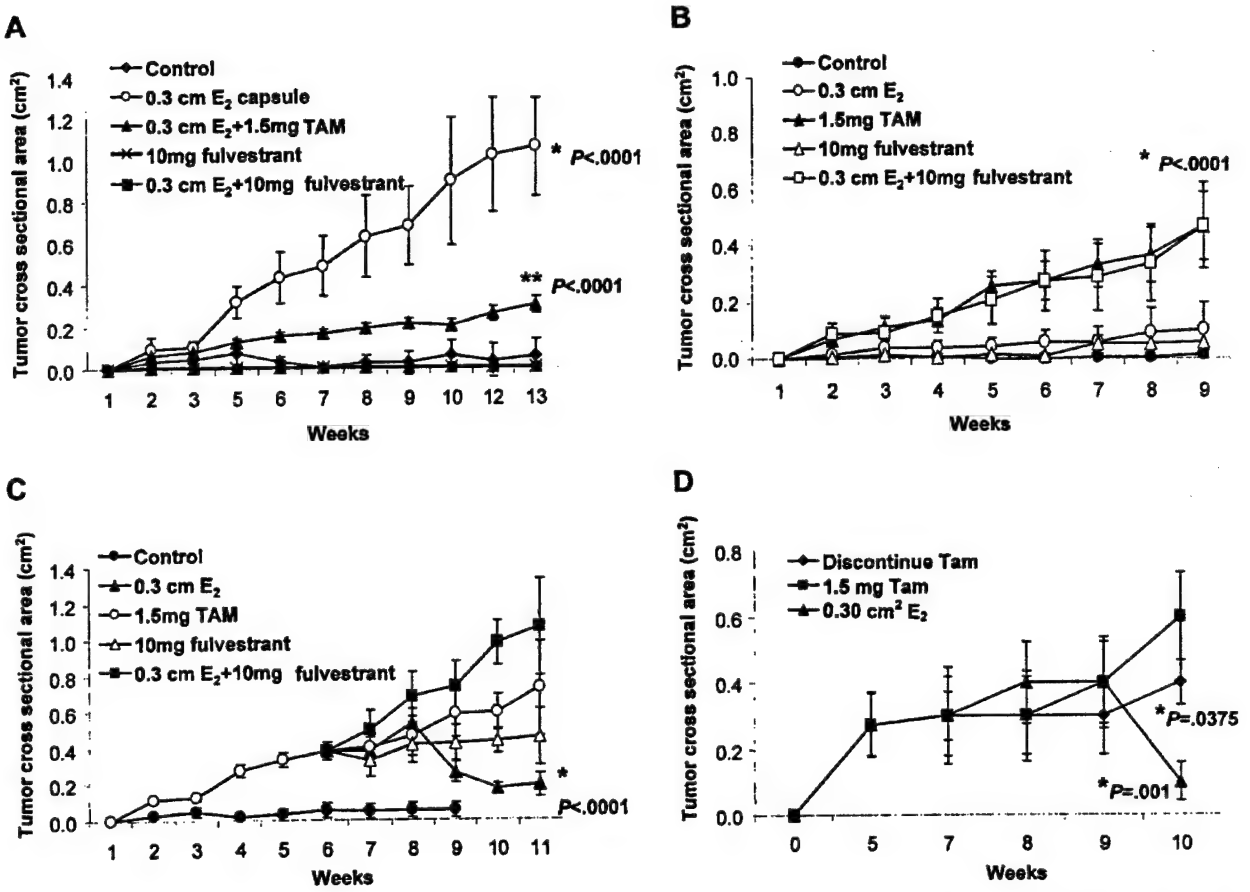

Fig. 1. Growth of MCF-7E_2 and MCF-7TAMLT tumors in athymic mice. Estradiol (E_2) was given as a 0.30-cm silastic capsule subcutaneously, tamoxifen (TAM) was given orally by gavage at 1.5 mg/day, and 10 mg of fulvestrant was given subcutaneously as a 5-mg dose twice a week. For all panels, tumor areas were measured weekly with vernier calipers. Cross-sectional areas were calculated by multiplying the length (l) by the width (w) and by π and dividing the product by 4 (i.e., $lw\pi/4$). **A)** MCF-7E_2 tumors. Fifty ovariectomized athymic mice were bi-transplanted with tamoxifen-naive MCF-7E_2 tumors, and groups of 10 mice were randomly assigned to the following treatments: vehicle (control), estradiol alone, estradiol plus tamoxifen, estradiol plus fulvestrant, or fulvestrant alone. *Cross-sectional area at 13 weeks of estradiol-treated tumors was statistically significantly different from that of tumors treated with control vehicle, estradiol plus tamoxifen, fulvestrant alone, or estradiol plus fulvestrant. **Cross-sectional area of tumors at 13 weeks treated with estradiol plus tamoxifen was statistically significantly different from that of tumors treated with vehicle control, fulvestrant alone, or estradiol plus fulvestrant. **B)** MCF-7TAMLT tumors. Another 50 athymic mice were bi-transplanted with MCF-7TAMLT tumors, and groups of 10 mice were randomly assigned to the following treatments: vehicle control, tamoxifen alone, estradiol alone, estradiol plus fulvestrant, or fulvestrant alone. *Cross-sectional area at 9 weeks of tumors treated with tamoxifen or with estradiol plus fulvestrant was statistically significantly different from that of tumors treated with vehicle control, fulvestrant alone, or estradiol. **C)** Tamoxifen-treated MCF-7TAMLT tumors. Fifty mice were bi-transplanted with MCF-7TAMLT tumors, of which 40 were treated with tamoxifen until tumors had an area of 0.35 cm^2, and 10 were given vehicle from the beginning (control). Tamoxifen was withdrawn from the tamoxifen-treated mice, and groups of 10 mice were randomly assigned to the following treatments: tamoxifen alone, estradiol alone, fulvestrant alone, or estradiol plus fulvestrant. *Cross-sectional area at 10 weeks of tumors treated with estradiol was statistically significantly different than that of tumors treated with tamoxifen alone, fulvestrant alone, or estradiol plus fulvestrant. **D)** Tamoxifen withdrawal. Thirty mice were bi-transplanted with MCF-7TAMLT tumors and treated with tamoxifen until tumors had an area of 0.32 cm^2. Tamoxifen was withdrawn, and groups of 10 mice were randomly assigned to the following treatments: tamoxifen, estradiol, or no treatment. *Cross-sectional area at 10 weeks of tumors treated with estradiol or withdrawn from tamoxifen was statistically significantly different from that of tumors treated with tamoxifen alone. At the conclusion of the experiment, one tumor from each mouse was fixed in 10% buffered formalin and sectioned for analysis and the other was snap-frozen in liquid nitrogen and maintained at −80 °C for future use. Data are from a representative experiment; results of other experiments are similar. Each experiment was repeated at least three times, with 10 mice per group. Error bars = 95% confidence intervals. All statistical tests were two-sided.

(1.7%, 95% CI = 0.7% to 2.7%) (Fig. 2, A) or 20% (95% CI = 7% to 33%; P = .038) apoptotic cells compared with tumors withdrawn from tamoxifen (Fig. 2, B). More importantly, apoptosis was completely blocked (2.5%, 95% CI = 1.5% to 3.5%) in tumors treated with the combination of estradiol plus fulvestrant (Fig. 2, A), indicating that estradiol-induced MCF-7TAMLT tumor regression is the result of apoptosis mediated through the ERα pathway.

Expression and Function of ERα in MCF-7E_2 and MCF-7TAMLT Tumors

To determined whether ERα expression and function are altered in MCF-7TAMLT tumors by long-term exposure to tamoxifen, we used western blot analysis to measure the level of ERα protein and real-time RT–PCR to measure ERα activity as reflected by the expression of TGF-α mRNA, an

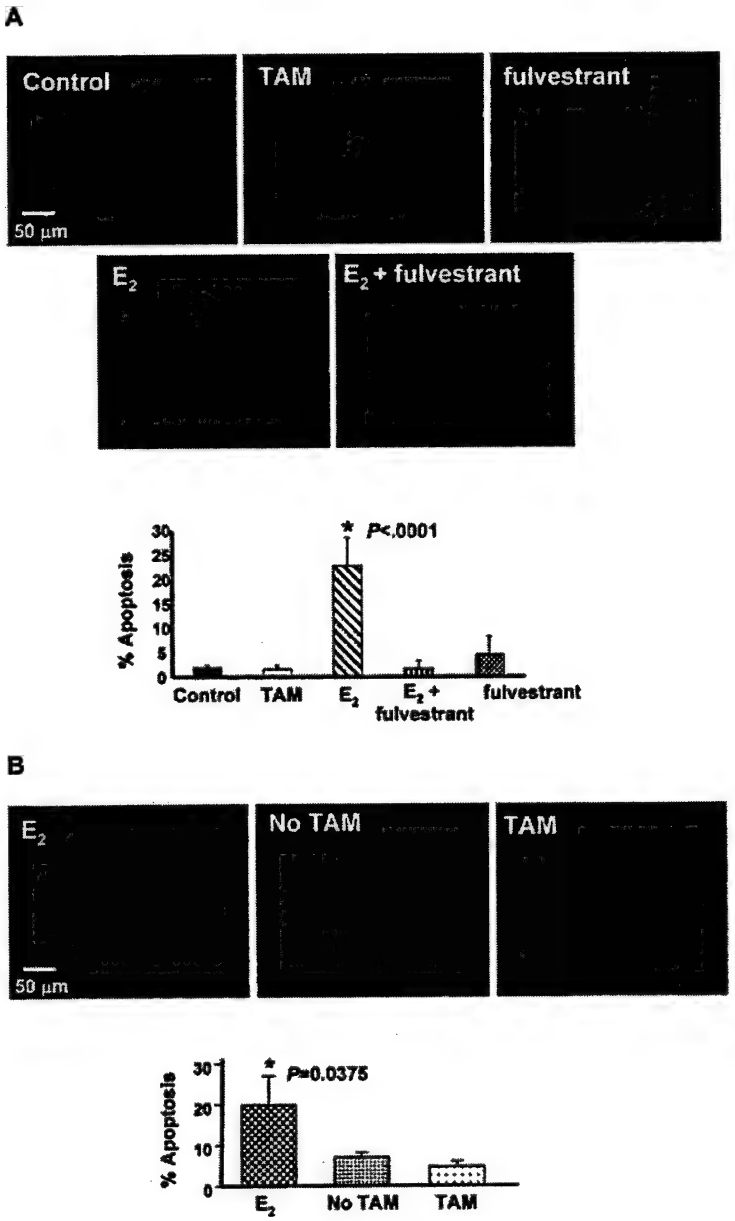

Fig. 2. Apoptosis in MCF-7TAMLT tumors after various treatments. **A)** MCF-7TAMLT tumors were bi-transplanted into the mammary fat pads of 50 mice. Ten control mice were treated with vehicle; 40 mice were treated with tamoxifen (TAM) at 1.5 mg/day until the cross-sectional area of the tumor was 0.35 cm^2. At this time, tamoxifen was stopped and groups of 10 mice were randomly assigned to receive tamoxifen alone (1.5 mg/day), estradiol (E_2; 0.3-cm capsule), fulvestrant alone (10 mg/wk), or estradiol plus fulvestrant. At 10 weeks, tumors were fixed and sectioned, and sections were placed on slides. An *in situ* death assay with the tetramethylrhodamine deoxyuridine 5′-triphosphate (TMR) red detection system (Roche Diagnostics) was used to detect apoptotic cells, according to the manufacturer's instructions. Four independent tumors from each treatment group, as described in Fig. 1, C, were tested. Slides were examined under ×40 magnification with a fluorescence microscope. *$P<.001$ for the estradiol-treated group versus all other groups. **B)** Thirty mice were bi-transplanted with MCF-7TAMLT tumors and treated with tamoxifen, as in **panel A**, until tumors were 0.32 cm^2. At this time, tamoxifen was withdrawn and groups of 10 mice were randomly assigned to no tamoxifen (discontinue TAM), to receive tamoxifen (continue TAM), or to receive estradiol (E_2; 0.30-cm capsule). At 10 weeks, four independent tumors from each treatment as described in Fig. 1, D, were examined with the terminal deoxynucleotidyltransferase–mediated deoxyuridine triphosphate nick-end labeling (TUNEL) assay for apoptosis. *$P = .038$ for the estradiol-treated group versus all other groups (one-factor analysis of variance). All statistical tests were two-sided. **A** and **B)** Apoptosis was quantified as the number of TUNEL-positive cells per total epithelial cells, as determined by hematoxylin-eosin staining (not shown). The number of apoptotic cells in four random fields was measured from each tumor section, and representative fields are shown. **Scale bars** = 50 μm. The percentage of apoptosis was calculated for both panels A and B by dividing the total number of TUNEL-positive cells in each field by the total number of epithelial cells and multiplying by 100. Data are the mean and 95% confidence intervals of four experiments.

endogenous human-specific estrogen-responsive gene *(30,31)*. Estradiol treatment reduced the level of ERα protein in both parental estradiol-dependent MCF-7 tumors and MCF-7TAMLT tumors compared with that in corresponding control tumors (Fig. 3, A). Tamoxifen treatment of MCF-$7E_2$ or MCF-7TAMLT tumors almost restored levels of ERα protein to that detected in corresponding control tumors. ERα activity in MCF-$7E_2$ and MCF-7TAMLT tumors followed a similar trend; estradiol treatment increased the expression of TGF-α in MCF-$7E_2$ and MCF-7TAMLT tumors (both $P<.001$) compared with that in control tumors (Fig. 3, B). The estradiol-induced expression of TGF-α mRNA was inhibited by tamoxifen in both MCF-$7E_2$ and MCF-7TAMLT tumors and by fulvestrant in MCF-7TAMLT tumors. Because fulvestrant-treated MCF-$7E_2$ tumors did not grow, they were not available for further analysis. In both MCF-$7E_2$ and MCF-7TAMLT tumors, as measured by real-time RT–PCR, the level of ERβ mRNA was much lower (<1%; $P<.001$) than that of ERα mRNA (data not shown), indicating that ERβ plays little, if any, role in estradiol-induced apoptosis in MCF-7TAMLT tumors. Thus, the ERα in MCF-7TAMLT tumors is apparently not dysregulated, and the paradoxical increase in the estradiol-induced apoptosis observed in such tumors may be mediated through the ERα pathway.

Roles of FasL and Fas in Estradiol-Induced Apoptosis

Song et al. *(19)* suggested that estradiol treatment of MCF-7LTED cells promoted apoptosis by increasing the expression of FasL, an estrogen-responsive gene belonging to the tumor necrosis factor α family, and thus activating the Fas death pathway. We detected similar levels of FasL protein in both MCF-$7E_2$ and MCF-7TAMLT tumors, regardless of treatment (Fig. 4, A), a result indicating that FasL is not a likely target for estradiol-

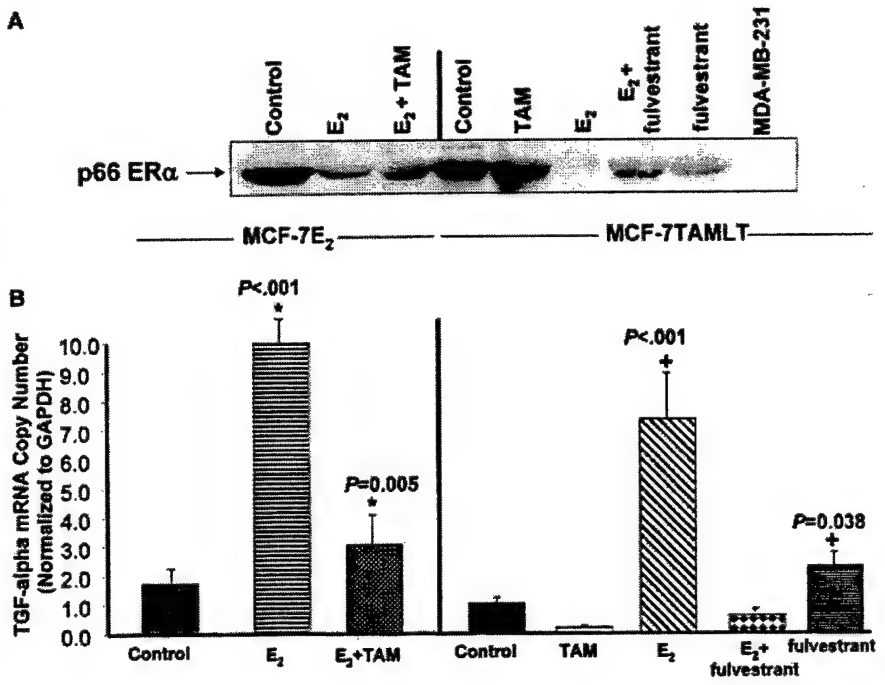

Fig. 3. Estrogen receptor α (ERα) protein expression and function. **A)** Western blot analysis of ERα (p66) in parental MCF-$7E_2$ and MCF-7TAMLT tumors (Fig. 1, C, at week 10) treated as previously described in Fig. 1, C. Each lane was loaded with 50 μg of protein extract, and ERα was detected with an ERα antibody (Santa Cruz Biotechnology). The negative control for ERα protein expression is the MDA-MB-231 cell lysate. The experiment was repeated at least three times with three independent tumors. A representative blot is shown; other blots were similar. **B)** ERα activity assessed by the estrogen-responsive expression of transforming growth factor α (TGF-α) mRNA. Total RNA from parental MCF-$7E_2$ and MCF-7TAMLT tumors, treated as described above, was reverse-transcribed to total cDNA, and real-time polymerase chain reaction was used to detect human TGF-α mRNA. Glyceraldehyde 3-phosphate dehydrogenase (GAPDH) mRNA was used as a loading control in all samples. TGF-α mRNA cycle threshold (CT) values (which are proportional to mRNA copy number) were normalized to Ct values for GAPDH mRNA by subtracting the Ct value for GAPDH from the Ct value for TGF-α. Data are the mean TGF-α mRNA copy numbers and 95% confidence intervals normalized to the loading control in three independent tumors with three replicates per tumor. *Compared with MCF-$7E_2$ control group (one-factor analysis of variance). +Compared with MCF-7TAMLT control group (one-factor analysis of variance). All statistical tests were two-sided.

induced apoptosis in MCF-7TAMLT tumors. To determine whether Fas plays a role in estradiol-induced apoptosis in MCF-7TAMLT tumors, we measured levels of Fas protein and mRNA in extracts of MCF-$7E_2$ and MCF-7TAMLT tumors. Fas protein was expressed in parental MCF-$7E_2$ tumors treated with estradiol plus tamoxifen and in MCF-7TAMLT tumors treated with estradiol (Fig. 4, A). The expression of human Fas mRNA was increased by 2.5-fold (95% CI = 2.3- to 2.7-fold; $P<.001$) in estradiol-dependent parental MCF-$7E_2$ tumors treated with estradiol plus tamoxifen compared with that in control tumors, and

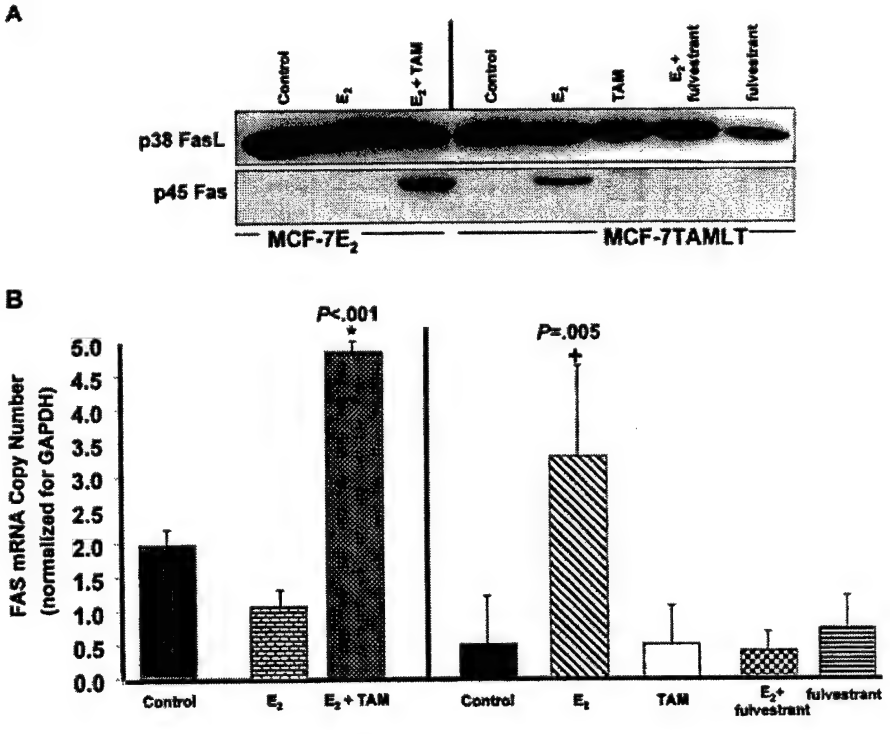

Fig. 4. Expression of Fas ligand (FasL) protein, Fas protein, and mRNA in parental MCF-$7E_2$ and tamoxifen (TAM)-stimulated MCF-7TAMLT tumors. **A)** Western blot analysis for human FasL protein (p38) and for human Fas protein (p45) in both parental MCF-$7E_2$ and MCF-7TAMLT tumors at 10 weeks treated as previously described in Fig. 1, C. Blots shown are representative of three independent experiments, all with similar results. **B)** Human Fas mRNA copy number detected by real-time reverse transcription–polymerase chain reaction. Copy number was normalized as described in Fig. 3, B. *$P<.001$ compared with MCF-$7E_2$ control group (one-factor analysis of variance). +$P = .005$ compared with MCF-7TAMLT control group (one-factor analysis of variance). All statistical tests were two-sided.

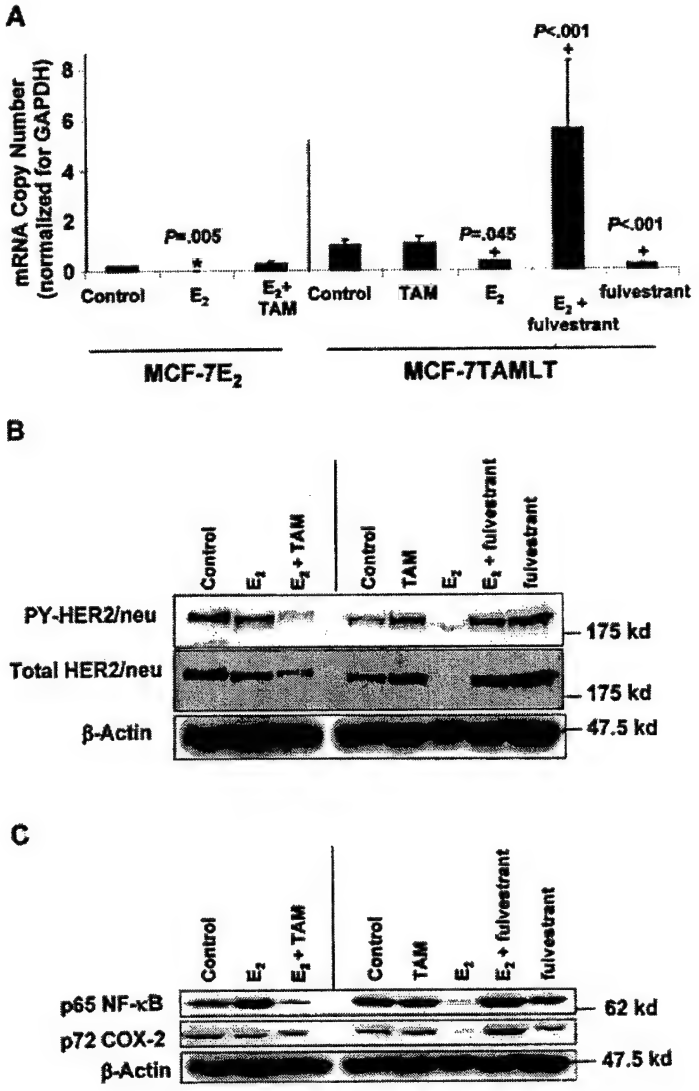

Fig. 5. Expression and function of HER2/neu and nuclear factorκB (NF-κB) in parental MCF-7E_2 and tamoxifen (TAM)-stimulated MCF-7TAMLT tumors. **A)** Total RNA (2 μg) from the tumors as previously described in Fig. 1, C, was reverse transcribed to cDNA, and real-time polymerase chain reaction was performed to detect human HER2/neu mRNA. Glyceraldehyde 3-phosphate dehydrogenase (GAPDH) cDNA was measured for an internal positive control. Copy number was normalized as described in Fig. 3, B. *Compared with MCF-7E_2 control group (one-factor analysis of variance). +Compared with MCF-7TAMLT control group (one-factor analysis of variance). All statistical tests were two-sided. **B** and **C)** Western blot analyses to detect phosphorylated (PY-HER2/neu) and total (Total HER2/neu) human HER2/neu protein (**B**) and human nuclear factor κB (NF-κB) p65 protein (p65 NF-κB) and cyclooxygenase 2 protein (p72 COX-2) (**C**) in both parental MCF-7E_2 and MCF-7TAMLT tumors, as indicated. Equal loading was assessed by stripping membranes and reprobing with a mouse anti-human β-actin monoclonal antibody followed by the appropriate secondary antibody. Western blots shown are representative of three independent experiments with three distinct tumors; results of other experiments were similar.

Fas mRNA expression was increased 3.3-fold (95% CI = 2.6- to 4.0-fold; P = .005) in tamoxifen-dependent MCF-7TAMLT tumors treated with estradiol compared with that in control tumors (Fig. 4, B). Thus, the expression of the Fas gene appears to be associated with estradiol-induced tumor regression of tamoxifen-stimulated breast cancer.

Expression and Function of HER2/neu in MCF-7E_2 and MCF-7TAMLT Tumors

The ERα pathway regulates expression of the oncogene HER2/neu *(36),* and overexpression and/or amplification of HER2/neu is sufficient to promote resistance to tamoxifen *in vitro* and *in vivo (37)*. To investigate whether the ERα pathway modulates estradiol-induced regression of MCF-7TAMLT tumors by regulating HER2/neu, we measured HER2/neu mRNA with real-time RT–PCR and measured phosphorylated and total HER2/neu protein with western blot analyses in tumor extracts. Levels of HER2/neu mRNA were lower in MCF-7E_2 (decrease of 9.2-fold, 95% CI = 9.1- to 9.3-fold; P = .005) and MCF-7TAMLT tumors (decrease of 5.1-fold, 95% CI = 2.3- to 7.9-fold; P = .045) treated with estradiol than in their respective control tumors (Fig. 5, A). Remarkably, treatment with the combination of estradiol plus fulvestrant resulted in an increase of 5.5-fold (95% CI = 3.7- to 8.3-fold; P<.001) of HER2/neu mRNA in MCF-7TAMLT tumors compared with that in vehicle-treated control tumors (Fig. 5, A). Levels of phosphorylated and total HER2/neu protein were decreased in regressing MCF-7E_2 tumors treated with estradiol plus tamoxifen compared with vehicle-treated control tumors and barely detected in estradiol-treated MCF-7TAMLT tumors (Fig. 5, B). MCF-7TAMLT tumors treated with fulvestrant plus estradiol expressed approximately fivefold more phosphorylated and total HER2/neu protein than control tumors (Fig. 5, B). Interestingly, mRNA levels do not appear to be consistent with steady-state protein levels; thus, this observation merits further analysis.

Expression and Function of NF-κB in MCF-7E_2 and MCF-7TAMLT Tumors

The ERα *(38)* and HER2/neu *(39,40)* pathways regulate expression and function of NF-κB, an antiapoptotic transcription

factor *(29)*, and the Fas gene promoter contains κB-binding sites *(28,29,41)*. To investigate whether ERα acts through NF-κB to mediate the induction of Fas and thus estradiol-induced apoptosis in MCF-7TAMLT tumors, we determined the levels of NF-κB protein and measured its activity in tumors. The level of the NF-κB p65 subunit protein was almost undetectable by western blot analysis in estradiol-treated MCF-7TAMLT tumors in contrast to that in tumors treated with vehicle control, tamoxifen, fulvestrant, or estradiol plus fulvestrant (Fig. 5, C), suggesting that the estradiol–ERα complex has an as yet undetermined role in the regulation of NF-κB p65 protein levels in MCF-7TAMLT tumors. Thus, a mechanism other than simple hormonal regulation appears to mediate the expression of NF-κB in estradiol-treated MCF-7TAMLT tumors. To assess activity of NF-κB protein in tumors after various treatments, we examined the expression of COX-2, an NF-κB responsive gene *(42,43)*. The level of cyclooxygenase 2 protein was lower in estradiol-treated MCF-7TAMLT tumors than in untreated MCF-7TAMLT tumors, whereas the level of COX-2 protein was lower in tamoxifen-treated MCF-$7E_2$ tumors than in untreated MCF-$7E_2$ tumors (Fig. 5, C). These data indicate a novel mechanism in which ERα appears to mediate estradiol-induced apoptosis and tumor regression of MCF-7TAMLT tumors by suppressing the prosurvival/antiapoptotic factors HER2/neu and NF-κB and inducing the death receptor Fas.

Discussion

We demonstrated, to our knowledge for the first time, that the regression of tamoxifen-stimulated human breast cancer tumors *in vivo* induced by physiologic levels of estradiol appears to be mediated by increased apoptosis through suppression of the prosurvival/antiapoptotic factors HER2/neu and NF-κB and induction of the death receptor Fas. In such tumors, the pure antiestrogen fulvestrant completely blocked the growth inhibitory effect of estradiol and paradoxically stimulated growth when given in combination with estradiol. These results strongly suggest that regulation of Fas, HER2/neu, and NF-κB in response to treatment with estradiol is mediated by the ERα pathway.

Currently, postmenopausal women with ERα-positive breast cancer are treated with tamoxifen, aromatase inhibitors, or fulvestrant. Tamoxifen is recommended as a 5-year adjuvant therapy for women with ERα-positive, lymph node–positive and –negative breast cancer and as a chemopreventive agent to women at high risk for breast cancer. During long-term adjuvant therapy, tumors can acquire resistance to tamoxifen. The evolution of acquired resistance consists of at least three phases *(44)*. During the treatment phase, breast tumors grow in the presence of estradiol and regress in the presence of tamoxifen or an aromatase inhibitor (estrogen withdrawal) *(45)*. In phase I resistance, acquired resistance to tamoxifen occurs when breast tumors grow in response to either tamoxifen or estradiol *(15)* and regress when either an aromatase inhibitor or fulvestrant is given after tamoxifen fails to inhibit growth *(16)*. Phase II resistance is observed after 5 years of therapy with tamoxifen (long-term treatment phase). Our current *in vivo* model used in this article, in which MCF-7 breast tumors that have been exposed to tamoxifen for more than 5 years and have become resistant to it, represents an example of phase II drug resistance. The growth of these breast tumors is dependent on tamoxifen, and tumors rapidly regress in the presence of physiologic levels of estradiol *(17)*. Phase II drug resistance is also observed in MCF-7 cells treated with raloxifene for more than 1 year *in vitro*, as described by Liu et al. *(46)*. Thus, phase II drug resistance is not limited to tamoxifen or to development of tamoxifen-stimulated MCF-7 tumors *in vivo* but might result from a long-term exposure of breast cancer cells to tamoxifen or raloxifene. Our data (Fig. 1, B and C) suggest that the clinical use of fulvestrant to treat ER-positive tumors might not be beneficial during phase II resistance because the growth of such tumors is stimulated by treatment with estradiol plus fulvestrant. Furthermore, the use of aromatase inhibitors to block estradiol synthesis might stabilize disease rather than cause regression.

Before the use of tamoxifen *(47–49)* or first-generation aromatase inhibitors *(50)*, postmenopausal women with breast cancer were treated with high-dose estrogens, such as diethylstilbestrol or ethinyl estradiol *(49,51,52)*. Results from our study suggest that low levels of estradiol (83.8 pg/mL in serum) *(32)* are sufficient to induce apoptosis and the regression of tamoxifen-stimulated breast tumors. A study by Lonning et al. *(53)* showed that standard high-dose estrogen (5 mg of diethylstilbestrol, given three times per day) has a substantial antitumor effect in postmenopausal breast cancer patients who have been exposed to multiple endocrine therapies. Four of the 32 patients in that study achieved complete remission, six had partial remission, five had objective responses to high-dose diethylstilbestrol, and three had stable disease lasting from 6 months to more than 1 year. Clearly, there could be a profound advantage for patients if an apoptotic regimen targeting ER-positive tumors could be integrated into the overall treatment plan, especially because a recent laboratory study *(17)* shows that tamoxifen is again effective after such estrogen therapy.

Song et al. *(19)* suggested that overexpression of FasL is important for estradiol-induced apoptosis of Fas-expressing breast cancer cells after long-term estrogen deprivation *in vitro*. In contrast, we demonstrate in this article that FasL protein is expressed at essentially the same level in both tamoxifen-naive and tamoxifen-stimulated MCF-7 tumors (Fig. 4, A), regardless of the treatment, and thus would not be a limiting factor. Moreover, we show that both Fas mRNA and protein are induced in regressing tumors in response to tamoxifen in parental MCF-$7E_2$ or to estradiol in MCF-7TAMLT tumors (Fig. 4, A) and could regulate apoptosis. Thus, apoptosis—induced initially by tamoxifen and later by estradiol—appears to be mediated by a common pathway. In estradiol-treated MCF-7TAMLT tumors, fulvestrant treatment completely blocked estradiol-induced regression, enhanced tumor growth (Fig. 1, B and C), and, most importantly, blocked the estradiol-induced expression of Fas (Fig. 4, A). Thus, both apoptosis and Fas expression appear to be mediated by the estradiol–ERα complex.

The finding that the pure antiestrogen fulvestrant could switch an estradiol-induced apoptotic signal to an estradiol-induced growth signal is intriguing. Fulvestrant is a steroidal compound with a 7α-alkylamide hydrocarbon side chain that reduces the level of cellular ERs *(54)* by disrupting dimerization of the ER; the protein monomer subsequently is targeted for ubiquitin-mediated degradation by the proteosome *(13)*. We have observed a novel action of fulvestrant—that the combined treatment of fulvestrant with estradiol stimulates the growth of breast tumors exposed to tamoxifen treatment for 5 years (Fig. 1, B and C). Unexpectedly, fulvestrant partially blocked the

estradiol-induced decrease in the ERα protein level (Fig. 3, A). Thus, long-term exposure of breast tumors to tamoxifen leads to a situation in which the combined treatment of fulvestrant and estradiol does not efficiently lead to ERα degradation and actually promotes growth. Because the combined treatment with estradiol plus fulvestrant enhanced tumor growth but did not induce the expression of TGF-α mRNA (Fig. 3, B), nongenomic actions of ERα (i.e., actions not dependent on ERα–DNA interaction), such as extranuclear ERα to activate the MAPK/ERK1/2 pathway, or ERα-mediated activation of other transcription factors may contribute to cell survival and proliferation stimulated by such treatment. We have initiated studies to address whether ERα is sequestered and redistributed in MCF-7TAMLT tumors.

The exact role played by the ERα in the estradiol-induced expression of Fas and subsequent apoptosis of MCF-7TAMLT tumors remains unclear. However, transcription of the Fas gene is inactivated in many types of cancers by epigenetic events, such as hypermethylation of the promoter at specific κB sites *(41)*. Our results demonstrate that estradiol decreases the expression and activity of NF-κB, an antiapoptotic factor, that has been shown to induce expression of apoptotic inhibitors such as Bcl-x(L) *(55)* and inhibitors of apoptosis, a group of proteins that inhibit caspases *(56)*, in MCF-7TAMLT tumors (Fig. 5) and that fulvestrant inhibits this effect. These results suggest that the estradiol–ERα complex might act by decreasing NF-κB protein levels and thus allowing apoptosis mediated by the FasL/Fas death pathway to proceed.

Our data suggest that long-term exposure of MCF-7 breast tumors to tamoxifen results in supersensitivity to estradiol, so that perhaps only physiologic levels of estradiol are required to induce tumor regression. Similar observations were reported in a raloxifene-resistant MCF-7 tumor model *in vitro* and *in vivo* *(46)*. These laboratory results have important clinical implications, particularly for the use of aromatase inhibitors and the pure antiestrogen fulvestrant as second-line therapies after tamoxifen. For patients with a recurrence of ER-positive, tamoxifen-dependent breast cancer after 5 years of adjuvant therapy (phase II resistance), second-line treatment with fulvestrant or aromatase inhibitors may produce tumor stasis or growth. More important, the use of fulvestrant in the patient with sufficient levels of circulating estrogen may exacerbate the disease by stimulating growth, as illustrated in this study. Paradoxically, a strategy of treatment with estrogen alone, either exogenous estrogen or the woman's endogenous estrogen may be sufficient to produce short-term control of disease progression. In the latter clinical scenario, it may be informative to document how long tamoxifen withdrawal responses occur in women with high levels of circulating estrogen after extended antihormonal therapy (i.e., tamoxifen or aromatase inhibitors). For the future, it may also be important to consider developing an estrogen challenge test or gene profile to distinguish between patients with phase I and those with phase II acquired resistance to tamoxifen or long-term estrogen deprivation.

In conclusion, the use of a tamoxifen-stimulated human breast cancer model *in vivo* demonstrates that long-term tamoxifen treatment results in supersensitivity to estradiol in which apoptosis and tumor regression are induced by physiologic levels of estradiol. Moreover, we show that combined treatment with estradiol plus fulvestrant promotes the growth of MCF-7TAMLT tumors, strongly implicating the ERα pathway and suggesting that estradiol is required to induce tumor regression in tamoxifen-stimulated breast cancer. Furthermore, our study suggests a novel mechanism in which estradiol induces apoptosis of MCF-7TAMLT tumors by inducing the death receptor Fas and suppressing the prosurvival/antiapoptotic factors HER2/neu and NF-κB. Future studies to integrate these novel results into clinical practice require a focus on enhancing estrogen-induced apoptosis with chemotherapy or radiation therapy and blocking tumor cell survival pathways with antibodies or tyrosine kinase inhibitors to HER2/neu and/or epidermal growth factor receptor. We believe that if these concepts can be tested in the clinic, a new strategy of extended adjuvant therapy, through progressive schedules of antihormonal and hormonal therapies, may be possible by exploiting ERα further as a drug target.

References

(1) Osborne CK. Tamoxifen in the treatment of breast cancer. N Engl J Med 1998;339:1609–18.

(2) Fisher B, Costantino JP, Wickerham DL, Redmond CK, Kavanah M, Cronin WM, et al. Tamoxifen for prevention of breast cancer: report of the National Surgical Adjuvant Breast and Bowel Project P-1 Study. J Natl Cancer Inst 1998;90:1371–88.

(3) Cuzick J, Forbes J, Edwards R, Baum M, Cawthorn S, Coates A, et al. First results from the International Breast Cancer Intervention Study (IBIS-I): a randomised prevention trial. Lancet 2002;360:817–24.

(4) Tamoxifen for early breast cancer: an overview of the randomised trials. Early Breast Cancer Trialists' Collaborative Group. Lancet 1998;351: 1451–67.

(5) Howell A, Dodwell DJ, Anderson H, Redford J. Response after withdrawal of tamoxifen and progestogens in advanced breast cancer. Ann Oncol 1992;3:611–7.

(6) Canney PA, Griffiths T, Latief TN, Priestman TJ. Clinical significance of tamoxifen withdrawal response. Lancet 1987;1:36.

(7) Baum M, Budzar AU, Cuzick J, Forbes J, Houghton JH, Klijh JG, et al. Anastrozole alone or in combination with tamoxifen versus tamoxifen alone for adjuvant treatment of postmenopausal women with early breast cancer: first results of the ATAC randomised trial. Lancet 2002;359: 2131–9.

(8) Piccart MJ, Cardoso F, Atalay G. Letrozole's superiority over progestins and tamoxifen challenges standards of care in endocrine therapy for metastatic breast cancer. Eur J Cancer 2002;38 Suppl 6:S52–4.

(9) Winer EP, Hudis C, Burstein HJ, Chlebowski RT, Ingle JN, Edge SB, et al. American Society of Clinical Oncology technology assessment on the use of aromatase inhibitors as adjuvant therapy for women with hormone receptor-positive breast cancer: status report 2002. J Clin Oncol 2002;20: 3317–27.

(10) Howell A, Robertson JF, Quaresma Albano J, Aschermannova A, Mauriac L, Kleeberg UR, et al. Fulvestrant, formerly ICI 182,780, is as effective as anastrozole in postmenopausal women with advanced breast cancer progressing after prior endocrine treatment. J Clin Oncol 2002; 20:3396–403.

(11) Osborne CK, Pippen J, Jones SE, Parker LM, Ellis M, Come S, et al. Double-blind, randomized trial comparing the efficacy and tolerability of fulvestrant versus anastrozole in postmenopausal women with advanced breast cancer progressing on prior endocrine therapy: results of a North American trial. J Clin Oncol 2002;20:3386–95.

(12) Dauvois S, White R, Parker MG. The antiestrogen ICI 182780 disrupts estrogen receptor nucleocytoplasmic shuttling. J Cell Sci 1993;106 (Pt 4):1377–88.

(13) Wijayaratne AL, McDonnell DP. The human estrogen receptor-alpha is a ubiquitinated protein whose stability is affected differentially by agonists, antagonists, and selective estrogen receptor modulators. J Biol Chem 2001;276:35684–92.

(14) Osborne CK, Coronado EB, Robinson JP. Human breast cancer in the athymic nude mouse: cytostatic effects of long-term antiestrogen therapy. Eur J Cancer Clin Oncol 1987;23:1189–96.

(15) Gottardis MM, Jordan VC. Development of tamoxifen-stimulated growth of MCF-7 tumors in athymic mice after long-term antiestrogen administration. Cancer Res 1988;48:5183–7.

(16) Osborne CK, Coronado-Heinsohn EB, Hilsenbeck SG, McCue BL, Wakeling AE, McClelland RA, et al. Comparison of the effects of a pure steroidal antiestrogen with those of tamoxifen in a model of human breast cancer. J Natl Cancer Inst 1995;87:746–50.

(17) Yao K, Lee ES, Bentrem DJ, England G, Schafer JI, O'Regan RM, et al. Antitumor action of physiological estradiol on tamoxifen-stimulated breast tumors grown in athymic mice. Clin Cancer Res 2000;6:2028–36.

(18) Wolf DM, Jordan VC. A laboratory model to explain the survival advantage observed in patients taking adjuvant tamoxifen therapy. Recent Results Cancer Res 1993;127:23–33.

(19) Song RX, Mor G, Naftolin F, McPherson RA, Song J, Zhang Z, et al. Effect of long-term estrogen deprivation on apoptotic responses of breast cancer cells to 17beta-estradiol. J Natl Cancer Inst 2001;93:1714–23.

(20) Brunner T, Mogil RJ, LaFace D, Yoo NJ, Mahboubi A, Echeverri F, et al. Cell-autonomous Fas (CD95)/Fas-ligand interaction mediates activation-induced apoptosis in T-cell hybridomas. Nature 1995;373:441–4.

(21) Ashkenazi A, Dixit VM. Death receptors: signaling and modulation. Science 1998;281:1305–8.

(22) Gutierrez LS, Eliza M, Niven-Fairchild T, Naftolin F, Mor G. The Fas/Fas-ligand system: a mechanism for immune evasion in human breast carcinomas. Breast Cancer Res Treat 1999;54:245–53.

(23) Song J, Sapi E, Brown W, Nilsen J, Tartaro K, Kacinski BM, et al. Roles of Fas and Fas ligand during mammary gland remodeling. J Clin Invest 2000;106:1209–20.

(24) Mullauer L, Mosberger I, Grusch M, Rudas M, Chott A. Fas ligand is expressed in normal breast epithelial cells and is frequently up-regulated in breast cancer. J Pathol 2000;190:20–30.

(25) Mor G, Kohen F, Garcia-Velasco J, Nilsen J, Brown W, Song J, et al. Regulation of fas ligand expression in breast cancer cells by estrogen: functional differences between estradiol and tamoxifen. J Steroid Biochem Mol Biol 2000;73:185–94.

(26) Slamon DJ, Clark GM, Wong SG, Levin WJ, Ullrich A, McGuire WL. Human breast cancer: correlation of relapse and survival with amplification of the HER-2/neu oncogene. Science 1987;235:177–82.

(27) Revillion F, Bonneterre J, Peyrat JP. ERBB2 oncogene in human breast cancer and its clinical significance. Eur J Cancer 1998;34:791–808.

(28) Bhat-Nakshatri P, Sweeney CJ, Nakshatri H. Identification of signal transduction pathways involved in constitutive NF-kappaB activation in breast cancer cells. Oncogene 2002;21:2066–78.

(29) Karin M, Cao Y, Greten FR, Li ZW. NF-kappaB in cancer: from innocent bystander to major culprit. Nat Rev Cancer 2002;2:301–10.

(30) Bates SE, Davidson NE, Valverius EM, Freter CE, Dickson RB, Tam JP, et al. Expression of transforming growth factor alpha and its messenger ribonucleic acid in human breast cancer: its regulation by estrogen and its possible functional significance. Mol Endocrinol 1988;2:543–55.

(31) Saeki T, Cristiano A, Lynch MJ, Brattain M, Kim N, Normanno N, et al. Regulation by estrogen through the 5′-flanking region of the transforming growth factor alpha gene. Mol Endocrinol 1991;5:1955–63.

(32) O'Regan RM, Cisneros A, England GM, MacGregor JI, Muenzner HD, Assikis VJ, et al. Effects of the antiestrogens tamoxifen, toremifene, and ICI 182,780 on endometrial cancer growth. J Natl Cancer Inst 1998;90:1552–8.

(33) O'Regan RM, England ME, MacGregor JI, Yao KA, Muenzner HD, Takei H, et al. Laboratory models of breast and endometrial cancer to develop strategies for antiestrogen therapy. Breast Cancer 1998;5:211–7.

(34) Robinson SP, Jordan VC. Antiestrogenic action of toremifene on hormone-dependent, -independent, and heterogeneous breast tumor growth in the athymic mouse. Cancer Res 1989;49:1758–62.

(35) Schafer JM, Lee ES, O'Regan RM, Yao K, Jordan VC. Rapid development of tamoxifen-stimulated mutant p53 breast tumors (T47D) in athymic mice. Clin Cancer Res 2000;6:4373–80.

(36) Newman SP, Bates NP, Vernimmen D, Parker MG, Hurst HC. Cofactor competition between the ligand-bound oestrogen receptor and an intron 1 enhancer leads to oestrogen repression of ERBB2 expression in breast cancer. Oncogene 2000;19:490–7.

(37) Benz CC, Scott GK, Sarup JC, Johnson RM, Tripathy D, Coronado E, et al. Estrogen-dependent, tamoxifen-resistant tumorigenic growth of MCF-7 cells transfected with HER2/neu. Breast Cancer Res Treat 1993;24:85–95.

(38) Cerillo G, Rees A, Manchanda N, Reilly C, Brogan I, White A, et al. The oestrogen receptor regulates NFkappaB and AP-1 activity in a cell-specific manner. J Steroid Biochem Mol Biol 1998;67:79–88.

(39) Pianetti S, Arsura M, Romieu-Mourez R, Coffey RJ, Sonenshein GE. Her-2/neu overexpression induces NF-kappaB via a PI3-kinase/Akt pathway involving calpain-mediated degradation of IkappaB-alpha that can be inhibited by the tumor suppressor PTEN. Oncogene 2001;20:1287–99.

(40) Romieu-Mourez R, Landesman-Bollag E, Seldin DC, Sonenshein GE. Protein kinase CK2 promotes aberrant activation of nuclear factor-kappaB, transformed phenotype, and survival of breast cancer cells. Cancer Res 2002;62:6770–8.

(41) Santourlidis S, Warskulat U, Florl AR, Maas S, Pulte T, Fischer J, et al. Hypermethylation of the tumor necrosis factor receptor superfamily 6 (APT1, Fas, CD95/Apo-1) gene promoter at rel/nuclear factor kappaB sites in prostatic carcinoma. Mol Carcinog 2001;32:36–43.

(42) Newton R, Kuitert LM, Bergmann M, Adcock IM, Barnes PJ. Evidence for involvement of NF-kappaB in the transcriptional control of COX-2 gene expression by IL-1beta. Biochem Biophys Res Commun 1997;237:28–32.

(43) D'Acquisto F, Iuvone T, Rombola L, Sautebin L, Di Rosa M, Carnuccio R. Involvement of NF-kappaB in the regulation of cyclooxygenase-2 protein expression in LPS-stimulated J774 macrophages. FEBS Lett 1997;418:175–8.

(44) Jordan VC, Osipo C, MacGregor Schafer J, Fox JE, Cheng D, Liu H. Changing role of the oestrogen receptor in the life and death of breast cancer cells. Breast. In press 2003.

(45) Osborne CK, Hobbs K, Clark GM. Effect of estrogens and antiestrogens on growth of human breast cancer cells in athymic nude mice. Cancer Res 1985;45:584–90.

(46) Liu H, Lee ES, Gajdos C, Pearce ST, Chen B, Osipo C, et al. Apoptotic action of 17beta-estradiol in raloxifene-resistant MCF-7 cells in vitro and in vivo. J Natl Cancer Inst 2003;95:1586–97.

(47) Cole MP, Jones CT, Todd ID. A new anti-oestrogenic agent in late breast cancer. An early clinical appraisal of ICI46474. Br J Cancer 1971;25:270–5.

(48) Ward HW. Anti-oestrogen therapy for breast cancer: a trial of tamoxifen at two dose levels. Br Med J 1973;1:13–4.

(49) Ingle JN, Ahmann DL, Green SJ, Edmonson JH, Bisel HF, Kvols LK, et al. Randomized clinical trial of diethylstilbestrol versus tamoxifen in postmenopausal women with advanced breast cancer. N Engl J Med 1981;304:16–21.

(50) Santen RJ, Lipton A, Kendall J. Successful medical adrenalectomy with amino-glutethimide. Role of altered drug metabolism. JAMA 1974;230:1661–5.

(51) Carter AC, Sedransk N, Kelley RM, Ansfield FJ, Ravdin RG, Talley RW, et al. Diethylstilbestrol: recommended dosages for different categories of breast cancer patients. Report of the Cooperative Breast Cancer Group. JAMA 1977;237:2079–88.

(52) Beex L, Pieters G, Smals A, Koenders A, Benraad T, Kloppenborg P. Tamoxifen versus ethinyl estradiol in the treatment of postmenopausal women with advanced breast cancer. Cancer Treat Rep 1981;65:179–85.

(53) Lonning PE, Taylor PD, Anker G, Iddon J, Wie L, Jorgensen LM, et al. High-dose estrogen treatment in postmenopausal breast cancer patients heavily exposed to endocrine therapy. Breast Cancer Res Treat 2001;67:111–6.

(54) Parker MG. Action of "pure" antiestrogens in inhibiting estrogen receptor action. Breast Cancer Res Treat 1993;26:131–7.

(55) Chen C, Edelstein LC, Gelinas C. The Rel/NF-kappaB family directly activates expression of the apoptosis inhibitor Bcl-x(L). Mol Cell Biol 2000;20:2687–95.

(56) LaCasse EC, Baird S, Korneluk RG, MacKenzie AE. The inhibitors of apoptosis (IAPs) and their emerging role in cancer. Oncogene 1998;17:3247–59.

NOTES

C. Osipo and C. Gajdos contributed equally to the studies.

Supported by the Avon Foundation, Specialized Programs of Research Excellence (SPORE) grant CA89018-03 in breast cancer research (to V. C. Jordan) from the National Cancer Institute, National Institutes of Health, Department of Health and Human Services, and the Lynn Sage Breast Cancer Research Foundation. C. Osipo is funded by the Judy Dlugie Memorial Fund Fellowship for Breast Cancer Research.

We thank Dr. Alfred Rademaker for his assistance in determining which statistical tests were necessary for our studies, Dr. Ruth O'Regan for her helpful discussion during the writing of this article, and Kathy Meeke for her assistance in performing the TUNEL assay.

Manuscript received February 10, 2003; revised August 21, 2003; accepted August 29, 2003.

Apoptotic Action of 17β-Estradiol in Raloxifene-Resistant MCF-7 Cells *In Vitro* and *In Vivo*

Hong Liu, Eun-Sook Lee, Csaba Gajdos, Sandra Timm Pearce, Bin Chen, Clodia Osipo, Jessica Loweth, Kevin McKian, Alexander De Los Reyes, Laura Wing, V. Craig Jordan

Background: **Resistance to tamoxifen, a selective estrogen receptor modulator (SERM), involves changes that prevent apoptosis and enhance cell proliferation and survival. Paradoxically, estrogen treatment inhibits the growth of long-term tamoxifen-treated breast tumors. Because of the increasing use of raloxifene, another SERM, to prevent osteoporosis and potentially reduce breast cancer risk, some women will develop raloxifene-resistant breast cancer. We developed a raloxifene-resistant MCF-7 cell model (MCF-7/Ral) and investigated the nature of raloxifene-resistant breast cancer and its response to estradiol.** ***Methods:*** **Raloxifene resistance and hormone responsiveness were assessed by proliferation assays and cell cycle analysis in parental MCF-7 and MCF-7/Ral cells. Nuclear factor κB (NF-κB) activity was investigated with a transient transfection assay. Apoptosis was investigated by annexin V staining, mRNA was measured by real-time polymerase chain reaction, and protein was measured by western blotting. Tumorigenesis was studied by injecting MCF-7 or MCF-7/Ral cells into ovariectomized athymic mice (10 per group) and monitoring tumor size weekly. All statistical tests were two-sided.** ***Results:*** **Basal NF-κB activity was higher in MCF-7/Ral cells (1.6 U, 95% confidence interval [CI] = 1.2 to 2.0 U) than in MCF-7 cells (0.8 U, 95% CI = 0.4 to 1.1 U; $P = .004$). When cultured with 1 μM raloxifene, MCF-7/Ral cells grew statistically significantly ($P<.001$) faster than MCF-7 cells. Estradiol treatment of MCF-7/Ral cells arrested cells in G_2/M phase of the cell cycle, decreased NF-κB activity (0.2 U, 95% CI = 0.2 to 0.3 U; $P<.001$), increased expression of Fas protein and mRNA (4.5-fold, 95% CI = 2.8- to 6.3-fold versus 0.5-fold, 95% CI = 0.3- to 0.8-fold for control treatment; $P<.001$), and induced apoptosis. Treatment with either raloxifene or tamoxifen stimulated MCF-7/Ral tumor growth, suggesting that such tumors were resistant to both drugs. When a 9-week raloxifene or tamoxifen treatment was followed by a 5-week estradiol treatment, estradiol statistically significantly reduced the size of tumors stimulated by raloxifene or tamoxifen (at week 14, $P = .004$ for raloxifene and $P<.001$ for tamoxifen).** ***Conclusions:*** **Growth of raloxifene-resistant MCF-7/Ral cells *in vitro* and *in vivo* is repressed by estradiol treatment by a mechanism involving G_2/M-phase arrest, decreased NF-κB activity, and increased Fas expression to induce apoptosis. [J Natl Cancer Inst 2003;95:1586–97]**

Selective estrogen receptor modulators (SERMs) are a novel class of compounds that have multiple applications in women's health. Tamoxifen, the first clinically useful SERM, has antiestrogenic effects in breast tissue and can be used to treat *(1)* or

Affiliations of authors: Robert H. Lurie Comprehensive Cancer Center, Feinberg School of Medicine, Northwestern University, Chicago, IL (HL, CG, STP, BC, CO, JL, KM, ADLR, LW, VCJ); National Cancer Center, Goyang, Gyeonggi, Korea (ESL).

Correspondence to: V. Craig Jordan, OBE, PhD, DSc, Robert H. Lurie Comprehensive Cancer Center, Feinberg School of Medicine, Northwestern University, 8258 Olson, 303 E. Chicago Ave., Chicago, IL 60611 (e-mail: vcjordan@northwestern.edu).

See "Notes" following "References."

DOI: 10.1093/jnci/djg080

Journal of the National Cancer Institute, Vol. 95, No. 21,

prevent *(2)* breast cancer. SERMs also have estrogen-like activity in bone and can be used to treat and prevent osteoporosis *(3)*. Raloxifene is the first SERM approved for the treatment and prevention of osteoporosis in postmenopausal women *(4)*. In a randomized clinical trial of patients with osteoporosis, raloxifene treatment was found to be associated with a statistically significant decrease in the incidence of breast cancer *(5,6)*. Consequently, raloxifene is currently being evaluated to determine whether it is an effective chemopreventive agent in women who were determined by the Gail model to be at high risk for breast cancer *(7)*. The Study of Tamoxifen and Raloxifene (STAR) trial is recruiting 19 000 high-risk postmenopausal women to establish whether raloxifene is more or less effective than tamoxifen, the current standard of care, as a chemoprevention agent for breast cancer but with fewer side effects.

Resistance to tamoxifen, in the form of tamoxifen-stimulated growth, is well documented in the laboratory and the clinic *(8–10)*. In contrast, there is only limited information about the development of resistance to raloxifene. The widespread use of raloxifene to prevent osteoporosis, or perhaps in the future to prevent breast cancer, means that increasing numbers of women will be developing raloxifene-exposed breast cancer. Thus, it is important to elucidate the mechanism of raloxifene resistance in breast cancer and to develop an effective therapy for raloxifene-resistant tumors.

Resistance to SERMs results from a complex series of changes that prevent apoptosis and thus enhance cell proliferation and survival. Alterations in several signal transduction pathways have been described for tamoxifen resistance, including enhanced activity of the activating protein 1 (AP1) *(11–13)* and phosphatidylinositol 3-kinase/protein kinase B (PKB or AKT) pathways *(14,15)* and altered expression of protein kinase Cα *(16)*, erbB-2 *(17–19)*, and insulin-like growth factor I *(20)*; all of these events have been linked to the activation of nuclear factor κB (NF-κB) *(21–24)*. Increased NF-κB activity is also important for hormone-independent growth and for ICI 182,780 (fulvestrant) resistance *(25,26)*. Thus, NF-κB pathways may also play a central role in raloxifene resistance. After resistance to one SERM appears, the breast tumors often exhibit cross-resistance to other antiestrogens *(27–31)*, which limits the effectiveness of secondary endocrine therapy. However, the process that causes resistance to SERMs appears to begin with a stage in which both estrogen and the SERM stimulate growth through the estrogen receptor (ER) *(8)* and then progress to a stage in which cell proliferation is dependent on the SERM or on prolonged estrogen deprivation but is inhibited by estrogen. Physiologic levels of estrogen inhibit the growth of long-term tamoxifen-stimulated breast tumors *(32,33)*, T47D cells stably transfected with protein kinase Cα (T47D:protein kinase Cα cells) inoculated into athymic mice *(16)*, long-term estrogen-deprived T47D and MCF-7 cells in culture *(34–36)*, and raloxifene-resistant ECC1 endometrial cancer cells *(37)*. Therefore, we propose that a patient's own estrogens might ultimately destroy SERM-resistant tumor cells after the SERM therapy is stopped.

In this article, we report the development of a reproducible raloxifene-resistant cell model, termed MCF-7/Ral. We used this model to investigate raloxifene resistance in breast cancer and to provide a preclinical basis for possible therapy for raloxifene-resistant tumors. We also used this model to explore the mechanism for raloxifene resistance and responsiveness to 17β-estradiol (hereafter estradiol), with particular attention to the regulation of NF-κB activity and apoptosis initiated through Fas, a member of the tumor necrosis factor receptor family *(38,39)*.

Materials and Methods

Breast Cancer Cells

MCF-7 cells used in this study *(40)* were cloned from an ERα-positive human MCF-7 breast cancer cells originally obtained from the American Type Culture Collection (Manassas, VA). They were maintained in full serum medium composed of RPMI-1640 medium, 10% fetal bovine serum, 2 m*M* glutamine, penicillin at 100 U/mL, streptomycin at 100 μg/mL, 1× nonessential amino acids (all from Invitrogen, Carlsbad, CA), and bovine insulin at 6 ng/mL (Sigma-Aldrich, St. Louis, MO). Raloxifene-resistant MCF-7 (termed MCF-7/Ral) cells were derived by culturing MCF-7 cells for more than 12 months in 1 μ*M* raloxifene in estrogen-free medium composed of phenol red–free minimal essential medium, 5% calf serum (treated three times with dextran-coated charcoal), 2 m*M* glutamine, bovine insulin at 6 ng/mL, penicillin at 100 U/mL, streptomycin at 100 μg/mL, and 1× nonessential amino acids. 4-Hydroxytamoxifen and estradiol were purchased from Sigma-Aldrich. Raloxifene used in cell cultures was a generous gift from Lilly Research Laboratories (Indianapolis, IN). Raloxifene (Evista) tablets used in animal studies were commercially available (Lilly Research Laboratories). ICI 182,780 (fulvestrant) and tamoxifen were provided by AstraZeneca Pharmaceuticals (Macclesfield, U.K.).

Proliferation Assays

MCF-7 or MCF-7/Ral cells were cultured in estrogen-free medium for 4 days before beginning the proliferation assay (day 0) by plating 1.5×10^4 cells in 1 mL of estrogen-free medium per well in 24-well plates. Medium containing the appropriate test compound was added on day 1. All compounds were dissolved in 100% ethanol (i.e., vehicle) and added to the medium at a 1 : 1000 dilution. Compound-containing medium was changed on days 3 and 5, and the experiment was stopped on day 7. The DNA content of cells was measured as described previously *(41)* with a VersaFluor fluorometer (Bio-Rad Laboratories, Hercules, CA).

To measure cell proliferation rates, 7.5×10^4 MCF-7 or MCF-7/Ral cells were plated into T-25 flasks in 5 mL of medium. Medium containing the appropriate test compound was added on day 1, and the cell number was counted each day with a hemacytometer.

To determine the effect of extended estradiol treatment on the proliferation of MCF-7/Ral cells, the cells were grown in estrogen-free medium without raloxifene for 4 days before starting experiments. For passage 0, cultures containing 2.5×10^5 cells were treated with vehicle control, 1 μ*M* raloxifene, 1 n*M* estradiol, or a combination of 1 μ*M* raloxifene and 1 n*M* estradiol for 6 days. After trypsinization, the cells in a single-cell suspension were counted with a hemacytometer. For passage 1, 2.5×10^5 cells from each treatment group were plated and continuously treated with the respective treatment for another 6 days. The cells were trypsinized and counted. This procedure was repeated for passages 2 and 3.

Cell Cycle Analysis

Cell cycle analysis was performed in the flow cytometry core facility (Robert H. Lurie Comprehensive Cancer Center, Northwestern University, Chicago, IL), as described *(42,43)*. Briefly, single-cell suspensions of MCF-7 or MCF-7/Ral cells were washed with phosphate-buffered saline and resuspended at 1×10^6 cells per milliliter, and 1 mL of cell suspension was mixed with 1 mL of a solution containing propidium iodide at 50 μg/mL, RNase at 180 U/mL, 0.1% Triton X-100, and 3% polyethylene glycol in 3.36 m*M* sodium citrate (pH 7.8). After a 20-minute incubation at room temperature in the dark, 1 mL of a solution containing propidium iodide at 50 μg/mL, 0.1% Triton X-100, 3.56 *M* NaCl, and 0.3% polyethylene glycol was added. The tubes were incubated at 4 °C in the dark for a minimum of 6 hours before flow cytometry analysis (Beckman Coulter Epics XL-MCL; Beckman Coulter, Miami, FL). Data were analyzed with Modfit (version 5.2; Verity Software House, Topsham, ME).

Apoptosis

Approximately 2×10^5 cells from a treatment group were stained with an annexin V fluorescein isothiocyanate kit (Beckman Coulter), and the number of apoptotic cells was determined by flow cytometry. To visualize apoptotic cells, the cells were grown on cover slides and stained with annexin V. Micrographs were taken with a Zeiss LSM510 confocal microscope (Carl Zeiss, Thornwood, NY). Phase-contrast live cell images were also taken with a Zeiss Invertoskop inverted microscope (Carl Zeiss).

Western Blot Analysis

Whole-cell lysates were extracted in protein extraction buffer, as described previously *(44)*. Protein concentration was measured with the Bio-Rad Protein Assay kit (Bio-Rad Laboratories). Antibodies against ERα (product G-20) and Fas (products B-10 and C-20) were from Santa Cruz Biotechnology (Santa Cruz, CA). Antibodies against Fas ligand (FasL; product F37720) and retinoblastoma protein (product 554136) were from BD Biosciences (San Jose, CA). Antibody against NF-κB p65 (product 06-418) was from Upstate Biotechnology (Waltham, MA). Antibody against β-actin (product AC-15; Sigma-Aldrich) was used to standardize loading. The appropriate secondary antibody conjugated to horseradish peroxidase (Santa Cruz Biotechnology) was used to visualize bands with an enhanced chemiluminescence (ECL) visualization kit (Amersham, Arlington Heights, IL).

Transient Transfection and Luciferase Assays

MCF-7 or MCF-7/Ral cells were grown in the estrogen-free medium 4 days before the transient transfection assay. Approximately 5×10^6 cells were mixed with 1 μg of a reporter plasmid, either $VitA_2$-ERE_3-luciferase (where $VitA_2$ is vitellogenin A_2 and ERE_3 is three estrogen response elements) *(45)* or pNF-κB-Luc (where Luc is luciferase; product 6053-1; BD Biosciences Clontech, Palo Alto, CA), and 0.2 μg of pCMV-β-galactosidase (where CMV is cytomegalovirus). Cells were electroporated (950 μF, 320 V) with a Bio-Rad Gene Pulser II (Bio-Rad Laboratories). Luciferase and β-galactosidase activities were measured as previously described *(45)*.

Athymic Mouse Model

Approximately 1×10^7 MCF-7 or MCF-7/Ral cells suspended in saline solution (product 20012027; Invitrogen) were bilaterally inoculated into mammary fat pads of ovariectomized BALB/c nu/nu mice (Harlan Sprague Dawley, Madison, WI) as described previously *(46)*. Inoculated mice were randomly divided into groups of 10 and were treated with estradiol, tamoxifen, or raloxifene or were not treated. For the estradiol treatment, silastic estradiol capsules [1 cm long *(47)*] were implanted subcutaneously in the mouse's back on the day of cell inoculation and replaced after 8–10 weeks of treatment. These capsules produced a mean serum estradiol level of 380 pg/mL *(48)*. Preparation of tamoxifen and raloxifene were described in detail previously *(31)*. Tamoxifen and raloxifene were administered orally by gavage at 1.5 mg/day per mouse for 5 days a week for 9 or 14 weeks, as indicated. Tumors were measured weekly with vernier calipers. The cross-sectional tumor area was calculated by multiplying the length (l) by the width (w) and π and dividing by 4 (i.e., $lw\pi/4$).

The Animal Care and Use Committee of Northwestern University approved all of the procedures involving animals.

Real-Time Polymerase Chain Reaction

Total RNA (100 ng) was reverse transcribed by use of random hexamers (TaqMan Reverse Transcription Reagents; Applied Biosystems, Foster City, CA). Primers and probes for Fas and glyceraldehyde-3-phosphate dehydrogenase (GAPDH) were designed with Primer Express 1.5 software (Applied Biosystems). The sequences for all primers and probes are as follows: GAPDH forward primer, 5′-GAAGGTGAAGGTCGGAGTCA-3′; GAPDH reverse primer, 5′-GAAGATGGTGATGGGATTTC-3′; GAPDH probe, 5′-FAM-CAAGCTTCCCGTTCTCAGCC-QSY7–3′; Fas forward primer, 5′-TGGAAGGCCTGCAT-CATGA-3′; Fas reverse primer, 5′-CAGTCCCTAGCTTTCC-TTTCACC-3′; and Fas probe, 5′-FAM-CCAATTCTGCC-ATAAGCCCTGTCCTCC-3′. All probes were labeled with 6-carboxyfluorescein (FAM) as reporter and with QSY7 (a nonfluorescent diarylrhodamine derivative) as quencher. The primers and probes were synthesized by MegaBases (Evanston, IL). The TaqMan polymerase chain reaction (PCR) Core Reagent Kit (Applied Biosystems) was used for PCR. A 25-μL reaction mixture contained 2 μL of the cDNA, probe at 100 n*M*, and each primer at 200 n*M*. PCRs were performed with the ABI Prism 7700 Sequence Detection System (Applied Biosystems). The PCR conditions were 50 °C for 2 minutes and 95 °C for 10 minutes, followed by 40 cycles of 95 °C for 15 seconds and 60 °C for 1 minute. Human GAPDH was used as an internal control, and each total RNA sample was normalized to the content of GAPDH mRNA.

Statistical Analysis

All data are expressed as the mean (with 95% confidence interval [CI]) of at least three determinations, unless stated otherwise. Paired t test was used when only two groups were compared. The interaction between estradiol and raloxifene was determined with a two-way analysis of variance (SPSS software; SPSS, Chicago, IL). When the interaction was statistically significant, each pairwise comparison was made with a one-way analysis of variance followed by Tukey's honestly significant difference. All statistical tests were two-sided.

RESULTS

Raloxifene Resistance of MCF-7 Cells *In Vitro*

Growth characteristics of raloxifene-resistant MCF-7/Ral cells and parental MCF-7 cells were investigated. When cultured with 1 μM raloxifene, MCF-7/Ral cells (at day 6, 152×10^4 cells, 95% CI = 130×10^4 to 174×10^4 cells; $P = .006$) grew statistically significantly faster than MCF-7 cells (at day 6, 55×10^4 cells, 95% CI = 44×10^4 to 64×10^4 cells) (Fig. 1, A). In fact, raloxifene at 1 μM statistically significantly (on day 4, $P = .001$; on day 5 and day 6, $P < .001$) inhibited the growth of cultured MCF-7 cells (Fig. 1, A), as reported previously *(49)*, and cell cycle analyses demonstrated that such MCF-7 cells were arrested in G_0/G_1 phase (Fig. 1, B).

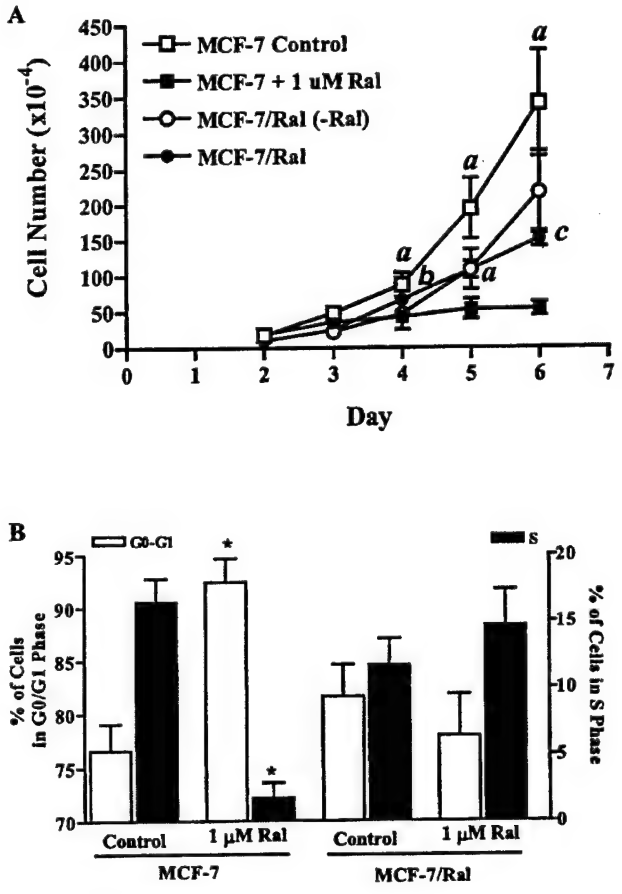

Fig. 1. Proliferation of MCF-7 and MCF-7/Ral cells *in vitro*. **A)** Proliferation rate. Approximately 7.5×10^4 MCF-7 or MCF-7/Ral cells were plated in T-25 flasks. MCF-7 cells were treated with ethanol vehicle (MCF-7 Control) or 1 μM raloxifene (MCF-7 + 1 μM Ral) in full serum medium. MCF-7/Ral cells were grown in estrogen-free medium alone [MCF-7/Ral (-Ral)] or containing 1 μM raloxifene (MCF-7/Ral). Three samples were counted every day. Data are the means; **error bars** are 95% confidence intervals. Statistically significant differences compared with MCF-7 treated with 1 μM raloxifene cells are as follows: *a*, $P < .001$; *b*, $P = .041$; *c*, $P = .006$. The experiment was repeated twice. **B)** Cell cycle analysis. MCF-7 cells were grown in full serum medium containing ethanol vehicle (Control) or 1 μM raloxifene (Ral) for 4 days, and MCF-7/Ral cells were grown in medium containing vehicle (Control) or 1 μM raloxifene for 4 days. * $P < .001$ compared with the corresponding control. All statistical tests were two-sided.

Because the ERα plays an important role in the development and growth of breast cancer *(3)*, raloxifene resistance could be a consequence of changes in the expression and/or transactivation activity of ERα. We measured the level of ERα protein by western blot analysis in MCF-7 and MCF-7/Ral cells and found that ERα protein levels were slightly lower in MCF-7/Ral cells than in MCF-7 cells (Fig. 2, A). In both cell lines, addition of 1 μM raloxifene had essentially no effect on the level of ERα protein, whereas addition of 1 nM estradiol decreased the level of ERα protein dramatically. Both cell lines had similar basal ERE_3–luciferase activities. Addition of 1 nM estradiol statistically significantly increased ER transcriptional activity ($P < .001$), and addition of 1 μM raloxifene inhibited the estradiol-induced ER transactivation activity in both cell lines (Fig. 2, B). Addition of estradiol also induced expression of endogenous ER-regulated genes, such as cyclin D1, p53, and BCL2 in both MCF-7 and MCF-7/Ral cells (data not shown). Because MCF-7/Ral cells appeared to express a functional ERα, as do MCF-7 cells, and raloxifene did not increase ER transactivation activity, enhanced estrogenic activity of the raloxifene–ERα complex is probably not the primary mechanism of raloxifene resistance in MCF-7 cells.

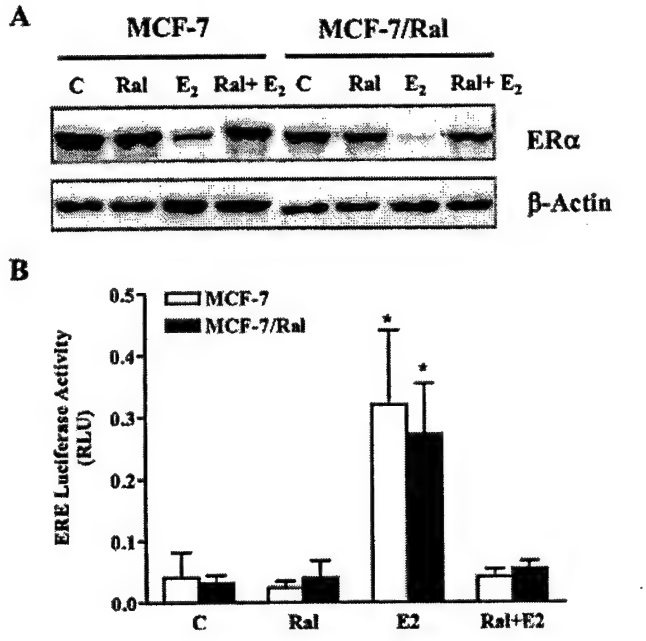

Fig. 2. Expression of functional estrogen receptor α (ERα) in MCF-7 and MCF-7/Ral cells. **A)** Western blot analysis for ERα in MCF-7 and MCF-7/Ral cells grown in estrogen-free medium. The cells were treated with ethanol vehicle (**lanes C**), 1 μM raloxifene (**lanes Ral**), 1 nM estradiol (**lanes E_2**), or a combination of 1 μM raloxifene and 1 nM estradiol (lanes Ral + E_2) for 4 days. β-Actin was used as the loading control. The blot is representative of three experiments, all with similar results. **B)** Transcriptional activity of the estrogen receptor in MCF-7 and MCF-7/Ral cells, as measured by $VitA_2$-ERE_3-luciferase transient transfection assays (where $VitA_2$ is vitellogenin A_2 and ERE_3 is three copies of estrogen response elements). RLU = relative light units. *$P < .001$ compared with the corresponding control groups. All statistical tests were two-sided.

Enhanced NF-κB Activity in MCF-7/Ral Cells

We next investigated whether NF-κB activity plays a role in raloxifene resistance. Short-term treatment (up to 48 hours) with estradiol or raloxifene had essentially no effect on NF-κB activity in either cell line, as measured with NF-κB reporter activity (data not shown). However, as shown in Fig. 3, statistically significantly higher basal NF-κB activity was detected in MCF-7/Ral cells (1.6 U, 95% CI = 1.2 to 2.0 U) than in MCF-7 cells (0.8 U, 95% CI = 0.4 to 1.1 U; P = .004). In addition, a higher level of NF-κB p65 protein, as measured by western blot analysis, was found in MCF-7/Ral cells than in MCF-7 cells (Fig. 3, inset). Thus, enhanced NF-κB activity may play a role in raloxifene resistance in MCF-7 cells.

Inhibitory Effect of Estradiol in MCF-7/Ral Cells

To investigate potential cross-resistance to other SERMs, we used DNA assays to measure the proliferation in MCF-7 and MCF-7/Ral cells treated with vehicle control, 1 nM estradiol, 1 μM raloxifene, or 1 μM 4-hydroxytamoxifen for 6 days. As shown in Fig. 4, A, proliferation of MCF-7 cells was statistically significantly higher in estradiol-treated cultures than in untreated control cell cultures (P<.001; Fig. 4, A). Both raloxifene and 4-hydroxytamoxifen inhibited estradiol-induced increased proliferation of MCF-7 cells (data not shown). MCF-7/Ral cells proliferated more rapidly than MCF-7 cells (P<.001) in estrogen-free medium. Although a 6-day estradiol treatment did not appreciably affect the proliferation of MCF-7/Ral cells (Fig. 4, A), cells were larger in estradiol-treated cultures than in untreated cultures, and apoptotic-like and multinucleated cells were observed in estradiol-treated cultures (Fig. 4, B). In contrast, MCF-7/Ral cultures treated for 6 days with a combination of raloxifene and estradiol contained normal-sized cells (Fig. 4, B). Thus, estradiol may be involved in the regulation of cell proliferation and apoptosis in raloxifene-resistant cells.

To study long-term effects of estradiol, MCF-7/Ral cells were treated with vehicle control, 1 μM raloxifene, 1 nM estradiol, or a combination of raloxifene and estradiol for four passages (passages 0–3). As shown in Fig. 4, C, treatment with estradiol statistically significantly inhibited the proliferation of MCF-7/Ral cells after 12–24 days compared with cells in raloxifene-treated cultures (for example, for passage 3, P = .001). Interestingly, extended estradiol treatment of MCF-7/Ral cells also statistically significantly inhibited NF-κB activity (0.2 U, 95% CI = 0.2 to 0.3 U, compared with 1.6 U, 95% CI = 1.2 to 2.0 U for baseline control; P<.001) (Fig. 4, D) without affecting the level of NF-κB p65 protein (data not shown). This result suggests that elevated NF-κB activity plays a role in raloxifene resistance in MCF-7 cells. In contrast, estradiol treatment did not statistically significantly affect NF-κB activity in MCF-7 parental cells (estradiol = 0.6 U, 95% CI = 0.4 to 0.8 U; control = 0.8 U, 95% CI = 0.5 to 1.1 U; P = .225).

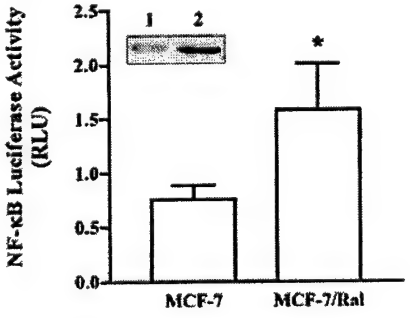

Fig. 3. Basal activity of nuclear factor-κB (NF-κB) in MCF-7 and MCF-7/Ral cells. Activity was measured by NF-κB-luciferase transient transfection assays. MCF-7 and MCF-7/Ral cells were grown in estrogen-free medium for 4 days before the assays. **Inset)** Protein levels of NF-κB p65 measured by western blot analysis in MCF-7 **(lane 1)** and MCF-7/Ral **(lane 2)** cells. RLU = relative light units. *P = .004 compared with MCF-7 cells. All statistical tests were two-sided.

Effect of Estradiol on the Cell Cycle and Apoptosis in MCF-7/Ral Cells

Because a decrease in cell number can result from decreased cell proliferation, increased cell death, or both, we first evaluated the effect of estradiol on the cell cycle in MCF-7 and MCF-7/Ral cells. In parental MCF-7 cells, estrogen deprivation blocked the transition from G_1 phase to S phase, whereas treatment with 1 nM estradiol relieved the block as shown by the decreased number of cells in G_0/G_1 phase and the increased number in S phase (for both, P<.001), apparently by inducing phosphorylation of the retinoblastoma protein (Rb) (Fig. 5, A). The estradiol-mediated Rb phosphorylation was blocked by raloxifene. In contrast, a 6-day estradiol treatment did not affect the cell cycle of MCF-7/Ral cells (data not shown), but a treatment of 2 weeks or longer with 1 nM estradiol statistically significantly increased the percentage of cells in G_2/M phase to 12.5% (95% CI = 10.6% to 14.3%) compared with 7.6% for vehicle control treatment (95% CI = 5.1% to 10.0%; P = .003), 7.7% for raloxifene (95% CI = 5.6% to 9.8%; P = .004), and 7.6% for estradiol plus raloxifene (95% CI = 4.9% to 10.2%; P = .003). A treatment of 2 weeks or longer with 1 nM estradiol also statistically significantly decreased the percentage of cells in G_0/G_1 phase to 69.7% (95% CI = 65.0% to 74.4%) compared with 80.1% for vehicle control treatment (95% CI = 74.2% to 85.9%; P = .006), 77.5% for raloxifene (95% CI = 72.1% to 82.8%; P = .041), and 77.3% for estradiol plus raloxifene (95% CI = 72.7% to 82.0%; P = .045) (Fig. 5, B). Rb was phosphorylated in raloxifene-treated MCF-7/Ral cells, and addition of estradiol did not induce additional phosphorylation of Rb (Fig. 5, B, lower panel).

Estradiol induces apoptosis in long-term estrogen-deprived cells *(36)* and, in fact, we observed apoptotic cells in MCF-7/Ral cultures treated with estradiol for 6 days (Fig. 4, B). To confirm that apoptotic cells were present in estradiol-treated MCF-7/Ral cultures, we used annexin V binding. Untreated control MCF-7/Ral cultures or MCF-7/Ral cultures treated with 1 μM raloxifene for up to 24 days had a minimal number of apoptotic cells (Fig. 6, B), an observation that reflects enhanced survival of MCF-7/Ral cells (Fig. 3) that may be mediated by their high activity of NF-κB, a known survival factor *(50–54)*. After a 6-day estradiol treatment (passage 0), the percentage of apoptotic MCF-7/Ral cells was not statistically significantly different than that in untreated control cultures or cultures treated with 1 μM raloxifene or a combination of estradiol and raloxifene (P = .063). Extended estradiol treatment (passages 1–3; 12–24 days), however, increased the percentage of apoptotic cells, and the addition of raloxifene essentially blocked this effect

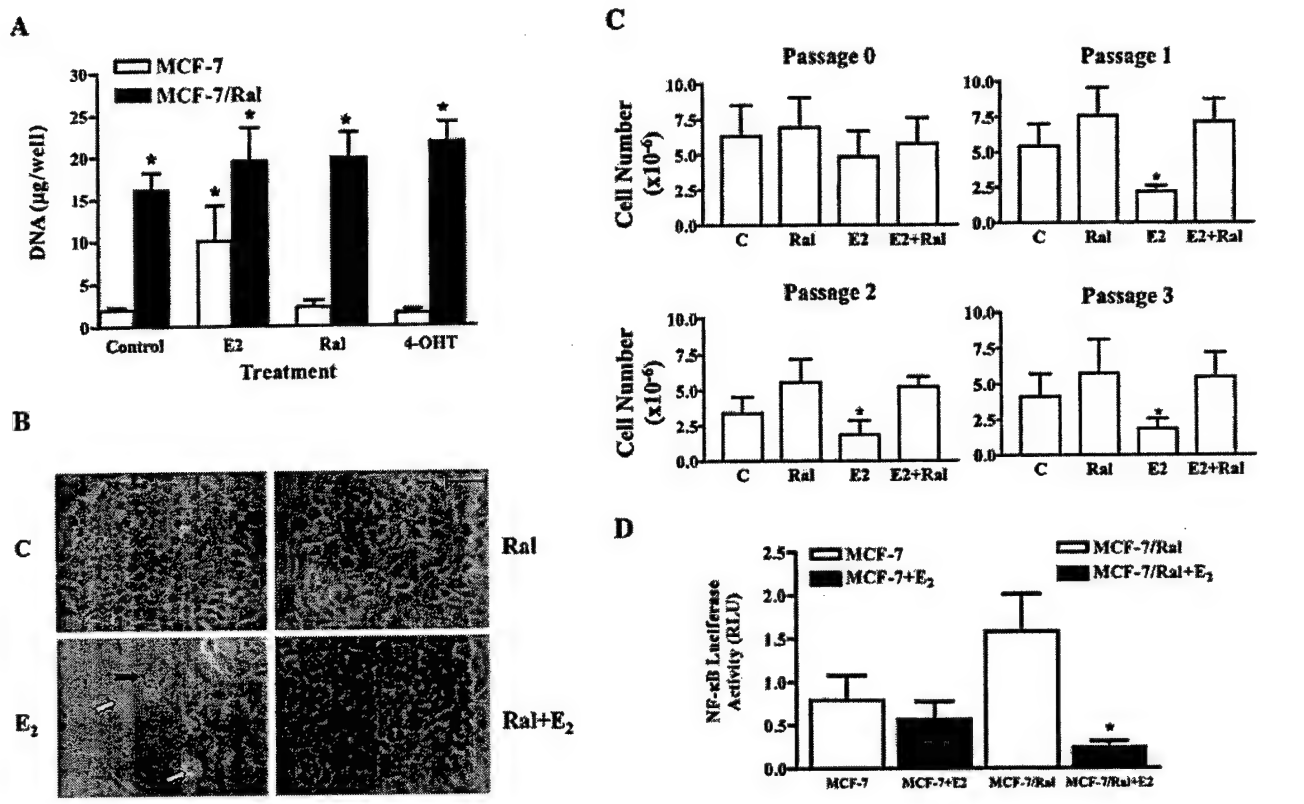

Fig. 4. Hormone-dependent growth of MCF-7 and MCF-7/Ral cells. All cells were grown in estrogen-free medium for 4 days before the assays. Cells were treated with ethanol vehicle (C or control), 1 n*M* 17β-estradiol (E_2), 1 µ*M* raloxifene (Ral), or 1 µ*M* 4-hydroxytamoxifen (4-OHT) for 6 days. **A)** DNA assay. For MCF-7 cells, values were as follows: control = 2.0 µg of DNA per well (95% CI = 1.6 to 2.3 µg); E_2 = 10.0 µg (95% CI = 5.8 to 14.3 µg); Ral = 2.2 µg (95% CI = 1.5 to 3.0 µg); and 4-OHT = 1.5 µg (95% CI = 1.1 to 1.9 µg). For MCF-7/Ral cells, values were as follows: control = 16.1 µg (95% CI = 14.1 to 18.2 µg); E_2 = 19.6 µg (95% CI = 15.6 to 23.6 µg); Ral = 19.8 µg (95% CI = 16.7 to 22.9 µg); and 4-OHT = 21.7 µg (95% CI = 19.3 to 24.1 µg). * $P<.001$ compared with the MCF-7 control cells. **B)** Cell morphology. Micrographs are phase-contrast images. **Open arrow** = apoptotic-like cells; **solid arrow** = double nuclei. **Scale bar** = 50 µm. **C)** Estradiol inhibition of MCF-7/Ral cell growth after an extended treatment *in vitro*. Approximately 2.5 × 10^4 cells were grown in estrogen-free medium for each passage (0–3) in the absence (C) or presence of 1 µ*M* raloxifene (Ral), 1 n*M* estradiol (E_2), or the combination of raloxifene and estradiol (E_2 + Ral). Experiments were repeated five times. The statistical interaction of estradiol and raloxifene was determined with a two-way analysis of variance. The interaction was statistically significant in passages 1 (P = .022), 2 (P = .023), and 3 (P = .029). All six pairwise comparisons among the four groups were calculated with Tukey's honestly significant difference. *Statistically significant compared with the values in raloxifene treatment group as follows: for passage 1, $P<.001$; for passage 2, P = .006; and for passage 3, P = .001. **D)** Estradiol treatment and nuclear factor κB (NF-κB) activity in MCF-7 and MCF-7/Ral cells. MCF-7 or MCF-7/Ral cells were grown in estrogen-free medium for 4 days before the NF-κB-luciferase transient transfection assay. MCF-7 + E_2 or MCF-7/Ral + E_2 cells were treated with 1 n*M* estradiol for 6 days and then grown in estrogen-free medium for 4 days before the transient transfection assay. * $P<.001$ compared with MCF-7/Ral cells. All statistical tests were two-sided.

(Fig. 6, B). Apoptosis was observed in untreated control and raloxifene-treated MCF-7 cell cultures, and estradiol treatment decreased the percentage of apoptotic MCF-7 cells (Fig. 6, B). Thus, estradiol treatment inhibited apoptosis in parental MCF-7 cells, and estradiol treatment promoted apoptosis in raloxifene-resistant MCF-7/Ral cells.

Estradiol and the Induction of Fas Expression

Estradiol regulates FasL expression in a variety of cells and tissues *(55–59)*, including long-term estrogen-deprived MCF-7 cells *(36)*. Untreated MCF-7 cells express a low or nondetectable level of Fas receptor *(36,60)*, but long-term estrogen deprivation of MCF-7 cells increases Fas expression *(36)*.

We investigated whether estradiol plays a role in the regulation of the Fas/FasL system in MCF-7/Ral and MCF-7 cells by determining their levels of Fas and FasL expression. Both MCF-7 and MCF-7/Ral cells expressed FasL but in an estradiol-independent manner. Although more apoptotic cells were observed in untreated control and raloxifene-treated MCF-7 cultures (Fig. 6, B), Fas protein was barely detected in MCF-7 cells. Estradiol treatment of parental MCF-7 cells did not appreciably affect Fas expression (Fig. 6, C) but did prevent apoptosis (Fig. 6, B), indicating that apoptosis in MCF-7 cells does not appear to be mediated by the Fas/FasL pathway. Fas protein was not detected in untreated control or raloxifene-treated MCF-7/Ral cells (Fig. 6, C). Estradiol treatment dramatically increased the level of Fas protein and mRNA in MCF-7/Ral cells (Fig. 6, C and D). For example, Fas mRNA levels increased 4.5-fold (95% CI = 2.8- to 6.3-fold) after estradiol treatment compared with 0.5-fold (95% CI = 0.3- to 0.8-fold) after control treatment, 0.8-fold (95% CI = 0.7- to 1.0-fold) after 1 µ*M* raloxifene, and 0.7-fold (95% CI = 0.4- to 1.1-fold) after raloxifene plus estradiol (all $P<.001$). Addition of raloxifene blocked estradiol-induced increases in Fas protein and mRNA levels (Fig. 6, C and

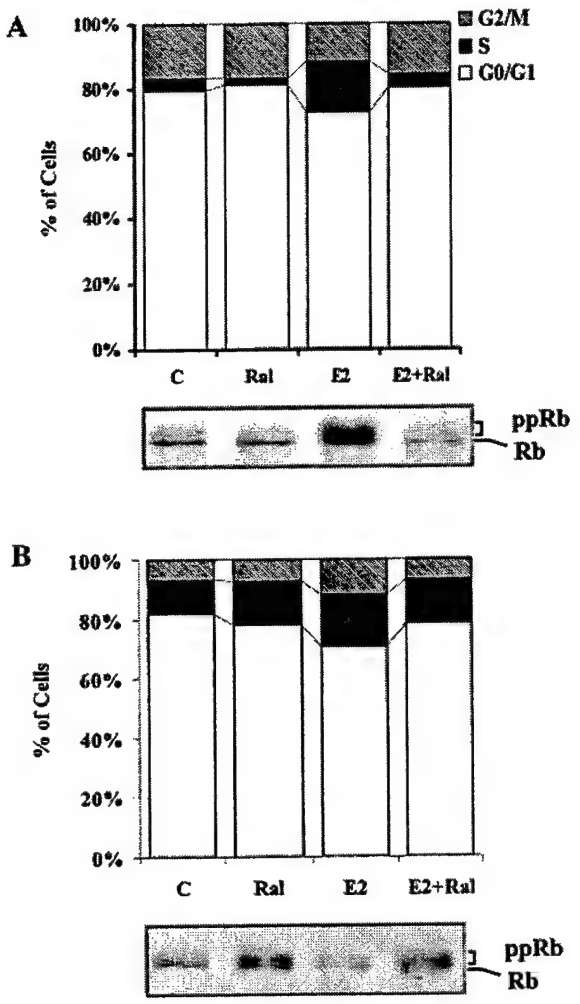

Fig. 5. Hormone-dependent effects on the cell cycle in MCF-7 (A) and MCF-7/Ral (B) cells. Cell cycle analysis is shown in the **upper panels**, and western blot analysis for the retinoblastoma protein (Rb) and phosphorylated Rb (ppRb) is shown in the **lower panels**. MCF-7 cells (A) and MCF-7/Ral cells (B) were treated with vehicle control (C), 1 μ*M* raloxifene (Ral), 1 n*M* 17β-estradiol (E_2), or 1 μ*M* raloxifene plus 1 n*M* 17β-estradiol (E_2 + Ral) for 6 days. Because there was no statistically significant difference in results from MCF-7/Ral cells in passages 1–3, the results from these passages were pooled for analysis.

D). In MCF-7/Ral cells, the effects of estradiol on Fas expression correspond to those on apoptosis and indicate that estradiol-induced apoptosis might be mediated by the Fas/FasL pathway in these cells.

Hormone-Dependent Growth of MCF-7/Ral Cells *In Vivo*

To further study raloxifene resistance and examine the unique inhibitory effect of estradiol on the growth of SERM-sensitized breast cancer cells, we examined the ability of MCF-7/Ral cells and parental MCF-7 cells to form tumors in athymic mice. As previously reported *(8,61)*, treatment with estradiol, but not with raloxifene, stimulated the growth of MCF-7 cell tumors in ovariectomized athymic mice (Fig. 7, A). MCF-7/Ral tumors, in contrast, required treatment with a SERM to grow; both raloxifene and tamoxifen, but not estradiol, statistically significantly stimulated the growth of MCF-7/Ral tumors in athymic mice (Fig. 7, B). Furthermore, if SERM treatment of the tumor-bearing athymic mice was stopped after 9 weeks and replaced by estradiol treatment for 5 weeks, tumors decreased in size in both groups of mice ($P = .004$ for raloxifene and $P<.001$ for tamoxifen), and some tumors disappeared altogether. These data are consistent with the effect of estradiol on the MCF-7/Ral cells *in vitro*.

Discussion

The increased use of SERMs to prevent breast cancer (with tamoxifen) or osteoporosis (with raloxifene) has added a new therapeutic dimension to clinical practice. The results of clinical trials now underway may establish SERMs as multifunctional medicines for the prevention of osteoporosis, coronary heart disease, and breast cancer *(3)*. However, the clinical use of these agents must be accompanied by rigorous laboratory studies to elucidate the mechanisms involved in the development of SERM-resistant breast cancer. The process of tamoxifen-resistant breast cancer development is well documented, but it is important to examine the potential for drug resistance to SERMs in general. We now report data from a new study of the evolution of raloxifene-resistant breast cancer in the laboratory that builds on our previous studies with tamoxifen *(8,29,30,33,62)*. Understanding the mechanism of raloxifene resistance should contribute important information for effective breast cancer therapy. We have confirmed and extended our original observation that low concentrations of estrogen shift the survival of SERM-resistant breast cancer cells by initiating apoptosis. Unlike our previous work that was entirely *in vivo (32,33,63)*, we now report results from both *in vitro* and *in vivo* studies using a new model of raloxifene-resistant breast cancer cells, MCF-7/Ral cells. We have defined the shift from cell survival induced by raloxifene in breast cancer to cell death induced by a modest concentration (1 n*M*) of estradiol in pre-sensitized cells.

Most research on SERM-resistant breast cancer has previously focused on tamoxifen. Apparent increased expression of ERα *(64,65)* and decreased expression of the nuclear receptor corepressor (i.e., N-CoR) *(66)* were detected in tamoxifen-resistant cells and tumors. An altered balance between ER coactivators and corepressors has been suggested as the mechanism for tamoxifen resistance *(67,68)*. Consequently, we initially examined the expression of ERα, ER coactivators (such as steroid receptor coactivators SRC-1, SRC-2, and SRC-3, and p300/CBP [cAMP response element–binding protein binding protein]), and ER corepressors (N-CoR and silencing mediator for retinoid and thyroid receptors) in MCF-7 and MCF-7/Ral cells with real-time PCR. We found no statistically significant differences in the expression levels of ERα and the ERα coregulators in MCF-7 cells and MCF-7/Ral cells grown in estrogen-free medium or treated with 1 μ*M* raloxifene for 24 or 48 hours (data not shown). Therefore, we conclude that changes in the expression of ERα or ER coregulators are not the primary mechanism for raloxifene resistance.

NF-κB is a key transcriptional factor for cell growth *(69)* and survival *(50–54)*. Increased NF-κB activity is involved in drug resistance in breast cancer *(70–72)*, and ERα represses NF-κB activity in the presence of estradiol *(52–54,73,74)*. Because raloxifene is an antiestrogen, we anticipated that raloxifene would block estradiol-mediated repression of NF-κB activity and thus increase NF-κB activity. In fact, we found higher levels of NF-κB p65 protein and activity in MCF-7/Ral cells than in

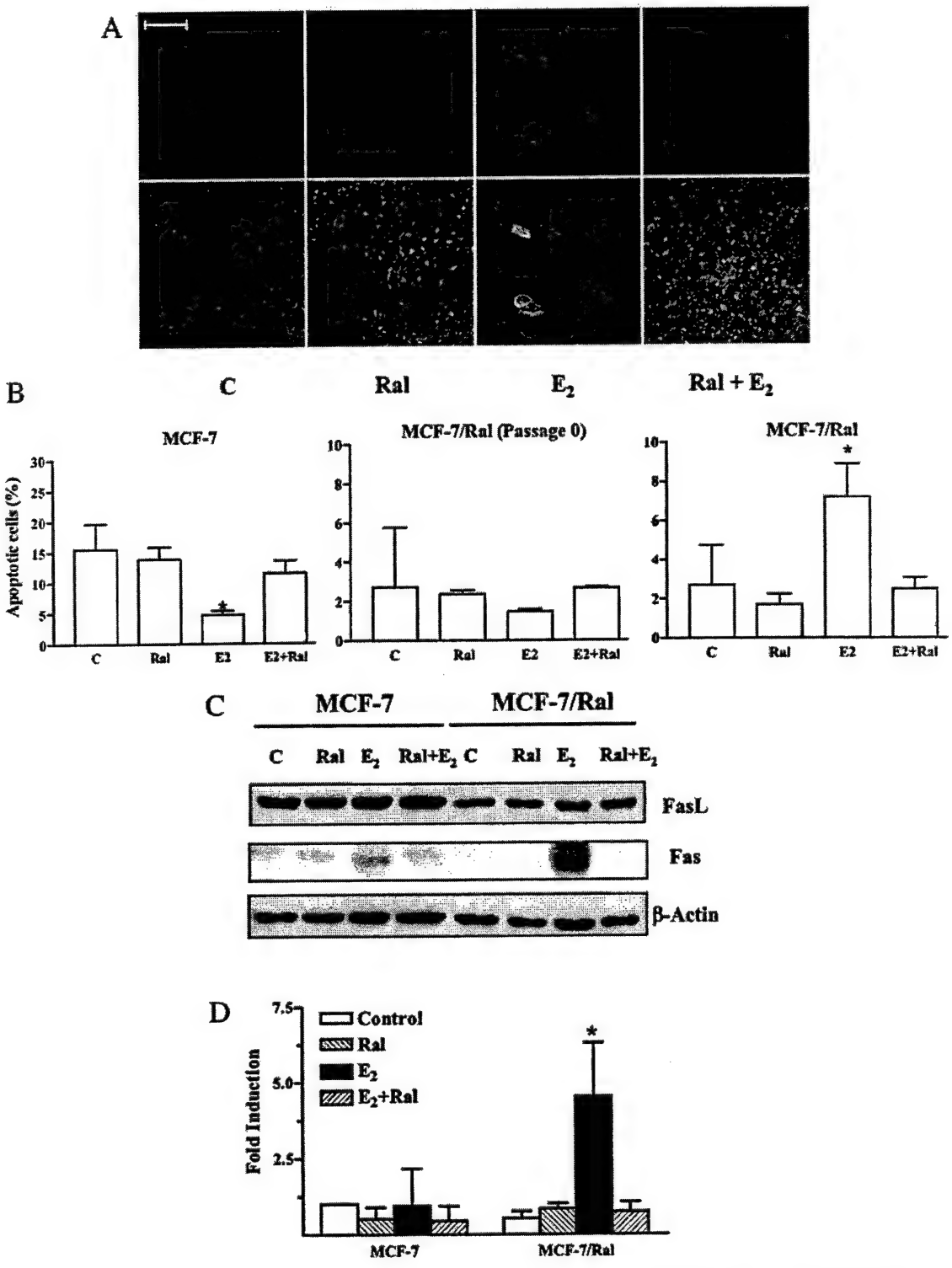

Fig. 6. Hormones and apoptosis in MCF-7 and MCF-7/Ral cells. C = vehicle control; Ral = raloxifene; E_2 = estradiol. **A)** Confocal images of annexin V staining in MCF-7/Ral cells. **Upper panel** = annexin V staining; **lower panel** = phase-contrast image. **Scale bar** = 50 μm. **B)** Apoptosis as measured by annexin V staining and flow cytometry. For panels MCF-7 and MCF-7/Ral (passage 0), cells were treated for 6 days with vehicle control, 1 μ*M* raloxifene, 1 n*M* estradiol, or 1 μ*M* raloxifene plus 1 n*M* estradiol. For panel MCF-7/Ral, cells were treated as indicated for passages 1–3 (12–24 days) and data from passages 1–3 were pooled. **C)** Western blot analysis for Fas and FasL in MCF-7 and MCF-7/Ral cells treated as indicated for two passages. β-Actin was used as the loading control. **D)** Real-time polymerase chain reaction analysis of Fas mRNA expression. MCF-7 cells were treated as indicated for 6 days, and MCF-7/Ral cells were treated as indicated for passages 0–3 (12–24 days). * $P<.001$ compared with any other group of MCF-7/Ral cells. All statistical tests were two-sided.

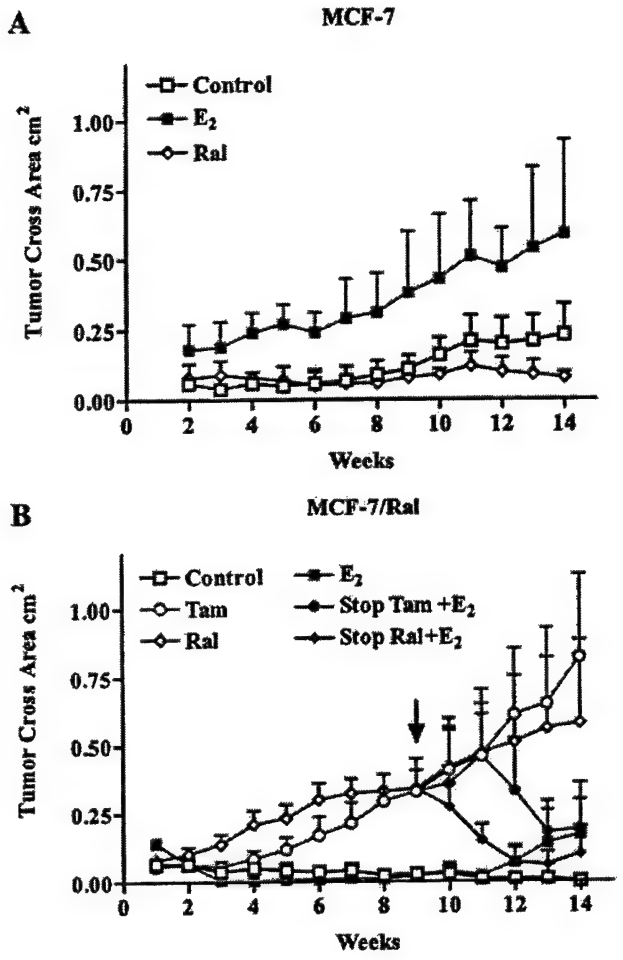

Fig. 7. Growth of MCF-7 (A) and MCF-7/Ral (B) tumors in ovariectomized athymic mice. Each group had 10 mice. The mice were treated with a 1-cm estradiol (E_2) capsule, 1.5 mg of tamoxifen (Tam), 1.5 mg of raloxifene (Ral), or vehicle control. At week 9 (**arrow**), raloxifene- and tamoxifen-stimulated MCF-7/Ral tumors were split into two arms: 1) continue raloxifene or tamoxifen treatment or 2) stop raloxifene or tamoxifen treatment and start estradiol treatment for 5 weeks (i.e., Stop Ral + E_2 or Stop Tam + E_2). For both treatments in the second arm, tumors at 14 weeks were statistically significantly decreased in size in both groups of mice (P = .004 for raloxifene and P<.001 for tamoxifen). Results are shown as mean tumor size with 95% confidence interval (only the upper confidence limit for each point is shown).

MCF-7 cells (Fig. 3). Thus, the NF-κB signal transduction pathway could be involved in the survival of raloxifene-resistant MCF-7/Ral cells.

The finding that raloxifene-resistant MCF-7/Ral cells are also resistant to tamoxifen has important therapeutic implications. Tamoxifen is used to treat all stages of ER-positive breast cancer and is used as a chemopreventive agent in women at high risk for breast cancer *(2)*. *In vitro* (Fig. 4, A) and *in vivo* (Fig. 7) data show that cells and/or tumors resistant to raloxifene are also resistant to tamoxifen and indicate that tamoxifen should not be given to patients with raloxifene-exposed breast cancer. The converse is also true *(31)*. It is perhaps prudent to consider treatment with an aromatase inhibitor or fulvestrant (i.e., Faslodex), a pure antiestrogen, in patients who have been exposed to raloxifene.

However, the most important observation for the outcome of long-term SERM-resistant breast cancer is the effectiveness of estrogen to induce apoptosis. Antitumor activity of estradiol has been reported for estrogen-deprived breast cancer cells *in vitro (34–36)*, tamoxifen-stimulated breast tumors *in vivo (16,32,33)*, and raloxifene-resistant ECC1 endometrial cancers *in vivo (37)*. More important, these findings have been extended to clinic settings, where estrogen is an effective treatment for breast cancers that have developed resistance to successive antiestrogenic therapies *(75)*. In this study, we found that a 6-day estradiol treatment (passage 0) did not inhibit MCF-7/Ral cell growth (Figs. 4, A, and 6, B), whereas an extended estradiol treatment (passages 1–3) of 12–24 days statistically significantly inhibited MCF-7/Ral cell growth (Fig. 4, C). Although the causes of the delayed inhibitory effect of estradiol are still not known, estradiol treatment also caused a delayed decrease in NF-κB activity (Fig. 4, D) without changing the level of NF-κB p65 protein (data not shown). Estradiol binds to ERα, and the estradiol–ERα complex suppresses NF-κB activity by inhibiting the binding of NF-κB to DNA or by competing with p300/CBP *(52,53,76,77)*, independent of new protein synthesis. However, because a 24- or 48-hour estradiol treatment did not inhibit NF-κB activity in MCF-7 and MCF-7/Ral cells (data not shown), the delayed inhibitory effect of estradiol on NF-κB activity may require the synthesis of new protein(s). This hypothesis is consistent with the report that estradiol inhibits NF-κB activity by increasing the expression of p105, the precursor of NF-κB *(78)*. However, further studies are necessary to understand the mechanism through which estradiol induces the delayed inhibition of NF-κB activity and growth in MCF-7/Ral cells.

If NF-κB plays an important role in raloxifene resistance, the decreased NF-κB activity induced by estradiol should increase the number of cells undergoing apoptosis. In fact, we observed that an extended estradiol treatment statistically significantly increased the number of apoptotic MCF-7/Ral cells (Fig. 6, A and B), as reported in long-term estrogen-deprived MCF-7 cells *(36)* and in T47D:protein kinase Cα cells *(16)*. Song et al. *(36)* suggested that estradiol induces apoptosis in long-term estrogen-deprived MCF-7 cells via the Fas/FasL pathway, and they noted that the level of Fas is elevated in the long-term estrogen-deprived MCF-7 cells and that treatment with estradiol increases the expression level of FasL and induces apoptosis through the elevated level of Fas. Consequently, we examined the expression of Fas and FasL in MCF-7 and MCF-7/Ral cells in response to estradiol treatment. We found that estradiol did not induce expression of FasL in MCF-7 or MCF-7/Ral cells or the expression of Fas in MCF-7 cells but did induce the expression of Fas protein and mRNA in MCF-7/Ral cells (Fig. 6, D). This result is perplexing because, to our knowledge, there are no reports that estrogen stimulates the expression of Fas; however, increased Fas expression is observed in tamoxifen-resistant MCF-7 cells treated with estradiol, which presages apoptosis *in vivo (63)*.

In MCF-7/Ral cells, estradiol treatment induced cell cycle arrest at G_2/M phase (Fig. 5, B) and generated multinucleated cells (Fig. 4, B), although the mechanism is currently unclear. Estradiol stimulates the expression of genes that are involved in both inhibiting and promoting G_2/M-phase arrest. In MCF-7 cells, estrogen induces the estrogen-responsive finger protein *(79,80)*, which targets the 14–3–3σ protein for proteolysis. [14–3–3σ is a p53-regulated gene that, along with $p21^{Cip-1/Waf-1}$, plays a role in p53-mediated cell cycle arrest at G_2/M phase *(81,82)*.] Because estradiol also induces p53 *(83)*, the estrogen-responsive finger protein and p53 might be involved in the

estradiol-mediated G_2/M-phase arrest observed in MCF-7/Ral cells. We are currently investigating this hypothesis.

In summary, the MCF-7/Ral model is the first reproducible raloxifene-resistant breast cancer grown in athymic mice. Using this model, we demonstrated that breast tumors and/or cells resistant to tamoxifen are also resistant to raloxifene, and so tamoxifen would not be an appropriate therapy for breast cancer after raloxifene resistance is diagnosed. More importantly, we have established that estradiol treatment causes tumor regression in SERM-sensitized cells by inducing G_2/M-phase arrest and apoptosis. Although the mechanism is not completely elucidated, the balance between survival and apoptosis may be mediated through the Fas/FasL pathway by the increasing Fas expression and the decreasing NF-κB activity. Overall, these data, and those in the companion study *(63)* using a tamoxifen-resistant model *in vivo,* suggest that it is possible for a patient's own estrogen to act as an anticancer agent in SERM-resistant breast cancers. Clearly, a clinical strategy to use an aromatase inhibitor after SERM resistance may have some short-term benefit for patients, but it is possible that a novel strategy of briefly treating patients with estrogen before re-instituting estrogen-deprivation therapy may benefit certain women. Indeed, preliminary studies *(75)* have demonstrated the beneficial effects of estrogen in patients for whom repeated estrogen-deprivation treatments have failed.

References

(1) Tamoxifen for early breast cancer: an overview of the randomised trials. Early Breast Cancer Trialists' Collaborative Group. Lancet 1998;351:1451–67.

(2) Fisher B, Costantino JP, Wickerham DL, Redmond CK, Kavanah M, Cronin WM, et al. Tamoxifen for prevention of breast cancer: report of the National Surgical Adjuvant Breast and Bowel Project P-1 Study. J Natl Cancer Inst 1998;90:1371–88.

(3) Jordan VC, Gapstur S, Morrow M. Selective estrogen receptor modulation and reduction in risk of breast cancer, osteoporosis, and coronary heart disease. J Natl Cancer Inst 2001;93:1449–57.

(4) Ettinger B, Black DM, Mitlak BH, Knickerbocker RK, Nickelsen T, Genant HK, et al. Reduction of vertebral fracture risk in postmenopausal women with osteoporosis treated with raloxifene: results from a 3-year randomized clinical trial. Multiple Outcomes of Raloxifene Evaluation (MORE) Investigators [published erratum appears in JAMA 1999;282: 2124]. JAMA 1999;282:637–45.

(5) Cummings SR, Eckert S, Krueger KA, Grady D, Powles TJ, Cauley JA, et al. The effect of raloxifene on risk of breast cancer in postmenopausal women: results from the MORE randomized trial. Multiple Outcomes of Raloxifene Evaluation. JAMA 1999;281:2189–97.

(6) Cauley JA, Norton L, Lippman ME, Eckert S, Krueger KA, Purdie DW, et al. Continued breast cancer risk reduction in postmenopausal women treated with raloxifene: 4-year results from the MORE trial. Multiple Outcomes of Raloxifene Evaluation. Breast Cancer Res Treat 2001;65:125–34.

(7) Gail MH, Brinton LA, Byar DP, Corle DK, Green SB, Schairer C, et al. Projecting individualized probabilities of developing breast cancer for white females who are being examined annually. J Natl Cancer Inst 1989;81:1879–86.

(8) Gottardis MM, Jordan VC. Development of tamoxifen-stimulated growth of MCF-7 tumors in athymic mice after long-term antiestrogen administration. Cancer Res 1988;48:5183–7.

(9) Howell A, Dodwell DJ, Anderson H, Redford J. Response after withdrawal of tamoxifen and progestogens in advanced breast cancer. Ann Oncol 1992;3:611–7.

(10) Schafer JM, Lee ES, O'Regan RM, Yao K, Jordan VC. Rapid development of tamoxifen-stimulated mutant p53 breast tumors (T47D) in athymic mice. Clin Cancer Res 2000;6:4373–80.

(11) Dumont JA, Bitonti AJ, Wallace CD, Baumann RJ, Cashman EA, Cross-Doersen DE. Progression of MCF-7 breast cancer cells to antiestrogen-resistant phenotype is accompanied by elevated levels of AP-1 DNA-binding activity. Cell Growth Differ 1996;7:351–9.

(12) Johnston SR, Lu B, Scott GK, Kushner PJ, Smith IE, Dowsett M, et al. Increased activator protein-1 DNA binding and c-Jun NH2-terminal kinase activity in human breast tumors with acquired tamoxifen resistance. Clin Cancer Res 1999;5:251–6.

(13) Schiff R, Reddy P, Ahotupa M, Coronado-Heinsohn E, Grim M, Hilsenbeck SG, et al. Oxidative stress and AP-1 activity in tamoxifen-resistant breast tumors in vivo. J Natl Cancer Inst 2000;92:1926–34.

(14) Campbell RA, Bhat-Nakshatri P, Patel NM, Constantinidou D, Ali S, Nakshatri H. Phosphatidylinositol 3-kinase/AKT-mediated activation of estrogen receptor alpha: a new model for anti-estrogen resistance. J Biol Chem 2001;276:9817–24.

(15) Sun M, Paciga JE, Feldman RI, Yuan Z, Coppola D, Lu YY, et al. Phosphatidylinositol-3-OH kinase (PI3K)/AKT2, activated in breast cancer, regulates and is induced by estrogen receptor alpha (ERalpha) via interaction between ERalpha and PI3K. Cancer Res 2001;61:5985–91.

(16) Chisamore MJ, Ahmed Y, Bentrem DJ, Jordan VC, Tonetti DA. Novel antitumor effect of estradiol in athymic mice injected with a T47D breast cancer cell line overexpressing protein kinase Calpha. Clin Cancer Res 2001;7:3156–65.

(17) Pietras RJ, Arboleda J, Reese DM, Wongvipat N, Pegram MD, Ramos L, et al. HER-2 tyrosine kinase pathway targets estrogen receptor and promotes hormone-independent growth in human breast cancer cells. Oncogene 1995;10:2435–46.

(18) Kurokawa H, Lenferink AE, Simpson JF, Pisacane PI, Sliwkowski MX, Forbes JT, et al. Inhibition of HER2/neu (erbB-2) and mitogen-activated protein kinases enhances tamoxifen action against HER2-overexpressing, tamoxifen-resistant breast cancer cells. Cancer Res 2000;60:5887–94.

(19) Chung YL, Sheu ML, Yang SC, Lin CH, Yen SH. Resistance to tamoxifen-induced apoptosis is associated with direct interaction between HER2/neu and cell membrane estrogen receptor in breast cancer. Int J Cancer 2002;97:306–12.

(20) Parisot JP, Hu XF, DeLuise M, Zalcberg JR. Altered expression of the IGF-1 receptor in a tamoxifen-resistant human breast cancer cell line. Br J Cancer 1999;79:693–700.

(21) Vertegaal AC, Kuiperij HB, Yamaoka S, Courtois G, van der Eb AJ, Zantema A. Protein kinase C-alpha is an upstream activator of the IkappaB kinase complex in the TPA signal transduction pathway to NF-kappaB in U2OS cells. Cell Signal 2000;12:759–68.

(22) Zhou BP, Hu MC, Miller SA, Yu Z, Xia W, Lin SY, et al. HER-2/neu blocks tumor necrosis factor-induced apoptosis via the Akt/NF-kappaB pathway. J Biol Chem 2000;275:8027–31.

(23) Pianetti S, Arsura M, Romieu-Mourez R, Coffey RJ, Sonenshein GE. Her-2/neu overexpression induces NF-kappaB via a PI3-kinase/Akt pathway involving calpain-mediated degradation of IkappaB-alpha that can be inhibited by the tumor suppressor PTEN. Oncogene 2001;20:1287–99.

(24) Bhat-Nakshatri P, Sweeney CJ, Nakshatri H. Identification of signal transduction pathways involved in constitutive NF-kappaB activation in breast cancer cells. Oncogene 2002;21:2066–78.

(25) Nakshatri H, Bhat-Nakshatri P, Martin DA, Goulet RJ Jr, Sledge GW Jr. Constitutive activation of NF-kappaB during progression of breast cancer to hormone-independent growth. Mol Cell Biol 1997;17:3629–39.

(26) Gu Z, Lee RY, Skaar TC, Bouker KB, Welch JN, Lu J, et al. Association of interferon regulatory factor-1, nucleophosmin, nuclear factor-kappaB, and cyclic AMP response element binding with acquired resistance to Faslodex (ICI 182,780). Cancer Res 2002;62:3428–37.

(27) Brunner N, Boysen B, Jirus S, Skaar TC, Holst-Hansen C, Lippman J, et al. MCF7/LCC9: an antiestrogen-resistant MCF-7 variant in which acquired resistance to the steroidal antiestrogen ICI 182,780 confers an early cross-resistance to the nonsteroidal antiestrogen tamoxifen. Cancer Res 1997;57: 3486–93.

(28) McLeskey SW, Zhang L, El-Ashry D, Trock BJ, Lopez CA, Kharbanda S, et al. Tamoxifen-resistant fibroblast growth factor-transfected MCF-7 cells are cross-resistant in vivo to the antiestrogen ICI 182,780 and two aromatase inhibitors. Clin Cancer Res 1998;4:697–711.

(29) Lee ES, Schafer JM, Yao K, England G, O'Regan RM, De Los Reyes A, et al. Cross-resistance of triphenylethylene-type antiestrogens but not ICI 182,780 in tamoxifen-stimulated breast tumors grown in athymic mice. Clin Cancer Res 2000;6:4893–9.

(30) Schafer JM, Lee ES, Dardes RC, Bentrem D, O'Regan RM, De Los Reyes A, et al. Analysis of cross-resistance of the selective estrogen receptor modulators arzoxifene (LY353381) and LY117018 in tamoxifen-stimulated breast cancer xenografts. Clin Cancer Res 2001;7:2505–12.

(31) O'Regan RM, Gajdos C, Dardes RC, De Los Reyes A, Park W, Rademaker AW, et al. Effects of raloxifene after tamoxifen on breast and endometrial tumor growth in athymic mice. J Natl Cancer Inst 2002;94:274–83.

(32) Wolf DM, Jordan VC. A laboratory model to explain the survival advantage observed in patients taking adjuvent tamoxifen therapy. Recent results in cancer research. Vol. 127. Heidelberg (Germany): Springer-Verlag; 1993. p. 23–33.

(33) Yao K, Lee ES, Bentrem DJ, England G, Schafer JI, O'Regan RM, et al. Antitumor action of physiological estradiol on tamoxifen-stimulated breast tumors grown in athymic mice. Clin Cancer Res 2000;6:2028–36.

(34) Fernandez P, Wilson C, Hoivik D, Safe SH. Altered phenotypic characteristics of T47d human breast cancer cells after prolonged growth in estrogen-deficient medium. Cell Biol Int 1998;22:623–33.

(35) Liu H, Lee ES, De Los Reyes A, Jordan VC. Antitumor action of estradiol on estrogen-deprived or raloxifene-resistant human breast cancer cells. Breast Cancer Res Treat 2000;64:134.

(36) Song RX, Mor G, Naftolin F, McPherson RA, Song J, Zhang Z, et al. Effect of long-term estrogen deprivation on apoptotic responses of breast cancer cells to 17beta-estradiol. J Natl Cancer Inst 2001;93:1714–23.

(37) Dardes R, Liu H, Gajdos C, O'Regan R, De Los Reyes A, Jordan V. Raloxifene stimulated endometrial cancer grown in athymic mice: cross-resistance with ICI 182,780 and antitumor action of estradiol. Breast Cancer Res Treat 2001;69:288.

(38) Itoh N, Yonehara S, Ishii A, Yonehara M, Mizushima S, Sameshima M, et al. The polypeptide encoded by the cDNA for human cell surface antigen Fas can mediate apoptosis. Cell 1991;66:233–43.

(39) Oehm A, Behrmann I, Falk W, Pawlita M, Maier G, Klas C, et al. Purification and molecular cloning of the APO-1 cell surface antigen, a member of the tumor necrosis factor/nerve growth factor receptor superfamily sequence identity with the Fas antigen. J Biol Chem 1992;267:10709–15.

(40) Pink JJ, Jordan VC. Models of estrogen receptor regulation by estrogens and antiestrogens in breast cancer cell lines. Cancer Res 1996;56:2321–30.

(41) Labarca C, Paigen K. A simple, rapid, and sensitive DNA assay procedure. Anal Biochem 1980; 102:344–52.

(42) Vindelov LL, Christensen IJ, Nissen NI. A detergent-trypsin method for the preparation of nuclei for flow cytometric DNA analysis. Cytometry 1983; 3:323–7.

(43) Robinson JK, Rademaker AW, Goolsby C, Traczyk TN, Zoladz C. DNA ploidy in nonmelanoma skin cancer. Cancer 1996;77:284–91.

(44) Schafer JM, Liu H, Bentrem DJ, Zapf JW, Jordan VC. Allosteric silencing of activating function 1 in the 4-hydroxytamoxifen estrogen receptor complex is induced by substituting glycine for aspartate at amino acid 351. Cancer Res 2000;60:5097–105.

(45) Catherino WH, Jordan VC. Increasing the number of tandem estrogen response elements increases the estrogenic activity of a tamoxifen analogue. Cancer Lett 1995;92:39–47.

(46) Gottardis MM, Robinson SP, Jordan VC. Estradiol-stimulated growth of MCF-7 tumors implanted in athymic mice: a model to study the tumoristatic action of tamoxifen. J Steroid Biochem 1988;30:311–4.

(47) Robinson S, Jordan V. Antiestrogenic action of toremifene on hormone-dependent, -independent, and heterogeneous breast tumor growth in the athymic mouse. Cancer Res 1989;49:1758–62.

(48) O'Regan RM, Cisneros A, England GM, MacGregor JI, Meunzner HD, Assikis VJ, et al. Effects of the antiestrogens tamoxifen, toremifene, and ICI 182,780 on endometrial cancer growth. J Natl Cancer Inst 1998;90:1552–8.

(49) Thompson EW, Reich R, Shima TB, Albini A, Graf J, Martin GR, et al. Differential regulation of growth and invasiveness of MCF-7 breast cancer cells by antiestrogens. Cancer Res 1988;48:6764–8.

(50) Sonenshein GE. Rel/NF-kappa B transcription factors and the control of apoptosis. Semin Cancer Biol 1997;8:113–9.

(51) Schwartz SA, Hernandez A, Mark Evers B. The role of NF-kappaB/IkappaB proteins in cancer: implications for novel treatment strategies. Surg Oncol 1999;8:143–53.

(52) Galien R, Garcia T. Estrogen receptor impairs interleukin-6 expression by preventing protein binding on the NF-kappaB site. Nucleic Acids Res 1997;25:2424–9.

(53) Harnish DC, Scicchitano MS, Adelman SJ, Lyttle CR, Karathanasis SK. The role of CBP in estrogen receptor cross-talk with nuclear factor-kappaB in HepG2 cells. Endocrinology 2000;141:3403–11.

(54) Evans MJ, Eckert A, Lai K, Adelman SJ, Harnish DC. Reciprocal antagonism between estrogen receptor and NF-kappaB activity in vivo. Circ Res 2001;89:823–30.

(55) Nilsen J, Mor G, Naftolin F. Estrogen-regulated developmental neuronal apoptosis is determined by estrogen receptor subtype and the Fas/Fas ligand system. J Neurobiol 2000;43:64–78.

(56) Mor G, Kohen F, Garcia-Velasco J, Nilsen J, Brown W, Song J, et al. Regulation of fas ligand expression in breast cancer cells by estrogen: functional differences between estradiol and tamoxifen. J Steroid Biochem Mol Biol 2000;73:185–94.

(57) Amant C, Holm P, Xu SH, Tritman N, Kearney M, Losordo DW. Estrogen receptor-mediated, nitric oxide-dependent modulation of the immunologic barrier function of the endothelium: regulation of fas ligand expression by estradiol. Circulation 2001;104:2576–81.

(58) Mor G, Munoz A, Redlinger R Jr, Silva I, Song J, Lim C, et al. The role of the Fas/Fas ligand system in estrogen-induced thymic alteration. Am J Reprod Immunol 2001;46:298–307.

(59) Sapi E, Brown WD, Aschkenazi S, Lim C, Munoz A, Kacinski BM, et al. Regulation of Fas ligand expression by estrogen in normal ovary. J Soc Gynecol Investig 2002;9:243–50.

(60) Yan Y, Haas JP, Kim M, Sgagias MK, Cowan KH. BRCA1-induced apoptosis involves inactivation of ERK1/2 activities. J Biol Chem 2002; 277:33422–30.

(61) Osborne CK, Hobbs K, Clark GM. Effect of estrogens and antiestrogens on growth of human breast cancer cells in athymic nude mice. Cancer Res 1985;45:584–90.

(62) Gottardis MM, Jiang SY, Jeng MH, Jordan VC. Inhibition of tamoxifen-stimulated growth of an MCF-7 tumor variant in athymic mice by novel steroidal antiestrogens. Cancer Res 1989;49:4090–3.

(63) Osipo C, Gajdos C, Liu H, Chen B, Jordan VC. Paradoxical action of fulvestrant in estradiol-induced regression of tamoxifen-stimulated breast cancer. Natl Cancer Inst 2003;95:000–000.

(64) Speirs V, Malone C, Walton DS, Kerin MJ, Atkin SL. Increased expression of estrogen receptor beta mRNA in tamoxifen-resistant breast cancer patients. Cancer Res 1999;59:5421–4.

(65) Speirs V, Kerin MJ. Prognostic significance of oestrogen receptor beta in breast cancer. Br J Surg 2000;87:405–9.

(66) Lavinsky RM, Jepsen K, Heinzel T, Torchia J, Mullen TM, Schiff R, et al. Diverse signaling pathways modulate nuclear receptor recruitment of N-CoR and SMRT complexes. Proc Natl Acad Sci U S A 1998;95:2920–5.

(67) Graham JD, Bain DL, Richer JK, Jackson TA, Tung L, Horwitz KB. Thoughts on tamoxifen resistant breast cancer. Are coregulators the answer or just a red herring? J Steroid Biochem Mol Biol 2000;74:255–9.

(68) Ratajczak T. Protein coregulators that mediate estrogen receptor function. Reprod Fertil Dev 2001;13:221–9.

(69) Tantini B, Pignatti C, Fattori M, Flamigni F, Stefanelli C, Giordano E, et al. NF-kappaB and ERK cooperate to stimulate DNA synthesis by inducing ornithine decarboxylase and nitric oxide synthase in cardiomyocytes treated with TNF and LPS. FEBS Lett 2002;512:75–9.

(70) Keane MM, Rubinstein Y, Cuello M, Ettenberg SA, Banerjee P, Nau MM, et al. Inhibition of NF-kappaB activity enhances TRAIL mediated apoptosis in breast cancer cell lines. Breast Cancer Res Treat 2000;64:211–9.

(71) Bhoumik A, Ivanov V, Ronai Z. Activating transcription factor 2-derived peptides alter resistance of human tumor cell lines to ultraviolet irradiation and chemical treatment. Clin Cancer Res 2001;7:331–42.

(72) Weldon CB, Burow ME, Rolfe KW, Clayton JL, Jaffe BM, Beckman BS. NF-kappa B-mediated chemoresistance in breast cancer cells. Surgery 2001;130:143–50.

(73) Pelzer T, Neumann M, de Jager T, Jazbutyte V, Neyses L. Estrogen effects in the myocardium: inhibition of NF-kappaB DNA binding by estrogen receptor-alpha and -beta. Biochem Biophys Res Commun 2001;286:1153–7.

(74) Sharma RV, Gurjar MV, Bhalla RC. Selected contribution: estrogen receptor-alpha gene transfer inhibits proliferation and NF-kappaB activation in VSM cells from female rats. J Appl Physiol 2001;91:2400–6.

(75) Lønning PE, Taylor PD, Anker G, Iddon J, Wie L, Jorgensen LM, et al. High-dose estrogen treatment in postmenopausal breast cancer patients heavily exposed to endocrine therapy. Breast Cancer Res Treat 2001;67:111–6.

(76) Ray P, Ghosh SK, Zhang DH, Ray A. Repression of interleukin-6 gene expression by 17 beta-estradiol: inhibition of the DNA-binding activity of the transcription factors NF-IL6 and NF-kappa B by the estrogen receptor. FEBS Lett 1997;409:79–85.

(77) Speir E, Yu ZX, Takeda K, Ferrans VJ, Cannon RO 3rd. Competition for p300 regulates transcription by estrogen receptors and nuclear factor-kappaB in human coronary smooth muscle cells. Circ Res 2000;87:1006–11.

(78) Hsu SM, Chen YC, Jiang MC. 17 beta-estradiol inhibits tumor necrosis factor-alpha-induced nuclear factor-kappa B activation by increasing nuclear factor-kappa B p105 level in MCF-7 breast cancer cells. Biochem Biophys Res Commun 2000;279:47–52.

(79) Inoue S, Orimo A, Hosoi T, Kondo S, Toyoshima H, Kondo T, et al. Genomic binding-site cloning reveals an estrogen-responsive gene that encodes a RING finger protein. Proc Natl Acad Sci U S A 1993;90:11117–21.

(80) Ikeda K, Orimo A, Higashi Y, Muramatsu M, Inoue S. Efp as a primary estrogen-responsive gene in human breast cancer. FEBS Lett 2000;472:9–13.

(81) Urano T, Saito T, Tsukui T, Fujita M, Hosoi T, Muramatsu M, et al. Efp targets 14–3-3 sigma for proteolysis and promotes breast tumour growth. Nature 2002;417:871–5.

(82) Taylor WR, Stark GR. Regulation of the G2/M transition by p53. Oncogene 2001;20:1803–15.

(83) Qin C, Nguyen T, Stewart J, Samudio I, Burghardt R, Safe S. Estrogen up-regulation of p53 gene expression in MCF-7 breast cancer cells is mediated by calmodulin kinase IV-dependent activation of a nuclear factor kappaB/CCAAT-binding transcription factor-1 complex. Mol Endocrinol 2002;16:1793–809.

NOTES

Supported by Specialized Programs of Research Excellence (SPORE) grant CA89018-01 (to V. C. Jordan) from the National Cancer Institute, National Institutes of Health, Department of Health and Human Services, grant DAMD 17-00-1-0386 (to V. C. Jordan) from the Department of Defense, and the Avon Foundation.

We thank Dr. Joan Lewis for her valuable discussion and Dr. Alfred Rademaker for his statistical advice.

Manuscript received February 10, 2003; revised August 21, 2003; accepted August 29, 2003.

Electrophoresis 2002, *23*, 1375–1385

Review

Igor V. Kourkine
Christa N. Hestekin
Annelise E. Barron

Northwestern University,
Department of Chemical
Engineering,
Evanston, IL, USA

Technical challenges in applying capillary electrophoresis-single strand conformation polymorphism for routine genetic analysis

Recent and future advances in population genetics will have a significant impact on health care practices and the economics of health care provision only if a spectrum of patient-tailored, effective methods of DNA screening for sequence alterations has been developed. Genetic screening by capillary electrophoresis-single strand conformation polymorphism (CE-SSCP), which is based upon the differences in electrophoretic mobilities of wild-type and mutant DNA species, offers an important complement to other presently available techniques such as Sanger sequencing and DNA hybridization arrays due to its simplicity, versatility, and low cost of analysis. A two-part review of CE-SSCP that discusses its advantages and limitations is presented. Emphasis is placed on technological aspects of CE-SSCP (including such rarely addressed issues as sample preparation protocols and the nature of the polymeric DNA separation matrix) as well as on the potential of CE-SSCP for routine genetic analysis. An attempt is made to organize and present the information in sufficient detail to allow the use of SSCP for routine genetic screening even by those inexperienced in CE. Some discussion of CE-based heteroduplex analysis (HA) is also presented.

Keywords: Capillary electrophoresis / Heteroduplex analysis / Mutation detection / Review / Single-strand conformation polymorphism

EL 4949

CE and CEC

Contents

Correspondence: Professor Annelise E. Barron, Northwestern University, Department of Chemical Engineering, 2145 Sheridan Road, Evanston, IL 60208, USA
E-mail: a-barron@northwestern.edu
Fax: + 847-491-3728

Abbreviations: CAE, capillary array electrophoresis; **HA**, heteroduplex analysis; **LPA**, linear polyacrylamide

1 Introduction

The development of low-cost, high-throughput genetic screening technologies promises to enable a systematic search within populations for individuals possessing particular genotypes that are either associated with, predispose to, or directly lead to the development of disease [1]. The goals of genetic screening include medical diagnosis, management or treatment of illness, the provision of reproductive information, genetic mutation enumeration (estimation of prevalence of mutant alleles, their distribution and biological significance), and genetic research. Routine genotyping and genetic testing of large numbers of individuals is not without troubling implications and potential roadblocks, which can be broadly classified as either psychosocial or technical in nature. From the psychosocial viewpoint, it is important to differentiate between the screening for inherited mutations (germline mutations) and for genetic changes accumulated throughout the lifetime of an individual as a result of environmental exposures or other unexplained events (somatic mutations). Testing for somatic mutations is not troubled with the same "worrisome implications" as screening for inherited genetic mutations might be. For example, the detection of such "acquired" mutations hold no major ethical considerations such as the issue of impact on other family members or possible psychological trauma.

0173-0835/02/1005–1375 $17.50+.50/0

From the technological perspective, there are real issues with the sensitivity of mutation detection. Routine genetic testing technology may fail to identify existent mutations in anywhere from 25 to 75% of the cases [2].

Single-strand conformation polymorphism (SSCP) is one of the most common, versatile, and inexpensive indirect methods for genetic screening, as evidenced by thousands of publications since its invention in 1989 by Orita *et al.* [3]. Unlike direct methods for genetic screening such as Sanger DNA sequencing or DNA hybridization arrays (*a.k.a.* GeneChips™), SSCP can determine the mutation status of a gene through a comparison to wild-type, but does not provide information on the exact nature of the mutation, *i.e.* the specific change in DNA sequence. SSCP is based on the principal that an alteration in DNA nucleotide sequence caused by a mutation will affect single-stranded DNA (ssDNA) folding and, hence, the electrophoretic mobility of a DNA fragment analyzed under native (nondenaturing) conditions. Traditionally, SSCP has involved time-consuming (up to 14 h), labor-intensive, and cumbersome electrophoresis of radioactively labeled DNA samples in a highly resolving separation medium such as a large-format, cross-linked 20% polyacrylamide gel. DNA bands typically were detected by long exposure of the gel to X-ray film (Fig. 1). These practical difficulties associated with slab-gel SSCP, which are ultimately technique-related, have resulted in selective and limited application of SSCP-based techniques in clinical medicine. The recent advent of capillary electrophoresis (CE), in which electrophoretic separation is carried out within arrays of microbore fused-silica capillaries of 50–75 μm inner diameter, not only provides a viable alternative to slab-gel SSCP, but also offers much higher throughput and sensitivity as well as greater reproducibility and full method automation [4, 5].

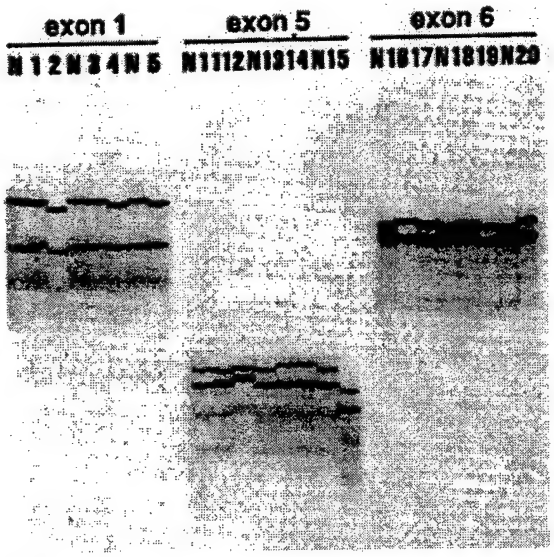

Figure 1. An example of genetic screening of the Factor IX exons 1 (424 bp), 5 (338 bp) and 6 (389 bp) by slab-gel SSCP, electrophoresed for 5 h. Lanes labeled N are loaded with wild-type controls, while those labeled 1–20 are loaded with samples of DNA obtained from hemophilia patients. Reprinted from Kukita *et al., Hum. Mutat.* 1997, *10*, 400–407, with permission.

While slab-gel SSCP protocols have been optimized extensively for sensitive mutation detection, precise, rational, and comprehensive information on the best methods for CE-SSCP is lacking. A few important CE-SSCP variables such as temperature, buffer composition and pH, and DNA size and sequence have been investigated with relative thoroughness. Others, such as the nature of the DNA separation matrix, capillary wall coating, and DNA sample preparation procedures, have received little or no attention. Moreover, information on CE-SSCP is presently fragmented and scattered throughout the literature, making it practically difficult for a novice in the field to start applying CE-SSCP to their needs.

In the first part of this review, we analyze the impact of DNA sample preparation methods and CE parameters on the sensitivity of mutation detection by CE-SSCP. In the second part, we outline some considerations related to the potential of CE-SSCP as an effective method for genetic screening in a clinical setting. The goal of this paper is to highlight the technical details of CE-SSCP protocols that are essential for reproducible and sensitive mutation detection, in order to facilitate the development of rational CE-SSCP protocols that will be useful in a clinical medicine, such as in the diagnosis and treatment of cancer.

2 CE-SSCP parameter optimization

2.1 PCR amplification

As indicated in many research papers and summarized in a recent review by Ren [6], two modes of detection can be used for CE-SSCP: fluorescence detection and UV (260 nm) detection. The use of UV detection dominated the field in the early 90's, but is now almost completely replaced by fluorescence detection due to the much higher sensitivity of the latter [7, 8]. Fluorescent labels may be introduced into dsDNA by PCR amplification with fluorescent primers, or by post-PCR fluorescent labeling using alkaline phosphatase and Klenow fragment enzymes. The latter method was pioneered by Inazuka *et al.* [9] and yields much cleaner and more homogeneous DNA samples, as well as easier-to-interpret CE-SSCP electropherograms. However, post-PCR labeling has yet

to gain widespread popularity, presumably because it is more involved than direct PCR primer fluorescent labeling, especially for the analysis of a small number of DNA samples (*i.e.*, without the aid of sample preparation robots). An alternative approach, recently described by Nishimura and Tsuhako [10], involves use of the intercalating dye YO-PRO-1, which was added to the DNA separation matrix and used for fluorescence detection of unlabeled SSCP conformers of the *N-ras* oncogene. The authors tested a variety of other intercalating dyes, none of which resulted in successful mutation detection. They also optimized the YO-PRO-1 concentration (optimum 0.2 μM) and observed that high concentrations of YO-PRO-1 led to decreased resolution, which was attributed to "disruption of higher-order structure of the ssDNAs [10]." Similarly, Zhang *et al.* [11] successfully utilized thiazole orange, another intercalating dye, for SSCP mutation detection in the *K-ras* gene.

The need for post-PCR purification is not well documented for CE-SSCP. Crude PCR samples contain a multitude of charged species including salt, unincorporated fluorescently labeled primers, excess dNTPs, and enzymes that reduce the efficiency of electrokinetic injection, which is the preferred way to introduce DNA samples into the capillary. More importantly, however, unincorporated primers can anneal to SSCP conformers to form primer-ssDNA constructs during denaturing and cooling prior to CE. The electrophoretic mobilities of these ssDNA-primer constructs can be very similar to those of SSCP conformers, and can complicate peak assignments [12].

Partial purification of crude PCR products by use of a Microcon-PCR (Millipore, Bedford, MA, USA) filtration device or QIAquick PCR Purification Kit (Qiagen, Valencia, CA, USA) reduces the amount of primer-ssDNA constructs [6, 13], while complete purification of crude PCR samples by preparative slab-gel electrophoresis can eliminate them entirely [14]. If additional PCR product purification is undesired or impossible, a similar but less pronounced beneficial reduction in primer-ssDNA annealing can be achieved by a mere decrease in initial primer concentration during PCR amplification [14]. Debernardi *et al.* [15] suggested an unconventional approach for pre-electrophoretic sample purification, in which they used biotinylated primers to perform PCR amplifications. Following the PCR amplifications, the resulting biotinylated DNA amplicons were purified from the buffer, salts, dNTPs, and primers with Dynabeads (M-280 Streptavidin; Dynal Biotech, Lake Success, NY, USA) and used for CE-SSCP with UV detection.

Fluorescent labeling of both the forward and reverse DNA strands offers several advantages over labeling of just one DNA strand, and requires little extra effort and moderate additional cost [16]. Notably, it increases the chances of mutation detection, as evidenced by many studies [17–19]. Two-color fluorescent labeling, in which the forward DNA strands are labeled with one type of dye and the reverse DNA strands with another type of dye, is superior to one-color fluorescent labeling in which only one dye is used. Not only does it allow for a straightforward identification of the peaks representing the forward and reverse ssDNA strands, but it also provides the means to differentiate between ssDNA and dsDNA species, including primer-ssDNA constructs, as described below [14, 18, 20].

We have observed that in two-color detection mode (forward strand – FAM, reverse strand – JOE), dsDNA exhibits two perfectly overlapping signals of two different colors in CE-SSCP electropherograms, while ssDNA shows only one major peak, of one color (often accompanied by a minor peak of the second color, Fig. 2) [14]. The minor peak, which can be attributed to minor overlap of the emission spectra of the two dyes, is centered in the same region as the major peak, but is of much lower intensity. We have used this feature to precisely and unambiguously assign all the peaks in electropherograms of 32 mutant DNA samples of the *p53* gene analyzed by combined CE-SSCP/heteroduplex analysis (HA) [20]. On the other hand, when a one-color detection mode (both strands – FAM) is employed, differentiation between SSCP conformers and ssDNA-primer constructs is virtually impossible, because the peaks look very similar in the two cases and have similar electrophoretic mobilities.

Attaching fluorescent dyes to DNA can lead to certain complications such as changes in DNA electrophoretic mobility due to the charge, hydrophobicity, or steric bulk of the dye [21]. If wild-type and mutant DNA are mixed and analyzed simultaneously, this complication can be addressed in a practical manner by labeling of the two corresponding ssDNA strands with the same dye (*i.e.*, both forward strands – FAM; both reverse strands – JOE), to cancel out or at least minimize these effects. Little is known about whether the nature of the dye affects folding of ssDNA during the formation of SSCP conformers, but it is very likely that it may have some effect. For the reasons of differences in mobility based on differences in dye structure, we do not recommend the use of four different dyes (*i.e.*, the use of different labels on each of the mutant and wild-type forward and reverse strands).

2.2 Additives and thermal treatment of samples

Denaturing agents, such as formamide, are commonly used to dilute CE-SSCP DNA samples prior to thermal denaturation. To our knowledge, there are no published

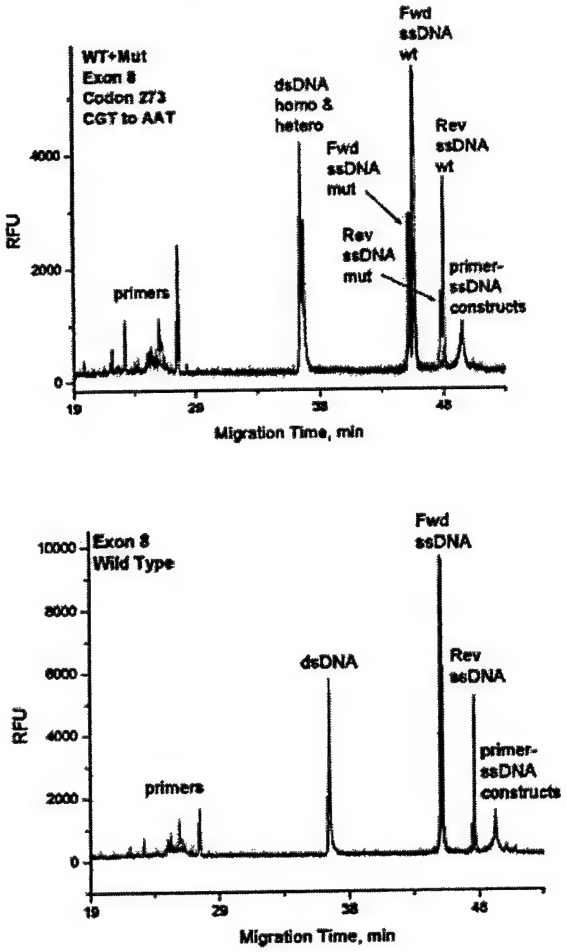

Figure 2. An example of genetic screening of a mutant DNA sample derived from the *p53* exon 8 (200 bp) by tandem capillary electrophoresis SSCP/HA using DNA samples prepared according to optimized protocols [20]. MegaBACE™ CAE instrument; total capillary array length 64 cm; effective capillary array length 40 cm; capillary inner diameter 75 μm; bare fused-silica dynamically coated with poly-*N*-hydroxyethyl acrylamide (polyDuramide™), LPA DNA separation matrices (6% w/v M_w 600 kDa); pre-electrophoresis 5 min at 140 V/cm; injection 230 V/cm for 25 s; electrophoresis at 180 V/cm at 27°C with an associated current of 10–12 μA.

reports that explain the reason for the adoption of this approach. However, in a related study, Casey and Davidson [22] investigated the melting of dsDNA and found that formamide simultaneously decreased the melting temperature (T_m) of the samples and improved the chances for complete denaturation. Elsewhere it was reported that high formamide concentrations (*i.e.*, 95%) depressed the T_m of dsDNA by as much as 60°C [23]. Therefore, we suppose that formamide has been added to SSCP samples prior to denaturation in order to ensure the completeness of initial DNA strand dissociation and unfolding.

Interestingly, Yip *et al.* [24] have added denaturants (formamide or urea) to the running buffer in slab-gel SSCP to "sharpen the bands of ssDNA fragments and clear the background that might otherwise obscure the bands that are diagnostic of a polymorphism," and cited other studies that have used these and other additives (*i.e.*, SDS or PEG) for the same purpose. To explain this approach, the authors suggested that a mildly denaturing environment in the gel created by formamide reduced the number of different SSCP conformers and thus cleared up the smearing of DNA bands. Another potent denaturant, methylmercuric hydroxide (CH_3HgOH), was used by Weghorst and Buzard [25] to improve the crispness of DNA bands by facilitating sample denaturing and preventing the formation of partially annealed conformations that might be confused with true SSCPs. Sodium hydroxide is another chemical that is commonly added in a small amount to the DNA solution prior to denaturation, presumably to assist DNA denaturation by increasing pH. One report suggested that NaOH did not improve DNA denaturation, but did affect the mobility of SSCP conformers [18]. Clearly, the pH and ionic strength of the sample solution are both strongly affected by the addition of NaOH. However, another report has shown that high pH (11–12) can be used to fully denature DNA for sequencing [26].

Salt concentration in the sample is another variable that can have a significant impact on the outcome of CE-SSCP analysis. Prior to electrophoresis, PCR products are usually diluted 10–100 X in aqueous buffer or formamide to prevent fluorescence detector saturation and to conserve the sample, a process that affects the final salt concentration present in the sample. Although concentrations of > 50 mM NaCl (or KCl) are generally used for the determination of T_m of dsDNA to ensure correct nucleotide base pairing, no strict guidelines exist for salt content in samples to be analyzed by CE-SSCP, as required to effect partial nucleotide base pairing. An increase in salt concentration from 20–50 to 100 mM is reported to raise the T_m of dsDNA by 5–10°C, showing an opposite trend to formamide effects on the T_m and potentially complicating dsDNA denaturation [23]. At the same time, high salt concentrations will definitely decrease the amount of sample injected into a capillary electrokinetically, and thus can hamper mutation detection by decreasing the signal-to-noise ratio in the analysis.

We have recently optimized sample preparation methods for combined CE-SSCP/HA for PCR products amplified from the *p53* gene, and determined that no formamide or

extra salt are required if a PCR product is diluted 20–40 X with 1 X Tris-HCl buffer (pH 8.5) [14]. We also observed that snap-cooling the sample on ice reduced the percentage of primer-ssDNA constructs in the final mixture, in comparison to the distribution obtained when one allows the denatured dsDNA sample to cool at ambient temperature. Although addition of formamide may be helpful for the accomplishment of full, initial denaturation of DNA samples with high GC content, at this point, we consider its use in routine CE-SSCP to be unnecessary.

2.3 DNA size and sequence

About a dozen different genes have been analyzed by CE-SSCP, of which *p53*, ras, BRCA1, and BRCA2 have received the most attention. It is definitely easier to detect mutations in some gene regions than others, perhaps reflecting the impact of DNA sequence on chain folding. Many CE-SSCP researchers have concluded that as DNA fragment length increases, the sensitivity of mutation detection by CE-SSCP decreases [6]. While the optimal DNA size for SSCP analysis is believed to be in the range of 175–400 bp, even longer DNA fragments (503–650 bp [27]; 740 bp [9]; 1223 bp [28]) have been analyzed for mutations with reported success. At the other extreme, Arakawa *et al.* [8] have reported CE-SSCP analysis of DNA fragments as short as 71 bp.

The GC content of the DNA sequence also seems to have some impact on how easy it is to detect mutations by CE-SSCP. Nataraj *et al.* [29] reported that they had better mutation detection sensitivity for fragments with high GC content (~60%) than for fragments with lower GC content (~40%), under the same conditions of the analysis. Presumably, the greater number of G-C base pairs provides SSCP conformers of greater average stability. Although one might expect that the sensitivity of CE-SSCP mutation detection should be lower for sequence alterations located near the ends of DNA fragments (as in the case for HA), in at least one study no such correlation was observed [28].

2.4 Temperature, buffer composition and pH

These three variables have been discussed thoroughly by Ren [6] in his recent review. Herein, we would like to reiterate that the optimum temperature and pH conditions for sensitive mutation detection seem to be highly sequence-specific, and probably cannot be determined *a priori* because of the absence of a first-principles understanding and prediction of three-dimensional SSCP structures due to the idiosyncratic nature of DNA folding. Ellis *et al.* [21] attempted to model SSCP folding using the program Mfold, but the results were not consistent enough to be applied. While analysis temperatures between 20 and 30°C typically are recommended as a starting point in temperature optimization for attempts to analyze novel DNA fragments by SSCP, one needs to keep in mind that lower or higher temperatures may in fact provide more sensitive analysis. Tris-borate-EDTA (TBE) running buffer that contains 10% glycerol remains the top choice in most CE-SSCP protocols, but other buffers such as Tris-HEPES and Tris-MES-EDTA have also been used successfully [13]. Gelfi *et al.* [30] evaluated the combined effects of temperature, sieving matrix, applied voltage, capillary length, capillary inner diameter, and pH on CE-SSCP, and noted a significant improvement in the resolution and sensitivity of CE-SSCP when a low-pH buffer (Tris-MES-EDTA, pH 6.8) was used; at the same time, no beneficial changes were recorded when the temperature of analysis was lowered.

2.5 DNA separation matrices

In CE, the "sieving" of DNA is accomplished with fluid solutions of highly entangled, water-soluble polymers. These entangled polymers form a dynamic mesh of obstacles through which the SSCP conformers must negotiate or force a path. To engender differences in electrophoretic mobility for these small, folded DNA strands, which differ only in their shape, requires a relatively dense polymer solution. Normally, for the high-resolution separation of any distinct class of DNA samples (oligonucleotides, dsDNA fragments, DNA sequencing fragments), the polymer matrix must be optimized with respect to the chemical nature of the polymer, physical nature of the polymer (polymer molar mass distribution), and polymer concentration in the buffer.

The same is, of course, true for SSCP conformers; it is not yet clear what the true optimum matrix for CE-SSCP will be, as significant work remains to be done in this area. As described in several studies and summarized in the recent review by Ren [6], a number of different polymers such as hydroxyethylcellulose (HEC), polyvinylpyrrolidone (PVP), methylcellulose (MC), POP™ from ABI and linear polyacrylamide (LPA) have been applied to CE-SSCP analysis, with varying degrees of success. A related novel copolymer, LPA-polydimethylacrylamide (PDMA) was recently shown by Ren and Fang [31] to have good potential for use in CE-SSCP, but has yet to be optimized with respect to polymer molar mass and concentration. The stated advantage of LPA-PDMA is that it combines the excellent sieving ability of LPA with the intrinsic capillary-coating properties of PDMA, and hence allows for SSCP analysis in uncoated capillaries. These studies shed some light on the chemical compositions suitable

for polymers employed in CE-SSCP. However, there is a relative paucity of studies aimed at investigating the influence of the physical nature of the polymers (average molar mass (M_w), persistence length in aqueous solution, and polydispersity) on CE-SSCP performance. Previously, Barron *et al.* [32] showed for hydroxypropylcellulose (HPC) polymers that a minimum M_w of 300 kDa is required for the decent separation of dsDNA larger that 1 kbp, and also determined that "stiff" polymers such as HEC can be used in more dilute solutions than HPC or LPA to afford similar DNA separation ability. SSCP conformers are much more compact, and hence more challenging to separate than dsDNA fragments. Therefore, it is likely that adjusting the physical nature of the polymer that acts as a CE-SSCP matrix will also have significant impact on its separating ability and optimum useful concentration. To our knowledge, there is only one study that has touched upon this subject. Ren *et al.* [33] demonstrated that homemade, short-chain LPA could be used for SSCP detection of single point mutations in a number of genes, and yielded DNA separation matrices that also were relatively easy to load into the capillary because of their low viscosity. No exact information on the LPA molecular weight, or the effects of M_w on CE resolution, were provided.

This present lack of published information on the impact of polymer physical characteristics on CE-SSCP separation is most likely due to the general absence of the means and/or the desire among the majority of CE-SSCP researchers to synthesize and precisely characterize polymeric materials suitable for CE. Most of the aforementioned polymers used in CE-SSCP (HEC, HPC, MC) are modified natural products, and are only available in certain molecular weight ranges, which also vary substantially from batch to batch. Therefore, these natural polymers are unsuitable for precise and reliable studies of the effects of M_w on the sensitivity of mutation detection by CE methods.

In the absence of a large choice of polymers, some efforts have been directed at optimizing polymer concentrations, primarily POP™, in the DNA separation matrix. POP™ is a polymer of undisclosed chemical nature and molecular weight, which has been commercially available as a DNA separation matrix (dissolved form) only from Applied Biosystems for a number of years. Not surprisingly, most of these studies found that higher POP™ polymer concentrations (up to 5%, the maximum (stock) concentration), which were increasingly difficult to use because of the increased viscosity of the polymer solutions, yielded better results [9, 17, 18]. In addition to POP™, a few other polymers have also been briefly investigated for CE-SSCP, and followed the same trend of the dependency of their separation ability on concentration. For instance, Nishimura and Tsuhako [10] reported that an optimal MC concentration was 1%, while matrices with MC concentration < 0.7% afforded no resolution and those with MC concentration > 1.2% were too viscous to load into the capillary. Ren *et al.* [34] studied 2–6% LPA solutions as SSCP separation matrices and reported that 6% provided the best resolution.

Recently, we have conducted what we believe is the first systematic study of the impact of the molecular weight of LPA on CE-SSCP analysis using a high-throughput MegaBACE™ (Molecular Dynamics, Sunnyvale, CA, USA) capillary array electrophoresis (CAE) instrument [20]. In our study, we simultaneously varied the concentration (2, 4, 6% w/v) and M_w (200, 600, 1000 kDa, and 2400 kDa) of LPA, and applied a combined CE-SSCP/HA analysis to more than a dozen different mutant DNA samples derived from exons 7 and 8 of the *p53* gene (size 139–300 bp). The optimum DNA separation matrix for these samples was determined to be 6% w/v of 600 kDa LPA. LPA of lower molar mass (200 kDa) did not provide adequate SSCP resolution at any concentration, while the use of a higher molar mass (2400 kDa) polymer did not offer any advantage over the optimum M_w, and furthermore complicated capillary loading due to high viscosity of its solutions (Fig. 3). Use of the M_w 2400 kDa polymer matrix also led to significantly longer analysis times (1 h *vs.* 20–30 min for lower-M_w polymers). We plan to extend this study to longer DNA fragments and to other polymer compositions (*i.e.*, more hydrophobic PDMA) in an attempt to establish the generality of the results cited above, and to formulate a universal SSCP separation matrix (*i.e.*, mixtures of high and low M_w versions of the same polymer or, perhaps, polymers of different chemical compositions) that will allow for a high sensitivity of SSCP detection without case-by-case fine-tuning of other variables, most importantly, the temperature of analysis.

2.6 Capillary coating

Another greatly understudied CE-SSCP variable is the nature of the polymer coating applied to the inner walls of a capillary, which is aimed at greatly reducing the velocity of electroosmotic flow and minimizing the adsorption of the analytes to the capillary wall. While a detailed description of capillary wall coatings is beyond the scope of this review, we would like to stress that the presence of a stable coating with the proper chemistry has the utmost impact on the sensitivity of CE-SSCP mutation detection, in our experience. One particularly relevant study came from Tian *et al.*, [35], in which the authors emphasized that the efficacy of CE-HA, a genetic screening method closely related to CE-SSCP, was dependent on both the

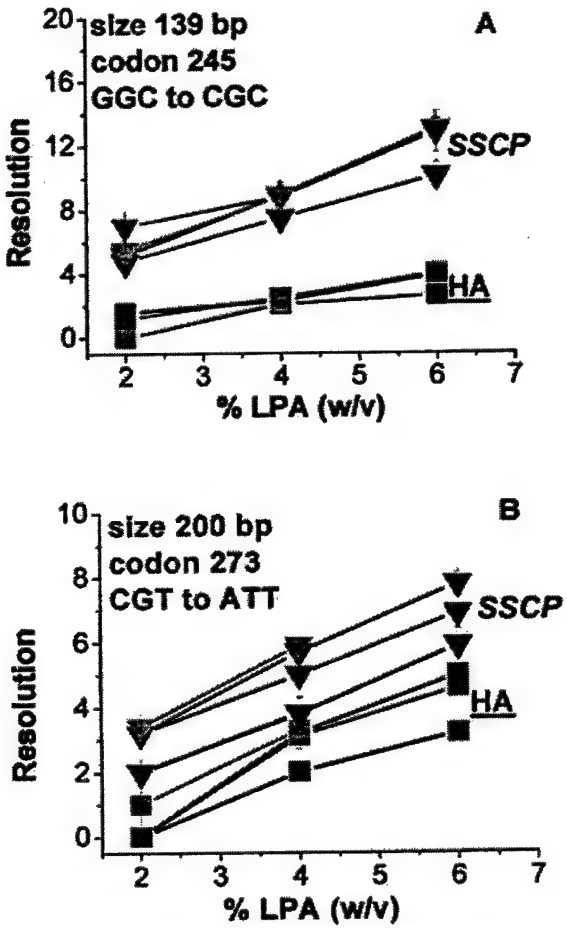

Figure 3. Combined impact of LPA M_w and matrix concentration on the resolution of capillary CE-SSCP and HA samples derived from (A) exon 7 and (B) 8 of the *p53* gene, performed in (--▼---■--) LPA M_w 200 kDa; (--▼---■--) LPA M_w 600 kDa; (--▼---■--) LPA M_w 1 kDa; (--▼---■--) LPA M_w 2.4 MDa. ▼, SSCP samples; ■, HA samples [20]. Conditions as in Fig. 2.

effective passivation of the capillary surface and on the choice of the correct polymer matrix for sieving. The authors tested a variety of silanizing reagents, polymer coatings, and DNA separation matrices for the analysis of fragments of the BRCA1 gene (DNA size *ca.* 200 bp) and found that the optimum performance for CE-HA was achieved when chlorodimethyloctasilane, PVP, and HEC were used in combination as the silanizing reagent, protective wall coating, and separation matrix, respectively (Fig. 4).

In a recent study, we have noticed that, under otherwise identical conditions, bare fused-silica capillaries dynamically coated with polyDuramide™, a novel adsorptive polymer jointly developed by BioWhittaker Molecular Applications (Walkersville, MD, USA) and our laboratory, provides much better CE-SSCP resolution than commercial capillary arrays covalently coated with LPA [20]. Interestingly, the same LPA-coated capillaries continued to provide high-quality DNA sequencing data while failing for SSCP, suggesting that the nature of folded ssDNA conformers and/or the CE conditions for SSCP place more stringent demands on the quality of the protective capillary wall coating. In particular, the absence of urea during SSCP separations may increase the tendency for analyte adsorption on the wall, which can lead to band-broadening and hence loss of peak resolution.

It is noteworthy that the pH of the buffer has a pronounced impact on the stability of some capillary wall coatings. For example, Ren *et al.* [34] showed that at pH 8.3 a dynamically applied dimethylacrylamide coating deteriorated faster than at pH 7.8. Similarly, we have noted that an LPA coating covalently bound to silica degrades rapidly during CE-SSCP analysis (*vide supra*) and compromises the sensitivity of mutation detection. This suggests a possibility that the apparent improvements in CE-SSCP sensitivity of mutation detection in low pH buffers may be at least partially due to the higher stability of protective capillary wall coatings at low pH.

3 The outlook for routine use of CE-SSCP for genetic screening

3.1 Sensitivity and specificity

For clinical genetic screening, it is essential to know the frequency of the incidents of false positives (specificity = 100 – frequency of false positives) and of false negatives (sensitivity = 100 – frequency of false negatives) of mutation detection in CE-SSCP. Both the specificity and the sensitivity of CE-SSCP mutation detection need to be at least 97%; lower sensitivity would impair confident mutation detection, while a lower specificity would unnecessarily disturb too great a number of patients.

The sensitivity of CE-SSCP has been anecdotally evaluated in several different studies, and is reputed to approach 100% if more than one experimental condition is employed [36–39]. However, the specificity of CE-SSCP has been much less investigated. According to some studies, SSCP analysis has produced no false positives [21, 37]. In another study, O'Connell *et al.* [36] analyzed 15 samples and identified 3 false positives. Elsewhere, Liechti-Gallati *et al.* [39] confirmed that some false positives resulted from the annealing of primers to SSCP conformers, and the consequent production of spurious peaks. The presence of these constructs led to the identi-

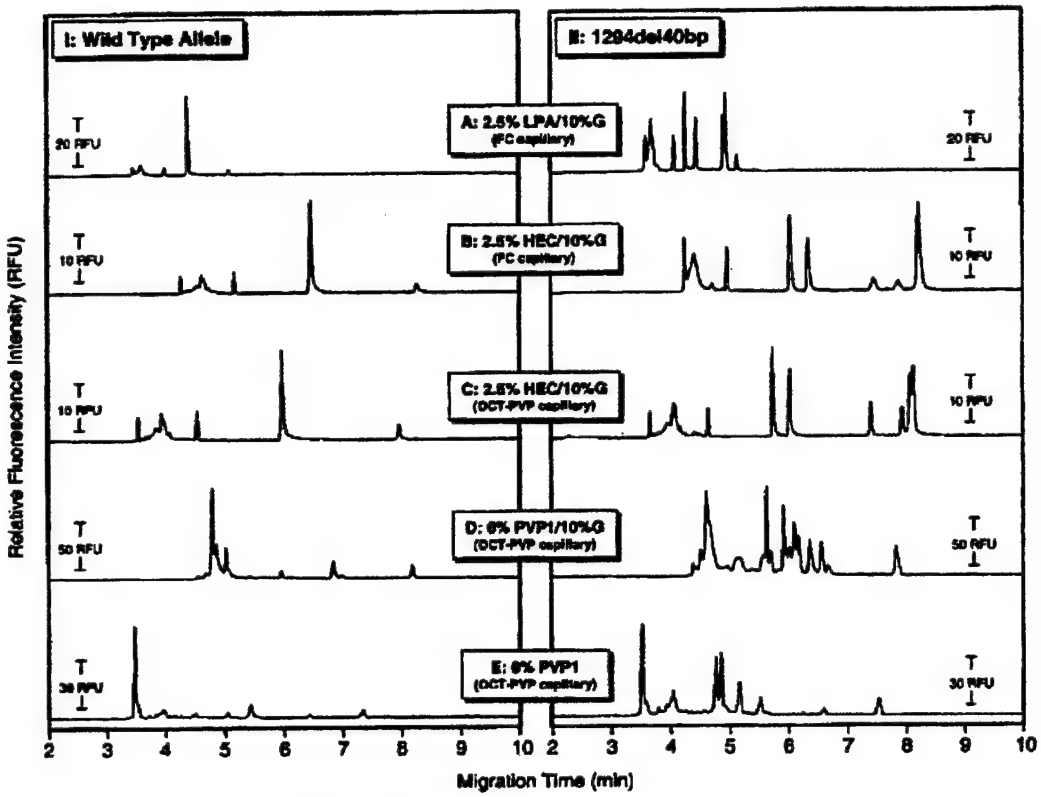

Figure 4. Comparison of different capillary wall coatings and separation matrices for CE based heteroduplex analysis. Reprinted from [35], with permission.

fication of some of the wild-type samples as mutants. While Ru *et al.* [37] concluded from their results that false positives should be more common in slab-gel SSCP than in CE-SSCP, Hayashi [12] stated in a recent review that false positives are unavoidable in genetic mutation detection in general since PCR products (which can be contaminated and/or imperfectly amplified by the enzymes) are used as starting materials for analysis.

Very few blinded studies, which can statistically assess the frequencies of false positives and false negatives, have been done in CE-SSCP. Notably, Wenz *et al.* [40] conducted two blind CE-SSCP studies. In the first study, 20 DNA samples containing two common mutations implicated in hereditary hemochromatosis were screened, and the results were in accord with those generated by restriction fragment length polymorphism (with 100% sensitivity). In the second study, ten *p53* gene exon 7 samples were analyzed by CE-SSCP against four reference samples, and again CE-SSCP correctly assigned the mutation status with 100% sensitivity [17]. Inazuka *et al.* [9] reasoned that the use of sophisticated computer software to assign the DNA mutation status should eliminate the need for blind studies. However, as long as a human factor is involved, blind studies are required for clinical assay validations regardless of the tools used for the data analysis.

The sensitivity of mutation detection by CE-SSCP and, as a matter of fact, most other mutation screening methodologies, is evaluated against and therefore cannot be better than the sensitivity of direct Sanger dideoxynucleotide sequencing (considered to be the "gold standard") in detecting sequence alterations. However, the latter method is not infallible either. For instance, Ahrendt *et al.* [41] used direct DNA sequencing to analyze a conserved region of the *p53* gene by slab-gel with automated fluorescence detection and detected only 76% of the mutations present (no information on number of repeat analyses is given). On the other hand, using the *p53* GeneChip™ hybridization assay, the authors detected 46 of 53 missense mutations (88% sensitivity) but none of the 5 frameshift mutations analyzed (0% sensitivity). Since even direct Sanger DNA sequencing or hybridization analysis does not give 100% sensitivity from a single analysis, it is important to ensure that sequencing of both the

forward and reverse DNA strands is done, with a sufficient number of repeats (3–5), to provide an accurate assessment of the genetic mutation methodologies to be tested.

Perhaps the best way to improve the sensitivity of an indirect mutation detection method such as CE-SSCP is to combine it with HA [39]. Similarly to SSCP, HA is based on the premise that dsDNA consisting of perfectly complementary strands (homoduplexes), will oftentimes exhibit different (usually higher) electrophoretic mobilities than "imperfect" DNA duplexes that contain nucleotide base mismatches (heteroduplexes). HA is reputed to be more useful for the detection of deletion and insertion mutations than for single-base substitutions, most of which typically remain undetected, especially in a slab-gel electrophoresis format [29, 42–44]. Typically, DNA samples being prepared for SSCP analysis are denatured at 95°C and cooled rapidly, while those destined for HA are denatured and cooled slowly over a period of 30–60 min to ensure complete dsDNA re-annealing. Combined SSCP/HA can be conducted by separately preparing SSCP and HA samples and analyzing them either simultaneously, or in a sequential fashion [39, 45, 46]. Recently, Ravnick-Glavač *et al.* [47] observed in their slab-gel electrophoresis experiments that SSCP/HA conformers suitable for tandem analysis can be generated simultaneously in the same vessel by utilizing the SSCP cooling protocols. Previously, doubts remained about whether the kinetics of annealing during fast cooling might yield incompletely re-annealed duplexes, that could result in false positives [48]. In the more recent study, Kozlowski and Krzyzosiak [27] for the first time demonstrated the possibility and utility of combined SSCP/HA in CE. In the latest development, we have investigated the effects of DNA sample preparation protocols and the physical nature of the DNA separation matrix on the resolution and sensitivity of combined CE-SSCP/HA performed in high-throughput CAE mode [14, 20].

In terms of sensitivity, Axton *et al.* [49] have reported that combined slab-gel SSCP/HA was able to detect 12 out of 12 (100%) mutations in the PAX6 gene, five of which were deletions and insertions and the rest single-base substitutions. Slab-gel SSCP alone correctly identified 10 out of 12 mutations; the remaining two undetected mutations (one deletion, one insertion) were identified by HA. It was unclear from the report what were the sizes of the analyzed DNA fragments. Ravnick-Glavač *et al.* [47] applied combined slab-gel SSCP/HA to the analysis of 27 mutated specimens of the CFTR gene (size 309–579) and were also able to achieve 100% sensitivity. Two mutations (one deletion, one insertion), which were indistinguishable by SSCP, showed different HA patterns. The authors again emphasized the need for the use of multiple running conditions for the most sensitive mutation detection, but identified a single gel condition (10% acrylamide/1.3% C; 10% glycerol) that produced a reasonably high sensitivity.

Recently, Kozlowski and Krzyzosiak [27] analyzed 31 mutant DNA samples of BRCA1 and BRCA2 (size 200–500 bp), most of which were single-base substitutions, by combined CE-SSCP/HA, and reported 100% sensitivity. For comparison, CE-SSCP alone detected 28 out of 31 mutations (~90%), and CE-HA alone detected 25 out of 31 (~80%) mutations. As expected, HA in CE mode was much more capable of detecting single-base substitutions than in a slab-gel electrophoresis mode. Interestingly, the authors reported two mutations in the BRCA1 gene (4427T/C and 3667 A/C) that actually showed two peaks in HA, one of which was assigned to two overlapping heteroduplexes and one homoduplex and the other of which was attributed to the second homoduplex. Thus, in these cases the presence of the mutation could be detected by the difference in electrophoretic mobilities of the two homoduplexes. Based on this observation, the authors argued that the correct name for the analysis should be SSCP/duplex analysis (DA) and not SSCP/heteroduplex analysis.

A potential problem with the use of SSCP for long-range genetic screening is the high occurrence of single nucleotide polymorphisms (SNPs) in the human genome (*ca.* 1 in 1000 bases in coding regions), which increases the probability of an SNP occurring in a large fragment of DNA that might be analyzed. Orban *et al.* [50] observed that SNPs masked detection of some mutants of BRCA1 and BRCA2 in slab-gel electrophoresis SSCP. However, Larsen *et al.* [45] have suggested that the high repeatability of SSCP, when run under the proper conditions, could be used to generate mutation and SNP "fingerprint" databases against which samples could be referenced. More studies need to be conducted to determine the extent of SNP effects on mutation detection. Notably, CE-SSCP has also been used for SNP detection [51, 52].

3.2 Throughput

Multiplexing, which involves the screening of a large number of DNA samples simultaneously, is desirable for clinical applications because of its higher throughput. Using multicapillary CE instruments equipped with multicolor laser-induced fluorescence detectors (*i.e.* the 4-color Applied Biosystems 3100™ or 3700™, or the MegaBACE™ CAE instrument), and labeling DNA with four different dyes instead of just two can further increase the throughput. In practice, Walz *et al.* [53] reported the ability to detect mutations in "seven pairs of exons" at the same time by multiplexing, without any loss of their SSCP-detection ability in

CE. However, Larsen *et al.* [45] in their study of the LQTS gene by combined CE-SSCP/HA cautioned that multiplexing might lead to decreased sensitivity of the analysis, due to the large number of DNA bands present, some of which may mask abnormal conformers. Optimization of the size of the DNA fragments analyzed by SSCP, as well as the use of high-resolution CE methods, can at least partially alleviate this problem [38, 54]. Another problem in multiplexing is that various rates of PCR amplification for different templates may result in unequal amounts of PCR end-products, which can lead to selective "drop-out" or overloading of some SSCP species relative to others [38].

3.3 Direct mutation detection

Generally, CE-SSCP is classified as an indirect mutation detection method that is capable of documenting the absence or presence of mutations only, but that cannot determine their position or nature. However, several reports have suggested that SSCP profiles are highly mutant-specific. For instance, years ago, Ravnik-Glavač *et al.* [47] observed that their samples gave distinct patterns in slab-gel electrophoresis that were "directly recognizable". In the previously mentioned study on the *p53* gene, Wenz *et al.* [17] screened ten unknown mutants against a panel of four reference mutants. Based on electrophoretic peak patterns, six samples were identified as having reference mutations, two were identified as having wild-type status, and two were shown to possess non-reference mutations. Characteristic SSCP/HA peak patterns could probably be determined for all of the "hot-spot" mutants of the *p53* gene, to facilitate the efficiency of analysis. Larsen *et al.* [28] reported that according to their CE-SSCP analyses, each of 34 mutant DNA samples of the KVLQT1, HERG, and MYH7 genes possessed its own distinct SSCP pattern, and that each allele could be identified without subsequent DNA sequencing [28].

Several studies have addressed the issue of the high reproducibility of CE-SSCP that would be required for reliable DNA fingerprinting. For instance, Ellis *et al.* [21] noted that they had less than 0.02% standard deviation of peak migration times during multiple runs of their control [21]. Nishimura *et al.* [10] observed a relative standard deviation of 0.5% for the migration time and mobility of each peak for 9 repeat injections. Wenz *et al.* [17] found that their relative standard deviation was 0.01–0.05% for multiple injections of the same sample. Atha *et al.* [55] reported that standard deviations of the mobility of the sense and antisense DNA strands of the *p53* gene samples were 2.1 scans (0.47 s) and 0.79 scans (0.18 s). Hence, even though SSCP may not have a general reputation for high precision and reproducibility, these recent capillary-based studies would suggest that it deserves one.

4 Conclusions

In conclusion, we would like to cite B. Vogelstein [56], a well-known cancer researcher at John Hopkins University, who pointed out in a recent publication in *Science* that "Genetic testing in the future will no doubt involve a combination of methods designed to fit the mutation spectrum of specific patients and genes. ... The best diagnostic medical tests have sensitivities and specificities approaching 100%, and it is not overly optimistic to expect that genetic testing will meet such exacting standards in the future". CE-SSCP, either alone or in combination with HA, may provide a cost-effective alternative for cases in which the sole purpose of analysis is to determine the presence or absence of a mutation to reduce the total frequency and cost of using direct mutation detection methodologies, which provide information on the precise nature of the mutation. In the latter case, DNA specimens can be efficiently prescreened by CE-SSCP/HA to identify mutant DNA specimens, which may then be analyzed by DNA sequencing, DNA hybridization arrays, or any other suitable direct technique.

Given the generally much higher cost of methods for direct mutation detection in comparison to CE-SSCP/HA, and the fact that only a relatively small percentage of patient samples may possess mutations (*i.e., ca.* 25% for the *p53* gene in breast cancer patients) CE-SSCP/HA can be used as a complementary method that will provide cancer researchers with significant cost and efficiency benefits. Further progress in the development of optimal materials and methods for CE-SSCP/HA analysis, as well as the implementation of these technologies on large sets of real patient samples to quantitate sensitivity and specificity for different genes of medical importance, will facilitate the transition of this technology into the clinical environment. Such routine application of low-cost genotyping technologies promises to make a substantial positive impact on human health in the new millennium.

Received December 17, 2001

5 References

[1] Gitzelman, R., *Hum. Genet. B: Med. Aspects* 1982, *84*, 425–436.
[2] van Ommen, G. J., Bakker, E., den Dunnen, J. T., *Lancet* 1999, *354*, SI5.
[3] Orita, M., Suzuki, Y., Sekiya, T., Hayashi, K., *Genomics* 1989, *5*, 874–879.
[4] Beale, S. C., *Anal. Chem.* 1998, *70*, 279R-300R.
[5] Haleem, I. J., *Electrophoresis* 2000, *21*, 1921–1939.
[6] Ren, J., *J. Chromatogr. B* 2000, *741*, 115–128.
[7] Oto, M., *Methods Mol. Med.* 1999, *27*, 127–138.

[8] Arakawa, H., Tsuji, A., Maeda, M., Kamahori, M., Kambara, H., *J. Pharm. Biomed. Anal.* 1997, *15*, 1537–1544.

[9] Inazuka, M., Wenz, H. M., Sakabe, M., Tahira, T., Hayashi, K., *Genome Methods* 1997, *7*, 1094–1103.

[10] Nishimura, A., Tsuhako, M., *Chem. Pharm. Bull.* 2000, *48*, 774–778.

[11] Zhang, Z., Wu, Y., Cheng, W., Wu, R., *Clin. Chim. Acta* 2000, *301*, 205–211.

[12] Hayashi, K., *Genet. Anal.* 1999, *14*, 193–196.

[13] Ren, J., Ueland, P. M., *Hum. Mutat.* 1999, *13*, 458–463.

[14] Kourkine, I. V., Hestekin, C. N., Magnusdottir, S. O., Barron, A. E., *BioTechniques* 2002, in press.

[15] Debernardi, S., Luzzana, M., De Bellis, G., *Frontiers Biosci.* 1996, *1*, c1–3.

[16] Merkelbach-Bruse, S., Kose, S., Losen, I., Bosserhoff, A. K., Buettner, R., *Combin. Chem. High Throughput Screen.* 2000, *3*, 519–524.

[17] Wenz, H. M., Ramachandra, S., O'Connell, C. D., Atha, D., *Mutat. Res. Genom.* 1998, *382*, 121–132.

[18] Ghozzi, R., Morand, P., Ferroni, A., Beretti, J. L., Bingen, E., Segonds, C., Husson, M.-D., Izard, D., Berche, P., Gaillard, J., *J. Clin. Microbiol.* 1999, *37*, 3374–3379.

[19] Cooksey, R. C., Morlock, G. P., Holloway, B. P., Mazurek, G. H., Abaddi, S., Jackson, L. K., Buzard, G. S., Crawford, J. T., *Mol. Diagn.* 1998, *3*, 73–80.

[20] Kourkine, I. V., Hestekin, C. N., Buchholz, B., Barron, A. E., *Anal. Chem.* 2002, in press.

[21] Ellis, L. A., Taylor, C. F., Taylor, G., *Hum. Mutat.* 2000, *15*, 556–564.

[22] Casey, J., Davidson, N., *Nucleic Acids Res.* 1977, *4*, 1539–1552.

[23] Bonner, G., Klibanov, A. M., *Biotech. Bioeng.* 2000, *68*, 339–344.

[24] Yip, S. P., Hopkinson, D. A., Whitehouse, D., *BioTechniques* 1999, *27*, 20–24.

[25] Weghorst, C. M., Buzard, G. S., *BioTechniques* 1993, *15*, 395–400.

[26] Mala, Z., Kleparnik, K., Boček, P., *J. Chromatogr. A* 1999, *853*, 371–379.

[27] Kozlowski, P., Krzyzosiak, W. J., *Nucleic Acids Res.* 2001, *29*, e71.

[28] Larsen, L. A., Christiansen, M., Vuust, J., Andersen, P. S., *Hum. Mutat.* 1999, *13*, 318–327.

[29] Nataraj, A. J., Olivos-Glander, I., Kusukawa, N., Highsmith, W. E., Jr., *Electrophoresis* 1999, *20*, 1177–1185.

[30] Gelfi, C., Vigano, A., Curcio, M., Righetti, P. G., Righetti, S. C., Corna, E., Zunino, F., *Electrophoresis* 2000, *21*, 785–791.

[31] Ren, J., Fang, Z., *Chin. Chem. Lett.* 2000, *11*, 1015–1018.

[32] Barron, A. E., Sunada, W. M., Blanch, H. W., *Electrophoresis* 1996, *17*, 744–757.

[33] Ren, J., Ulvik, A., Refsum, H., Ueland, P. M., *Anal. Biochem.* 1999, *276*, 188–194.

[34] Ren, J., Ulvik, A., Ueland, P. M., Refsum, H., *Anal. Biochem.* 1997, *245*, 79–84.

[35] Tian, H., Brody, L. C., Mao, D., Landers, J. P., *Anal. Chem.* 2000, *72*, 5483–5492.

[36] O'Connell, C. D., Atha, D. H., Oldenburg, M., Tian, J., Siebert, M., Handrow, R., Grooms, K., Heisler, L., de Arruda, M., *Electrophoresis* 1999, *20*, 1211–1223.

[37] Ru, Q. H., Jing, H., Luo, G.-A., Huang, Q., *J. Chromatogr. A* 2000, *894*, 171–177.

[38] Larsen, L. A., Christiansen, M., Vuust, J., Andersen, P., *Combin. Chem. High Throughput Screen.* 2000, *3*, 393–409.

[39] Liechti-Gallati, S., Schneider, V., Neeser, D., Kraemer, R., *Eur. J. Hum. Genet.* 1999, *7*, 590–598.

[40] Wenz, H. M., Baumhueter, S., Ramachandra, S., Worwood, M., *Hum. Genet.* 1999, *104*, 29–35.

[41] Ahrendt, S. A., Halachmi, S., Chow, J. T., Wu, L., Halachmi, N., Yang, S. C., Wehage, S., Jen, J., Sidransky, D., *Proc. Natl. Acad. Sci. USA* 1999, *96*, 7382–7387.

[42] Tian, H., Brody, L., Landers, J. P., *Genome Res.* 2000, *10*, 1403–1413.

[43] Wikman, F. P., Katballe, N., Christensen, M., Laurberg, S., Ørntoft, T. F., *Genet. Testing* 2000, *4*, 15–21.

[44] Jackson, H. A., Bowen, D. J., Worwood, M., *Brit. J. Haematol.* 1997, *98*, 856–859.

[45] Larsen, L. A., Andersen, P. S., Kanters, J. K., Jacobsen, J., Vuust, J., Christiansen, M., *Clin. Chim. Acta* 1999, *280*, 113–125.

[46] Pursall, M. C., Clay, T. M., Bidwell, J. L., *Eur. J. Immunogenet.* 1996, *26*, 41–53.

[47] Ravnik-Glavac, M., Glavač, D., Dean, M., *Hum. Mol. Genet.* 1994, *3*, 801–807.

[48] Hongyo, T., Buzard, G. S., Calvert, R. J., Weghorst, C. M., *Nucleic Acids Res.* 1993, *21*, 3637–3642.

[49] Axton, R. A., Hanson, I. M., Love, J., Seawright, A., Prosser, J., van Heyningen, V., *Mol. Cell. Probes* 1997, *11*, 287–292.

[50] Orban, T. I., Csokay, B., Olah, E., *BioTechniques* 2000, *29*, 94–98.

[51] Gonen, D., Veenstra-VanderWeele, J., Yang, Z., Leventhal, B., Cook, E. H. Jr., *Mol. Psychiat.* 1999, *4*, 339–343.

[52] Sasaki, T. I., Tahira, T., Suzuki, A., Higasa, K., Kukita, Y., Baba, S., Hayashi, K., *Am. J. Hum. Genet.* 2001, *68*, 214–218.

[53] Walz, T., Geisel, J., Bodis, M., Knapp, J.-P., Herrmann, W., *Electrophoresis* 2000, *21*, 375–379.

[54] Geisel, J., Walz, T., Bodis, M., Nauck, M., Oette, K., Herrmann, W., *J. Chromatogr. B* 1999, *724*, 239–247.

[55] Atha, D. H., Wenz, H. M., Morehead, H., Tian, J., O'Connell, C. D., *Electrophoresis* 1998, *19*, 172–179.

[56] Yan, H., Kinzler, K. W., Vogelstein, B., *Science* 2000, *289*, 1890–1892.

Anal. Chem. 2002, *74*, 2565−2572

High-Throughput, High-Sensitivity Genetic Mutation Detection by Tandem Single-Strand Conformation Polymorphism/Heteroduplex Analysis Capillary Array Electrophoresis

Igor V. Kourkine, Christa N. Hestekin, Brett A. Buchholz, and Annelise E. Barron*

Department of Chemical Engineering, Northwestern University, Evanston, Illinois 60208

We present the first optimization of linear polyacrylamide (LPA)-based DNA separation matrixes for an automated *tandem* microchannel single-strand conformation polymorphism (SSCP)/heteroduplex analysis (HA) method, implemented in capillary arrays dynamically coated with poly(*N*-hydroxyethylacrylamide) (polyDuramide). An optimized protocol for sample preparation allowed both SSCP and HA species to be produced in one step in a single tube and distinguished in a single electrophoretic analysis. A simple, two-color fluorescent sample labeling and detection strategy enabled unambiguous identification of all DNA species in the electropherogram, both single- and double-stranded. Using these protocols and a panel of 11 p53 mutant DNA samples in comparison with wild-type, we employed high-throughput capillary array electrophoresis (CAE) to carry out a systematic and simultaneous optimization of LPA weight-average molar mass (M_w) and concentration for SSCP/HA peak separation. The combination of the optimized LPA matrix (6% LPA, M_w 600 kDa) and a hydrophilic, adsorbed polyDuramide wall coating was found to be essential for resolution of CAE-SSCP/HA peaks and yielded sensitive mutation detection in all 11 p53 samples initially studied. A larger set of 32 mutant DNA specimens was then analyzed using these optimized tandem CAE-SSCP/HA protocols and materials and yielded 100% sensitivity of mutation detection, whereas each individual method yielded lower sensitivity on its own (93% for SSCP and 75% for HA). This simple, highly sensitive tandem SSCP/HA mutation detection method should be easily translatable to electrophoretic analyses on microfluidic devices, due to the ease of the capillary coating protocol and the low viscosity of the matrix.

Single-strand conformation polymorphism (SSCP) is based on the principal that, even in DNA fragments of equal length, an altered DNA nucleotide sequence caused by a mutation can affect single-strand DNA (ssDNA) folding and, hence, can be detected as a difference in electrophoretic mobility.[1,2] Similarly, heteroduplex analysis (HA) is based on the premise that dsDNA fragments of a given length consisting of perfectly complementary strands (homoduplexes) often exhibit electrophoretic mobilities different from those of dsDNA that contain sequence mismatches (heteroduplexes).[3] Generally, both SSCP and HA are relatively difficult DNA separations to achieve. Traditionally, the two methods are performed separately and involve PCR amplification of the DNA region of interest with ^{32}P-labeled (radioactive) primers, thermal denaturation, and cooling of the resulting dsDNA to form either single-strand conformers or mixed homo- and heteroduplexes, electrophoresis in highly resolving cross-linked polyacrylamide slab gels, and finally autoradiographic detection. The major practical weakness of SSCP is the perceived need to conduct the analysis under more than one set of experimental conditions to obtain a high sensitivity of mutation detection, while the major disadvantage of HA is its generally low sensitivity for the detection of single-base substitutions.[1] Another weakness of SSCP as a diagnostic tool is its empirical nature, which results from the inability to predict ssDNA folding and to correlate it with the electrophoretic mobility of the resulting single-strand conformers.[4]

More recently, there has been interest in performing SSCP and HA in tandem. If a mixture of the wild-type and mutant dsDNA species is thermally denatured and rapidly cooled to form ssDNA conformers under the correct buffer conditions, a significant portion of the mixture also reanneals to form homo- and heteroduplexes, allowing one to conduct both SSCP and HA *simultaneously* using a single sample. The sensitivity of mutation detection with this combined methodology exceeds that of SSCP or HA alone (60−90% typically) and can approach 100%, as evidenced by several slab gel electrophoresis studies.[5-8] These studies

* Corresponding author: Email: a-barron@northwestern.edu. Fax: +847-491-3728.

10.1021/ac020025b CCC: $22.00
Published on Web 05/03/2002

(1) Nataraj, A. J.; Olivos-Glander, I.; Kusukawa, N.; Highsmith, W. E., Jr. *Electrophoresis* **1999**, *20*, 1177−1185.
(2) Orita, M.; Suzuki, Y.; Sekiya, T.; Hayashi, K. *Genomics* **1989**, *5*, 874−879.
(3) Nagamine, C. M.; Chan, K.; Lau, Y.-F. C. *Am. J. Hum. Genet.* **1989**, *45*, 337−339.
(4) Ellis, L. A.; Taylor, C. F.; Taylor, G. R. *Hum. Mutat.* **2000**, *15*, 556−564.
(5) Axton, R. A.; Hanson, I. M.; Love, J.; Seawright, A.; Prosser, J.; van Heyningen, V. *Mol. Cell. Probes* **1997**, *11*, 287−292.
(6) Larsen, L. A.; Andersen, P. S.; Kanters, J. K.; Jacobsen, J.; Vuust, J.; Christiansen, M. *Clin. Chim. Acta* **1999**, *280*, 113−125.

also document the high specificity of combined SSCP/HA and alleviate some earlier concerns that fast hybridization kinetics might lead to partial reannealing of the dsDNA, which could result in spurious peaks and false positives.[9]

Genetic analyses designed for slab gels can often be accomplished more efficiently using microchannel electrophoresis formats such as capillary electrophoresis (CE), capillary array electrophoresis (CAE), and microchip electrophoresis (ME).[10-12] In C(A)E, electrophoretic separation is carried out within microbore fused-silica capillaries, while in ME, electrophoretic separation is conducted in tiny grooves manufactured on the surface of glass or plastic chips. Both C(A)E and ME formats offer access to process streamlining, including automated loading of separation matrix between runs and automated injection of DNA samples, and provide much faster separations than slab gels due to the higher electric fields applied.[10] C(A)E and ME can be equipped with laser-induced fluorescence (LIF) detectors that eliminate the inconvenience of radioactive labeling while maintaining high sensitivity of analyte detection. Finally, ME offers the potential of so-called "lab-on-a-chip" devices that are capable of integrating all of the steps required for genetic screening on a single microfluidic chip, including DNA extraction, purification, PCR amplification, and electrophoretic separation.[13]

In order for C(A)E and ME technologies to work well for genetic screening by tandem SSCP/HA, it is critical that optimal DNA separation matrixes for these types of samples be developed for microchannel formats. In slab gel electrophoresis SSCP, such optimization studies have focused on the ratio of *N,N*-methylene bisacrylamide (cross-linker) to acrylamide monomer and have yielded matrixes with a low ratio of the former to the latter, which are more flexible and therefore more efficient for mutation detection.[14] In CE-SSCP and CE-HA, which employ non-cross-linked (linear) entangled polymer matrixes, such optimization must focus on the chemical (i.e., composition and hydrophobicity) and physical properties (i.e., molecular weight, persistence length, and polydispersity) of the polymers that form DNA separation matrixes. These chemical and physical polymer characteristics are important since they determine the properties of the entangled polymer network that is formed and, hence, the matrix "mesh size" and ability to provide high-resolution DNA separations.[15] Previously, several polymers such as hydroxyethylcellulose (HEC), poly(vinylpyrrolidone) (PVP), methylcellulose (MC), ABI POP, and linear polyacrylamide (LPA) were applied to CE-SSCP or CE-HA with varying degrees of success, and these studies have shed some light on the impact of polymer chemical composition on the performance of these analyses.[16]

Only one study touched upon the impact of polymer physical properties on the sensitivity of mutation detection by CE-SSCP and CE-HA. Notably, Ren et al. demonstrated that DNA separation matrixes based upon short-chain LPA of unspecified average molar mass can be used for CE-SSCP mutation detection and are easier to load into capillaries than those composed of long-chain LPA because of the lower polymer solution viscosity of the former.[17,18] But in order to achieve a systematic study of the influence of polymer physical characteristics on CE-SSCP and CE-HA performance, it is necessary to both synthesize and characterize polymers suitable for CE. The majority of the polymers studied for this purpose to date are commercially available only in certain chain lengths, which for naturally occurring polymers (i.e., HEC and MC) also tend to vary from batch to batch, precluding precise and reliable evaluation of the impact of their physical nature on CE separations. In the absence of a large choice of polymers, some efforts have been directed at optimizing the concentrations of commercially available polymers for CE-SSCP, primarily POP, a DNA sieving polymer supplied by Applied Biosystems. Not surprisingly, more concentrated POP matrixes have yielded better results, but also complicated capillary loading due to their high viscosities.[19-21]

Research projects in our group place emphasis on the controlled synthesis of polymers suitable for CE applications and on their complete and precise physical characterization by gel permeation chromatography (GPC) in tandem with refractive index and multiangle laser light scattering (MALLS) detection, resulting in the determination of both polymer molar mass distribution and the average radius of gyration in the solvent of interest.[22] With this knowledge in hand, we recently carried out detailed studies of the impact of polymer properties on DNA sequencing separations by capillary electrophoresis.[23] Herein, we extend our correlations of matrix properties with CE performance of genetic analysis and describe the first thorough investigation of the combined impact of the weight-average molar mass (M_w) of LPA and its concentration in the DNA separation matrix on the resolution of tandem CAE-SSCP/HA, resulting in the formulation of an optimized DNA separation matrix for this important application. The dynamic coating we used for passivation of bare fused-silica capillary arrays is based upon polyDuramide (poly-*N*-hydroxyethyl acrylamide), a novel polymer developed in our laboratory in collaboration with BioWhittaker Molecular Applications (Walkersville, MD).[24] Precoating the capillaries with a dilute solution of polyDuramide provides a low-cost solution for the lack of self-coating ability of LPA and allows for highly efficient and reproducible electrophoretic peak patterns of SSCP and HA

(7) Ravnik-Glavac, M.; Glavac, D.; Dean, M. *Hum. Mol. Genet.* **1994**, *3*, 801–807.
(8) Pursall, M. C.; Clay, T. M.; Bidwell, J. L. *Eur. J. Immunogenet.* **1996**, *26*, 41–53.
(9) Hongyo, T.; Buzard, G. S.; Calvert, R. J.; Weghorst, C. M. *Nucleic Acids Res.* **1993**, *21*, 3637–3642.
(10) Dolnik, V.; Liu, S.; Jovanovich, S. *Electrophoresis* **2000**, *21*, 41–54.
(11) Beale, S. C. *Anal. Chem.* **1998**, *70*, 279R–300R.
(12) Haleem, I. J. *Electrophoresis* **2000**, *21*, 1921–1939.
(13) Service, R. F. *Science* **1998**, *282*, 399–401.
(14) Cotton, R. G. H., Edkins, E., Forrest, S., Eds. *Mutation Detection: A Practical Approach*; Oxford University Press: New York, 1998; pp 7–34.
(15) Albarghouthi, M. N.; Barron, A. E. *Electrophoresis* **2000**, *21*, 4096–4111.
(16) Ren, J. *J. Chromatogr., B* **2000**, *741*, 115–128.
(17) Ren, J.; Ulvik, A.; Refsum, H.; Ueland, P. M. *Anal. Biochem.* **1999**, *276*, 188–194.
(18) Ren, J.; Ulvik, A.; Ueland, P. M.; Refsum, H. *Anal. Biochem.* **1997**, *245*, 79–84.
(19) Inazuka, M.; Wenz, H. M.; Sakabe, M.; Tahira, T.; Hayashi, K. *Genome Methods* **1997**, *7*, 1094–1103.
(20) Ghozzi, R.; Morand, P.; Ferroni, A.; Beretti, J. L.; Bingen, E.; Segonds, C.; Husson, M.; Izard, D.; Berche, P.; Gaillard, J.-L. *J. Clin. Microbiol.* **1999**, *37*, 3374–3379.
(21) Wenz, H. M.; Ramachandra, S.; O'Connell, C. D.; Atha, D. H. *Mutat. Res. Genomics* **1998**, *382*, 121–132.
(22) Buchholz, B. A.; Barron, A. E. *Electrophoresis* **2001**, *22*, 4118–4128.
(23) Albarghouthi, M. N.; Buchholz, B. A.; Doherty, E. A. S.; Bogdan, F. M.; Zhou, H.; Barron, A. E. *Electrophoresis* **2001**, *22*, 737–747.
(24) Albarghouthi, M. N.; Buchholz, B. A.; Hulberts, P. J.; Stein, T. M.; Barron, A. E. *Electrophoresis*, in press.

Table 1. Data Detailing Preparation and Characterization of a Set of LPAs

	monomer, g	H_2O, mL	2-propanol, mL	APS, 10% (w/v) aq, mL	TEMED, 10% (v/v) aq, mL	M_w, kDa	R_g, nm	PDI
LPA200K	10	110	5.8	0.625	0.625	200	63	1.51
LPA600K	10	110	0.7	0.5	0.5	600	64	1.8
LPA1M	10	110	none	0.4	0.4	1000	73	1.94
LPA2.4M	10	110	none	0.625	0.625	2400	116	2.91

samples. The optimized LPA matrix in combination with polyDuramide dynamic coating was utilized for the screening of 32 mutant DNA specimens of the p53 gene, which is the most frequently mutated gene in human cancer.[25,26] When used in concert with two-color LIF detection at 27 °C and optimized sample preparation protocols, tandem CE-SSCP/HA afforded 100% sensitivity of mutation detection coupled with complete and unambiguous peak assignments in the resulting electropherograms. On the other hand, CE-SSCP and CE-HA applied individually to the same set of p53 gene samples revealed only 93 and 75% of existing mutations, respectively, making these techniques unsuitable for implementation in a clinical setting, for which the NIH presently recommends a sensitivity of at least 97%.

EXPERIMENTAL SECTION

Reagents and Equipment. The following materials and reagents were purchased from commercial suppliers and were used as received: boric acid; ethylenediaminetetraacetic acid tetrasodium salt (EDTA), tris(hydroxymethyl)aminomethane (Tris), ethidium bromide, ammonium persulfate (APS), TEMED, acrylamide (all from Amresco, Solon, OH); 2-propanol, HCl, NaOH (Fisher, Brightwaters, NY), dialysis cellulose ester membranes (MWCO 100K, Spectrum Laboratories, Rancho Domingues, CA); compressed N_2 (Air Products and Chemicals, Allentown, PA), and glycerol (Aldrich, Milwaukee, WI). Mutant DNA specimens of the p53 gene (exon 7, size 139 bp; exon 8, size 200 bp) were supplied by the National Institute of Standards and Technology (NIST, Gaithersburg, MD) in the form of PCR amplicons and used as stock solutions of SSCP and HA samples without further purification. P53 cell lines (genomic DNA) that contain mutations in the p53 exon 7 were purchased from American Type Culture Collection (ATCC, Manassas, VA). These were PCR-amplified (amplicon size 300 bp) with forward (FAM-CCT GCT TGC CAC AGG TCT) and reverse (JOE-GTG ATG AGA GGT GGA TGG GT) primers, purified as described elsewhere[27] and then used as stock solutions in this study. PolyDuramide polymer (M_w 4 MDa), which was used for dynamic capillary coating, was prepared, purified, and characterized in our laboratory as described by Albarghouthi et al.[24]

The following equipment was used in this study: a GPC 2690 Separations Module (Waters, Milford, MA) with Shodex (New York, NY) OHpak columns SB-806 HQ, SB-804 HQ, and SB-802.5 HQ connected in series, a MALLS DAWN-Optilab system (Wyatt Technology, Santa Barbara, CA), a PTC200 DNA Engine thermocycler (MJ Research, Waltham, MA), and a MegaBACE DNA sequencing system with uncoated fused-silica capillary arrays (Molecular Dynamics, Sunnyvale, CA).

Polymer Synthesis and Characterization. Two samples of short-chained (M_w 200 and 600 kDa) and two samples of long-chained linear polyacrylamide (M_w 1 and 2.4 MDa) were synthesized by radically induced aqueous polymerization. In a typical procedure, a solution of acrylamide (10 g) in deionized water (110 mL) was placed into a 300-mL airtight flask, immersed in a water bath kept at 50 °C, and degassed by bubbling N_2 for 30 min (for more details see Table 1). Next, 2-propanol (2.5−5 mL), APS (0.625 mL, 10% w/v aqueous), and TEMED (0.625 mL, 10% v/v aqueous) were added in a consecutive fashion, and the resulting mixture was kept at 50 °C under N_2 flow for 1.5 h to ensure anaerobic conditions. During this time, the acrylamide monomer underwent radically induced polymerization, as evidenced by the increased viscosity of the resulting LPA solution. LPA was then loaded into a tubular cellulose ester membrane and dialyzed against distilled, deionized water for 10 days with daily water changes. Purified LPA was lyophilized and characterized by tandem GPC-MALLS as described elsewhere (see Table 1 for polymer data).[28] Dry polymers were dissolved at 2, 4, and 6% (w/v) in 1× TBE buffer (89 mM Tris, 89 mM boric acid, 2 mM EDTA) containing 10% glycerol to afford a set of 12 different DNA separation matrixes (stored at 4 °C throughout the present study).

SSCP/HA Sample Preparation and CE. Fluorescently labeled DNA amplicons (forward strand, FAM; reverse strand, JOE) of exons 7 and 8 of the p53 gene were diluted 10×−40× with Tris-HCl (10 mM, pH 8.5). The diluted PCR products or their mixtures were loaded onto a 96-well plate (5 μL into each well), denatured at 95 °C for 3 min using a PTC200 thermocycler, and snap-cooled on ice. Prior to CE-SSCP/HA runs, uncoated MegaBACE capillary arrays (total length 64 cm, effective length 40 cm, inner diameter 75 μm) were conditioned and dynamically coated by rinsing them with the following: NaOH (aqueous, 0.1 M, 4 mL) for 30 min at low pressure (100 psi), deionized water (2 mL) for 30 s at high pressure (1000 psi), HCl (aqueous, 0.1 M, 4 mL) for 30 min at low pressure (100 psi), water (2 mL) for 30 s at high pressure (1000 psi), polyDuramide (coating reagent, aqueous, 0.5%, 0.3 mL) for 30 min at low pressure (100 psi), and water (2 mL) for 30 s at high pressure (1000 psi). Throughout this study, the arrays were reconditioned by this procedure every 10−14 runs to ensure high-performance separations. The capillary arrays were loaded with the LPA-based DNA separation matrixes for 0.5−1.5 min and temperature-equilibrated for 20 min at 27 °C. Pre-electrophoresis was performed for 5 min at 140 V/cm. The DNA amplicons were injected at 230 V/cm for 25 s and

(25) Sidransky, D.; Hollstein, M. *Annu. Rev. Med.* **1996**, *47*, 285−301.
(26) Greenblatt, M. S.; Bennet, W. P.; Hollstein, M. *Cancer Res.* **1994**, *54*, 4855−4878.
(27) Kourkine, I. V.; Hestekin, C. N.; Magnusdottir, S. O.; E., B. A. *Biotechniques*, in press.
(28) Zhou, H.; Miller, A. W.; Sosic, Z.; Buchholz, B.; Barron, A. E.; Kotler, L.; Karger, B. L. *Anal. Chem.* **2000**, *72*, 1045−1052.

Table 2. Results of Genetic Screening of the P53 Gene by Tandem CAE-SSCP/HA, Utilizing an Optimized DNA Separation Matrix[a,b]

	p53 exon 7 (size 139 bp)				p53 exon 8 (size 200 bp)	
codon no.	242	245	248	249	273	282
wild-type sequence	TGC	GGC	CGG	AGG	CGT	CGG
mutant DNA specimens	AGC (+/+)	AGC (+/+)	AGG (++/++)	AGC (++/++)[c]	AAT (+/++)	*GGG (−/+)*
	AAC (+/+)	CGC (++/++)[c]	CAG (++/++)	*AGT (−/++)*	ACT (+/+)[c]	*AGG (−/+)*[c]
	ACC (++/+)[c]	GCC (+/++)	GGG (++/++)[c]		*AGT (−/+)*	**TGG (+/−)**
	ATC (++/+)[c]	*GTC (-/++)*	TGG (+/++)		ATT (+/++)	
	CAC (++/+)	*TGC (-/++)*			*CAT (−/+)*[c]	
	CTC (++/+)				CTT (+/+)	
	GGC (+/+)				TAT (+/++)	
	TCC (+/+)				**TCT (+/−)**[c]	
	TTC (+/+)				*TGT (−/+)*	
no. of samples	9	5	4	2	9	3
					total no. of samples: 32	

[a] Key: (−/+) homo and heteroduplexes overlap, wild-type (wt) differs from mutant in only one ssDNA strand; (−/++) homo- and heteroduplexes overlap, wt differs from mutant in both ssDNA; (+/+) one separate heteroduplex, wt differs from mutant in only one ssDNA strand; (+/++) one separate heteroduplex, wt differs from mutant in both ssDNA; (++/+) two separate heteroduplexes, wt differs from mutant in only one ssDNA strand; (++/++) two separate heteroduplexes, wt differs from mutant in both ssDNA; (+/−) one separate heteroduplex, wt does not differ from mutant in either ssDNA strand. [b] Shown in Italic type are mutations that were not detected by HA; while mutations not detected by SSCP are shown in boldface type. [c] DNA specimens used for LPA optimization.

electrophoresed at 180 V/cm with an associated current of 10−12 μA at 27 °C.

RESULTS AND DISCUSSION

Polymer Synthesis and Characterization. LPA was selected from among other synthetic polymers suitable for CE for its high hydrophilicity, efficient DNA separation ability, ease of synthesis, and low cost.[15] Several batches of LPA were synthesized by radically induced aqueous polymerization under anaerobic conditions according to a procedure previously established in our laboratory.[23] The amounts of monomer (acrylamide), catalyst (APS), cocatalyst (TEMED), and chain terminator (2-propanol) were systematically adjusted to afford a set of polymers having weight-average molar mass between 200 kDa and 2 MDa. Following the synthesis, the polymers were purified by dialysis, lyophilized, and analyzed by tandem gel permeation chromatography/multiangle laser light scattering (GPC/MALLS), which is a versatile and accurate method of characterization of polymers and copolymers suitable for CE applications.[22] Based on the results of the GPC/MALLS analysis, a set of four polymers, LPA200K, LPA600K, LPA1M, and LPA2.4M, was selected (Table 1). Each of the polymers was dissolved in 1× TBE buffer containing 10% glycerol—the most ubiquitously used CE-SSCP buffer[16]—at 2, 4, and 6% to afford a set of 12 different matrixes (4 M_w × 3 concentrations = 12) that were tested as DNA separation matrixes in CAE-SSCP/HA experiments.

Fluorescently Labeled p53 DNA Samples. Seven mutant DNA samples amplified from exon 7 of the p53 gene (size 139 and 300 bp) and four mutant DNA samples from exon 8 of the p53 gene (size 200 bp) were used in this study for LPA matrix optimization. These DNA specimens were selected so that they include three different DNA sizes, both single- and two-base substitutions, and several different mutation positions (Table 2) in order to establish general trends in the impact of polymer physical nature on the resolution of CAE-SSCP/HA samples. The short DNA fragments (size 139 and 200 bp) were used as received from NIST in the form of PCR amplicons that were fluorescently labeled with FAM on the forward strands and with JOE on the reverse strands. The longer DNA fragments (300 bp), obtained from ATCC, were PCR-amplified from genomic DNA with FAM- and JOE-labeled fluorescent primers, purified by a preparative slab gel electrophoresis/cellulose membrane method, and partially desalted by filtration through Microcon-PCR filtration device. This labeling scheme allowed for two-color LIF detection and facilitated the unambiguous assignment of DNA peaks in the CAE-SSCP/HA electropherograms. The final concentration of purified DNA mutant specimens was not measured, but was estimated to be 20 pmol/μL for exon 7 wild-type and 5−20 pmol/μL for all other amplicons by the brightness of the DNA sample bands during slab gel electrophoresis relative to the brightness of selected DNA samples whose precise concentration had been calculated on the basis of their OD_{260} values.

Tandem SSCP/HA Sample Preparation. In the literature, CE-SSCP samples are commonly diluted with 50−95% deionized formamide as well as a small amount of NaOH, without any clear justification for the presence of these additives (that we have found). We recently conducted a systematic study of the effects of formamide on CAE-SSCP and CAE-HA and concluded that it does not provide any benefits for the CAE analysis of the p53 gene, but instead significantly decreases the efficiency of electrokinetic injection and possibly adversely affects the resolution of the homo- and heteroduplexes.[27] In the same study, we also thoroughly evaluated the effects of the salt concentration in the sample on CAE-SSCP and CAE-HA and determined that 1× Tris-HCl (10 mM, pH 8.5) without any other additives is an ideal diluent for the tandem CE-SSCP/HA method.

The diluted DNA samples were denatured at 95 °C for 3 min and snap-cooled on ice. Previously, we noticed that snap-cooling has advantages over allowing the denatured DNA sample to cool naturally, in that it provides faster hybridization kinetics and minimizes the undesired annealing of primers to the SSCP conformers, while at the same time allowing for the formation of homo- and heteroduplexes (vide infra). On the other hand, attempts at slow annealing of the denatured samples over a period

of 10−60 min yields dsDNA exclusively, which can only be used for CAE-HA and not for CAE-SSCP analysis.[27]

Immediately prior to CE, a cold solution of a mutant DNA sample was mixed with a cold solution of the corresponding wild-type DNA species in ~1:1 ratio, split into three fractions (to allow three repeats of the analysis), and loaded into a 96-well plate. Additionally, chilled solutions of the same mutant and wild-type DNA specimens were each split into three fractions, loaded into the same 96-well plate separately, and used as references for the peak assignments. Successful analyses of mixtures containing only 20% of mutant DNA (one part of exon 7 wild-type at ~20 pmol/μL mixed with one part of exon 7 mutant at ~5 pmol/μL) confirm the potential of tandem CE-SSCP/HA for sensitive detection of genetic mutations in heterozygous individuals and in DNA samples derived from tumors containing a significant fraction of normal tissue. It is likely that tandem CE-SSCP/HA can detect even lower concentrations of mutant DNA since it is reported elsewhere that CE-HA can detect as little as 1% mutant DNA diluted with 99% of the wild-type DNA,[29] while CE-SSCP can identify mutations in a mixture consisting of 10% mutant and 90% wild-type DNA.[30]

Typically, 2 of the 6 capillary arrays (each consisting of 16 capillaries) available in the MegaBACE instrument were used simultaneously, allowing for screening of 2−3 mutant DNA samples and 1 matrix composition at a time. The high-throughput ability of the MegaBACE instrument proved indispensable for this study, which required only ~65 separate CAE runs (2000 single CE analyses!) to analyze all of the desired permutations of the polymer M_w and separation matrix concentrations. The already high throughput of the instrument could be further increased for a clinical application of these methods by utilizing all of the 96 capillaries and a 4-color LIF detection mode that would allow for the analysis of two different mutant DNA species labeled with two different sets of dyes in a single capillary (multiplexing).

Tandem CE-SSCP/HA was performed at 27 °C since this temperature falls within the range of those most often recommended for CE-SSCP (20−30 °C)[16] and because it was the lowest temperature possible in the MegaBACE instrument available to us (temperature range 27−44 °C). Although higher temperatures may be beneficial for HA due to larger heteroduplex perturbations at the point of mismatch, leading to larger differences in homo/heteroduplex electrophoretic mobilities and hence higher sensitivity of mutation detection, at least one study reports only a minor improvement in the sensitivity of mutation detection by CE-HA upon temperature increase from 30 to 60 °C.[31] Additionally, the optimum temperature for sensitive mutation detection by both CE-SSCP and CE-HA is believed to be highly sequence-specific and, hence, probably cannot be determined a priori.[4] Because of these considerations, we chose to focus on creating optimized separation matrixes that would allow for high sensitivity of mutation detection without case-by-case fine-tuning of the temperature of analysis, which was fixed at 27 °C throughout our study.

Dynamic Capillary Coating. Custom-made bare fused-silica capillary arrays used in this study were coated with adsorbed polyDuramide prior to loading of the LPA separation matrix. Typically, these dynamically coated capillary arrays afforded high-quality results with LPA matrixes for about 10−14 runs, after which time they were recoated using the procedure outlined in the Experimental Section. Unlike polyDuramide-coated arrays, commercially available covalently LPA-coated capillary arrays designed for DNA sequencing applications showed much less robust performance for SSCP/HA analysis. Following five to seven successful CAE-SSCP/HA runs in these covalently coated capillaries, the electropherograms started to show broad, irreproducible, and unresolved peaks, especially for SSCP conformers, pointing to a fast irreversible deterioration or fouling of the protective LPA coating. Notably, the same LPA-coated arrays continued to perform adequately for DNA sequencing separations (M13 standard), suggesting that either the nature of SSCP conformers (i.e., increased hydrophobicity of ssDNA vs dsDNA) or the SSCP running conditions (i.e., 1× TBE buffer with glycerol for SSCP vs 1X TTE buffer with 7M urea for sequencing) place different requirements on the protective coating. For comparison, we also performed tandem CE-SSCP/HA in bare fused-silica capillary arrays dynamically coated with long-chained PDMA (M_w 3−4 MDa), another self-coating polymer prepared in our laboratory, but again we were not able to obtain reproducible, sharp, and resolved SSCP/HA peaks. We attributed this to detrimental interactions of the borate ions present in the 1× TBE buffer with the PDMA coating and confirmed it by registering high electroosmotic flow in a PDMA-coated capillary in the presence of borate ions (unpublished results). These results support some earlier studies that demonstrated the importance of the protective coating and its interactions with the DNA separation matrix for high-resolution CE-HA.[32] At this stage, it was also discovered that the matrix composed of 6% of the long-chained LPA2.4M was too viscous to be loaded into the capillaries, and so it was excluded from the study.

Analysis of SSCP/HA Electropherograms. Typical tandem SSCP/HA electropherograms obtained in this study are presented in Figure 1. In the figure, different single-stranded and double-stranded DNA species are distinguished, and peaks are labeled (a−g). Electropherograms can be broadly divided into three clearly separate regions, which are listed here in the order of increasing migration times: (1) primers, which elute at ~20−30 min (see Supporting Information), (2) homoduplex (peaks labeled (a)) and heteroduplex dsDNA (e), and (3) ssDNA conformers (b, c, f, g) and primer−ssDNA constructs (d). Facile differentiation between all of these DNA species was made possible by the two-color labeling and LIF detection scheme. Specifically, the homo- and heteroduplexes each demonstrate two perfectly overlapping peaks of red (reverse strand, JOE) and blue (forward strand, FAM) colors as expected from two comigrating DNA strands. Single-strand conformers exhibit two overlapping peaks of different intensities, the smaller of which results from a minor overlap of the emission spectra for the two dyes picked up by the detector. Peaks representing primer−ssDNA constructs are clustered around the peaks for the ssDNA conformers and are composed of two perfectly overlapping peaks of the two LIF colors. An unambiguous assignment of the peaks resulting from annealed primer−ssDNA species was confirmed by an experiment in which

(29) Tian, H.; Brody, L.; Landers, J. *Genome Res.* **2000**, *10*, 1403−1413.
(30) Cooksey, R. C.; Morlock, G. P.; Holloway, B. P.; Mazurek, G. H.; Abaddi, S.; Jackson, L. K.; Buzard, G. S.; Crawford, J. T. *Mol. Diagn.* **1998**, *3*, 73−80.
(31) Kozłowski, P.; Krzyzosiak, W. J. *Nucleic Acids Res.* **2001**, *29*, 71.
(32) Tian, H.; Brody, L.; Mao, D.; Landers, J. *Anal. Chem.* **2000**, *72*, 5483−5492.

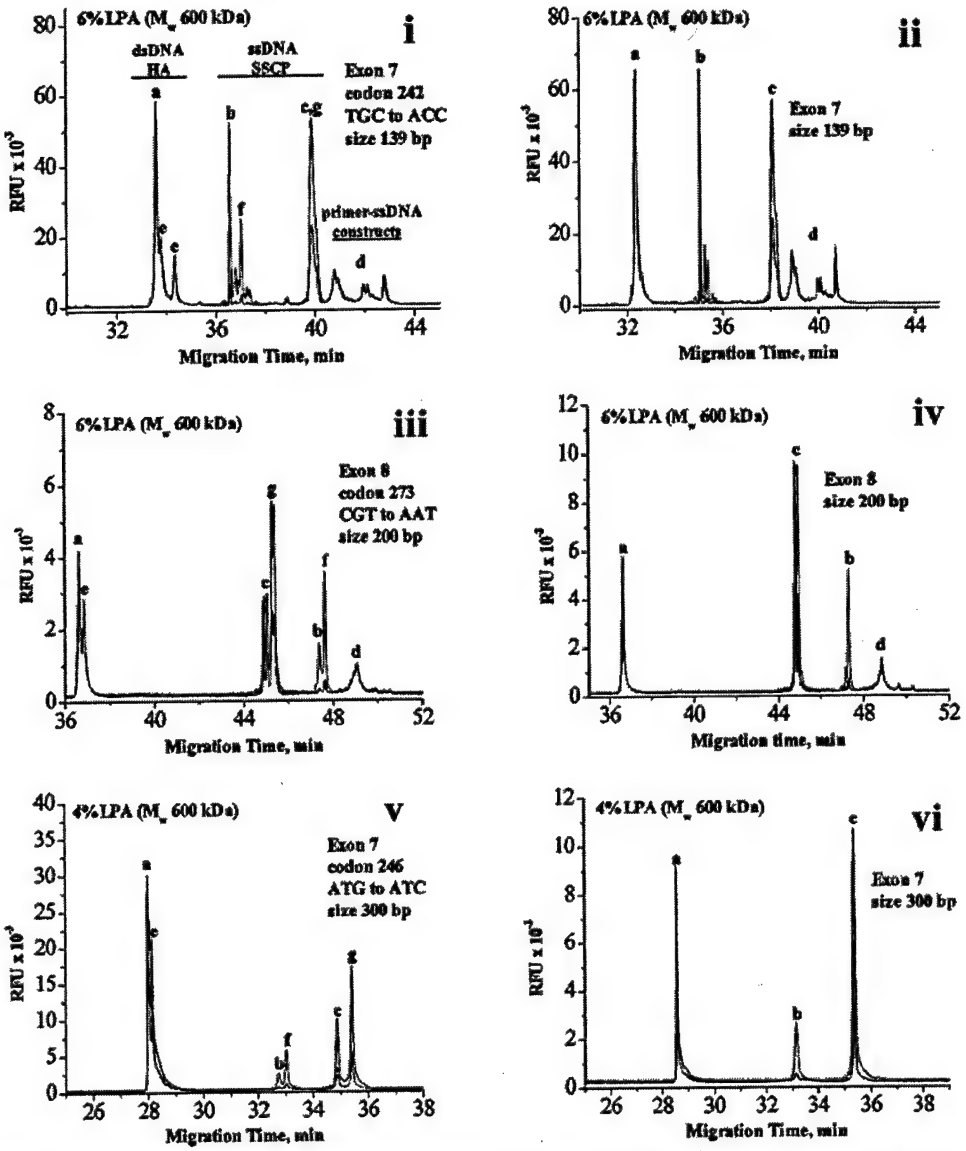

Figure 1. Precise identification of CAE-SSCP/HA peaks associated with genetic screening of p53 gene samples labeled with FAM on the forward strand (blue) and with JOE on the reverse-strand (red): (a) homoduplex; (b) wild-type reverse-strand SSCP; (c) wild-type forward-strand SSCP; (d) primer-ssDNA constructs; (e) heteroduplex; (f) mutant reverse-strand SSCP; (g) mutant forward-strand SSCP.

removal of the primers led to the disappearance of primer−ssDNA constructs, and their addition resulted in their reappearance, as evidenced by CE.[27]

Interpretation of Electropherograms. During early stages of this study, we attempted to evaluate the LPA matrix performance for CE-SSCP/HA by simply comparing the time of separation between the wild-type and mutant DNA peaks, a fairly common approach adopted in other studies that have looked at the effects of polymer concentration on CE-SSCP performance.[19-21] However, as the study progressed, we deemed this methodology inadequate, because more concentrated matrixes based upon long-chain LPA resulted in longer DNA migration times and more widely separated and broader peaks than those obtained in less concentrated matrixes and in those of lower LPA M_w. At this point, we decided that resolution is a much better gauge for the performance of the different LPAs. The migration times of the wild-type DNA (t_{wt}) and mutant DNA (t_{mut}) were determined from the electropherograms, and resolution (R) was calculated according to the following classical equation

$$R = 2(t_{wt} - t_{mut})/(w_{wt} - w_{mut})$$

where w_{wt} and w_{mut} are wild-type and mutant DNA peak widths, respectively.

Since peak widths could vary from capillary to capillary and from run to run by as much as 50%, they were modeled in the

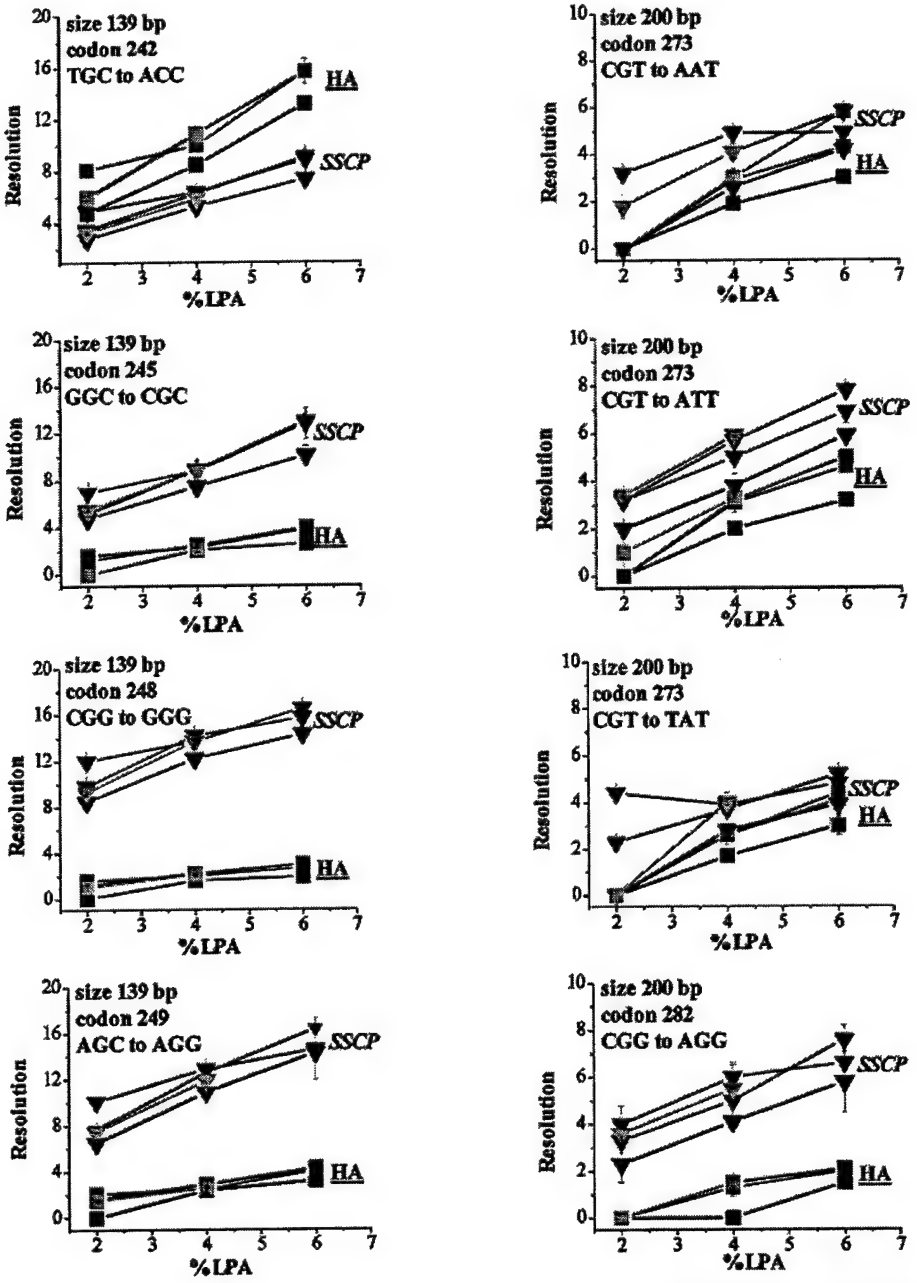

Figure 2. Combined impact of LPA weight-average molar mass and matrix concentration on the resolution of CAE-SSCP and CAE-HA for eight different DNA samples of the p53 gene, for separations performed in LPA200K (black), LPA600K (red), LPA1M (blue), and LPA 2.4M (green). Squares represent HA data, and inverted triangles represent SSCP data.

following fashion. Three mutant DNAs that possessed the most distinct and clear peak patterns were identified from the SSCP/HA electropherograms, and the peak widths recorded in all 12 matrixes were modeled in ORIGIN (Gaussian fit) and measured. The data were plotted as peak width versus peak migration time, and the plot showed an excellent linear fit ($w_{wt,\ mut} = 0.00131 t_{wt,\ mut}$), which was used for all the peak width estimations used in resolution calculations (Figure 34S, Supporting Information).

LPA Optimization for Sensitive CAE-SSCP/HA Mutation Detection. Plots of R versus LPA concentration (%) were constructed for all of the separation matrixes, and each includes the data for both SSCP and HA (Figure 2). If a mutant species was resolved from the wild-type in both forward and reverse SSCP strands and also in both heteroduplexes, only one heteroduplex and one SSCP strand were taken into account and used for R calculations. Each data point in these plots represents an individual analysis that was repeated at least 3 times; typical standard deviation of mobilities in these analyses was 3%. It is evident from the plots that resolution increases with increased LPA concentration in an almost linear fashion. We found that extremely short-chained LPA200K provided relatively poor resolution of SSCP/HA species at any concentration. LPA600K and LPA1M both

offered good resolution of CE-SSCP and CE-HA analysis for short DNA fragments (139 and 200 bp), while longer LPA2.4M polymer did not offer further improvements and also slowed the analyses and hindered capillary loading due to its higher matrix viscosity. With the exception of two DNA samples of p53 exon 7 that contained 2-bp substitutions (Figure 2), resolution of mutant species from wild-type was always higher for SSCP than HA.

Attempts at analyzing longer DNA fragments from exon 7 (300 bp) of the p53 gene proved to be less successful. Tandem CAE-SSCP/HA of one mutant DNA sample gave higher resolution in LPA1M than in LPA200K and even LPA600K. Additionally, in the LPA1M matrix resolution did not necessarily depend linearly on the concentration of LPA (not shown), as in the case of shorter DNA fragments, and was higher in 4% LPA solutions than in 6% LPA solutions. These trends, however, have not yet been confirmed because SSCP/HA analysis of the rest of the limited number of the long DNA fragments we have studied so far yielded inconsistent results. We are continuing to evaluate these phenomena.

Although the highest resolution of SSCP/HA conformers was achieved in 6% LPA1M (Figure 2), its routine use for tandem CE-SSCP/HA was compromised by the increased number of failed runs and excessive CE noise, presumably as a result of high viscosity of this polymer solution. Therefore, 6% LPA600K, which provides comparable resolution, but does not have the shortcomings associated with LPA1M, was selected as the optimized DNA separation matrix. The optimized DNA separation matrix was utilized to screen 32 mutant DNA samples of p53 exons 7 and 8 that include both single-base and double-base substitutions. CAE-SSCP was able to detect 30 of 32 mutations (93% sensitivity), and CAE-HA was able to detect 24 of 32 mutations (75% sensitivity) (Table 2). Since only 6% LPA600K allows for highly sensitive genetic screening, while other polymer compositions demonstrated much lower sensitivity due to poor resolution, excessive noise, or a large number of failed CE runs, it is likely that a higher than usual individual sensitivity of mutation detection by CE-SSCP or CE-HA is due to the powerful separation capability of the optimally synthesized polymer. Significantly, *tandem* CAE-SSCP/HA was able to identify all 32 mutations (100% sensitivity), and this perfect sensitivity of mutation detection is attributed to the complimentary abilities of CE-SSCP and CE-HA. Generally, the resolutions and sensitivity were higher for the smaller p53 exon 7 fragments than for the larger exon 8 samples, which can only be nonspecifically attributed to differences in either DNA sequence or size. Moreover, three p53 exon 7 mutant DNA specimens were successfully screened for mutations by SSCP performed on a plastic microchip during proof-of-concept experiments in our laboratory (data not shown). The microchannels (length 18 cm) were filled with the optimized polymer matrix (LPA600K, 6%), and the separations were achieved in less than 13 min. Further tandem SSCP/HA studies in plastic and glass microfluidic chips are ongoing in our laboratory.

(33) Wolfgang, G.; Kotler, L.; Carrilho, E.; Ruiz-Martinez, M. C.; Salas-Solano, O.; Karger, B. L. *Electrophoresis* **1998**, *19*, 242–248.

CONCLUSIONS

We have conducted the first systematic investigation of the combined impact of the average molar mass of LPAs and their concentration in the DNA separation matrix on the resolution of tandem capillary array electrophoresis single-strand conformation polymorphism/heteroduplex analysis, coupled with complete and precise assignment of all of the peaks in the electropherograms. We conclude that moderately short LPA (~600 kDa) dissolved at ~6% in 1× TBE serves as an optimal DNA separation matrix for the analysis of short DNA fragments (<200 bp) of the p53 gene and can afford 100% sensitivity of mutation detection by tandem SSCP/HA. Unlike *tandem* SSCP/HA, SSCP and HA applied separately to the same set of p53 gene samples afforded only 93 and 75% sensitivity of mutation detection, respectively, and at this level would not be applicable for clinical patient genetic screening, for which a sensitivity of at least 97% is desirable.

It was shown that the sensitivity of CAE-SSCP/HA strongly depends on a simultaneous optimization of both the protective capillary wall coating and the DNA separation matrix and that polyDuramide, a novel self-coating polymer, is essential for dynamic capillary coating employed in CAE-SSCP/HA. Neither a covalent LPA coating nor a dynamic PDMA coating gave reproducible SSCP/HA results with efficient DNA peaks.

We are presently applying these optimized tandem CE-SSCP/HA protocols to the mutation analysis of the PTEN and β-catenin genes derived from human prostate tumors, to test their broader generality. We are also working to transfer CAE-SSCP/HA to a microchip electrophoresis format, a task for which these optimized LPA-based matrixes are particularly well suited given their good separation ability, moderately low viscosities, and high shear thinning rate.[33] Preliminary results suggest that analogous mutation detection separations can be achieved on plastic microchips in less than 13 min, using optimized LPA as the DNA separation matrix.

ACKNOWLEDGMENT

We thank Dr. Catherine O'Connell of NIST for supplying us with mutant DNA samples of the p53 gene, BioWhittaker Molecular Applications for the gift of the Duramide monomer, and Erin Doherty and Methal Albarghouthi for preparing polyDuramide.

SUPPORTING INFORMATION AVAILABLE

Plot showing peak width vs peak migration time, tandem CE-SSCP/HA electropherograms illustrating mutation detection in all 32 screened DNA mutant specimens. This material is available free of charge via the Internet at http://pubs.acs.org.

Received for review January 11, 2002. Accepted March 26, 2002.

AC020025B

also can be cleaved by *Dpn*I. A 12-fold overdigestion with *Dpn*I results in hemimethylated DNA digestion that could be interpreted as suggesting replication failure, where in fact significant replication actually took place. Three- or 6-fold overdigestion digested the fully methylated DNA but preserved approximately half of hemimethylated product (Figure 2). The differential *Dpn*I digestion of fully methylated DNA compared to hemimethylated DNA is not present when the methyl insensitive *Sau*3AI is used on the two substrates. Comparing the *Dpn*I digestion intensity to undigested DNA, the 3–6-fold overdigestions cleave roughly half of the hemimethylated form while completely eliminating the fully methylated form (Figure 3).

Discriminating replicated plasmid from plasmid with radionucleotide incorporation due to repair or short primer extensions is critical for interpreting in vitro replication studies. Underdigestion with *Dpn*I will result in bands that have not been fully replicated, and overdigestion will result in loss of signal from fully replicated plasmid. Rao and Martin (10) have suggested that only the supercoiled band of *Dpn*I-resistant plasmid represents actual replication, while other non-supercoiled bands may not represent true replication. This observation also could be compatible with an underdigestion by *Dpn*I, or the digestion was sufficient to cleave the hemimethylated strand, leading to only cleaved and open circular molecules, though the concise nature of the manuscript precludes a definite conclusion on these possibilities.

The SV40 replication system has illuminated a great deal of information about the role of the large T antigen and human replication protein A in replication (5,6). However, this is a specific viral system and is not shared across all eukaryotes. Unlike the yeast origin of replication, which contains a recognizable consensus sequence, mammals appear to have a more complex mechanism of origin recognition and initiation of replication (4). Clarifying the digestion requirements for *Dpn*I detection of replicated DNA may simplify the analysis of potential mammalian origins of replication using an in vitro system. By working out precise parameters of the interaction of *Dpn*I with hemimethylated DNA, such a technique may be used as a screen for origin-like activity before going to more arduous techniques such as 2-D replication gels (1,14).

REFERENCES

1. **Berberich, S., A. Trivedi, D.C. Daniel, E.M. Johnson, and M. Leffak.** 1995. In vitro replication of plasmids containing human c-myc DNA. J. Mol. Biol. *245*:92-109.
2. **Carty, M.P., S. el-Saleh, M. Zernik-Kobak, and K. Dixon.** 1995. Analysis of mutations induced by replication of UV-damaged plasmid DNA in HeLa cell extracts. Environ. Mol. Mutagen. *26*:139-146.
3. **Carty, M.P., C.W. Lawrence, and K. Dixon.** 1996. Complete replication of plasmid DNA containing a single UV-induced lesion in human cell extracts. J. Biol. Chem. *271*:9637-9647.
4. **DePamphilis, M.L.** 1999. Replication origins in metazoan chromosomes: fact or fiction? Bioessays *21*:5-16.
5. **Iftode, C. and J.A. Borowiec.** 1997. Denaturation of the simian virus 40 origin of replication mediated by human replication protein A. Mol. Cell. Biol. *17*:3876-3883.
6. **Iftode, C. and J.A. Borowiec.** 1998. Unwinding of origin-specific structures by human replication protein A occurs in a two-step process. Nucleic Acids Res. *26*:5636-5643.
7. **Lacks, S.A.** 1980. Purification and properties of the complementary endonucleases *Dpn*I and *Dpn*II. Methods Enzymol. *65*:138-146.
8. **Li, J.J. and T.J. Kelly.** 1985. Simian virus 40 DNA replication in vitro: specificity of initiation and evidence for bidirectional replication. Mol. Cell. Biol. *5*:1238-1246.
9. **Palmer, B.R. and M.G. Marinus.** 1994. The dam and dcm strains of *Escherichia coli*—a review. Gene *143*:1-12.
10. **Rao, B.S. and R.G. Martin.** 1988. *Dpn*I assay for DNA replication in animal cells: enzyme-resistant material can result from factors not related to replication. Nucleic Acids Res. *16*:4171.
11. **Sambrook, J., E.F. Fritsch, and T. Maniatis.** 1989. Molecular Cloning: A Laboratory Manual. CSH Laboratory Press, Cold Spring Harbor, NY.
12. **Sanchez, J.A., D. Marek, and L.J. Wangh.** 1992. The efficiency and timing of plasmid DNA replication in *Xenopus* eggs: correlations to the extent of prior chromatin assembly. J. Cell Sci. *103*:907-918.
13. **Seidman, M.M., K. Dixon, A. Razzaque, R.J. Zagursky, and M.L. Berman.** 1985. A shuttle vector plasmid for studying carcinogen-induced point mutations in mammalian cells. Gene *38*:233-237.
14. **Snapka, R.M.** 1996. The SV40 Replicon Model for Analysis of Cancer Drugs. R.G. Landes Company, San Diego.

This work was supported by a grant from the PKD Foundation. Address correspondence to Dr. John J. Bissler, Children's Hospital Research Foundation, R5, 3333 Burnet Ave., Cincinnati, OH 45229-3039, USA. e-mail: john.bissler@chmcc.org

Received 26 November 2001; accepted 16 April 2002.

Lu Lu, Hiren Patel, and John J. Bissler
The Children's Hospital Research Foundation
Cincinnati, OH, USA

Optimized Sample Preparation for Tandem Capillary Electrophoresis Single-Stranded Conformational Polymorphism/ Heteroduplex Analysis

BioTechniques 33:318-325(August 2002)

ABSTRACT

Here we describe DNA sample preparation methods that allow the rapid, simultaneous generation of both single-stranded conformational polymorphism (SSCP) and heteroduplex DNA elements from a single sample in a single tube, which are suitable for direct injection into a capillary electrophoresis (CE) instrument with excellent sensitivity of genetic mutation detection. The p53 gene was used as a model DNA region for this study, which was performed on a high-throughput MegaBACE™ 96-capillary array electrophoresis instrument. We found that, contrary to the practice common in slab-gel SSCP analysis, denaturants such as formamide are incompatible with this novel technique because they result in homo- and heteroduplex peak broadening in

CE (possibly as a result of incomplete dsDNA re-hybridization) that reduces the peak resolution and hence the sensitivity of mutation detection. We also have found that PCR buffers, which are typically used to suspend samples for slab-gel heteroduplex analysis (HA), but which are less suitable for CE because of the presence of extra salt that reduces the efficiency of electrokinetic injection, may be substituted with a 10 mM Tris-HCl buffer (pH 8.5). The use of this Tris-HCl buffer for sample preparation provides both a high sensitivity of mutation detection by tandem SSCP/HA and high efficiency of electrokinetic injection by CE. In a related study (published elsewhere), we have applied this optimized protocol to the screening of a set of 32 mutant DNA samples from p53 exons 7 and 8 and recorded 100% sensitivity of mutation detection for tandem CE-SSCP/HA, whereas each individual method yielded lower sensitivity on its own (93% for SSCP and 75% for HA).

INTRODUCTION

In the past 10 years, single-stranded conformational polymorphism (SSCP) and heteroduplex analysis (HA) have rapidly gained popularity as two of the most straightforward and versatile methods to screen for DNA alterations (12). Traditionally, SSCP and HA are performed separately and have involved time-consuming (12–14 h), labor-intensive, and cumbersome electrophoresis of radioactively labeled DNA samples under nondenaturing conditions in a highly resolving cross-linked polyacrylamide slab gel and afforded relatively low sensitivity of mutation detection (60%–90%) (12). More recently, however, the advent of automated capillary electrophoresis (CE), in which electrophoretic separation of fluorescently labeled DNA is carried out within a microbore fused-silica capillary filled with an entangled polymer solution to serve as the "gel", has offered a viable alternative to slab-gel SSCP and slab-gel HA and allowed for the potential of much higher throughput, automation, sensitivity (reportedly >90%), and reproducibility of analysis (3,6).

Because of its nature, CE has a much lower tolerance than slab-gel electrophoresis for common sample impurities such as oligonucleotide primers, proteins, salt, and additives such as formamide and NaOH. Yet, to our knowledge, there have been no reports on the development of optimized DNA sample preparation protocols for CE-SSCP or CE-HA. Instead, published reports have mostly focused on the effects of temperature, pH, and DNA chain length on CE-SSCP performance (8,15), while using sample preparation protocols common in slab-gel electrophoresis, including routine

addition of formamide and NaOH to the sample. Studies of CE-HA are more rare in the literature.

We were motivated to carry out the following study of sample preparation protocols for CE-SSCP/HA when we found that these "standard" protocols for slab gels consistently yielded poor CE results (low signal-to-noise ratios, failed injections, and poor resolution of SSCP and HA DNA species). In the course of our studies, we have discovered what seems to be an optimal set of conditions that allow SSCP and HA to be carried out in tandem by CE, a method that involves simultaneous thermal generation and analysis of SSCP and HA conformers from a single sample (10,11,14). This novel technique requires both partial and complete re-annealing of dsDNA to form SSCP and HA conformers, respectively, which places even more stringent requirements on the amount of salt and denaturant contained in the DNA sample, since these additives affect dsDNA hybridization as well as the CE injection and separation performance. To date, there has been only one report on the use of tandem SSCP/HA in CE mode (9), and these critical sample preparation issues have not been discussed there or anywhere else.

MATERIALS AND METHODS

Tandem SSCP/HA

Two wild-type and two mutant DNA sample templates of exons 7 and 8 of the p53 gene (codon 248, CGG→GGG, and codon 273, CGT→AAT) were provided by the National Institute of Standards and Technology (Gaithersburg, MD, USA). PCR amplifications were done on a PTC-150 Minicycler™ (MJ Research, Waltham, MA, USA) using 10 pmol template DNA and a thermal cycling protocol and primers reported elsewhere (13). Crude PCR products, fluorescently labeled with FAM on the forward strand and with JOE on the reverse strand, were purified using either a Microcon®-PCR filtration device (Millipore, Bedford, MA, USA) or a QIAquick™ PCR Purification Kit (Qiagen, Valencia, CA, USA) according to the manufacturers' instructions. Two microliters of the DNA stock solutions were diluted with 10–40 µL of a 10 mM Tris-HCl buffer (pH 8.5) containing NaCl (0, 10, 20, 50 mM; Aldrich Chemical, Milwaukee, WI, USA) and formamide (0%, 50%, 95%; Aldrich Chemical) to make an SSCP/HA mixture. Formamide was deionized before use with mixed-bed ion exchange resin (Bio-Rad Laboratories, Hercules, CA, USA) according to the procedure recommended by the resin supplier. A 96-

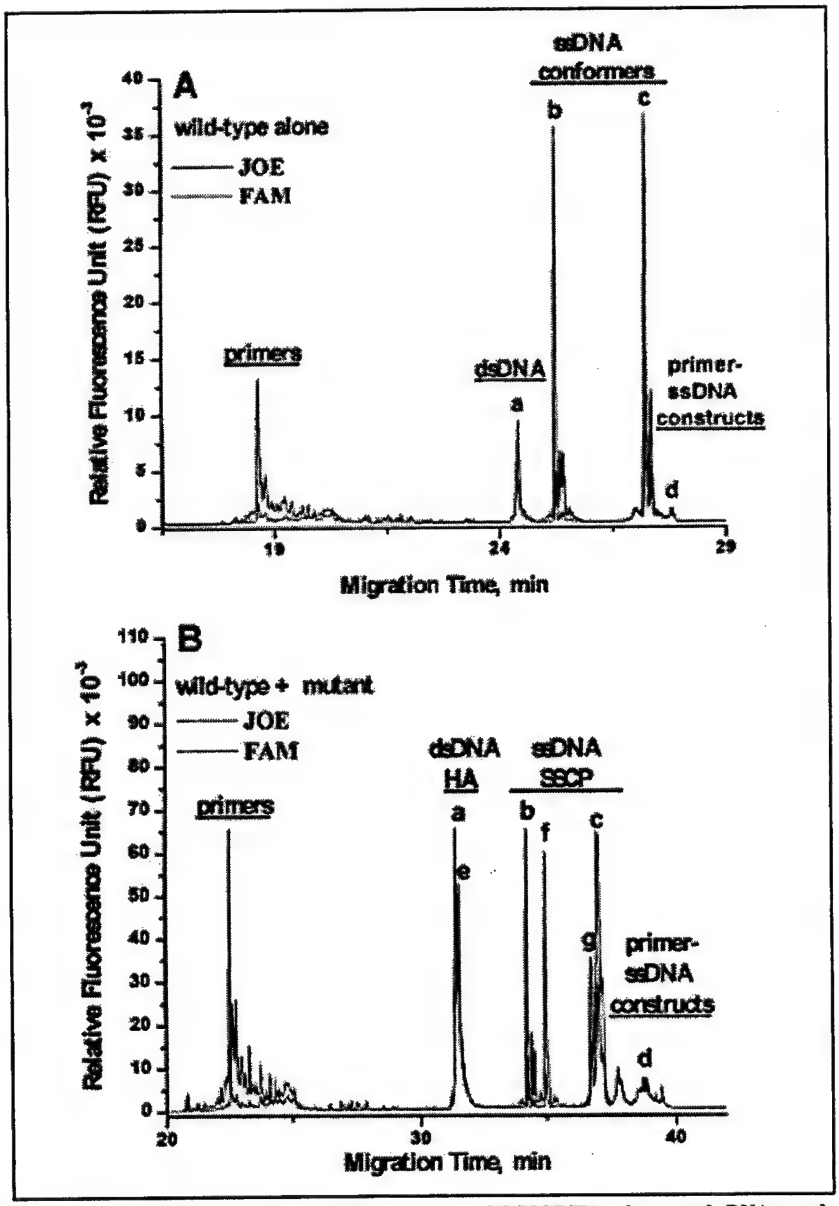

Figure 1. An example of mutation detection by tandem CE-SSCP/HA using a crude DNA sample prepared according to the optimized protocols. (A) p53 gene, exon 7, wild-type alone. (B) p53 gene, exon 7 wild-type + mutant (codon 248 CGG to GGG). a, homoduplexes (FAM + JOE); b, wild-type DNA reverse-strand SSCP (JOE); c, wild-type DNA forward-strand SSCP (FAM); d, primer-ssDNA constructs (FAM + JOE); e, heteroduplexes (FAM + JOE); f, mutant DNA reverse-strand SSCP (JOE); g, mutant DNA forward-strand SSCP (FAM). Electrophoresis conditions: injection 240 V/cm, 25–40 s, 27°C; CE 190 V/cm, 12 µA, 25–40 min, 27°C; bare fused-silica capillaries dynamically coated with polyDuramide (1) and filled with an optimized DNA separation matrix [a 4% (w/v) solution of linear polyacrylamide (M_r, 600 kDa) in a TBE buffer] (7).

well plate (Amersham Biosciences, Piscataway, NJ, USA) was loaded with SSCP/HA mixtures (three repeats for each sample) containing 5 μL DNA and denatured at 95°C for 3 min using a PTC-200™ thermal cycler (MJ Research). After denaturation, the plate was cooled, loaded into a 96-capillary MegaBACE™ (Amersham Biosciences) automated capillary electrophoresis instrument, and analyzed by CE with laser-induced fluorescence detection at 27°C. Raw data were converted to text files and processed using ORIGIN (Microcal Software, Northampton, MA, USA). Although only two MegaBACE arrays were used in this study, all six arrays could be used to screen 96 DNA specimens simultaneously for studies involving larger number of samples. The DNA samples could be kept at 4°C for at least 24 h and analyzed with no detrimental effects on the sensitivity of mutation detection.

RESULTS AND DISCUSSION

The tandem CE-SSCP/HA technique described here first involves the CE analysis of the wild-type p53 DNA (exon 7, 139 bp), as shown in Figure 1A. In the two-color detection mode, dsDNA (homo- and heteroduplexes) exhibits two peaks in the two fluorescence detection channels that are perfectly overlapping with respect to both position and amplitude, while ssDNA (SSCP conformers) shows just one major peak of one color, accompanied by a minor peak of the second color. The minor peak, which is due to some minimal overlap of FAM and JOE dye emission spectra, is centered in the same region as the major one, but the two peaks do not overlap in amplitude. Forward-strand ssDNA labeled with FAM is easily distinguished from reverse-strand ssDNA labeled with JOE. Based on these considerations, we are able to make the following unambiguous assignments of the major peaks seen in Figure 1A: peak labeled a, dsDNA (unresolved homoduplexes); b, reverse-strand SSCPs; c, forward-strand SSCPs (peaks labeled d will be discussed below). In the next phase of mutation detection, we perform a CE analysis of the mixture of the wild-type and the unknown (patient) DNA of interest, as shown in Figure 1B. A genetic sample is scored as containing mutant DNA if the electropherogram of a mixture of the wild-type and mutant DNA exhibits additional peaks associated with either dsDNA (heteroduplexes; Figure 1B, peaks labeled e), reverse-strand SSCPs (Figure 1B, peaks labeled f), or forward-strand SSCPs (Figure 1B, peaks labeled g), which are not found in the electropherogram of the separately analyzed wild-type DNA (Figure 1A, peaks labeled a, b, and c). Note that these peak patterns were highly reproducible from run to run.

Although salt concentrations of greater than 50 mM NaCl or KCl are recommended for the determination of the T_m of dsDNA to screen charge repulsion of phosphate groups in the DNA backbone and ensure its correct re-annealing, no strict guidelines exist for salt content in homo/heteroduplex DNA samples analyzed by CE-HA, or a combined CE-SSCP/HA analysis, despite the fact that these methods involve rapid DNA sample cooling and may require a substantial salt content to effect correct DNA folding or hybridization. At the same time, high salt content reduces the efficiency of electrokinetic injection into capillaries and is hence undesirable for CE analyses. Moreover, for SSCP analysis, PCR products are commonly diluted 10–100× with 50%–95% aqueous formamide, a potent denaturant, which further alters DNA hybridization kinetics. For example, high formamide concentrations (i.e., 95%) will depress the T_m of dsDNA by as much as 60°C, while an increase in salt concentration from 20–50 to 100 mM will increase the T_m by 5°C–10°C (4,5). These observations clearly warrant a more thorough study of the effects of these additives on the sensitivity of CE mutation detection by SSCP, HA, and tandem SSCP/HA.

We have investigated the combined effects of additives such as NaCl and formamide on the sensitivity of tandem CE-SSCP/HA (data not shown). Two wild-type and two mutant p53 gene specimens were used to prepare 12 sample solutions in 10 mM Tris-HCl buffer (pH 8.5) with varying ratios of NaCl and formamide. Our earlier experiments revealed that SSCP samples diluted with pure water in the absence of salt—conditions that are highly desirable in CE because of the efficient electrokinetic injection they allow—yield extremely broad peaks for poorly folded DNA (>20 s width at half-heights) that are unsuitable for mutation detection, confirming similar observations made earlier by Tian et al. (16). Significantly, we later found that 10 mM Tris-HCl (pH 8.5), a common DNA analysis buffer, used as a diluent does not require additional salt for the production of sharp (2–5 s width at half-heights) and reproducible (<2% standard deviation on peak positions) SSCP and HA peaks from a single sample. Therefore, this buffer was selected as a starting point in our optimization of the additives (formamide and NaCl). While these additives seemed to have little effect on SSCP patterns, reproducibility, or peak width, their presence reduced the efficiency of electrokinetic injection. Although the addition of formamide may perhaps be necessary in the preparation of DNA samples with high GC content to ensure complete denaturing, we did not find it useful in routine SSCP analysis of exons 7 and 8 of the p53 gene. Moreover, it reduced the intensity of the peaks for homo- and heteroduplexes and also made them broader, and hence less easily resolved. Therefore, we conclude that 10 mM Tris-HCl buffer (pH 8.5) without added salt or formamide is an excellent sample medium for tandem CE-SSCP/HA.

Typically, samples designated for SSCP analysis are denatured at 95°C and then either snap-cooled or allowed to cool naturally at room temperature, while those analyzed by HA are denatured and cooled slowly over a period of 30–60 min to ensure complete re-annealing. Although it was previously observed that some homo- and heteroduplexes can be formed during snap-cooling, doubts remained until recently about whether the fast kinetics of annealing allow for a perfect re-formation of the duplexes (2). To evaluate the effects of the cooling rate on the preparation of samples for tandem SSCP/HA, we denatured a DNA sample in a 10 mM Tris-HCl buffer (pH 8.5) and then either snap-cooled it, allowed it to cool naturally at room temperature, or gradually cooled it at a linear rate over

10, 20, 30, or 40 min. We observed that the first two modes of cooling yielded very similar electropherograms, in which SSCPs comprised 60%–80% and homo- and heteroduplexes comprised 20%–40% of the injected DNA (data not shown). However, snap-cooling produced less of the unwanted primer-ssDNA constructs. Apparently, during snap-cooling, fewer primers have sufficient time to find their complementary ssDNA and anneal to them. More gradual cooling of the denatured DNA samples was also attempted to balance the relative concentrations of homo- and heteroduplexes and SSCP conformers but led in all cases to the formation of homo- and heteroduplexes exclusively and a complete disappearance of the SSCP peaks.

The impact of the method of post-PCR DNA purification has also been investigated. Salt or oligonucleotides (DNA primers) present in the crude sample interfere with the electrokinetic injection of larger biomolecules, since these low-molecular weight charged species have higher electrophoretic mobilities than the SSCP/HA analytes and hence are preferentially injected. Also, as mentioned above, free primers can anneal to SSCP conformers during the cooling stage before CE analysis to form primer-ssDNA constructs. The peaks associated with these constructs showed two perfectly overlapping signals of the two different colors and had migration times similar to those of the SSCP conformers (Figure 1, A and B, peaks labeled d). The presence of these peaks correlated with a decrease in the intensity of the SSCP peaks and varied from mutant DNA sample to mutant DNA sample. Hence, these are spurious peaks that are not useful for the analysis. This peak assignment was confirmed by experiments in which SSCP/HA was done on a sample of p53 exon 8 that had been purified by preparative slab-gel electrophoresis and subsequently titrated with varying amounts of either the forward or reverse primer. It was observed that addition of the reverse primer led to the appearance of the extra peaks and concomitant disappearance of the forward-strand SSCP conformer. The formation of these primer-ssDNA constructs, which complicates the analysis and peak assignment of electropherograms, is most likely ubiquitous in the literature. We have found that this problem can be minimized by reducing concentrations of the stock solutions of primers from 20 pmol/μL (the standard PCR protocol) to 2–4 pmol/μL.

In summary, we have developed optimal sample preparation protocols for a tandem CE-SSCP/HA mutation detection of the p53 gene (exons 7 and 8) and can conclude that the best ap-

proach is PCR amplification of a template with a reduced primer content (2–4 pmol/μL), followed by 20–40× dilution with 10 mM Tris-HCl (pH 8.5) without additives (salt or formamide), denaturation at 95°C for 3 min, and snap-cooling on ice. In the interpretation of the resulting electropherograms, a two-color fluorescent labeling scheme was key to high-sensitivity, unambiguous mutation detection. We have used this optimized sample preparation protocol, along with an optimized linear polyacrylamide separation matrix, for the screening of a set of 32 mutant DNA samples derived from p53 exons 7 and 8, selected to include three different DNA sizes (139, 200, and 300 bp), both single- and two-base substitutions, and several different mutation positions (codons 242, 245, 248, 249, 273, and 282) (7). For this larger set of samples, we observed 100% sensitivity of mutation detection by a tandem CE-SSCP/HA approach (all 32 mutations were detected), whereas each individual method yielded lower sensitivity on its own (7). In particular, 30 of 32 mutations (93%) were detected by CE-SSCP, while 24 of 32 mutations (75%) were detected by CE-HA. For clinical implementation of a mutation detection method, sensitivity greater than 97% is desired. It seems reasonable to assume that these protocols will work well for any DNA sample. We are currently testing these sample preparation methods for the mutation analysis of the PTEN and β-catenin genes derived from human prostate tumors to test their broader generality.

REFERENCES

1. **Albarghouthi, M.N., B.A. Buchholz, P.J. Huiberts, T.M. Stein, and A.E. Barron.** 2002. Poly-*N*-hydroxyethylacrylamide (poly-Duramide™): a novel, hydrophilic, self-coating polymer matrix for DNA sequencing by capillary electrophoresis. Electrophoresis *23*:1429-1440.
2. **Axton, R.A., I.M. Hanson, J. Love, A. Seawright, J. Prosser, and V. van Heyningen.** 1997. Combined SSCP/heteroduplex analysis in the screening for PAX6 mutations. Mol. Cell. Probes *11*:287-292.
3. **Beale, S.C.** 1998. Capillary electrophoresis. Anal. Chem. *70*:279R-300R.
4. **Bonner, G. and A.M. Klibanov.** 2000. Structural stability of DNA in nonaqueous solvents. Biotech. Bioeng. *68*:339-344.
5. **Casey, J. and N. Davidson.** 1977. Rates of formation and thermal stabilities of RNA:DNA and DNA:DNA duplexes at high concentrations of formamide. Nucleic Acids Res. *4*:1539-1552.
6. **Haleem, I.J.** 2000. A decade of capillary electrophoresis. Electrophoresis *21*:1921-1939.
7. **Kourkine, I.V., C.N. Hestekin, B. Buchholz, and A.E. Barron.** 2002. High-throughput, high-sensitivity mutation detection by tandem single-strand conformation polymorphism (SSCP) -heteroduplex analysis (HA) capillary array electrophoresis (CAE). Anal. Chem. *74*:2565-2572.
8. **Kourkine, I.V., C.N. Hestekin, and A.E. Barron.** 2002. Technical challenges in applying capillary electrophoresis (CE)-single strand conformation polymorphism (SSCP) for routine genetic analysis. Electrophoresis *23*:1375-1385.
9. **Kozlowski, P. and W.J. Krzyzosiak.** 2001. Combined SSCP/duplex analysis by capillary electrophoresis for more efficient mutation detection. Nucleic Acids Res. *29*:e71.
10. **Larsen, L.A., P.S. Andersen, J.K. Kanters, J.R. Jacobsen, J. Vuust, and M. Christiansen.** 1999. A single strand conformation polymorphism/heteroduplex (SSCP/HA) method for detection of mutations in 15 exons of the KVLQT1 gene, associated with long QT syndrome. Clin. Chim. Acta *280*:113-125.
11. **Liechti-Gallati, S., V. Schneider, D. Neeser, and R. Kraemer.** 1999. Two buffer PAGE system-based SSCP/HD analysis: a general protocol for rapid and sensitive mutation screening in cystic fibrosis and any other human genetic disease. Eur. J. Hum. Genet. *7*:590-598.
12. **Nataraj, A.J., I. Olivos-Glander, N. Kusukawa, and W.E. Highsmith, Jr.** 1999. Single-strand conformation polymorphism and heteroduplex analysis for gel-based mutation detection. Electrophoresis *20*:1177-1185.
13. **O'Connell, C.D., D.H. Atha, M. Oldenburg, J. Tian, M. Siebert, R. Handrow, K. Grooms, L. Heisler, and M. de Arruda.** 1999. Detection of p53 gene mutation: analysis by single-strand conformation polymorphism and Cleavase fragment length polymorphism. Electrophoresis *20*:1211-1223.
14. **Ravnik-Glavac, M., D. Glavac, and M. Dean.** 1994. Sensitivity of single-strand conformation polymorphism and heteroduplex method for mutation detection in the cystic fibrosis gene. Hum. Mol. Genet. *3*:801-807.
15. **Ren, J.** 2000. High-throughput single-strand conformation polymorphism analysis by capillary electrophoresis. J. Chromatogr. B *741*:115-128.
16. **Tian, H., L.C. Brody, and J.P. Landers.** 2000. Rapid detection of deletion, insertion, and substitution mutations via heteroduplex analysis using capillary- and microchip-based electrophoresis. Genome Res. *10*:1403-1413.

We thank Dr. Catherine O'Connell of the National Institute of Standards and Technology for providing us with 32 mutant DNA specimens of the p53 gene and Dr. Karin Klein of Northwestern Hospital for helpful discussions on PCR protocols. We also thank Erin Doherty and Methal Albarghouthi for their helpful comments, BioWhittaker for the polyDuramide monomer, and Amersham Biosciences Molecular Dynamics for the loan of the MegaBACE instrument.

Address correspondence to Prof. Annelise E. Barron, Northwestern University, Department of Chemical Engineering, 2145 Sheridan Road, Evanston, IL 60208, USA. e-mail: a-barron@northwestern.edu

Received 11 January 2002; accepted 19 April 2002.

Igor V. Kourkine, Christa N. Hestekin, Soffia O. Magnusdottir, and Annelise E. Barron
Northwestern University
Evanston, IL, USA

THE JOURNAL OF BIOLOGICAL CHEMISTRY
Vol. 277, No. 41, Issue of October 11, pp. 38159–38167, 2002
Printed in U.S.A.

Proteinase Suppression by E-cadherin-mediated Cell-Cell Attachment in Premalignant Oral Keratinocytes*

Received for publication, March 12, 2002, and in revised form, July 16, 2002
Published, JBC Papers in Press, July 23, 2002, DOI 10.1074/jbc.M202384200

Hidayatullah G. Munshi‡§¶‖, Supurna Ghosh¶, Subhendu Mukhopadhyay**, Yi I. Wu**, Ratna Sen**, Kathleen J. Green§ §§, and M. Sharon Stack§**‡‡¶¶**

*From the ‡Division of Hematology/Oncology, Department of Medicine, Departments of **Cell and Molecular Biology, ‡‡Obstetrics and Gynecology, §§Pathology and Dermatology, Feinberg School of Medicine, Northwestern University and the §Robert H. Lurie Comprehensive Cancer Center of Northwestern University, Chicago, Illinois 60611*

The expression and activity of epithelial proteinases is under stringent control to prevent aberrant hydrolysis of structural proteins and disruption of tissue architecture. E-cadherin-dependent cell-cell adhesion is also important for maintenance of epithelial structural integrity, and loss of E-cadherin expression has been correlated with enhanced invasive potential in multiple tumor models. To address the hypothesis that there is a functional link between E-cadherin and proteinase expression, we have examined the role of E-cadherin in proteinase regulation. By using a calcium switch protocol to manipulate junction assembly, our data demonstrate that initiation of *de novo* E-cadherin-mediated adhesive contacts suppresses expression of both relative matrix metalloproteinase-9 levels and net urinary-type plasminogen activator activity. E-cadherin-mediated cell-cell adhesion increases both phosphatidylinositol 3′-kinase (PI3-kinase)-dependent AKT phosphorylation and epidermal growth factor receptor-dependent MAPK/ERK activation. Pharmacologic inhibition of the PI3-kinase pathway, but not the epidermal growth factor receptor/MAPK pathway, prevents E-cadherin-mediated suppression of proteinases and delays junction assembly. Moreover, inhibition of junction assembly with a function-blocking anti-E-cadherin antibody stimulates proteinase-dependent Matrigel invasion. As matrix metalloproteinase-9 and urinary-type plasminogen activator potentiate the invasive activity of oral squamous cell carcinoma, these data suggest E-cadherin-mediated signaling through PI3-kinase can regulate the invasive behavior of cells by modulating proteinase secretion.

Degradation of the extracellular matrix by proteolytic enzymes is necessary for a number of normal and pathological processes, including embryonic development, tissue resorption and remodeling, angiogenesis, and wound healing (1–3). Proteinases have also been implicated in the invasion and metastasis of malignant cells (4–6). Predominant among these enzymes are the matrix metalloproteinases (MMPs)[1] and the plasminogen activator (PA) urinary-type PA (uPA) (7–10). MMPs are a large family of metalloendopeptidases with activity directed against a variety of extracellular matrix substrates (11). MMP-9 (gelatinase B), a 92-kDa gelatinase that efficiently degrades native type IV collagen, has been implicated in tumor dissemination, as evidenced by enhanced MMP-9 expression in tumor samples exhibiting matrix invasion and distant metastases (12). This is supported by studies using tumor-bearing MMP-9-deficient mice, which exhibit decreased propensity to develop metastatic foci, indicating that MMP-9 plays a critical role in tumor development (5). Post-translational regulation of MMP-9 activity is mediated by interaction with tissue inhibitor of metalloproteinases (TIMP)-1 which forms a 1:1 noncovalent inactive enzyme-inhibitor complex (12). Under many conditions, secretion of MMP-9 and TIMP-1 is coordinately regulated (12).

In addition to MMP-9, up-regulation of uPA expression has also been correlated with malignant progression of a wide variety of neoplasms (9). uPA is a serine proteinase that functions in the conversion of the circulating zymogen plasminogen to the active enzyme plasmin (9). Plasmin is a broad spectrum serine proteinase that can directly cleave a number of protein substrates (9), as well as activate many additional proteinase zymogens including pro-MMP-9 (13). uPA is localized to the cell surface via interaction with a glycosylphosphatidylinositol-anchored receptor, designated uPA receptor or uPAR (9). Proteolytic activity is also regulated by the serpin plasminogen activator inhibitor 1 (PAI-1) which forms a covalent enzyme-inhibitor complex with both free and receptor-localized uPA (9). In a number of tumor models, down-regulation of either uPA or its receptor decreases invasion and reduces metastatic potential (14, 15).

Like proteolytic enzymes, dysregulation of adhesion molecules is often observed in malignant cells. Cadherins are a family of cell surface adhesion molecules that participate in Ca^{2+}-dependent cell-cell adhesion (16) and thus are essential for maintenance of tissue integrity. E-cadherin is a widely distributed transmembrane intercellular adhesion molecule

* This work was supported in part by NIDCR Research Grant PO1 DE12328 from the National Institutes of Health (to M. S. S. and K. J. G.) and National Institutes of Health Grant RO1 CA 85870 (to M. S. S.). The costs of publication of this article were defrayed in part by the payment of page charges. This article must therefore be hereby marked "*advertisement*" in accordance with 18 U.S.C. Section 1734 solely to indicate this fact.

¶ Both authors contributed equally to this work.

‖ Supported by NCI Clinical Oncology Research Training Program Grant T32 CA79447 from the National Institutes of Health.

¶¶ To whom correspondence should be addressed: Dept. of Cell and Molecular Biology, Northwestern University Medical School, 303 E. Chicago Ave., Tarry 8-715, Chicago IL 60611. Tel.: 312-908-8216; Fax: 312-503-7912; E-mail: mss130@northwestern.edu.

[1] The abbreviations used are: MMP-9, matrix metalloproteinase 9; TIMP-1, tissue of inhibitor of metalloproteinases 1; uPA, urinary-type plasminogen activator; uPAR, uPA receptor; PAI-1, plasminogen activator inhibitor 1; MEK, mitogen-activated protein kinase/extracellular signal-regulated kinase kinase; MAPK, mitogen-activated protein kinase; ERK, extracellular signal-regulated kinase; PI3-kinase, phosphatidylinositol 3′-kinase; ELISA, enzyme-linked immunosorbent assay; EGFR, epidermal growth factor receptor; PBS, phosphate-buffered saline; pp, phosphoprotein.

(17). In addition to functioning in cell-cell adhesion, the cytoplasmic tail of E-cadherin binds to β- or γ-catenin/plakoglobin, thereby providing a mechanism for association with additional proteins, including signaling molecules such as phosphatidylinositol 3′-kinase (PI3-kinase) and epidermal growth factor receptor (18–21). Loss of E-cadherin expression is frequently observed in carcinomas (22, 23), and transfection of ectopic E-cadherin into breast (24), colon (25), and prostate cancer cells (26) decreases cellular invasion.

In multiple tumor models, loss of E-cadherin expression and increased proteinase activity correlate with more invasive and metastatic tumors (9, 12, 14, 15, 22, 23, 27). To address the hypothesis that there is a functional link between E-cadherin and proteinase expression, in the current study we have examined the role of E-cadherin in the regulation of proteinase expression in premalignant oral keratinocytes. Our data demonstrate that initiation of *de novo* E-cadherin-mediated cell-cell adhesion suppresses both relative MMP-9 levels and net uPA activity in premalignant oral keratinocytes. Concomitant with decreased proteinase expression, secretion of TIMP-1 and PAI-1 is also down-regulated. E-cadherin-mediated cell-cell adhesion increases PI3-kinase-dependent AKT activation and epidermal growth factor receptor (EGFR)-dependent mitogen-activated protein kinase (MAPK)/extracellular signal regulated kinase (ERK) activation. Inhibition of the PI3-kinase pathway, but not the EGFR-MAPK pathway, interferes with formation of adherens junctions and prevents E-cadherin-mediated suppression of proteinases. Furthermore, prevention of junction assembly with a function-blocking E-cadherin antibody stimulates proteinase-dependent Matrigel invasion. Together these data support the hypothesis that E-cadherin-mediated signaling via PI3-kinase can regulate the invasive behavior of cells by modulating proteinase expression.

EXPERIMENTAL PROCEDURES

Materials—Gelatin, cell culture reagents, D-Val-Leu-Lys-*p*-nitroanilide, rat anti-E-cadherin (DECMA clone), and peroxidase-conjugated secondary antibodies were purchased from Sigma. Keratinocyte-SFM was obtained from Invitrogen. Plasminogen was purified by affinity chromatography from outdated human plasma as described previously (28). Anti-mouse E-cadherin (HECD-1 clone) and isotype-specific IgG1 antibodies were obtained from Calbiochem; anti-phosphorylated p42/p44 (MAPK/ERK) was obtained from Promega (Madison, WI); anti-ERK1/2 (anti-p42/p44) antibody and anti-AKT antibody were purchased from Santa Cruz Biotechnology (Santa Cruz, CA); anti-phosphorylated AKT (Thr-308) was obtained from Upstate Biotechnology, Inc.; anti-uPAR antibody (399R) and function-blocking anti-uPA antibody (394) were obtained from American Diagnostica (Greenwich, CT); and Alexa Fluor 594 goat anti-mouse and anti-rat antibodies were from Molecular Probes (Eugene, OR). TIMP-1 and MMP-9 ELISA kits were from Oncogene Research Products (Boston, MA), and PAI-1 ELISA kit was purchased from American Diagnostica. The mitogen-activated protein kinase/extracellular signal-regulated kinase kinase (MEK) inhibitor PD98059, PI3-kinase inhibitor LY294002, and EGFR-specific inhibitor AG1478 were obtained from Calbiochem. The MMP inhibitor GM6001 was purchased from Chemicon (Temecula, CA). Polyvinylidene difluoride membrane was from Amersham Biosciences (Arlington Heights, IL). Supersignal enhanced chemiluminescence (ECL) reagent, EZ-Link Sulfo-NHS-Biotin, and UltraLink Immobilized Streptavadin Gel were obtained from Pierce. Microcon 10 microconcentrators were purchased from Millipore (Bedford, MA).

Cell Cultures—Premalignant oral keratinocytes (pp126 cells) were the gift of Dr. D. Oda (University of Washington, Seattle, WA) (29, 30). Early passage (between 3 and 8) pp126 cells were maintained at 37 °C in a humidified atmosphere of 5% CO_2 in keratinocyte-SFM containing 0.09 mM calcium and supplemented with 100 units/ml penicillin, 100 ng/ml EGF, and 50 μg/ml bovine pituitary extract.

E-cadherin Activation—The calcium switch method was utilized to assess the consequences of *de novo* E-cadherin activation (19–21, 31, 32). Briefly, pp126 cells were seeded at a constant density (1.5×10^5 cells/well) in 12-well tissue culture plates. After 24 h, the cells were starved for 6–8 h, and calcium was removed by incubation with Keratinocyte-SFM containing 4 mM EGTA and 1 mM $MgCl_2$ at 37 °C. After 30 min the calcium-free medium was removed, and Keratinocyte-SFM containing 0.09 mM calcium was immediately added to induce E-cadherin mediated cell-cell interactions (designated "E-cadherin activation +"). In control experiments, cells received fresh media in the absence of EGTA such that original junctions are maintained, but *de novo* activation of E-cadherin is not induced (designated "E-cadherin activation −"). In selected experiments, either anti-E-cadherin antibody (HECD-1 clone) or isotype-specific control antibody was added to the calcium-containing medium at 10 μg/ml. In additional studies, the PI3-kinase inhibitor LY294002 (10 μM), the MEK inhibitor PD98059 (5 μM), the EGFR inhibitor AG1478 (250 nM), or the appropriate vehicle was added to the medium. Conditioned medium was collected for proteinase analysis after 24–36 h.

Immunfluorescence Microscopy—pp126 cells were grown on glass coverslips at 37 °C in Keratinocyte-SFM. Following a 30-min incubation with serum-free medium containing 4 mM EGTA and 1 mM $MgCl_2$, cells were incubated with Keratinocyte-SFM containing 0.09 mM Ca^{2+} in the presence of either control IgG antibody or anti-E-cadherin antibody (HECD-1, 10 μg/ml). In additional studies, the PI3-kinase inhibitor LY294002 (10 μM), the MEK inhibitor PD98059 (5 μM), the EGFR inhibitor AG1478 (250 nM), or the appropriate vehicle was added to the medium. For immunofluorescence staining, cells were washed with PBS and fixed with ice-cold methanol for 2 min or with 3.7% formaldehyde for 5 min followed by 0.5% Triton X-100 for 7 min. After washing with PBS, cells were blocked with 1% bovine serum albumin in PBS and incubated with mouse anti-E-cadherin antibody (HECD-1) or rat anti-E-cadherin antibody (DECMA) for 1 h at 37 °C. After three washes with PBS, cells were incubated for 1 h at room temperature with Alexa Fluor 594-labeled goat anti-mouse or anti-rat antibody. Glass coverslips were washed with PBS three times, mounted, and examined under a UV microscope (Nikon) using the appropriate filter.

Analysis of MMP-9 and TIMP-1 Expression—Gelatinase activities in the conditioned media at 36 h were determined using SDS-PAGE gelatin zymography as described previously (33). Briefly, SDS-PAGE gels (9% acrylamide) were co-polymerized with 0.1% gelatin, and samples were electrophoresed without reduction or boiling using 5× Laemmli sample buffer (34). SDS was removed through a 30-min incubation in 2.5% Triton X-100, and gels were incubated in 20 mM glycine, pH 8.3, 10 mM $CaCl_2$, 1 μM $ZnCl_2$ at 37 °C for 24–36 h. The gels were stained with Coomassie Blue to visualize zones of gelatinolytic activity. MMP-9 levels in the conditioned media were also quantified by ELISA (Oncogene Research Products) following concentration of the conditioned media 25–30-fold with Microcon 10. Levels of TIMP-1 protein in the conditioned media were quantified by ELISA (Oncogene Research Products) according to the manufacturer's specifications.

Analysis of uPA Activity and PAI-1 Protein Levels—Net uPA activity in the conditioned media at 24 h was quantified using a coupled assay to monitor plasminogen activation and resulting hydrolysis of a colorimetric substrate (Val-Leu-Lys-*p*-nitroanilide) as described previously (28). Levels of PAI-1 protein in the conditioned media were quantified by ELISA (American Diagnostica) according to the manufacturer's specifications.

Cell Surface Biotinylation—pp126 cells were grown in a 6-well plate, washed with ice-cold PBS, and incubated at 4 °C with gentle shaking for 30 min with 0.5 mg/ml cell-impermeable Sulfo-NHS-Biotin in ice-cold PBS, followed by washing with 100 mM glycine to quench free biotin. Cells were then detached by scraping, lysed in modified RIPA buffer (50 mM Tris, pH 7.4, 150 mM NaCl, 5 mM EDTA, 1% Triton X-100, and 0.1% SDS) with proteinase inhibitors, and clarified by centrifugation. To isolate biotinylated cell-surface proteins, equal amounts of protein from each of the samples were incubated with streptavidin beads at 4 °C for 14 h, followed by centrifugation. After boiling in Laemmli sample dilution buffer (34) to dissociate streptavidin bead-biotin complexes, the samples were analyzed by SDS-PAGE (9% gels) and immunoblotted for uPAR (1:1000, American Diagnostica, clone 399R).

MAPK and AKT Activation—E-cadherin was activated by the calcium switch method as described above, and at the indicated time points cells were lysed in modified RIPA buffer containing 20 mM sodium fluoride, 10 mM sodium pyrophosphate, 1 mM sodium orthovanadate, 1 μg/ml aprotinin, 1 μM pepstatin, and 10 μM leupeptin. The samples were analyzed by SDS-PAGE (9% gels), and the blots were probed with anti-ERK1/2 antibody (1:1000) or with anti-AKT antibody (1:1000) to detect total ERK1/2 or AKT expression or with anti-phosphorylated ERK1/2 antibody (1:1000) or anti-phosphorylated AKT antibody (1:1000) to detect active (phosphorylated) forms of ERK or AKT.

Analysis of Invasion—Invasive activity was quantified using a Boyden Chamber (8-μm pore size) coated with Matrigel (10 μg). Cells (2×10^5) were added to the chamber in 500 μl of serum-free medium with 25 μg/ml of E-cadherin function-blocking antibody (HECD-1 clone) or isotype-specific control antibody, followed by incubation for 40 h. Nonmigrating cells were removed from the upper chamber with a cotton swab; filters were fixed and stained with Diff-Quik Stain, and migrating cells adherent to the underside of the filter were enumerated using an ocular micrometer and counting a minimum of 10 high-powered fields. Data are expressed as relative migration (number of cells/field). In selected experiments, the proteinase dependence of invasion was determined by quantifying invasion in the presence of the MMP inhibitor GM6001 (2.5 μM) (Chemicon) or the function-blocking anti-uPA antibody (15 μg/ml) (American Diagnostica, clone 394).

RESULTS

Calcium-dependent Cell-Cell Adhesion Modulates Proteinase and Inhibitor Expression—E-cadherin dependent cell-cell adhesion is important for the maintenance of epithelial structural integrity, and the loss of E-cadherin expression has been shown to correlate with increased invasive potential of both carcinoma cell lines and human tumor samples (21, 22, 27, 35). Recent data demonstrate that specific proteinases, including tumor-associated MMPs, can modulate cell-cell adhesion by cleaving E-cadherin (36–38). As E-cadherin itself couples to signal transduction pathways (18–21), the hypothesis that E-cadherin may participate in proteinase regulation was tested in premalignant gingival keratinocytes (pp126 cells). The calcium switch method, in which E-cadherin-mediated cell-cell adhesion was disrupted with EGTA treatment and restored by replacing Ca^{2+}, was utilized to initiate *de novo* adherens junction assembly (19–21, 31, 32). Control cells present a typical pattern of E-cadherin staining at the level of cell-cell contacts (Fig. 1*A*); however, in cells treated with EGTA, E-cadherin is absent from cell junctions (Fig. 1*B*). After addition of calcium, adherens junctions are again formed (Fig. 1*C*), with complete restoration by 1 h of treatment (Fig. 1*D*). To evaluate the effect of E-cadherin activation on proteinase expression, after 24–36 h conditioned media were collected and analyzed. Gelatin zymography demonstrated that calcium-mediated cell-cell adhesion (designated *E-cad Actn* +) decreased relative MMP-9 levels (Fig. 1*E*). This was confirmed using an ELISA kit that recognizes both free and TIMP-1-complexed MMP-9, demonstrating a 6.5-fold decrease in MMP-9 levels in concentrated conditioned media following calcium-mediated cell-cell adhesion (Fig. 1*E*). Concomitant with MMP-9 down-regulation, *net* uPA activity was also decreased by 2–3-fold (Fig. 1*F*). Evaluation of proteinase inhibitor expression by ELISA indicated a coordinate decrease in both TIMP-1 and PAI-1 levels (Table I). Disruption of cell-cell junctions using the calcium switch method did not affect cell proliferation (data not shown).

Proteinase Suppression Following Cell-Cell Adhesion Requires Engagement of E-cadherin—To confirm that proteinase suppression is due to E-cadherin engagement and is not an unrelated consequence of calcium modulation, a function-blocking anti-E-cadherin antibody (HECD-1 clone) was utilized. To verify that the HECD-1 antibody blocked cell-cell attachment following the calcium switch protocol, cells were treated with EGTA to dissociate cell-cell junctions and then incubated for 40 min in calcium-containing medium in the presence of either function-blocking E-cadherin antibody (HECD-1, 10 μg/ml) or isotype-matched control IgG. Cells were then processed for immunofluorescence microscopy using rat anti-E-cadherin antibody (DECMA clone). Similar to the control experiment shown in Fig. 1*B*, no E-cadherin staining is visible at cell-cell junctions following EGTA treatment (Fig. 2*A*). Following calcium restoration, junctional E-cadherin is prevalent in IgG-treated cells (Fig. 2*B*), but not in anti-E-cadherin-treated cells (Fig. 2*C*), demonstrating that the antibody indeed blocks cell-cell attachment. To assess the effect of E-cadherin function blocking antibodies on proteinase suppression, cell-cell junctions were disrupted by calcium chelation, and junction assembly was initiated by the addition of calcium in the presence of

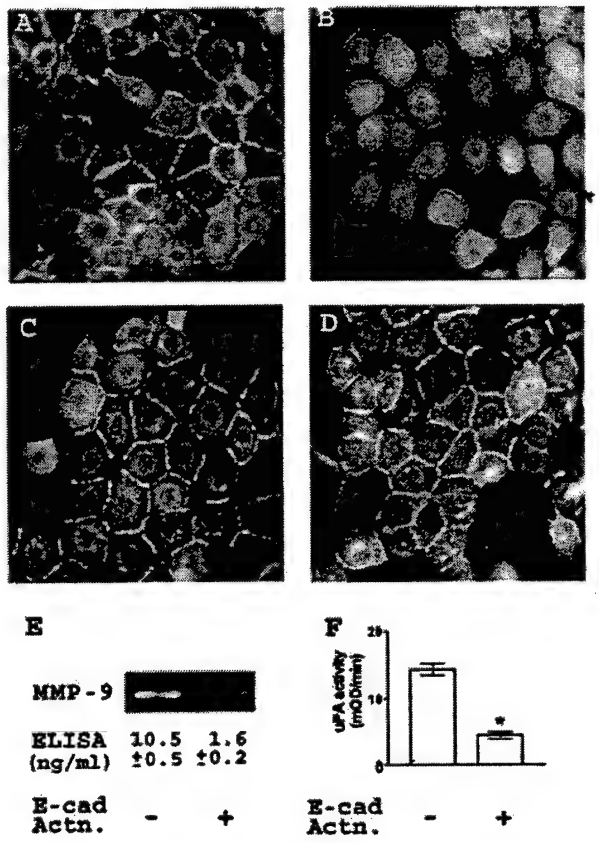

FIG. 1. **Calcium-mediated cell-cell adhesion decreases proteinase expression.** *A–D*, pp126 cells were left untreated (*A*) or treated with 4 mM EGTA for 30 min (*B–D*). To induce E-cadherin activation, the EGTA-containing medium was then replaced with calcium-containing Keratinocyte-SFM (0.09 mM) for 30 min (*C*) or 1 h (*D*). Cells were fixed, incubated with anti-E-cadherin antibody (HECD-1), and detected with Alexa Fluor 594-conjugated anti-mouse antibody. *E*, E-cadherin was activated (designated *E-cad Actn.* +) in pp126 cells using the calcium switch method as described under "Experimental Procedures." Control cells (designated *E-cad Actn.* −) were left untreated. Conditioned media were collected at 36 h and analyzed for MMP-9 expression by gelatin zymography and by ELISA as described under "Experimental Procedures." *F*, uPA activity was analyzed in the conditioned media at 24 h using a coupled colorimetric plasminogen activation assay as described under "Experimental Procedures." The results represent the mean ± S.E. of five different experiments. *, significantly different from control with $p < 0.001$.

TABLE I

Calcium-mediated cell-cell attachment suppresses TIMP-1 and PAI-1

E-cadherin (E-cad)-mediated cell-cell adhesion was disrupted by incubating pp 126 cells with 4 mM EGTA for 30 min and then re-initiated by replacing the medium with calcium-containing keratinocyte-SFM (0.09 mM, designated E-cad activation +). Conditioned media were collected after 24–36 h, and TIMP-1 and PAI-1 levels were analyzed by ELISA according to the manufacturer's specifications. The results represent the mean ± S.E. of three individual experiments.

E-cad activation	TIMP-1	PAI-1
	ng/ml	
−	72 ± 3	40 ± 2
+	45 ± 3[a]	16 ± 1[b]

[a] Value significantly different from control with $p < 0.005$.
[b] Value significantly different from control with $p < 0.001$.

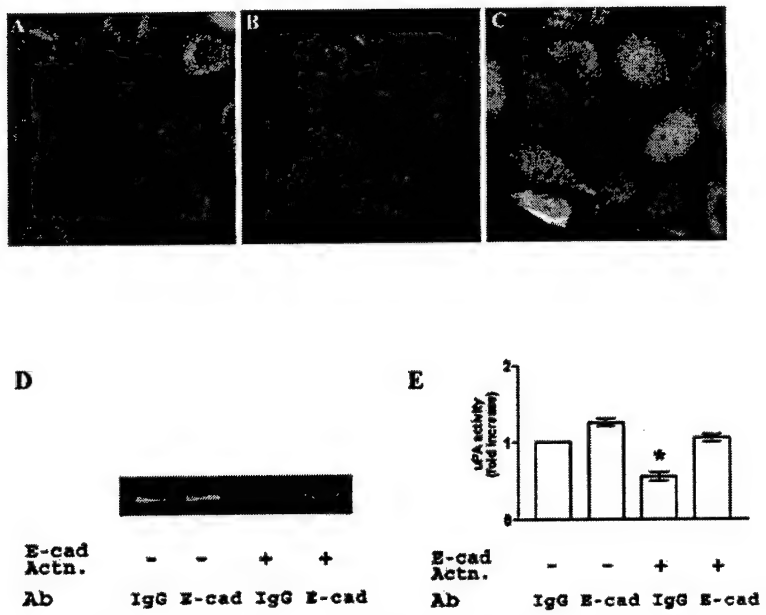

FIG. 2. **Proteinase suppression following cell adhesion requires engagement of E-cadherin.** *A–C*, pp126 cells were treated with 4 mM EGTA for 30 min (*A–C*). The EGTA-containing medium was replaced with Keratinocyte-SFM containing 0.09 mM calcium for 45 min in the presence of control IgG (10 μg/ml) (*B*) or function-blocking anti-E-cadherin antibody (HECD-1, 10 μg/ml) (*C*). Cells were fixed, incubated with anti-E-cadherin antibody (DECMA), and detected with Alexa Fluor 594-conjugated anti-rat antibody. *D* and *E*, cells were either left untreated or underwent activation of E-cadherin using the calcium switch method in the presence of function-blocking anti-E-cadherin antibody (*Ab*) (HECD-1, 10 μg/ml) or isotype-matched IgG (10 μg/ml) as described under "Experimental Procedures." *D*, conditioned media were collected at 36 h and analyzed for MMP-9 activity by gelatin zymography. *E*, uPA activity was analyzed in the conditioned media at 24 h using a coupled colorimetric plasminogen activation assay as described under "Experimental Procedures." The results represent the mean ± S.E. of three different experiments. *, significantly different from control with $p < 0.01$.

blocking antibody (10 μg/ml) to prevent formation of adherens junctions. Control samples contained an equal concentration of isotype-specific IgG. In additional controls, antibodies were added without prior disruption of cell-cell junctions by calcium chelation (designated *E-cad Actn* −). Blocking E-cadherin engagement prevented the adhesion-mediated suppression of both the relative MMP-9 levels (Fig. 2*D*, *4th lane*) and the net uPA activity (Fig. 2*E*). Addition of the function-blocking HECD-1 antibody at 10 μg/ml without prior junction disruption (designated *E-cad Actn* −) was ineffective (Fig. 2, *D*, *2nd lane*, and *E*). Moreover, in IgG-treated control samples, in which junction reformation was not prevented, proteinase expression was suppressed (Fig. 2, *D*, *3rd lane*, and *E*). Similar results were obtained for TIMP-1 and PAI-1, in which suppression of expression by E-cadherin engagement was also blocked by anti-E-cadherin antibody (Table II). In control experiments, treatment of cells with EGTA in the presence or absence of blocking antibody did not alter proliferation (data not shown). Together these data demonstrate that *de novo* E-cadherin engagement suppresses proteinase expression.

Because uPA activity can also be modulated by cell surface association (9), the effect of E-cadherin-mediated cell-cell adhesion on uPAR expression was evaluated. Cell-cell junctions were disrupted by calcium chelation, and the samples were treated with either HECD-1 blocking antibody or control IgG as described above. Cells were then incubated with cell-impermeable NHS-biotin to label surface proteins and lysed in modified RIPA buffer. Following precipitation of surface-labeled proteins with streptavidin beads, samples were electrophoresed and probed for uPAR by immunoblotting. There was no change in uPAR surface expression induced by E-cadherin-mediated cell-cell adhesion (Fig. 3). In addition, there was no change in total cellular uPAR protein levels (surface and cytoplasmic) as measured by Western blot (data not shown). These data suggest that, although the net uPA activity is suppressed, the receptor remains available.

TABLE II
Suppression of TIMP-1 and PAI-1 following cell adhesion requires E-cadherin

E-cadherin (E-cad)-mediated cell-cell adhesion was disrupted by incubating pp 126 cells with 4 mM EGTA for 30 min and then re-initiated by replacing the medium with calcium-containing keratinocyte-SFM (0.09 mM, designated E-cad activation +) in the presence of anti-E-cadherin antibody (HECD-1, 10 μg/ml) or isotype-matched IgG (10 μg/ml). Conditioned media were collected after 24–36 h, and TIMP-1 and PAI-1 levels in the conditioned media were analyzed by ELISA according to the manufacturer's specifications.

Antibody	E-cad activation	TIMP-1	PAI-1
		ng/ml	
IgG	−	94 ± 6	25 ± 2
E-cad	−	83 ± 5	23 ± 2
IgG	+	46 ± 3[a]	13 ± 1[b]
E-cad	+	70 ± 5	21 ± 1

[a] Values significantly different from control with $p < 0.001$.
[b] Values significantly different from control with $p < 0.01$.

Inhibition of MAPK Does Not Block E-cadherin-mediated Suppression of Proteinases—Because we have reported previously (30) that MAPK activation regulates proteinase expression in pp126 cells, levels of phosphorylated (active) ERK1/2 were assessed in pp126 cells following the calcium switch. Cells were lysed at various time points after calcium-induced initiation of junction assembly, and samples were analyzed by Western blotting using antibodies directed against total ERK1/2 or the phosphorylated (active) species of ERK 1/2. A time-dependent phosphorylation of ERK1/2 following *de novo* engagement of E-cadherin was observed in pp126 cells (Fig. 4*A*), with maximal MAPK activation at ~15 min. There was no change in the total amount of ERK1/2 protein (Fig. 4*A*). To confirm that

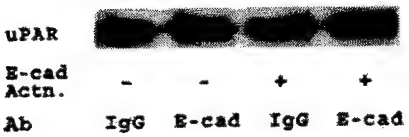

FIG. 3. **E-cadherin-mediated cell-cell adhesion does not affect surface uPAR expression.** Cells were either left untreated (designated *E-cad Actn.* −) or underwent activation of E-cadherin (designated *E-cad Actn.* +) using the calcium switch method in the presence of function-blocking anti-E-cadherin antibody (*Ab*) (HECD-1, 10 μg/ml) or isotype-matched IgG (10 μg/ml) as described under "Experimental Procedures." After 24 h the cells were surface-biotinylated and lysed. Samples were immunoprecipitated with streptavidin beads to isolate cell-surface proteins and electrophoresed on a 9% SDS-polyacrylamide gel. The membranes were immunoblotted with anti-uPAR antibody followed by peroxidase-conjugated secondary antibody and enhanced chemiluminescence detection.

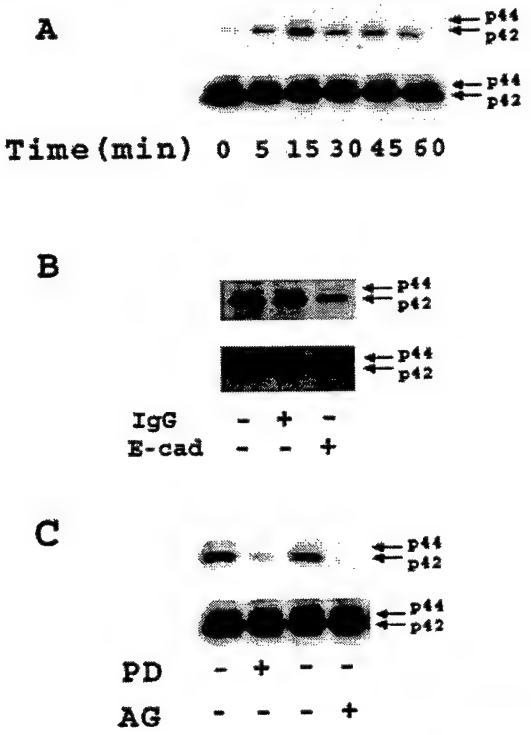

FIG. 4. **E-cadherin-mediated adhesion enhances EGFR-mediated MAPK activity.** *A*, using the calcium switch method, E-cadherin was activated in pp126 cells. The cells were lysed at the indicated times following E-cadherin activation. The lysates were separated by SDS-PAGE (9% gels), transferred to polyvinylidene difluoride membrane, and probed with anti-phospho-ERK1/2 antibody to detect the phosphorylated, active form of ERK (*upper panel*) or with anti-ERK1/2 antibody to detect total ERK1/2 expression (*lower panel*). *B*, pp126 cells underwent activation of E-cadherin using the calcium switch method in the presence of function-blocking anti-E-cadherin antibody (HECD-1, 10 μg/ml) or isotype-matched IgG (10 μg/ml) as described under "Experimental Procedures." The cells were lysed at 15 min after calcium restoration. The lysates were analyzed for phospho-ERK (*upper panel*) or for total ERK expression (*lower panel*). *C*, pp126 cells were treated with the MEK inhibitor, PD98059 (*PD*, 5 μM), EGFR inhibitor, AG1478 (*AG*, 250 nM), or with an equal amount of Me_2SO vehicle as control at the time of disruption of cell-cell junctions as described above. The cells were lysed at 15 min after calcium restoration. The lysates were analyzed for phospho-ERK (*upper panel*) or for total ERK expression (*lower panel*). The results are representative of three independent experiments.

MAPK phosphorylation was a specific consequence of E-cadherin engagement, junction assembly was initiated in the presence of the function-blocking anti-E-cadherin antibody or control IgG as described above. Inhibition of E-cadherin engagement decreased ERK1/2 phosphorylation, indicating that engagement of E-cadherin leads to MAPK activation (Fig. 4*B*). Moreover, E-cadherin-mediated MAPK activation was blocked with the MEK inhibitor PD98059, demonstrating the involvement of the MEK-ERK pathway (Fig. 4*C*). Interestingly, the epidermal growth factor receptor (EGFR)-specific tyrphostin AG1478 also completely abrogated E-cadherin-mediated MAPK activation (Fig. 4*C*), supporting the observation that E-cadherin-mediated activation of MAPK is dependent on EGFR (20).

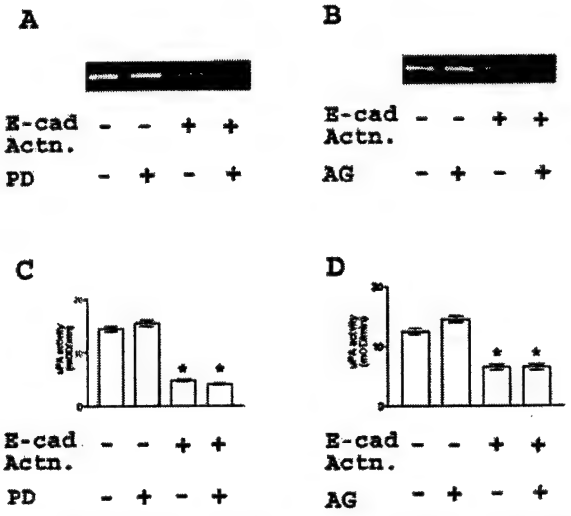

FIG. 5. **EGFR-MAPK pathway is not involved in E-cadherin-mediated suppression of proteinases.** Serum-starved pp126 cells were either left untreated (designated *E-cad Actn.* −) or underwent activation of E-cadherin (designated *E-cad Actn.* +) using the calcium switch method in the presence of 5 μM PD98059 (*PD*), 250 nM AG1478 (*AG*), or an equal volume of Me_2SO as described under "Experimental Procedures." *A* and *B*, conditioned media were collected at 36 h and analyzed for MMP-9 activity by gelatin zymography. *C* and *D*, uPA activity was analyzed in the conditioned media at 24 h using a coupled colorimetric plasminogen activation assay. The results represent the mean ± S.E. of three different experiments. *, significantly different from control with $p < 0.005$.

By using the MEK inhibitor PD98059, the role of MAPK in the E-cadherin mediated suppression of proteinases was evaluated. Cells were incubated with EGTA and 5 μM PD98059 or an equal amount of Me_2SO vehicle for 30 min before the addition of calcium-replete medium containing either 5 μM PD98059 or Me_2SO. Under basal conditions (designated *E-cad Actn* −), PD98059 did not affect the relative MMP-9 levels or the net uPA activity (Fig. 5, *A*, *2nd lane*, and *C*). However following E-cadherin activation by EGTA treatment and calcium restoration, inhibition of MEK activity did not prevent the suppression of proteinase expression (Fig. 5, *A*, *4th lane*, and *C*). Similar results were obtained with TIMP-1 and PAI-1 (data not shown).

To evaluate further the role of MAPK in the control of E-cadherin-regulated proteinase expression, the EGFR kinase-specific inhibitor tyrphostin AG1478 was employed. Cells were treated with EGTA followed by calcium restoration in the presence of AG1478 (250 nM). Under basal conditions (designated *E-cad Actn* −) AG1478 (250 nM) did not affect MMP-9 or uPA expression (Fig. 5, *B*, *2nd lane*, and *D*). Similar to the results obtained with PD98059, specific inhibition of the EGFR kinase also failed to abrogate the suppressive effect of E-cadherin engagement on the relative MMP-9 levels or the net uPA activity (Fig. 5, *B*, *4th lane*, and *D*). Together these data demonstrate that, although E-cadherin engagement can activate

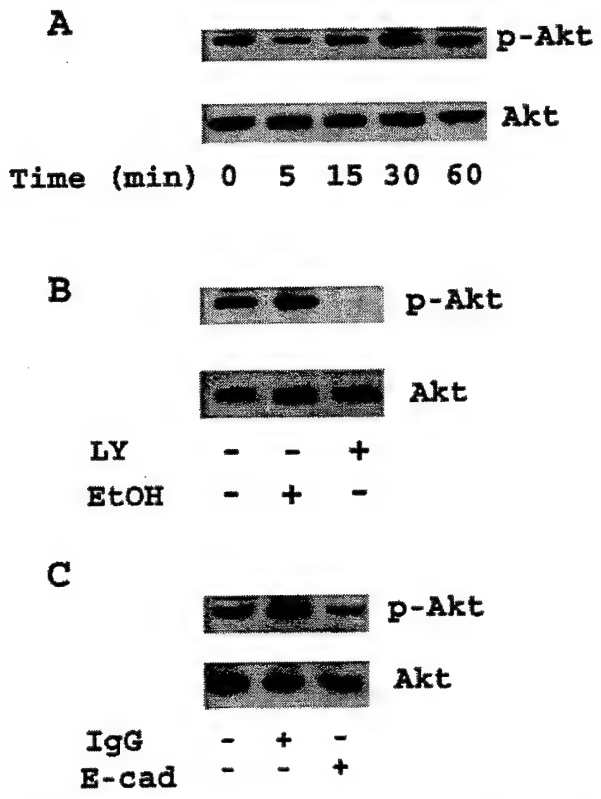

FIG. 6. **E-cadherin-mediated adhesion induces PI3-kinase mediated AKT activity.** *A*, using the calcium switch method, E-cadherin was activated in pp126 cells. The cells were lysed at the indicated times following E-cadherin activation. The lysates were separated by SDS-PAGE (9% gels), transferred to polyvinylidene difluoride membrane, and probed with an antibody that specifically recognizes phosphorylation on Thr-308 (phospho-AKT). The membrane was then reprobed with an antibody against total AKT. *B*, pp126 cells were treated with the PI3-kinase inhibitor, LY294002 (*LY*, 10 μM), or an equal volume of ethanol for 30 min at the time of disruption of cell-cell junctions as described above. The cells were lysed at 30 min after calcium restoration and analyzed for phospho-AKT (*upper panel*) and total AKT (*lower panel*) as described above. *C*, pp126 cells were either left untreated or underwent activation of E-cadherin using the calcium switch method in the presence of function-blocking anti-E-cadherin antibody (HECD-1, 10 μg/ml) or isotype-matched IgG (10 μg/ml) as described under "Experimental Procedures." The cells were lysed at 30 min after calcium restoration and analyzed for phospho-AKT or for total AKT expression as described above. The results are representative of three independent experiments.

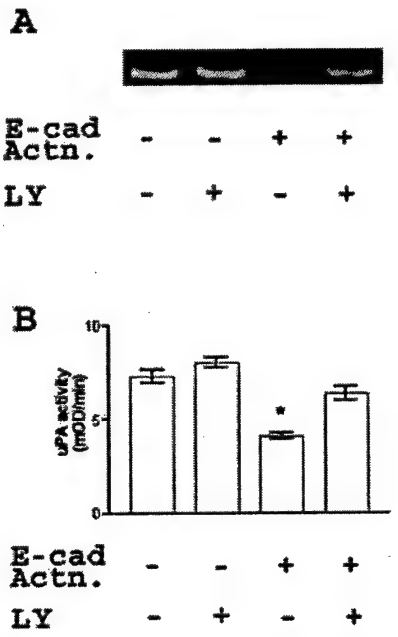

FIG. 7. **Inhibition of PI3-kinase blocks E-cadherin-mediated suppression of proteinases.** Serum-starved pp126 cells were either left untreated (designated *E-cad Actn.* −) or underwent activation of E-cadherin (designated *E-cad Actn.* +) using the calcium switch method in the presence of 10 μM LY294002 (*LY*) or an equal volume of ethanol for 30 min as described under "Experimental Procedures." *A*, conditioned media were collected at 36 h and analyzed for MMP-9 activity by gelatin zymography. *B*, uPA activity was analyzed in the conditioned media at 24 h using a coupled colorimetric plasminogen activation assay. The results represent the mean ± S.E. of three different experiments. * significantly different from control with $p < 0.05$.

MAPK in pp126 cells via a mechanism involving the EGFR kinase, this signaling pathway does not modulate E-cadherin regulation of proteinase expression.

Inhibition of PI3-kinase Blocks E-cadherin-mediated Suppression of Proteinases—Formation of *de novo* E-cadherin-mediated cell-cell contact activates PI3-kinase (19–21, 31, 32, 39–41) and induces physical association of PI3-kinase with E-cadherin (see Refs. 19 and 21 and data not shown). To determine whether PI3-kinase activation may play a role in the E-cadherin regulation of proteinase expression, activation of PI3-kinase was assessed in pp126 cells following calcium-induced adherens junction assembly by evaluating activation (phosphorylation) of the downstream substrate AKT. Cells were lysed at various time points and samples analyzed by Western blotting using antibodies directed against total AKT or the phosphorylated (active) species. A time-dependent phosphorylation of AKT following E-cadherin activation was observed in pp126 cells (Fig. 6*A*, *upper panel*) with no change in total AKT protein (Fig. 6*A*, *lower panel*). AKT activation was blocked with the PI3-kinase inhibitor LY294002, demonstrating the involvement of the PI3-kinase-AKT pathway (Fig. 6*B*). To confirm that AKT activation resulted from E-cadherin engagement, junction assembly was initiated in the presence of the function-blocking anti-E-cadherin antibody or control IgG as described above. Inhibition of E-cadherin engagement decreased AKT activation (Fig. 6*C*), indicating that engagement of E-cadherin leads to PI3-kinase activation.

By using the inhibitor LY294002, the role of PI3-kinase in E-cadherin-mediated suppression of MMP-9 and uPA expression was evaluated. Cells were preincubated with EGTA and LY294002 (10 μM) or an equal amount of ethanol vehicle for 30 min before the addition of calcium-replete medium containing LY294002 or ethanol. Under control conditions when the adherens junctions were not disrupted with EGTA treatment (designated *E-cad Actn* −), LY294002 did not alter the relative MMP-9 levels or the net uPA activity (Fig. 7, *A*, *2nd lane*, and *B*). In EGTA-treated cells, calcium-induced engagement of E-cadherin decreased the relative MMP-9 levels and the net uPA activity, as demonstrated previously (Fig. 7, *A*, *3rd lane*, and *B*). However, concomitant treatment with LY294002 abrogated the E-cadherin-mediated proteinase suppression and restored the relative MMP-9 levels and the net uPA activity (Fig. 7, *A*, *4th lane*, and *B*), implicating PI3-kinase in E-cadherin-mediated proteinase regulation. Similar results were obtained with TIMP-1 and PAI-1 (data not shown).

PI3-Kinase Controls Integrity of Adherens Junctions in pp126 Cells—Recent data indicate that PI3-kinase can regulate either the assembly or maintenance of adherens junctions (21, 32). As both PI3-kinase inhibition (using LY294002) and prevention of E-cadherin junction formation (with blocking an-

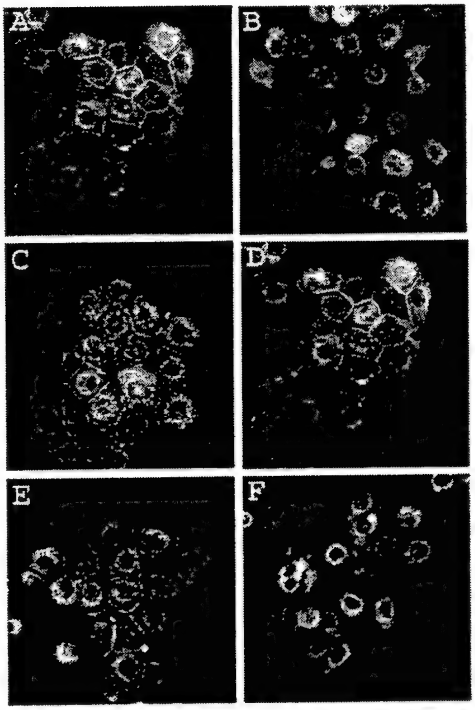

FIG. 8. **PI3-kinase controls the integrity of adherens junctions in pp126 cells.** Serum-starved pp126 cells were either left untreated (*A*) or treated with 4 mM EGTA for 30 min (*B–F*) containing either Me_2SO as control (*A–C*), 5 μM PD98059 (*D*), 250 nM AG1478 (*E*), or 10 μM LY294008 (*F*). The EGTA containing medium was then replaced with Keratinocyte-SFM (0.09 mM Ca^{2+}) containing Me_2SO or the corresponding inhibitor for 45 min. Cells were fixed, incubated with anti-E-cadherin antibody (HECD-1), and detected with Alexa Fluor 594-conjugated anti-mouse antibody.

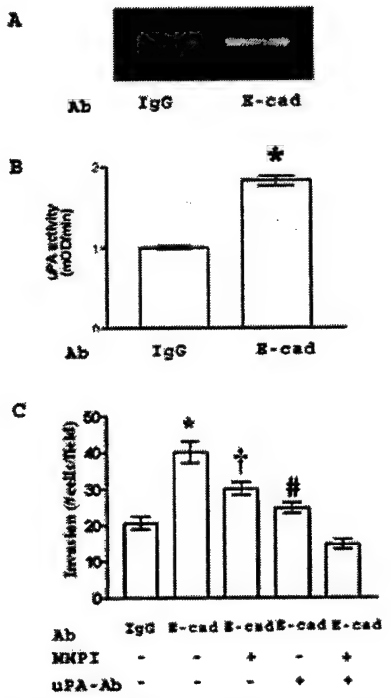

FIG. 9. **Disruption of cell-cell adhesion enhances pp126 cell invasion.** pp126 cells were plated with either control antibody (*Ab*) (*IgG*) or anti-E-cadherin antibody (HECD-1, designated *E-cad*). *A*, conditioned media were collected at 36 h and analyzed for MMP-9 activity by gelatin zymography. *B*, uPA activity was analyzed in the conditioned media at 24 h using a coupled colorimetric plasminogen activation assay. *, significantly different from control with $p < 0.001$. *C*, cells (2×10^5/500 μl) were added to porous polycarbonate filters (8-μm pore) coated with Matrigel (10 μg) in the presence 25 μg/ml of control antibody (*IgG*) or anti-E-cadherin antibody (HECD-1, designated *E-cad*) for 40 h. In wells containing E-cadherin antibody, either MMP inhibitor, GM6001 (2.5 μM), function-blocking uPA antibody (American Diagnostica number 394, 15 μg/ml), or both were added. Nonmigrating cells were removed from the upper chamber, and filters were fixed and stained, and invading cells were enumerated using an ocular micrometer. The results represent the mean ± S.E. of three different experiments. *, significantly different from IgG treated cells with $p < 0.001$. †, significantly different from E-cadherin antibody treated cells with $p < 0.05$. #, significantly different from E-cadherin antibody treated cells with $p < 0.01$.

tibodies) restored proteinase expression, these data suggest that PI3-kinase may participate in regulation of E-cadherin junctions in pp126 cells. To test this hypothesis, the effect of PI3-kinase inhibition (10 μM LY294002) on junction formation was evaluated. Control experiments included inhibitors of EGFR tyrosine kinase (250 nM AG1478) or MEK (5 μM PD98059). Cells were pre-incubated with EGTA in the presence of inhibitor or Me_2SO vehicle for 30 min before the addition of calcium-replete medium containing the specific inhibitor or Me_2SO. After 45 min, cells were processed for immunofluorescence microscopy using anti-E-cadherin antibody. Control cells present a typical pattern of E-cadherin staining at the level of cell-cell contacts (Fig. 8*A*). After 30 min of treatment with EGTA, E-cadherin was absent from sites of cell-cell contact (Fig. 8*B*). Following calcium addition, E-cadherin-mediated adherens junctions were again formed at 45 min (Fig. 8*C*). Similar results were observed in cells treated with PD98059 or AG1478 (Fig. 8, *D* and *E*). In contrast, cells treated with LY294002 showed significantly reduced E-cadherin staining at sites of cell-cell contact (Fig. 8*F*), indicating that PI3-kinase participates in the formation of *de novo* E-cadherin-mediated adherens junctions in pp126 cells.

Prevention of Cell-Cell Adhesion Enhances pp126 Cell Invasion—To assess the functional consequences of E-cadherin-regulated proteinase expression, the impact of preventing cell-cell adhesion on cellular invasive activity was evaluated. pp126 cells were seeded into Boyden chambers overlaid with Matrigel to provide a three-dimensional, protein-rich barrier to invasion in the presence of E-cadherin blocking antibody (HECD-1) or control IgG. Prevention of *de novo* E-cadherin cell-cell contacts resulted in an increase in the relative MMP-9 levels and the net uPA activity (Fig. 9, *A* and *B*). Concomitant with enhanced proteinase expression, inhibition of junction formation significantly increased Matrigel invasion (Fig. 9*C*). The enhanced invasive activity was partially blocked with either a broad spectrum MMP inhibitor (2.5 μM GM6001) or by a function-blocking anti-uPA antibody (15 μg/ml) and was completely abrogated by a mixture of the two inhibitors (Fig. 9*C*), implicating both MMP-9 and uPA in Matrigel invasion by pp126 cells. These data demonstrate that the proteinase up-regulation resulting from inhibition of E-cadherin engagement can promote cellular invasive behavior.

DISCUSSION

Studies using multiple cancer models have demonstrated that loss of E-cadherin-mediated adherens junctions leads to increased invasion and metastases (22, 23, 27, 35, 42). Additional data suggest a correlation between E-cadherin status and proteinase levels. For example, down-regulation of E-cadherin increased MMP-9 secretion in murine skin carcinoma cell lines (43), whereas overexpression of E-cadherin decreased MMP-2 activity in prostate cancer cells (26) and MT1-MMP in squamous cancer cells (44). However a mechanistic examina-

tion of the potential functional link between cell-cell adhesion and proteolysis has not been reported. Our current data demonstrate that E-cadherin plays a direct role in proteinase regulation in premalignant oral keratinocytes. Initiation of *de novo* E-cadherin-mediated cell-cell junctions resulted in suppression of MMP-9 and uPA expression. Conversely, prevention of junction formation enhanced proteinase expression and consequent cellular invasive behavior, suggesting a biochemical mechanism by which down-regulation of E-cadherin may promote metastasis.

The detailed signal transduction pathway through which E-cadherin regulates proteinase gene expression is unknown. However, our data support a role for PI3-kinase activity in the E-cadherin-mediated suppression of MMP-9 and uPA expression. Formation of *de novo* E-cadherin junctions activates PI3-kinase (Fig. 6) (19–21, 31, 32, 39–41) and leads to the physical association of PI3-kinase with E-cadherin (see Refs. 19 and 21 and data not shown). Activation of PI3-kinase recruits the GTP exchange factor Tiam-1 to the adherens junctions, resulting in activation of Rac-GTPase (45). In keratinocytes, Rac-GTPases play an important role in forming and stabilizing adherens junctions by recruiting F-actin to these junctions (46, 47). Supporting this model, inhibition of PI3-kinase blocks the recruitment of F-actin to sites of cell-cell contact in intestinal epithelial cells (21) and destabilizes adherens junctions in mammary epithelial cells (48). Moreover, additional data indicate that PI3-kinase may participate in maturation and maintenance of cadherin-based adhesions (32, 40), in part via regulation of productive adhesive contact formation following initial homophilic ligation (32). Our current data support the hypothesis that PI3-kinase activity also functions to regulate formation of adherens junctions in pp126 cells. Thus, inhibition of PI3-kinase activity with LY294002 destabilizes junctions, thereby abrogating the suppressive effect of E-cadherin engagement on proteinase expression.

In addition to activation of PI3-kinase, E-cadherin engagement has also been shown to enhance MAPK activity through the recruitment and activation of EGFR (20). A similar effect was observed in the current study, wherein junction formation induced maximal MAPK activation in pp126 cells at 15 min. MAPK activation was completely abrogated with the EGFR kinase inhibitor AG1478, implicating EGFR signaling in MAPK activation. However, inhibition of MEK (with PD98059) or EGFR kinase (with AG1478) was insufficient to restore proteinase expression, suggesting that E-cadherin-mediated proteinase regulation does not involve EGFR-initiated MAPK signaling. Furthermore, inhibition of MEK and EGFR kinase activity at the time of calcium switch did not prevent adherens junction re-formation in pp126 cells. It should be noted, however, that the MAPK pathway is important in both growth factor-induced secretion of MMP-9 in carcinoma cells (49) and in integrin-mediated up-regulation of uPA in pp126 cells (30). These data support the hypothesis that the signaling pathways that regulate formation of adherens junctions (PI3-kinase) may also regulate cadherin-mediated suppression of proteinases. This effect may be, in part, due to sequestration of β-catenin at cell-cell junctions as part of E-cadherin-catenin complex (50, 51). β-catenin can translocate to the nucleus and form a complex with proteins of the T cell factor/lymphoid-enhancer factor family (52). T cell factor/lymphoid-enhancer factor proteins act as transcription factors and have been shown to activate genes that are important in cancer progression including MMP-7, MMP-26, and uPAR (50, 51, 53–58). A number of other MMP promoters, including MMP-9, have T cell factor 4-binding sites and, consequently, may be regulated by β-catenin (54, 57). Although we have not formally addressed the potential contribution of β-catenin signaling, no change in uPAR expression was observed following E-cadherin activation in our system, suggesting that additional mechanisms of proteinase regulation are engaged. Thus, it is interesting to speculate that net extracellular proteinase activity may result from a balance between signaling pathways differentially activated by engagement of cell-cell *versus* cell-matrix adhesion molecules.

In addition to enhanced proteinase expression (uPA, MMP-9) induced by E-cadherin disruption, a coordinate increase in the corresponding inhibitors (PAI-1, TIMP-1) was also observed. Although a coordinate regulation of uPA and PAI-1 is apparent, a *net* increase in uPA activity is obtained following E-cadherin disruption, and this functionally contributes to the increased Matrigel invasion. Similarly, the Matrigel invasion data also suggest that a net increase in MMP-9 activity is also likely. It has been shown previously (24) in T47D and MCF-7 breast cancer cells that disruption of cell junctions with anti-E-cadherin antibodies increases uPA expression and collagen invasion. The enhanced collagen invasion was partially blocked using anti-catalytic uPA antibodies; however, the effect of MMP inhibitors was not evaluated (24). The current data demonstrate that Matrigel invasion by pp126 cells is dependent on both uPA and MMP-9, as inhibiting both proteinases simultaneously completely abrogated the increase in Matrigel invasion by pp126 cells.

Recent studies (36–38) have shown that proteinase expression may regulate cell-cell junction integrity by cleaving E-cadherin. Conversely, our data demonstrate that E-cadherin participates in proteinase regulation via a PI3-kinase-dependent mechanism, providing novel evidence for a bi-directional communication between proteinases and cadherins. As proteinases play a central role in a number of important cellular processes, these findings may provide a framework for a more detailed understanding of the mechanism by which E-cadherin-mediated cell-cell contacts regulate both normal epithelial cell behavior and the invasiveness of carcinoma cells.

REFERENCES

1. Werb, Z. (1997) *Cell* **91,** 439–442
2. Sternlicht, M. D., and Werb, Z. (2001) *Annu. Rev. Cell Dev. Biol.* **17,** 463–516
3. Ellis, V., and Murphy, G. (2001) *FEBS Lett.* **506,** 1–5
4. Westermarck, J., and Kahari, V. M. (1999) *FASEB J.* **13,** 781–792
5. Itoh, T., Tanioka, M., Matsuda, H., Nishimoto, H., Yoshioka, T., Suzuki, R., and Uehira, M. (1999) *Clin. Exp. Metastasis* **17,** 177–181
6. Murphy, G., and Gavrilovic, J. (1999) *Curr. Opin. Cell Biol.* **11,** 614–621
7. Nagase, H., and Woessner, J. F., Jr. (1999) *J. Biol. Chem.* **274,** 21491–21494
8. Vu, T. H., and Werb, Z. (2000) *Genes Dev.* **14,** 2123–2133
9. Andreasen, P. A., Kjoller, L., Christensen, L., and Duffy, M. J. (1997) *Int. J. Cancer* **72,** 1–22
10. Ghosh, S., Ellerbroek, S. M., Wu, Y., and Stack, M. S. (2000) *Fibrinolysis Proteolysis* **14,** 87–97
11. Parks, W. C., and Mecham, R. P. (1998) *Matrix Metalloproteinases*, Academic Press, San Diego
12. Vu, T. H., and Werb Z. (1998) in *Matrix Metalloproteinases* (Parks, W. C., and Mecham, R. P., eds) pp. 115–48, Academic Press, San Diego
13. Mignatti, P., and Rifkin, D. B. (2000) *Adv. Cancer Res.* **78,** 103–157
14. Yu, H. R., and Schultz, R. M. (1990) *Cancer Res.* **50,** 7623–7633
15. Kook, Y. H., Adamski, J., Zelent, A., and Ossowski, L. (1994) *EMBO J.* **13,** 3983–3991
16. Angst, B. D., Marcozzi, C., and Magee, A. I. (2001) *J. Cell Sci.* **114,** 629–641
17. Takeichi, M. (1991) *Science* **251,** 1451–1455
18. Provost, E., and Rimm, D. L. (1999) *Curr. Opin. Cell Biol.* **11,** 567–572
19. Pece, S., Chiariello, M., Murga, C., and Gutkind, J. S. (1999) *J. Biol. Chem.* **274,** 19347–19351
20. Pece, S., and Gutkind, J. S. (2000) *J. Biol. Chem.* **275,** 41227–41233
21. Laprise, P., Chailler, P., Houde, M., Beaulieu, J. F., Boucher, M. J., and Rivard, N. (2001) *J. Biol. Chem.* **276,** 21885–21894
22. Noe, V., Chastre, E., Bruyneel, E., Gespach, C., and Mareel, M. (1999) *Biochem. Soc. Symp.* **65,** 43–62
23. Van Aken, E., De Wever, O., Correia da Rocha, A. S., and Mareel, M. (2001) *Virchows Arch.* **439,** 725–751
24. Frixen, U. H., and Nagamine, Y. (1993) *Cancer Res.* **53,** 3618–3623
25. Miyaki, M., Tanaka, K., Kikuchi-Yanoshita, R., Muraoka, M., Konishi, M., and Takeichi, M. (1995) *Oncogene* **11,** 2547–2552
26. Luo, J., Lubaroff, D. M., and Hendrix, M. J. (1999) *Cancer Res.* **59,** 3552–3556
27. Wijnhoven, B. P., Dinjens, W. N., and Pignatelli, M. (2000) *Br. J. Surg.* **87,** 992–1005
28. Stack, S., Gonzalez-Gronow, M., and Pizzo, S. V. (1990) *Biochemistry* **29,** 4966–4970

29. Oda, D., Bigler, L., Lee, P., and Blanton, R. (1996) *Exp. Cell Res.* **226,** 164–169
30. Ghosh, S., Brown, R., Jones, J. C., Ellerbroek, S. M., and Stack, M. S. (2000) *J. Biol. Chem.* **275,** 23869–23876
31. Kim, S. H., Li, Z., and Sacks, D. B. (2000) *J. Biol. Chem.* **275,** 36999–37005
32. Nakagawa, M., Fukata, M., Yamaga, M., Itoh, N., and Kaibuchi, K. (2001) *J. Cell Sci.* **114,** 1829–1838
33. Munshi, H. G., and Stack, M. S. (2002) *Methods Cell Biol.* **69,** 195–205
34. Laemmli, U. K. (1970) *Nature* **227,** 680–685
35. Frixen, U. H., Behrens, J., Sachs, M., Eberle, G., Voss, B., Warda, A., Lochner, D., and Birchmeier, W. (1991) *J. Cell Biol.* **113,** 173–185
36. Noe, V., Fingleton, B., Jacobs, K., Crawford, H. C., Vermeulen, S., Steelant, W., Bruyneel, E., Matrisian, L. M., and Mareel, M. (2001) *J. Cell Sci.* **114,** 111–118
37. Steinhusen, U., Weiske, J., Badock, V., Tauber, R., Bommert, K., and Huber, O. (2001) *J. Biol. Chem.* **276,** 4972–4980
38. Ryniers, F., Stove, C., Goethals, M., Brackenier, L., Noe, V., Bracke, M., Vandekerckhove, J., Mareel, M., and Bruyneel, E. (2002) *Biol. Chem.* **383,** 159–165
39. Li, G., Satyamoorthy, K., and Herlyn, M. (2001) *Cancer Res.* **61,** 3819–3825
40. Kovacs, E. M., Ali, R. G., McCormack, A. J., and Yap, A. S. (2002) *J. Biol. Chem.* **277,** 6708–6718
41. Shinohara, M., Kodama, A., Matozaki, T., Fukuhara, A., Tachibana, K., Nakanishi, H., and Takai, Y. (2001) *J. Biol. Chem.* **276,** 18941–18946
42. Schipper, J. H., Frixen, U. H., Behrens, J., Unger, A., Jahnke, K., and Birchmeier, W. (1991) *Cancer Res.* **51,** 6328–6337
43. Llorens, A., Rodrigo, I., Lopez-Barcons, L., Gonzalez-Garrigues, M., Lozano, E., Vinyals, A., Quintanilla, M., Cano, A., and Fabra, A. (1998) *Lab. Invest.* **78,** 1131–1142
44. Ara, T., Deyama, Y., Yoshimura, Y., Higashino, F., Shindoh, M., Matsumoto, A., and Fukuda, H. (2000) *Cancer Lett.* **157,** 115–121
45. Sander, E. E., van Delft, S., ten Klooster, J. P., Reid, T., van der Kammen, R. A., Michiels, F., and Collard, J. G. (1998) *J. Cell Biol.* **143,** 1385–1398
46. Braga, V. M., Machesky, L. M., Hall, A., and Hotchin, N. A. (1997) *J. Cell Biol.* **137,** 1421–1431
47. Braga, V. M., Del Maschio, A., Machesky, L., and Dejana, E. (1999) *Mol. Biol. Cell* **10,** 9–22
48. Somasiri, A., Wu, C., Ellchuk, T., Turley, S., and Roskelley, C. D. (2000) *Differentiation* **66,** 116–125
49. McCawley, L. J., Li, S., Wattenberg, E. V., and Hudson, L. G. (1999) *J. Biol. Chem.* **274,** 4347–4353
50. Barker, N., and Clevers, H. (2000) *Bioessays* **22,** 961–965
51. Huber, A. H., and Weis, W. I. (2001) *Cell* **105,** 391–402
52. Love, J. J., Li, X., Case, D. A., Giese, K., Grosschedl, R., and Wright, P. E. (1995) *Nature* **376,** 791–795
53. Wong, N. A., and Pignatelli, M. (2002) *Am. J. Pathol.* **160,** 389–401
54. Brabletz, T., Jung, A., Dag, S., Hlubek, F., and Kirchner, T. (1999) *Am. J. Pathol.* **155,** 1033–1038
55. Crawford, H. C., Fingleton, B., Gustavson, M. D., Kurpios, N., Wagenaar, R. A., Hassell, J. A., and Matrisian, L. M. (2001) *Mol. Cell. Biol.* **21,** 1370–1383
56. Crawford, H. C., Fingleton, B. M., Rudolph-Owen, L. A., Goss, K. J., Rubinfeld, B., Polakis, P., and Matrisian, L. M. (1999) *Oncogene* **18,** 2883–2891
57. Marchenko, G. N., Marchenko, N. D., Leng, J., and Strongin, A. Y. (2002) *Biochem. J.* **363,** 253–262
58. Mann, B., Gelos, M., Siedow, A., Hanski, M. L., Gratchev, A., Ilyas, M., Bodmer, W. F., Moyer, M. P., Riecken, E. O., Buhr, H. J., and Hanski, C. (1999) *Proc. Natl. Acad. Sci. U. S. A.* **96,** 1603–1608

THE JOURNAL OF BIOLOGICAL CHEMISTRY
Vol. 277, No. 41, Issue of October 11, pp. 39005–39014, 2002
Printed in U.S.A.

Collagen Binding Properties of the Membrane Type-1 Matrix Metalloproteinase (MT1-MMP) Hemopexin C Domain

THE ECTODOMAIN OF THE 44-kDa AUTOCATALYTIC PRODUCT OF MT1-MMP INHIBITS CELL INVASION BY DISRUPTING NATIVE TYPE I COLLAGEN CLEAVAGE*

Received for publication, July 10, 2002
Published, JBC Papers in Press, July 26, 2002, DOI 10.1074/jbc.M206874200

Eric M. Tam‡§, Yi I. Wu¶‖, Georgina S. Butler, M. Sharon Stack¶, and Christopher M. Overall‡**‡‡**

*From the C.I.H.R. Group in Matrix Dynamics, Departments of ‡Biochemistry and Molecular Biology, **Oral Biological and Medical Sciences, University of British Columbia, Vancouver, British Columbia V6T 1Z3, Canada and the ¶Department of Cell and Molecular Biology, Northwestern University Medical School, Chicago, Illinois 60611*

Up-regulation of the collagenolytic membrane type-1 matrix metalloproteinase (MT1-MMP) leads to increased MMP2 (gelatinase A) activation and MT1-MMP autolysis. The autocatalytic degradation product is a cell surface 44-kDa fragment of MT1-MMP (Gly^{285}–Val^{582}) in which the ectodomain consists of only the linker, hemopexin C domain and the stalk segment found before the transmembrane sequence. In the collagenases, hemopexin C domain exosites bind native collagen, which is required for triple helicase activity during collagen cleavage. Here we investigated the collagen binding properties and the role of the hemopexin C domain of MT1-MMP and of the 44-kDa MT1-MMP ectodomain in collagenolysis. Recombinant proteins, MT1-LCD (Gly^{285}–Cys^{508}), consisting of the linker and the hemopexin C domain, and MT1-CD (Gly^{315}–Cys^{508}), which consists of the hemopexin C domain only, were found to bind native type I collagen but not gelatin. Functionally, MT1-LCD inhibited collagen-induced MMP2 activation in fibroblasts, suggesting that interactions between collagen and endogenous MT1-MMP directly stimulate the cellular activation of pro-MMP2. MT1-LCD, but not MT1-CD, also blocked the cleavage of native type I collagen by MT1-MMP *in vitro*, indicating an important role for the MT1-MMP linker region in triple helicase activity. Similarly, soluble MT1-LCD, but not MT1-CD or peptide analogs of the MT1-MMP linker, reduced the invasion of type I collagen matrices by MDA-MB-231 cells as did the expression of recombinant 44-kDa MT1-MMP on the cell surface. Together, these studies demonstrate that generation of the 44-kDa MT1-MMP autolysis product regulates collagenolytic activity and subsequent invasive potential, suggesting a novel feedback mechanism for the control of pericellular proteolysis.

Type I collagen is the most abundant protein of the extracellular matrix and is an important structural component in blood vessels, skin, tendons, ligaments, and bone (1). Accordingly, the synthesis and degradation of type I collagen is tightly regulated. Disruptions in this homeostasis can lead to diseases such as pulmonary fibrosis, scleroderma, arthritis, and osteoporosis, which, if untreated, can result in loss of tissue function and integrity. In a number of cancer cells, the capacity to degrade type I collagen and invade through type I collagen matrices often correlates with metastatic potential (2), a characteristic that is as important for the local dissemination of tumor cells as type IV collagen degradation and basement membrane penetration is for metastasis (3). Despite the importance of maintaining correct collagen homeostasis in tissues, the proteases responsible for type I collagen degradation *in vivo* remain unclear. An intracellular pathway may play an important role in collagen degradation (4) that, in bone, utilizes the cysteine protease cathepsin K at low pH (5). Extracellularly, fibrillar type I collagen may be degraded at neutral pH by several matrix metalloproteinases (MMPs),[1] a 24-member family of zinc-dependent endopeptidases in humans (2). The major collagenolytic MMPs are the secreted collagenases, MMP1, MMP8, and MMP13 (6), and the cell surface membrane type 1 (MT1)-MMP (7, 8). MT1-MMP also activates collagenase-2 (MMP13) (9) and is the primary activator of MMP2 (10), a gelatinase that exhibits weak native type I collagenolytic activity (11–13).

MMPs share a common overall structure consisting of a propeptide, catalytic domain, linker (also called a hinge), and a hemopexin C domain (14). Whereas the majority of MMPs are secreted as latent zymogens, MT-MMPs, the largest subgroup of MMPs, are membrane-anchored by the presence of a type I transmembrane sequence and cytoplasmic tail (MT1-, MT2-, MT3-, and MT5-MMP) or by glycosylphosphatidylinositol linkage (MT4- and MT6-MMP) (14). MT1-MMP is activated intracellularly by proprotein convertase-dependent and -independent pathways (15, 16) and is expressed as an active protease on the surface of many normal and pathological cell types (10, 17). The importance of MT1-MMP is indicated by its requirement for the invasion of endothelial and cancer cells through type I collagen matrices (18–20). Moreover, mice deficient in MT1-

* This work was supported by grants from the National Cancer Institute of Canada, Canadian Institutes for Health Research, and the National Institutes of Health Research. The costs of publication of this article were defrayed in part by the payment of page charges. This article must therefore be hereby marked "*advertisement*" in accordance with 18 U.S.C. Section 1734 solely to indicate this fact.

§ Supported by a Roman Babicki Scholarship and Canadian Arthritis Network Trainee Award.

‖ Supported by a United States Army MRMC Training Grant.

‡‡ Supported by a Canada Research Chair in Metalloproteinase Biology. To whom correspondence should be addressed: University of British Columbia, 2199 Wesbrook Mall, J.B. Macdonald Bldg., Vancouver, British Columbia V6T 1Z3, Canada. Tel.: 604-822-2958; Fax: 604-822-3562; E-mail: chris.overall@ubc.ca; Website: www.clip.ubc.co.

[1] The abbreviations used are: MMP, matrix metalloproteinase; MT, membrane type; CD, C domain; LCD, C domain with linker; sMT1-MMP, soluble MT1-MMP; TIMP, tissue inhibitor of metalloproteinases; DMEM, Dulbecco's modified Eagle's medium; BSA, bovine serum albumin; ConA, concanavalin A; PBS, phosphate-buffered saline; HRP, horseradish peroxidase; Mca, 7-methoxycoumarin-4-yl)acetyl.

MMP developed severe aberrations in type I collagen-abundant tissues, such as bone and skin, and the mice exhibited arthritis and scleroderma (21, 22). In humans, homoallelic loss-of-function mutations in the *MMP2* gene result in excessive bone resorption and arthritis (23). This condition resembles the phenotype of the MT1-MMP knockout mouse, supporting the close functional connection of MMP2 and MT1-MMP in regulating pericellular collagen homeostasis in mice and humans.

Native type I collagen consists of two α1(I) chains and one α2(I) chain interwound in a right-handed triple helix that is resistant to cleavage by most proteinases at neutral pH with the exception of the MMP collagenases (14). Because the active site of collagenolytic MMPs can only accommodate a single α-chain, cleavage of the three α-chains occurs sequentially at the single collagenase-susceptible site, Gly^{775}-Ile/Leu^{776}, to generate ¾ and ¼ collagen fragments. To achieve this, the collagen helix must be initially unwound by a triple helicase mechanism in order to expose the scissile bonds. This critical step requires the presence of collagen-binding exosites (14), in addition to elements within the active site (24–26). In MMP1, MMP8, and MMP13, the hemopexin C domain supports binding to collagen and is required for native collagen cleavage (27–32). Deletion or mutation of the MMP8 linker also reduces collagenolysis (33, 34). Furthermore, synthetic peptide analogs of the MMP1 linker bound collagen and inhibited collagen cleavage (35). Interestingly, the 35-amino acid residue linker of MT1-MMP is twice the length of other collagenase linkers (18 residues); however, the significance of this and its role in collagen cleavage have yet to be examined.

The regulation of MT1-MMP activity, MMP2 activation and pericellular type I collagen levels is complex. In a variety of cells, stimulation by fibrillar type I collagen has been shown to increase the cell surface expression of MT1-MMP and induce the cellular activation of pro-MMP2 (36–42). This response is in part dependent on β_1 integrin clustering and signaling (40, 42, 43) and is potentially self-regulating, since type I collagen is susceptible to MT1-MMP and MMP2 proteolysis (14, 44). Concentration of MT1-MMP by overexpression (45, 46) or clustering interactions (47–50) favors MMP2 activation and collagenolysis (50). Concomitant with increased MT1-MMP expression and MMP2 activation is the autocatalytic processing of MT1-MMP at Gly^{284}–Gly^{285} to shed the catalytic domain from the hemopexin C domain, which is retained on the cell membrane (40, 46, 51). Hence, the ectodomain of the residual 44-kDa MT1-MMP fragment (Gly^{285}–Val^{582}) on the cell surface consists of the linker, hemopexin C domain, and stalk segment only (see Fig. 1*A*, *ii*) and thus is catalytically inactive. The significance of the 44-kDa MT1-MMP *in vivo* is not clear. In addition to being present following cell binding to type I collagen, the 44-kDa MT1-MMP has also been detected on the surface of tumor cells (40, 51). During MMP2 activation, TIMP-2-free MT1-MMP must be in close proximity to a trimeric complex of MT1-MMP·TIMP-2·pro-MMP2 in order to activate the bound pro-MMP2 (52). The mechanisms of MT1-MMP oligomerization are not clear. The recombinant hemopexin C domain of MT1-MMP did not form oligomers in solution or modulate MMP2 activation when added to cells (47). Recent reports using transmembrane MT1-MMP chimera and deletion mutants have suggested that the hemopexin C domain can mediate homophilic complex formation of cellular MT1-MMP for efficient MMP2 activation (48, 49). Expression of a transmembrane-tethered MT1-MMP hemopexin C domain lacking the linker, termed PEX (Thr^{313}–Val^{582}), in HT1080 cells inhibited MT1-MMP oligomerization, the cellular activation of pro-MMP2, and Matrigel invasion (48), a function previously attributed to MMP2 proteolytic activity against type IV collagen (53).

Considering that MT1-MMP is a collagenase, we hypothesized that exosites on the hemopexin C domain would bind to type I collagen and be essential for collagenolytic activity. Thus, the autolytically generated 44-kDa MT1-MMP ectodomain would be predicted to modulate pericellular collagenolysis on the membrane through dominant-negative interactions. Since native type I collagen stimulates MMP2 activation, we also hypothesized that collagen binding by the hemopexin C domain of MT1-MMP would modulate MMP2 activation with 44-kDa MT1-MMP opposing these effects *in vivo*. Experiments reported here demonstrate that collagen binding by the MT1-MMP hemopexin C domain is essential for collagenolytic activity and enhancement of MMP2 activation by MT1-MMP. Inhibition of this interaction either *in vitro* or on the cell surface inhibits collagen degradation. Together, these studies suggest a novel feedback mechanism through which generation of the 44-kDa MT1-MMP autolysis product regulates pericellular collagenolytic activity and subsequent invasive potential.

EXPERIMENTAL PROCEDURES

Materials—Rat tail type I collagen was prepared as previously described (54). Vitrogen® was purchased from Cohesion (Palo Alto, CA). Biotin-labeled type I collagen was prepared as previously described (55). Human placental type I collagen was purchased from Sigma. The triple helical nature of collagen was confirmed by the absence of trypsin sensitivity at an enzyme/substrate ratio of 1:10 over 3 h, 28 °C. The general hydroxamate inhibitor BB2116 was provided by British Biotech Pharmaceuticals (Oxford, UK). Hydroxamate inhibitor GM6001 and AB8102 (blocking antibody raised against the human MT1-MMP catalytic domain) were purchased from Chemicon (Temecula, CA). The polyclonal antibody RP1MMP-14 (raised against the MT1-MMP linker) was purchased from Triple Point Biologics (Portland, OR). The affinity-purified polyclonal antibodies αMT1-CD and αHis_6 were described previously (47).

Synthetic Peptides and Recombinant Proteins—The MT1-MMP linker peptide analogs MT1-L18 (^{302}RPSVPDKPKNPTYGPNIC^{319}) (University of Victoria, Victoria, Canada) and MT1-L35 (^{285}GESGFPTKMPPQPRTTSRPSVPDKPKNPTYGPNIC^{319}) (Tufts University, Medford, MA) (Fig. 1*A*, *iii*) were synthesized and verified by mass spectrometry. Recombinant domains of human MT1-MMP and MMP2 were expressed in *Escherichia coli* as N-terminal His-tagged proteins. The MT1-MMP hemopexin C domain (CD) with or without the linker (L) (MT1-LCD, Gly^{285}–Cys^{508}; MT1-CD, Gly^{315}–Cys^{508}) (*see* Fig. 1*A*) and the MMP2 hemopexin C domain with the linker (MMP2-LCD, Gly^{446}–Cys^{660}) were prepared as previously described (47). Recombinant human MMP2-CBD (Val^{220}–Gln^{393}) (collagen binding domain consisting of three fibronectin type II modules) was prepared previously (54). Any bacterial endotoxins in purified recombinant protein preparations were removed by polymyxin B-agarose columns (Sigma). The fidelity of purified recombinant proteins was confirmed by electrospray ionization mass spectrometry (47) and N-terminal Edman sequencing of protein bands cut from the membrane of Western blots. Human soluble MT1-MMP, truncated C-terminal to the hemopexin C domain (sMT1-MMP), was kindly provided by British Biotech Pharmaceuticals. Recombinant human MMP2, TIMP-1, and TIMP-2 were expressed in a mammalian cell system and purified as previously described (56) or kindly provided by Dr. H. Nagase (Imperial College School of Medicine, London, UK).

Electrophoretic Techniques—Samples in reducing (65 mM dithiothreitol) or nonreducing sample buffer (125 mM Tris-HCl, pH 6.8, 2.0% SDS, 2.0 M urea, 0.05% bromphenol blue) were separated on 15% SDS-PAGE gels and analyzed by either silver nitrate staining or by Western blotting using αMT1-CD and αHis_6 antibodies. ECL detection was performed according to the manufacturer's instructions (Amersham Biosciences). For zymographic analysis, samples were separated under nonreducing conditions on 10% SDS-PAGE gels co-polymerized with 0.5 mg/ml gelatin. Gels were washed for 30 min with 2.5% Triton X-100, rinsed with deionized water, and incubated with assay buffer (100 mM Tris, pH 8.0, 30 mM $CaCl_2$, 0.05% Brij, 0.025% NaN_3) at 37 °C for 4 h before staining with Coomassie Brilliant Blue G250.

Gel Filtration Chromatography—Purified MT1-LCD (0.5 mg) was subjected to gel filtration chromatography on a Superdex 75 column equilibrated with PBS (10 mM Na_2HPO_4, 1.8 mM NaH_2PO_4, 2.7 mM KCl,

140 mM NaCl, pH 7.4) and run on an AKTA purifier (Amersham Biosciences). Protein elution was monitored at 215 nm. Molecular mass standards used were BSA (67 kDa), ovalbumin (43 kDa), chymotrypsin A (25 kDa), and ribonuclease A (13.7 kDa).

Solid Phase Binding Assays—Native and heat-denatured type I collagen (rat tail) (5 μg/ml) were diluted in 15 mM Na_2CO_3, 35 mM $NaHCO_3$, 0.02% NaN_3, pH 9.6 (100 μl), and coated onto 96-microwell plates (Falcon) overnight at 4 °C as described previously (54, 57). Wells coated with myoglobin served as a control for nonspecific binding. The coated wells were blocked with 1% BSA to which serially diluted recombinant proteins in PBS (100 μl total volume) were added and incubated for 1 h at room temperature. After extensive washes, bound proteins were quantitated using affinity-purified polyclonal antibodies followed by incubation with goat anti-rabbit alkaline phosphatase-conjugated secondary antibody. Substrate, *p*-nitrophenyl phosphate disodium (Sigma), was added to the wells, and color development was monitored at 405 nm in a Thermomax plate reader (Molecular Devices).

Ligand Blot Assays—Proteins (5 μg) in 50 mM Tris-HCl, pH 8.0, 150 mM NaCl were filtered onto an Immobilon-P® membrane (Millipore Corp.) by vacuum. Membranes were blocked with 1% BSA in PBS and incubated with biotin-labeled native type I collagen in PBS/Tween 20 for 1 h. Bound collagen was visualized using horseradish peroxidase (HRP)-conjugated streptavidin and ECL detection.

Enzyme Assays—Biotin-labeled type I collagen (0.025 pmol) was incubated with either sMT1-MMP or MMP2 in assay buffer (50 mM Tris-HCl, pH 7.4, 200 mM NaCl, 5 mM $CaCl_2$, 3.8 mM NaN_3, 0.05% Brij) for 18 h at 28 °C. MMPs were activated with 2 mM 4-aminophenylmercuric acetate. Recombinant proteins and BB2116 in assay buffer were added to the reactions where indicated. Following digestion, samples were separated by 7.5% SDS-PAGE and analyzed by Western blotting using streptavidin-HRP and ECL detection. α1(I) and α2(I) chains were quantitated by scanning densitometry, and the percentage of native collagen cleavage was calculated as previously described (58). Cleavage of the quenched fluorescent substrate, Mca-Pro-Leu-Gly-Dpa-Ala-Arg-NH_2, was performed as described previously (56). MT1-LCD and MT1-CD in assay buffer (100 mM Tris-HCl, pH 7.4, 100 mM NaCl, 10 mM $CaCl_2$, 0.05% Brij) were added to the reaction where indicated.

Transmembrane MT1-MMP and MT1-MMP Hemopexin C Domain Constructs—The mammalian expression vector pCR3.1-Uni (Invitrogen) carrying human MT1-MMP cDNA was the generous gift of Dr. D. Pei (University of Minnesota). To express cell surface (c) transmembrane MT1-MMP hemoperin C domain, cMT1-CD (Δ112–315) and cMT1-LCD (Δ112–284), two-step overlapping PCR was used with T7 and reverse primer as external primers and either 5′-CGAAGGAAGCGCCCCAACATCTGTGACGGGAAC-3′ and 5′-ACAGATGTTGGGGCGCTTCCTTCGAACATTGGC-3′ (cMT1-CD, Δ112–315) or 5′-CGAAGGAAGCGCGGTGAGTCAGGGTTCCCCACC-3′ and 5′-CCCTGACTCACCGCGCTTCCTTCGAACATTGGCC-3′ (cMT1-LCD, Δ112–284) as internal primer pairs. The catalytically inactive MT1-MMP (E240A) mutant construct was generated using 5′-GGTGGCTGTGCACGCGCTGGGCCATGCC-3′ and 5′-GGCATGGCCCAGCGCGTGCACAGCCACC-3′ (E240A) primers. Full-length constructs were synthesized by PCR with T7 and reverse primers, digested with *Hin*dIII and *Eco*RI, ligated back to pCR3.1-Uni vector, and fully sequenced.

Cell Culture and Stable Transfection—Early passage human gingival fibroblasts were kindly provided by Dr. D. Brunette (University of British Columbia, Vancouver, Canada) and maintained in Dulbecco's modified Eagle's medium (DMEM) containing 10% newborn calf serum (Invitrogen). MDA-MB-231 breast carcinoma cells were kindly provided by Dr. V. G. Jordan (Northwestern University, Chicago, IL) and cultured in DMEM (Cellgro) supplemented with 10% fetal bovine serum (U.S. Bio-Technologies Inc.). MDA-MB-231 cells were transfected with MT1-MMP cDNA constructs using FuGENE 6 (Roche Molecular Biochemicals) according to the manufacturer's instructions. Stable cell lines were clone-selected and maintained in medium containing 1 mg/ml G418 (Mediatech Inc.). For each line, five clones were pooled and used in the experiments.

Transwell Invasion and Migration Assay—MDA-MB-231 cell invasion and migration assays through type I collagen (human placental) were performed as described previously (42). Endotoxin-free recombinant proteins, linker peptide analogs and antibodies in PBS were added to the cell media with BSA or IgG as controls. GM6001 was added to the cells in Me_2SO.

Collagen Gels—To prepare collagen gels, 8 volumes of Vitrogen was neutralized with 1 volume of 10× concentrated PBS and 1 volume of 0.1 M NaOH. Fibroblasts were detached with PBS containing 0.54 mM EDTA and 1.1 mM glucose and resuspended in a neutralized Vitrogen solution (2.0 mg/ml) containing 11.3% DMEM and 2.5% new born calf serum. The cell/collagen solution (75 μl) was then transferred into 96-well tissue culture plates and incubated at 37 °C for 1 h to allow for collagen polymerization. Cells were supplemented with DMEM containing 2.5% newborn calf serum for 18 h. Collagen gels were then rinsed with DMEM, and cells were cultured under serum-free conditions with or without MT1-LCD (endotoxin-free, in PBS) for the duration of the experiment. Cell conditioned medium was replaced every 24 h and analyzed by gelatin zymography after 72 h.

Latex Beads—Native and denatured type I collagen (100 μg/ml) were incubated with latex beads (1%) (Sigma) for 1 h at room temperature to allow for adsorption. The beads were then washed with PBS and blocked with 1% BSA for 1 h. Beads not absorbed with collagen served as a control. Blocked beads were rinsed with PBS and resuspended in DMEM at a concentration of 0.2% (v/v). Fibroblasts cultured in 96-well tissue culture plates were rinsed and incubated in serum-free medium for 1 h prior to incubation with the latex beads in DMEM (100 μl). Endotoxin-free MT1-LCD in PBS was added to the latex bead preparations where indicated. Cells were cultured for 24 h, after which the conditioned cell medium was analyzed by gelatin zymography.

RESULTS

Recombinant Protein Expression—To characterize the hemopexin C domain of MT1-MMP and the ectodomain of 44-kDa MT1-MMP, two forms of the MT1-MMP hemopexin C domain were cloned and expressed in *E. coli*. MT1-LCD (Gly^{285}–Cys^{508}) corresponds to the N terminus of 44-kDa MT1-MMP and includes both the linker and the hemopexin C domain (Fig. 1*A*, *iv*). MT1-CD (Gly^{315}–Cys^{508}) consists of the hemopexin C domain only (Fig. 1*A*, *iv*). Yields of purified protein were typically ~20 mg from 3 liters of liquid culture. The identities of the purified proteins were confirmed by Western blotting with αMT1-CD antibody (Fig. 1*B*) and αHis_6 (data not shown). Nonreducing SDS-PAGE analysis demonstrated the absence of dimeric intermolecular disulfide cross-linked aggregates (Fig. 1*B*). Reducing SDS-PAGE and electrospray ionization mass spectrometry determination of the purified protein masses were consistent with the predicted masses. As shown in Fig. 1*B*, both MT1-LCD (27,894 Da) and MT1-CD (24,612 Da) were within 1–2 Da of the predicted mass after accounting for the removal of the N-terminal methionine and hydrogen atoms after disulfide bond formation. Edman sequencing also confirmed N-terminal methionine processing and the presence of the N-terminal His_6 tag (Fig. 1*B*). MT1-LCD did not form noncovalent multimeric complexes under native conditions in solution as shown by the elution of a single peak at 28 kDa corresponding to the monomeric form of MT1-LCD upon gel filtration chromatography (Fig 1*C*).

Collagen Binding Properties of the MT1-MMP Hemopexin C Domain—We first assessed the collagen binding properties of the MT1-MMP hemopexin C domain by performing solid phase binding assays with type I collagen, the preferred collagen substrate of MT1-MMP. As shown in Fig. 2*A*, binding of MT1-CD and MT1-LCD to native collagen films was similar, indicating that the linker had little apparent affect on collagen binding affinity. Unlike MMP2-CBD, both MT1-CD and MT1-LCD did not bind denatured collagen (Fig. 2*B*), confirming specificity. As a control, MMP2-LCD did not bind native or denatured type I collagen as shown previously (57). Binding of soluble native type I collagen to MT1-CD and MT1-LCD was confirmed by ligand blot analysis with MMP2-LCD and BSA serving as negative controls (Fig. 2*C*).

Collagen/MT1-MMP Hemopexin C Domain Interactions during Collagen-induced MMP2 Activation—Physical clustering of MT1-MMP was previously shown to facilitate the pro-MMP2 activation reaction by increasing the proximity of catalytically active MT1-MMP to the trimeric activation complex (52). Due to the collagen binding properties of the MT1-MMP hemopexin C domain, we postulated that type I collagen may function as an *in vivo* mechanism to directly bind and concentrate cell surface MT1-MMP to facilitate the cellular activation of pro-

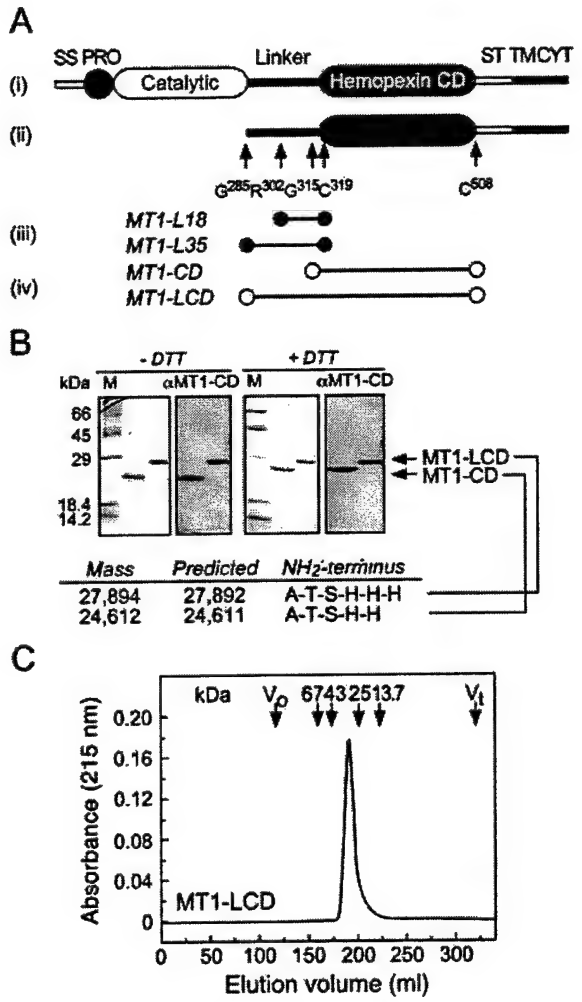

FIG. 1. **MT1-MMP hemopexin C domain constructs and linker peptide analogs.** *A*, the domain structures of pro-MT1-MMP (*i*) and 44-kDa MT1-MMP (*ii*) are shown in a linear diagram. The signal sequence (*SS*), propeptide domain (*PRO*), stalk segment (*ST*), transmembrane sequence (*TM*), and cytoplasmic tail (*CYT*) of MT1-MMP are indicated. Schematic representations of MT1-MMP linker peptide analogs MT1-L18 and MT1-L35 (*iii*) and hemopexin C domain constructs MT1-CD and MT1-LCD (*iv*) are shown with N- and C-terminal residues indicated. *B*, purified MT1-CD and MT1-LCD (0.1 μg) were electrophoresed on SDS-PAGE (15%) gels under reducing (+*DTT*) and nonreducing (−*DTT*) conditions. Gels were analyzed by either silver staining or by Western blotting using αMT1-CD antibody. Protein masses measured by electrospray ionization mass spectrometry (*Mass*), predicted masses, and N-terminal Edman sequence analysis are indicated. *C*, MT1-LCD was subjected to FPLC gel filtration chromatography on a Superdex 75 column, and elution was monitored at 215 nm. The elution volumes of the void volume (V_o) and column volume (V_t) and molecular weight standards are indicated.

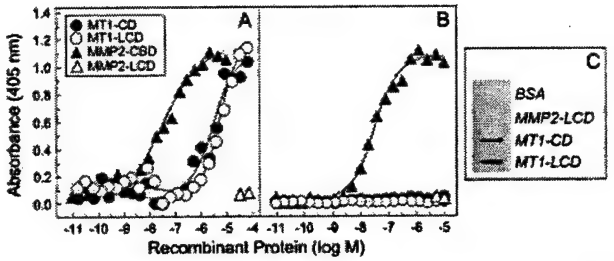

FIG. 2. **Type I collagen binding properties of MT1-MMP hemopexin C domain constructs.** Serial dilutions of MT1-CD and MT1-LCD were incubated in the same 96-microwell plates coated with native (*A*) or heat-denatured (65 °C for 1 h) (*B*) type I collagen (0.5 μg/well) as described under "Experimental Procedures." MMP2-CBD and MMP2-LCD were included as positive (54) and negative controls (57), respectively. Bound recombinant domains were detected using α-His_6 antibody. *C*, ligand blot assay. Immobilized MT1-CD and MT1-LCD and control proteins, BSA and MMP2-LCD (5 μg each), were incubated with biotin-labeled type I collagen (0.1 μg/ml) in PBS as described under "Experimental Procedures." Bound collagen was detected using streptavidin-HRP and ECL detection.

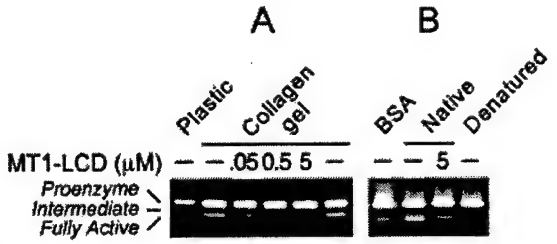

FIG. 3. **Recombinant MT1-MMP hemopexin C domain reduces collagen-induced activation of MMP2.** *A*, fibroblasts (1×10^4) grown on tissue culture plastic or within type I collagen gels (2.0 mg/ml) were incubated with MT1-LCD (0, 0.05–5 μM) in DMEM for 72 h. MMP2 in the conditioned cell media was visualized by gelatin zymography. *B*, fibroblasts (1×10^4) grown on plastic were incubated with latex beads adsorbed with type I collagen (native or denatured) or BSA in DMEM for 24 h. Exogenous MT1-LCD (5 μM) was added to the cultures where indicated. Conditioned cell media were analyzed by gelatin zymography. Lanes presented in both *A* and *B* are from the same zymogram.

MMP2. To test this, human gingival fibroblasts were cultured in three-dimensional type I collagen gels for 72 h to stimulate the activation of pro-MMP2. Soluble MT1-LCD was added to the cultures to compete with endogenous MT1-MMP for collagen binding. As shown in Fig. 3*A*, activation of pro-MMP2 in the cell cultures was reduced with increasing concentrations of MT1-LCD. Control cells cultured on plastic did not activate pro-MMP2. To confirm this response, latex beads coated with type I collagen were found to stimulate pro-MMP2 activation in fibroblasts cultured on plastic (Fig. 3*B*). Consistent with our observations of cells in collagen gels, induction of pro-MMP2 activation by native collagen-adsorbed beads was reduced by the presence of MT1-LCD to the levels seen with BSA-adsorbed beads (Fig. 3*B*). The requirement for fibrillar collagen was confirmed, since gelatin-adsorbed beads did not stimulate pro-MMP2 activation. In the absence of latex beads, the addition of soluble native collagen to fibroblasts cultured on plastic produced inconsistent and variable levels of activation (data not shown). Together, these results demonstrate that native type I fibrillar collagen interactions with the MT1-MMP hemopexin C domain in fibroblasts may concentrate cell surface MT1-MMP to stimulate the cellular activation of pro-MMP2.

Effect of Exogenous MT1-MMP Hemopexin C Domain on Collagenolysis by sMT1-MMP and MMP2—Studies of collagenases have shown that the hemopexin C domain is required to support binding to and cleavage of collagen (27–29, 31, 32, 59). To examine the role of the hemopexin C domain in MT1-MMP collagenolysis, recombinant hemopexin C domain constructs were incubated with sMT1-MMP and biotin-labeled type I collagen. Reactions were performed at 28 °C to maintain collagen triple helicity, as confirmed by the lack of collagen cleavage in the presence of trypsin even at a 1:10 enzyme/substrate molar ratio (data not shown). sMT1-MMP cleaved native type I collagen (Fig. 4*A*) and was inhibited by TIMP-2 and BB2116 (data not shown). As seen in Fig. 4*A* (*left panel*), the sMT1-MMP cleavage of native type I collagen was inhibited by the presence of MT1-LCD in a concentration-dependent manner. In contrast, neither MT1-CD (Fig. 4*A*, *right panel*) nor the control protein, MMP2-LCD, had any effect on cleavage. The percent-

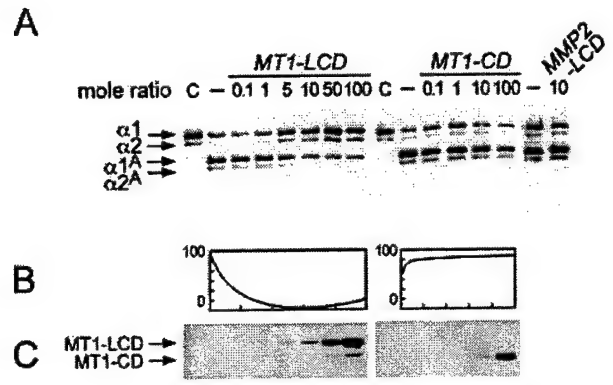

FIG. 4. **Recombinant MT1-MMP hemopexin C domain reduces MT1-MMP collagenolysis.** *A*, biotin-labeled type I collagen was incubated in the absence (*C*) or presence of sMT1-MMP (1 pmol) for 18 h at 28 °C. Recombinant proteins, MT1-LCD, MT1-CD, and MMP2-LCD were added at the indicated molar equivalents relative to sMT1-MMP. Reactions were separated by SDS-PAGE (7.5%), followed by Western blotting using streptavidin-HRP. *B*, percentage of α-chain cleavage was determined by densitometric analysis as described under "Experimental Procedures" and plotted against the amount of recombinant hemopexin C domain added. *C*, MT1-LCD and MT1-CD were detected in reaction samples by SDS-PAGE (15%) and Western blotting using the αMT1-CD antibody.

TABLE I

Quenched fluorescent peptide cleavage by sMT1-MMP

Mca-Pro-Leu-Gly-Dpa-Ala-Arg-NH_2 (0.1 nmol) was incubated with (control) or without (buffer) sMT1-MMP (0.035 pmol) for 1 h at 37 °C. MT1-LCD and MT1-CD were added to the reaction at a 100-fold molar excess to sMT1-MMP. RFU, relative fluorescence units.

	Buffer	Control	MT1-LCD	MT1-CD
Rate of cleavage (RFU × $10^{-3} \cdot s^{-1}$)	0.05	6.7	7.0	7.0

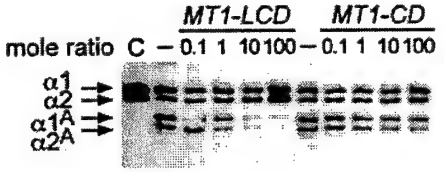

FIG. 5. **Recombinant MT1-MMP hemopexin C domain blocks MMP2 cleavage of native collagen.** *A*, biotin-labeled type I collagen was incubated in the absence (*C*) or presence of MMP2 (0.84 pmol) for 18 h at 28 °C. MT1-LCD and MT1-CD (0.1–100-fold molar equivalents) were added to the reactions where indicated. Following digestion, samples were separated by SDS-PAGE (7.5%), followed by Western blotting using streptavidin-HRP.

age of α-chain cleavage for each reaction was quantitated by scanning densitometry and graphically plotted against the amount of MT1-LCD or MT1-CD added (Fig. 4*B*). The presence of hemopexin C domain proteins at the end of each reaction was confirmed by Western blot analysis (Fig. 4*C*). As a control, MT1-CD and MT1-LCD did not affect sMT1-MMP activity against the quenched fluorescent peptide, Mca-Pro-Leu-Gly-Dpa-Ala-Arg-NH_2 (Table I), demonstrating that inhibition by MT1-LCD is specific for triple helical substrates and that peptide bond cleavage by MT1-MMP does not require the hemopexin C domain. Due to the unique association between MT1-MMP and MMP2 *in vivo*, we assessed whether the MT1-MMP hemopexin C domain may affect MMP2 collagenolysis. Similar to that observed for MT1-MMP, MT1-LCD, but not MT1-CD, disrupted MMP2 cleavage of native type I collagen (Fig. 5).

Collagen Binding Properties of MT1-MMP Linker Peptide Analogs and the Effect on Collagenolysis—Although both MT1-MMP hemopexin C domain constructs share similar collagen binding properties, only MT1-LCD disrupted collagenolysis. Since this result indicated an important role for the linker in native collagen cleavage, we generated two synthetic peptide linker analogs to further study the effect of the MT1-MMP linker on MT1-MMP collagenolysis. From clustal alignments, we synthesized the peptide analog MT1-L18 (Arg^{302}–Cys^{319}), which corresponds to an 18-amino acid residue region of similarity possessed by the collagenolytic MMPs, MMP1, MMP2, MMP8, and MMP13 (Fig. 6*A*). MT1-L35 (Gly^{285}–Cys^{319}) encompasses the entire MT1-MMP linker and includes the unique 17-amino acid residue region that is N-terminal to the homologous 18-amino acid residue region (Fig. 6*A*). As shown in Fig. 6*B*, neither MT1-L18 nor MT1-L35 showed affinity for native (Fig. 6*B*, *i*) or denatured type I collagen (Fig. 6*B*, *ii*), indicating that the MT1-MMP linker alone does not contribute to collagen binding or that the collagen binding site spans the junction of the linker and hemopexin C domain. Similarly, both peptide analogs did not disrupt native type I collagen cleavage by sMT1-MMP, even at a 1000-fold molar excess (Fig. 6*C*). To determine whether either linker peptide sequence could confer regulatory activity on the MT1-CD polypeptide, MT1-L18 or MT1-L35 was added to the reaction mixture containing MT1-CD. As shown in Fig. 6*C*, no inhibition of collagenolysis was observed. In a second set of experiments, MT1-LCD inhibited collagen cleavage as previously observed (Fig. 4), regardless of whether MT1-L18 or MT1-L35 was added. Since the presence of the linker sequence and the hemopexin C domain together as separate polypeptides is not sufficient for disrupting cleavage, these data suggest that the ability of the MT1-LCD to inhibit collagenolysis is context- and/or conformation-specific.

Cellular Invasion of Type I Collagen is Inhibited by a 44-kDa MT1-MMP Ectodomain Fragment—Active MT1-MMP is efficiently processed to a 44-kDa ectodomain fragment containing the MT1-LCD sequence (Gly^{285}–Cys^{508}) that is retained on the cell membrane (40, 46, 51). Since the soluble MT1-LCD inhibits native collagen cleavage by sMT1-MMP, we hypothesized that 44-kDa MT1-MMP may also function in a similar manner at the cell surface to modulate the collagenolytic activity of transmembrane MT1-MMP. To test this hypothesis, we used MDA-MB-231 breast carcinoma cells, which express endogenous MT1-MMP in the absence of detectable levels of MMP2. Invasion of three-dimensional collagen gels overlaid onto a porous polycarbonate filter requires collagenolytic activity (42). In control experiments, MDA-MB-231 cellular invasive activity was inhibited by the hydroxamate inhibitor GM6001, indicating a requirement for metalloproteinase activity (Fig. 7*A*). TIMP-2 significantly reduced invasion ($p < 0.05$), whereas TIMP-1 or the BSA control had no effect, confirming the dependence for MT-MMPs (60) in MDA-MB-231 cell invasion. A blocking antibody against the MT1-MMP active site (Fig. 7*A*, *anti-MT1*) also reduced invasion compared with IgG controls ($p < 0.05$), identifying MT1-MMP as the critical protease in this process. Indeed, overexpression of MT1-MMP on MDA-MB-231 cells increased collagen invasion ~2.5-fold compared with vector transfectants ($p < 0.05$, Fig. 7*A*, *black bars*). Furthermore, expression of the inactive mutant, MT1-MMP (E240A), on MDA-MB-231 cells resulted in inhibition of invasion to below control values, suggesting that this species may function in a dominant negative manner.

To determine whether the MT1-LCD could inhibit cell-associated collagenolytic activity, cells were incubated with MT1-LCD, MT1-L35, or BSA. At low concentrations (4 μM), the invasion of MT1-MMP transfected (Fig. 7*B*) or parental (data not shown) MDA-MB-231 cells was unaffected. MT1-L35 did not affect invasion at any concentration tested (data not

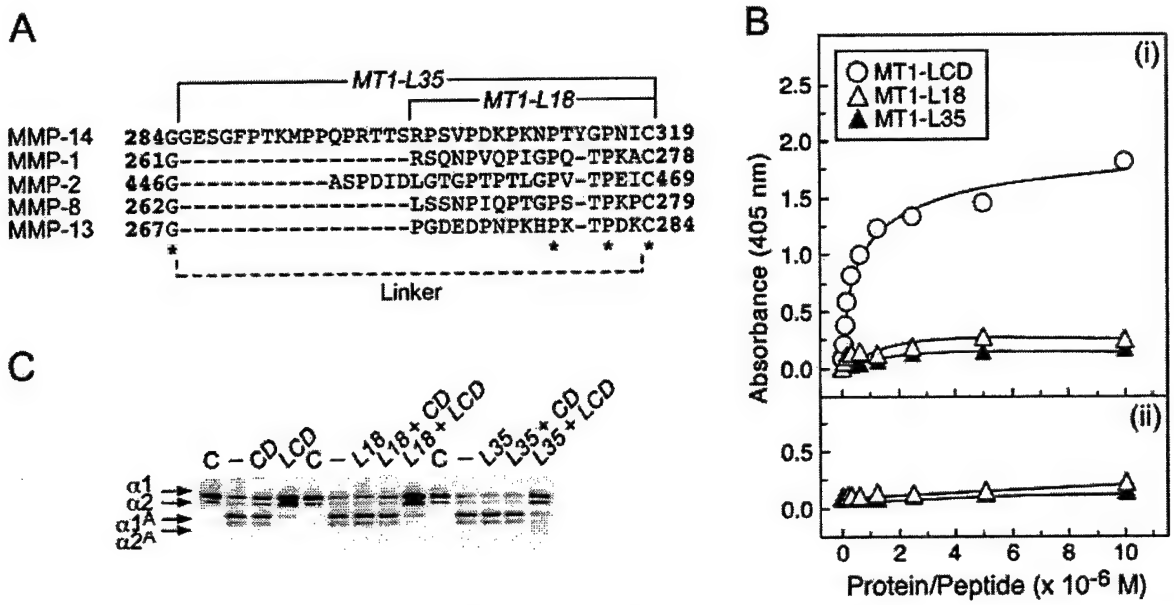

FIG. 6. **Characterization of MT1-MMP peptide linker analogs.** *A*, sequence alignment of collagenolytic MMP linkers using Megalign (DNASTAR Inc.) (Clustal method). Conserved residues are denoted with *asterisks*. Sequences of the peptide analogs of MT1-MMP are indicated. *B*, a 96-well plate was coated with either native (*i*) or denatured (*ii*) type I collagen (rat tail) (0.5 μg/well). Serial dilutions of MT1-LCD, MT1-L18, and MT1-L35 were added, and bound protein/peptide was detected using RP1MMP-14 antibody, which recognizes the linker. *C*, biotin-labeled type I collagen was incubated in the absence (*C*) or presence of sMT1-MMP (1 pmol) for 18 h at 28 °C. Molar excesses of MT1-MMP hemopexin C domain constructs (*CD* and *LCD*) (100-fold) and linker peptide analogs (*L18* and *L35*) (1000-fold) were added to the reaction where indicated. Reactions were separated by SDS-PAGE (7.5%), followed by Western blotting using streptavidin-HRP.

shown). However, since MT1-LCD binds native collagen, the effective concentration of free protein available to the cells may be reduced by binding to the collagen filters. Therefore, the highest concentration possible with these protein preparations (30 μM) was used to ensure saturation of binding sites within the collagen-coated filters and availability of free protein at the cell surface to interact with MT1-MMP. Under these conditions, collagen invasion was significantly reduced ($p < 0.05$; Fig. 7*B*), demonstrating inhibition of cell-associated MT1-MMP collagenolytic activity and confirming the *in vitro* analysis of MT1-LCD inhibiting collagen cleavage.

Because autolysis of transmembrane MT1-MMP leads to the accumulation of a cell surface 44-kDa MT1-MMP ectodomain fragment containing the linker and hemopexin C domain but lacking the active site, the effect of this cell-associated product on cellular MT1-MMP-mediated collagenolysis was assessed. For this experiment, transmembrane constructs of MT1-LCD (Gly^{285}–Val^{582}, designated cMT1-LCD) and MT1-CD (Pro^{316}–Val^{582}, designated cMT1-CD) (Fig. 8*A*) were expressed in MDA-MB-231 cells, and type I collagen invasion was assessed relative to vector-transfected controls. Intracellular furin processing of these constructs at Arg^{111} generates the 44-kDa MT1-MMP and the linker-deleted form thereof. Expression of cMT1-LCD significantly reduced invasion by 50% to levels similar to those seen with soluble MT1-LCD when compared with cells expressing cMT1-CD ($p < 0.05$; Fig. 8*B*). This confirms the above results and the *in vitro* biochemical analyses and demonstrates the importance of the MT1-MMP linker-hemopexin C domain in native collagen cleavage by cellular MTI-MMP. In control experiments, migration of MDA-MB-231 cells toward type I collagen, a process independent of collagenase activity (42, 61), was unaffected by expression of cMT1-LCD or cMT1-CD (Fig. 8*C*). Since these data clearly demonstrate the ability of cMT1-LCD to modulate type I collagen cleavage by transmembrane MT1-MMP, our results suggest that a function of the endogenous MT1-MMP autolysis product, 44-kDa MT1-MMP, is to regulate pericellular collagenolytic activity.

DISCUSSION

As an integral membrane protein, MT1-MMP appears suited for coordinating the homeostatic catabolism of pericellular type I collagen under the guide of the cell (62–65). MT1-MMP mediates collagen degradation directly by cleaving native collagen and, indirectly, by activating MMP13 (9) and the gelatinase and weak collagenase, MMP2 (11–13). Spatially and temporally, these two distinct activities of MT1-MMP regulate collagenolytic and gelatinolytic activities on the cell surface. Since MT1-MMP is a critical initiator and effector in the pericellular collagenolytic cascade, the regulation of its biological activity is very important in physiological and pathological collagen remodeling. The studies reported here have revealed the importance of the MT1-MMP hemopexin C domain and linker in the mechanism of collagen cleavage and demonstrated the role of collagen binding to MT1-MMP in stimulating MMP2 activation by cells. Moreover, these actions may be modulated in a dominant negative manner by the 44-kDa remnant form of MT1-MMP on the cell surface, revealing a novel regulatory function in proteolysis for an autolytic fragment of a protease.

The structure of collagen presents a challenge for proteolytic cleavage, as indicated by the low k_{cat}/K_m values for collagenases (66). Despite several studies from a number of laboratories, the triple helicase mechanism remains enigmatic (14). Our use of recombinant domains and polypeptides to probe the exosite requirements of MT1-MMP for collagenolysis revealed similar domain requirements for triple helicase activity as the secreted collagenases. The binding of the MT1-MMP hemopexin C domain, with or without the linker, to native collagen is consistent with previous reports for the collagenolytic MMPs (27, 30–32). The hemopexin C domain of MMP2, in contrast, does bind native collagen stably (57). Interestingly, the MT1-MMP hemopexin C domain does not bind denatured collagen. This suggests that, following cleavage, subsequent denaturation of the collagen would result in the release of MT1-MMP from the cleaved substrate facilitating turnover.

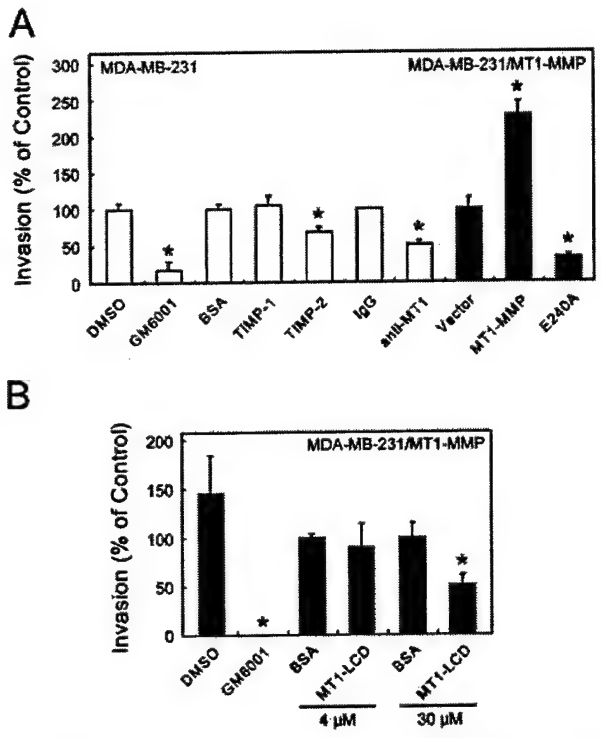

FIG. 7. **Invasion of MDA-MB-231 cells is MT1-MMP-dependent and is inhibited by recombinant MT1-MMP hemopexin C domain.** *A* and *B*, invasion of type I collagen. Cells (2.5×10^5) were seeded onto Transwell filters (8-μm pore) coated with a type I collagen gel (20 μg) and allowed to invade for 24 h as described under "Experimental Procedures." Noninvading cells were removed from the upper chamber with a cotton swab. Filters were then stained, and cells, adherent to the underside of the filter, were enumerated using an ocular micrometer. The average of triplicate experiments were normalized to corresponding controls (designated 100%) and are presented with S.D. value shown (*, $p < 0.05$). *A*, parental MDA-MB-231 cells (*white*) were allowed to invade in the presence of Me_2SO (*DMSO*), GM6001 (10 μM), BSA (10 nM), TIMP-1 (10 nM), TIMP-2 (10 nM), purified rabbit IgG (*IgG*; 10 μg/ml), or AB8102 antibody (*anti-MT1*; 10 μg/ml). MDA-MB-231 cells expressing MT1-MMP or MT1-MMP(E240A) (*black*) were also analyzed. Results are expressed as percentage of control invasion (*versus BSA* and *Vector*, as appropriate). *B*, MDA-MB-231 cells expressing MT1-MMP (2.5×10^5) were incubated with Me_2SO, GM6001 (10 μM), MT1-LCD, and BSA (4 and 30 μM) and allowed to invade for 24 h. Results are expressed as percentage of control invasion (*versus* BSA).

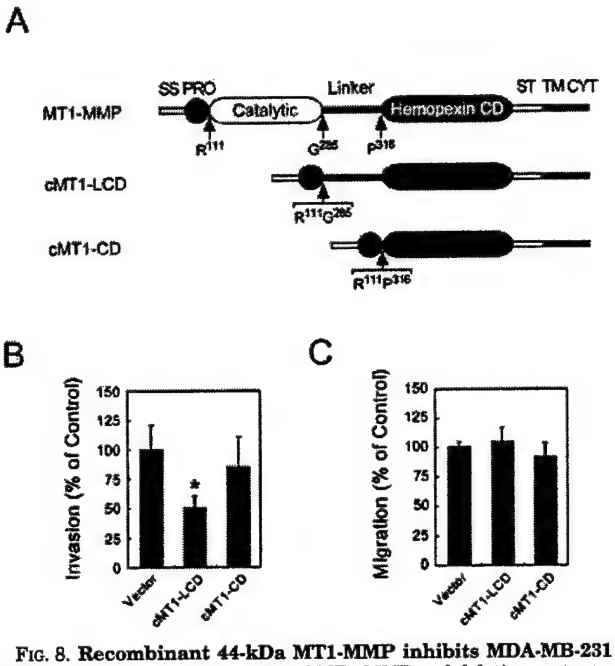

FIG. 8. **Recombinant 44-kDa MT1-MMP inhibits MDA-MB-231 cell invasion.** *A*, linear diagram of MT1-MMP and deletion mutants, cMT1-LCD (Δ112–284) and cMT1-CD (Δ112–315). The signal sequence (*SS*), propeptide domain (*PRO*), stalk segment (*ST*), transmembrane sequence (*TM*), and cytoplasmic tail (*CYT*) are indicated. Invasion of type I collagen (*B*) and migration (*C*) of MDA-MB-231 cells expressing MT1-MMP deletion mutants, cMT1-LCD and cMT1-CD, were assessed. *B*, cells (2.5×10^5) were seeded onto Transwell filters (8-μm pore) coated with a type I collagen gel (20 μg) and allowed to invade for 24 h as described under "Experimental Procedures." *C*, cells (2.5×10^5) were seeded onto Transwell filters coated with a thin layer of collagen on the underside and incubated for 1.5 h to permit migration. In both assays, noninvading or nonmigrating cells were removed from the upper chamber with a cotton swab. Filters were then stained, and cells, adherent to the underside of the filter, were enumerated using an ocular micrometer. The averages of triplicate experiments were normalized to the vector control (designated 100%) and are presented with S.D. value as shown (*, $p < 0.05$).

Inhibition of sMT1-MMP collagen cleavage using MT1-MMP hemopexin C domain constructs required the presence of the linker, indicating that collagen binding, by the hemopexin C domain alone, is not sufficient to disrupt collagenolysis. This requirement was also observed in MMP2 collagenolysis, since MT1-LCD, but not MT1-CD, blocked MMP2 cleavage of native collagen. Protein engineering studies of MMP1 and MMP8 have previously shown a role for the linker in triple helicase activity (33–35); however, our studies have revealed some unique features of the MT1-MMP linker. De Souza *et al.* (67) proposed that the MMP1 collagenase linker, due to its proline content, intercalates with the collagen triple helix, thereby displacing individual α-chains for cleavage. We found that MT1-MMP linker peptide analogs of either the full-length 35-amino acid residue linker or the 18-amino acid residue region, corresponding to that found in the secreted collagenases, did not bind native or denatured type I collagen. These results indicate that the MT1-MMP linker may not bind or intercalate with the collagen triple helix as proposed for the MMP1 linker. Indeed, the low glycine content renders triple helix formation by these linkers impossible. Potentially, the full collagen binding exosite of the MT1-MMP hemopexin C domain that recognizes the ¾-¼ collagen site may span the linker/hemopexin C domain junction, thereby accounting for the lack of collagen binding by the linker analogs alone and the ineffectiveness of MTI-CD in blocking collagenolysis. The MT1-MMP linker, when connected to the hemopexin C domain, may act as a specificity determinant directing binding of the protease to the ¾-¼ collagen cleavage site. Thus, competition from MT1-LCD, but not MT1-CD, may block MT1-MMP from binding collagen here and so inhibit cleavage. Topographically, the MT1-MMP, and other collagenase linkers, may also correctly configure the catalytic domain relative to the hemopexin C domain for collagenolytic competence. Indeed, the MT1-MMP linker has predicted rigidity due to the presence of 9 proline residues, and we interpret the x-ray crystallographic structure of the MMP1 linker (68) to also indicate that the linker is not as flexible as generally thought. Hence, MT1-LCD binding of collagen may sterically disrupt the collagenolytic configuration of sMT1-MMP at the ¾-¼ collagen cleavage site, thereby inhibiting cleavage.

The importance of MT1-MMP in collagen homeostasis is supported by the finding that fibrillar type I collagen induces cell surface expression of MT1-MMP and subsequent MMP2 activation through transcriptional and nontranscriptional pathways (36–41, 69). Induction of MT1-MMP transcription is dependent on β_1 integrin receptors and actin cytoskeleton rearrangement (38, 43). Clustering of β_1 integrins by collagen

ligation or antibody cross-linking induces *de novo* expression of MT1-MMP and subsequent MMP2 activation (40, 42). Interestingly, our data reveal that collagen may also assemble MT1-MMP on the cell surface via binding to the hemopexin C domain, thereby increasing the local concentration of MT1-MMP for collagenolysis and efficient MMP2 activation. In view of the demonstrated absence of oligomer formation by the MT1-LCD used here and previously reported (47), we interpret the reduction in collagen-induced MMP2 activation by MT1-LCD to be the result of competitive binding for collagen between the exogenous MT1-LCD and cell surface MT1-MMP, rather than competitively disrupting any MT1-MMP·MT1-MMP binding interactions. Indeed, this interaction between MT1-MMP and collagen may represent a biological mechanism similar to that observed with ConA, which clusters MT1-MMP on the cell surface during MMP2 activation (47). As originally shown, ConA increases the matrix-degradative phenotype of the cell through transcriptional and post-transcriptional regulation of MMP and TIMP genes that was reflected by extensive endogenous collagen degradation in the conditioned media and in biochemical assays (50). Cleavage of β_1 integrin-ligated collagen also releases bound pro-MMP2, which can now enter the activation pathway, which otherwise is recalcitrant to activation (70). Hence, pericellular collagen has multiple effects in binding and regulating the activities of collagenolytic MMPs, representing an unusual relationship between a protease and cognate substrate that appears to contribute to the homeostatic maintenance of collagen levels.

MT1-MMP activity on the cell surface is further regulated by endocytosis (71, 72), TIMP binding (45, 56, 73), and trimolecular complex formation (56, 74) as well as the autolytic shedding of the catalytic domain to yield 44-kDa MT1-MMP (46, 51, 75, 76). Currently, the role of 44-kDa MT1-MMP *in vivo* is not clear. It has been reported recently that the hemopexin C domain and the cytoplasmic tail of MT1-MMP mediate homophilic interactions that increase MMP2 activation (48, 49). Using HT1080 cells, Itoh *et al.* (48) found that expression of MT1-MMP PEX (Thr^{313}–Val^{582}), a truncated form of 44-kDa MT1-MMP that lacks most of the linker and hence is similar to cMT1-CD used here, reduced MMP2 activation and subsequent Matrigel invasion, presumed to be by disrupting the formation of oligomeric MT1-MMP complexes. PEX is unfortunately a confusing designation for the MT1-MMP hemopexin C domain, since PEX was already the name of a cell surface zinc metallopeptidase belonging to the neprilysin family (77, 78). As reported here and previously (47), we have found no evidence for oligomerization using MT1-LCD or MT1-CD, emphasizing the importance of cell membrane context or the stalk segment, transmembrane sequence, and cytoplasmic tail in these proposed complexes. Our recent data[2] indicate that the stalk segment also does not dimerize or drive oligomerization of 44-kDa MT1-MMP. Unlike the effects of MT1-LCD in disrupting the collagen-induced activation of MMP2 shown here, the inability of soluble MT1-LCD or MT1-CD to competitively block ConA-induced MMP2 activation in cells cultured on plastic reported previously (47) indicates the importance of cellular context for these effects and highlights the difference in collagen-mediated activation of MMP2, which is blocked by MT1-LCD, from activation induced by MT1-MMP overexpression or ConA, which is not.

In our previous studies of chemokine cleavage by MMP2, we found that MCP-3 and SDF-1α binding to the hemopexin C domain markedly improved the catalytic efficiency of cleavage (79, 80). Notably, the addition of recombinant MMP2 hemopexin C domain to mixtures of chemokine and active MMP2 in enzyme assays could entirely block substrate cleavage (80). Therefore, the presence of the entire 35-amino acid residue linker and hemopexin C domain in the 44-kDa MT1-MMP ectodomain suggested to us that this autolytic product has the potential to antagonize the proteolytic activity of MT1-MMP in a dominant-negative manner by interacting with native collagen. Our data demonstrate that expression of cMT1-LCD (Gly^{285}–Val^{582}), representing the 44-kDa MT1-MMP in its entirety (46, 76), on MDA-MB-231 cells inhibits MT1-MMP-mediated type I collagen cleavage and cell invasion. The inhibitory effect of cMT1-LCD expression on cell invasion was confirmed by the addition of soluble MT1-LCD to MT1-MMP-transfected cells. Since MDA-MB-231 cells do not express MMP2, the effect of cMT1-LCD expression and MT1-LCD on collagenolysis and cell invasion is distinct from that reported previously (48) and discussed above. Nonetheless, the capacity of MT1-LCD to also block MMP2 native collagen cleavage may amplify the down-regulation of collagenolysis *in vivo* by blocking MMP2 in addition to MT1-MMP but sparing MMP2 gelatinolysis. Invasion was also inhibited with the expression of MT1-MMP (E240A), a dominant-negative mutant mimicking TIMP-2-inhibited MT1-MMP, further supporting the role of MT1-MMP in collagen invasion and of inactive MT1-MMP forms in competing for collagen binding and down-regulating collagen cleavage. Consistent with our biochemical analysis, neither the expression of cMT1-CD nor the addition of soluble MT1-CD (data not shown) affected cell invasion to a significant degree, confirming the importance of the MT1-MMP linker in context with the hemopexin C domain in collagenolysis. In view of these effects, we propose that 44-kDa MT1-MMP may reduce MMP2 activation by reducing MT1-MMP clustering mediated by pericellular collagen. Together, these results clearly reveal the 44-kDa MT1-MMP as a novel inhibitor of pericellular type I collagen cleavage by MT1-MMP and MMP2 activities. Our studies also demonstrate the feasibility of designing new MMP inhibitors that target the substrate rather than the protease (81). This new class of inhibitors may exert highly selective substrate-specific protease inhibition while sparing the cleavage of other substrates in the protease degradome. Similarly, targeting the protease exosite rather than the active site may also represent new avenues of substrate-specific inhibition to achieve levels of specificity not possible with active site inhibitors (81).

The degradation of pericellular type I collagen is revealed to be a dynamic self-regulated process. We have previously proposed models regarding the regulation of pericellular type I collagen levels upon β_1 integrin stimulation of MT1-MMP and MMP2 activity (14, 40, 70). Our investigation into the role of the 44-kDa MT1-MMP ectodomain adds a new dimension to this homeostatic process. As modeled in Fig. 9, fibrillar type I collagen induces a β_1 integrin-dependent increase in MT1-MMP expression on the cell surface, thus favoring an initial collagenolytic phase. Our data show that the collagen binding properties of the MT1-MMP hemopexin C domain are necessary for native collagen cleavage (Fig. 9*A*). As suggested previously (70), the release of collagen-bound pro-MMP2 from the cell surface following collagen cleavage by MT1-MMP allows pro-MMP2 reservoirs to be optimally activated temporally and spatially in relation to its substrate. Collagen binding by the MT1-MMP hemopexin C domain also potentiates MMP2 activation, most likely by concentrating MT1-MMP·TIMP-2·pro-MMP2 complexes with TIMP-free MT1-MMP (Fig. 9*A*). Furthermore, in the MMP2 activation process, MT1-MMP collagenolytic activities are suppressed by TIMP-2 binding to form the trimolecular pro-MMP2 complex and by MT1-MMP autolysis, converting the proteolytic signature of the cell from

[2] E. M. Tam and C. M. Overall, unpublished data.

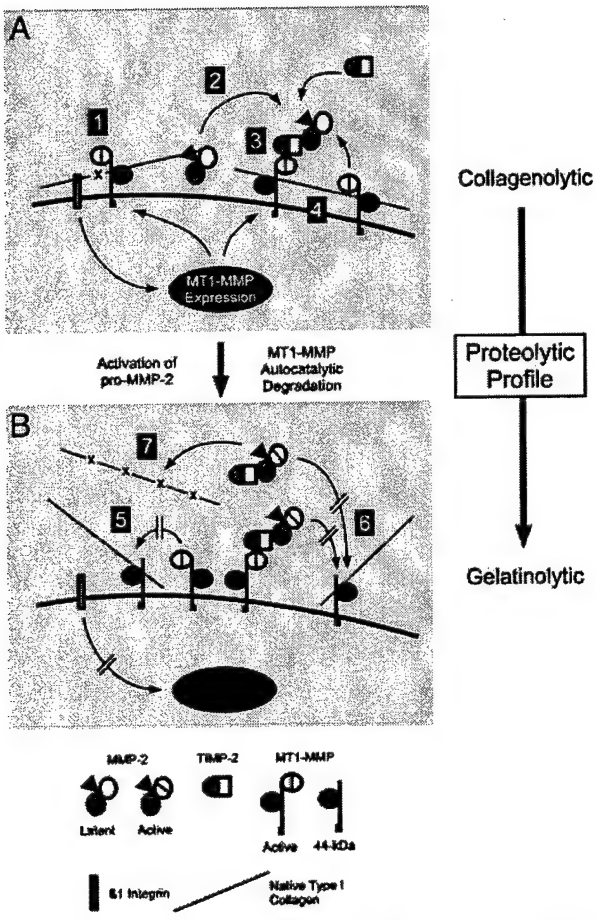

FIG. 9. **Potential role of the 44-kDa MT1-MMP in pericellular collagen degradation.** *A*, collagenolytic cell profile. Upon collagen-induced engagement of β_1 integrins and intracellular signaling, expression of MT1-MMP is up-regulated on the cell surface. Increased MT1-MMP expression promotes the cleavage of native collagen (*1*) and the release of collagen-bound pro-MMP2, which now enters into the activation pathway (*2*). The conversion from collagenolysis to gelatinolysis commences with the formation of the trimolecular complex (*3*), which reduces MT1-MMP collagenolytic activity, and the activation of pro-MMP2, which is enhanced by the collagen-mediated assembly of MT1-MMP (*4*). Collagen binding by TIMP-2-inhibited MT1-MMP in the trimolecular complex may also block collagen cleavage by uninhibited MT1-MMP. *B*, gelatinolytic cell profile. Following pro-MMP2 activation and MT1-MMP autolysis, the 44-kDa MT1-MMP accumulates on the cell surface, binds native collagen, and suppresses collagen degradation by inhibiting MT1-MMP (*5*) and MMP2 (*6*) collagenolysis but not MMP2 gelatinolysis (*7*). Stimulation of cell surface MT1-MMP expression is reduced due to the absence of native collagen and β_1 integrin engagement which together allow collagen levels to increase.

collagenolytic to gelatinolytic. Following MT1-MMP autolytic shedding, our data show that the 44-kDa MT1-MMP continues to bind collagen, further reducing pericellular collagenolysis by MT1-MMP and MMP-2 (Fig. 9*B*). Overall, these intimately related and complex events allow for a conversion of proteolytic activity to take place on the cell surface. This shift from a collagenolytic to a gelatinolytic profile may be important for maintaining pericellular collagen levels. Thus, collagen is a unique substrate; by binding the proteases responsible for its cleavage, these interactions recruit and regulate collagenolytic and gelatinolytic activities in a homeostatic manner. Hence, the studies reported here reveal several new aspects in the biology of MT1-MMP as a consequence of native type I collagen binding by the hemopexin C domain. This also provides a novel explanation for the generation of MT1-MMP clusters on the cell surface and adds a new layer of control to the complex regulation of focal proteolysis by MT1-MMP and MMP2.

REFERENCES

1. Vuorio, E., and de Crombrugghe, B. (1990) *Annu. Rev. Biochem.* **59**, 837–872
2. Egeblad, M., and Werb, Z. (2002) *Nat. Rev. Cancer* **2**, 161–174
3. Stetler-Stevenson, W. G., and Yu, A. E. (2001) *Semin. Cancer Biol.* **11**, 143–152
4. Overall, C. M., and Sodek, J. (1988) in *Biological Mechanisms of Tooth Eruption and Root Resorption* (Davidovitch, Z., ed) pp. 303–312, EBSCO Media, Birmingham, Alabama
5. Saftig, P., Hunziker, E., Wehmeyer, O., Jones, S., Boyde, A., Rommerskirch, W., Moritz, J. D., Schu, P., and von Figura, K. (1998) *Proc. Natl. Acad. Sci. U. S. A.* **95**, 13453–13458
6. Nagase, H., and Woessner, J. F., Jr. (1999) *J. Biol. Chem.* **274**, 21491–21494
7. Pei, D., and Weiss, S. J. (1996) *J. Biol. Chem.* **271**, 9135–9140
8. Ohuchi, E., Imai, K., Fujii, Y., Sato, H., Seiki, M., and Okada, Y. (1997) *J. Biol. Chem.* **272**, 2446–2451
9. Cowell, S., Knauper, V., Stewart, M. L., D'Ortho, M. P., Stanton, H., Hembry, R. M., Lopez-Otin, C., Reynolds, J. J., and Murphy, G. (1998) *Biochem. J.* **331**, 453–458
10. Sato, H., Takino, T., Okada, Y., Cao, J., Shinagawa, A., Yamamoto, E., and Seiki, M. (1994) *Nature* **370**, 61–65
11. Sodek, J., and Overall, C. M. (1992) *Matrix Suppl.* **1**, 352–362
12. Aimes, R. T., and Quigley, J. P. (1995) *J. Biol. Chem.* **270**, 5872–5876
13. Patterson, M. L., Atkinson, S. J., Knauper, V., and Murphy, G. (2001) *FEBS Lett.* **503**, 158–162
14. Overall, C. M. (2001) *Methods Mol. Biol.* **151**, 79–120
15. Yana, I., and Weiss, S. J. (2000) *Mol. Biol. Cell* **11**, 2387–2401
16. Rozanov, D. V., Deryugina, E. I., Ratnikov, B. I., Monosov, E. Z., Marchenko, G. N., Quigley, J. P., and Strongin, A. Y. (2001) *J. Biol. Chem.* **276**, 25705–25714
17. Takino, T., Sato, H., Yamamoto, E., and Seiki, M. (1995) *Gene (Amst.)* **155**, 293–298
18. Galvez, B. G., Matias-Roman, S., Albar, J. P., Sanchez-Madrid, F., and Arroyo, A. G. (2001) *J. Biol. Chem.* **276**, 37491–37500
19. Belien, A. T., Paganetti, P. A., and Schwab, M. E. (1999) *J. Cell Biol.* **144**, 373–384
20. Aznavoorian, S., Moore, B. A., Alexander-Lister, L. D., Hallit, S. L., Windsor, L. J., and Engler, J. A. (2001) *Cancer Res.* **61**, 6264–6275
21. Holmbeck, K., Bianco, P., Caterina, J., Yamada, S., Kromer, M., Kuznetsov, S. A., Mankani, M., Robey, P. G., Poole, A. R., Pidoux, I., Ward, J. M., and Birkedal-Hansen, H. (1999) *Cell* **99**, 81–92
22. Zhou, Z., Apte, S. S., Soininen, R., Cao, R., Baaklini, G. Y., Rauser, R. W., Wang, J., Cao, Y., and Tryggvason, K. (2000) *Proc. Natl. Acad. Sci. U. S. A.* **97**, 4052–4057
23. Martignetti, J. A., Aqeel, A. A., Sewairi, W. A., Boumah, C. E., Kambouris, M., Mayouf, S. A., Sheth, K. V., Eid, W. A., Dowling, O., Harris, J., Glucksman, M. J., Bahabri, S., Meyer, B. F., and Desnick, R. J. (2001) *Nat. Genet.* **28**, 261–265
24. Knauper, V., Patterson, M. L., Gomis-Ruth, F. X., Smith, B., Lyons, A., Docherty, A. J., and Murphy, G. (2001) *Eur. J. Biochem.* **268**, 1888–1896
25. Chung, L., Shimokawa, K., Dinakarpandian, D., Grams, F., Fields, G. B., and Nagase, H. (2000) *J. Biol. Chem.* **275**, 29610–29617
26. Brandstetter, H., Grams, F., Glitz, D., Lang, A., Huber, R., Bode, W., Krell, H. W., and Engh, R. A. (2001) *J. Biol. Chem.* **276**, 17405–17412
27. Allan, J. A., Hembry, R. M., Angal, S., Reynolds, J. J., and Murphy, G. (1991) *J. Cell Sci.* **99**, 789–795
28. Clark, I. M., and Cawston, T. E. (1989) *Biochem. J.* **263**, 201–206
29. Windsor, L. J., Birkedal-Hansen, H., Birkedal-Hansen, B., and Engler, J. A. (1991) *Biochemistry* **30**, 641–647
30. Murphy, G., Allan, J. A., Willenbrock, F., Cockett, M. I., O'Connell, J. P., and Docherty, A. J. (1992) *J. Biol. Chem.* **267**, 9612–9618
31. Knauper, V., Osthues, A., DeClerck, Y. A., Langley, K. E., Blaser, J., and Tschesche, H. (1993) *Biochem. J.* **291**, 847–854
32. Knauper, V., Cowell, S., Smith, B., Lopez-Otin, C., O'Shea, M., Morris, H., Zardi, L., and Murphy, G. (1997) *J. Biol. Chem.* **272**, 7608–7616
33. Hirose, T., Patterson, C., Pourmotabbed, T., Mainardi, C. L., and Hasty, K. A. (1993) *Proc. Natl. Acad. Sci. U. S. A.* **90**, 2569–2573
34. Knauper, V., Docherty, A. J., Smith, B., Tschesche, H., and Murphy, G. (1997) *FEBS Lett.* **405**, 60–64
35. de Souza, S. J., and Brentani, R. (1992) *J. Biol. Chem.* **267**, 13763–13767
36. Azzam, H. S., and Thompson, E. W. (1992) *Cancer Res.* **52**, 4540–4544
37. Gilles, C., Polette, M., Seiki, M., Birembaut, P., and Thompson, E. W. (1997) *Lab. Invest.* **76**, 651–660
38. Tomasek, J. J., Halliday, N. L., Updike, D. L., Ahern-Moore, J. S., Vu, T. K., Liu, R. W., and Howard, E. W. (1997) *J. Biol. Chem.* **272**, 7482–7487
39. Haas, T. L., Davis, S. J., and Madri, J. A. (1998) *J. Biol. Chem.* **273**, 3604–3610
40. Ellerbroek, S. M., Fishman, D. A., Kearns, A. S., Bafetti, L. M., and Stack, M. S. (1999) *Cancer Res.* **59**, 1635–1641
41. Ruangpanit, N., Chan, D., Holmbeck, K., Birkedal-Hansen, H., Polarek, J., Yang, C., Bateman, J. F., and Thompson, E. W. (2001) *Matrix Biol.* **20**, 193–203
42. Ellerbroek, S. M., Wu, Y. I., Overall, C. M., and Stack, M. S. (2001) *J. Biol. Chem.* **276**, 24833–24842
43. Seltzer, J. L., Lee, A. Y., Akers, K. T., Sudbeck, B., Southon, E. A., Wayner, E. A., and Eisen, A. Z. (1994) *Exp. Cell Res.* **213**, 365–374
44. Ellerbroek, S. M., and Stack, M. S. (1999) *Bioessays* **21**, 940–949
45. Butler, G. S., Butler, M. J., Atkinson, S. J., Will, H., Tamura, T., van Westrum, S. S., Crabbe, T., Clements, J., d'Ortho, M. P., and Murphy, G. (1998) *J. Biol. Chem.* **273**, 871–880
46. Hernandez-Barrantes, S., Toth, M., Bernardo, M. M., Yurkova, M., Gervasi, D. C., Raz, Y., Sang, Q. A., and Fridman, R. (2000) *J. Biol. Chem.* **275**,

12080–12089
47. Overall, C. M., Tam, E., McQuibban, G. A., Morrison, C., Wallon, U. M., Bigg, H. F., King, A. E., and Roberts, C. R. (2000) *J. Biol. Chem.* **275,** 39497–39506
48. Itoh, Y., Takamura, A., Ito, N., Maru, Y., Sato, H., Suenaga, N., Aoki, T., and Seiki, M. (2001) *EMBO J.* **20,** 4782–4793
49. Lehti, K., Lohi, J., Juntunen, M. M., Pei, D., and Keski-Oja, J. (2002) *J. Biol. Chem.* **277,** 8440–8448
50. Overall, C. M., and Sodek, J. (1990) *J. Biol. Chem.* **265,** 21141–21151
51. Lehti, K., Lohi, J., Valtanen, H., and Keski-Oja, J. (1998) *Biochem. J.* **334,** 345–353
52. Kinoshita, T., Sato, H., Okada, A., Ohuchi, E., Imai, K., Okada, Y., and Seiki, M. (1998) *J. Biol. Chem.* **273,** 16098–16103
53. Albini, A., Melchiori, A., Santi, L., Liotta, L. A., Brown, P. D., and Stetler-Stevenson, W. G. (1991) *J. Natl. Cancer Inst.* **83,** 775–779
54. Steffensen, B., Wallon, U. M., and Overall, C. M. (1995) *J. Biol. Chem.* **270,** 11555–11566
55. Mancini, S., Romanelli, R., Laschinger, C. A., Overall, C. M., Sodek, J., and McCulloch, C. A. (1999) *J. Periodontol.* **70,** 1292–1302
56. Bigg, H. F., Morrison, C. J., Butler, G. S., Bogoyevitch, M. A., Wang, Z., Soloway, P. D., and Overall, C. M. (2001) *Cancer Res.* **61,** 3610–3618
57. Wallon, U. M., and Overall, C. M. (1997) *J. Biol. Chem.* **272,** 7473–7481
58. Overall, C. M., and Sodek, J. (1987) *J. Dent. Res.* **66,** 1271–1282
59. d'Ortho, M. P., Will, H., Atkinson, S., Butler, G., Messent, A., Gavrilovic, J., Smith, B., Timpl, R., Zardi, L., and Murphy, G. (1997) *Eur. J. Biochem.* **250,** 751–757
60. Strongin, A. Y., Marmer, B. L., Grant, G. A., and Goldberg, G. I. (1993) *J. Biol. Chem.* **268,** 14033–14039
61. Fishman, D. A., Liu, Y., Ellerbroek, S. M., and Stack, M. S. (2001) *Cancer Res.* **61,** 3194–3199
62. Nakahara, H., Howard, L., Thompson, E. W., Sato, H., Seiki, M., Yeh, Y., and Chen, W. T. (1997) *Proc. Natl. Acad. Sci. U. S. A.* **94,** 7959–7964
63. Nabeshima, K., Inoue, T., Shimao, Y., Okada, Y., Itoh, Y., Seiki, M., and Koono, M. (2000) *Cancer Res.* **60,** 3364–3369
64. Lehti, K., Valtanen, H., Wickstrom, S., Lohi, J., and Keski-Oja, J. (2000) *J. Biol. Chem.* **275,** 15006–15013
65. Hotary, K., Allen, E., Punturieri, A., Yana, I., and Weiss, S. J. (2000) *J. Cell Biol.* **149,** 1309–1323
66. Welgus, H. G., Jeffrey, J. J., Stricklin, G. P., Roswit, W. T., and Eisen, A. Z. (1980) *J. Biol. Chem.* **255,** 6806–6813
67. De Souza, S. J., Pereira, H. M., Jacchieri, S., and Brentani, R. R. (1996) *FASEB J.* **10,** 927–930
68. Li, J., Brick, P., O'Hare, M. C., Skarzynski, T., Lloyd, L. F., Curry, V. A., Clark, I. M., Bigg, H. F., Hazleman, B. L., and Cawston, T. E. (1995) *Structure* **3,** 541–549
69. Gilles, C., Bassuk, J. A., Pulyaeva, H., Sage, E. H., Foidart, J. M., and Thompson, E. W. (1998) *Cancer Res.* **58,** 5529–5536
70. Steffensen, B., Bigg, H. F., and Overall, C. M. (1998) *J. Biol. Chem.* **273,** 20622–20628
71. Jiang, A., Lehti, K., Wang, X., Weiss, S. J., Keski-Oja, J., and Pei, D. (2001) *Proc. Natl. Acad. Sci. U. S. A.* **98,** 13693–13698
72. Uekita, T., Itoh, Y., Yana, I., Ohno, H., and Seiki, M. (2001) *J. Cell Biol.* **155,** 1345–1356
73. Will, H., Atkinson, S. J., Butler, G. S., Smith, B., and Murphy, G. (1996) *J. Biol. Chem.* **271,** 17119–17123
74. Strongin, A. Y., Collier, I., Bannikov, G., Marmer, B. L., Grant, G. A., and Goldberg, G. I. (1995) *J. Biol. Chem.* **270,** 5331–5338
75. Stanton, H., Gavrilovic, J., Atkinson, S. J., d'Ortho, M. P., Yamada, K. M., Zardi, L., and Murphy, G. (1998) *J. Cell Sci.* **111,** 2789–2798
76. Toth, M., Hernandez-Barrantes, S., Osenkowski, P., Bernardo, M. M., Gervasi, D. C., Shimura, Y., Meroueh, O., Kotra, L. P., Gatvez, B. G., Arroyo, A. G., Mobashery, S., and Fridman, R. (2002) *J. Biol. Chem.* **277,** 26340–26350
77. Consortium, T. H. (1995) *Nat. Genet.* **11,** 130–136
78. Turner, A. J., Isaac, R. E., and Coates, D. (2001) *Bioessays* **23,** 261–269
79. McQuibban, G. A., Gong, J. H., Tam, E. M., McCulloch, C. A., Clark-Lewis, I., and Overall, C. M. (2000) *Science* **289,** 1202–1206
80. McQuibban, G. A., Butler, G. S., Gong, J. H., Bendall, L., Power, C., Clark-Lewis, I., and Overall, C. M. (2001) *J. Biol. Chem.* **276,** 43503–43508
81. Overall, C. M., and Lopéz-Otín, C. (2002) *Nat. Rev. Cancer* **2,** 657–672

THE JOURNAL OF BIOLOGICAL CHEMISTRY
Vol. 279, No. 9, Issue of February 27, pp. 8278–8289, 2004
Printed in U.S.A.

Glycosylation Broadens the Substrate Profile of Membrane Type 1 Matrix Metalloproteinase*

Received for publication, October 29, 2003, and in revised form, December 5, 2003
Published, JBC Papers in Press, December 11, 2003, DOI 10.1074/jbc.M311870200

Yi I. Wu‡§, Hidayatullah G. Munshi§¶, Ratna Sen‡§, Scott J. Snipas‖, Guy S. Salvesen‖, Rafael Fridman, and M. Sharon Stack‡§‡‡**

*From the ‡Department of Cell & Molecular Biology and ¶Division of Hematology/Oncology, Department of Medicine, Feinberg School of Medicine, and the §Robert H. Lurie Comprehensive Cancer Center, Northwestern University, Chicago, Illinois 60611, the ‖Program in Apoptosis and Cell Death Research, Burnham Institute, La Jolla, California 92037, and the **Department of Pathology, Wayne State University, Detroit, Michigan 48202*

Membrane type 1 matrix metalloproteinase (MT1-MMP) is a collagenolytic enzyme that has been implicated in normal development and in pathological processes such as cancer metastasis. The activity of MT1-MMP is regulated extensively at the post-translational level, and the current data support the hypothesis that MT1-MMP activity is modulated by glycosylation. Enzymatic deglycosylation, site-directed mutagenesis, and lectin precipitation assays were used to demonstrate that MT1-MMP contains *O*-linked complex carbohydrates on the Thr^{291}, Thr^{299}, Thr^{300}, and/or Ser^{301} residues in the proline-rich linker region. MT1-MMP glycoforms were detected in human cancer cell lines, suggesting that MT1-MMP activity may be regulated by differential glycosylation *in vivo*. Although the autolytic processing and interstitial collagenase activity of MT1-MMP were not impaired in glycosylation-deficient mutants, cell surface MT1-MMP-catalyzed activation of pro-matrix metalloproteinase-2 (proMMP-2) required proper glycosylation of MT1-MMP. The inability of carbohydrate-free MT1-MMP to activate proMMP-2 was not a result of defective MT1-MMP zymogen activation, aberrant protein stability, or inability of the mature enzyme to oligomerize. Rather, our data support a mechanism whereby glycosylation affects the recruitment of tissue inhibitor of metalloproteinases-2 (TIMP-2) to the cell surface, resulting in defective formation of the MT1-MMP/TIMP-2/proMMP-2 trimeric activation complex. These data provide evidence for an additional mechanism for post-translational control of MT1-MMP activity and suggest that glycosylation of MT1-MMP may regulate its substrate targeting.

Matrix metalloproteinases (MMPs)[1] are a family of zinc-dependent proteinases (1–3) with activity against a variety of extracellular matrix proteins including collagens, laminins, and fibronectin (4). Recent research has identified a variety of non-traditional MMP activities including shedding of growth factors, cytokines and their receptors (5–8), disruption of cell-matrix and cell-cell junctional protein complexes (9–11), and initiation of proteinase cascades that impact much broader substrates (12, 13). As a result, MMPs play a central role in many physiological and pathological processes, including development, wound healing, tissue resorption, angiogenesis, and tumor invasion (3, 14, 15). Most MMPs are secreted proteins and share a similar modular domain structure including propeptide, catalytic domain, linker region, and hemopexin-like domain (2). However, a subgroup of MMPs, designated membrane type (MT)-MMPs, contains either an additional transmembrane and cytoplasmic domain (16–19) or a glycosylphosphatidylinositol anchor (20, 21), suggesting unique substrate specificity and distinct regulatory mechanisms as a consequence of cell surface localization (22).

Among MT-MMPs, MT1-MMP is the most extensively studied and the best characterized. A primary function of MT1-MMP is pericelluar collagenolysis (reviewed in Ref. 23). This is supported by both *in vitro* experiments in which MT1-MMP was shown to promote cellular invasion of type I collagen (24, 25), and *in vivo* studies of mice genetically deficient in MT1-MMP expression (MT1-MMP−/−) (26, 27). These mice developed craniofacial dysmorphism, arthritis, osteopenia, dwarfism, and fibrosis of soft tissues because of the inability to process interstitial collagen (26). In addition to direct cleavage of matrix proteins, MT1-MMP also mediates activation of proMMP-2, which leads to a broader impact on pericelluar proteolysis (16). ProMMP-2 activation involves formation of a ternary complex consisting of MT1-MMP, TIMP-2, and proMMP-2 (28–30). In this model, TIMP-2 bridges the catalytic domain of MT1-MMP (31) and the hemopexin-like domain of proMMP-2 (32), thereby facilitating the recruitment of proMMP-2 to the cell surface. A catalytically competent MT1-MMP (TIMP-2 free) then mediates an initial cleavage of proMMP-2 (72 kDa) to generate an intermediate form (68 kDa), which undergoes autolysis to generate fully activated MMP-2 (62 kDa) (33, 34). Recent studies indicate that activation of proMMP-2 is regulated by oligomerization of MT1-MMP via hemopexin-like domain interactions (35, 36).

The proteolytic activity of MT1-MMP is tightly regulated under normal physiological conditions (22, 23). In addition to controls on protein expression, the activity of MT1-MMP is extensively regulated post-translationally by zymogen activation, inhibition by TIMPs, autolytic degradation, shedding, oligomerization, and membrane trafficking (34–40). MT1-MMP is expressed in a zymogen form (64 kDa) and activated in the

* This work was supported by Grant DAMD170010386 (to Y. I. W.) from United States Army Medical Research and Materiel Command, and by Grants K08CA94877 (to H. G. M.) and R01CA85870 (to M. S. S.) from the National Cancer Institute. The costs of publication of this article were defrayed in part by the payment of page charges. This article must therefore be hereby marked "*advertisement*" in accordance with 18 U.S.C. Section 1734 solely to indicate this fact.

‡‡ To whom correspondence should be addressed: Dept. of Cell and Molecular Biology, Northwestern University Medical School, 303 E. Chicago Ave., Tarry 8-715, Chicago, IL 60611. Tel.: 312-908-8216; Fax: 312-503-7912; E-mail: mss130@northwestern.edu.

[1] The abbreviations used are: MMP, matrix metalloproteinase; MT, membrane type; TIMP, tissue inhibitor of metalloproteinases; PC, proprotein convertase; PI, proteinase inhibitor; CHO, Chinese hamster ovary; TUG, transverse urea gradient; BGN, benzyl-2-acetamido-2-deoxy-α-D-galactopyranoside.

secretory pathway by furin or furin-like proprotein convertases (PCs) (41–43). These proprotein convertases cleave proMT1-MMP after the $R^{108}RKR^{111}$ sequence to generate the active species (55 kDa). This is supported by studies using an engineered mutant of α1-proteinase inhibitor (α1-PI) with furin/PC inhibitory activity, designated α1-PI_{PDX} (44), to block proMT1-MMP zymogen activation (43). Active MT1-MMP is inhibited by TIMP-2, but is unaffected by TIMP-1 (34). MT1-MMP also undergoes autolytic degradation at $Gly^{284}\downarrow Gly^{285}$ in the linker region, generating a catalytically inactive species (calculated molecular mass of 34 kDa) (39). Finally, as a trans-membrane protein, MT1-MMP is also regulated by membrane trafficking and cell surface localization (37, 45–47).

The current study tested the hypothesis that glycosylation of MT1-MMP functions as an additional mechanism for post-translational regulation of enzymatic activity and demonstrates that MT1-MMP is an *O*-glycoprotein. Although glycosylation was not required for collagenase activity, formation of a stable MT1-MMP/TIMP-2/proMMP-2 ternary complex and subsequent cell surface activation of MMP-2 was blocked in glycosylation-defective mutants. Distinct glycoforms of MT1-MMP were detected in human cancer cell lines, suggesting that MT1-MMP activity may be regulated by differential glycosylation *in vivo*. These data support a model in which glycosylation regulates substrate targeting and suggest a cellular mechanism for controlling the initiation of MMP-2 dependent proteolysis.

EXPERIMENTAL PROCEDURES

Materials—Anti-FLAG monoclonal M1 and M2 antibody, anti-Myc monoclonal antibody (9E10), rabbit polyclonal antibody that recognizes the linker region of MT1-MMP, peroxidase-conjugated secondary antibodies, gelatin, rat tail collagen, *O*-glycosylation inhibitor, benzyl-2-acetamido-2-deoxy-α-D-galactopyranoside (GalNAc-α-*O*-benzyl (BGN)), and *N*-glycosylation inhibitor tunicamycin were purchased from Sigma. The broad spectrum metalloproteinase inhibitor GM6001 and rabbit polyclonal TIMP-2 antibody (AB801) were purchased from Chemicon (Temecula, CA). Anti-transferrin receptor monoclonal antibody was purchased from Zymed Laboratories Inc. (South San Francisco, CA). Human TIMP-2 and proMMP-2 were purified as previously described (48, 49).

Sequence Analyses of MT-MMPs—The amino acid sequences of MT1- to MT6-MMP were obtained from Swiss-Prot P50281, P51511, P51512, Q9ULZ9, Q9Y5R2, and Q9NPA2, respectively. The prediction of *O*- and *N*-glycosylation sites was performed using full-length sequences on the NetOGlyc 2.0 server (www.cbs.dtu.dk/services/NetOGlyc/) (50) and NetNGlyc 1.0 server (www.cbs.dtu.dk/services/NetNGlyc/), respectively. The alignment of the MT-MMP linker domains was performed on the server of T-Coffee multiple sequence alignment (www.ch.embnet.org/software/TCoffee.html) (51).

Cell Culture—COS-7 cells (generous gift of Dr. Kathleen J. Green, Northwestern University Medical School, Chicago, IL) and MDA-MB-231 cells (generous gift of Dr. V. Craig Jordan, Northwestern University Medical School, Chicago, IL) were maintained in Dulbecco's modified Eagle's medium containing 10% fetal bovine serum. The ovarian cancer cell lines DOV13, OVCA429, and OVCA433 were kindly provided by Dr. Robert Bast, Jr. (M. D. Anderson Cancer Center, Houston, TX), and were maintained in minimal essential medium containing 10% fetal bovine serum. Cell culture media and reagents were purchased from Mediatech (Herndon, VA).

DNA Constructs—The human MT1-MMP cDNA was kindly provided by Dr. Duanqing Pei (University of Minnesota, Minneapolis, MN). The complete coding sequence of MT1-MMP was amplified by PCR using forward primer, 5′-ACCATGTCTCCCGCCCCAAGAC-3′ and reverse primer, 5′-TCAGACCTTGTCCAGCAGGGAAC-3′, and subcloned into eukaryotic expression vector pCR3.1-Uni (Invitrogen, Carlsbad, CA) to obtain the untagged wild type construct. The wild type construct was further FLAG (DYKDDDDK)-tagged in the stalk region (stalk) or after the furin/PC cleavage site (f112), or Myc (EQKLISEEDL)- tagged in the stalk region (Fig. 1*B*). Subsequently different deletions (ΔCat) or point mutations (E240A, CHO-1, CHO-3, and CHO-4; see below) were generated on the wild type cDNA and on the tagged constructs using a two-step overlapping PCR strategy. Briefly, two fragments covering the complete cDNA were generated in the first step PCR, with an overlapping region carrying tag or mutation(s). In the second step of PCR, both fragments were used as templates to generate the complete cDNA carrying the tag or mutation, followed by subcloning back into the pCR3.1-Uni vector using HindIII and EcoRI sites. The outer primers in this strategy are the sequencing primers provided by Invitrogen. The inner primers are 5′-GGCCGGCCGGATTATAAGGATGATGATGATAAGGAGGTGATCATCATTG-3′ and 5′-CAATGATGATCACCTCCTTATCATCATCATCCTTATATTCCGGCCGGCC-3′ for FLAGtag (stalk); 5′-GACTATAAAGATGATGATGATAAATACGCCATCCAGGGTCTCAAATG-3′ and 5′-TTTATCATCATCATCTTTATAATCGCGCTTCCTTCGAACATTGGC-3′ for FLAG tag (f112); 5′-GAACAAAAACTTATCAGTGAAGAAGATCTGGGCCGGCCGGATGAGfsGGGAC-3′ and 5′-CAGATCTTCTTCACTGATAAGTTTTTGTTCTCCCGATGGGCAGCCCATCC-3′ for Myc tag (stalk); 5′-GTCAGGGTTCCCCGCCAAGATGCCCCC-3′ and 5′GGGGGCATCTTGGCGGGGAACCCTGAC-3′ for CHO-1 (T291A); 5′-AGGGCTGCTGCTCGGCCTTCTGTTCCTGAT-3′ and 5′-GGCCGAGCAGCAGCCCTGGGTTGAGGGGGCAT-3′ for CHO-3 (T299A/T300A/S301A); 5′-GGTGGCTGTGCACGCGCTGGGCCATGCC-3′ and 5′-GGCATGGCCCAGCGCGTGCACAGCCACC-3′ for E240A; and 5′-CGAAGGAAGCGCGGTGAGTCAGGGTTCCCCACC-3′ and 5′-CCCTGACTCACCGCGCTTCCTTCGAACATTGGCC-3′ for ΔCat (Δ112–284).

In addition to the above mutants of MT1-MMP, soluble FLAG-tagged (f112) MT1-MMP (sMT1-MMP) and CHO-4 mutant (sCHO-4) were also generated using TA cloning approach from the corresponding membrane-anchored constructs. The primers used to delete the transmembrane and cytoplasmic domain (soluble) are forward primer (5′-ACCATGTCTCCCGCCCCAAGAC-3′) and reverse primer (5′-TCAAGCCGCGCTCACCGCCCCGCC-3′).

The DNA constructs of wild type α1-PI and α1-PI_{PDX} in pcDNA3 vector (Invitrogen) were generated by the laboratory of Dr. Guy S. Salvesen (Burnham Institute, La Jolla, CA). The PCR reactions were performed using high fidelity *Pfu* Turbo polymerase (Stratagene, La Jolla, CA), and the plasmids were verified by DNA sequencing.

Immunoprecipitation with Anti-FLAG M2 Affinity Gel—COS-7 cells were transfected with plasmid DNA indicated using FuGENE 6 (Roche, Switzerland) according to instructions from the manufacturer. After 24 h, cells were lysed in lysis buffer (50 mM Tris buffer, pH 7.5, 150 mM NaCl, 1% Triton X-100) supplemented with 5 mM EDTA and protease inhibitor mixture (Roche). Immunoprecipitation of FLAG-tagged proteins was performed using anti-FLAG M2 affinity gel according to instructions from the manufacturer (Sigma) and Handee spin cup columns (Pierce). The cell lysates were incubated with M2 affinity gel at 4 °C for 2 h, washed three times with washing buffer containing 50 mM Tris, pH7.5, 150 mM NaCl, and 0.1% Triton X-100, and eluted with 200 μg/ml 3× FLAG peptide (Sigma) in washing buffer. In co-immunoprecipitation experiments, EDTA was omitted from lysis buffer, and both lysis buffer and washing buffer were supplemented with 2 mM $CaCl_2$ and 2 mM $MgCl_2$. The cell lysates and immunoprecipitates were analyzed by Western blot and gelatin zymography as previously described (24, 40, 52).

Enzymatic Deglycosylation—Enzymatic deglycosylation was performed according to instructions from the manufacturer (ProZyme, San Leandro, CA). Briefly, FLAG-tagged MT1-MMP or glycosylation mutants were purified using M2 affinity gel as described above. The purified protein was heat-denatured in SDS buffer provided, neutralized with Triton X-100, and digested with buffer control or different glycosidases for 24 h. Several glycosidases, including sialidase A, endo-*O*-glycosidase, β(1–4)-galactosidase, glucosaminidase, and peptide-*N*-glycosidase F were used either individually or in combinations as described under "Results." The digestion was stopped by boiling in SDS sample dilution buffer, and the samples were analyzed by Western blot.

Lectin Precipitation Assay—Biotinylated lectins, including concanavalin A, soybean agglutinin, *Ulex europaeus* agglutinin I, wheat germ agglutinin, succinylated wheat germ agglutinin, *Maackia amurensis* lectin II, and *Sambucus nigra* lectin were purchased from Vector Laboratories (Burlingame, CA). These biotinylated lectins were immobilized by incubating with neutravidin-conjugated beads (Pierce) at 4 °C for 1 h, followed by three washes with washing buffer supplemented with 2 mM $CaCl_2$ and $MgCl_2$. At the same time, cell lysates were prepared using lysis buffer without EDTA and supplemented with 2 mM $CaCl_2$ and $MgCl_2$. These immobilized lectins were incubated with the cell lysates overnight, followed by washes with washing buffer containing 2 mM $CaCl_2$ and $MgCl_2$. The precipitated proteins were eluted by boiling in SDS sample dilution buffer and analyzed by Western blot.

Collagen Invasion Assay—Collagen invasion assays were performed and analyzed as previously described (24, 52). Briefly, cell culture inserts (24 wells, 8.0-μm pore, Becton Dickinson, Bedford, MA) were

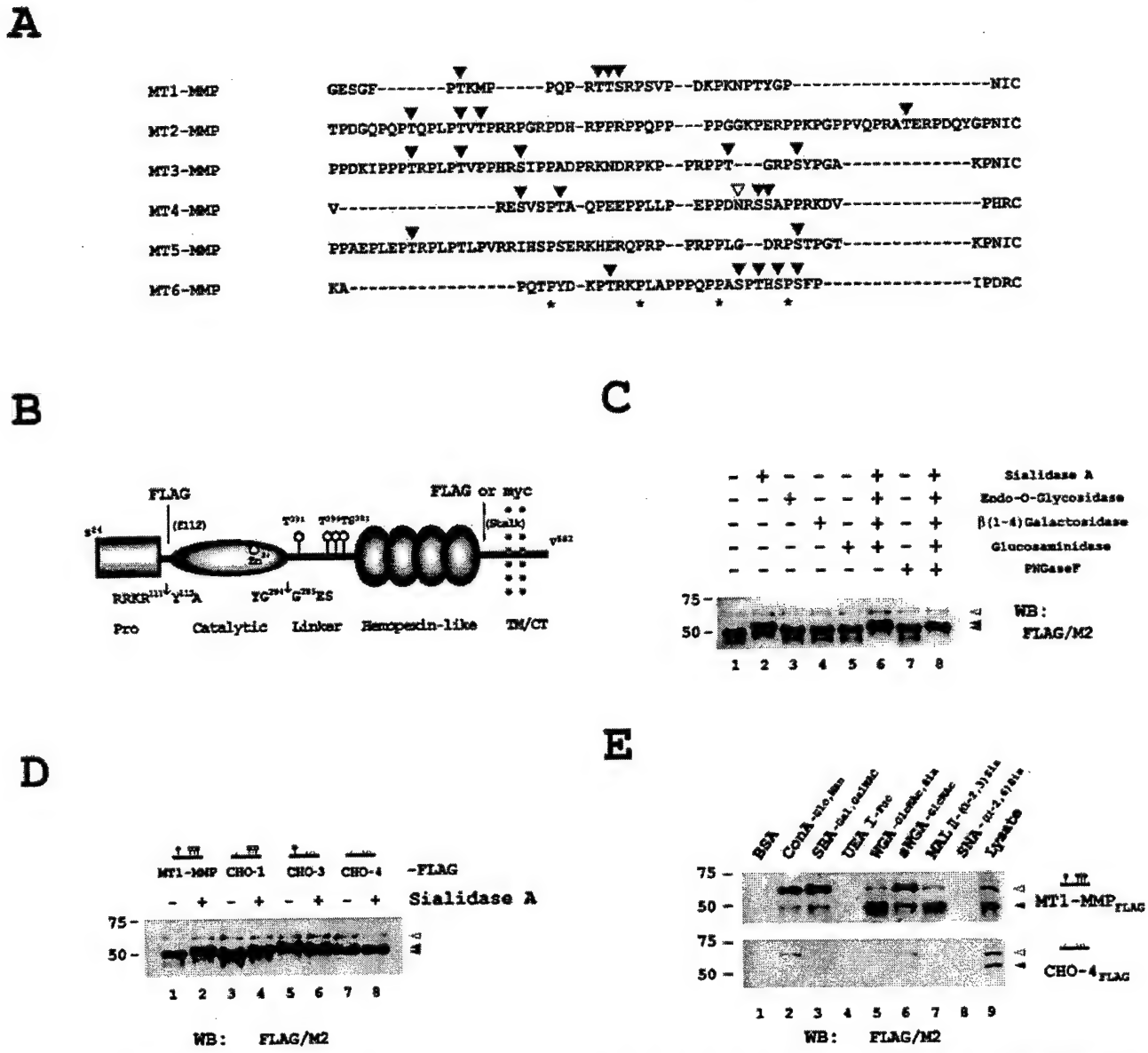

FIG. 1. **MT1-MMP is *O*-glycosylated with complex carbohydrates.** *A*, the amino acid sequences from the linker domains of MT-MMPs are aligned in a clustal format, with the conserved residues denoted with *asterisks*. The predicted *O*- and *N*-glycosylation sites within these sequences are *highlighted* with ▼ and ▽, respectively. *B*, schematic diagram of MT1-MMP (Ser^{24}–Val^{582}) consisting of propeptide (*Pro*), catalytic, linker, hemopexin-like, and transmembrane/cytoplasmic (*TM/CT*) domains. The predicted *O*-glycosylation sites, Thr^{291}, Thr^{299}, Thr^{300}, and Ser^{301}, were indicated with ○ on the linker domain. Different FLAG- and Myc-tagged MT1-MMP plasmid constructs were generated in the following studies. The tagging sites are, as indicated in each experiment, either after furin/PC cleavage site (*RRKR*^{111} ↓ *Y*^{112}*A*, *f112*) or in the stalk region between hemopexin-like and TM/CT domains. The site of autolysis is also indicated (*YG*^{284} ↓ *G*^{285}*ES*). *C*, FLAG-tagged (stalk) MT1-MMP was purified from transiently transfected COS-7 cells and digested with sialidase A, endo-*O*-glycosidase, β(1–4)-galactosidase, glucosaminidase, and peptide-*N*-glycosidase F (*PNGase F*) as indicated. The reaction mixtures were fractionated on a 10% SDS-PAGE followed by Western blot (*WB*) with anti-FLAG M2 antibody. *D*, FLAG-tagged (stalk) glycosylation mutants CHO-1 (T291A), CHO-3 (T299A/T300A/S301A), and CHO-4 (T291A/T299A/T300A/S301A), as well as wild type MT1-MMP were purified from COS-7 cells, digested with sialidase A, and analyzed by Western blot with anti-FLAG M2 antibody. *E*, lysates from COS-7 cells expressing FLAG-tagged (stalk) wild type or CHO-4 mutant MT1-MMP were incubated with BSA, biotinylated lectins, including concanavalin A (*ConA*), soybean agglutinin (*SBA*), *U. europaeus* agglutinin I (*UEA I*), wheat germ agglutinin (*WGA*), succinylated wheat germ agglutinin (*sWGA*), *M. amurensis* lectin II (*MAL II*), or *S. nigra* lectin (*SNA*), followed by neutravidin precipitation as described under "Experimental Procedures." The carbohydrate group(s) that interacts with each lectin was indicated. *Glc*, glucose; *Man*, mannose; *Gal*, galactose; *GalNAc*, *N*-acetylgalactosamine; *Fuc*, fucose; *GlcNAc*, *N*-acetylglucosamine; and *Sia*, sialic acid. The precipitates along with 10% of corresponding lysate input were analyzed by Western blot with anti-FLAG M2 antibody. The pro- and active forms of MT1-MMP are indicated as ◁ and ◀, respectively.

coated with rat tail type I collagen (10 μg/well) in 100 mM Na_2CO_3 and allowed to air-dry overnight. Collagen-coated inserts were then washed with Dulbecco's modified Eagle's medium three times to remove salts and used immediately. Transfected COS-7 cells were trypsinized, washed with cultured medium, and 1×10^5 cells were added to the inner invasion chamber in 250 μl of culture medium. The outer wells contained 400 μl of culture medium. To evaluate the MMP dependence of invasion, 25 μM GM6001 was added to the inner and outer chambers as indicated. Cells were allowed to invade for 24 h, non-invading cells were removed from inner wells using a cotton swab, and invading cells adherent to the bottom of membrane were fixed and stained using a Diff-Quick staining kit (Dade AG, Miami, FL). Invading cells were enumerated as described previously (24, 40).

Transverse Urea Gradient (TUG) PAGE—TUG gel electrophoresis

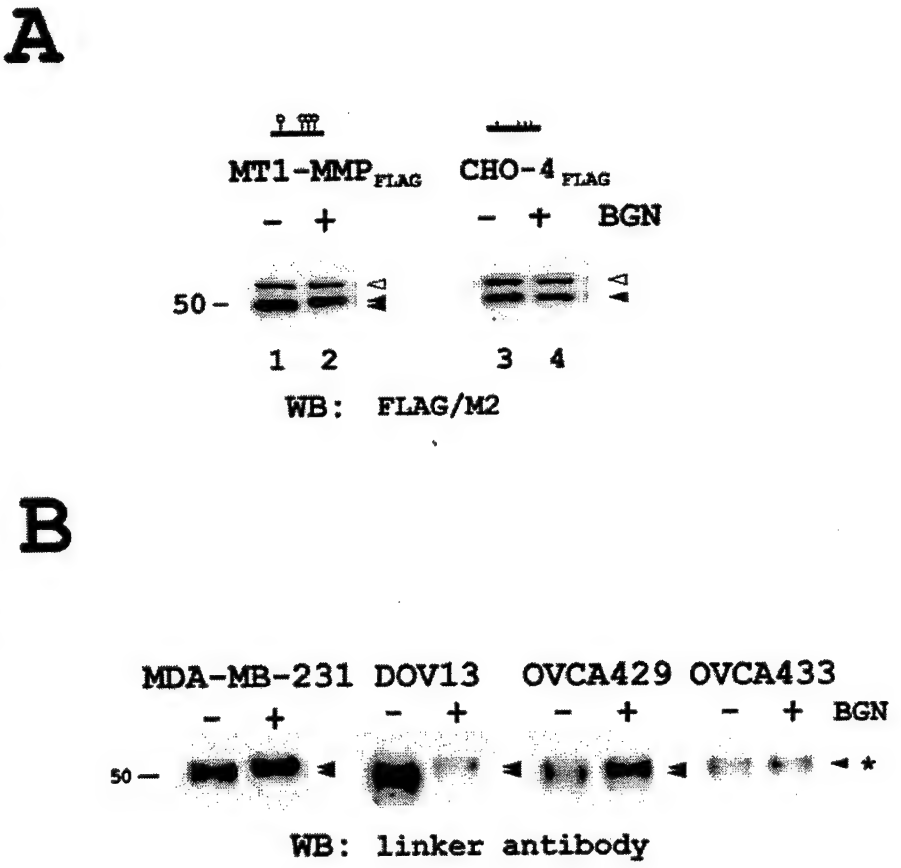

FIG. 2. **Differential glycosylation of MT1-MMP in cancer cells.** *A*, COS-7 cells were transfected with FLAG-tagged (stalk) wild type (*left panel*) or CHO-4 mutant (*right panel*) MT1-MMP in the absence or presence of 2 mM *O*-glycosylation inhibitor BGN. The cell lysates were fractionated on a 10% SDS-PAGE followed by Western blot with anti-FLAG M2 antibody. *B*, breast cancer MDA-MB-231 cells, and ovarian cancer OVCA-R3, DOV13, and OVCA433 cells were cultured in the presence or absence of *O*-glycosylation inhibitor BGN for 48 h. GM6001 was added 24 h before lysing the cells. The cell surface proteins from these cells were purified as described under "Experimental Procedures" and analyzed by Western blot (*WB*) with anti-MT1-MMP antibody. The pro- and active forms of MT1-MMP are indicated as ◁ and ◀, respectively.

was performed as previously described (53). Briefly, 7% polyacrylamide gels containing a continuous 0–8 M urea gradient were cast in batch using a multiple gradient caster (Owl Scientific, Woburn, MA). The gels were rotated 90°, and a single sample of purified protein, FLAG-tagged (f112) sMT1-MMP or sCHO-4 in a 200-μl total volume was loaded evenly across the top of the gel. Electrophoresis was performed in the absence of SDS. The fractionated proteins were transferred to polyvinylidene difluoride membranes and analyzed by Western blot analysis using anti-FLAG M1 antibody (1:1000 dilution) and peroxidase-conjugated secondary antibody (1:10,000 dilution) followed by ECL detection (Pierce).

Labeling and Purification of Cell Surface Proteins—Labeling of cell surface proteins was performed as described previously (40). Briefly, cells were washed with phosphate-buffered saline and incubated with Sulfo-NHS-LC-LC-Biotin (Pierce) for 10 min on ice and washed with 100 mM glycine to quench remaining NHS groups. The cells were then lysed in lysis buffer, incubated with neutravidin-conjugated beads (Pierce) for 1 h, and eluted by boiling in SDS sample dilution buffer for 15 min followed by Western blot analysis.

Immunostaining of Endocytosed MT1-MMP—COS-7 cells were transfected with FLAG-tagged (stalk) MT1-MMP, CHO-4, and E240A mutant in the presence of 25 μM GM6001. Cell surface FLAG-tagged proteins were labeled with FLAG/M2 antibody (1:1000 dilution) on ice for 1 h. The unbound antibody was washed off with medium, and 25 μM GM6001 alone or 25 μM GM6001 and 25 nM TIMP-2 were added back to the chamber slides. Cells were shifted to 37 °C to allow endocytosis to take place. After 15 min, the cells were placed on ice, washed with wash buffer (500 mM acetic acid and 150 mM NaCl) (47) and phosphate-buffered saline, fixed with 3.7% formaldehyde, and permeabilized with 0.2% Triton X-100. The cells were further stained with rabbit polyclonal antibody (Sigma) that recognizes the linker domain of MT1-MMP (1:2000 dilution). The bound FLAG/M2 antibody and linker antibody were detected with corresponding secondary antibody (1:500 dilution) conjugated with Alexa Fluor 488 and 546 (Molecular Probes, Eugene, OR), respectively. The nucleus was counterstained with TO-PRO-3 iodide (Molecular Probes). The images were taken using a Zeiss LSM510 laser scanning confocal microscope at the Northwestern University Cell Imaging Facility, and edited using Adobe PhotoShop 7.0 software.

RESULTS

MT1-MMP Is Post-translationally Modified by O-Glycosylation—To determine whether MT1-MMP is post-translationally modified by glycosylation, the glycosylation potentials of MT1-MMP were examined on the Center for Biological Sequence Analysis server (NetNGlyc and NetOGlyc programs for *N*-linked and *O*-linked glycosylation, respectively). The results of analysis indicated that MT1-MMP is not likely to be *N*-glycosylated; however, four potential *O*-glycosylation sites (Thr^{291}, Thr^{299}, Thr^{300}, and Ser^{301}) were identified (Fig. 1, *A* and *B*). These sites were all located in the proline-rich linker (also known as hinge) region, proposed to be critical for the proteinase activity of MT1-MMP (54). Similar to MT1-MMP, MT2- to MT6-MMP were all predicted to be glycosylated in the linker region (Fig. 1A), suggesting a conserved post-translational modification indicative of a potential regulatory function. Enzymatic deglycosylation was subsequently used to test the prediction that MT1-MMP is a glycoprotein. Affinity-purified MT1-MMP from COS-7 cells was digested with specific glycosidases and evaluated by SDS-PAGE. Because glycosylation can cause a change in the mass and/or charge of a protein, both positive and negative changes in relative electrophoretic mobility were interpreted in support of carbohydrate removal. Without digestion, the purified protein migrated as a 64-kDa proMT1-MMP species and a 50-kDa active MT1-MMP species (Fig. 1*C*, *lane 1*). Treatment of MT1-MMP with peptide-*N*-glycosidase F, which efficiently removes *N*-linked sugars, did not result in any detectable mobility shift in either the pro- or active MT1-MMP (Fig. 1*C*, *lane 7*), supporting the prediction that MT1-MMP is not *N*-glycosylated. Similarly, treatment with several *O*-glycosidases (endo-*O*-glycosidase, β(1–4)-galactosidase, and glucosaminidase) did not alter the electrophoretic

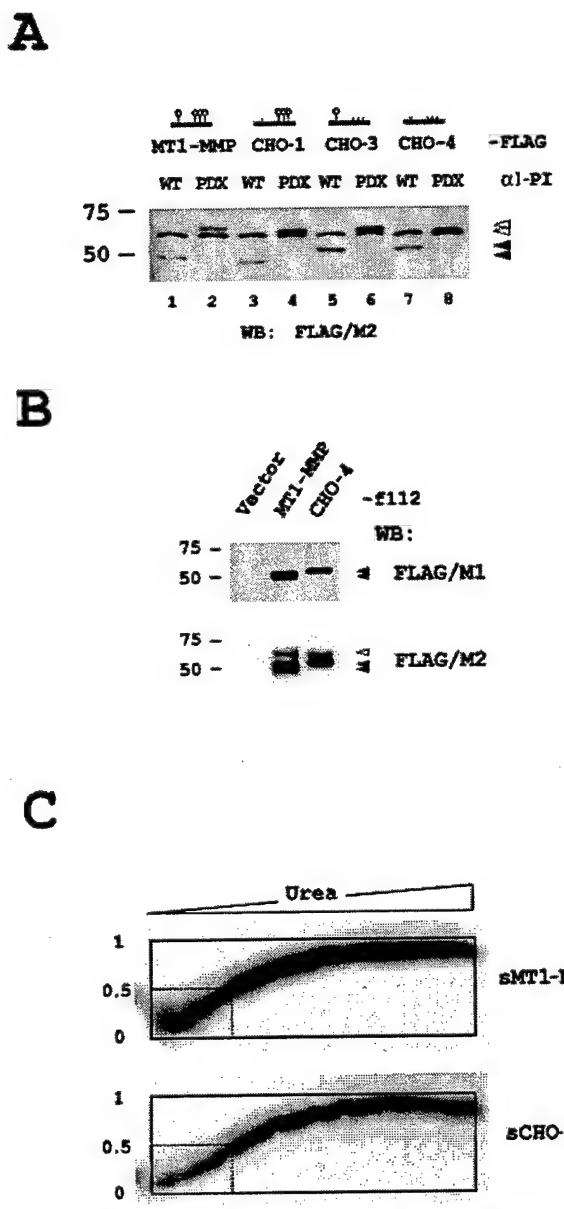

FIG. 3. **Glycosylation of MT1-MMP does not affect its zymogen activation or folding.** *A*, COS-7 cells were co-transfected with different FLAG-tagged (stalk) MT1-MMP glycosylation variants and wild type α1-PI (*WT*) or α1-PI$_{PDX}$ mutant in the presence of 25 μM GM6001. After 24 h, cell lysates were fractionated on 10% SDS-PAGE and analyzed by Western blot (*WB*) using anti-FLAG M2 antibody. *B*, COS-7 cells were transfected with vector, FLAG-tagged (f112) wild type MT1-MMP or CHO-4 mutant in the presence of 25 μM GM6001. After 24 h, cell lysates were fractionated on 10% SDS-PAGE and analyzed by Western blot using anti-FLAG M1 (*upper panel*) and M2 (*lower panel*) antibody. *C*, soluble FLAG-tagged (f112) MT1-MMP and CHO-4 mutant were purified from transfected COS-7 cells and analyzed by TUG-PAGE as described under "Experimental Procedures." The FLAG-tagged proteins were detected using anti-FLAG M1 antibody. The pro- and active forms of MT1-MMP are indicated as ◁ and ◀, respectively.

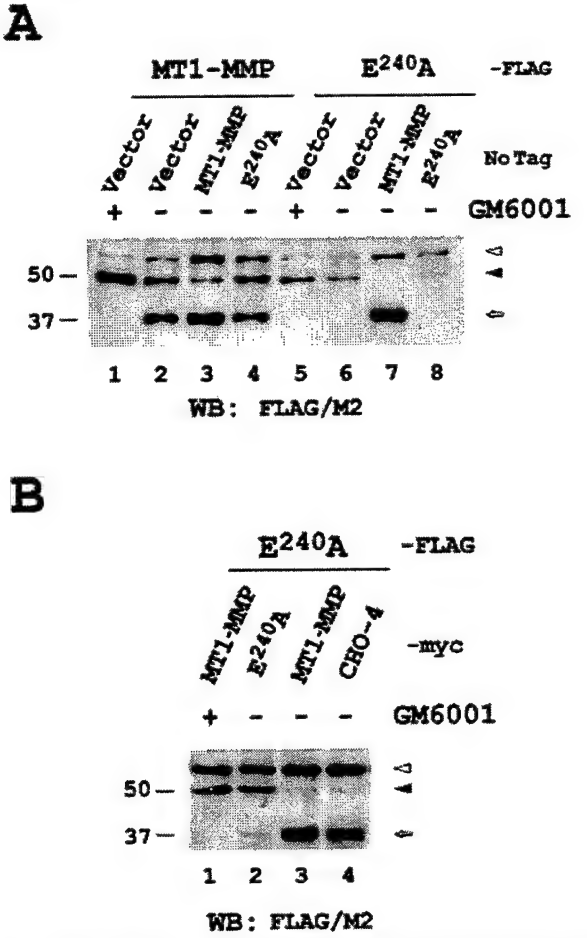

FIG. 4. **Glycosylation of MT1-MMP does not affect its autolysis *in trans*.** COS-7 cells were co-transfected with different FLAG-tagged (stalk) and untagged MT1-MMP plasmids in the presence or absence of 25 μM GM6001 as indicated. The cell lysates were fractionated on 10% SDS-PAGE and analyzed by Western blot (*WB*) using anti-FLAG M2 antibody. *B*, COS-7 cells were co-transfected with FLAG-tagged (stalk) E240A mutant and different Myc-tagged MT1-MMP plasmids in the presence or absence of 25 μM GM6001. The cell lysates were fractionated on 10% SDS-PAGE and analyzed by Western blot using anti-FLAG M2 antibody. The pro-, active, and autolytic products of MT1-MMP are indicated as ◁, ◀, and ⇐, respectively.

migration of MT1-MMPs (Fig. 1*C*, *lanes 3–5*), potentially because of the poor efficiency of these *O*-glycosidases against complex *O*-linked carbohydrates. However, treatment of MT1-MMP with sialidase A consistently resulted in an altered relative mobility of the active MT1-MMP species (Fig. 1*C*, *lanes 2*, *6*, and *8*). A similar decrease in relative mobility after desialylation has been shown in several other glycoproteins including MUC1, endolyn, and CD44 (55–57) and presumably reflects alterations in SDS binding properties of the modified proteins. Of note, there is no mobility shift detected in the proMT1-MMP species following treatment with sialidase A, suggesting that the sialylation likely follows activation of proMT1-MMP in the *trans*-Golgi network (58).

To confirm the prediction that MT1-MMP contains *O*-linked carbohydrate, three alanine mutants were generated, in which Thr^{291} (designated CHO-1), Thr^{299}-Thr-Ser^{301} (CHO-3), or all four predicted *O*-glycosylation sites (Thr^{291} and Thr^{299}-Thr-Ser^{301}, designated CHO-4) were mutated to alanine(s) (schematic of linker region shown in Fig. 1*D*, *top panel*). The CHO-1 mutant, which preserves three predicted glycosylation sites, exhibited a relative electrophoretic mobility shift following desialylation similar to the wild type protein (Fig. 1*D*, *lanes* 2 and *4*). Removal of all four potential *O*-glycosylation site(s) (CHO-4, Fig. 1*D*, *lane 7*) resulted in a mutant with electrophoretic mobility similar to desialylated wild type MT1-MMP (Fig. 1*D*, *lane 2*). Further, this mutant was insensitive to sialidase A treatment (Fig. 1*D*, *lane 8*), suggesting that sialic acids are added to MT1-MMP via *O*-linked carbohydrates and all potential *O*-glycosylation sites were identified. To further character-

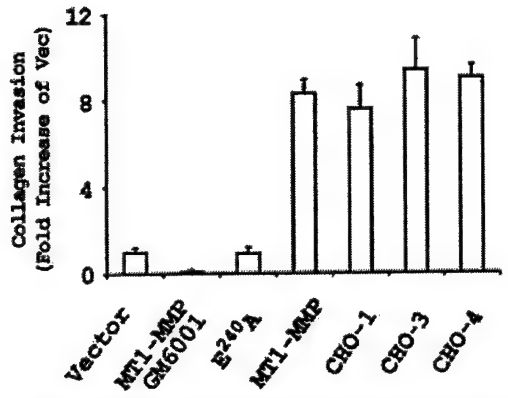

FIG. 5. **Glycosylation of MT1-MMP does not affect collagen invasion.** COS-7 cells were transfected with vector, MT1-MMP, E240A, and different glycosylation mutants as indicated. After 12 h, these cells were trypsinized, seeded (1×10^5/well) onto cell culture inserts (24 well, 8.0 μm pore) coated with a type I collagen (10 μg/well), and allowed to invade for 24 h as described under "Experimental Procedures." Non-invading cells were removed from the upper chamber with a cotton swab. Filters were then stained, and cells, adherent to the underside of the filter, were enumerated using an ocular micrometer. The average values of triplicate experiments were normalized to cells transfected with vector alone (designated *1*) and were presented with S.D. *error bar*. GM6001 (25 μM) was added in the well indicated.

ize the glycosylation of MT1-MMP, cells were transfected with either wild type or CHO-4 mutant MT1-MMP and the lysates were precipitated with various immobilized lectins. Negligible CHO-4 MT1-MMP was precipitated by any lectin (Fig. 1*E*, *lower panel*), suggesting that MT1-MMP has very low carbohydrate-independent interaction with lectins. In contrast wild type MT1-MMP was precipitated with both concanavalin A, which binds to glucose and mannose (Fig. 1*E*, *lane 2*), and soybean agglutinin, which binds to galactose and *N*-acetylgalactosamine (Fig. 1*E*, *lane 3*). Interestingly, a preferential interaction with proMT1-MMP was observed, suggesting that partial deglycosylation of the proenzyme may accompany zymogen activation. Wheat germ agglutinin, which binds to *N*-acetylglucosamine and sialic acid, also precipitated MT1-MMP, with preferential binding to the active MT1-MMP species (Fig. 1*E*, *lane 5*). Succinylated wheat germ agglutinin, which no longer binds to sialic acid but preserves its interaction with *N*-acetylglucosamine, differentially recognizes proMT1-MMP (Fig. 1*E*, *lane 6*), providing additional evidence that active MT1-MMP is sialylated. To determine the subtype of sialic acid on MT1-MMP, interaction with the (α-2,3) linkage-specific lectin *M. amurensis* lectin II and the (α-2,6) linkage-specific lectin *S. nigra* lectin was evaluated. Only *M. amurensis* lectin II was found to interact with MT1-MMP (Fig. 1*E*, *lanes 7* and *8*), indicating the sialic acid was added via (α-2,3) linkage. These data support the conclusion that MT1-MMP is a glycoprotein with *O*-linked complex carbohydrates.

In addition to mutational analysis and lectin precipitation, the *O*-glycosylation inhibitor benzyl-2-acetamido-2-deoxy-α-D-galactopyranoside (GalNAc-α-*O*-benzyl, or BGN) (59, 60) and the *N*-glycosylation inhibitor tunicamycin were used to evaluate glycosylation of MT1-MMP. Culture of cells overexpressing wild type MT1-MMP with BGN resulted in expression of an MT1-MMP species (Fig. 2*A*, *lane 2*) with relative electrophoretic migration similar to the carbohydrate-free CHO-4 mutant (Fig. 2*A*, *lane 3*), providing additional evidence that MT1-MMP is *O*-glycosylated. No change in mobility was observed upon treatment of CHO-4-expressing cells with BGN (Fig. 2*A*, *lane 4*). In control experiments, treatment with the *N*-glycosylation inhibitor tunicamycin did not alter the electrophoretic mobility of either wild type or CHO-4 MT1-MMP (data not shown). To determine whether endogenously expressed MT1-MMP is also glycosylated in cancer cells, breast and ovarian cancer cell lines were cultured in the presence and absence of BGN. Because of low expression levels, the endogenous MT1-MMP was enriched by purification of cell surface proteins. The active species of endogenous MT1-MMP was detected when probed with an antibody that recognizes the linker region in Western blot analysis (Fig. 2*B*). The treatment with BGN resulted in a similar mobility shift of the active MT1-MMP species in MDA-MB-231, DOV13, and OVCA429 cells, suggesting that endogenous MT1-MMP is also glycosylated. Interestingly, no mobility shift was detected upon BGN treatment of OVCA433 cells, with the active species of MT1-MMP detected at the higher apparent molecular weight corresponding to underglycosylated MT1-MMP. These data demonstrate that endogenous MT1-MMP is *O*-glycosylated and indicate the presence of differential MT1-MMP glycoforms in human cancer cells.

Glycosylation Does Not Affect Zymogen Activation and Folding of MT1-MMP—The distinct lectin binding properties of pro- and active MT1-MMP (Fig. 1*E*) suggest a temporal relationship between MT1-MMP activation and glycosylation. ProMT1-MMP is activated by a specific cleavage following the $R^{108}RKR^{111}$ sequence by furin or other PCs and zymogen activation can be inhibited by an engineered mutant of αl-PI designated α1-PI_{PDX} (43). To evaluate the relationship between proMT1-MMP activation and glycosylation, wild type or glycosylation-defective MT1-MMP was co-expressed with wild type α1-PI or α1-PI_{PDX}. In the presence of wild type α1-PI (inactive against furin/PC), all proMT1-MMP glycoforms were converted to the active species in the same relative ratio as the wild type protein, suggesting glycosylation is not required for MT1-MMP activation (Fig. 3*A*, *lanes 1*, *3*, *5*, and *7*). Co-expression of α1-PI_{PDX} inhibited proMT1-MMP activation in all glycoforms (Fig. 3*A*, *lanes 2*, *4*, *6*, and *8*), indicating the conversion was furin/PC-dependent. The accumulated proMT1-MMP appeared to be glycosylated at the same sites in the linker region, because the pro-form of the CHO-4 mutant did not exhibit a similar mobility shift (Fig. 3*A*, *lane 8*). These data indicate that glycosylation of MT1-MMP is not required for efficient zymogen activation.

Because differential NH_2-terminal proteolytic processing of active MT1-MMP has been reported (61, 62), control experiments were performed to examine whether the altered mobility of CHO-4 was the result of unusual NH_2-terminal processing. This was achieved by taking advantage of the anti-FLAG M1 antibody, which recognizes the FLAG epitope only when it is at the NH_2 terminus. Additional tagged wild type MT1-MMP and CHO-4 constructs were generated in which the FLAG sequence was inserted immediately after furin/PC cleavage site (designated f112), instead of the stalk region (Fig. 1*B*). The f112-tagged constructs were expressed in COS-7 cells and initially probed with M2 antibody, which detects the FLAG epitope irrespective of location in the protein primary structure. Both the pro- and active species of wild type and CHO-4 MT1-MMP were recognized (Fig. 3*B*, *lower panel*). When probed with M1 antibody, only the active species were detected, because of exposure of the NH_2-terminal FLAG epitope following furin/PC processing (Fig. 3*B*, *upper panel*). The CHO-4 mutant as well as wild type MT1-MMP was recognized, indicating that the amino terminus of the CHO-4 mutant is identical to that of wild type MT1-MMP. These data confirm that the altered relative electrophoretic mobility observed in the CHO-4 mutant reflects lack of glycosylation rather than differential proteolysis. Because glycosylation has been shown to be important for protein folding in many proteins, the stability of the carbohydrate-free

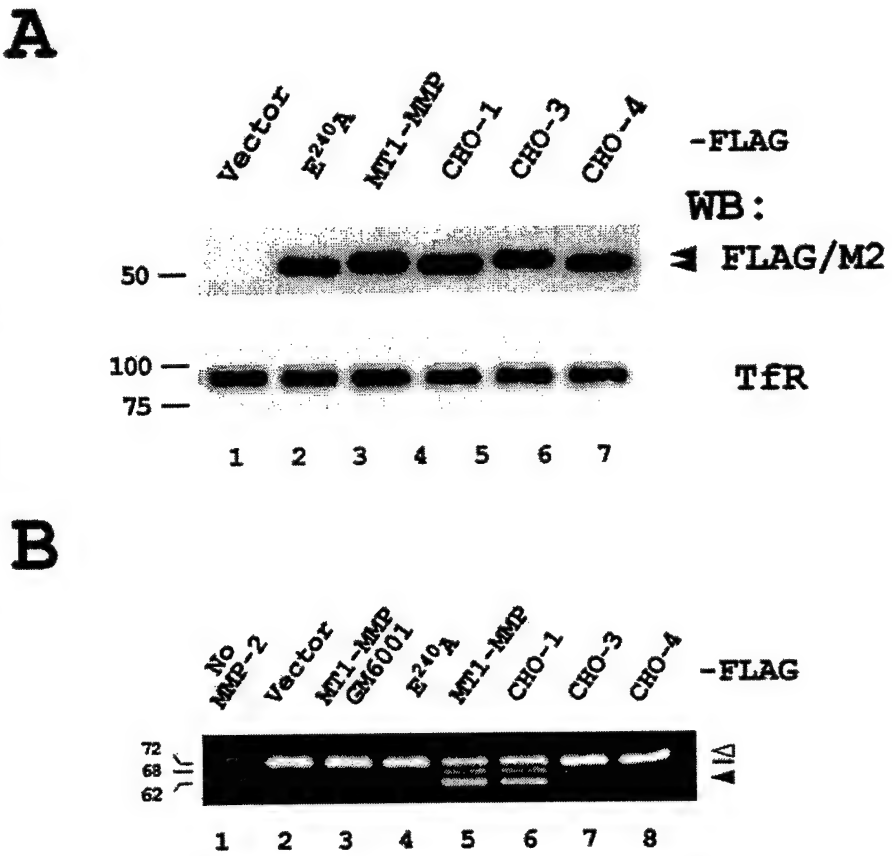

FIG. 6. **Glycosylation of MT1-MMP is required for MMP-2 activation.** The transfected COS-7 cells in Fig. 5 were also plated on 6-well plates coated with thin layer of type I collagen at the same time. *A*, after attachment, cells were incubated with 25 μM GM6001 for 12 h. Cell surface proteins were labeled with Sulfo-NHS-LC-LC-Biotin, purified with neutravidin as described under "Experimental Procedures," and analyzed by Western blot (*WB*) using anti-FLAG M2 antibody and anti-transferrin receptor (*TfR*) antibody. The active MT1-MMP are indicated as ◀. *B*, cells were also incubated with 1 nM of purified proMMP-2 in serum-free media for 24 h. The conditioned media were collected and analyzed by zymography as described under "Experimental Procedures." The pro-, intermediate, and active form of MMP-2 are indicated as ◁, —, and ◀, respectively.

CHO-4 mutant relative to wild-type MT1-MMP was evaluated. Soluble MT1-MMP was generated on the background of either wild type (sMT1-MMP) or CHO-4 mutant (sCHO-4). Comparison of sMT1-MMP and sCHO-4 by TUG-gel electrophoresis showed an identical unfolding transition, indicating similarity in stability and folding of the wild type and mutant soluble proteins (Fig. 3*C*).

Glycosylation Regulates Substrate Targeting of MT1-MMP—To evaluate the potential functional consequences of post-translational glycosylation of MT1-MMP, the proteolytic activity of the enzyme was evaluated against several key substrates. MT1-MMP activity can be down-regulated by autolytic cleavage at the start of the linker region ($Gly^{284} \downarrow Gly^{285}$, Fig. 1*B*), generating a catalytically inactive species (39). Because the predicted glycosylation sites are close to the reported cleavage site, the effect of glycosylation on MT1-MMP autolysis was investigated. In initial control experiments, FLAG-tagged MT1-MMP was co-expressed with untagged wild type MT1-MMP, inactive MT1-MMP (E240A) or control vector. The cell lysates were probed with anti-FLAG antibody to monitor processing of only the FLAG-tagged proteins. The conversion of active wild-type MT1-MMP (50 kDa) to a 37-kDa species was blocked by GM6001 (Fig. 4*A*, *lanes 1* and *2*). Co-expression of an untagged MT1-MMP increased the cleavage of the FLAG-tagged protein (Fig. 4*A*, *lane 3*), whereas co-transfection of the catalytically inactive E240A mutant did not affect conversion (Fig. 4*A*, *lane 4*), supporting a model of autolysis *in trans*. To further examine the autolysis model, similar experiments were performed with FLAG-tagged E240A MT1-MMP mutant. Consistent with the loss of proteinase activity in the E240A mutant, no autolysis was detected in the presence or absence of GM6001 (Fig. 4*A*, *lanes 5* and *6*). Co-expression of the untagged wild type MT1-MMP, but not the untagged E240A mutant, however, substantially converted the active species to the degradation product (Fig. 4*A*, *lanes 7* and *8*). These data clearly indicate that proteolytic processing of MT1-MMP is mediated by autolysis *in trans*. To test whether glycosylation affects autolytic processing of MT1-MMP, FLAG-tagged inactive E240A MT1-MMP was co-expressed with Myc-tagged wild type, E240A, or CHO-4 MT1-MMP and the cell lysates were probed with anti-FLAG antibody. Consistent with results in Fig. 4*A*, wild type MT1-MMP cleaved the inactive E240A mutant and this processing was blocked by GM6001 (Fig. 4*B*, *lanes 1* and *3*). Similar results were obtained using CHO-4-MT1-MMP (Fig. 4*B*, *lane 4*), indicating that glycosylation does not regulate the catalytic activity of MT1-MMP against other MT1-MMP species.

Because the linker region of MT1-MMP is important for its collagenolytic activity (54) and our results demonstrate that MT1-MMP is glycosylated in this domain, the effect of glycosylation on collagenolysis was examined using a previously established three-dimensional collagen gel invasion assay (24). Expression of MT1-MMP resulted in an 8-fold increase in collagen invasion (Fig. 5). The proteolytic activity of MT1-MMP is required for invasion, as base-line levels of invasion are observed in cells treated with the broad spectrum metalloproteinase inhibitor GM6001 as well as in cells expressing the catalytically inactive E240A mutant. All three glycosylation-defective mutants promoted collagen invasion as efficiently as wild type MT1-MMP (Fig. 5), demonstrating that collagenolytic activity is not regulated by glycosylation. In control surface-labeling experiments, wild-type MT1-MMP and glycosylation-deficient mutants were presented on the cell surface at equal levels (Fig. 6*A*).

In addition to type I collagen, proMMP-2 is a major substrate of MT1-MMP. To test whether glycosylation of MT1-MMP affects activation of proMMP-2, COS-7 cells were transfected with wild type MT1-MMP or various glycosylation mutants and

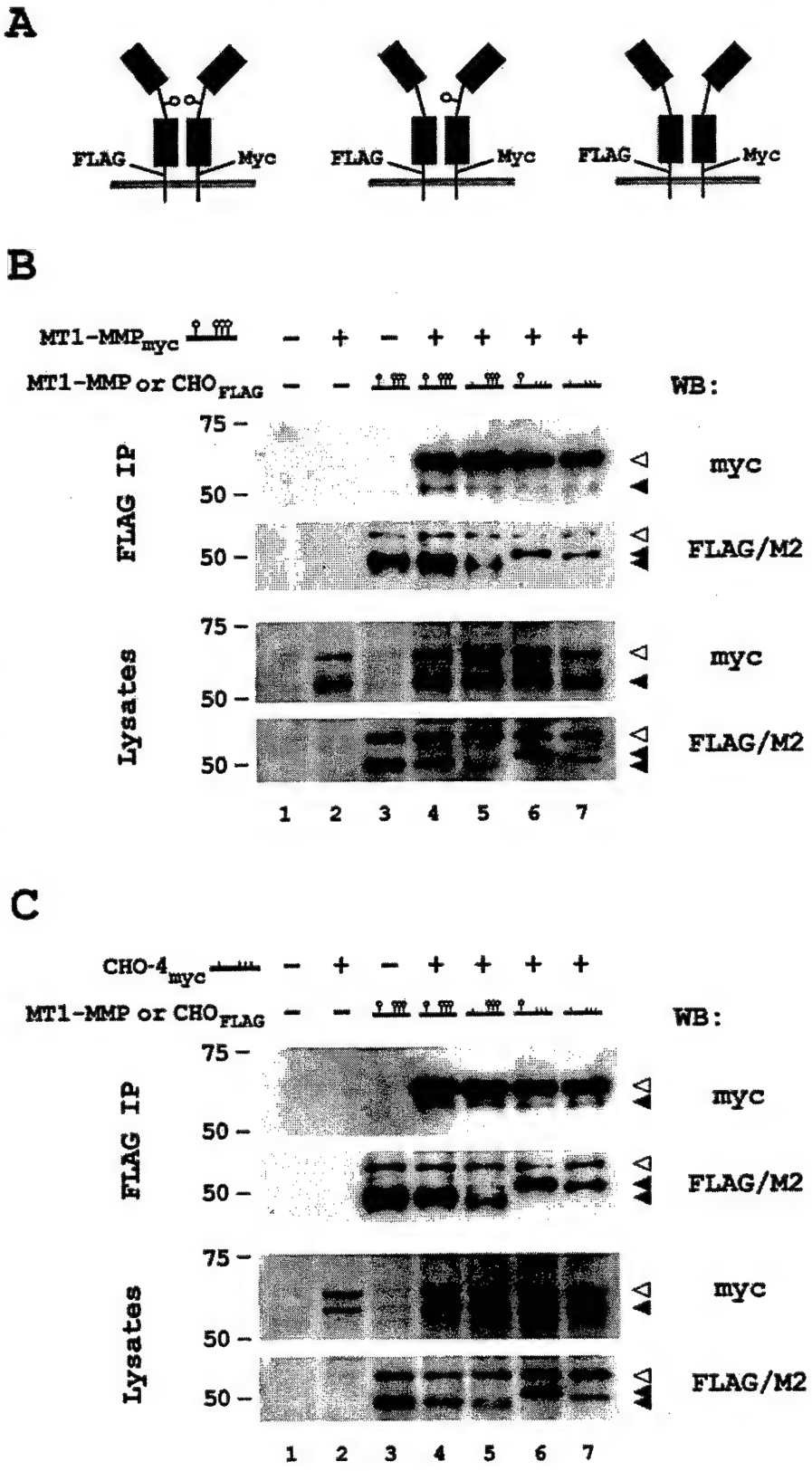

FIG. 7. **Oligomerization of MT1-MMP is not affected by its glycosylation.** *A*, schematic diagram of MT1-MMP oligomerization. FLAG- and Myc-tagged (stalk) MT1-MMP and its CHO-4 mutant were generated to test whether glycosylation interferes with oligomerization. *B*, COS-7 cells were co-transfected with Myc-tagged MT1-MMP and FLAG-tagged different glycosylation variants of MT1-MMP. Cell lysates were immunoprecipitated with anti-FLAG M2 antibody and probe back with anti-Myc (9E10) and anti-FLAG M2 antibody (*upper panel*). Cell lysates were also analyzed for equal expression (*lower panel*). Similar experiments were performed in *C* with Myc-tagged CHO-4 mutant. The pro- and active MT1-MMPs are indicated as ◁ and ◀, respectively. *WB*, Western blot.

incubated with purified proMMP-2, followed by analysis of zymogen activation by gelatin zymography. Cells transfected with wild type MT1-MMP processed proMMP-2 (72 kDa) to a 68-kDa intermediate and a 62-kDa active species (Fig. 6*B*, *lane 5*). The catalytic activity of MT1-MMP is required, because the activation of proMMP-2 was blocked by GM6001 (Fig. 6*B*, *lane 3*) and transfection of the MT1-MMP E240A mutant failed to activate proMMP-2 (Fig. 6*B*, *lane 4*). Cells transfected with glycosylation-deficient mutants demonstrated a distinct activation profile. Whereas the CHO-1 mutant activated proMMP-2

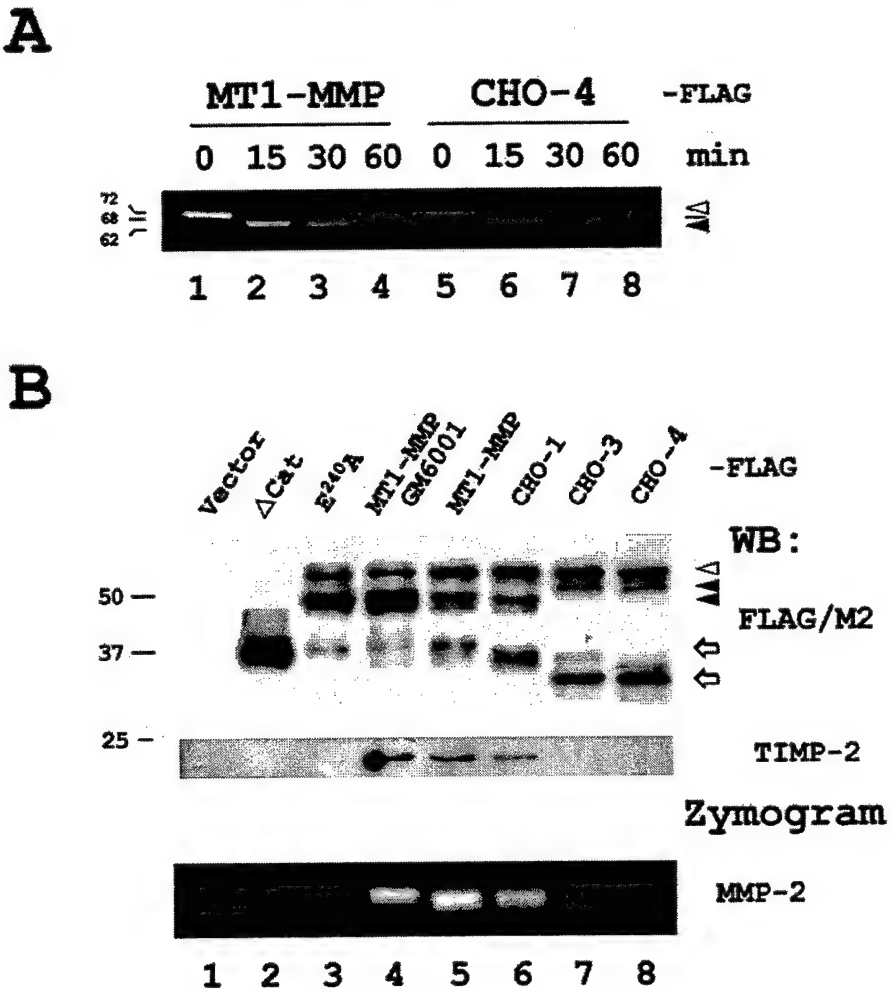

FIG. 8. **Glycosylation of MT1-MMP is required for MT1-MMP/TIMP-2/MMP-2 trimeric complex formation.** *A*, COS-7 cells were transfected with FLAG-tagged MT1-MMP or CHO-4 mutant in the presence of 25 μM GM6001. After 24 h, cells were incubated with 10 nM TIMP-2 and 10 nM proMMP-2 in the presence of 25 μM GM6001 for 1 h. Unbound TIMP-2 and proMMP-2, as well as GM6001, were then removed to allow activation of cell surface-bound MMP-2. Cell lysates were obtained at 0, 15, 30, and 60 min and analyzed by gelatin zymography as described under "Experimental Procedures." The pro-, intermediate, and active form of MMP-2 are indicated as ◁, —, and ◀, respectively. *B*, COS-7 cells were transfected with vector, Δ Cat, E240A, and different glycosylation variants of MT1-MMP in the presence of 25 μM GM6001. After 24 h, cells were incubated with 10 nM TIMP-2 and 10 nM proMMP-2 for 1 h followed by co-immunoprecipitation with anti-FLAG M2 antibody. The immunoprecipitates were analyzed by Western blot (*WB*) using anti-FLAG M2 and anti-TIMP-2 antibodies, and analyzed by gelatin zymography. The pro-, active, and autolytic products of MT1-MMP are indicated as ◁, ◀, and ⇐, respectively.

to the same extent as the wild type protein (Fig. 6*B*, *lane 6*), mutation of the ^{299}Thr-Thr-Ser^{301} sites in CHO-3 and CHO-4 significantly blocked proMMP-2 activation (Fig. 6*B*, *lanes 7* and *8*). These data demonstrate a differential effect of glycosylation on the substrate cleavage profile of MT1-MMP. Although wild type MT1-MMP promotes collagenolysis, autolysis, and gelatinolysis (via proMMP-2 activation), the carbohydrate free enzyme does not initiate gelatinolysis.

Oligomerization of MT1-MMP Is Not Regulated by Glycosylation—It was recently reported that hemopexin domain-dependent oligomerization of MT1-MMP is required for efficient proMMP-2 activation (35). To determine whether the defect in proMMP-2 activation described above results from the inability of the CHO-deficient mutants to oligomerize, differentially epitope-tagged MT1-MMP constructs were generated. Wild-type or CHO-4 MT1-MMP expressing the Myc epitope tag was generated and co-expressed with FLAG-tagged MT1-MMP or the individual CHO-1, CHO-3, or CHO-4 mutants. Following expression, cellular extracts were immunoprecipitated with immobilized FLAG antibody (M2), electrophoresed, and blots were probed with either the FLAG or Myc epitope tag antibodies. Potential dimer pairings between wild type and CHO-deficient MT1-MMP species are shown schematically in Fig. 7*A* (only one CHO chain is included for simplicity). Consistent with the observation of Itoh and co-workers (35), immunoprecipitation through the FLAG epitope tag also precipitated Myc-tagged MT1-MMP (Fig. 7*B*, *lane 4*), supporting the hypothesis that protein-protein interactions occur between adjacent MT1-MMP species. This interaction was not affected by the glycosylation status of MT1-MMP, as similar amounts of Myc-tagged MT1-MMP were co-immunoprecipitated with the FLAG-tagged CHO-1, -3, and -4 glycosylation-defective mutants (Fig. 7*B*, *lanes 5–7*). Similar results were obtained using Myc-tagged CHO-4 MT1-MMP (Fig. 7*C*), demonstrating that oligomerization is independent of glycosylation. Further, these data indicate that the inability of the CHO-3 and CHO-4 mutants to effectively catalyze proMMP-2 activation is not a result of inefficient oligomerization.

Glycosylation Affects the Presentation of a Stable MT1-MMP/TIMP-2/ProMMP-2 Trimeric Complex and Modulates TIMP-2/MT1-MMP Interaction—MT1-MMP mediates MMP-2 activation through the formation of a trimeric complex consisting MT1-MMP, TIMP-2 and proMMP-2. To examine the effect of glycosylation on the formation of the trimeric complex, FLAG-tagged MT1-MMP species were expressed in COS-7 cells in the presence of GM6001 to prevent autolytic degradation. After 24 h, the cells were incubated with TIMP-2 and proMMP-2 in the presence of GM6001 for 1 h. Cells were washed to remove unbound protein and inhibitors, and cellular activation of MMP-2 was monitored with time. As indicated in Fig. 8*A*, proMMP-2 initially associates with MT1-MMP transfected cells, and is processed to the intermediate and active species within 1 h (Fig. 8*C*, *lanes 1–4*). In contrast, interaction of proMMP-2 with CHO-4 mutant MT1-MMP transfected cells was substantially decreased (Fig. 8*A*, *lanes 5–8*), suggesting altered association and/or dissociation kinetics. This was con-

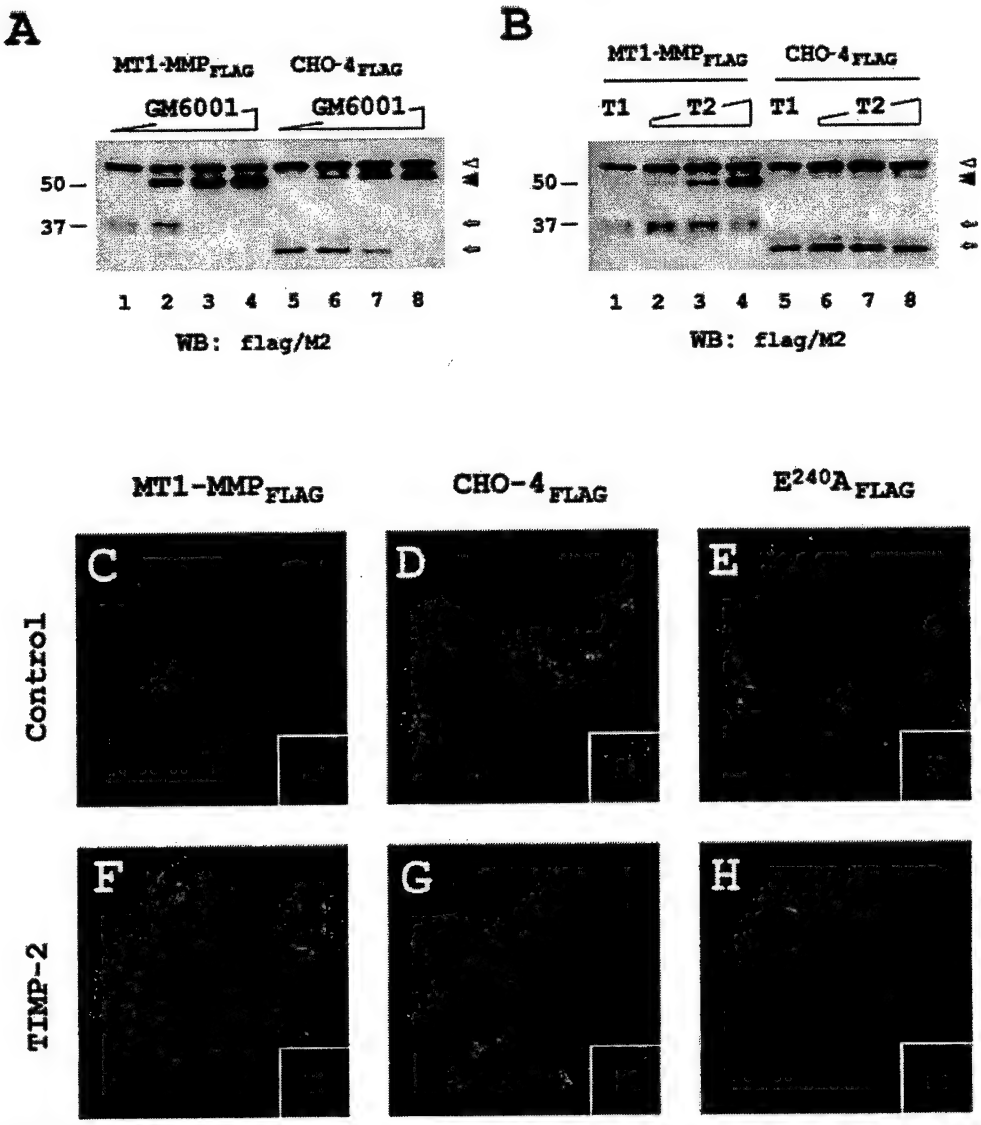

FIG. 9. **Glycosylation of MT1-MMP affects TIMP-2 inhibition of autolysis and TIMP-2-dependent endocytosis of MT1-MMP.** COS-7 cells were transfected with FLAG-tagged (stalk) MT1-MMP or CHO-4 mutant in the presence of increasing concentrations of GM6001 (*A*, 0, 1, 10, and 100 μM), or in *B*, TIMP-1 (100 nM) or increasing concentrations of TIMP-2 (1, 10, and 100 nM). After 24 h, cell lysates were fractionated on 10% SDS-PAGE and analyzed by Western blot using anti-FLAG M2 antibody. The pro-, active, and autolytic products of MT1-MMP are indicated as ◁, ◀, and ⇐, respectively. *C–H*, COS-7 cells were transfected with FLAG-tagged (stalk) MT1-MMP (*C* and *F*), CHO-4 (*D* and *G*), and E240A (*E* and *H*) mutant in the presence of 25 μM GM6001. Cell surface FLAG-tagged proteins were labeled with anti-FLAG M2 antibody on ice for 1 h. After washing off unbound antibody, cells were put back to 37 °C to allow endocytosis for 15 min. Cells were then fixed with formaldehyde and permeabilized with saponin, followed by Alexa Fluor 488-conjugated goat anti-mouse secondary antibody (in *green*). Total expression of MT1-MMP or its mutants were also stained with anti-linker antibody followed by Alexa Fluor 546-conjugated goat anti-rabbit secondary antibody (*inset*, in *red*). The nuclei were counterstained using TO-PRO iodide (642/661) (in *blue*). The images were taken using a Zeiss LSM510 laser scanning confocal microscope.

firmed by co-immunoprecipitation experiments in which wild type or mutant MT1-MMP species were immunoprecipitated with anti-FLAG antibody, and analyzed for the presence of TIMP-2 by Western blot and MMP-2 by gelatin zymography. Both TIMP-2 and MMP-2 were co-precipitated with wild type MT1-MMP (Fig. 8*B*, *lanes 4* and *5*). In control experiments, no complex was generated with the ΔCat mutant lacking the active site (Fig. 8*B*, *lane 2*) and negligible MMP-2 was associated with the inactive E240A mutant, presumably through direct interaction with the catalytic domain of MT1-MMP (63) (Fig. 8*B*, *lane 3*). Although similar levels of expression of CHO-deficient MT1-MMP mutants were obtained, no TIMP-2 was precipitated with the CHO-3 and CHO-4 mutants, and associated MMP-2 was substantially decreased to the level of E240A mutant (Fig. 8B, *lanes 7* and *8*). In control experiments, purified soluble MT1-MMP or the CHO-4 mutant (lacking the transmembrane and cytoplasmic domains) bound to TIMP-2 with similar efficiency (data not shown). These data suggest an inability to efficiently recruit TIMP-2 and proMMP-2 to cell surface localized carbohydrate-deficient MT1-MMP, indicating that glycosylation directly affects the presentation of a functional MT1-MMP/TIMP-2/proMMP-2 ternary complex on the cell surface and thereby inhibits cell surface proMMP -2 activation.

To further characterize the effect of glycosylation on the MT1-MMP/TIMP-2 interaction, the interaction of MT1-MMP with synthetic metalloproteinase inhibitor GM6001 and the endogenous inhibitor TIMP-2 was examined. GM6001 inhibited the autolysis of both wild type and CHO-4 MT1-MMP in a dose-dependent manner and with a similar inhibitory profile,

with partial inhibition at 1 and 10 μM, and complete blockade at 100 μM (Fig. 9*A*). In contrast, the inhibitory profiles of TIMP-2 against the two glycoforms were quite distinct. Although TIMP-2 stabilized the 50-kDa active species of wild type MT1-MMP in a dose-dependent manner (Fig. 9*B*, *lanes 2–4*), very little of the active species of CHO-4 mutant MT1-MMP was preserved even at 100 nM concentration of TIMP-2 (Fig. 9*B*, *lanes 6–8*). These data suggest that under *in vivo* conditions wherein TIMP-2 is the primary inhibitor of MT1-MMP, glycosylation of MT1-MMP may protect against autolysis and thus stabilize active MT1-MMP.

As a recent report demonstrated that TIMP-2 undergoes endocytosis with MT1-MMP (47, 64, 65), the effect of TIMP-2 on wild type and CHO-4 mutant MT1-MMP endocytosis was evaluated. Cells expressing FLAG epitope-tagged wild type, CHO-4, or E240A-MT1-MMP were incubated at 4 °C to prevent endocytosis and labeled with anti-FLAG antibody. Cells were then incubated in the presence or absence of TIMP-2 and shifted to 37 °C for 15 min to promote endocytosis. To prevent autolysis and shedding of MT1-MMP, GM6001 was kept throughout the experiment (38, 39). After endocytosis, antibody remaining on the cell surface was removed by low pH washing, and endocytosed antibody (indicative of endocytosed MT1-MMP) was detected with a secondary antibody probe. Control experiments using an antibody directed against the MT1-MMP linker domain demonstrated similar levels of expression of the various MT1-MMP species (Fig. 9, *C–H*, *index box*). Similar patterns of endocytosis were observed among wild type, carbohydrate-free, and catalytically inactive MT1-MMP (Fig. 9, *C–E*). Addition of TIMP-2 to wild-type MT1-MMP significantly increased endocytosis (Fig. 9*F*), whereas TIMP-2 had no effect on endocytosis of either inactive E240A MT1-MMP or carbohydrate-free CHO-4 MT1-MMP (Fig. 9, *G* and *H*). These data suggest that the inability of cell surface CHO-4 MT1-MMP to bind TIMP-2 may modulate the cell surface retention of the protein.

DISCUSSION

Results of the current study demonstrate that MT1-MMP is post-translationally modified by *O*-glycosylation at Thr^{291}, Thr^{299}, Thr^{300}, and/or Ser^{301} residues in the proline-rich linker region. Although the detailed carbohydrate composition was not analyzed, lectin precipitation experiments suggest that the carbohydrate moiety contains complex sugar structures. Using glycosylation inhibitors, evidence for glycosylation of endogenously expressed MT1-MMP in human cancer cells was provided. Distinct glycoforms of MT1-MMP were detected in human cancer cell lines, suggesting that MT1-MMP activity may be regulated by differential glycosylation *in vivo*. Moreover, putative glycosylation sites are predicted to exist in the linker regions of all known MT-MMPs, suggesting a conserved post-translational modification indicative of a potential regulatory function. Although the role of glycosylation among MMP family members has not been extensively evaluated, the secreted proteinase MMP-9 is known to be both *O*- and *N*-glycosylated and terminally sialylated. Interestingly, desialylation of MMP-9 has been shown to increase the hydrolysis of peptide substrate in the presence of TIMP-1 (66), suggesting TIMP-dependent inhibition of MMP activity could be modulated by glycosylation.

To evaluate the potential role of glycosylation in modifying MT1-MMP function, initial studies focused on analysis of collagenase activity, as recent studies have proposed that the linker domains of MMPs may play a crucial role in collagenolysis. For example, introduction of a single amino acid mutation in the linker region of MMP-1 (collagenase-1) dramatically decreased collagenase activity without affecting gelatinolysis, suggesting a direct role of this domain in collagen cleavage (67). Regulation of collagenase activity by the MT1-MMP linker region has also been demonstrated. MT1-MMP-mediated collagen cleavage was blocked by a recombinant protein containing the linker and hemopexin-like domains of MT1-MMP, whereas the hemopexin-like domain fragment in the absence of the linker was ineffective (54). Results of the current study show effective collagen gel invasion, regardless of the glycosylation status of the MT1-MMP linker region, suggesting that the relative efficiency of pericellular collagenolysis is not altered by carbohydrate.

In addition to interstitial collagen, proMMP-2 is a predominant MT1-MMP substrate, and results of the current study demonstrate that cell surface activation of proMMP-2 is blocked in glycosylation-defective mutants. The mechanism by which glycosylation of MT1-MMP affects MMP-2 activation was explored in detail. Experiments using α1-PI_{PDX} to block furin/PC activity indicated that the zymogen of MT1-MMP was activated with equal efficiency in the wild type enzyme or carbohydrate deficient mutants. To determine whether the inability to activate MMP-2 resulted from failure of the carbohydrate-free mutant to oligomerize, differentially epitope-tagged MT1-MMP species were employed as recently described (35). Our results confirm published reports that protein-protein interactions between neighboring MT1-MMP species accompany proMMP-2 activation; however, MT1-MMP oligomerization was independent of glycosylation status. The current data support the hypothesis that carbohydrate-free MT1-MMP does not form an effective ternary activation complex owing to an inability to recruit TIMP-2 to the cell surface proteinase. Although soluble recombinant MT1-MMP lacking the transmembrane and cytoplasmic domains can bind to TIMP-2 in solution, co-precipitation analyses demonstrate a lack of ternary complex formation with the cell-associated carbohydrate-free mutant. This result is supported by data showing an inability of TIMP-2 to block autolysis of cell surface carbohydrate-free MT1-MMP. Although the biochemical basis for the lack of TIMP-2 binding by the cell surface carbohydrate-free MT1-MMP species is unclear, an unidentified carbohydrate-binding protein may be necessary to induce or stabilize the active conformation of MT1-MMP prior to TIMP-2 binding. Alternatively the carbohydrate moiety may participate in the trafficking of MT1-MMP (55, 68). Indeed, our data demonstrate that, although TIMP-2 promotes endocytosis of wild-type MT1-MMP, internalization of the carbohydrate-defective MT1-MMP mutant is unaltered by TIMP-2, suggesting that glycosylation may regulate TIMP-2-driven endocytosis of MT1-MMP. Together these data support a model wherein glycosylation regulates substrate targeting and suggest a cellular mechanism by which post-translational processing may control MT1-MMP surface presentation and proMMP-2 activation.

REFERENCES

1. Brinckerhoff, C. E., and Matrisian, L. M. (2002) *Nat. Rev. Mol. Cell. Biol.* **3**, 207–214
2. Nagase, H., and Woessner, J. F., Jr. (1999) *J. Biol. Chem.* **274**, 21491–21494
3. Sternlicht, M. D., and Werb, Z. (2001) *Annu. Rev. Cell Dev. Biol.* **17**, 463–516
4. Werb, Z. (1997) *Cell* **91**, 439–442
5. Yu, Q., and Stamenkovic, I. (2000) *Genes Dev.* **14**, 163–176
6. Levi, E., Fridman, R., Miao, H. Q., Ma, Y. S., Yayon, A., and Vlodavsky, I. (1996) *Proc. Natl. Acad. Sci. U. S. A.* **93**, 7069–7074
7. Suzuki, M., Raab, G., Moses, M. A., Fernandez, C. A., and Klagsbrun, M. (1997) *J. Biol. Chem.* **272**, 31730–31737
8. English, W. R., Puente, X. S., Freije, J. M., Knauper, V., Amour, A., Merryweather, A., Lopez-Otin, C., and Murphy, G. (2000) *J. Biol. Chem.* **275**, 14046–14055
9. Noe, V., Fingleton, B., Jacobs, K., Crawford, H. C., Vermeulen, S., Steelant, W., Bruyneel, E., Matrisian, L. M., and Mareel, M. (2001) *J. Cell Sci.* **114**, 111–118
10. Deryugina, E. I., Ratnikov, B., Monosov, E., Postnova, T. I., DiScipio, R., Smith, J. W., and Strongin, A. Y. (2001) *Exp. Cell Res.* **263**, 209–223
11. Preece, G., Murphy, G., and Ager, A. (1996) *J. Biol. Chem.* **271**, 11634–11640
12. Knauper, V., Will, H., Lopez-Otin, C., Smith, B., Atkinson, S. J., Stanton, H., Hembry, R. M., and Murphy, G. (1996) *J. Biol. Chem.* **271**, 17124–17131

13. Murphy, G., Stanton, H., Cowell, S., Butler, G., Knauper, V., Atkinson, S., and Gavrilovic, J. (1999) *APMIS* **107,** 38–44
14. Overall, C. M., and Lopez-Otin, C. (2002) *Nat. Rev. Cancer* **2,** 657–672
15. Nelson, A. R., Fingleton, B., Rothenberg, M. L., and Matrisian, L. M. (2000) *J. Clin. Oncol.* **18,** 1135–1149
16. Sato, H., Takino, T., Okada, Y., Cao, J., Shinagawa, A., Yamamoto, E., and Seiki, M. (1994) *Nature* **370,** 61–65
17. Takino, T., Sato, H., Shinagawa, A., and Seiki, M. (1995) *J. Biol. Chem.* **270,** 23013–23020
18. Will, H., and Hinzmann, B. (1995) *Eur. J. Biochem.* **231,** 602–608
19. Pei, D. (1999) *J. Biol. Chem.* **274,** 8925–8932
20. Itoh, Y., Kajita, M., Kinoh, H., Mori, H., Okada, A., and Seiki, M. (1999) *J. Biol. Chem.* **274,** 34260–34266
21. Kojima, S., Itoh, Y., Matsumoto, S., Masuho, Y., and Seiki, M. (2000) *FEBS Lett.* **480,** 142–146
22. Seiki, M. (2002) *Curr. Opin. Cell Biol.* **14,** 624–632
23. Seiki, M. (2003) *Cancer Lett.* **194,** 1–11
24. Ellerbroek, S. M., Wu, Y. I., Overall, C. M., and Stack, M. S. (2001) *J. Biol. Chem.* **276,** 24833–24842
25. Hotary, K., Allen, E., Punturieri, A., Yana, I., and Weiss, S. J. (2000) *J. Cell Biol.* **149,** 1309–1323
26. Holmbeck, K., Bianco, P., Caterina, J., Yamada, S., Kromer, M., Kuznetsov, S. A., Mankani, M., Robey, P. G., Poole, A. R., Pidoux, I., Ward, J. M., and Birkedal-Hansen, H. (1999) *Cell* **99,** 81–92
27. Zhou, Z., Apte, S. S., Soininen, R., Cao, R., Baaklini, G. Y., Rauser, R. W., Wang, J., Cao, Y., and Tryggvason, K. (2000) *Proc. Natl. Acad. Sci. U. S. A.* **97,** 4052–4057
28. Strongin, A. Y., Collier, I., Bannikov, G., Marmer, B. L., Grant, G. A., and Goldberg, G. I. (1995) *J. Biol. Chem.* **270,** 5331–5338
29. Butler, G. S., Butler, M. J., Atkinson, S. J., Will, H., Tamura, T., van Westrum, S. S., Crabbe, T., Clements, J., d'Ortho, M. P., and Murphy, G. (1998) *J. Biol. Chem.* **273,** 871–880
30. Kinoshita, T., Sato, H., Okada, A., Ohuchi, E., Imai, K., Okada, Y., and Seiki, M. (1998) *J. Biol. Chem.* **273,** 16098–16103
31. Zucker, S., Drews, M., Conner, C., Foda, H. D., DeClerck, Y. A., Langley, K. E., Bahou, W. F., Docherty, A. J., and Cao, J. (1998) *J. Biol. Chem.* **273,** 1216–1222
32. Overall, C. M., King, A. E., Sam, D. K., Ong, A. D., Lau, T. T., Wallon, U. M., DeClerck, Y. A., and Atherstone, J. (1999) *J. Biol. Chem.* **274,** 4421–4429
33. Atkinson, S. J., Crabbe, T., Cowell, S., Ward, R. V., Butler, M. J., Sato, H., Seiki, M., Reynolds, J. J., and Murphy, G. (1995) *J. Biol. Chem.* **270,** 30479–30485
34. Will, H., Atkinson, S. J., Butler, G. S., Smith, B., and Murphy, G. (1996) *J. Biol. Chem.* **271,** 17119–17123
35. Itoh, Y., Takamura, A., Ito, N., Maru, Y., Sato, H., Suenaga, N., Aoki, T., and Seiki, M. (2001) *EMBO J.* **20,** 4782–4793
36. Lehti, K., Lohi, J., Juntunen, M. M., Pei, D., and Keski-Oja, J. (2002) *J. Biol. Chem.* **277,** 8440–8448
37. Jiang, A., Lehti, K., Wang, X., Weiss, S. J., Keski-Oja, J., and Pei, D. (2001) *Proc. Natl. Acad. Sci. U. S. A.* **98,** 13693–13698
38. Toth, M., Hernandez-Barrantes, S., Osenkowski, P., Bernardo, M. M., Gervasi, D. C., Shimura, Y., Meroueh, O., Kotra, L. P., Galvez, B. G., Arroyo, A. G., Mobashery, S., and Fridman, R. (2002) *J. Biol. Chem.* **277,** 26340–26350
39. Hernandez-Barrantes, S., Toth, M., Bernardo, M. M., Yurkova, M., Gervasi, D. C., Raz, Y., Sang, Q. A., and Fridman, R. (2000) *J. Biol. Chem.* **275,** 12080–12089
40. Munshi, H. G., Wu, Y. I., Ariztia, E. V., and Stack, M. S. (2002) *J. Biol. Chem.* **277,** 41480–41488
41. Pei, D., and Weiss, S. J. (1995) *Nature* **375,** 244–247
42. Maquoi, E., Noel, A., Frankenne, F., Angliker, H., Murphy, G., and Foidart, J. M. (1998) *FEBS Lett.* **424,** 262–266
43. Yana, I., and Weiss, S. J. (2000) *Mol. Biol. Cell* **11,** 2387–2401
44. Anderson, E. D., Thomas, L., Hayflick, J. S., and Thomas, G. (1993) *J. Biol. Chem.* **268,** 24887–24891
45. Mori, H., Tomari, T., Koshikawa, N., Kajita, M., Itoh, Y., Sato, H., Tojo, H., Yana, I., and Seiki, M. (2002) *EMBO J.* **21,** 3949–3959
46. Galvez, B. G., Matias-Roman, S., Yanez-Mo, M., Sanchez-Madrid, F., and Arroyo, A. G. (2002) *J. Cell Biol.* **159,** 509–521
47. Uekita, T., Itoh, Y., Yana, I., Ohno, H., and Seiki, M. (2001) *J. Cell Biol.* **155,** 1345–1356
48. Toth, M., Bernardo, M. M., Gervasi, D. C., Soloway, P. D., Wang, Z., Bigg, H. F., Overall, C. M., DeClerck, Y. A., Tschesche, H., Cher, M. L., Brown, S., Mobashery, S., and Fridman, R. (2000) *J. Biol. Chem.* **275,** 41415–41423
49. Olson, M. W., Gervasi, D. C., Mobashery, S., and Fridman, R. (1997) *J. Biol. Chem.* **272,** 29975–29983
50. Hansen, J. E., Lund, O., Rapacki, K., and Brunak, S. (1997) *Nucleic Acids Res.* **25,** 278–282
51. Notredame, C., Higgins, D. G., and Heringa, J. (2000) *J. Mol. Biol.* **302,** 205–217
52. Munshi, H. G., and Stack, M. S. (2002) *Methods Cell Biol.* **69,** 195–205
53. Mast, A. E., Enghild, J. J., Pizzo, S. V., and Salvesen, G. (1991) *Biochemistry* **30,** 1723–1730
54. Tam, E. M., Wu, Y. I., Butler, G. S., Stack, M. S., and Overall, C. M. (2002) *J. Biol. Chem.* **277,** 39005–39014
55. Altschuler, Y., Kinlough, C. L., Poland, P. A., Bruns, J. B., Apodaca, G., Weisz, O. A., and Hughey, R. P. (2000) *Mol. Biol. Cell* **11,** 819–831
56. Huet, G., Hennebicq-Reig, S., de Bolos, C., Ulloa, F., Lesuffleur, T., Barbat, A., Carriere, V., Kim, I., Real, F. X., Delannoy, P., and Zweibaum, A. (1998) *J. Cell Biol.* **141,** 1311–1322
57. Ihrke, G., Bruns, J. R., Luzio, J. P., and Weisz, O. A. (2001) *EMBO J.* **20,** 6256–6264
58. Molloy, S. S., Anderson, E. D., Jean, F., and Thomas, G. (1999) *Trends Cell Biol.* **9,** 28–35
59. Kuan, S. F., Byrd, J. C., Basbaum, C., and Kim, Y. S. (1989) *J. Biol. Chem.* **264,** 19271–19277
60. Huet, G., Kim, I., de Bolos, C., Lo-Guidice, J. M., Moreau, O., Hemon, B., Richet, C., Delannoy, P., Real, F. X., and Degand, P. (1995) *J. Cell Sci.* **108,** 1275–1285
61. Rozanov, D. V., and Strongin, A. Y. (2003) *J. Biol. Chem.* **278,** 8257–8260
62. Koo, H. M., Kim, J. H., Hwang, I. K., Lee, S. J., Kim, T. H., Rhee, K. H., and Lee, S. T. (2002) *Mol. Cell* **13,** 118–124
63. English, W. R., Holtz, B., Vogt, G., Knauper, V., and Murphy, G. (2001) *J. Biol. Chem.* **276,** 42018–42026
64. Remacle, A., Murphy, G., and Roghi, C. (2003) *J. Cell Sci.* **116,** 3905–3916
65. Maquoi, E., Frankenne, F., Baramova, E., Munaut, C., Sounni, N. E., Remacle, A., Noel, A., Murphy, G., and Foidart, J. M. (2000) *J. Biol. Chem.* **275,** 11368–11378
66. Van den Steen, P. E., Opdenakker, G., Wormald, M. R., Dwek, R. A., and Rudd, P. M. (2001) *Biochim. Biophys. Acta* **1528,** 61–73
67. Tsukada, H., and Pourmotabbed, T. (2002) *J. Biol. Chem.* **277,** 27378–27384
68. Yeaman, C., Le Gall, A. H., Baldwin, A. N., Monlauzeur, L., Le Bivic, A., and Rodriguez-Boulan, E. (1997) *J. Cell Biol.* **139,** 929–940

THE JOURNAL OF BIOLOGICAL CHEMISTRY
Vol. 277, No. 44, Issue of November 1, pp. 41480–41488, 2002
Printed in U.S.A.

Calcium Regulation of Matrix Metalloproteinase-mediated Migration in Oral Squamous Cell Carcinoma Cells*

Received for publication, July 30, 2002
Published, JBC Papers in Press, August 22, 2002, DOI 10.1074/jbc.M207695200

Hidayatullah G. Munshi‡§¶, Yi I. Wu‖, Edgardo V. Ariztia‖, and M. Sharon Stack§‖**

From the ‡Division of Hematology/Oncology, Department of Medicine and ‖Department of Cell and Molecular Biology, Feinberg School of Medicine, Northwestern University, and the §Robert H. Lurie Comprehensive Cancer Center of Northwestern University, Chicago, Illinois 60611

Activation of matrix metalloproteinase 2 (MMP-2) has been shown to play a significant role in the behavior of cancer cells, affecting both migration and invasion. The activation process requires multimolecular complex formation involving pro-MMP-2, membrane type 1-MMP (MT1-MMP), and tissue inhibitor of metalloproteinases-2 (TIMP-2). Because calcium is an important regulator of keratinocyte function, we evaluated the effect of calcium on MMP regulation in an oral squamous cell carcinoma line (SCC25). Increasing extracellular calcium (0.09–1.2 mM) resulted in a dose-dependent increase in MT1-MMP-dependent pro-MMP-2 activation. Despite the requirement for MT1-MMP in the activation process, no changes in MT1-MMP expression, cell surface localization, or endocytosis were apparent. However, increased generation of the catalytically inactive 43-kDa MT1-MMP autolysis product and decline in the TIMP-2 levels in conditioned media were observed. The decrease in TIMP-2 levels in the conditioned media was prevented by a broad spectrum MMP inhibitor, suggesting that calcium promotes recruitment of TIMP-2 to MT1-MMP on the cell surface. Despite the decline in soluble TIMP-2, no accumulation of TIMP-2 in cell lysates was seen. Blocking TIMP-2 degradation with bafilomycin A1 significantly increased cell-associated TIMP-2 levels in the presence of high calcium. These data suggest that the decline in TIMP-2 is because of increased calcium-mediated MT1-MMP-dependent degradation of TIMP-2. In functional studies, increasing calcium enhanced MMP-dependent cellular migration on laminin-5-rich matrix using an *in vitro* colony dispersion assay. Taken together, these results suggest that changes in extracellular calcium can regulate post-translational MMP dynamics and thus affect the cellular behavior of oral squamous cell carcinoma.

Oral squamous cell carcinoma (OSCC)[1] is characterized by local, regional, and distant spread of the disease; however, the cellular and molecular events that control the invasive behavior are poorly understood (1, 2). Immunohistochemical studies have implicated enzymes belonging to the matrix metalloproteinase (MMP) family in basement membrane proteolysis and tissue invasion in OSCC (3). MMPs are a large family of metallo-endopeptidases with activity directed against a variety of extracellular matrix substrates (4–7). Expression of MMP-2 (gelatinase A, a 72-kDa type IV collagenase) is observed in invasive and metastatic cases of OSCC (3, 8). Furthermore, increased expression of MMP-2 is associated with decreased staining of extracellular matrix in OSCC, suggesting that MMP-2 promotes matrix breakdown (3, 8). MMP-2 is secreted from cells as a zymogen (pro-MMP-2) and is activated post-translationally by a trans-membrane MMP designated as membrane type 1-MMP (MT1-MMP) (9–11). MT1-MMP is also up-regulated in OSCC, and increased expression is observed in highly invasive and metastatic cases (3, 8). Pro-MT1-MMP is synthesized as a 63–66-kDa zymogen and is activated intracellularly to a 55-kDa species by the serine proteinase furin, a member of the proprotein convertase family (12–14).

The activation of pro-MMP-2 is regulated by a complex mechanism involving formation of a trimolecular complex with MT1-MMP and tissue inhibitor of metalloproteinase-2 (TIMP-2) (10, 15–17). In this model, TIMP-2 plays a dual role in the regulation of MMP-2 activation, functioning both to promote and to inhibit the activation process in a concentration-dependent manner (16, 18). TIMP-2 bridges the interaction between the MMP-2 zymogen and MT1-MMP via N-terminal binding to the active site of MT1-MMP with the concomitant C-terminal binding to the pro-MMP-2 hemopexin domain (10, 15–20). Thus, at low TIMP-2 concentration, an adjacent TIMP-2-free MT1-MMP can effectively process the cell surface-bound pro-MMP-2 to a 68-kDa intermediate species, which undergoes autolytic processing to the mature 62-kDa active species. However at high TIMP-2 concentration, all of the cell surface MT1-MMPs undergo complex formation with TIMP-2, thereby inhibiting pro-MMP-2 activation (10, 15–20).

As stringent control of MMP activity plays an important role in keratinocyte behavior (21–23) and dysregulation of MMP activity has been correlated with metastatic progression, factors that control acquisition of net MMP activity in OSCC were evaluated. Of the many agents that are known to affect keratinocyte behavior, calcium is one of the key factors (24–27). There is a steep calcium gradient within the epidermis, with

* This work was supported in part by NIDCR Grant PO1 DE12328 (to M. S. S.) from the National Institutes of Health. The costs of publication of this article were defrayed in part by the payment of page charges. This article must therefore be hereby marked "*advertisement*" in accordance with 18 U.S.C. Section 1734 solely to indicate this fact.

¶ Supported in part by Grant 5T32 CA70085 from the National Institutes of Health to the RHL Comprehensive Cancer Center's Training Program in Signal Transduction and Cancer and is the recipient of the 2002 American Society of Clinical Oncology Young Investigator Award.

** To whom correspondence should be addressed: Dept. of Cell and Molecular Biology, Northwestern University Medical School, 303 E. Chicago Ave., Tarry 8-715, Chicago IL 60611. Tel.: 312-908-8216; Fax: 312-503-7912; E-mail: mss130@northwestern.edu.

[1] The abbreviations used are: OSCC, oral squamous cell carcinoma; MMP, matrix metalloproteinase; MT1-MMP, membrane type 1-MMP; TIMP, tissue of inhibitor of metalloproteinases; RVKR, decanoyl-Arg-Val-Lys-Arg-chloromethyl ketone; DMEM, Dulbecco's modified Eagle's media; PBS, phosphate-buffered saline; PMA, phorbol 12-myristate 13-acetate; MESNA, mercaptoethanesulfonic acid; EGF, epidermal growth factor; ELISA, enzyme-linked immunosorbent assay; RT, reverse transcriptase; GAPDH, glyceraldehyde-3-phosphate dehydrogenase.

higher calcium present in the uppermost layers (28–30). Moreover, altering extracellular calcium has been used to effectively model *in vitro* physiologic changes in keratinocytes that occur within the epidermis as cells migrate from the basal to the uppermost layers. Interestingly, recent studies (31–33) have demonstrated a relationship between extracellular calcium and enhanced matrix metalloproteinase gene expression in primary human keratinocytes.

Because calcium is an important regulator of keratinocyte function, we evaluated the effect of calcium on MMP regulation in an oral squamous cell carcinoma line (SCC25). Increasing extracellular calcium resulted in a dose-dependent increase in pro-MMP-2 activation, accompanied by enhanced MT1-MMP autolytic processing and a decline in the levels of soluble TIMP-2. The decrease in TIMP-2 levels in the conditioned media was prevented by a broad spectrum MMP inhibitor, suggesting that calcium promotes recruitment of TIMP-2 to MT1-MMP on the cell surface. Despite the decline in soluble TIMP-2, no accumulation of TIMP-2 in cell lysates was seen. However, blocking TIMP-2 degradation with bafilomycin A1 significantly increased cell-associated TIMP-2 levels in the presence of high calcium. These data suggest that the decline in TIMP-2 is due to increased calcium-mediated MT1-MMP-dependent degradation of TIMP-2. Moreover, calcium enhanced MMP-dependent cellular migration on laminin-5-rich matrix. These results suggest that changes in extracellular calcium can regulate post-translational MMP dynamics and thus affect the cellular behavior of OSCC.

EXPERIMENTAL PROCEDURES

Materials—Gelatin, type I collagen, cell culture reagents, Chelex 100, MESNA, peroxidase-conjugated secondary antibodies, and the MT1-MMP antibody directed against the hinge region were purchased from Sigma. Phorbol 12-myristate 13-acetate (PMA), epidermal growth factor (EGF), and bafilomycin A1 were from Calbiochem. Dulbecco's modified Eagle's media (DMEM), DMEM without calcium, Ham's F-12, G418, Trizol, and One-step RT-PCR kits were purchased from Invitrogen. Purified TIMP-1 and TIMP-2 proteins, rabbit polyclonal TIMP-2 antibody, and the broad spectrum MMP inhibitor GM6001 were purchased from Chemicon (Temecula, CA). TIMP-2 ELISA kit was from Oncogene Research Products (Boston, MA). SuperSignal enhanced chemiluminescence (ECL) reagent, EZ-Link Sulfo-NHS-LC-Biotin, EZ-Link Sulfo-NHS-SS-Biotin, and UltraLink immobilized streptavidin gel were obtained from Pierce. The furin inhibitor decanoyl-Arg-Val-Lys-Arg-chloromethyl ketone (RVKR) was from Alexis Biochemicals (San Diego, CA). Microcon 10 microconcentrators and polyvinylidene difluoride membranes were purchased from Millipore (Bedford, MA). FuGENE 6 was obtained from Roche Molecular Biochemicals. RQ1 DNase was from Promega (Madison, WI).

Cell Cultures—SCC25 cells were obtained from American Type Culture Collection (ATCC). SCC25 cells were routinely maintained in DMEM/Ham's F-12 = 1:1 media containing 10% fetal calf serum and supplemented with 100 units/ml penicillin. SCC25 and SCC25-MT (defined below) cells were plated in DMEM containing 0.09 mM calcium and supplemented with Chelex-treated 10% fetal calf serum. After overnight serum starvation, the cells were switched to serum-free DMEM containing the indicated calcium concentration. In additional experiments, inhibitors or other chemical reagents were added 30 min prior to the medium change.

In some experiments, cells were cultured on thin layer or three-dimensional collagen surfaces (34). Briefly, acid-solubilized rat tail type I collagen was diluted to 50 μg/ml in 0.02 N acetic acid and added to the tissue culture plate for 1 h at 18 °C. The solution was aspirated, and the plate was rinsed three times with PBS. Three-dimensional collagen gels were prepared by diluting acid-solubilized type I collagen to a concentration of 1 mg/ml in cold DMEM (calcium-free), neutralizing with sodium hydroxide, and then allowing to gel (700 μl in 12-well plates) for 30 min at 37 °C prior to plating cells.

Generation of SCC25-MT Cells—Human MT1-MMP cDNA (a kind gift from Duanqing Pei, University of Minnesota) was cloned into pCR3.1-Uni (Invitrogen) mammalian expression vector. SCC25 cells were stably transfected using FuGENE 6 according to the manufacturer's instructions. Cell clones resistant to 0.8 mg/ml G418 were chosen and screened for MMP-2 activation by zymography as described below and for MT1-MMP expression by Western blotting using antibody directed against the hinge region. Six different clones with high levels of MT1-MMP expression were selected for subsequent experiments. The cells were then maintained in DMEM/Ham's F12 media = 1:1 supplemented with 10% fetal calf serum, 100 units/ml penicillin, and 0.65 mg/ml G418.

Analysis of MMP-2 and TIMP-2 Expression—Gelatinase activities in 24-h serum-free conditioned media were determined using SDS-PAGE gelatin zymography as described previously (34). Briefly, SDS-PAGE gels (9% acrylamide) were co-polymerized with 0.1% gelatin, and samples were electrophoresed without reduction or boiling using 5× Laemmli sample buffer (35). SDS was removed through a 30-min incubation in 2.5% Triton X-100, and gels were incubated in 20 mM glycine, pH 8.3, 10 mM $CaCl_2$, 1 μM $ZnCl_2$ at 37 °C for 24–36 h. The gels were stained with Coomassie Blue to visualize zones of gelatinolytic activity. The conditioned media were concentrated 15–20-fold using Microcon 10 microconcentrators, boiled in Laemmli sample dilution buffer (35), analyzed for TIMP-2 by SDS-PAGE (15% gels), and immunoblotted with rabbit polyclonal antibody (Chemicon). Levels of TIMP-2 protein in the cell lysates were quantified by ELISA (Oncogene Research Products) according to the manufacturer's specifications.

MT1-MMP and TIMP-2 RNA Levels—Total RNA was isolated from SCC25 and SCC25-MT cells using Trizol reagent according to the manufacturer's instructions. Following digestion with RQ1 DNase for 30 min at 37 °C, the total RNA concentration was determined by spectrophotometric measurement. Primer pairs for human MT1-MMP, human TIMP-2, and human GAPDH were as follows: forward primer 5′-GCCCATTGGCCAGTTCTGGCGGG-3′ and reverse primer 5′-CCTCGTCCACCTCAATGATGATC-3′ for MT1-MMP; forward primer 5′-GGCGTTTTGCAATGCAGATGTAG-3′ and reverse primer 5′-CACAGGAGCCGTCACTTCTCTTG-3′ for TIMP-2; and forward primer 5′-CGGAGTCAACGGATTTGGTCGTAT-3′ and reverse primer 5′-AGCCTTCTCCATGGTGGTGAAGAC-3′ for GAPDH (36). The length of the MT1-MMP, TIMP-2, and GAPDH amplicons were 530, 497, and 307 bp, respectively. RT-PCR was performed using the One-step RT-PCR kit where reverse transcription and DNA amplification occur in the same reaction. Briefly, 1 μg of total RNA was used as template in a reaction that included the appropriate primers in the presence of both reverse transcriptase and *Taq* polymerase. The mixture was incubated at 45 °C for 30 min and cycled 30 times at 94 °C for 30 s, 55 °C for 30 s, and 72 °C for 2 min. Appropriate negative controls of amplification included reactions without reverse transcriptase. PCR products were visualized by UV transillumination of 1.5% agarose gels stained with ethidium bromide.

Cell Surface Biotinylation—To label cell surface proteins, SCC25-MT cells were grown to confluence in a 6-well plate, washed with ice-cold PBS, and incubated at 4 °C with gentle shaking for 30 min with 0.5 mg/ml cell-impermeable Sulfo-NHS-LC-Biotin in ice-cold PBS, followed by washing with 100 mM glycine to quench free biotin. Cells were detached by scraping, lysed in modified RIPA buffer (50 mM Tris, pH 7.4, 150 mM NaCl, 5 mM EDTA, 1% Triton X-100 and 0.1% SDS) with proteinase inhibitors (1 μg/ml aprotinin, 1 μM pepstatin, and 10 μM leupeptin), and clarified by centrifugation. To isolate biotinylated cell surface proteins, equal amounts of protein from each sample were incubated with streptavidin beads at 4 °C for 14 h, followed by centrifugation. After boiling in Laemmli sample dilution buffer (35) to dissociate streptavidin bead-biotin complexes, the biotin-labeled samples were analyzed by SDS-PAGE (9% gels) and immunoblotted for MT1-MMP.

MT1-MMP Endocytosis—To determine whether calcium affects MT1-MMP endocytosis, SCC25-MT cells grown to confluence in a 6-cm dish were washed with ice-cold PBS and then incubated with cleavable cell-impermeable sulfo-NHS-SS-biotin (1 mg/ml) for 20 min in an ice bath. Biotinylation was stopped by washing with ice-cold PBS followed by 100 mM glycine in PBS to quench free biotin. Cells were then incubated with DMEM containing either 0.09 mM or 1.2 mM calcium at 37 °C for 40 min to initiate endocytosis. Endocytosis of cell surface proteins was then stopped by placing the cells on ice and washing them with ice-cold PBS. Biotin was then cleaved off the exposed cell surface by incubating the cells with membrane-impermeable reducing agent MESNA (100 mM) for 30 min at 4 °C (37). The cells were lysed in modified RIPA buffer with proteinase inhibitors (1 μg/ml aprotinin, 1 μM pepstatin, and 10 μM leupeptin) and clarified by centrifugation. To isolate biotinylated proteins (representing endocytosed surface-labeled species), equal amounts of protein from each of the samples were incubated with streptavidin beads at 4 °C for 14 h, followed by centrifugation. After boiling in Laemmli sample dilution buffer (35) to disso-

ciate streptavidin bead-biotin complexes, the samples were analyzed by SDS-PAGE (9% gels) and immunoblotted for MT1-MMP. In control experiments to determine the efficiency of surface stripping with MESNA, cells were maintained on ice for the duration of the experiment and were not induced to undergo endocytosis via a temperature shift. In additional control experiments, the MESNA stripping step was omitted such that total labeled protein (endocytosed and the cell surface pool) was analyzed.

Generation of Laminin-5-enriched Matrix and Cell Dispersion Assays—The extracellular matrix deposited by SCC25 cells was generated as described previously (34, 38). Briefly, SCC25 cells were grown in 12-well plates to 48–72 h post-confluence prior to treatment for 7 min with 20 mM ammonium hydroxide to remove cells. After 3 rapid washes each in sterile distilled water and PBS, the laminin-5-enriched matrix was then used for *in vitro* migration assays. The effect of calcium on laminin-5-induced migration was assessed using a cell dispersion assay as described previously (39). Briefly, SCC25 and SCC25-MT cells (3×10^4) were plated in DMEM (0.09 mM calcium) inside a cloning cylinder placed in the middle of a 12-well plate coated with laminin-5-enriched matrix. After the cells have attached and spread, the cloning cylinder was removed, and the cells were washed twice with DMEM containing 0.09 mM calcium and serum-starved for an additional 3 h. The media were then switched to DMEM containing either 0.09 or 1.2 mM calcium supplemented with 20 ng/ml EGF. In selected experiments, the proteinase dependence of migration was determined by adding the MMP inhibitor GM6001 (10 μM). To quantify the relative motility, the migratory front was photographed every 12 h for 48 h, and the percentage of cells crossing a line designated "migratory max" was enumerated.

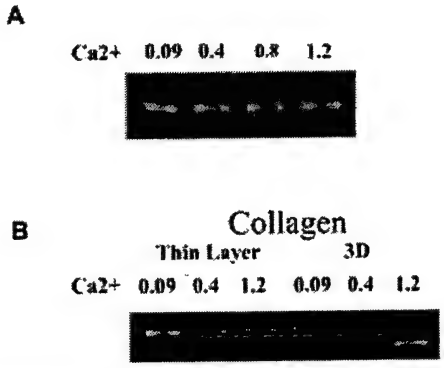

FIG. 1. **Extracellular calcium regulates pro-MMP-2 activation.** *A*, SCC25 cells were plated on plastic in medium containing 0.09 mM calcium. Following overnight serum starvation, cells were transferred to medium containing the indicated calcium concentration (0.09–1.2 mM). The conditioned media were collected at 24 h and analyzed for MMP activity by gelatin zymography. *B*, SCC25 cells were plated in medium containing 0.09 mM calcium on thin layer or three-dimensional (*3-D*) collagen as described under "Experimental Procedures." Following serum starvation, media were replaced with serum-free medium at the indicated calcium concentration. The conditioned media were collected at 24 h and analyzed for MMP activity by gelatin zymography. The results are representative of at least four independent experiments.

RESULTS

Extracellular Calcium Regulates Pro-MMP-2 Activation—MMP activity is subject to complex post-translational regulation by a number of processes including zymogen activation, enzyme-inhibitor binding, endocytosis, and shedding (4–7, 40, 41); however, the biologic factors that control and coordinate these processes are poorly understood. As keratinocytes are subjected to fluctuations in extracellular calcium in the epidermal milieu, the effect of calcium on MMP activation was evaluated in SCC25 cells. The predominant soluble MMP expressed by SCC25 cells is MMP-2, with low level expression of MMP-9. SCC25 cells were plated in low calcium media (0.09 mM), serum-starved, and incubated with fresh serum-free media containing increasing calcium. Conditioned media were collected at 24 h and analyzed for MMP activity by gelatin zymography. Whereas cells cultured in 0.09 mM calcium concentration expressed pro-MMP-2 (Fig. 1*A*, *1st lane*), increasing calcium concentration resulted in a dose-dependent MMP-2 activation (Fig. 1*A*, *2nd* to *4th lanes*). There was no change in MMP-9 expression with increasing calcium concentration in these cells (data not shown). Because collagen has been shown to affect MMP-2 expression and/or processing (42–48), the effect of calcium on collagen-induced MMP-2 activation was examined. Similar to the results obtained with SCC25 cells on plastic (Fig. 1*A*), cells plated on thin layer collagen demonstrated MMP-2 activation with increasing calcium concentration (Fig. 1*B*, *1st* to *3rd lanes*). Although cells cultured on three-dimensional collagen gels had a more pronounced base-line MMP-2 activation (Fig. 1*B*, *4th lane*), a calcium-dependent increase in MMP-2 activation was observed (Fig. 1*B*, *5th* and *6th lanes*). These data indicate that extracellular calcium-mediated regulation of MMP-2 activation in SCC25 cells may act in synergy with collagen-induced pro-MMP-2 processing.

To investigate the proteolytic process leading to MMP-2 activation, SCC25 cells were treated with a broad spectrum MMP inhibitor, GM6001, or vehicle (Me_2SO) control. GM6001 inhibited calcium-induced pro-MMP-2 activation, demonstrating the involvement of an MMP in the activation process (Fig. 2*A*, *lanes 3* and *4*). To investigate MMP dependence further, SCC25 cells were treated with TIMP-1 and TIMP-2. TIMP-2 blocks both MMP-2 and MT1-MMP activities, whereas MT1-MMP activity is not inhibited by TIMP-1 (49, 50). TIMP-1 had no effect on calcium-induced MMP-2 activation (Fig. 2*A*, *lanes 5* and *6*), whereas TIMP-2 completely abrogated the response (Fig. 2*A*, *lanes 7* and *8*), implicating MT1-MMP-in the calcium-induced pro-MMP-2 activation reaction.

To investigate further the involvement of MT1-MMP in calcium-dependent pro-MMP-2 activation, SCC25 cells were treated with a furin inhibitor decanoyl-Arg-Val-Lys-Arg-chloromethyl ketone (RVKR), which has been shown to block activation of pro-MT1-MMP (51). Treatment of SCC25 cells with RVKR inhibited calcium-mediated MMP-2 activation, further implicating MT1-MMP in the calcium-induced pro-MMP-2 activation (compare Fig. 2*B*, *lanes 1* and *3*, with Fig. 2*B*, *lanes 5* and *7*). To determine whether calcium can act in synergy with PMA, another agent that has been shown to induce MMP-2 activation via MT1-MMP (11, 52), cells were cultured in low *versus* high calcium concentration in the presence of PMA and various proteinase inhibitors. As reported previously (52, 53), PMA induced pro-MMP-9 expression, irrespective of calcium concentration (Fig. 2*C*, compare *lanes 1* and *2* with *lanes 5* and *6*). In contrast, expression of pro-MMP-2 was not affected; however, activation was stimulated (Fig. 2*C*, *lanes 1* and *2* and *lanes 5* and *6*). Addition of calcium further increased PMA-induced pro-MMP-2 activation (compare Fig. 2*C*, *lanes 2* and *6*), indicative of synergistic stimulation of MMP processing. In control experiments, activation was blocked by both RVKR and GM6001 (Fig. 2*C*, *lanes 3* and *7* and *4* and *8*, respectively).

Overexpression of MT1-MMP in SCC25 Cells—To investigate further the involvement of MT1-MMP in calcium-dependent pro-MMP-2 activation, SCC25 cells overexpressing MT1-MMP (designated SCC25-MT) were generated (Fig. 3*A*). Overexpression of MT1-MMP in SCC25-MT cells was verified by Western blotting of whole cell lysates, indicating the presence of the 55-kDa active species and the 43-kDa catalytically inactive autolysis product (Fig. 3*A*). As reported previously (54, 55), GM6001 prevents autolysis of MT1-MMP and thus increases the accumulation of the 55-kDa species (Fig. 3*A*, *2nd lane*). Correlating with the enhanced MT1-MMP expression in SCC25-MT cells (Fig. 3*A*, *4th lane*), a significantly increased MMP-2 activation is observed (Fig. 3*A*, *lower panel, 4th lane*). Similar to wild-type SCC25 cells, calcium increased pro-MMP-2 activation by SCC25-MT cells in a dose-dependent manner (Fig.

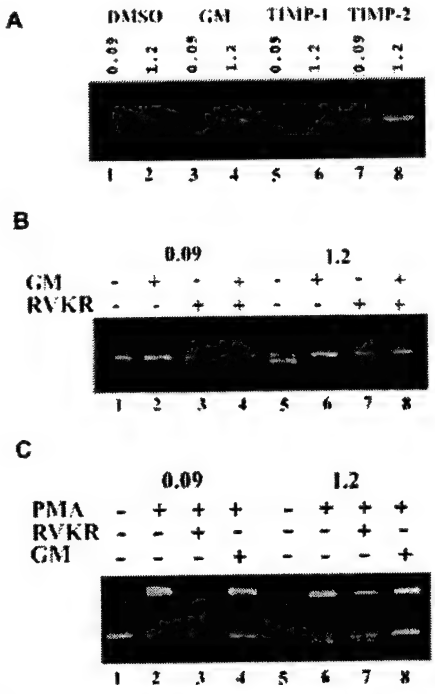

FIG. 2. **Calcium-induced pro-MMP-2 activation involves MT1-MMP.** *A*, SCC25 cells were plated on plastic in medium containing 0.09 mM calcium, subjected to overnight serum starvation, and transferred to fresh medium at the indicated calcium concentration. At the time of calcium switch, the cells were treated with Me_2SO (*DMSO*, vehicle control), MMP inhibitor GM6001 (*GM*, 10 μM), TIMP-1 (20 ng/ml), or TIMP-2 (20 ng/ml). The conditioned media were collected at 24 h and analyzed for MMP activity by gelatin zymography. *B* and *C*, SCC25 cells were plated on plastic in medium containing 0.09 mM calcium, subjected to overnight serum starvation, and transferred to fresh medium at the indicated calcium concentration. At the time of calcium switch, the cells were treated with PMA (20 nM), MMP inhibitor GM6001 (10 μM), and/or furin inhibitor decanoyl-Arg-Val-Lys-Arg-chloromethyl ketone (RVKR, 20 μM). The conditioned media were collected at 24 h and analyzed for MMP activity by gelatin zymography. The results are representative of three independent experiments.

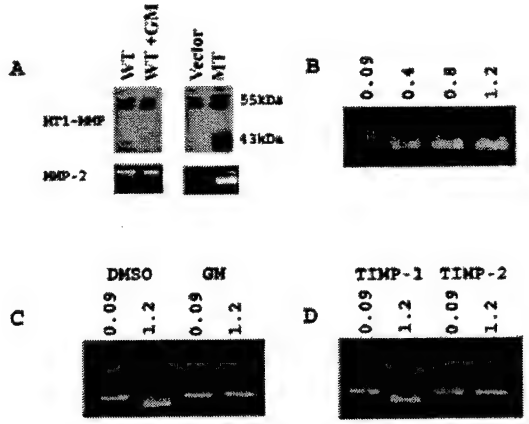

FIG. 3. **Overexpression of MT1-MMP in SCC25 cells.** *A*, SCC25 cells overexpressing MT1-MMP (SCC25-MT) were generated as described under "Experimental Procedures." At 24 h the cell lysates from wild-type (*WT*) SCC25 and SCC25-MT cells were analyzed for MT1-MMP expression by Western blotting and the conditioned media for MMP-2 activity by gelatin zymography. The membranes were immunoblotted with anti-MT1-MMP antibody followed by peroxidase-conjugated secondary antibody and enhanced chemiluminescence detection. *B*, SCC25-MT cells were plated on plastic in medium containing 0.09 mM calcium. Following overnight serum starvation, cells were transferred to medium containing the indicated calcium concentration (0.09–1.2 mM). Conditioned media were collected at 24 h and analyzed for MMP activity by gelatin zymography. *C* and *D*, SCC25-MT cells were plated on plastic in medium containing 0.09 mM calcium, and following overnight serum starvation, the media were changed to either 0.09 or 1.2 mM calcium concentration. At the time of calcium switch, the cells were treated with Me_2SO (*DMSO*, vehicle control), MMP inhibitor GM6001 (*GM*, 10 μM), TIMP-1 (20 ng/ml) or TIMP-2 (20 ng/ml). The conditioned media were collected at 24 h and analyzed for MMP activity by gelatin zymography. The results are representative of two independent experiments.

3*B*). Activation was inhibited by the broad spectrum MMP inhibitor GM6001 (Fig. 3*C*) and by TIMP-2 (Fig. 3*D*).

Effect of Extracellular Calcium on MT1-MMP—To determine whether the calcium-induced increases in pro-MMP-2 activation are the result of enhanced MT1-MMP expression, the MT1-MMP mRNA levels from SCC25 and SCC25-MT cells were analyzed by RT-PCR. Changes in the message levels for GAPDH were used as internal control. SCC25-MT cells expressed higher levels of MT1-MMP message compared with SCC25 cells; however, calcium did not alter the steady state levels of MT1-MMP mRNA (Fig. 4*A*).

As the RT-PCR data indicated that MT1-MMP expression levels were unaffected by calcium, post-translational mechanisms of MT1-MMP regulation were investigated. To evaluate the effect of calcium on MT1-MMP processing, SCC25-MT cells were plated in low calcium, serum-starved, and incubated in fresh medium containing low (0.09 mM) or high (1.2 mM) calcium concentration in the presence or absence of GM6001 to prevent autocatalytic processing of MT1-MMP to the 43-kDa species. After 24 h, the cell lysates were probed for MT1-MMP by Western blotting. In agreement with the RT-PCR data, no significant change in overall MT1-MMP protein expression was observed (Fig. 4*B*, *upper panel*). However, increased processing of MT1-MMP to the 43-kDa autolysis product was observed in high calcium, indicative of enhanced MT1-MMP activity, as further supported by zymogram data showing increased pro-MMP-2 activation (Fig. 4*B*, *lower panel, 3rd lane*).

To determine whether MT1-MMP activity is enhanced via increased cell surface association, surface biotinylation was used to probe calcium-induced changes in the cell surface MT1-MMP species. Serum-starved SCC25-MT cells were maintained in low or high calcium for 24 h as indicated and then incubated with cell-impermeable NHS-biotin to label cell surface proteins and lysed in modified RIPA buffer. Following precipitation of surface-labeled proteins with streptavidin beads, samples were electrophoresed and probed for MT1-MMP by immunoblotting. Similar to the results obtained with whole cell lysates, calcium had no effect on the surface expression of MT1-MMP (Fig. 4*C*). Enhanced surface levels of 43-kDa autolysis product were also observed, providing additional evidence for increased cell surface MT1-MMP activity.

Rapid Kinetics of Calcium-induced Pro-MMP-2 Activation—To evaluate the kinetics of pro-MMP-2 activation, serum-starved SCC25 and SCC25-MT cells were first incubated in low calcium medium (0.09 mM) to accumulate pro-MMP-2 and TIMP-2 in the conditioned media. After 24 h, activation was initiated by the addition of calcium from a concentrated stock solution to a final concentration of 1.2 mM. At various time points, conditioned media and cell lysates were collected, and the relative kinetics of pro-MMP-2 activation were analyzed by gelatin zymography. Rapid MMP-2 activation was detected at the cell surface within 30 min following calcium restoration in both wild-type and MT1-MMP-overexpressing SCC25 cells (Fig. 5, *A* and *B*). Surface activation was followed by a more gradual release of MMP-2 as evidenced by accumulation of activated MMP-2 in the conditioned media (Fig. 5, *C* and *D*). The rapid calcium-induced activation of pro-MMP-2 was blocked by GM6001 (data not shown).

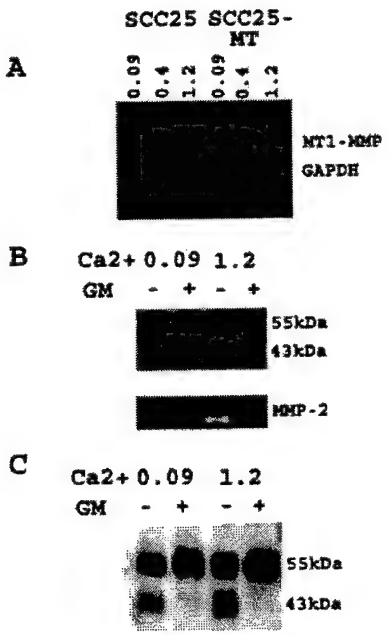

FIG. 4. **Effect of extracellular calcium on MT1-MMP.** *A*, SCC25 (*1st to 3rd lanes*) and SCC25-MT (*4th to 6th lanes*) cells were cultured for 24 h in medium at the indicated calcium concentration. Total RNA was isolated using Trizol reagent and quantified, and RT-PCR for MT1-MMP message was performed using primers as detailed under "Experimental Procedures." As loading control, amplification primers for GAPDH were used. PCR products were visualized by UV transillumination of 1.5% agarose gels stained with ethidium bromide. *B*, SCC25-MT cells were cultured in calcium-containing medium as indicated in the presence or absence of GM6001 (*GM*, 10 μM). Cells were lysed at 24 h in modified RIPA buffer containing proteinase inhibitors. Equal amounts of cell lysates were separated by SDS-PAGE, and the membranes were immunoblotted with anti-MT1-MMP antibody followed by peroxidase-conjugated secondary antibody and enhanced chemiluminescence detection (*upper panel*). The conditioned media were analyzed for MMP-2 activation using gelatin zymography (*lower panel*). *C*, SCC25-MT cells were cultured in calcium-containing medium as indicated in the presence or absence of GM6001 (10 μM). After 24 h the cells were surface-biotinylated and lysed. Samples were immunoprecipitated with streptavidin beads at 4 °C for 14 h to isolate cell surface (biotinylated) proteins and electrophoresed on a 9% SDS-polyacrylamide gel. The membranes were immunoblotted with anti-MT1-MMP antibody followed by peroxidase-conjugated secondary antibody and enhanced chemiluminescence detection. The results are representative of at least two independent experiments.

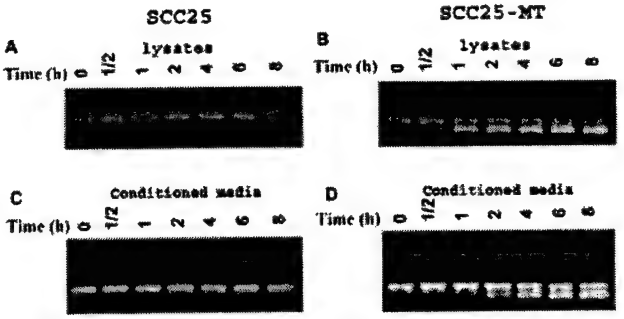

FIG. 5. **Calcium induces rapid surface activation of pro-MMP-2.** SCC25 and SCC25-MT cells were serum-starved overnight and incubated for an additional 24 h in medium containing 0.09 mM calcium. Calcium from a concentrated solution was added to the conditioned media to a final concentration of 1.2 mM, and at the indicated times (in hours) the cell lysates and conditioned media (*CM*) from SCC25 (*A* and *C*) and SCC25-MT (*B* and *D*) cells were analyzed for MMP-2 activation by gelatin zymography. The results are representative of four independent experiments.

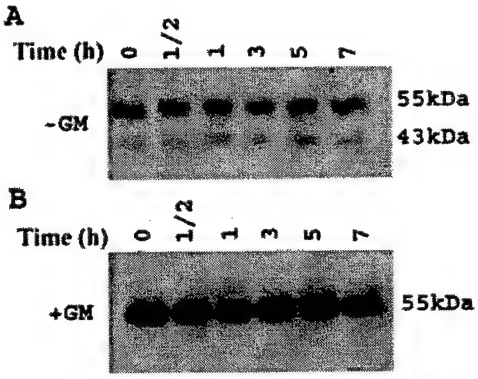

FIG. 6. **Calcium does not affect cell surface MT1-MMP levels.** SCC25-MT cells were serum-starved overnight and then incubated for an additional 24 h with Me_2SO or GM6001 (*GM*, 10 μM) in medium containing 0.09 mM calcium. Calcium from a concentrated solution was added to the conditioned media to a final concentration of 1.2 mM, and at the indicated times the samples were surface-labeled with biotin, immunoprecipitated with streptavidin, and electrophoresed on a 9% SDS-polyacrylamide gel as described under "Experimental Procedures." The membranes were immunoblotted with anti-MT1-MMP antibody, followed by peroxidase-conjugated secondary antibody and enhanced chemiluminescence detection. The results are representative of three independent experiments.

Because MMP-2 activation occurs rapidly following calcium addition, two distinct approaches were utilized to address the potential for rapid calcium-induced changes in the surface localization of MT1-MMP. In initial experiments, cells were cultured in low calcium medium (0.09 mM), switched to high calcium (1.2 mM), and at the indicated times cell surface proteins were labeled with NHS-biotin followed by lysis in modified RIPA buffer. The surface-labeled proteins were immunoprecipitated with streptavidin beads and probed for MT1-MMP by immunoblotting. No significant changes in the surface levels of the 55-kDa MT1-MMP species were induced by calcium supplementation (Fig. 6*A*), although GM6001 stabilized cell surface MT1-MMP against autolysis (Fig. 6*B*).

Recent data demonstrate that MT1-MMP can be regulated post-translationally via internalization from the cell surface (56, 57). To determine whether calcium induces dynamic turnover of MT1-MMP and thereby regulates MMP-2 activation, we evaluated MT1-MMP endocytosis in SCC25-MT cells. SCC25-MT cells were surface-biotinylated with cleavable cell-impermeable NHS-SS-biotin at 4 °C to block endocytosis and then transferred to 37 °C in 0.09 or 1.2 mM calcium-containing medium to allow for internalization (Fig. 7*A*, [*1*]). Control cells were maintained at 4 °C to prevent internalization (Fig. 7*A*, [*2*]). After a 40-min incubation at 37 °C, the cells were returned to 4 °C to stabilize surface protein profiles and block further internalization (Fig. 7*A*, [*3*]). Biotin on the remaining cell surface proteins was then removed using the reducing agent MESNA (Fig. 7*A*, [*4*]). In control experiments, MESNA was omitted to enable evaluation of total labeled proteins (*i.e.* surface and internalized) (Fig. 7*A*, [*5*]). Cells were washed with ice-cold PBS and lysed, and labeled proteins were precipitated with streptavidin beads (Fig. 7*A*, [*6–8*]), electrophoresed, and probed for MT1-MMP by immunoblotting. In cells not subject to the temperature shift prior to reduction (Fig. 7*A*, (*a*)), no MT1-MMP was detected, demonstrating the efficacy of MESNA in removing the biotin from surface-labeled MT1-MMP (Fig. 7*B*, *lanes 1* and *4*). In contrast, cells incubated at 37 °C contained a protected, MESNA-resistant pool of MT1-MMP (Fig. 7*A*, (*b*)), demonstrating internalization of MT1-MMP in SCC25-MT cells (Fig. 7*B*, *lanes 2* and *5*). Treatment of cells with GM6001 for 40 min did not affect internalization of the

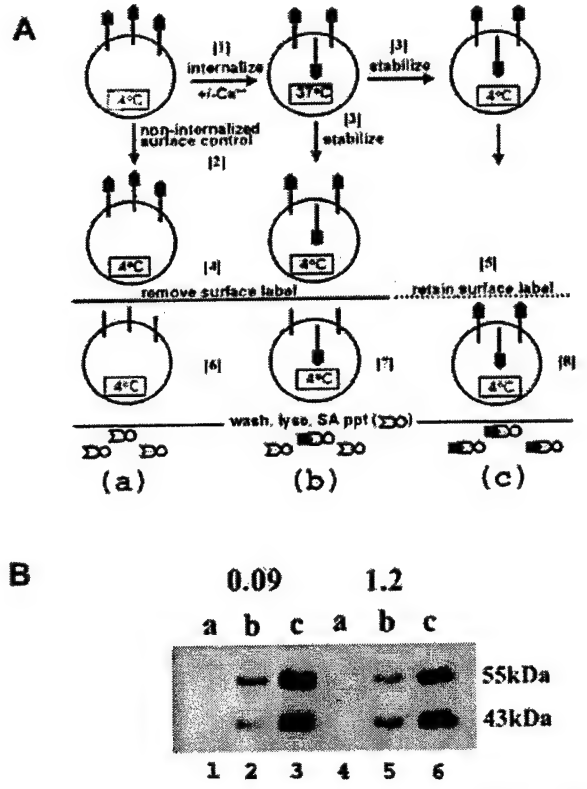

FIG. 7. **Calcium does not affect MT1-MMP endocytosis.** *A*, schematic of endocytosis protocol. *[1]*, SCC25-MT cells were surface-biotinylated on ice to block endocytosis with cleavable sulfo-NHS-SS-biotin and transferred to 37 °C in medium containing 0.09 or 1.2 mM calcium. *[2]*, control cells were maintained at 4 °C. *[3]*, after a 40-min incubation, cells were returned to 4 °C to block further internalization. *[4]*, surface biotin was removed with 100 mM MESNA. *[5]*, in control experiments, MESNA was omitted to assess total labeled protein (surface and internalized). *[6–8]*, cells were washed with ice-cold PBS, lysed, and labeled proteins precipitated at 4 °C for 14 h with streptavidin beads to isolate labeled proteins. *B*, samples prepared as described above were boiled, electrophoresed on a 9% SDS-polyacrylamide gel, and immunoblotted with anti-MT1-MMP antibody, followed by peroxidase-conjugated secondary antibody and enhanced chemiluminescence detection. The results are representative of three independent experiments.

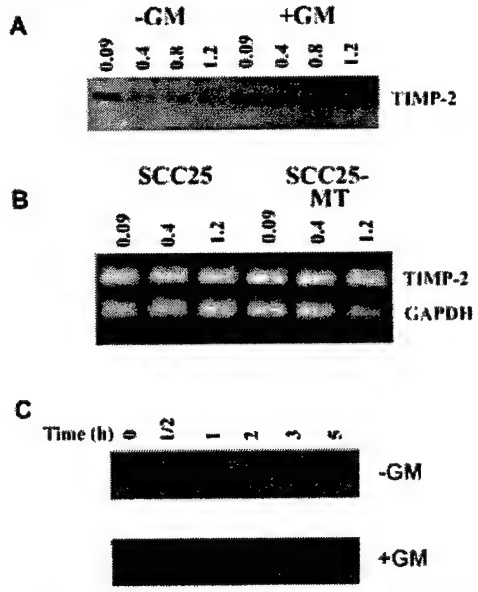

FIG. 8. **Calcium decreases soluble TIMP-2.** *A*, SCC25-MT cells were cultured for 24 h in medium at the indicated calcium concentration in the presence or absence of GM6001 (*GM*, 10 μM). The conditioned media were collected at 24 h, concentrated 15–20-fold using Micron 10 microconcentrators, electrophoresed on a 15% SDS-polyacrylamide gel, and immunoblotted with anti-TIMP-2 antibody followed by peroxidase-conjugated secondary antibody and enhanced chemiluminescence detection. *B*, SCC25 (*1st* to *3rd lanes*) and SCC25-MT (*4th* to *6th lanes*) cells were cultured for 24 h in medium at the indicated calcium concentrations. Total RNA was isolated using Trizol reagent and quantified, and RT-PCR for TIMP-2 message was performed using primers described under "Experimental Procedures." As loading control, amplification primers for GAPDH were used. The samples were electrophoresed on a 1.5% agarose gel, stained with ethidium bromide, and visualized by UV transillumination. *C*, SCC25-MT cells were serum-starved overnight and incubated for an additional 24 h in medium containing 0.09 mM calcium in the presence or absence of GM6001 (10 μM). Calcium from a concentrated solution was added to the conditioned media to a final concentration of 1.2 mM, and at the indicated times the conditioned medium was harvested, concentrated 15–20-fold, electrophoresed on a 15% SDS-polyacrylamide gel, and immunoblotted with anti-TIMP-2 antibody followed by peroxidase-conjugated secondary antibody and enhanced chemiluminescence detection. The results are representative of at least three independent experiments.

55-kDa MT1-MMP species (data not shown). To evaluate the effect of calcium on MT1-MMP endocytosis, calcium levels in the medium were modulated at the time of temperature shift. MT1-MMP was effectively internalized in both low (0.09) and high (1.2 mM) calcium conditions (Fig. 7*B*, *lanes 2* and *5*). Analysis of total cellular MT1-MMP (Fig. 7*A*, (*c*); surface and internalized) confirmed previous results and indicated no change in the overall expression levels (Fig. 7*B*, *lanes 3* and *6*). Together, these data demonstrate that MT1-MMP is regulated by endocytosis under both low and high calcium conditions. However, the rapid calcium-induced changes in pro-MMP-2 activation kinetics are not mirrored by corresponding changes in surface MT1-MMP expression or endocytosis.

Calcium Regulates TIMP-2 Levels—TIMP-2 plays an important role in pro-MMP-2 activation (10, 15–20); at low concentrations it facilitates activation by bridging trimolecular-activation complex formation, whereas at higher concentrations the activation is inhibited via interaction of TIMP-2 with the catalytically competent MT1-MMP active site. Because the calcium-induced pro-MMP-2 activation could not be attributed to changes in either MT1-MMP expression or to surface localization, the remaining component of the trimolecular complex, TIMP-2, was evaluated. Following serum starvation in low calcium, SCC25-MT cells were maintained in medium containing the indicated calcium concentration in the presence or absence of GM6001. Conditioned media were collected at 24 h, concentrated 15–20-fold, and TIMP-2 analyzed by Western blotting. A dose-dependent decrease in soluble TIMP-2 was observed (Fig. 8*A*, *1st* to *4th lanes*). To determine whether the calcium-induced decrease in soluble TIMP-2 results from decreased expression, the TIMP-2 message levels from SCC25 and SCC25-MT cells were analyzed by RT-PCR. No calcium-induced changes in TIMP-2 message levels were observed either in SCC25 or SCC25-MT cells (Fig. 8*B*). However, analysis of soluble TIMP-2 protein levels in cells cultured with GM6001 indicated that GM6001 blocked the calcium-mediated decline in soluble TIMP-2 (Fig. 8*A*, *5th* to *8th lanes*). Together, these data suggest that blocking the MT1-MMP active site with GM6001 may prevent the loss of soluble TIMP-2 by affecting recruitment of TIMP-2 to the cell surface-activation complex, providing evidence that calcium regulates TIMP-2 at the post-translational level.

To determine whether the rapid calcium-mediated induction of pro-MMP-2 activation reflects changes in surface-associated TIMP-2 levels, the effect of calcium on the kinetics of TIMP-2 loss from the conditioned media was examined. SCC25-MT cells were incubated in low calcium (0.09 mM) medium to accu-

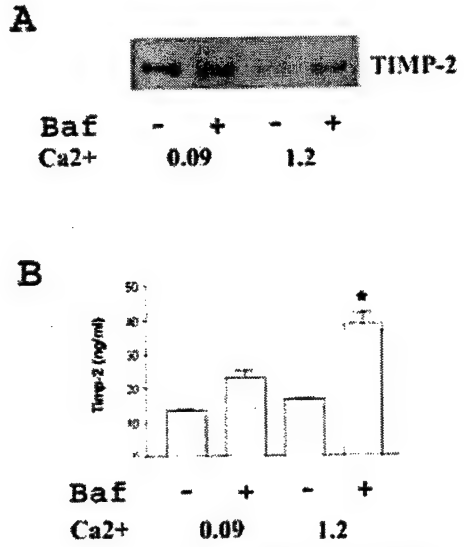

FIG. 9. **Calcium promotes degradation of TIMP-2.** SCC25-MT cells were serum-starved overnight and incubated for an additional 24 h at the indicated calcium concentration in the presence or absence of bafilomycin A1 (75 nM). *A*, conditioned media were concentrated 15–20-fold using Micron 10 microconcentrators and electrophoresed on a 15% SDS-polyacrylamide gel. The membranes were immunoblotted with anti-TIMP-2 antibody followed by peroxidase-conjugated secondary antibody and enhanced chemiluminescence detection. *B*, TIMP-2 levels in the cell lysates were quantified using ELISA according to the manufacturer's specifications. The results are representative of at least two independent experiments. *, significantly different from control (Ca^{2+} 0.09, *Baf*−) with $p < 0.05$.

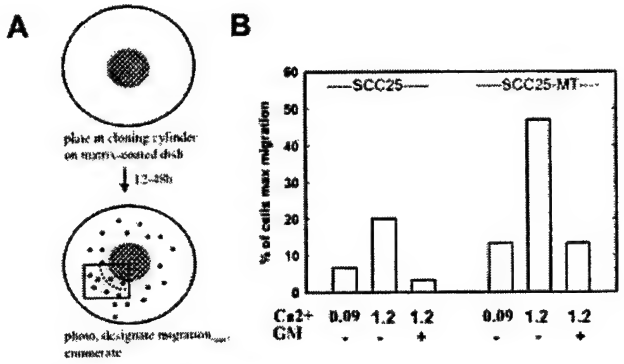

FIG. 10. **Calcium promotes cell migration.** *A*, schematic of migration protocol. Cells were plated in medium containing 0.09 mM calcium on laminin-5-enriched matrix inside a glass ring. After removal of the ring, the cells were serum-starved for 3 h, and then fresh serum-free medium containing either 0.09 or 1.2 mM calcium supplemented with 20 ng/ml EGF was added. Cells were allowed to migrate for 12–48 h. To quantify the relative motility, the migratory front was photographed every 12 h for 48 h, and the percentage of cells crossing a line designated "migratory max" was enumerated. *B*, SCC25 and SCC25-MT cells were allowed to migrate as described above in the presence or absence of GM6001 (*GM*, 10 μM). In a representative experiment, the relative motility at 24 h was quantified by determining the percentage of the SCC25 and SCC25-MT cells crossing the migratory max line. The results are representative of three independent experiments.

mulate pro-MMP-2 and TIMP-2 in the conditioned media. After 24 h, calcium from a concentrated stock solution was added to a final concentration of 1.2 mM. At the indicated times, the conditioned media were collected, concentrated, and TIMP-2 analyzed by Western blotting. TIMP-2 levels in the conditioned media changed with time, with the decrease apparent at 2 h following calcium restoration (Fig. 8*C, upper panel*). The presence of GM6001 blocked the decline (Fig. 8*C, lower panel*), further supporting the hypothesis that calcium promotes MT1-MMP dependent recruitment of TIMP-2 to the cell surface trimolecular activation complex.

To differentiate whether the calcium-induced decrease in soluble TIMP-2 levels reflected enhanced surface accumulation *versus* increased degradation of TIMP-2, the vacuolar ATPase inhibitor bafilomycin A1 was utilized. The rationale for this experiment was based on previous studies (58) showing that PMA-induced stimulation of pro-MMP-2 activation and corresponding loss of soluble TIMP-2 resulted from MT1-MMP-mediated TIMP-2 internalization and subsequent intracellular degradation in endosomal and/or lysosomal compartments. Increasing the pH of these compartments with bafilomycin A1 blocked TIMP-2 degradation, leading to a build-up of cellular TIMP-2 levels (58). Thus, SCC25-MT cells were cultured in 0.09 or 1.2 mM calcium for 24 h in the presence or absence of bafilomycin A1 (75 nM), and conditioned media were collected, concentrated 15–20-fold, and evaluated for TIMP-2 by Western blotting. In addition, the cell lysates at 24 h were collected and analyzed for TIMP-2 by ELISA. As shown above (Fig. 8*A*), calcium decreased the TIMP-2 levels in the conditioned media (Fig. 9*A, 1st* and *3rd lanes*) but did not affect the levels of TIMP-2 in the cell lysates (Fig. 9*B*). Together, these data indicate that the calcium-mediated decline in soluble TIMP-2 is not due to cell surface accumulation of the inhibitor and suggest that TIMP-2 degradation is increased in high calcium. This is supported by experiments using bafilomycin A1, which partially blocked the calcium-mediated decline in soluble TIMP-2 (Fig. 9*A, 4th lane*). Because bafilomycin A1 blocks TIMP-2 degradation (58), these data support the hypothesis that the decline in soluble TIMP-2 observed under high calcium conditions reflects increased degradation of TIMP-2.

Calcium Promotes SCC25 Cell Migration—To evaluate the functional consequences of calcium-induced MMP-2 activation, the effect of calcium on SCC25 and SCC25-MT cell migration on laminin-5-rich matrix was examined. Migration was quantified using an *in vitro* cell dispersion assay (39), in which cells are plated at high density in a glass ring and allowed to migrate after removal of the ring (Fig. 10*A*). After the cells have attached and spread, the ring is removed, serum-starved for 3 h, and the media switched to either low (0.09 mM) or high (1.2 mM) calcium supplemented with 20 ng/ml EGF, and migration is quantified at 12–48 h. In a representative experiment quantified at 24 h, SCC25 cells migrated on laminin 5-rich matrix, with SCC25-MT cells displaying increased migration relative to wild-type cells (Fig. 10*B*). Calcium enhanced the motility of both wild-type and MT1-MMP-overexpressing SCC25 cells. Calcium-induced migration was blocked by GM6001, indicating that the enhanced migration observed can be attributed to increased MMP activity.

DISCUSSION

Studies using multiple cancer models have shown that MMP-2 activation is important in cellular behavior (59–62). The activation of MMP-2 *in vitro* is associated with increased migration and invasiveness of cancer cells (63–65). Furthermore, there is increased MMP-2 activation with lymph node metastasis in a number of different cancers, including OSCC (3, 8, 66). Hence, the regulation of MMP-2 activation has been studied extensively. Previously, it was shown that MMP-2 activation could be promoted with non-physiological agents like PMA (11, 52) and concanavalin A (67, 68) and also by proteins of the extracellular matrix such as collagen and fibronectin (42–48, 69, 70). In this study, we show that calcium also regulates pro-MMP-2 activation without altering expression of the zymogen. Increasing extracellular calcium resulted in a dose-dependent activation of pro-MMP-2, accompanied by enhanced

generation of 43-kDa catalytically inactive MT1-MMP species and a decline in the levels of soluble TIMP-2. Calcium did not affect the steady state levels of TIMP-2 in the cell lysates, suggesting that calcium induces TIMP-2 degradation. As a functional consequence, calcium promoted cellular migration, suggesting that calcium may control keratinocyte migration via regulation of MMP-2 activation.

Calcium-mediated MMP-2 activation was MT1-MMP-dependent; however, calcium did not affect MT1-MMP message or cell surface protein levels, consistent with the observation that calcium-mediated activation of MMP-2 occurs rapidly at the cell surface. Increased generation of the catalytically inactive 43-kDa MT1-MMP species autolysis product was also observed. These data are in agreement with the recent reports (58, 69, 70) showing that MMP-2 activation induced by fibronectin and PMA increased accumulation of the 43-kDa MT1-MMP species without affecting the levels of the 55-kDa MT1-MMP species. Despite the rapid activation of MMP-2 at the cell surface, calcium did not affect MT1-MMP endocytosis.

Calcium-induced MMP-2 activation was associated with an MT1-MMP-dependent decline in soluble TIMP-2. A similar phenomenon has been reported recently (58, 69, 71) in other model systems. For example, PMA and type IV collagen-induced MMP-2 activation in HT1080 cells is coupled with TIMP-2 degradation (58, 69). In SCC25 cells, the calcium-induced decline in TIMP-2 also likely results from degradation as treatment with bafilomycin A1, a highly specific inhibitor of vacuolar ATPase that was previously shown to block MT1-MMP-mediated degradation of TIMP-2 (58), restored soluble TIMP-2 levels. This is in contrast to the loss of soluble TIMP-2 that accompanies concanavalin A-induced pro-MMP-2 activation, which results from enhanced cell surface binding rather than degradation (58, 69, 72). The mechanism by which changes in extracellular calcium promote TIMP-2 internalization and degradation is currently under investigation. Nevertheless, it is interesting to note that an inverse relationship between MMP-2 activation and soluble TIMP-2 has been observed in many human cancer cell lines (22, 51, 72).

The calcium-induced changes in post-translational MMP regulation correlated with increased migration over laminin-5-enriched matrix. Several reports (63, 64, 74, 75) have demonstrated involvement of active MMP-2 in cellular migration, including laminin-5-driven motility (73, 76). MT1-MMP has also been implicated in epithelial cell migration over laminin-5 matrix (39, 73). Our data demonstrate that migration on laminin-5 is enhanced both in MT1-MMP-overexpressing cells and under conditions that promote MMP-2 activation. Because calcium is a key regulator of keratinocyte function, these data suggest that localized changes in calcium in the extracellular milieu may function as a fine regulatory mechanism for post-translational control of MMP activity and MMP-influenced cellular behaviors such as migration and invasion.

REFERENCES

1. Liotta, L. A., Tryggvason, K., Garbisa, S., Hart, I., Foltz, C. M., and Shafie, S. (1980) *Nature* **284,** 67–68
2. Forastiere, A., Koch, W., Trotti, A., and Sidransky, D. (2001) *N. Engl. J. Med.* **345,** 1890–1900
3. Kurahara, S., Shinohara, M., Ikebe, T., Nakamura, S., Beppu, M., Hiraki, A., Takeuchi, H., and Shirasuna, K. (1999) *Head Neck* **21,** 627–638
4. Werb, Z. (1997) *Cell* **91,** 439–442
5. Nagase, H., and Woessner, J. F., Jr. (1999) *J. Biol. Chem.* **274,** 21491–21494
6. Sternlicht, M. D., and Werb, Z. (2001) *Annu. Rev. Cell Dev. Biol.* **17,** 463–516
7. Egeblad, M., and Werb, Z. (2002) *Nat. Rev. Cancer* **2,** 161–174
8. Shimada, T., Nakamura, H., Yamashita, K., Kawata, R., Murakami, Y., Fujimoto, N., Sato, H., Seiki, M., and Okada, Y. (2000) *Clin. Exp. Metastasis* **18,** 179–188
9. Sato, H., Takino, T., Okada, Y., Cao, J., Shinagawa, A., Yamamoto, E., and Seiki, M. (1994) *Nature* **370,** 61–65
10. Butler, G. S., Butler, M. J., Atkinson, S. J., Will, H., Tamura, T., van Westrum, S. S., Crabbe, T., Clements, J., d'Ortho, M. P., and Murphy, G. (1998) *J. Biol. Chem.* **273,** 871–880
11. Lehti, K., Lohi, J., Valtanen, H., and Keski-Oja, J. (1998) *Biochem. J.* **334,** 345–353
12. Sato, H., Kinoshita, T., Takino, T., Nakayama, K., and Seiki, M. (1996) *FEBS Lett.* **393,** 101–104
13. Maquoi, E., Noel, A., Frankenne, F., Angliker, H., Murphy, G., and Foidart, J. M. (1998) *FEBS Lett.* **424,** 262–266
14. Yana, I., and Weiss, S. J. (2000) *Mol. Biol. Cell* **11,** 2387–2401
15. Strongin, A. Y., Collier, I., Bannikov, G., Marmer, B. L., Grant, G. A., and Goldberg, G. I. (1995) *J. Biol. Chem.* **270,** 5331–5338
16. Itoh, Y., Ito, A., Iwata, K., Tanzawa, K., Mori, Y., and Nagase, H. (1998) *J. Biol. Chem.* **273,** 24360–24367
17. Zucker, S., Drews, M., Conner, C., Foda, H. D., DeClerck, Y. A., Langley, K. E., Bahou, W. F., Docherty, A. J., and Cao, J. (1998) *J. Biol. Chem.* **273,** 1216–1222
18. Jo, Y., Yeon, J., Kim, H. J., and Lee, S. T. (2000) *Biochem. J.* **345,** 511–519
19. Overall, C. M., King, A. E., Sam, D. K., Ong, A. D., Lau, T. T., Wallon, U. M., DeClerck, Y. A., and Atherstone, J. (1999) *J. Biol. Chem.* **274,** 4421–4429
20. Toth, M., Bernardo, M. M., Gervasi, D. C., Soloway, P. D., Wang, Z., Bigg, H. F., Overall, C. M., DeClerck, Y. A., Tschesche, H., Cher, M. L., Brown, S., Mobashery, S., and Fridman, R. (2000) *J. Biol. Chem.* **275,** 41415–41423
21. Madlener, M., Parks, W. C., and Werner, S. (1998) *Exp. Cell Res.* **242,** 201–210
22. Baumann, P., Zigrino, P., Mauch, C., Breitkreutz, D., and Nischt, R. (2000) *Br. J. Cancer* **83,** 1387–1393
23. Nagavarapu, U., Relloma, K., and Herron, G. S. (2002) *J. Invest. Dermatol.* **118,** 573–581
24. Hennings, H., Michael, D., Cheng, C., Steinert, P., Holbrook, K., and Yuspa, S. H. (1980) *Cell* **19,** 245–254
25. Hennings, H., and Holbrook, K. A. (1983) *Exp. Cell Res.* **143,** 127–142
26. Yuspa, S. H., Kilkenny, A. E., Steinert, P. M., and Roop, D. R. (1989) *J. Cell Biol.* **109,** 1207–1217
27. Bikle, D. D., Ng, D., Tu, C. L., Oda, Y., and Xie, Z. (2001) *Mol. Cell. Endocrinol.* **177,** 161–171
28. Menon, G. K., Grayson, S., and Elias, P. M. (1985) *J. Invest. Dermatol.* **84,** 508–512
29. Menon, G. K., Price, L. F., Bommannan, B., Elias, P. M., and Feingold, K. R. (1994) *J. Invest. Dermatol.* **102,** 789–795
30. Mauro, T., Bench, G., Sidderas-Haddad, E., Feingold, K., Elias, P., and Cullander, C. (1998) *J. Invest. Dermatol.* **111,** 1198–1201
31. Kobayashi, T., Hattori, S., Nagai, Y., Tajima, S., and Nishikawa, T. (1998) *Dermatology* **197,** 1–5
32. Kobayashi, T., Hattori, S., Nagai, Y., and Tajima, S. (2000) *IUBMB Life* **50,** 221–226
33. Kobayashi, T., Kishimoto, J., Ge, Y., Jin, W., Hudson, D. L., Ouahes, N., Ehama, R., Shinkai, H., and Burgeson, R. E. (2001) *EMBO Rep.* **2,** 604–608
34. Munshi, H. G., and Stack, M. S. (2002) *Methods Cell Biol.* **69,** 195–205
35. Laemmli, U. K. (1970) *Nature* **227,** 680–685
36. Wong, H., Muzik, H., Groft, L. L., Lafleur, M. A., Matouk, C., Forsyth, P. A., Schultz, G. A., Wall, S. J., and Edwards, D. R. (2001) *Methods Mol. Biol.* **151,** 305–320
37. Neuhaus, E. M., and Soldati, T. (2000) *J. Cell Biol.* **150,** 1013–1026
38. Gospodarowicz, D. (1984) in *Methods for Preparation of Media Supplements and Substrata* (Barnes, D. W., Sirbasku, D. A., and Stao, G. H., eds) pp. 275–293, Alan R. Liss, Inc., New York
39. Gilles, C., Polette, M., Coraux, C., Tournier, J. M., Meneguzzi, G., Munaut, C., Volders, L., Rousselle, P., Birembaut, P., and Foidart, J. M. (2001) *J. Cell Sci.* **114,** 2967–2976
40. Hernandez-Barrantes, S., Bernardo, M., Toth, M., and Fridman, R. (2002) *Semin. Cancer Biol.* **12,** 131–138
41. Toth, M., Hernandez-Barrantes, S., Osenkowski, P., Bernardo, M. M., Gervasi, D. C., Shimura, Y., Meroueh, O., Kotra, L. P., Galvez, B. G., Arroyo, A. G., Mobashery, S., and Fridman, R. (2002) *J. Biol. Chem.* **277,** 26340–26350
42. Azzam, H. S., and Thompson, E. W. (1992) *Cancer Res.* **52,** 4540–4544
43. Seltzer, J. L., Lee, A. Y., Akers, K. T., Sudbeck, B., Southon, E. A., Wayner, E. A., and Eisen, A. Z. (1994) *Exp. Cell Res.* **213,** 365–374
44. Gilles, C., Polette, M., Seiki, M., Birembaut, P., and Thompson, E. W. (1997) *Lab. Invest.* **76,** 651–660
45. Haas, T. L., Davis, S. J., and Madri, J. A. (1998) *J. Biol. Chem.* **273,** 3604–3610
46. Ellerbroek, S. M., Fishman, D. A., Kearns, A. S., Bafetti, L. M., and Stack, M. S. (1999) *Cancer Res.* **59,** 1635–1641
47. Ellerbroek, S. M., Wu, Y. I., Overall, C. M., and Stack, M. S. (2001) *J. Biol. Chem.* **276,** 24833–24842
48. Aznavoorian, S., Moore, B. A., Alexander-Lister, L. D., Hallit, S. L., Windsor, L. J., and Engler, J. A. (2001) *Cancer Res.* **61,** 6264–6275
49. Strongin, A. Y., Marmer, B. L., Grant, G. A., and Goldberg, G. I. (1993) *J. Biol. Chem.* **268,** 14033–14039
50. Will, H., Atkinson, S. J., Butler, G. S., Smith, B., and Murphy, G. (1996) *J. Biol. Chem.* **271,** 17119–17123
51. Kurschat, P., Zigrino, P., Nischt, R., Breitkopf, K., Steurer, P., Klein, C. E., Krieg, T., and Mauch, C. (1999) *J. Biol. Chem.* **274,** 21056–21062
52. Lohi, J., and Keski-Oja, J. (1995) *J. Biol. Chem.* **270,** 17602–17609
53. Simon, C., Goepfert, H., and Boyd, D. (1998) *Cancer Res.* **58,** 1135–1139
54. Yamamoto, M., Tsujishita, H., Hori, N., Ohishi, Y., Inoue, S., Ikeda, S., and Okada, Y. (1998) *J. Med. Chem.* **41,** 1209–1217
55. Rozanov, D. V., Deryugina, E. I., Ratnikov, B. I., Monosov, E. Z., Marchenko, G. N., Quigley, J. P., and Strongin, A. Y. (2001) *J. Biol. Chem.* **276,** 25705–25714
56. Jiang, A., Lehti, K., Wang, X., Weiss, S. J., Keski-Oja, J., and Pei, D. (2001) *Proc. Natl. Acad. Sci. U. S. A.* **98,** 13693–13698
57. Uekita, T., Itoh, Y., Yana, I., Ohno, H., and Seiki, M. (2001) *J. Cell Biol.* **155,** 1345–1356
58. Maquoi, E., Frankenne, F., Baramova, E., Munaut, C., Sounni, N. E., Remacle, A., Noel, A., Murphy, G., and Foidart, J. M. (2000) *J. Biol. Chem.* **275,** 11368–11378

59. Brown, P. D., Bloxidge, R. E., Stuart, N. S., Gatter, K. C., and Carmichael, J. (1993) *J. Natl. Cancer Inst.* **85,** 574–578
60. Nomura, H., Fujimoto, N., Seiki, M., Mai, M., and Okada, Y. (1996) *Int. J. Cancer* **69,** 9–16
61. Liabakk, N. B., Talbot, I., Smith, R. A., Wilkinson, K., and Balkwill, F. (1996) *Cancer Res.* **56,** 190–196
62. Crescimanno, C., Foidart, J. M., Noel, A., Polette, M., Maquoi, E., Birembaut, P., Baramova, E., Kaufmann, P., and Castellucci, M. (1996) *Exp. Cell Res.* **227,** 240–251
63. Deryugina, E. I., Bourdon, M. A., Luo, G. X., Reisfeld, R. A., and Strongin, A. (1997) *J. Cell Sci.* **110,** 2473–2482
64. Makela, M., Larjava, H., Pirila, E., Maisi, P., Salo, T., Sorsa, T., and Uitto, V. J. (1999) *Exp. Cell Res.* **251,** 67–78
65. Itoh, Y., Takamura, A., Ito, N., Maru, Y., Sato, H., Suenaga, N., Aoki, T., and Seiki, M. (2001) *EMBO J.* **20,** 4782–4793
66. Kawata, R., Shimada, T., Maruyama, S., Hisa, Y., Takenaka, H., and Murakami, Y. (2002) *Acta Oto-Laryngol.* **122,** 101–106
67. Overall, C. M., and Sodek, J. (1990) *J. Biol. Chem.* **265,** 21141–21151
68. Yu, M., Sato, H., Seiki, M., and Thompson, E. W. (1995) *Cancer Res.* **55,** 3272–3277
69. Maquoi, E., Frankenne, F., Noel, A., Krell, H. W., Grams, F., and Foidart, J. M. (2000) *Exp. Cell Res.* **261,** 348–359
70. Stanton, H., Gavrilovic, J., Atkinson, S. J., d'Ortho, M. P., Yamada, K. M., Zardi, L., and Murphy, G. (1998) *J. Cell Sci.* **111,** 2789–2798
71. Gilles, C., Bassuk, J. A., Pulyaeva, H., Sage, E. H., Foidart, J. M., and Thompson, E. W. (1998) *Cancer Res.* **58,** 5529–5536
72. Shofuda, K., Moriyama, K., Nishihashi, A., Higashi, S., Mizushima, H., Yasumitsu, H., Miki, K., Sato, H., Seiki, M., and Miyazaki, K. (1998) *J. Biochem.* (*Tokyo*) **124,** 462–470
73. Koshikawa, N., Giannelli, G., Cirulli, V., Miyazaki, K., and Quaranta, V. (2000) *J. Cell Biol.* **148,** 615–624
74. Nawrocki Raby, B., Polette, M., Gilles, C., Clavel, C., Strumane, K., Matos, M., Zahm, J. M., Van Roy, F., Bonnet, N., and Birembaut, P. (2001) *Int. J. Cancer* **93,** 644–652
75. Takahashi, K., Eto, H., and Tanabe, K. K. (1999) *Int. J. Cancer* **80,** 387–395
76. Giannelli, G., Falk-Marzillier, J., Schiraldi, O., Stetler-Stevenson, W. G., and Quaranta, V. (1997) *Science* **277,** 225–228

1: J Biol Chem. 2004 Jul 9 [Epub ahead of print]

Differential regulation of membrane-type 1 matrix metalloproteinase activity by ERK 1/2- and p38 MAPK-modulated tissue inhibitor of metalloproteinases 2 expression controls TGF-beta1-induced pericellular collagenolysis.

Munshi HG, Wu YI, Mukhopadhyay S, Ottaviano AJ, Sassano A, Koblinski JE, Platanias LC, Stack MS.

Cell and Molecular Biology, Northwestern University, Chicago, IL 60611.

Acquisition of matrix metalloproteinase-2 (MMP-2) activity is temporally associated with increased migration and invasiveness of cancer cells. ProMMP-2 activation requires multimolecular complex assembly involving proMMP-2, membrane type 1-MMP (MT1-MMP, MMP-14) and tissue inhibitor of metalloproteinases-2 (TIMP-2). Because transforming growth factor-b1 (TGF-ss1) promotes tumor invasion in advanced squamous cell carcinomas, the role of TGF-ss1 in the regulation of MMP activity in a cellular model o invasive oral squamous cell carcinoma (OSCC) was examined. Treatment of OSCC cells with TGF-ss1 promoted MMP-dependent cell scattering and collagen invasion, increased expression of MMP-2 and MT1-MMP, and enhanced MMP-2 activation. TGF-ss1 induced concomitant activation of ERK1/2 and p38 MAPK and kinase inhibition studies revealed a negative regulatory role for ERK1/2 in modulating acquisition of MMP-2 activity. Thus, a reciprocal effect on proMMP-2 activation was observed whereupon blocking ERK1/2 phosphorylation promoted proMMP-2 activation and MT1-MMP activity while inhibiting p38 MAPK activity decreased proteolytic potential. The cellular mechanism for control of MT1-MMP catalytic activity involved concurrent reciprocal modulation of TIMP-2 expression by ERK1/2 and p38 MAPKs, such that inhibition of ERK1/2 phosphorylation decreased TIMP-2 production while downregulation of p38 MAPK activity enhanced TIMP 2 synthesis. Further, p38 MAPK inhibition promoted ERK1/2 phosphorylation, providing additional evidence for cross-talk between MAPK pathways. These observations demonstrat the complex reciprocal effects of ERK1/2 and p38 MAPK in the regulation of MMP activity which could complicate the use of MAPK specific inhibitors as therapeutic agents to down-regulate the biologic effects of TGF-ss1 on pericellular collagen degradation and tumor invasion.

PMID: 15247230 [PubMed - as supplied by publisher]

Jul 27 2004 06:47:

1: Proc Natl Acad Sci U S A. 2004 May 4;101(18):6917-22. Epub 2004 Apr 26.

Membrane protease proteomics: Isotope-coded affinity tag MS identification of undescribed MT1-matrix metalloproteinase substrates.

Tam EM, Morrison CJ, Wu YI, Stack MS, Overall CM.

Department of Biochemistry and Molecular Biology, Centre for Blood Research and Canadian Institutes of Health Research Group in Matrix Dynamics, University of British Columbia, Vancouver, BC, Canada V6T 1Z3.

By proteolytic modification of low abundant signaling proteins and membrane receptors, proteases exert potent posttranslational control over cell behavior at the postsecretion level. Hence, substrate discovery is indispensable for understanding the biological role of protease in vivo. Indeed, matrix metalloproteinases (MMPs), long associated with extracellular matri: degradation, are increasingly recognized as important processing enzymes of bioactive molecules. MS is now the primary proteomic technique for detecting, identifying, and quantitating proteins in cells or tissues. Here we used isotopecoded affinity tag labeling and multidimensional liquid chromatography inline with tandem MS to identify MDA-MB-231 breast carcinoma cell proteins shed from the cell surface or the pericellular matrix and extracellular proteins that were degraded or processed after transfection with human membrane type 1-MMP (MT1-MMP). Potential substrates were identified as those having altered protein levels compared with the E240A inactive MT1-MMP mutant or vector transfectants. New substrates were biochemically confirmed by matrix-assisted laser desorption ionization-time-of-flight MS and Edman sequencing of cleavage fragments after incubation with recombinant soluble MT1-MMP in vitro. We report many previously uncharacterized substrates of MT1-MMP, including the neutrophil chemokine IL-8, secretor leukocyte protease inhibitor, pro-tumor necrosis factor alpha, death receptor-6, and connective tissue growth factor, indicating that MT1-MMP is an important signaling proteas in addition to its traditionally ascribed roles in pericellular matrix remodeling. Moreover, the high-throughput and quantitative nature of isotope-coded affinity tag labeling combined witl tandem MS sequencing is a previously undescribed degradomic screen for protease substrate discovery that should be generally adaptable to other classes of protease for exploring proteolytic function in complex and dynamic biological contexts.

PMID: 15118097 [PubMed - indexed for MEDLINE]

Jul 27 2004 06:47:

Membrane protease proteomics: Isotope-coded affinity tag MS identification of undescribed MT1–matrix metalloproteinase substrates

Eric M. Tam*, Charlotte J. Morrison†, Yi I. Wu‡, M. Sharon Stack‡, and Christopher M. Overall*†§

Departments of *Biochemistry and Molecular Biology and †Oral Biological and Medical Sciences, Centre for Blood Research and Canadian Institutes of Health Research Group in Matrix Dynamics, University of British Columbia, Vancouver, BC, Canada V6T 1Z3; and ‡Department of Cell and Molecular Biology, Northwestern University Medical School, Chicago, IL 60611

Edited by Jerome Gross, Massachusetts General Hospital, Charlestown, MA, and approved February 20, 2004 (received for review September 11, 2003)

By proteolytic modification of low abundant signaling proteins and membrane receptors, proteases exert potent posttranslational control over cell behavior at the postsecretion level. Hence, substrate discovery is indispensable for understanding the biological role of proteases *in vivo*. Indeed, matrix metalloproteinases (MMPs), long associated with extracellular matrix degradation, are increasingly recognized as important processing enzymes of bioactive molecules. MS is now the primary proteomic technique for detecting, identifying, and quantitating proteins in cells or tissues. Here we used isotope-coded affinity tag labeling and multidimensional liquid chromatography inline with tandem MS to identify MDA-MB-231 breast carcinoma cell proteins shed from the cell surface or the pericellular matrix and extracellular proteins that were degraded or processed after transfection with human membrane type 1-MMP (MT1-MMP). Potential substrates were identified as those having altered protein levels compared with the E240A inactive MT1-MMP mutant or vector transfectants. New substrates were biochemically confirmed by matrix-assisted laser desorption ionization–time-of-flight MS and Edman sequencing of cleavage fragments after incubation with recombinant soluble MT1-MMP *in vitro*. We report many previously uncharacterized substrates of MT1-MMP, including the neutrophil chemokine IL-8, secretory leukocyte protease inhibitor, pro-tumor necrosis factor α, death receptor-6, and connective tissue growth factor, indicating that MT1-MMP is an important signaling protease in addition to its traditionally ascribed roles in pericellular matrix remodeling. Moreover, the high-throughput and quantitative nature of isotope-coded affinity tag labeling combined with tandem MS sequencing is a previously undescribed degradomic screen for protease substrate discovery that should be generally adaptable to other classes of protease for exploring proteolytic function in complex and dynamic biological contexts.

In all living organisms, proteases exert high-order posttranslational control over a diverse range of cellular functions. Altered protease expression and substrate proteolysis are pivotal elements in the pathogenesis of many diseases (1) with 53 hereditary genetic diseases of proteolysis recognized (2). Indeed, proteases represent ≈10% of current drug targets (3). Elucidating the substrate repertoire of a protease is critical to understanding its biological role, but given the large number of proteases (>553) present in the human genome (2), this is a daunting task. Innovative approaches using combinatorial or positional scanning libraries of fluorogenic (4) and inhibitory peptides (5) and oriented (6) and phage display (7) peptide libraries can determine consensus protease cleavage sequences. However, bioinformatic identification of proteins containing these sequences followed by biochemical and *in vivo* validation of proteolytic susceptibility has led to the identification of relatively few biologically relevant new substrates. This is not surprising, because the majority of substrates *in vivo* are proteins and not peptides. Moreover, substrates must colocalize with proteases, spatially and temporally. Although useful, these techniques are inherently limited in their power, because they do not consider the influence of protein conformation, posttranslational modification, protease exosites, and substrate availability *in vivo* (8). Serial analysis of protein libraries and exosite scanning by yeast two-hybrid screens, although time consuming, have proven effective in identifying new protein substrates (9). Nonetheless, because proteases do not operate alone but more commonly in amplification cascades or regulatory circuits in the presence of a multitude of interacting proteins, substrates, and cleavage products, and often in distinct compartments, biologically relevant protease substrates *in vivo* may differ from theoretical activities inferred from *in vitro* experiments. In the face of such biochemical complexity, this emphasizes the need to identify protease-cleaved substrates and not just enzyme activities in cells, tissues, and whole organisms (10, 11). Thus, rapid techniques are needed to directly identify new substrates in biological settings and to quantitate differences in substrate processing as disease biomarkers and as surrogate markers of antiproteolytic drug treatment (3).

Proteomics offers the potential to identify protease substrates in complex biological samples in a system-wide approach that has been termed "degradomics" (12). However, apart from isolated reports (13), proteomic approaches for protease substrate identification have not been widely developed. In part, this may be due to difficulty in relating cleavage products with parent protein spots on 2D gels or to MS spectral peaks. Difficulties in quantification also hinder comparative analyses. Recently, techniques have been developed that incorporate stable isotopes into proteins by metabolic or posttranslational labeling (reviewed in ref. 14), thereby allowing MS quantification of the relative amounts of protein present in two samples (15). In isotope-coded affinity tag (ICAT) labeling (16), proteins in two samples that are to be compared are reduced and labeled by reductive alkylation of cysteines by using biotin-tagged reagents that are chemically identical but that differ in isotopic composition and mass. The two isotopically distinct labeled protein samples are then combined and thereafter treated identically, enabling quantitative comparisons to be made. Tryptic peptides are prepared, and the biotin-tagged cysteine-containing peptides only are avidin column purified for mass determination. Spectral peak analysis of the isotopically resolved identical peptides from the two sources enables relative quantitation. These proteins are then identified by tandem MS (MS/MS) sequencing in an iterative approach. ICAT has been recently refined by labeling with $[^{13}C]_9$ to avoid the slight alteration in hydrophobicity occurring in deuterium-labeled peptides and by the use of cleavable linkers to remove the biotin moiety after elution.

This paper was submitted directly (Track II) to the PNAS office.

Abbreviations: ICAT, isotope-coded affinity tag; MS/MS, tandem MS; MD-LC, multidimensional liquid chromatography; MMP, matrix metalloproteinase; MT, membrane type; sMT, soluble MT; TIMP, tissue inhibitor of metalloproteinases; GRO, growth-related oncogene; SLPI, secretory leukocyte protease inhibitor; CTGF, connective tissue growth factor; TNF, tumor necrosis factor; MALDI-TOF, matrix-assisted laser desorption ionization–time-of-flight.

§To whom correspondence should be addressed. E-mail: chris.overall@ubc.ca.

Matrix metalloproteinase (MMP)-14, or membrane type (MT)1-MMP, is one of 23 members of an important protease family historically associated with the cleavage of extracellular matrix proteins (17). MT1-MMP is constitutively activated by furin processing, is essential for normal growth and development (18), and is up-regulated in cancer and arthritis (19). MT1-MMP degrades fibrillar collagen and fibronectin (20, 21) and activates MMP-2 (gelatinase A) (22, 23), which is also heavily implicated in cancer metastasis. However, like most proteases, the breadth of potential *in vivo* substrates and biological role of MT1-MMP are largely unknown. This is important to address because, of all MMP gene knockouts, only the MT1-MMP$^{-/-}$ mouse exhibits strong developmental abnormalities (18).

Here we have developed a functional proteomic screen to identify new protease substrates in cell cultures. We hypothesized that the levels of individual proteins in conditioned culture medium would be differentially altered after cell transfection with MT1-MMP and thus would be amenable to ICAT and MS/MS identification. After proteolysis, secreted proteins may be reduced in amount if degraded or processed and subsequently cleared after reductions in stability, and other proteins may increase in quantity if proteolytically shed from the cell surface or released from the pericellular matrix. We report that ICAT is applicable to the proteomic analysis of proteolytic activity in complex cellular systems with the identification of multiple previously undescribed signaling molecules as substrates of MT1-MMP.

Experimental Procedures

Cell Culture. Human MDA-MB-231 breast carcinoma cells stably transfected with FLAG-tagged human MT1-MMP, a catalytically inactive MT1-MMP mutant (E240A) in which the active-site Glu is replaced, or pCR3.1 vector alone under G418 selection were as described (21). MT1-MMP expression was confirmed by Western blotting and flow cytometry. MT1-MMP activity was confirmed by zymographic analysis of MMP-2 activation when the transfected cells were incubated with human proMMP-2 expressed from *Timp2*$^{-/-}$ cells (23).

For protein analysis, confluent transfected MDA-MB-231 cells were grown in DMEM, 10% FBS, and G418 (1 mg/ml), washed with PBS, and incubated in DMEM alone to eliminate serum contamination. After 48 h, the medium was replaced with DMEM and ascorbic acid (50 μg/ml). The conditioned medium was harvested (48 h), protease inhibitors (6.7 μM EDTA, 1 mM PMSF, 10 μM leupeptin, and 1 μM pepstatin A) were immediately added, and the conditioned medium clarified by centrifugation (30 min, 1,000 $\times$ *g*) and filtration (0.22 μm). Amicon stirred cells and Centripreps (3-kDa cutoff, Millipore) were used to concentrate proteins 100–200×.

ICAT Labeling, Chromatography, and MS/MS. Conditioned medium proteins (100 μg) from MT1-MMP transfectants were labeled with isotopically heavy [^{13}C]$_9$-cleavable ICAT reagent (Applied Biosystems) (2 h, 37°C) for comparison with proteins from vector control or the E240A inactive MT1-MMP mutant-transfectant conditioned medium, which were labeled with the light [^{13}C]$_0$-ICAT reagent. Sample pairs were combined (MT1-MMP/vector or MT1-MMP/E240A), trypsin digested (18 h, 37°C), and fractionated on a cation-exchange column (4 $\times$ 15 mm) by elution with 350 mM KCl, pH 3.0, to remove the trypsin and free label. Labeled peptides were purified by using an avidin-affinity column (4 $\times$ 15 mm) and eluted with 20% acetonitrile/0.4% trifluoroacetic acid (TFA). Dried samples were incubated in 95% TFA (2 h, 37°C) to cleave the biotin tag from the ICAT-labeled peptides. The biotin tab was then cleaved with 95% TFA. Samples were fractionated by multidimensional liquid chromatography (MD-LC), first on a 500-μm i.d. $\times$ 15 mm BioX-SCX column (LC Packings, Sunnyvale, CA) and eluted as 50-μl fractions (25, 50, 75, 100, 150, 200, 250, 500, 1,000, or 2,000 mM ammonium acetate, pH 4.0). Eluted peptides were concentrated and desalted on a 300-μm i.d. $\times$ 1 mm PepMap nanotrapping column before loading onto a 75-μm i.d. $\times$ 15 cm PepMap nanoseparation column. Peptides were then fractionated by using an acetonitrile gradient (0–64%, 35 min) before entering the nanospray ionization source (New Objective, Woburn, MA). MS analysis of the separated peptides was performed by using a QStar PulsarI mass spectrometer (MDS-Sciex, Thornhill, ON, Canada). MS/MS fragmentation (2 s, 65–1,800 m/z) was performed on three of the most intense ions, as determined from a 1-s survey scan (300–1,500 m/z). ICAT ratios of isotopically heavy $^{13}C_9$- to light $^{13}C_0$-labeled tryptic peptides were determined by using PROICAT (Applied Biosystems) software and averaged for multiple peptides derived from a single parent protein. Using MASCOT (Matrix Science), proteins were identified from peptide sequences queried against the National Center for Biotechnology Information nonredundant protein database with human sequence filtering. Labeling and analysis were performed three times at the Genome BC Proteomic Centre (Victoria, BC, Canada).

Protease and Substrates. Soluble (s) human MT1-MMP lacking the transmembrane and cytoplasmic tail was expressed and purified (21). Human IL-8, growth-related oncogene (GRO)-α, and GRO-γ were chemically synthesized and purified (24). Human secretory leukocyte protease inhibitor (SLPI) (ICN) and human death receptor-6 fused via a Factor Xa site to the Fc region of IgG (R & D Systems) were purchased. Human connective tissue growth factor (CTGF) was a kind gift from D. Brigstock (Ohio State University, Columbus). Human pro-tumor necrosis factor (TNF)α fused to GST and a hydroxamate MMP inhibitor, BB2116, were provided by British Biotech (Oxford). Human tissue inhibitor of metalloproteinases (TIMP)-1 and -2 were expressed and purified (25). Monoclonal antibodies against human fibronectin (MAB1891, Chemicon) and death receptor-6 (MAB1441, R & D Systems) were purchased.

Assays. Recombinant and synthetic proteins were incubated with sMT1-MMP in 50 mM Tris·HCl/200 mM NaCl/5 mM $CaCl_2$/3.8 mM NaN_3/0.05% Brij 35, pH 7.4, for 18 h at 37°C. Reaction products were separated by Tris-glycine or -tricine SDS/PAGE and stained by Coomassie R-250 or Western blotted. The mass and sequence of the cleavage products were determined by matrix-assisted laser desorption ionization–time-of-flight (MALDI-TOF) MS and N-terminal Edman sequencing, respectively.

Results

MT1-MMP Expression. FLAG-tagged MT1-MMP and the 44-kDa form were detected on transfected cells (Fig. 1 *A* and *B*), which activated exogenous proMMP-2 (Fig. 1*C*), confirming the presence of active MT1-MMP on the cell surface. Vector transfectants expressed only very low levels of endogenous MT1-MMP (Fig. 1*B*). No secreted active MMPs were detected by using a general MMP-quenched fluorescent substrate (25) (data not shown).

ICAT and MD-LC MS/MS Analysis. In comparing the relative abundance ratios of ICAT-labeled peptides from MT1-MMP transfectants with those from the vector or E240A MT1-MMP controls, we hypothesized that those proteins with an average labeled-peptide ICAT ratio <1.0 (MT1-MMP/control) had undergone MT1-MMP-mediated degradation or processing that triggered clearance; proteins with ratios >1.0 were hypothesized to have been shed from the cell membrane or pericellular matrix by MT1-MMP activity. Although ICAT is sensitive and highly reproducible (14), to reduce the probability of false positives, we analyzed only proteins with ICAT ratios <0.5 or >1.5, which typically numbered from 100 to 150 identified proteins. Without inline MD-LC fractionation, the number of proteins so identified was reduced to <100. Intracellular proteins were not further considered. A selective list of the biologically interesting proteins that may be potential MT1-MMP sub-

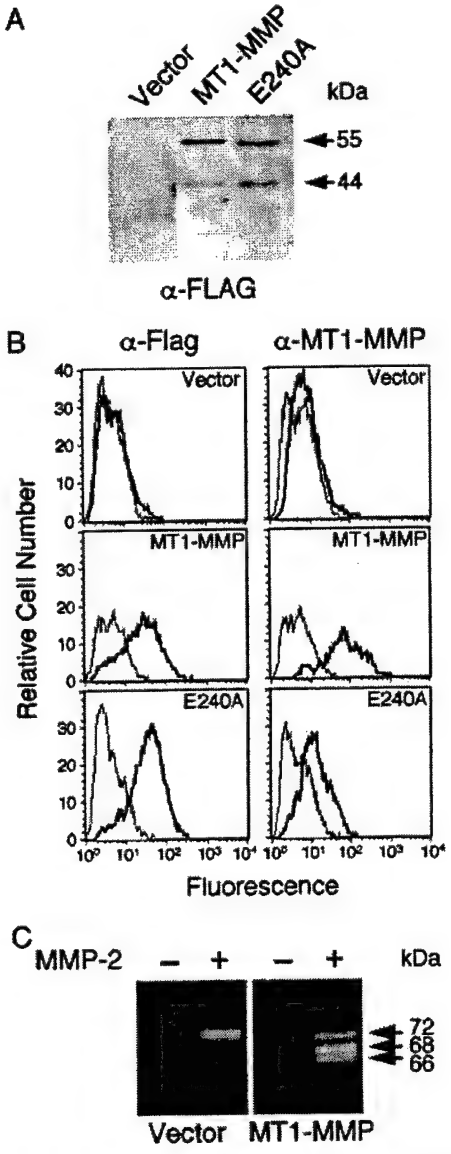

Fig. 1. Characterization of cells expressing MT1-MMP and inactive mutant E240A MT1-MMP. (*A*) Cell lysates from MT1-MMP, E240A, and vector-transfected MDA-MB-231 cells were analyzed by SDS/PAGE (10%) and Western blotting. Full-length MT1-MMP (55 kDa) and the 44-kDa form are indicated. (*B*) Cells labeled with either α-FLAG (Sigma) or α-human MT1-MMP antibody (AB815, Chemicon) (dark line) or no primary antibody (light line) were analyzed by fluorescent flow cytometry on a FACScan. (*C*) Media from MT1-MMP and vector-transfected cells, with or without exogenous proMMP-2 (72 kDa) added, were analyzed by gelatin zymography. Fully activated (62-kDa) and activation intermediate (68-kDa) MMP-2 are indicated.

strates was generated from the two data sets (Table 1) based on deduced roles in pathology and embryonic development. These included protease inhibitors (SLPI and skin-derived antileukoproteinase), chemokines (IL-8, GRO-α, GRO-γ, and macrophage migration inhibitory factor), cytokines (TNFα, CTGF), cell receptors (death receptor-6, neuropilin-1), latent transforming growth factor-binding protein-4S, and complement component-3. Extracellular matrix proteins (fibronectin, epidermal growth factor-containing fibulin-like extracellular matrix protein-1) and shed MT1-MMP and proMMP-1 (collagenase-1) were also elevated in the MT1-MMP cell-conditioned medium.

Table 1. Identification by ICAT and MS/MS analysis of cellular proteins in the conditioned medium of MDA-MB-231 cultures displaying altered abundance due to MT1-MMP activity

Protein*	MT1-MMP/control† mean ratio‡	Peptide sequences§
SLPI	4.95	CCMGMCGK
		YKKPECQSDWQCPGK
EFEMP-1	3.90	ADQVCINLR
		CVNHYGGYLCLPK
DR-6	3.79¶	VCSSCPVGTFTR
Fibronectin	3.04	EYLGAICSCTCFGGQR
		GEWTCIAYSQLR
		ISCTIANR
		LLCQCLGFGSGHFR
		TFYSCTTEGR
		TYLGNALVCTCYGGSR
		WCGTTQNYDADQK
		YQCYCYGR
		YSFCTDHTVLVQTR
MT1-MMP	2.61	CGVPDKFGAEIK‖
		WQHNEITFCIQNYTPK
ProMMP-1	2.05	ACDSKLTFDAITTIR
		CGVPDVAQFVLTEGNPR‖
Neuropilin-1	1.90	SPGFPEKYPNSLECTYIVFAPK
SKALP	1.85	CAMLNPPNR
		CLKDTDCPGIK
CTGF	1.74	DGAPCIFGGTVYR
LTBP-4S	1.73	AGPDLASCLDVDECRER
		DGGCSLPILR
		IQQCPGTETAEYQSLCPHGR
TNFα	1.29	SWLPAGCETAILFPMR
TIMP-1	1.25	EPGLCTWQSLR
		FVYTPAMESVCGYFHR
		LQSGTHCLWTDQLLQGSEK
MIF	0.49	LLCGLLAER
GRO-α	0.37	CQCLQTLQGIHPK
		KACLNPASPIVK
		SPGPHCAQTEVIATLK
IL-8	0.34	ELCLDPK
		LSDGRELCLDPK
		VIESGPHCANTEIIVK
GRO-γ	0.27	CQCLQTLQGIHLK
		SPGPHCAQTEVIATLK
C3	0.25	NTMILEICTR
		VFLDCCNYITELRR
		VYAYYNLEESCTR

*SLPI, secretory leukocyte protease inhibitor; EFEMP-1, EGF-containing fibulin-like extracellular matrix protein-1; DR-6, death receptor-6; SKALP, skin derived antileukoproteinase; CTGF, connective tissue growth factor; LTBP-4S, latent transforming growth factor-binding protein-4S; TIMP-1, tissue inhibitor of metalloproteinase-1; MIF, macrophage migration inhibitory factor; GRO-α, growth related oncogene-α; GRO-γ, growth related oncogene-γ; C3, complement component 3.

†Control protein was from vector transfected cells unless stated otherwise.

‡The relative abundance of the $^{13}C_9$-labeled peptides from the MT1-MMP transfected cell proteins compared with the $^{13}C_0$-labeled peptides from control cell protein were averaged to give a mean ratio.

§All peptides containing multiple Cys residues were quantitatively labeled by the ICAT reagent.

¶Control protein was from inactive MT1-MMP mutant transfected cells.

‖These peptides represent the Cys-switch motif of the MMP prodomain indicating increased expression of the zymogen form of these MMPs and that furin activation of MT1-MMP may occur on the cell surface.

Chemokine Processing. To test the hypothesis that ICAT can identify potential protease substrates, we biochemically analyzed a number of the proteins from Table 1 for cleavage by sMT1-MMP using

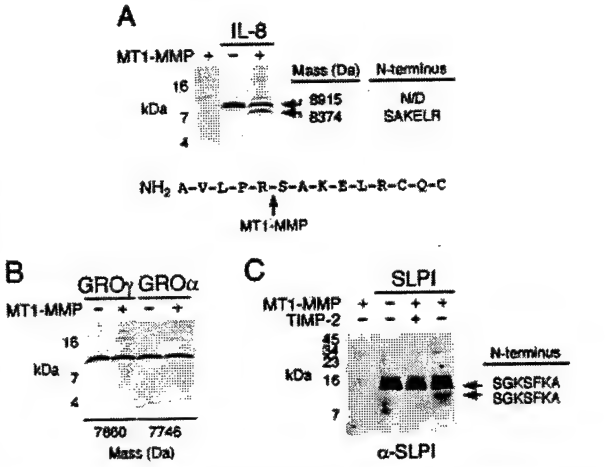

Fig. 2. MT1-MMP processing of IL-8 and SLPI. (*A–C*) CXC chemokines or SLPI were incubated with sMT1-MMP for 18 h at 37°C. Samples were then separated on 15% Tris-tricine gels under nonreducing conditions. (*A*) MT1-MMP cleavage of IL-8 and sequence of the cleavage site. (*B*) MT1-MMP did not cleave GRO-α or -γ as analyzed by SDS/PAGE. MALDI-TOF MS revealed identical masses for both chemokines in the presence or absence of MT1-MMP. (*C*) SLPI was detected by Western blotting by using α-SLPI antibody. SLPI cleavage was blocked by TIMP-2 added with sMT1-MMP or after preincubation (not shown). N-terminal sequences are shown.

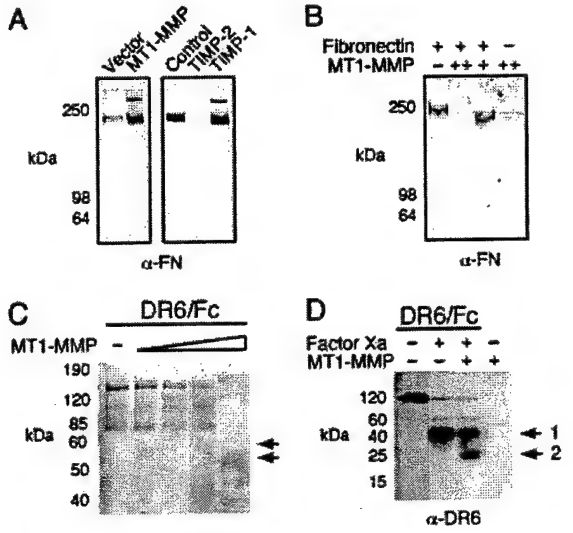

Fig. 3. MT1-MMP shedding of fibronectin and death receptor-6. (*A*) MT1-MMP and vector-transfected MDA-MB-231 cells were incubated in serum-free DMEM with or without inhibitors (TIMP-1 and -2, 100 nM). Shed fibronectin was then purified from the 48-h media by using a gelatin-Sepharose column and eluted with 8 M urea in PBS before analysis by SDS/PAGE (5%) and Western blotting with α-fibronectin monoclonal antibody. (*B*) Fibronectin was incubated with sMT1-MMP (+, ++) *in vitro* for 18 h at 37°C. (*C*) DR6/Fc fusion protein was treated with increasing amounts of sMT1-MMP and separated by SDS/PAGE (10%). Cleavage products are indicated by arrows. (*D*) DR6/Fc was cleaved with Factor Xa (5 h, 37°C) before digestion with sMT1-MMP (18 h, 37°C). Samples were then electrophoresed and Western blotted by using α-DR6 antibody. Factor Xa (1) and MT1-MMP (2) cleaved-DR6/Fc products are shown.

recombinant or synthetic proteins as substrates. Because chemokines are a recently recognized class of MMP substrates (9, 26–28), it was of interest that the chemokines IL-8, GRO-α, and GRO-γ showed decreased levels on MT1-MMP expression. N-terminal sequencing confirmed the proteolytic removal of the first five residues of IL-8 by sMT1-MMP *in vitro* to generate a truncated form beginning with the sequence SAKELR (Fig. 2*A*). However, SDS/PAGE and MALDI-TOF MS showed no change in mass for GRO-α and -γ after incubation with sMT1-MMP (Fig. 2*B*). Complement component-3, which displayed a similar ICAT ratio to GRO-γ (Table 1), was also not susceptible to MT1-MMP proteolysis *in vitro* (data not shown), revealing that MT1-MMP expression can decrease the levels of these proteins by indirect means.

Sheddase Activity. Levels of the secretory leukocyte protease inhibitor, SLPI, were greatly increased on MT1-MMP expression (Table 1). Biochemical assays revealed that sMT1-MMP cleaved SLPI in a TIMP-2-inhibitable manner to generate a single 12.3-kDa product with an N terminus of SGKSFKA (Fig. 2*C*). This sequence is identical to the intact inhibitor, and so cleavage occurred near the C terminus, which may release the cleaved SLPI from association with the cell layer proteins.

Medium levels of fibronectin, a known substrate of sMT1-MMP (20), were also significantly elevated upon MT1-MMP expression (Table 1), implying that MT1-MMP may shed fibronectin from the cell surface. This was confirmed by gelatin-Sepharose affinity purification and quantitation of fibronectin from the conditioned medium of the transfectants (Fig. 3*A*). Fibronectin shedding was inhibited by adding TIMP-2 but not -1 to the cultures. Because TIMP-1 spares MT1-MMP in its inhibitory profile, this confirms the specific requirement for MT1-MMP activity in the proteolytic release of fibronectin from the cell surface. Shed immunoreactive protein migrated with the expected molecular mass (220 kDa + DTT) of the full-length protein (Fig. 3*A*); cleaved fibronectin fragments were never observed in the conditioned medium; and the ICAT-labeled peptides ^{67}TYLGNALVCTCYGGSR^{84} and ^{2199}LLCQCLGFGSGHFR^{2214} (Table 1), which are proximal to the N and C termini of the molecule, displayed similar abundance ratios to the other fibronectin peptides. This indicates that the solubilized form of fibronectin is intact and that overexpressed MT1-MMP did not appear to degrade fibronectin in a cellular context, despite its activity on this protein in biochemical assays (Fig. 3*B*). Although processing of fibronectin cannot be discounted as a shedding mechanism, this indicates that cleavage of a fibronectin-binding cell surface molecule by MT1-MMP is the mechanism for release.

Death receptor-6 is a member of the TNF receptor family and consists of a 350-residue ectodomain and a cytoplasmic death domain (29). Using a death receptor-6 fusion protein, DR6/Fc, as a substrate for *in vitro* assays with sMT1-MMP, we found loss of intact protein and generation of two immunoreactive fragments at 55 and 50 kDa (Fig. 3*C*). To verify that cleavage occurred within the ectodomain and not the Fc region, DR6/Fc was first treated with Factor Xa to cleave a susceptible site between the ectodomain and the Fc region. Upon incubation with sMT1-MMP *in vitro*, a 25-kDa product was generated from the 40-kDa ectodomain confirming susceptibility of DR6 to MT1-MMP proteolysis (Fig. 3*D*).

Cytokine Substrates. The inflammatory cytokine, TNFα, had a MT1-MMP/vector ICAT ratio of 1.29 that indicated shedding to the medium. Although this was below our arbitrary 1.5 ICAT ratio cutoff, proTNFα can be shed by MMP-7 (30). Therefore, the susceptibility of proTNFα to sMT1-MMP processing was investigated by using a proTNFα/GST fusion protein as substrate. This was cleaved by sMT1-MMP to generate a product corresponding to the correct size of mature TNFα (≈16 kDa) (Fig. 4*A*). N-terminal sequencing revealed that, in addition to cleavage at the Ala-76—Val-77 bond, which generates the fully active TNFα, three other bonds in close proximity in the proregion of TNFα were also processed by sMT1-MMP *in vitro* (Fig. 4*A*).

Last, we analyzed CTGF, a member of the CCN (CTGF/cysteine-rich 61/nephroblastoma overexpressed) family of extra-

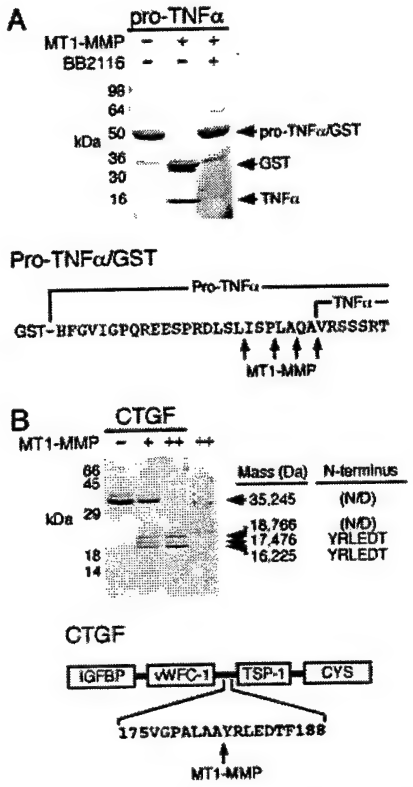

Fig. 4. MT1-MMP processing of proTNFα and CTGF. (*A*) ProTNFα/GST fusion protein was incubated with sMT1-MMP (18 h, 37°C) with or without BB2116. Samples were separated by SDS/PAGE (5–15%). MT1-MMP cleavage sites within the TNFα proregion were determined by N-terminal sequencing as schematically shown. Mature TNFα commences at VRSSSRT. (*B*) CTGF was treated with sMT1-MMP (+, ++) for 18 h at 37°C and analyzed by SDS/PAGE (15%) and MALDI-TOF MS. MT1-MMP cleavage sites were located by N-terminal sequencing to be in the CTGF linker. The IGF-binding protein module (IGFBP), von Willebrand factor type 1C module (vWFC-1), thrombospondin 1 module (TSP-1), and the cysteine-knot-containing C-terminal module (CYS) of CTGF are indicated. Insufficient protein was present to sequence the 18.8-kDa fragment. No sequence was attainable for intact CTGF, indicative of a modified N terminus.

cellular matrix-associated signaling molecules (31) for cleavage by sMT1-MMP. Three distinct lower molecular mass fragments were generated (Fig. 4*B*). Sequencing of the 17.5- and 16.2-kDa sMT1-MMP cleavage products revealed an identical N terminus, YRLEDT, corresponding to cleavage at the Ala-181—Tyr-182 bond (Fig. 4*B*).

Discussion

High-throughput protein quantitation and identification by ICAT and MD-LC MS/MS are powerful techniques that we have adapted for the proteomic investigation of protease function and substrate discovery in a dynamic cellular milieu. In MDA-MB-231 cells, we specifically identified a number of proteins that were biochemically confirmed as novel substrates of MT1-MMP, thereby validating the utility of ICAT MD-LC MS/MS for substrate discovery in cell-based systems. The majority of substrates discovered to date have been from serial approaches using available proteins or hypothesis-driven intuition using time-consuming biochemical and genetic approaches or peptide libraries and bioinformatics (12). The alternative of using proteomic techniques to screen for novel protease substrates is advantageous because of its coverage on a system-wide scale, speed, and resolution of even complex biological samples. However, to date there have been few proteomic studies except for using 2D-PAGE and stable isotope dilution (13). In comparison to gel-based analyses, LC MS approaches provide more extensive and rapid proteome coverage, the abundance of isotopically labeled peptides can be quantitated, and cell membrane proteins are amenable for MS analysis (reviewed in ref. 14). Nonetheless, protein abundance sets detection limits, and until improvements are made in sample preparation and chromatography before MS, it is not yet possible to localize cleaved substrates or to analyze whole tissues by ICAT because of the added sample complexity and variability. Moreover, differences in protein abundance as measured by ICAT must be interpreted with caution; some cleaved substrates may not change levels, and as we have found the levels of some uncleaved proteins may alter just by expression of the transfected gene, an important caveat for interpreting any study using protease-transfected cells. Thus, ICAT and MD-LC MS/MS should be considered as a screen for potential protease substrates that must be confirmed biochemically and *in vivo* when possible but that offers general applicability to other protease classes for functional proteomic investigation of protease function in complex samples.

The pool of potential substrates available to MT1-MMP expressed in MDA-MB231 cells will contain overlapping candidates with normal mammary epithelium as well as unique targets. The majority of proteins identified as potential MT1-MMP substrates were not extracellular matrix molecules. Rather, the levels of a variety of signaling proteins were specifically modulated on expression of MT1-MMP. Of these, IL-8, GRO-α, and GRO-γ are important for the regulation of leukocyte migration during wound healing (32, 33). MT1-MMP is also known to participate in wound healing and is expressed by monocytes. IL-8, GRO-α, and GRO-γ belong to the subgroup of CXC chemokine family members that contain the ELR motif near the N terminus, which is essential for neutrophil chemotactic activity (34). MT1-MMP processing of IL-8 removes the first five residues, which is more active than the untruncated form. In contrast to MMP-9, which processes a different site in IL-8 and also GROα (28), MT1-MMP does not cleave GRO-α or -γ, demonstrating selective susceptibility of CXC chemokines to MMP cleavage. Therefore, the reduction in the levels of these chemokines appears to be an indirect upstream response to the expression of MT1-MMP but biologically may be as important a consequence of MT1-MMP activity.

A number of protease inhibitors, including the plasma serine protease inhibitor SLPI, are also essential for normal wound repair. SLPI suppresses monocyte MMP production and is resistant to neutrophil collagenase (35). Here, ICAT identified SLPI as a potential MT1-MMP substrate, which we biochemically confirmed was processed near its C terminus. Because the inhibitory site of SLPI lies within the C domain (36), this reveals a previously undescribed intersection between the serine and metalloproteases in which the activity of a serine protease inhibitor is predicted to be abrogated on MT1-MMP proteolysis.

Expression of recombinant proteases may occur at levels greater than that seen in some normal tissues, thereby favoring proteolysis of less preferred or low abundant substrates. Although sMT1-MMP can degrade fibronectin *in vitro*, we found that in cell culture, MT1-MMP activity led only to the shedding of intact fibronectin from the MDA-MB-231 cell surface, suggesting that the levels of the recombinant MT1-MMP expressed were not artificially extreme or generated cleavage artifacts. This result not only highlights the importance of biochemically confirming proteomic data but equally important is the biological validation of biochemically determined proteolytic activity with cell-based and *in vivo* studies at the genetic or proteomic levels. Although the mode of fibronectin release is not clear, it has been reported that MT1-MMP degrades transglutaminase, a fibronectin coreceptor, thereby reducing both the adhesion and migration of cells on fibronectin (37).

We also found that MT1-MMP cleaved the ectodomain of death receptor-6, a transmembrane receptor that regulates apoptosis through its cytoplasmic death domain and activation of the

TRADD/FADD/caspase-8 pathway (29). Although the purpose of our study was to develop a novel proteomic approach for protease substrate discovery and not to fully explore here the biological ramifications of the cleavage of newly identified substrates, it is reasonable to hypothesize that MT1-MMP proteolysis of the ectodomain may regulate death receptor-6 signaling and apoptosis. Ligands that bind death receptor-6 belong to the TNF family of cytokines, one of which, TRANCE, is cleaved by MT1-MMP (38). Although ADAM-17 is the enzyme thought to be primarily responsible for the generation of mature TNFα from a membrane-bound precursor, particularly under lipopolysaccharide (LPS) stimulation (39, 40), MMP-7 can also process TNFα (30). Here, we extend the repertoire of MMPs that can cleave proTNFα by showing that MT1-MMP cleaves at the Ala-76—Val-77 bond within the proregion of TNFα to generate mature fully active TNFα, a potentially important mechanism in non-LPS-induced inflammation.

CTGF was also identified as a potential MT1-MMP substrate by ICAT that we then showed was cleaved by sMT1-MMP *in vitro* at the Ala-181—Tyr-182 bond. This site is within the linker that connects the insulin-like growth factor-binding protein domain and von Willebrand factor type-1C domain of CTGF with the thrombospondin-1 and C-terminal domains (Fig. 3*B*). Cleavage here potentially disengages matrix-binding domains from the signaling functions of CTGF, leading to release from the cell layer. Hashimoto *et al.* (41) also recently described CTGF cleavage by soluble MMPs 1, 3, 7, and 13 at Met-194-Ile-195 within the CTGF linker, with a minor cleavage site at Ala-181-Tyr-182. CTGF is unstable *in vivo*, being converted into low molecular mass forms (10–20 kDa) by an unidentified protease (42). Interestingly, conditioned medium from serum-stimulated mouse fibroblasts did not degrade CTGF (43), suggesting that a cell surface protease was responsible for CTGF processing. These results are consistent with our data demonstrating that the cell surface MT1-MMP can process CTGF in cell culture to generate ≈17-kDa fragments.

The substrates identified here reveal that MT1-MMP may be an important cell signaling protease and add to recent studies describing new MMP substrates that are redefining our outlook of the biological role of this protease family (12). Traditionally, MMPs have been viewed as enzymes of catabolism being primarily involved in the degradation and turnover of the extracellular matrix (17). MMPs are now known to process a diverse range of extracellular proteins other than those of the matrix (44). Like many proteases, MMPs regulate and refine many aspects of protein function, including activity, localization, shedding, exposure of cryptic binding sites, and release of neoproteins thereby achieving precise control over many cell processes. Thus, elucidating the substrate repertoires or degradomes of proteases is essential for understanding their *in vivo* roles. By establishing the physiological function of a protease, its role in pathology can be more readily ascertained. This in turn is a necessary prerequisite for drug target validation. No one technique will provide complete coverage of the protease substrate landscape, but overall MD-LC ICAT MS/MS provides a powerful functional degradomic approach that renders the quantitative analysis of proteolysis in defined cell cultures feasible, and one that should be generally applicable to elucidate the biological role of other proteases.

We thank Derek Smith for help with the ICAT data and Suzanne Perry for N-terminal sequencing and MALDI-TOF. E.M.T. is supported by a Canadian Institutes of Health Research Strategic Training Fellow Award in Cell Signals and a Canadian Arthritis Network Trainee Award. C.M.O. is supported by a Canada Research Chair in Metalloproteinase Biology. This work was supported by grants from Protein Engineering National Centres of Excellence National Cancer Institute of Canada and the Canadian Institutes of Health Research.

1. Barrett, A. J., Rawlings, N. D. & Woessner, J. F. (1998) *Handbook of Proteolytic Enzymes* (Academic, San Diego).
2. Puente, X. S., Sanchez, L. M., Overall, C. M. & López-Otín, C. (2003) *Nat. Rev. Genet.* **4**, 544–558.
3. Fingleton, B. (2003) *Expert Opin. Ther. Targets* **7**, 385–397.
4. Harris, J. L., Backes, B. J., Leonetti, F., Mahrus, S., Ellman, J. A. & Craik, C. S. (2000) *Proc. Natl. Acad. Sci. USA* **97**, 7754–7759.
5. Nazif, T. & Bogyo, M. (2001) *Proc. Natl. Acad. Sci. USA* **98**, 2967–2972.
6. Turk, B. E., Huang, L. L., Piro, E. T. & Cantley, L. C. (2001) *Nat. Biotechnol.* **19**, 661–667.
7. Deng, S. J., Bickett, D. M., Mitchell, J. L., Lambert, M. H., Blackburn, R. K., Carter, H. L., Neugebauer, J., Pahel, G., Weiner, M. P. & Moss, M. L. (2000) *J. Biol. Chem.* **275**, 31422–31427.
8. Overall, C. M., McQuibban, G. A. & Clark-Lewis, I. (2002) *Biol. Chem.* **383**, 1059–1066.
9. McQuibban, G. A., Gong, J. H., Tam, E. M., McCulloch, C. A., Clark-Lewis, I. & Overall, C. M. (2000) *Science* **289**, 1202–1206.
10. Overall, C. M., Wiebkin, O. W. and Thonard, J. C. (1987) *J. Periodont. Res.* **22**, 81–88.
11. Hughes, C. E., Caterson, B., Fosang, A. J., Roughley, P. J. & Mort, J. S. (1995) *Biochem. J.* **305**, 799–804.
12. Lopéz-Otín, C. & Overall, C. M. (2002) *Nat. Rev. Mol. Cell Biol.* **3**, 509–519.
13. Guo, L., Eisenman, J. R., Mahimkar, R. M., Peschon, J. J., Paxton, R. J., Black, R. A. & Johnson, R. S. (2002) *Mol. Cell. Proteomics* **1**, 30–36.
14. Abersold, R. & Mann, M. (2003) *Nature* **422**, 198–207.
15. De Leenheer, A. P. & Thienpont, L. M. (1992) *Mass Spectrom. Rev.* **11**, 249–307.
16. Gygi, S. P., Rist, B., Gerber, S. A., Turecek, F., Gelb, M. H. & Aebersold, R. (1999) *Nat. Biotechnol.* **17**, 994–999.
17. Nagase, H. & Woessner, J. F. (1999) *J. Biol. Chem.* **274**, 21491–21494.
18. Holmbeck, K., Bianco, P., Caterina, J., Yamada, S., Kromer, M., Kuznetsov, S. A., Mankani, M., Robey, P. G., Poole, A. R., Pidoux, I., *et al.* (1999) *Cell* **99**, 81–92.
19. Seiki, M. (2003) *Cancer Lett.* **194**, 1–11.
20. Ohuchi, E., Imai, K., Fujii, Y., Sato, H., Seiki, M. & Okada, Y. (1997) *J. Biol. Chem.* **272**, 2446–2451.
21. Tam, E. M., Wu, Y. I., Butler, G. S., Stack, M. S. & Overall, C. M. (2002) *J. Biol. Chem.* **277**, 39005–39014.
22. Sato, H., Takino, T., Okada, Y., Cao, J., Shinagawa, A., Yamamoto, E. & Seiki, M. (1994) *Nature* **370**, 61–65.
23. Morrison, C. J., Butler, G. S., Bigg, H. F., Roberts, C. R., Soloway, P. D. & Overall, C. M. (2001) *J. Biol. Chem.* **276**, 47402–47410.
24. Clark-Lewis, I., Vo, L., Owen, P. & Anderson, J. (1997) *Methods Enzymol.* **287**, 233–250.
25. Bigg, H. F., Morrison, C. J., Butler, G. S., Bogoyevitch, M. A., Wang, Z., Soloway, P. D. & Overall, C. M. (2001) *Cancer Res.* **61**, 3610–3618.
26. Zhang, K., McQuibban, G. A., Silva, C., Butler, G. S., Johnston, J. B., Holden, J., Clark-Lewis, I., Overall, C. M. & Power, C. (2003) *Nat. Neurosci.* **6**, 1064–1071.
27. Balbín, M., Fueyo, A., Tester, A. M., Pendás, A. M., Pitiot, A. S., Astudillo, A., Overall, C. M., Shapiro, S. & López-Otín, C. (2003) *Nat. Genet.* **35**, 252–257.
28. Van den Steen, P. E., Proost, P., Wuyts, A., Van Damme, J. & Opdenakker, G. (2000) *Blood* **96**, 2673–2681.
29. Pan, G., Bauer, J. H., Haridas, V., Wang, S., Liu, D., Yu, G., Vincenz, C., Aggarwal, B. B., Ni, J. & Dixit, V. M. (1998) *FEBS Lett.* **431**, 351–356.
30. Haro, H., Crawford, H. C., Fingleton, B., Shinomiya, K., Spengler, D. M. & Matrisian, L. M. (2000) *J. Clin. Invest.* **105**, 143–150.
31. Brigstock, D. R. (1999) *Endocr. Rev.* **20**, 189–206.
32. Olson, T. S. & Ley, K. (2002) *Am. J. Physiol.* **283**, R7–R28.
33. Ashcroft, G. S., Lei, K., Jin, W., Longenecker, G., Kulkarni, A. B., Greenwell-Wild, T., Hale-Donze, H., McGrady, G., Song, X. Y. & Wahl, S. M. (2000) *Nat. Med.* **6**, 1147–1153.
34. Van Damme, J., Decock, B., Conings, R., Lenaerts, J. P., Opdenakker, G. & Billiau, A. (1989) *Eur. J. Immunol.* **19**, 1189–1194.
35. Henry, M. T., McMahon, K., Costello, C., Fitzgerald, M. X. & O'Connor, C. M. (2002) *Exp. Lung Res.* **28**, 85–97.
36. Grutter, M. G., Fendrich, G., Huber, R. & Bode, W. (1988) *EMBO J.* **7**, 345–351.
37. Belkin, A. M., Akimov, S. S., Zaritskaya, L. S., Ratnikov, B. I., Deryugina, E. I. & Strongin, A. Y. (2001) *J. Biol. Chem.* **276**, 18415–18422.
38. Schlondorff, J., Lum, L. & Blobel, C. P. (2001) *J. Biol. Chem.* **276**, 14665–14674.
39. Black, R. A., Rauch, C. T., Kozlosky, C. J., Peschon, J. J., Slack, J. L., Wolfson, M. F., Castner, B. J., Stocking, K. L., Reddy, P., Srinivasan, S., *et al.* (1997) *Nature* **385**, 729–733.
40. Moss, M. L., Jin, S. L., Milla, M. E., Bickett, D. M., Burkhart, W., Carter, H. L., Chen, W. J., Clay, W. C., Didsbury, J. R., Hassler, D., *et al.* (1997) *Nature* **385**, 733–736.
41. Hashimoto, G., Inoki, I., Fujii, Y., Aoki, T., Ikeda, E. & Okada, Y. (2002) *J. Biol. Chem.* **277**, 36288–36295.
42. Ball, D. K., Surveyor, G. A., Diehl, J. R., Steffen, C. L., Uzumcu, M., Mirando, M. A. & Brigstock, D. R. (1998) *Biol. Reprod.* **59**, 828–835.
43. Kireeva, M. L., Latinkic, B. V., Kolesnikova, T. V., Chen, C., Yang, G., Abler, A. & Lau, L. F. (1997) *Exp. Cell Res.* **233**, 63–77.
44. Egeblad, M. & Werb, Z. (2002) *Nat. Rev. Cancer* **2**, 161–174.

THE JOURNAL OF BIOLOGICAL CHEMISTRY
Vol. 278, No. 40, Issue of October 3, pp. 38707–38714, 2003
Printed in U.S.A.

Crucial Role of the Specificity-determining Loop of the Integrin β_4 Subunit in the Binding of Cells to Laminin-5 and Outside-in Signal Transduction*

Received for publication, February 14, 2003, and in revised form, July 1, 2003
Published, JBC Papers in Press, July 16, 2003, DOI 10.1074/jbc.M301637200

Daisuke Tsuruta‡, Susan B. Hopkinson‡, Kimberly D. Lane, Michael E. Werner, Vincent L. Cryns, and Jonathan C. R. Jones§

From the Departments of Cell and Molecular Biology and Medicine, Feinberg School of Medicine at Northwestern University, Chicago, Illinois 60611

Within each hemidesmosome, $\alpha_6\beta_4$ integrin plays a crucial role in hemidesmosome assembly by binding to laminin-5 in the basement membrane zone of epithelial tissue. Recent analyses have implicated "specificity-determining loops" (SDLs) in the I-like domain of β integrin in regulating ligand binding. Here, we investigated the function of an SDL-like motif within the extracellular I-like domain of β_4 integrin. We generated point mutations within the SDL of β_4 integrin tagged with green fluorescent protein (GFP-β_4K150A and GFP-β_4Q155L). We also generated a mutation within the I-like domain of the β_4 integrin, lying outside the SDL region (GFP-β_4V284E). We transfected constructs encoding the mutated β_4 integrins and a GFP-conjugated wild type β_4 integrin (GFP-β_4WT) into 804G cells, which assemble hemidesmosomes, and human endothelial cells, which express little endogenous β_4 integrin. In transfected 804G cells, GFP-β_4WT and GFP-β_4V284E colocalize with hemidesmosome proteins, whereas hemidesmosomal components in cells expressing GFP-β_4K150A and GFP-β_4Q155L are aberrantly localized. In endothelial cells, GFP-β_4WT and mutant proteins are co-expressed at the cell surface with α_6 integrin. When transfected endothelial cells are plated onto laminin-5 matrix, GFP-β_4WT and GFP-β_4V284E localize with laminin-5, whereas GFP-β_4K150A and GFP-β_4Q155L do not. GFP-β_4WT and GFP-β_4V284E expressed in endothelial cells associate with the adaptor protein Shc when the cells are stimulated with laminin-5. However, GFP-β_4K150A and GFP-β_4Q155L fail to associate with Shc even when laminin-5 is present, thus impacting downstream signaling. These results provide evidence that the SDL segment of the β_4 integrin subunit is required for ligand binding and is involved in outside-in signaling.

Integrins are members of a family of cell surface receptor proteins involved in cell-matrix and cell-cell interactions (1, 2). A primary function of many integrins is to adhere cells to extracellular matrix molecules and to provide a structural link between the outside of the cell and the cytoskeleton (1–3). In addition, integrins mediate inside-out and outside-in signaling pathways, thereby regulating growth, differentiation, and migration of cells during development, wound healing, and in a variety of pathological conditions including tumor metastasis (4).

Each integrin is a heterodimer containing an α and a β subunit. At present 18 α and 8 β subunits have been identified, which combine to form 24 integrins (1, 2). Both subunits have large extracellular amino-terminal domains, single membrane-spanning regions, and short cytoplasmic tails of about 50 residues that interact with components of the microfilament cytoskeleton system (1, 2). One notable exception is the β_4 integrin subunit, whose cytoplasmic domain comprises over 1000 amino acids. It links to the keratin intermediate filament network at the site of hemidesmosomes in certain epithelial tissues via interaction with a transmembrane molecule of 180 kDa (BP180), a cytoplasmic structural protein of 230 kDa (BP230) and the cytoskeletal linker protein plectin (5, 6).

The binding of integrins to their extracellular ligands triggers outside-in signaling events that may include activation of tyrosine, serine/threonine, and lipid kinases as well as small GTP-binding proteins, including RhoA, RacI, and Cdc42 (4). Activation of these signaling pathways can lead to a variety of responses in the cell, including changes in cytoskeletal organization, cell division, differentiation, and apoptosis. Conversely, intracellular signals are believed to trigger conformational changes in the cytoplasmic domains of an integrin that are transmitted along the molecule to its extracellular domain. These conformational changes appear to regulate the affinity of integrins for their ligands (2).

Recent structural data, including crystallographic analyses, have shed new light onto how integrins bind ligand, how ligand-binding specificity is accomplished, and how signals are transmitted by integrin molecules across the membrane (2). For example, the extracellular domains of several of the α integrin subunits contain an "inserted" sequence, the I or A domain, of about 200 amino acids, that has been implicated in ligand binding (2). The β integrin subunit also possesses an extracellular I-like domain within which a short sequence of about 30 residues appears to specify ligand binding. This 30-residue domain has been termed the specificity-determining loop (SDL).[1] In particular, Takagi *et al.* (7) have shown that removal of the SDL blocks the ability of the $\alpha_5\beta_1$ integrin to bind its ligand, fibronectin. Moreover, when a seven-residue sequence contained within the SDL of β_1 integrin is switched

* This work is supported by National Institutes of Health Grant RO1(24) DK60589 (to J. C. R. J.). The costs of publication of this article were defrayed in part by the payment of page charges. This article must therefore be hereby marked "*advertisement*" in accordance with 18 U.S.C. Section 1734 solely to indicate this fact.

‡ These two authors contributed equally to this work.

§ To whom correspondence should be addressed: Dept. of Cell and Molecular Biology, Morton 4-616, Feinberg School of Medicine at Northwestern University, 303 E. Chicago Ave., Chicago, IL 60611. Tel.: 312-503-1412; Fax: 312-503-6475; E-mail: j-jones3@northwestern.edu.

[1] The abbreviations used are: SDL, specificity-determining loop; GFP, green fluorescent protein; TrHBMEC, transformed human bone marrow endothelial cells; PBS, phosphate-buffered saline; WT, wild type.

with a comparable sequence in β_3 integrin, ligand binding specificity of the mutated integrin is altered (8). In addition, the SDLs of the β_1 and β_2 integrin subunit appear to play an essential role in heterodimerization with specific α integrin subunits (namely $\alpha_6\beta_1$, $\alpha_v\beta_1$, and $\alpha_1\beta_2$) (7).

The SDL of the β_4 integrin does not appear to play a role in mediating its interaction with its α_6 integrin (7), its only known partner (1, 2). The $\alpha_6\beta_4$ integrin heterodimer is primarily expressed in epithelial cells and plays an essential role in the assembly of hemidesmosomes, certain matrix adhesion devices that stabilize the interaction of epithelia with the underlying connective tissue (5, 6, 9). The importance of the $\alpha_6\beta_4$ integrin in the adhesion of epithelial cells to the basement membrane is underscored by the blistering that occurs at the dermal-epidermal border in the skin of patients afflicted with junctional epidermolysis bullosa associated with pyloric atresia, in which expression of $\alpha_6\beta_4$ integrin is aberrant, and in genetically engineered mice in which expression of α_6 or β_4 integrin protein is inactivated by targeted disruption (5, 6, 10–12). The ligand of integrin $\alpha_6\beta_4$ is laminin-5, a major structural component of the basement membranes of epithelial tissues (5, 6). Indeed, the binding of $\alpha_6\beta_4$ integrin and laminin-5 is a necessary prerequisite to certain epithelial cell adhesion, migration, and morphogenetic events (5, 6). Yet, despite this importance, structural and molecular characterization of regions that regulate $\alpha_6\beta_4$ integrin binding to laminin-5 have not been investigated. Takagi *et al.* (7) have suggested that the SDLs of all β integrin subunits are involved in regulating ligand binding. However, to date no studies have addressed whether the SDL of β_4 integrin modulates $\alpha_6\beta_4$ integrin/laminin-5 interaction. Hence, we have undertaken assays of the function of the SDL of β_4 integrin with regard to both ligand binding and transduction of outside-in signals.

MATERIALS AND METHODS

Cell Culture and Transfection—Cells of the rat bladder epithelial cell line 804G were cultured and transiently transfected as previously reported (13–15). Briefly, 804G cells were cultured at 37 °C in minimum essential medium containing a final concentration of 2 mM L-glutamine, 10% fetal bovine serum, 50 units/ml penicillin, and 50 units/ml streptomycin. Prior to transfection, 804G cells were maintained for 48 h on 22-mm glass coverslips or 100-mm plastic dishes. They were transfected with 8.8 μg of plasmid DNA using the calcium phosphate protocol detailed elsewhere (14, 15). Immortalized human bone marrow-derived endothelial cells (TrHBMECs) were maintained in Dulbecco's modified Eagle's medium containing a final concentration of 2 mM L-glutamine, 10% fetal bovine serum, 50 units/ml penicillin, and 50 units/ml streptomycin and 1× RPMI 1640 vitamin solution (16). For transfection, TrHBMECs were trypsinized and resuspended in HEPES-buffered Dulbecco's modified Eagle's medium at about 1×10^6 cells/ml. The cells were electroporated with DNA at 950 microfarads, 196 ohms, and 210 V in a BTX Electro Cell Manipulator 600 (BTX, San Diego, CA) (17).

Construction of β_4 Integrin Wild Type Protein and Generation of Point Mutations—A mammalian expression vector encoding the sequence of the green fluorescent protein (GFP) fused to a full-length human integrin β_4 subunit (GFP-hβ_4WT) was described elsewhere (15). Point mutations were generated in the β_4 integrin sequence in this vector using the QuikChange XL site-directed mutagenesis kit from Stratagene (La Jolla, CA) following the procedure of the manufacturer. Plasmids were used to transform XL10-Gold Ultracompetent Cells (Stratagene), which were then plated on selective media and incubated overnight at 37 °C. DNA was prepared from the resultant colonies using the Wizard Plus Miniprep DNA Purification System (Promega, Madison, WI) and sequenced using Big Dye chemistry on an ABI Prism automated sequencer (Applied Biosystems, Foster City, CA) to confirm the presence of the appropriate point mutation. Plasmid DNA was purified by equilibrium centrifugation in $CsCl_2$-ethidium bromide gradient and was used to transform mammalian cells as described above.

Antibodies—Mouse monoclonal antibodies against GFP (clones 7.1 and 13.1), the dephosphorylated light chain of α_6 integrin subunit (4E9G8), and the β_4 integrin subunit (3E1) were purchased from Roche Applied Science, Immunotech (Marseille, France), and Chemicon International (Temecula, CA), respectively. 5E, a human monoclonal antibody against BP230, was a gift from Dr. Takashi Hashimoto (Kurume University, Fukuoka, Japan). Antibody 5C5 against the α_3 chain of laminin-5 was described previously (18, 19). Monoclonal antibodies against BP180 were characterized previously (13). The polyclonal anti-Shc antibody was purchased from Transduction Laboratories (Lexington, KY). Secondary antibodies conjugated to rhodamine or horseradish peroxidase were purchased from Jackson ImmunoResearch Laboratories, Inc. (West Grove, PA). Protein G-agarose was bought from Invitrogen. Plectin antibody 7A8 was obtained from Sigma, and the phosphotyrosine antibodies 4G10 and PY20 were purchased from Upstate Biotechnology, Inc. (Lake Placid, NY) and Transduction Laboratories, respectively.

Matrix Proteins—The laminin-5-rich matrix of 804G cells was prepared as described previously (18). In brief, 804G cells were plated onto either glass coverslips or 100-mm dishes and allowed to reach confluence. The culture medium was removed, and the cells were washed in sterile PBS. Cells were removed from their matrix by treatment for 10 min in sterile 20 mM NH_4OH. Any remaining cells were removed by three washes with sterile PBS.

Immunoblotting and Immunoprecipitation Protocols—For immunoblotting, confluent cell cultures of 804G cells and TrHBMECs were solubilized in sample buffer consisting of 8 M urea, 1% SDS in 10 mM Tris-HCl, pH 6.8, 15% β-mercaptoethanol. Proteins were separated by SDS-PAGE, transferred to nitrocellulose, and processed for immunoblotting (20, 21). Nitrocellulose-bound antibodies were detected by chemiluminescence using the ECL kit (Amersham Biosciences).

Proteins were immunoprecipitated from 804G cells or TrHBMECs by first extracting the cells with immunoprecipitation buffer consisting of 25 mM HEPES, pH 7.5, 1% Brij 97, 150 mM NaCl, 5 mM $MgCl_2$, 0.2% SDS, supplemented with a protease inhibitor mixture and 1 mM orthovanadate (Sigma). Integrin or GFP antibodies were added to the extract and incubated at 4 °C for 2 h. Subsequently, protein G-agarose (Invitrogen) was added to the mix for an additional 2 h. The protein G-agarose was collected by centrifugation, washed three times in immunoprecipitation buffer, and then solubilized in Laemmli type SDS-PAGE sample buffer (20). The resulting protein solution was processed for Western immunoblotting as detailed above.

Flow Cytometry—Cells were trypsinized and resuspended in either PBS or tissue culture medium containing a 50% dilution of normal goat serum. The cell suspension was then incubated with the monoclonal antibody 3E1 for 45 min at room temperature. Cells were washed, and Cy5-conjugated goat anti-mouse IgG (Jackson ImmunoResearch) was added to each of the samples. Following a 45-min incubation at room temperature, stained cells were washed, resuspended in 0.5% formaldehyde, and then analyzed by flow cytometry using a Beckman Coulter Elite PCS sorter (Beckman Coulter, Miami, FL).

Immunofluorescence Microscopy—Cells on glass coverslips were fixed in 3.7% formaldehyde in PBS for 1 min at room temperature and then extracted for 8 min in 0.5% Triton X-100 in PBS at 4 °C. Antibody was overlaid onto the cells, and the preparations were incubated for 37 °C for 60 min. The cells on coverslips were washed in three changes of PBS and then overlaid with fluorochrome-conjugated secondary antibody, placed at 37 °C for an additional 60 min, washed extensively, and then mounted on slides. All preparations were viewed in a Zeiss laser-scanning microscope (LSM) 510 confocal microscope (Zeiss Inc., Thornwood, NY). Microscope images were exported as TIFF files, and figures were generated using Adobe Photoshop 7.0 software. At least 50 cells were examined for each experimental condition.

RESULTS

Comparison of the SDLs of β Integrin Subunits—Fig. 1 shows the alignment of a relatively conserved sequence of amino acids within the extracellular domain of β integrin subunits. This region is located within the I-like domain and contains the so-called SDL, which is proposed to regulate ligand interaction (7). The residues at the amino-flanking region of the SDLs of all of the β integrins share a high level of homology, each being FGXXVX. However, the sequences of the SDLs themselves show more diversity. Interestingly, all of the SDLs of β integrin subunits, with the exception of β_4, possess a short region of 5–8 amino acids flanked by cysteine residues, which, at least in β_2 integrin, appears to play an important role in regulating ligand binding (22) (Fig. 1).

The divergence of the sequence of the β_4 integrin SDL, par-

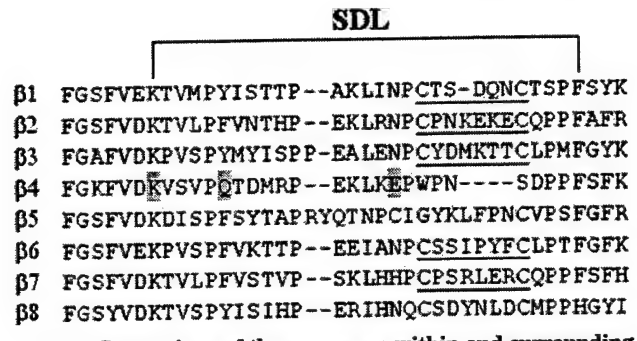

FIG. 1. **Comparison of the sequences within and surrounding the SDLs of β integrin subunits.** The putative sequence of each of the SDLs is demarcated by the *bracket*. The SDL of the β_4 integrin subunit spans residues 150–174. Note that, with the exception of the β_4 integrin subunit, cysteine residues border a series of between 5 and 8 residues (*underlined*) within each SDL. In our analyses, residues 150, 155, and 165 of the SDL of the β_4 integrin subunit were mutated (indicated by the *hatched boxes*).

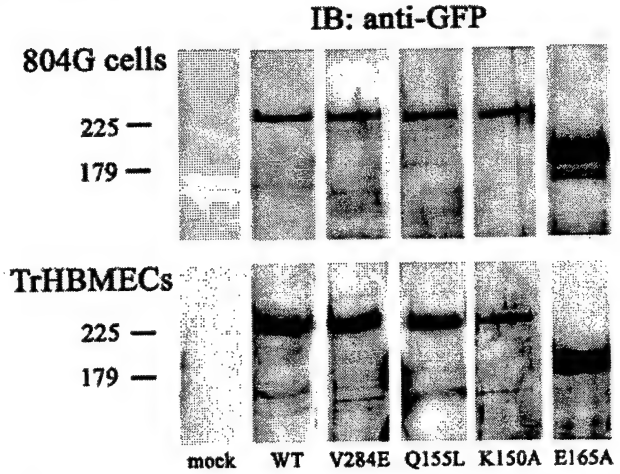

FIG. 2. **Western immunoblotting analysis of tagged β_4 integrin proteins.** Expression of GFP-tagged wild type and mutated β_4 integrin subunits in 804G cells (*upper panels*) and TrHBMECs (*lower panels*) was assessed by western immunoblotting of cell extracts using a GFP monoclonal antibody. The GFP antibody fails to recognize any polypeptides in mock-transfected cells (*lane mock*). In extracts derived from cells expressing GFP-β_4WT (*lane WT*), GFP-β_4V284E (*lane V284E*), GFP-β_4K150A (*lane K150A*), and GFP-β_4Q155L (*lane Q155L*), the GFP antibody recognizes a polypeptide of 227 kDa, whereas the same probe recognizes a 180-kDa polypeptide in extracts of cells expressing GFP-β_4E165A (*lane E165A*). Note that with the exception of extracts of cells expressing GFP-β_4E165A, comparable loadings of protein (20 μg) were loaded onto each lane. Approximately 50 μg of cells expressing GFP-β_4E165A was processed for immunoblotting (*IB*) in order to assess whether full-length tagged protein could be detected.

ticularly the absence of cysteine residues, motivated us to assess whether the β_4 integrin SDL is involved in the regulation of $\alpha_6\beta_4$ integrin binding to its ligand laminin-5 and, if so, to determine which residues are important in this pivotal function for a matrix receptor. To begin to do so, we first prepared a series of expression vectors encoding human GFP-tagged β_4 integrin subunit, in which residues within the SDL (residues 150, 155, and 165) or within the I-like extracellular domain of the β_4 integrin, which lies outside the SDL region (residue 284), were mutated (Fig. 1). We selected one conserved and two nonconserved residues within the β_4 integrin subunit SDL region for our mutational analyses. Each of the polar residues at positions 150, 155, and 165 was replaced by a small, nonpolar amino acid. We mutated residue 284 in the non-SDL region to a charged residue to increase the possibility of mutational effects. Constructs encoding the resulting tagged mutated proteins (GFP-β_4K150A, GFP-β_4Q155L, GFP-β_4E165A, and GFP-β_4V284E) as well as a GFP-tagged wild type β_4 integrin subunit (GFP-β_4WT) were transfected into either rat bladder 804G cells or immortalized TrHBMECs (16, 23). We chose 804G cells for this analysis, since they assemble mature hemidesmosomes *in vitro* and express all known hemidesmosome structural proteins (23). Thus, using this cell line, we would be able to assess the impact of expression of the mutated β_4 integrin subunits on the localization of other hemidesmosome proteins. In addition, an immortalized endothelial cell line was used in our studies, since these cells possess barely detectable levels of β_4 integrin subunit but express α_6 integrin, partnered with β_1 integrin as determined by fluorescence-activated cell sorting (see below) (24). Furthermore, when such endothelial cells are induced to express wild type β_4 integrin and are plated subsequently onto laminin-5-rich matrix derived from 804G cells, β_4 integrin clusters in the membrane at sites of cell-substratum interaction in a pattern that reflects the organization state of laminin-5 polymer on the substrate (25, 26) (see below). In other words, this endothelial cell model system provides a morphological readout of β_4 integrin subunit/ligand binding.

At 48 h following transfection of 804G cells and TrHBMECs with vectors encoding GFP-tagged wild type and mutated β_4 integrin subunits, extracts of the transfected cells were prepared for immunoblotting using an antibody against GFP to confirm expression of the appropriately sized protein (Fig. 2). Proteins of ~227 kDa are detected in extracts of the transfected cells using the GFP antibody probe with one exception. The GFP antibody recognizes a 180-kDa polypeptide in extracts of both 804G and endothelial cells expressing GFP-β_4E165A. This suggests that GFP-β_4E165A is subjected to proteolytic degradation, and, for this reason, we did not analyze this mutation further. We are currently investigating why this mutation makes the mutated β_4 integrin protein more susceptible to cleavage.

In transfected 804G cells and TrHBMECs, fluorescence-activated cell sorting analyses indicate that GFP-β_4WT, GFP-β_4K150A, GFP-β_4Q155L, and GFP-β_4V284E exist at the cell surface (Fig. 3*A* and Table I). Moreover, antibodies against human α_6 integrin subunit precipitate a 227-kDa protein recognized by anti-GFP antibodies in cells expressing GFP-tagged wild type and all of the mutated β_4 integrin subunit proteins (Fig. 3*B*). In addition, antibodies against GFP precipitate the integrin α_6 subunit from extracts of cells induced to express wild type and mutant human β_4 integrin subunits, confirming that wild type and all of our mutated GFP-tagged β_4 integrin subunits complex with α_6 integrin (Fig. 3*C*). We used antibody 4E9G8, which recognizes the 26-kDa light chain of the α_6 integrin subunit in these studies. In summary, these results confirm that all the tagged β_4 integrin proteins complex with α_6 integrin at the cell surface.

Expression of β_4 Integrin Subunit Protein Containing Point Mutations within the SDL and Its Impact on the Organization of Hemidesmosome Proteins in 804G Cells—We next assessed the fate of GFP-β_4WT, GFP-β_4K150A, GFP-β_4Q155L, and GFP-β_4V284E following their expression in 804G cells. GFP-β_4WT and GFP-β_4V284E localize in distinct cat paw arrays along the substratum-attached surface of transfected 804G cells (Fig. 4). This cat paw organization has been used by us as an indicator of hemidesmosome-like protein clusters (25–27). In contrast, in the majority of cells expressing GFP-β_4K150A and GFP-β_4Q155L, the GFP signal is diffusely distributed along the basal surface of the transfectants. We quantified these results by evaluating the localization of the four β_4 integrin proteins in at least 50 804G cells expressing each transgene protein product in multiple trials (Table II displays re-

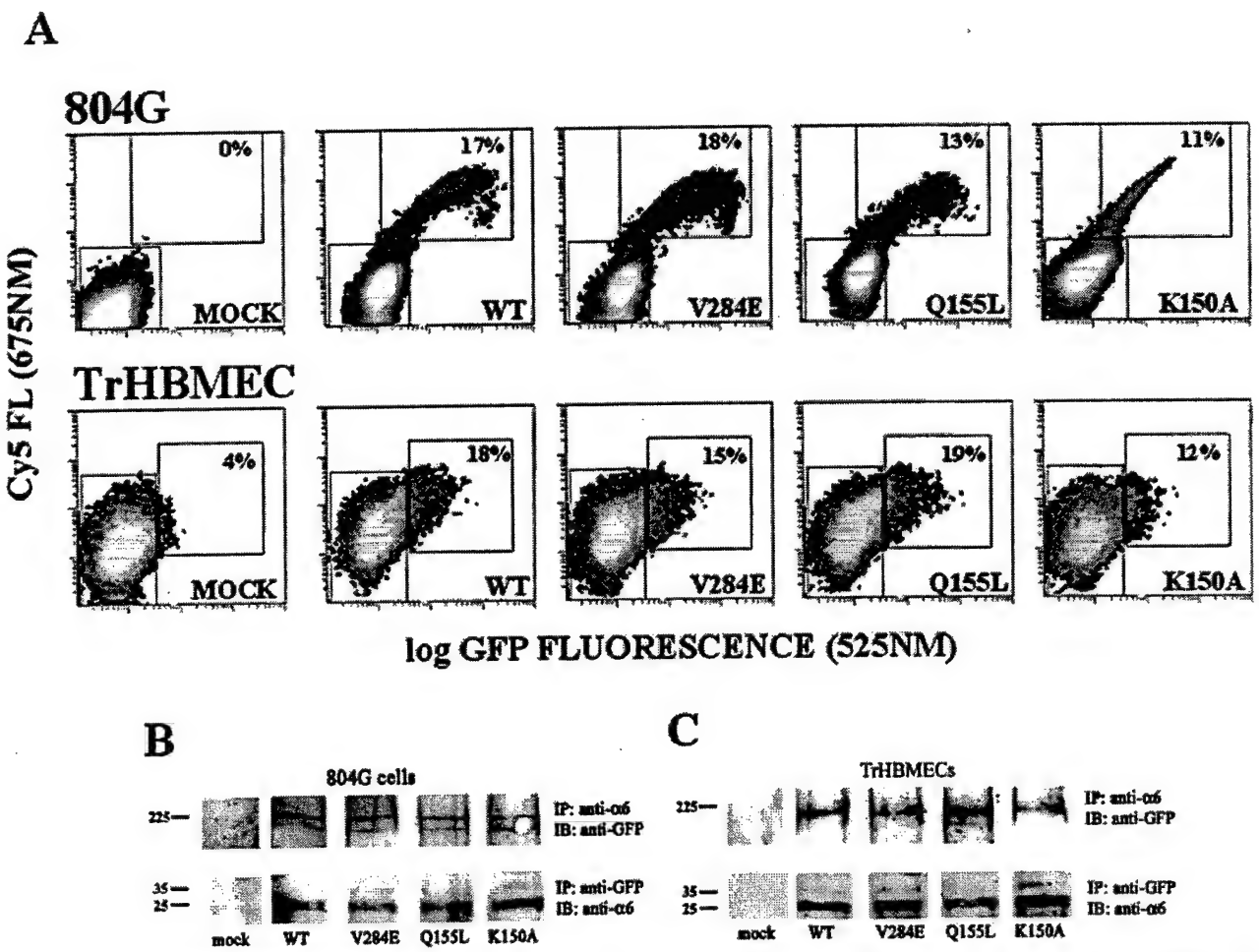

FIG. 3. **GFP-β_4 wild type and mutated integrin proteins are expressed at the cell surface with α_6 integrin in transfected 804G cells and TrHBMECs.** *A*, mock-transfected rat 804G cells (*upper row*) and TrHBMECs (*lower row*) or cells expressing GFP-β_4WT (*WT*), GFP-β_4V284E, GFP-β_4Q155L, and GFP-β_4K150A were prepared for fluorescence-activated cell sorting using antibody 3E1, which recognizes an extracellular epitope of the human β_4 integrin subunit and which does not recognize rat protein. *B* and *C*, sorting profiles were plotted according to fluorescence intensity for GFP (*x axis*) and Cy5 (*y axis*). *Left boxes* represent base-line fluorescence for the negative population of mock-transfected cells. *Boxes* on the *right* depict cells displaying fluorescence for both GFP and Cy5. The percentage of such double-positive cells is indicated in each *box*. Extracts of mock-transfected 804G cells (*B*) and TrHBMECs (*C*) or cells expressing GFP-β_4WT, GFP-β_4V284E, GFP-β_4Q155L, and GFP-β_4K150A (*lanes* marked *WT*, *V284E*, *Q155L*, and *K150A*) were processed for immunoprecipitation (*IP*) using either antibody 4E9G8 against the α_6 integrin light chain subunit (*upper panels*) or GFP antibody (*lower panels*). The precipitated proteins were prepared for immunoblotting (*IB*) using the GFP monoclonal antibody (*upper panels*) or 4E9G8 antibody (*lower panels*). Note that antibody 4E9G8 precipitates a 227-kDa polypeptide recognized by the GFP probe in the *last four lanes* of the *upper panels* in *B* and *C*, whereas the GFP probe precipitates a 26-kDa polypeptide recognized by antibody 4E9G8 in the *last four lanes* of the *lower panels* in *B* and *C*. No proteins are recognized by either the antibodies against the α_6 integrin or GFP in the precipitates of the mock-transfected cells (*lanes* at the *left*).

sults from a representative trial). We scored the GFP signal in transfected cells as being in an extensive cat paw pattern (greater than 50% of the basal cell surface exhibits cat paw arrays), in a partial cat paw pattern (less than 50% of the basal cell surface exhibits cat paw arrays), or diffuse/spotty.

Next, populations of 804G cells expressing GFP-β_4WT protein and cells expressing the various mutated β_4 integrins were analyzed by immunofluorescence microscopy to assess the impact of the protein products of the transgene on the organization of the endogenous cytoplasmic, transmembrane, and matrix proteins of hemidesmosomes. Specifically transfected cell populations were probed with antibodies against BP230, plectin, BP180, and the α_3 laminin subunit of laminin-5. GFP-β_4WT and GFP-β_4V284E proteins distribute precisely with BP230, plectin, and BP180 in extensive cat paw arrays along the substratum attached surface in all transfected 804G cells we have analyzed (Fig. 5, *A*, *B*, and *C* and *E*, *F*, and *G*, respectively). GFP-β_4WT and GFP-β_4V284E protein also co-localize

TABLE I
Fluorescence-activated cell sorting analysis of 804G and TrHBMEC cells

The median fluorescence intensity for both GFP and Cy5 derived from the data in Fig. 3 is represented numerically. The values were gated on light scatter to include intact, homogenously distributed cells (excluding debris and cells with altered scatler) and then gated on the fluorescence value based on the mock-transfected, negative controls.

	804G				TrHBMEC			
	Left box		Right box		Left box		Right box	
Mock	Cy5	0.2	Cy5	0	Cy5	1.7	Cy5	4.7
	GFP	0.5	GFP	0	GFP	0.8	GFP	5.6
GFP-β_4WT	Cy5	0.6	Cy5	37.7	Cy5	2.7	Cy5	13.3
	GFP	1.2	GFP	20.7	GFP	0.9	GFP	8.8
GFP-β_4V284E	Cy5	0.5	Cy5	27.8	Cy5	2.3	Cy5	8.7
	GFP	1.4	GFP	23.8	GFP	0.8	GFP	8
GFP-β_4Q155L	Cy5	0.9	Cy5	20.8	Cy5	2.3	Cy5	11.1
	GFP	1.5	GFP	17.3	GFP	0.8	GFP	8.9
GFP-β_4K150A	Cy5	0.9	Cy5	18.7	Cy5	1.9	Cy5	7.8
	GFP	0.7	GFP	3.7	GFP	0.7	GFP	8

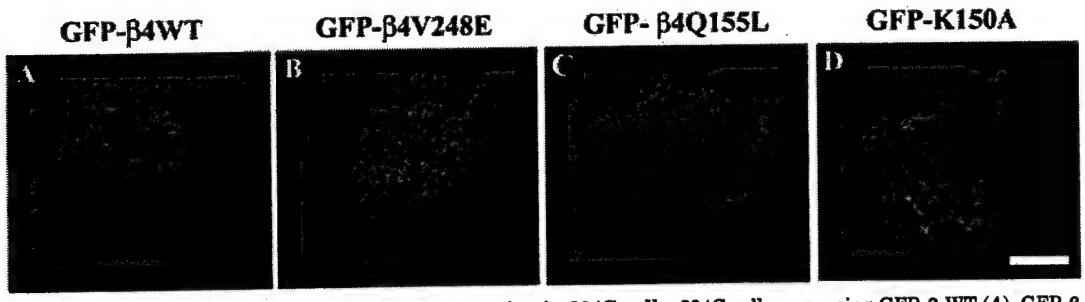

FIG. 4. **Expression of GFP-β_4 wild type and mutated integrins in 804G cells.** 804G cells expressing GFP-β_4WT (*A*), GFP-β_4V284E (*B*), GFP-β_4Q155L (*C*), and GFP-K150A (*D*) were visualized by confocal microscopy with the focal plane being at the substratum-attached surface of the cells. Note that in *A* and *B*, the GFP-tagged protein is organized into cat paw arrays, whereas in *C* and *D*, GFP-tagged protein appears primarily diffusely localized along the basal surface of the cells. *Bar*, 10 μm.

TABLE II

Localization of tagged β_4 integrin proteins in transfected 804G cells

Transfected cells were viewed by confocal microscopy, and the distribution of the transgene product was evaluated by focusing at the substratum-attached surface of the cells.

Protein	Percentage distribution
	%
GFP-β_4WT	
Extensive cat paw	95
Partial cat paw	5
Diffuse/spotty	0
GFP-β_4V284E	
Extensive cat paw	89
Partial cat paw	11
Diffuse/spotty	0
GFP-β_4K150A	
Extensive cat paw	14
Partial cat paw	28
Diffuse/spotty	58
GFP-β_4Q155L	
Extensive cat paw	6
Partial cat paw	43
Diffuse/spotty	51

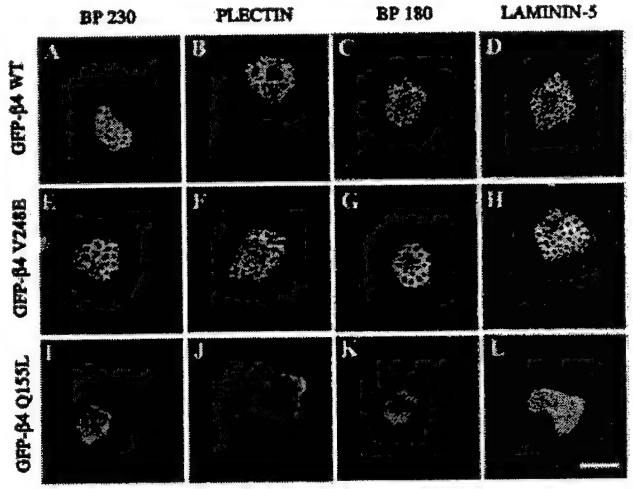

FIG. 5. **Impact of expression of GFP-β_4 wild type and mutated integrins on hemidesmosome protein localization in 804G cells.** 804G cells expressing GFP-β_4WT (*A–D*), GFP-β_4V284E (*E–H*), or GFP-β_4Q155L (*I–L*) protein were prepared for immunofluorescence microscopy using antibodies against BP230 (*A*, *E*, and *I*), plectin (*B*, *F*, and *J*), BP180 (*C*, *G*, and *K*), or the α_3 subunit of rat laminin 5 (*D*, *H*, and *L*). In each case, images of the GFP-tagged protein are shown overlaid on those generated by the antibodies. The *yellow color* indicates overlapping stain. In *I–L*, the *green color* shows lack of co-localization. Cells were viewed by confocal microscopy, and the focal plane for imaging is as close as possible to the substratum-attached surface of the cells. *Bar*, 10 μm.

with the α_3 laminin subunit in the extracellular matrix secreted by 804G cells (Fig. 5, *D* and *H*). In sharp contrast, in 804G cells expressing GFP-β_4K150A or GFP-β_4Q155L, the GFP-tagged proteins show minimal co-localization with other hemidesmosome proteins, and, in the majority of the same cells, the organization of BP230, plectin, and BP180 is also perturbed (Fig. 5, *I*, *J*, and *K*; only results where 804G cells are expressing GFP-β_4Q155L are shown) (Tables II and III). Although the degree of perturbation differs from cell to cell, in the majority of the transfected 804G cells, BP230, BP180, and plectin appear diffusely distributed or in a spotlike pattern (Fig. 5, *I*, *J*, and *K*). In all instances, expression of the mutated tagged β_4 integrin subunit had little, if any, impact on the organization of laminin-5 in the matrix of the transfected cells (Fig. 5*L*). At least 50 cells were counted for each condition in each trial, and these immunofluorescence observations are quantified in Table III. We assessed whether the endogenous plaque and transmembrane hemidesmosome proteins in cells expressing the tagged β_4 proteins organize into an extensive cat paw array or a partial cat paw array or appear diffusely/spottily distributed as above (Table III). These results indicate that both GFP-β_4K150A and GFP-β_4Q155L have a dominant negative impact on the ability of 804G cells to organize clusters of plaque and transmembrane hemidesmosome proteins.

Mutations in the β_4 Integrin SDL Inhibit the Interactions of $\alpha_6\beta_4$ Integrin and Laminin-5—Within 5 h of plating endothelial cells expressing GFP-β_4WT integrin onto laminin-5-rich matrix, GFP-β_4WT integrin clusters in the membrane at sites of cell-substratum interaction in a cat paw pattern that reflects

TABLE III

Localization of endogenous hemidesmosomal protein in transfected 804G cells

The organization of the endogenous hemidesmosomal proteins was evaluated by confocal microscopy in transfected cells.

	GFP-β4WT	GFP-β4V284E	GFP-β4K150A	GFP-β4Q155L
	%	%	%	%
BP230				
Extensive cat paw	85	89	8	4
Partial cat paw	15	11	21	32
Diffuse/spotty	0	0	71	64
Plectin				
Extensive cat paw	92	81	2	4
Partial cat paw	8	19	38	38
Diffuse/spotty	0	0	60	60
BP180				
Extensive cat paw	94	73	21	2
Partial cat paw	6	27	31	44
Diffuse/spotty	0	0	48	54

the organization of the laminin-5 on the substrate immediately underlying the transfected cell (18, 25) (Fig. 6, *A–C*). We used this *in vivo* morphological assay system to assess whether our

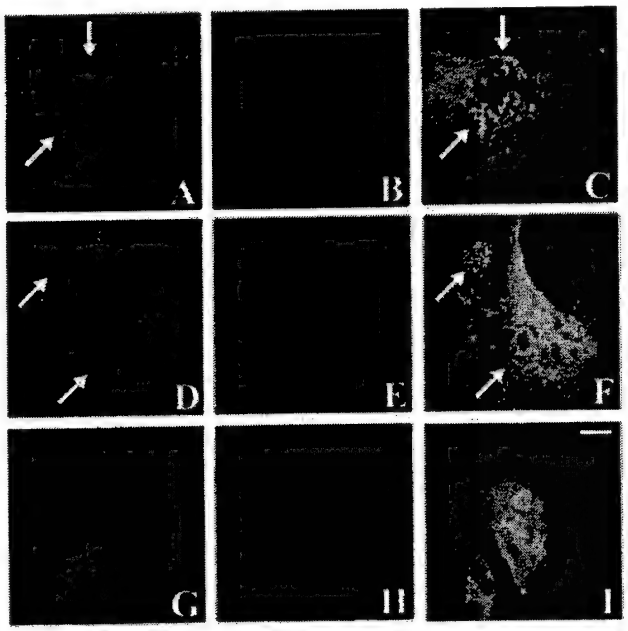

FIG. 6. **GFP-β_4 wild type and mutated integrin protein localization in endothelial cells plated onto a laminin-5-rich matrix.** TrHBMECs expressing GFP-β_4WT (*A–C*), GFP-β_4V284E (*D–F*), or GFP-β_4Q155L (*G–I*) were trypsinized and plated onto the laminin-5-rich matrix of 804G cells. At 5 h after plating, the samples were processed for immunofluorescence microscopy. The GFP signal from the cells is shown in *A*, *D*, and *G*. Localization of antibodies against the α_3 laminin subunit of laminin-5 is shown in *B*, *E*, and *H*. The *images* in the *two right panels* of each *row* were merged and are shown in *C*, *F*, and *I*, respectively. In *C* and *F*, there are numerous areas where GFP-tagged protein in transfected cells co-distributes in a cat paw arrangement that mirrors the stained laminin-5 matrix molecules immediately underlying the cells (*arrows*). In *I*, no cat paw arrays of GFP-tagged protein are observed, and there is no obvious co-distribution of mutated β_4 integrin subunit and the laminin-5 under the transfected cell. *Bar*, 5 μm.

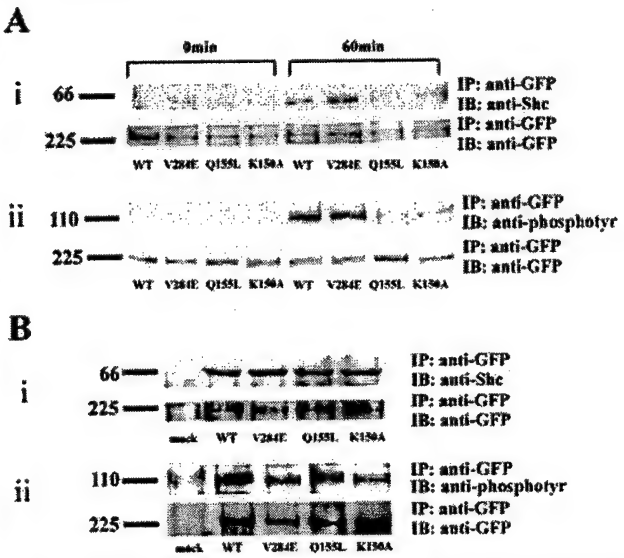

FIG. 7. **Signal transduction in endothelial cells mediated by wild type and mutated β_4 integrin subunit proteins.** *A*, mock-transfected endothelial cells and endothelial cells expressing GFP-β_4WT, GFP-β_4V284E, GFP-β_4Q155L, and GFP-β_4K150A were plated onto the laminin-5-rich matrix of 804G cells. At 0 and 60 min after plating, extracts of the cells were made and then processed for immunoprecipitation (*IP*) using GFP antibodies. The precipitated proteins were then subjected to immunoblotting (*IB*) using antibodies against Shc and GFP (*Ai*) or antibodies against phosphotyrosine and GFP (*Aii*). The GFP blots were performed to confirm successful precipitation of tagged β_4 integrin protein. In *B*, mock-transfected endothelial cells or endothelial cells express wild type, and the mutated β_4 integrin subunits were plated for 15 min onto β_4 antibody (3E1)-coated surfaces. Extracts of the cells were then subjected to immunoprecipitation (*IP*) using antibodies against GFP. The precipitates were then prepared for immunoblotting (*IB*) using antibodies against Shc and GFP (*Bi*) and antibodies against phosphotyrosine and GFP (*Bii*, as indicated).

mutated β_4 integrin proteins expressed in endothelial cells show co-distribution with organized laminin-5 arrays. Like GFP-β_4WT integrin, GFP-β_4V284E protein in transfected endothelial cells shows colocalization with laminin-5 matrix (Fig. 6, *D–F*). In sharp contrast, GFP-β_4K150A or GFP-β_4Q155L protein fails to co-distribute along endothelial cell-substratum adhesion sites in a pattern that mirrors that of laminin-5 in the matrix (Fig. 6, *G–I*; results for GFP-β_4Q155L only are shown).

Point Mutations in the β_4 Integrin SDL Impact Outside-in Signal Transduction—It has been established that ligand-induced clustering of β_4 integrin results in recruitment of the adapter protein Shc (28–30). Indeed, such outside-in signaling provides a measure of β_4 integrin/ligand interaction. Thus, to evaluate whether mutations in the SDL domain of the β_4 integrin subunit impact not only ligand interaction, as shown in Fig. 6, but, in so doing, interrupt outside-in signaling, we assayed the degree of Shc recruitment of wild type and mutated β_4 integrin when expressed in endothelial cells at 0 and 60 min after plating onto laminin-5-rich extracellular matrix. At each time point, β_4 integrin was precipitated from extracts of endothelial cells, and the precipitated protein was probed by immunoblotting using an antibody against Shc (Fig. 7*A*). GFP monoclonal antibody reactivity was used to confirm that tagged β_4 integrin was successfully precipitated. GFP-β_4WT and GFP-β_4V284E protein precipitated from transfected endothelial cells that had been maintained on a laminin-5-rich matrix for 60 min recruit the 66-kDa isoform of Shc (Fig. 7). In contrast, GFP-β_4K150A or GFP-β_4Q155L, which have been precipitated from transfected endothelial cells at 60 min after plating onto laminin-5-rich matrix do not do so. Moreover, during the course of these studies, we identified a 105-kDa endothelial cell protein that undergoes tyrosine phosphorylation only in the β_4 integrin precipitates derived from cells expressing GFP-β_4WT and GFP-β_4V284E but not from cells expressing GFP-β_4K150A or GFP-β_4Q155L (Fig. 7*A*). We have not yet determined the nature of this 105-kDa protein. Here we use its recognition by a phosphotyrosine antibody as a read-out of $\alpha_6\beta_4$ integrin-ligand interaction.

We also assayed the ability of wild type and mutated β_4 integrin to recruit Shc when $\alpha_6\beta_4$ integrin was clustered with the β_4 integrin monoclonal antibody 3E1. The 66-kDa isoform of Shc is clearly immunoprecipitated from extracts of endothelial cells expressing wild type and all of the mutated β_4 integrin subunits we analyzed within 15 min of plating the transfected cells onto a 3E1 antibody-coated surface (Fig. 7*B*). In addition, the β_4 integrin precipitates derived from such cells contain a 105-kDa tyrosine phosphorylated protein (Fig. 7*B*). Together these results indicate that the point mutations have no secondary, inhibitory effect on the ability of the cytoplasmic domain of β_4 integrin subunits to bind Shc protein and mediate signaling.

DISCUSSION

Recent structural analyses of integrin heterodimers, primarily of the $\alpha_v\beta_3$ integrin, have provided new clues to the structural basis and regulation of integrin-ligand binding. For example, the N-terminal halves of both the α and β integrin subunits comprise the region that binds ligand (2, 31). Binding of this region to ligand is regulated by a series of amino acids, termed the SDL, within the extracellular domain of the β integrin subunit (2, 31–33). In particular, Takagi *et al.* have reported that a motif, composed of CYDMKTTC, within the

SDL of the β_3 integrin subunit sequence is critically involved in specifying ligand binding of integrin $\alpha_v\beta_3$ (8). Moreover, a series of eight residues (CPNKEKEC) within the SDL region of the β_2 integrin subunit regulates binding of the $\alpha_L\beta_2$ heterodimer to its ligand (22).

In this work, we studied the functions of the I-like region in the β_4 integrin SDL. To do so, we generated point mutations in the SDL and in the α_5 extracellular domain of the β_4 integrin subunit. Wild type and mutated β_4 integrin subunits were then expressed in 804G cells or an immortalized endothelial cell type. In both cell types, wild type and mutated β_4 integrin is expressed at the cell surface and partners with α_6 integrin. In addition, point mutations within the β_4 subunit SDL have no impact on $\alpha_6\beta_4$ integrin heterodimer assembly. This is consistent with previous work showing that the SDLs of β_4, β_1, and β_3 integrin are not required for formation of $\alpha_6\beta_4$, $\alpha_5\beta_1$, $\alpha_4\beta_1$, and $\alpha_v\beta_3$ integrin complexes (7). In contrast, the SDLs of the β_1 and β_2 integrin subunits do appear to play an essential role in heterodimer formation with their α integrin partners (namely $\alpha_6\beta_1$, $\alpha_v\beta_1$, and $\alpha_l\beta_2$) (7).

We used endothelial cells to assess the ability of the β_4 integrin subunit-containing integrin complexes to interact with laminin-5 ligand. We did so by plating endothelial cells expressing wild type or mutated β_4 integrins onto the laminin-5-rich matrix secreted and organized by 804G cells into exquisite arrays on their substrate. Our analyses show that wild type β_4 integrin protein and β_4 integrin protein possessing a point mutation in a non-SDL region of the extracellular domain cluster in the endothelial cells in patterns that mirror the organized arrays of 804G cell laminin-5 to which they adhere. In sharp contrast, β_4 integrins that possess point mutations in their SDLs do not cluster and fail to organize in patterns that mimic the organization of laminin-5 ligand in the extracellular matrix. In other words, the SDL of β_4 integrin regulates $\alpha_6\beta_4$ integrin/laminin-5 interaction.

A number of mutations in the β_4 integrin extracellular domain have been linked to the pathogenesis of the blistering skin disease junctional epidermolysis bullosa. Most if not all of these mutations result in lack of expression of the protein. Interestingly, to date, no mutations in the SDL have been detailed. We suggest that expression of a β_4 subunit with mutations in its SDL may result in a more devastating phenotype than when no β_4 protein is produced at all. We provide some support for this, since we show that β_4 possessing mutations within its SDL act as dominant negatives in 804G cells.

Previous studies have shown that a chimeric β_4 integrin, whose extracellular domain has been replaced by the extracellular domain of the IL-2 receptor (*i.e.* a "headless" β_4 integrin), is able to cluster along sites of cell-substrate interaction and recruits plectin to such sites in a ligand-independent manner (34). Headless β_4 integrin also incorporates into formed hemidesmosome-like protein arrays in 804G cells and, unlike our mutated β_4 integrin, does not disrupt existing hemidesmosome-like structures (27, 34, 35). These and other results have led to a proposal that hemidesmosome assembly is driven primarily from within the cell (34, 35). These ideas, however, are not supported by the results we present here. Mutated β_4 integrin, which is incapable of binding ligand because of mutations in its SDL, destabilizes hemidesmosome protein arrays or prevents their assembly in 804G cells. Indeed, mutated β_4 integrin that does not interact with ligand acts as a "dominant negative" in transfected 804G cells and is not recruited into hemidesmosome-like protein arrays in either 804G cells or endothelial cells. How do we rationalize our results with those of Nievers *et al.* (34, 35)? We concur with the suggestion that headless β_4 integrin, which binds neither ligand nor α_6 integrin, is either "activated" via the action of intracellular regulators or is constitutively active and hence can both cluster and transduce signals when expressed as a chimeric or truncated protein at the cell surface (34–37). The data we present here, however, support the notion that "activation" of full-length wild type β_4 integrin by ligand is a necessary prerequisite to its incorporation into assembled and/or assembling hemidesmosome-like protein arrays, since mutated β_4 integrin (which fails to interact with ligand) does not cluster in endothelial cells. The latter provides support for the notion that ligand interaction is dominant in β_4 integrin activation, since intracellular regulators clearly fail to mediate clustering and "activation" of mutated β_4 integrin. That the cytoplasmic tail of the mutated β_4 integrin is in an "inactive" state of conformation is supported by those studies where we analyzed the ability of wild type and mutated β_4 integrin to mediate outside-in signaling. Mutated β_4 integrin only recruits the adaptor protein Shc to its cytoplasmic tail and mediates signaling that results in tyrosine phosphorylation of a 105-kDa protein when it is clustered by human β_4 integrin antibodies. Indeed, taken together, our results suggest that β_4 interaction with ligand on the outside of the cells has a dramatic impact on the binding properties of its cytoplasmic tail and is essential for outside-in signaling.

Since we also show that mutated β_4 integrin binds rat α_6 integrin, we suggest that mutated, "inactive" β_4 integrin partially or completely destabilizes hemidesmosome protein arrays in 804G cells by competing with endogenous wild type β_4 integrin for its α_6 partner. The degree of disruption induced by the mutated protein appears to reflect the amount of the protein product of the transgene expressed in the cells (not shown). In summary, our results support the idea that signals emanating from matrix on the outside of a cell predominate over cytoplasmic "cues" with regard to induction of hemidesmosome protein array assembly. This is consistent with the conclusions of some of our previous studies (18, 19, 38).

It is becoming clear that the diverse SDLs of β integrin subunits possess an essential role in regulating integrin function. The β_4 integrin subunit is no exception, since our findings emphasize the importance of its SDL in specifying ligand interaction, integrin clustering, and downstream signaling. Our data also imply that the activation of the cytoplasmic domain of the β_4 integrin is tightly controlled by its interaction with ligand. This phenomenon is all the more remarkable because of the size of the β_4 cytoplasmic tail, which is over 1000 amino acids. How signals emanating in the matrix influence the activation/conformation of this tail remains unclear, but we have provided the first evidence that the SDL is involved in regulating such signaling events.

Acknowledgment—We thank Mary Paniagua (Flow Cytometry Core Facility, Robert H. Lurie Comprehensive Cancer Center) for help and advice.

REFERENCES

1. Hynes, R. O. (1992) *Cell* **69**, 11–25
2. Hynes, R. O. (2002) *Cell* **110**, 673–687
3. Martin, K. H., Slack, J. K., Boerner, S. A., Martin, C. C., and Parsons, J. T. (2002) *Science* **296**, 1652–1653
4. Schwartz, M. A., and Ginsberg, M. H. (2002) *Nat Cell Biol.* **4**, E65–E68
5. Borradori, L., and Sonnenberg, A. (1999) *J. Invest. Dermatol.* **112**, 411–418
6. Jones, J. C. R., Hopkinson, S. B., and Goldfinger, L. E. (1998) *BioEssays* **20**, 488–494
7. Takagi, J., DeBottis, D. P., Erickson, H. P., and Springer, T. A. (2002) *Biochemistry* **41**, 4339–4347
8. Takagi, J., Kamata, T., Meredith, J., Puzon-McLaughlin, W., and Takada, Y. (1997) *J. Biol. Chem.* **272**, 19794–19800
9. Jones, J. C. R., Kurpakus, M. A., Cooper, H. M., and Quaranta, V. (1991) *Cell Regul.* **2**, 427–438
10. van der Neut, R., Krimpenfort, P., Calafat, J., Niessen, C. M., and Sonnenberg, A. (1996) *Nat. Genet.* **13**, 366–369
11. Dowling, J., Yu, Q.-C., and Fuchs, E. (1996) *J. Cell Biol.* **134**, 559–572
12. Georges-Labouesse, E., Messaddeq, N., Yehia, G., Cadalbert, L., Dierich, A., and Le Meur, M. (1996) *Nat. Genet.* **13**, 370–373

13. Riddelle, K. S., Hopkinson, S. B., and Jones, J. C. R. (1992) *J. Cell Sci.* **103,** 475–490
14. Hopkinson, S. B., Baker, S. E., and Jones, J. C. (1995) *J. Cell Biol.* **130,** 117–125
15. Tsuruta, D., Hopkinson, S. B., and Jones, J. C. R. (2003) *Cell Motil. Cytoskel.* **54,** 122–134
16. Schweitzer, K. M., Vicart, P., Delouis, C., Paulin, D., Drager, A. M., Langenhuijsen, M. M., and Weksler, B. B. (1997) *Lab. Invest.* **76,** 25–36
17. Tsuruta, D., Gonzales, M., Hopkinson, S. B., Otey, C., Khuon, S., Goldman, R. D., and Jones, J. C. (2002) *FASEB J.* **16,** 866–868
18. Langhofer, M., Hopkinson, S. B., and Jones, J. C. R. (1993) *J. Cell Sci.* **105,** 753–764
19. Baker, S. E., Hopkinson, S. B., Fitchmun, M., Andreason, G. L., Frasier, F., Plopper, G., Quaranta, V., and Jones, J. C. R. (1996) *J. Cell Sci.* **109,** 2509–2520
20. Laemmli, U. K. (1970) *Nature* **227,** 680–685
21. Harlow, E., and Lane, D. (1988) *Antibodies: A Laboratory Manual*, pp. 92–121, Cold Spring Harbor Laboratory, Cold Spring Harbor, NY
22. Kamata, T., Tieu, K. K., Tarui, T., Puzon-McLaughlin, W., Hogg, N., and Takada, Y. (2002) *J. Immunol.* **168,** 2296–2301
23. Riddelle, K. S., Green, K. J., and Jones, J. C. (1991) *J. Cell Biol.* **112,** 159–168
24. Gonzalez, A. M., Gonzales, M., Herron, G. S., Nagavarapu, U., Hopkinson, S. B., Tsuruta, D., and Jones, J. C. (2002) *Proc. Natl. Acad. Sci. U. S. A.* **99,** 16075–16080
25. Homan, S. M., Mercurio, A. M., and LaFlamme, S. E. (1998) *J. Cell Sci.* **111,** 2717–2728
26. Homan, S. M., Martinez, R., Benware, A., and LaFlamme, S. E. (2002) *Exp. Cell Res.* **281,** 107–114
27. Spinardi, L., Ren, Y.-L., Sanders, R., and Giancotti, F. G. (1993) *Mol. Biol. Cell* **4,** 871–884
28. Giancotti, F. G. (1999) *Nat. Cell Biol.* **2,** E13–E14
29. Mainiero, F., Pepe, A., Wary, K. K., Spinardi, L., Mohammadi, M., Schlessinger, J., and Giancotti, F. G. (1995) *EMBO J.* **14,** 4470–4481
30. Mainiero, F., Pepe, A., Yeon, M., Ren, Y., and Giancotti, F. G. (1996) *J. Cell Biol.* **134,** 241–253
31. Xiong, J.-P., Stehle, T., Diefenbach, B., Zhang, R., Dunker, R., Scoll, D. L., Joachimiak, A., Goodman, S. L., and Arnaout, M. A. (2001) *Science* **294,** 339–345
32. Takagi, J., Petre, B. M., Walz, T., and Springer, T. A. (2002) *Cell* **110,** 599–611
33. Tuckwell, D. S., Humphries, M. J. (1997) *FEBS Lett.* **400,** 297–303
34. Nievers, M. G., Schaapveld, R. Q. J., Oomen, L. C. J. M., Fontao, L., Geerts, D., Sonnenberg, A. (1998) *J. Cell Sci.* **111,** 1659–1672
35. Nievers, M. G., Kuikman, I., Geerts, D., Leigh, I. M., Sonnenberg, A. (2000) *J. Cell Sci.* **113,** 963–973
36. Spinardi, L., Einheber, S., Cullen, T., Milner, T. A., Giancotti, F. G. (1995) *J. Cell Biol.* **129,** 473–487
37. Trusolino, L., Bertotti, A., and Comoglio, P. M. (2001) *Cell* **107,** 643–654
38. Goldfinger, L. E., Stack, M. S., Jones, J. C. R. (1998) *J. Cell Biol.* **141,** 255–265

1: J Biol Chem. 2003 Oct 3;278(40):38707-14. Epub 2003 Jul 16.

Crucial role of the specificity-determining loop of the integrin beta4 subunit in the binding of cells to laminin-5 and outside-in signal transduction.

Tsuruta D, Hopkinson SB, Lane KD, Werner ME, Cryns VL, Jones JC.

Departments of Cell and Molecular Biology and Medicine, Feinberg School of Medicine at Northwestern University, Chicago, Illinois 60611, USA.

Within each hemidesmosome, alpha6beta4 integrin plays a crucial role in hemidesmosome assembly by binding to laminin-5 in the basement membrane zone of epithelial tissue. Recer analyses have implicated "specificity-determining loops" (SDLs) in the I-like domain of beta integrin in regulating ligand binding. Here, we investigated the function of an SDL-like mot within the extracellular I-like domain of beta4 integrin. We generated point mutations withir the SDL of beta4 integrin tagged with green fluorescent protein (GFP-beta4K150A and GFF beta4Q155L). We also generated a mutation within the I-like domain of the beta4 integrin, lying outside the SDL region (GFP-beta4V284E). We transfected constructs encoding the mutated beta4 integrins and a GFP-conjugated wild type beta4 integrin (GFP-beta4WT) into 804G cells, which assemble hemidesmosomes, and human endothelial cells, which express little endogenous beta4 integrin. In transfected 804G cells, GFP-beta4WT and GFP-beta4V284E colocalize with hemidesmosome proteins, whereas hemidesmosomal components in cells expressing GFP-beta4K150A and GFP-beta4Q155L are aberrantly localized. In endothelial cells, GFP-beta4WT and mutant proteins are co-expressed at the ce surface with alpha6 integrin. When transfected endothelial cells are plated onto laminin-5 matrix, GFP-beta4WT and GFP-beta4V284E localize with laminin-5, whereas GFP-beta4K150A and GFP-beta4Q155L do not. GFP-beta4WT and GFP-beta4V284E expressed in endothelial cells associate with the adaptor protein Shc when the cells are stimulated with laminin-5. However, GFP-beta4K150A and GFP-beta4Q155L fail to associate with Shc eve when laminin-5 is present, thus impacting downstream signaling. These results provide evidence that the SDL segment of the beta4 integrin subunit is required for ligand binding and is involved in outside-in signaling.

PMID: 12867433 [PubMed - indexed for MEDLINE]

THE JOURNAL OF BIOLOGICAL CHEMISTRY

Vol. 279, No. 26, Issue of June 25, pp. 27621–27632, 2004
Printed in U.S.A.

Neuronal Microtubule-associated Protein 2D Is a Dual A-kinase Anchoring Protein Expressed in Rat Ovarian Granulosa Cells*

Received for publication, March 17, 2004
Published, JBC Papers in Press, March 31, 2004, DOI 10.1074/jbc.M402980200

Lisa M. Salvador‡§, Maxfield P. Flynn‡, Jesús Avila¶, Scott Reierstad‡, Evelyn T. Maizels‡, Hena Alam‡, Youngkyu Park‡, John D. Scott‖, Daniel W. Carr, and Mary Hunzicker-Dunn‡ ‡‡**

*From the ‡Department of Cell and Molecular Biology, Northwestern University Feinberg School of Medicine, Chicago, Illinois 60611, **Veterans Affairs Medical Center and Oregon Health and Science University, Portland, Oregon 97201-3098, ¶Centro de Biologia Molecular "Severo Ochoa," Facultad de Ciencias, Universidad Autónoma de Madrid, Cantoblanco, 28049 Madrid, Spain, ‖Howard Hughes Medical Institute, Vollum Institute, Oregon Health and Science University, Portland, Oregon 97201-3098*

A-kinase anchoring proteins (AKAPs) function to target protein kinase A (PKA) to specific locations within the cell. AKAPs are functionally identified by their ability to bind the type II regulatory subunits (RII) of PKA in an *in vitro* overlay assay. We previously showed that follicle-stimulating hormone (FSH) induces the expression of an 80-kDa AKAP (AKAP 80) in ovarian granulosa cells as they mature from a preantral to a preovulatory phenotype. In this report, we identify AKAP 80 as microtubule-associated protein 2D (MAP2D), a low molecular weight splice variant of the neuronal MAP2 protein. MAP2D is induced in granulosa cells by dexamethasone and by FSH in a time-dependent manner that mimics that of AKAP 80, and immunoprecipitation of MAP2D depletes extracts of AKAP 80. MAP2D is the only MAP2 protein present in ovaries and is localized to granulosa cells of preovulatory follicles and to luteal cells. MAP2D is concentrated at the Golgi apparatus along with RI and RII and, based on coimmunoprecipitation results, appears to bind both RI and RII in granulosa cells. Reduced expression of MAP2D resulting from treatment of granulosa cells with antisense oligonucleotides to MAP2 inhibited the phosphorylation of cAMP-response element-binding protein. These results suggest that this classic neuronal RII AKAP is a dual RI/RII AKAP that performs unique functions in ovarian granulosa cells that contribute to the preovulatory phenotype.

Ovarian follicles house the oocyte and, upon maturation, produce steroid and protein hormones that regulate uterine receptivity and the reproductive axis. Follicles exist in a relatively dormant, preantral (PA)[1] state until they are recruited to grow and differentiate to a preovulatory (PO) phenotype by the pituitary hormone follicle-stimulating hormone (FSH) (1, 2). Maturation of follicles to a PO phenotype involves not only proliferation but also differentiation of the enclosed granulosa cells. FSH triggers these events by binding to its G-protein-coupled receptor, located exclusively on granulosa cells in female mammals, and activating adenylyl cyclase, which converts ATP to cAMP. cAMP then acts as a second messenger primarily by activating protein kinase A (PKA) (3).

PKA is a tetrameric enzyme that consists of a dimeric regulatory (R) subunit and two catalytic subunits (4). Upon binding of cAMP to the R subunits, a conformational change occurs that allows for dissociation of the active catalytic subunits, which can then phosphorylate neighboring substrates. Two classes of PKA holoenzymes, PKA I and PKA II, exist based on the association of two possible RI subunits (RIα and RIβ) or two possible RII subunits (RIIα and RIIβ) with four possible catalytic subunits (Cα, Cβ1, Cβ2, and Cγ) (5). In rat granulosa cells of PA and PO follicles, PKA IIα and PKA IIβ are the predominant PKA isoforms present, whereas less than 5% of PKA holoenzyme activity is contributed by PKA Iα (6–8).

The specificity of PKA action is accomplished by the targeting of PKA to specific cellular locales by virtue of its binding to a growing family of A-kinase anchoring proteins (AKAPs). Most known AKAPs anchor RII and exhibit at least a 100-fold lower affinity for RI (9). RII subunits of PKA bind with nanomolar affinity to AKAPs (5, 10). The domain on the AKAP responsible for RII binding comprises an amphipathic helix that binds to the N termini of the RII dimer (11). A growing number of "dual" AKAPs have been identified, although they still exhibit higher affinity for RII over RI (12–15). Recent reports, however, indicate that some AKAPs can preferentially bind RI (16–19). AKAPs anchor PKA to specific cellular locations, such as the actin cytoskeleton (20, 21), plasma membrane (22), mitochondria (23, 24), Golgi apparatus (25), centrosome (26), and nuclear envelope (27). The localization of PKA to distinct regions within the cell is generally thought to allow for both specific and efficient substrate phosphorylation in response to a specific stimulus (28).

FSH receptor signaling in PA granulosa cells stimulates the PKA-dependent phosphorylation of a number of signaling intermediates including histone H3 (29), cAMP-response element-binding protein (CREB) (30, 31), and an extracellular regulated kinase (ERK)-protein-tyrosine phosphatase that

* This work was funded by National Institutes of Health (NIH) Grant P01 HD21921 (to M. H. D.), a Veterans Affairs Merit Grant and NIH Grants HD36408 (to D. W. C.), and NIH Grant DK48239 (to J. D. S.). The costs of publication of this article were defrayed in part by the payment of page charges. This article must therefore be hereby marked "*advertisement*" in accordance with 18 U.S.C. Section 1734 solely to indicate this fact.

§ Present address: Center for Research in Reproduction and Women's Health, BRB II/II Rm. 1349A, 421 Curie Blvd., Philadelphia, PA 19104.

‡‡ To whom correspondence should be addressed: Northwestern University Medical School, 303 E. Chicago Ave., Chicago, IL 60611. Tel.: 312-503-8940; Fax: 312-503-0566; mhd@Northwestern.edu.

[1] The abbreviations used are: PA, preantral; AKAP, A-kinase anchoring protein; C subunit, catalytic subunit of PKA; CREB, cAMP-response element-binding protein; DEX, dexamethasone; DSP, dithiobis[succinimidylpropionate]; ERK, extracellular signal-regulated kinase; FSH, follicle-stimulating hormone; hCG, human chorionic gonadotropin; LH, luteinizing hormone; MAP2, microtubule-associated protein 2; NI, nonimmune; PKA, protein kinase A; PO, preovulatory; PMSG, pregnant mares serum gonadotropin; R subunit, PKA regulatory subunit; HA, hemagglutinin; DTT, dithiothreitol; PBS, phosphate-buffered saline.

leads to ERK activation (32). In addition, FSH receptor activation induces the transcription of a number of genes, including those for the luteinizing hormone (LH) receptor and inhibin-α as well as the P450 aromatase and side chain cleavage steroidogenic enzymes (33, 34). On the other hand, in granulosa cells of the PO follicle, LH receptor signaling causes an up-regulation in genes that encode for progesterone receptor and cyclooxgenase-2 while at the same time causing a down-regulation in genes that encode for the LH and FSH receptors, inhibin-α, and aromatase proteins (33, 35). Like FSH receptor signaling, LH receptor signaling also stimulates the PKA-dependent phosphorylation of key substrates such as histone H3, CREB, and an unidentified substrate upstream of ERK that leads to the activation of ERK (36). The fact that PKA plays a predominant role in the pleotrophic signaling events regulated by these hormones in PA *versus* PO granulosa cells led us to hypothesize that these cells may express different complements of AKAPs to localize PKA to distinct subcellular environments. In this report, we demonstrate that an 80-kDa AKAP that we previously showed is induced in ovarian granulosa cells by FSH (8, 37) is microtubule-associated protein 2D (MAP2D).

MAP2 is a microtubule- and microfilament-binding protein localized primarily to dendrites and to nonneuronal glial cells (38, 39). Most of the reports on MAP2 focus on its role in neurite outgrowth and dendrite development in the brain (40). MAP2 functions in the brain to stabilize microtubules, to stimulate microtubule assembly, and to regulate cell shape (41, 42). The MAP2 gene encodes high and low molecular weight protein isoforms that are generated by alternative splicing (43). MAP2A and MAP2B are high molecular mass isoforms (270 and 280 kDa, respectively), whereas MAP2C and MAP2D are low molecular mass isoforms (70 and 80 kDa, respectively) (44). The low molecular weight isoforms contain N- and C-terminal regions of the high molecular weight isoforms but lack the large central domain found in high molecular weight MAP2 isoforms. Each isoform contains at least three imperfect microtubule-binding domains in their C termini. MAP2D contains an additional 93-base pair insert, which comprises the fourth microtubule-binding domain that is absent from MAP2C (45, 46). MAP2 was the first protein to be recognized as an AKAP (47), and the RII-binding region was localized to amino acids 83–113 in the N-terminal region of the protein and is conserved among all MAP2 isoforms (48).

Our results show that the neuronal protein MAP2D is induced by FSH and localized to the granulosa cells of the PO follicle and that its expression is maintained in luteal cells following ovulation and corpus luteum formation. MAP2D appears to anchor both RI and RII to the Golgi apparatus in granulosa cells of PO follicles, and, based on antisense oligonucleotide experiments, MAP2D appears to participate in acute LH receptor signaling events. The function of MAP2D in ovarian granulosa cells is thus expected to be quite distinct from its established neuronal roles.

EXPERIMENTAL PROCEDURES

Materials—The following were purchased: ovine FSH (oFSH-20) from Dr. A. F. Parlow of the NIDDK, National Institutes of Health, National Hormone and Pituitary Program (Harbor-UCLA Medical Center, Torrance, CA); Profasi® hCG from Serono Laboratories Inc. (Randolph, MA); [γ-^{32}P]ATP, ammonium salt (3000 Ci/mmol), and [^{32}P]orthophosphate (~9000 Ci/mmol) from PerkinElmer Life Sciences; [2,8-^{3}H]cAMP sodium salt (15–40 Ci/mmol) from ICN Chemical and Radioisotope Division (Costa Mesa, CA); DEAE-cellulose (DE-52) and P-81 cellulose phosphate paper from Whatman (Clifton, NJ); ECL reagents, rainbow molecular weight markers, and Hybond-C nitrocellulose membranes from Amersham Biosciences; SDS-PAGE reagents from Bio-Rad; X-Omat AR film from Eastman Kodak Co.; all culture media from Invitrogen; brefeldin A from LC Laboratories (San Diego, CA); MAP2D scrambled and antisense oligonucleotides from Integrated DNA Technologies (Coralville, IA); MAP2D and glyceraldehyde-3-phosphate dehydrogenase PCR primers from Northwestern University Biotechnology Laboratory (Chicago, IL); DNase and reverse transcriptase-PCR reagents and buffers from Promega (Madison, WI); actin phalloidin from Molecular Probes, Inc. (Eugene, OR); and protein A+G-agarose from Santa Cruz Biotechnologies, Inc. (Santa Cruz, CA). All other biochemical reagents were purchased from Sigma, unless otherwise indicated.

Antibodies—Inhibin-α antibody was kindly provided by Dr. Wiley Vale of the Salk Institute for Biological Studies (San Diego, CA). The following were purchased: anti-MAP2 mouse monoclonal and anti-γ-tubulin from Sigma; anti-cyclin D2 polyclonal from Santa Cruz Biotechnologies; anti-PKA RI mouse monoclonal and anti-PKA RIIβ mouse monoclonal from BD Biosciences; anti-PKA RII (RIIα and -β) goat polyclonal and anti-phospho-CREB (S133) from Upstate Biotechnology, Inc. (Lake Placid, NY); goat anti-mouse rhodamine, goat anti-rabbit fluorescein, goat anti-rabbit rhodamine, donkey anti-goat rhodamine, donkey anti-mouse fluorescein, and goat anti-mouse fluorescein secondary antibodies from Jackson Immunochemicals (West Grove, PA); anti-Gm 130-fluorescein conjugate from BD Biosciences (Palo Alto, CA), and anti-hemagglutinin (HA) protein of human influenza virus from Roche Applied Science.

Primary Granulosa Cell Cultures—Sprague-Dawley rats were obtained at 15–18 days of age (Sasco, Baltimore, MD) and maintained in accordance with the National Institutes of Health Guide for the Care and Use of Laboratory Animals. Rats at 21–24 days of age were injected subcutaneously with either 1.5 mg/ml estrogen for 3 days to obtain PA ovaries or 10 IU of pregnant mares serum gonadotropin (PMSG) to obtain PO ovaries (harvested 48–50 h postinjection). Ovaries were trimmed to remove the bursa, fat, and oviducts and incubated for 15–30 min at 37 °C in 6 mM EGTA in Dulbecco's modified Eagle's medium/Ham's F-12 medium. Ovaries were then incubated for 5–20 min in 0.5 M sucrose in Dulbecco's modified Eagle's medium/Ham's F-12 medium. Granulosa cells from PA or PO ovaries were expressed by penetration of PA or large PO follicles, respectively, with a 30-gauge needle. The cells were plated at a density of 5–7 × 10^6 in serum-free Dulbecco's modified Eagle's medium/Ham's F-12 medium on plates coated with 0.5 μg/ml fibronectin (Invitrogen) and cultured as previously described (29, 37). Cells were treated the next day, as indicated under "Results."

Detergent-soluble Ovarian Extracts—21–24-Day-old Sprague-Dawley rats (Sasco) were not treated or were injected subcutaneously with 25 IU PMSG 48 h prior to injection with 25 IU hCG, as specified under "Results." Ovaries were harvested at various time points after injections; cooled to 4 °C in an iced 10 mM potassium phosphate buffer, pH 7.0; dissected free of bursa, fat, and oviducts; weighed; and homogenized (5:1 ratio of homogenization buffer/wet weight) in buffer A (10 mM potassium phosphate, pH 7.0, 1 mM EDTA, 5 mM EGTA, 10 mM $MgCl_2$, 50 mM β-glycerol phosphate, 1 mM sodium orthovanadate, 2 mM dithiothreitol (DTT), 40 μg/ml phenylmethylsulfonyl fluoride, 10 μg/ml E64, 0.5% Nonidet P-40, 0.1% deoxycholate) using 15–20 strokes with a ground glass homogenizer. A supernatant fraction was obtained by centrifugation at 10,000 × *g* for 10 min at 4 °C. Protein concentrations were determined by the Lowry protein assay (49) using bovine serum albumin as the standard.

Electrophoresis and Western Blotting—Total cell extracts were made by harvesting granulosa cells into 300 μl of SDS-PAGE sample buffer (50) and boiled. Protein concentrations were controlled by plating equal numbers of cells in each dish for each experiment followed by loading equal volumes onto an SDS-PAGE gel. These cells do not divide under serum-free conditions. The proteins in the cell extracts were separated by SDS-PAGE (51), electrotransferred to Hybond C-extra nitrocellulose overnight at 4 °C, and stained for protein loading using Ponceau S. The nitrocellulose blots were incubated with primary antibody at 4 °C overnight. Antigen-antibody complexes were detected using ECL.

DEAE-cellulose Chromatography and Sucrose Density Gradient Centrifugation—DEAE-cellulose chromatography was conducted as previously described (52), collecting fractions (~0.75 ml) in tubes containing 50 μl of a concentrated mixture of protease inhibitors (buffer B) at the indicated final concentrations: 10 mM benzamidine, 2 mM DTT, 5 μg/ml pepstatin, 10 μg/ml leupeptin, 5 μg/ml aprotinin, 40 μg/ml phenylmethylsulfonyl fluoride, 5 μg/ml soybean trypsin inhibitor, 10 μg/ml E-64. Protein kinase activity in DEAE fractions was determined in the presence of 0.5 μM cAMP and 71.5 μM Leu-Arg-Arg-Ala-Ser-Leu-Gly (Kemptide) as substrate (8). Total [^{3}H]cAMP binding sites on R subunits were determined by incubating sample with 0.3 μM [^{3}H]cAMP for 30 min at 30 °C (52). When indicated, DEAE-cellulose fractions (collected in the absence of DTT) were concentrated and subjected to sucrose density gradient centrifugation, as previously described (52), in the presence of

protease and phosphatase inhibitors. Following centrifugation, fractions were mixed with SDS-sample buffer, boiled, and subjected to SDS-PAGE and Western blotting.

RII Overlay Assay and cAMP-agarose Affinity Chromatography—Recombinant murine RIIα was expressed in *Escherichia coli* and purified by affinity chromatography on cAMP-Sepharose (53). For solid phase RII overlay assays, proteins were separated by SDS-PAGE and electrotransferred to Immobilon-P polyvinylidene difluoride (Millipore Corp.), and blots were probed with 0.5 μg of recombinant RIIα phosphorylated using [γ-^{32}P]ATP with the catalytic subunit of PKA and then subjected to autoradiography (54). For cAMP-agarose affinity chromatography, pooled and concentrated DEAE-cellulose fractions were added to cAMP-agarose (0.2-ml packed volume; Sigma) equilibrated in buffer C (10 mM Hepes, pH 7.0, 1 mM EDTA, 5 mM EGTA, 10 mM $MgCl_2$, 2 mM DTT, 10 μg/ml pepstatin, 10 μg/ml leupeptin, 5 μg/ml aprotinin, 10 μg/ml soybean trypsin inhibitor, 40 μg/ml phenylmethylsulfonyl fluoride, 1 mM sodium vanadate, 10 μM isobutylmethylxanthine, 20 mM benzamidine, and 10 μg/ml E-64) and incubated overnight at 4 °C on a Nutator (8). The flow-through fraction (~1.0 ml) was collected by centrifugation at 5000 × *g* for 5 min, an aliquot (0.1 ml) was diluted to 0.3 ml, mixed with 0.15 ml of 3-fold SDS-PAGE sample buffer, and boiled. The cAMP-agarose pellet was then washed three times by sequential centrifugations with a total of 3 ml of buffer C, three times with buffer C containing 1 M NaCl, and three times with buffer C containing 0.3 M NaCl, collecting an aliquot (0.3 ml) of the final 1.0-ml wash. cAMP-agarose was then incubated at room temperature for 30 min with 0.3 ml of 5 μM Ht31 peptide (residues 493–515) in buffer C containing 0.3 M NaCl, collecting eluate from agarose using a syringe followed by boiling after the addition of 3-fold SDS-PAGE sample buffer (0.15 ml). Finally, cAMP-agarose was incubated at room temperature for 30 min with 0.3 ml of 75 mM cAMP in buffer C containing 0.3 M NaCl, collecting eluate as described above.

RNA Isolation and Reverse Transcriptase-PCR—RNA was collected by lysing cultured granulosa cells in 1 ml of Trizol® reagent (Invitrogen) per 3 ml of medium according to the manufacturer's instructions. RNA (5 μg) was treated with DNase I (Promega) for 15 min at room temperature and heat-inactivated at 65 °C for 10 min. The reverse transcription reaction was performed using 2.5 μg of DNase-treated RNA and avian myeloblastosis virus reverse transcriptase (Promega) as described previously (55). PCR was performed using 500 ng of DNA using primers for MAP2 (forward, 5′-CAC AAG GAT CAG CCT GCA GCT CTG-3′; reverse, 5′-CAC CTG GCC TGT GAC GGA TGT TCT-3′) that generate a 756-base pair PCR product (45) or primers for glyceraldehyde-3-phosphate dehydrogenase (forward, 5′-CCCTTCATTGACCTCAACTA-3′; reverse, 5′-CCAAAGTTGTCATGGATGAC-3′) that generate a 350-bp PCR product (56). The PCR consisted of 24 cycles of 94 °C denaturation, 55 °C annealing, and 72 °C elongation steps. The reactions were analyzed on a 1.5% agarose gel containing ethidium bromide.

Immunofluorescence and Immunohistochemistry—For immunofluorescence analysis, granulosa cells from PA follicles were cultured on fibronectin-coated glass coverslips and treated as indicated under "Results." The cells were washed in phosphate-buffered saline (PBS), fixed for 10 min in 4% formaldehyde in PBS, and permeabilized with 0.1% Triton X-100. Coverslips were then washed three times with PBS and blocked for 1 h in 1% bovine serum albumin in PBS. Coverslips were incubated overnight at 4 °C in a humidified chamber with primary antibody at a 1:200 dilution (unless otherwise indicated). Coverslips were then washed three times with PBS, incubated for 2 h at 37 °C with secondary antibody conjugated to rhodamine or flourescein, as indicated, and washed three times with PBS. Coverslips were then allowed to dry and mounted onto glass slides using Vectashield® mounting medium (Vector Laboratories, Burlingame, CA). The slides were analyzed using a Zeiss LSM510 laser-scanning microscope.

For immunohistochemistry, whole ovaries were harvested in 4% paraformaldehyde, paraffin-embedded, sectioned at 4 μm onto glass slides, and subjected to enzyme-induced epitope retrieval immunohistochemistry according to the protocol developed by Northwestern University Robert H. Lurie Cancer Center Pathology Core (Chicago IL).

Immunoprecipitation—For immunoprecipitation of MAP2 from ovarian and brain extracts (see Fig. 3), extracts were prepared in buffer A and incubated with 10 μl of anti-MAP2 antibody and 30 μl of protein A+G-agarose for 4 h at 4 °C on a Nutator. The agarose was then washed with buffer D (20 mM Hepes, 150 mM NaCl, 10% glycerol, and 0.1% Triton-X). Proteins bound to the agarose were eluted by boiling in 50 μl of SDS-PAGE sample buffer. For PKA R subunit immunoprecipitations from ovarian extracts and DEAE fractions, samples (containing 500–800 μg of protein in ovarian extracts or 1 ml from pooled DEAE fractions collected in the absence of DTT) were incubated with 1 μM dithiobis[succinimidylpropionate] (DSP) (Pierce) in dimethyl sulfoxide for 15 min at room temperature. The cross-linking reaction was stopped by adding 1 M Tris-HCl, pH 7.5, to a final concentration of 25 mM and incubating samples at room temperature for 15 min. Antibody (10 μl of anti-MAP2 (Sigma), 25 μl of anti-RI (BD Biosciences), 20 μl of anti-RII (Upstate Biotechnology), 10 μl of anti-HA as a nonimmune (NI) control, 10 μl of anti-RIIβ (BD Biosciences Transduction Laboratories)) and 30 μl of protein A+G-agarose was added and incubated for 4 h at 4 °C. The agarose was then washed with buffer D. When indicated, proteins were eluted using Immunopure® elution buffer, pH 2.8, that contains a primary amine (Pierce) in three elution steps at 50 μl each for a total volume of 150 μl. Remaining proteins bound to agarose were eluted by boiling in 100 μl of SDS-PAGE sample buffer.

For MAP2D phosphorylation, PO granulosa cells from PMSG-treated rats were incubated for 1 h in phosphate-free medium and then incubated for 2 h in 1.25 mCi of $^{32}P_i$/6 × 10^6 cells. Cells were then treated with vehicle or hCG for 15 min and lysed in buffer A, and insoluble cell debris was removed by centrifugation at 10,000 × *g* for 2 min. Cell extracts were then incubated overnight with 10 μl of anti-MAP2 antibody or NI antibody plus 30 μl of protein A+G-agarose on a Nutator. Immunoprecipitates were washed with buffer D, mixed with SDS-PAGE sample buffer, and boiled, and proteins were separated by SDS-PAGE and subjected to autoradiography.

Antisense Oligonucleotide Transfection—Granulosa cells from PA follicles were plated in either 6-well or 60-mm plates coated with 100 ng/ml poly-L-lysine. Prior to hormone treatment, either a MAP2 antisense oligonucleotide (18-mer; CTC GTC AGC CAT CCT TCA) (41, 44) or a scrambled oligonucleotide (18-mer; ATT CCA GTA CGC TCC CCT), diluted in 10 mM Tris-HCl, pH 7.5, 1 mM EDTA buffer, was added to the cells at a concentration of 10 μg/ml. Oligonucleotides were added every 12 h during the 72-h incubation period. Total cell extracts were collected in SDS-PAGE sample buffer and analyzed by gel electrophoresis and Western blotting.

Purification of AKAP 80—Ovaries from 110 PMSG-primed rats were flash frozen in liquid nitrogen; ground with a mortar and pestle; scraped into buffer E (20 mM Hepes, pH 7.4, 20 mM NaCl, 5 mM EDTA, 2 mM DTT, 1 mM EGTA, 5 μg/ml pepsatin and aprotinin, 10 μg/ml leupeptin and E64, 50 μg/ml soybean trypsin inhibitor, 10 mM benzamidine), which was maintained at 100 °C; homogenized using a Polytron® homogenizer (Brinkman Instruments, Westbury, NY); and boiled for 20 min. The homogenate was chilled to 4 °C, fresh protease inhibitors as well as 10 μM isomethylbutylxanthine and 1 mM sodium vanadate were added, and a soluble extract was obtained upon centrifugation at 5000 × *g* for 10 min at 4 °C. Boiling was performed based on evidence that AKAP 80 was heat-stable (data not shown). The soluble extract was applied to 15 g of DEAE-cellulose, and AKAP 80 was batch-eluted with 0.1 M potassium phosphate, pH 7.0. The DEAE eluate was then incubated with 2 ml of cAMP-agarose beads complexed with 20 μg of recombinant RIIα and 35 μg of recombinant RIIβ subunits of PKA overnight at 4 °C. The cAMP-agarose was then washed extensively, and the bound AKAPs were eluted with 50 ml of 75 mM cAMP in buffer C containing 0.3 M NaCl. The proteins in the cAMP eluate were precipitated with 15% trichloroacetic acid, and the trichloroacetic acid pellet was washed with ethanol, resuspended in 100 μl of SDS-PAGE sample buffer, and boiled. Following confirmation (by RII overlay assay) that AKAP 80 was present in 0.5 μl of the reconstituted trichloroacetic acid pellet, the remaining 99 μl was subjected to SDS-PAGE. The portion of the gel ~80 kDa was cut and sent to the Harvard Microchemistry Facility for sequence analysis by microcapillary reverse-phase high pressure liquid chromatography nanoelectrospray tandem mass spectroscopy on a Finnigan LQC DECA quadrupole ion trap mass spectrometer. Peptide sequence identification was based on the Sequest algorithm.

RESULTS

FSH and Dexamethasone Induce the Expression of MAP2D—We previously reported that FSH induces the expression of an 80-kDa heat-stable AKAP as granulosa cells mature from a PA to a PO phenotype (8, 37, 58). AKAP 80 is also induced by dexamethasone (DEX) (58). AKAP 80 was partially purified by cAMP-agarose affinity chromatography from boiled ovarian extracts of PMSG-primed rats and subjected to SDS-PAGE, and peptides from ~80-kDa proteins were separated by mass spectrometry, as detailed under "Experimental Procedures." A BLAST search revealed sequence identity to a peptide (KIDFSK) unique to the fourth microtubule binding domain of the 80-kDa protein MAP2D. The high

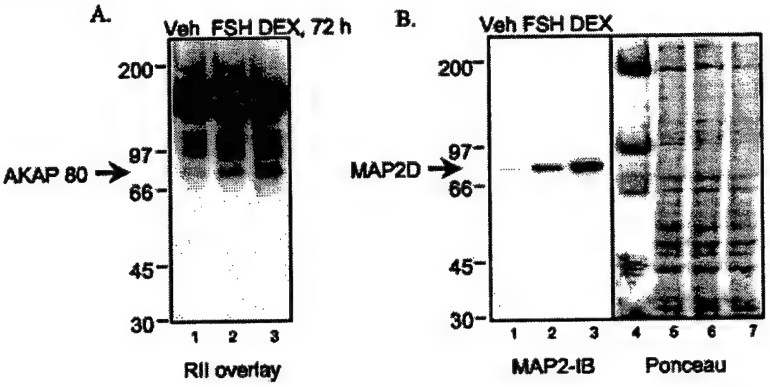

FIG. 1. **Effect of FSH and dexamethasone on the expression of AKAP 80/MAP2D.** Granulosa cells from estrogen-primed rats were treated for 72 h with vehicle (*Veh*), 50 ng/ml FSH, or 10 nM dexamethasone (*DEX*). Total cell extracts were subjected to either RII overlay assay (*A*) or immunoblotting (*IB*) using a mouse monoclonal MAP2 antibody at 1:1000 dilution (*B*). Ponceau S staining of the protein in *B* (*lanes 1–3*) is shown in *lanes 5–7*, respectively. *Lane 4*, molecular weight markers. See "Experimental Procedures" for details. Results are representative of two separate experiments.

molecular weight MAP2s were the first AKAPs to be identified and contain an N-terminal 31-amino acid RII binding domain that is conserved in the MAP2D splice variant (46).

We therefore hypothesized that AKAP 80 corresponded to MAP2D. To test this hypothesis, granulosa cells from PA follicles were treated for 72 h with vehicle, FSH, or DEX, and total cell extracts were subjected to an RII overlay assay and Western blotting using an antibody to MAP2 that detects MAP2A, -2B, -2C, and -2D (45). The RII overlay detects induction of AKAP 80 by FSH and an even greater induction by DEX (Fig. 1*A*). The corresponding Western blot shows that FSH and DEX induce a similar pattern of expression of a MAP2 isoform at 80 kDa (Fig. 1*B*). Additionally, two-dimensional gel electrophoresis showed an equivalent migration pattern for AKAP 80 (8) and MAP2D as detected by Western blotting (data not shown).

We compared the time course of expression of MAP2D and AKAP 80. Granulosa cells were treated with FSH for 0, 8, 24, 48, or 72 h. Total cell lysates were then subjected to both an RII overlay assay and an immunoblot with the MAP2 antibody (Fig. 2*A*). FSH treatment for 48 h promotes an increase in MAP2D expression that corresponds to the increase in AKAP 80. Both MAP2D and AKAP 80 expression remain elevated at 72 h post-FSH (Fig. 2*A*, *lanes 4* and *5*). Since heat stability is a defining characteristic of AKAP 80, we tested the heat stability of MAP2D. Granulosa cells treated for 72 h with FSH were collected in buffer A and boiled for 15 min. Soluble heat-stable proteins were obtained by centrifuging the boiled extract at 10,000 × *g* for 10 min at 4 °C. Results show that MAP2D, like AKAP 80, is heat-stable (Fig. 2*A*, *lane 6*), consistent with reports for MAP2 (59). To confirm that the 80-kDa AKAP induced by FSH as cells mature to the PO phenotype is MAP2D, ovarian extracts enriched in PO follicles were subjected to immunoprecipitation using the MAP2 antibody and a mouse monoclonal antibody as a NI control. The resulting immunoprecipitations were subjected to an RII overlay assay. As shown in Fig. 2*B*, the MAP2 antibody selectively immunoprecipitates RII binding activity exclusively at 80 kDa. Moreover, immunoprecipitation of MAP2D with anti-MAP2 antibody (Fig. 2*C*, *lane 2*) depletes extracts of AKAP 80 (Fig. 2*C*, *lane 1*). Taken together, these results confirm the identity of AKAP 80 as MAP2D.

In order to show that FSH increases the gene expression of MAP2D, reverse transcriptase-PCR was performed. Results showed that whereas there is detectable MAP2D mRNA expression in vehicle-treated cells, FSH up-regulates the expression of MAP2D mRNA by 48 h post-treatment (Fig. 2*D*, *lanes 2* and *3*). Glyceraldehyde-3-phosphate dehydrogenase was used as an internal loading control.

MAP2D Is the Only MAP2 Isoform Expressed in the Ovary and Is Expressed Only in Granulosa Cells of PO Follicles and the Corpus Luteum—Our identification of AKAP 80 as MAP2D is the first report of the expression of a member of the MAP2 protein family in the ovary. Since the MAP2 family of proteins was previously thought to be localized primarily to neural cells (40, 41, 60, 61), we sought to compare the expression of MAP2 in ovarian extracts with that of brain extracts. Rats were not injected or were injected with PMSG for 48 h to induce maturation of PA follicles to a PO phenotype or were injected with PMSG for 48 h followed by hCG for 1 h. The ovaries as well as the brains from PMSG-treated rats were harvested, homogenized in detergent-enriched buffer A, and subjected to immunoprecipitation with the MAP2 antibody. A Western blot using the MAP2 antibody revealed that whereas all four isoforms of MAP2 are present in the brain (Fig. 3, *lane 4*), only the MAP2D isoform is present in the ovary (Fig. 3, *lane 4* compared with *lanes 2* and *3*). These results also demonstrate that MAP2D is only present in ovarian extracts enriched in PO follicles (Fig. 3, *lanes 2* and *3*, compared with *lane 1*).

To further explore the expression of MAP2D in the ovary, whole ovarian extracts were analyzed for MAP2D protein during both the follicular and luteal phases of maturation. For Fig. 4*A*, rats were injected with 25 IU of PMSG to induce the maturation of PA to PO follicles. Some rats were also injected first with 25 IU of PMSG and 48 h later with 25 IU of hCG to induce ovulation (~12 h post-hCG injection) and corpus luteum formation. The ovaries were harvested at the indicated time points, and ovarian extracts were subjected to both an RII overlay assay and Western blot with the MAP2 antibody. Blots were also probed with an antibody to cyclin D2 as a loading control. Consistent with *in vitro* granulosa cell results seen in Fig. 2*A*, the expression of MAP2D *in vivo* is induced by PMSG by 48 h (Fig. 4*A*, *lane 4*). Treatment with hCG did not substantially alter the expression of MAP2D; MAP2D expression is maintained throughout the luteal phase (Fig. 4*A*, *lanes 5–10*). These results suggest that MAP2D may play a role not only in the PO follicle but also in the corpus luteum. To determine whether MAP2D was restricted to granulosa cells or was expressed in other ovarian cells, we performed immunohistochemistry on paraffin-embedded sections of whole rat ovaries. Rats were injected with PMSG for 48 h or injected with PMSG for 48 h and then with hCG for 48 h to stimulate ovulation and corpus luteum formation. Paraffin-embedded sections were incubated with antibodies to either MAP2 or, as a positive control, inhibin-α. Inhibin-α is induced by PMSG in granulosa cells of PO follicles and is absent from the corpus luteum (33, 62). Protein expression of both MAP2D and inhibin-α was low in PA follicles (Fig. 4*B*, *a* and *e*). PMSG induces the expression of both inhibin-α and MAP2D in the PO follicle (Fig. 4*B*, *b* and *f*). Like inhibin-α expression, the expression of MAP2D is localized to the granulosa cell layer of the PO follicle, with minimal expres-

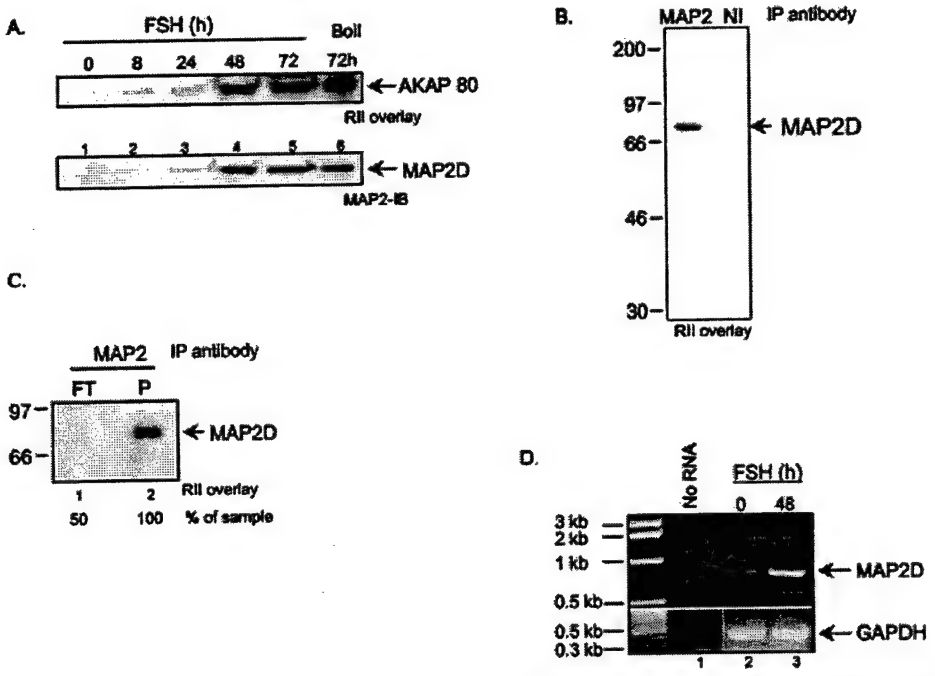

FIG. 2. ***In vitro* expression of MAP2D.** *A*, granulosa cells from estrogen-primed rats were treated with 50 ng/ml FSH for 0, 8, 24, 48, or 72 h. Total cell extracts were boiled in SDS-PAGE sample buffer and subjected to either RII overlay assay (*top*) or Western blotting using a mouse monoclonal MAP2 antibody (*bottom*). *Lane 6*, cells were harvested in buffer A, boiled for 10 min, and centrifuged at 10,000 × *g* for 10 min at 4 °C, and the supernatant fraction was loaded onto the gel. Results are representative of three separate experiments. *B*, detergent-soluble ovarian extracts from PMSG-treated rats (500 μg of protein) were subjected to immunoprecipitation using either the mouse monoclonal anti-MAP2 antibody (10 μl) or control NI mouse anti-HA antibody (10 μl) in the presence of protein A+G-agarose. The agarose pellets were washed in buffer D, and proteins were separated by SDS-PAGE, blotted to Immobilon, and subjected to an RII overlay assay as described under "Experimental Procedures." Results are representative of two separate experiments. *C*, detergent-soluble ovarian extracts from PMSG-treated rats (800 μg of protein) were subjected to immunoprecipitation using either the mouse monoclonal anti-MAP2 antibody (10 μl) or control NI mouse anti-HA antibody (10 μl) in the presence of protein A+G-agarose in a total volume of 200 μl. The flow-through (*FT*) collected upon pelleting the agarose was boiled, and 50% was subjected to SDS-PAGE. *P*, washed agarose pellet. Following SDS-PAGE, proteins were subjected to an RII overlay assay. Results are representative of two separate experiments. *D*, cells were treated with 50 ng/ml FSH for either 0 or 48 h. Cells were harvested in 1 ml of Trizol® reagent, and RNA was isolated by phenol/chloroform extraction and isopropyl alcohol precipitation. 500 ng of RNA was DNase-treated and subjected to reverse transcriptase-PCR using the primers and conditions described under "Experimental Procedures."

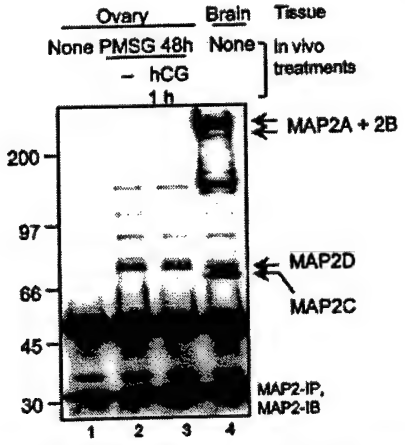

FIG. 3. **MAP2 isoform expression in rat ovary compared with brain.** Rats were injected with vehicle (*Veh*) or 25 IU of PMSG, and ovaries were harvested 48 h later. For hCG treatment, rats were injected with 25 IU of hCG 48 h post-PMSG injection, and ovaries were obtained 1 h post-hCG. Brain tissue was collected 48 h post-PMSG injection. Soluble extracts were made by homogenizing ovaries or brain in buffer A and centrifugation (10 min, 10,000 × *g*, 4 °C). MAP2 was immunoprecipitated from soluble extracts (500 μg of protein in a total volume of 500 μl) as described under "Experimental Procedures." Results are representative of three separate experiments.

sion in the thecal, stromal, and surface epithelial cells of the ovary (Fig. 4*B*, *c* and *g*). In contrast to inhibin-α expression, which is down-regulated in response to the preovulatory LH surge (62), MAP2D expression is maintained after ovulation and in the cells of the corpus luteum (Fig. 4*B*, *d* and *h*).

MAP2D Is Phosphorylated in Granulosa Cells—Phosphorylation of the MAP2 family of proteins has been extensively studied in the brain (43, 63). MAP2 phosphorylation has been shown to regulate its association with other proteins as well as the microtubule network (43, 63, 64). At least 15 of the 46 phosphorylation sites present in the high molecular weight MAP2 isoforms are conserved in MAP2D (43). We first sought to determine whether or not an acute treatment of PO granulosa cells with hCG stimulated MAP2 phosphorylation. To this end, granulosa cells from PMSG-primed rats were cultured overnight in the presence of $^{32}P_i$ and treated the next day for 10 min with either vehicle or hCG. Cell lysates were then subjected to immunoprecipitation using the MAP2 antibody or a mouse monoclonal NI control. MAP2D was already phosphorylated in vehicle-treated cells (Fig. 5*A*, *lane 1*), and acute treatment with hCG did not further increase the phosphorylation of MAP2D (Fig. 5*A*, *lane 2*). ^{32}P-Labeled MAP2D protein was absent from NI control immunoprecipitations (Fig. 5*A*, *lanes 3* and *4*). Since MAP2D was already phosphorylated in vehicle-treated cells, we sought to determine the time point at which MAP2D was phosphorylated relative to its expression using an antibody that recognizes MAP2 phosphorylation on Thr^{256} and/or Thr^{259} in the proline-rich domain (MAP2 305 antibody) (43). Granulosa cells from PA follicles were treated with FSH for 0, 24, 48, and 72 h, and total cell lysates were subjected to Western blotting. MAP2 phosphorylation on Thr^{256} and/or Thr^{259} matched the expression of MAP2D in

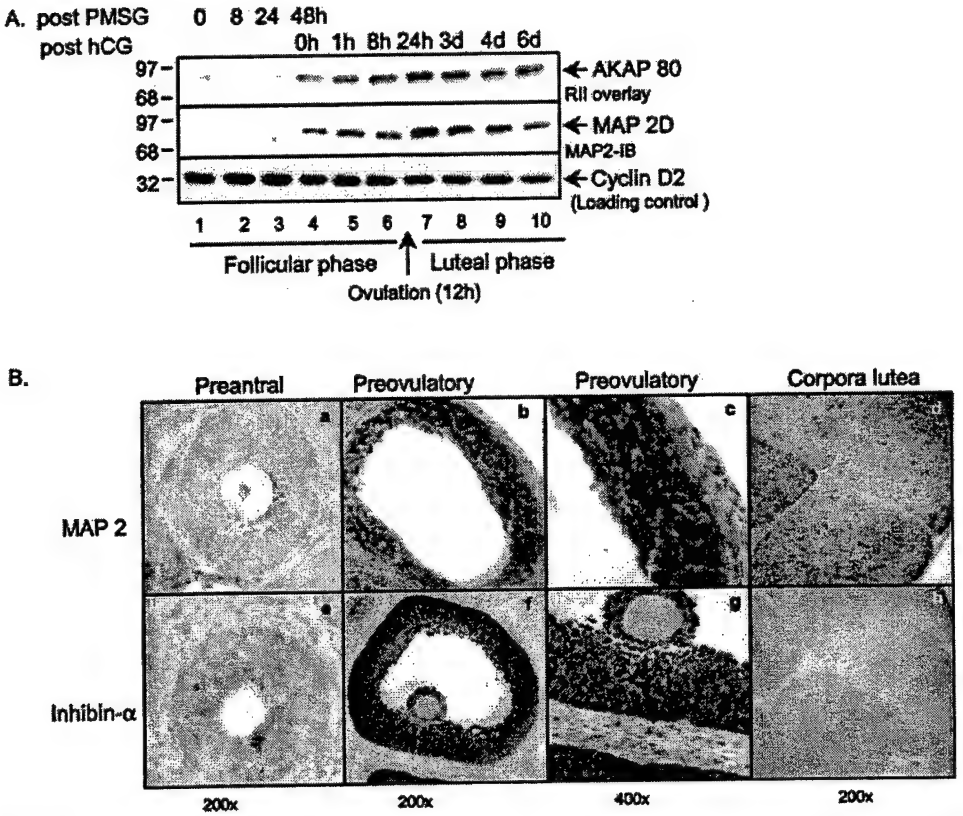

FIG. 4. **Expression of MAP2D during ovarian differentiation.** *A*, rats were not treated or were injected with either 25 IU of PMSG or with 25 IU of PMSG followed by 25 IU of hCG. Ovaries were harvested at the time points indicated after injections. Soluble extracts were made by homogenizing whole ovaries in buffer A, as described under "Experimental Procedures." Equal concentrations of protein (60 μg) were loaded. Following SDS-PAGE and transfer, blots were subjected to RII overlay assay (top) or Western blotting using anti-MAP2D antibody or, as a loading control, anti-cyclin D2 antibody. Results are representative of two separate experiments. *B*, rats were injected with either 25 IU of PMSG or with 25 IU of PMSG followed by 25 IU of hCG. Ovaries were harvested 48 h post-PMSG or 48 h post-hCG into 4% paraformaldehyde. Ovarian tissue was sectioned onto glass slides and subjected to immunohistochemistry. -Fold magnification is indicated at the *bottom*. Results are representative of two separate experiments.

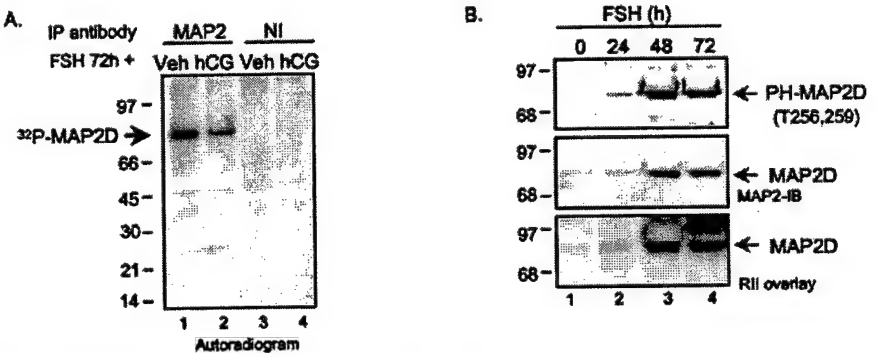

FIG. 5. **Phosphorylation of MAP2D in granulosa cells.** *A*, PO granulosa cells obtained from rats 48 h after injection of 10 IU of PMSG were incubated overnight with 0.5 mCi of $^{32}P_i$ to label cellular ATP pools. Granulosa cells were then treated for 10 min with vehicle or 1 IU/ml hCG. Cell extracts were prepared in buffer A and then subjected to immunoprecipitation with indicated antibodies, as detailed under "Experimental Procedures." Following SDS-PAGE, gel was dried and exposed to film. Results are representative of three separate experiments. *B*, granulosa cells were treated with 50 ng/ml FSH for the times indicated, and total cell extracts were subjected to Western blotting with either MAP2 antibody or anti-phospho-MAP2 (antibody 305) or to RII overlay. Results are representative of two separate experiments.

response to FSH treatment (Fig. 5*B*, compare *top* with *middle* and *lower panels*). These results suggest that MAP2D is phosphorylated either coincidentally with or soon after its synthesis at least on Thr^{256} and/or Thr^{259}.

MAP2D Associates with the R Subunits of PKA in Granulosa Cells of PO Follicles—We previously showed that AKAP 80 preferentially binds RIIα over RIIβ in an *in vitro* solid phase overlay assay (37). However, we also showed, following separation of PKA holoenzymes in ovarian extracts by DEAE-cellulose chromatography, that AKAP 80 copurified with DEAE fractions containing PKA IIβ holoenzyme as well as catalytic subunit-free RI and not with PKA IIα holoenzyme or the prominent peak of catalytic subunit-free RIIβ (8). We therefore sought to ascertain whether MAP2D additionally anchored RI as well as RII subunits in granulosa cells. Most known AKAPs predominately anchor RII and exhibit at least a 100-fold lower affinity for RI (9). A growing number of "dual" AKAPs readily bind RI (12–15, 18), yet these AKAPs still exhibit a 10–25-fold

preference for PKA II (65). However, some recently described AKAPs appear to preferentially bind RI (16–19).

To determine whether MAP2D additionally bound to RI, we performed immunoprecipitations from ovarian extracts. Under standard immunoprecipitation conditions, neither RI nor RII antibodies immunoprecipitated detectable levels of MAP2D (not shown). However, upon cross-linking of proteins with the reversible cross-linker DSP, RI antibodies immunoprecipitated primarily a slower migrating form of MAP2D from ovarian extracts, whereas detectable levels of MAP2D were never immunoprecipitated with RII antibodies (Fig. 6*A*). The reverse immunoprecipitations were unsuccessful, because we could not distinguish RI and RII from the prominent IgG bands in our immunoprecipitates. These results suggested that MAP2D could be an RI-preferential AKAP in ovarian extracts. If this is true, then MAP2D and RI should copurify.

We therefore sought to compare the DEAE-cellulose elution positions of MAP2D, RI, and RII. Ovarian PKAs are separated by DEAE-cellulose chromatography into three peaks of kinase activity (8, 52) (see Fig. 6*C*). We have previously established that peak 1 consists of the PKA I holoenzyme; peak 2 consists of catalytic subunit-free RI and a PKA IIβ holoenzyme; and peak 3 consists of a second PKA IIβ holoenzyme, a relatively minor PKA IIα holoenzyme, and a prominent peak of catalytic subunit-free RIIβ (8, 52). The elution positions of MAP2D, RI, RII, PKA activity, and the PKA C subunit are shown in Fig. 6, *B* and *C*. Notably, the highest concentrations of RI are detected in DEAE peak 2 (fractions 25–39), consistent with the more acidic elution of this prominent peak of catalytic subunit-free RI relative to PKA I holoenzyme (52, 66, 67). The majority of RII elutes in peak 3. The peak of MAP2D co-elutes with the PKA I holoenzyme in peak 1, although a portion of the MAP2D also elutes in the same fractions as RI and RII in peak 2. However, MAP2D does not coelute with the bulk of the RII protein in peak 3.

We then bound PKA R subunits in pooled fractions from DEAE peaks 1 plus 2 *versus* peak 3 to cAMP-agarose. We compared the elution of MAP2D and PKA R subunits using Ht31, a synthetic peptide derived from the amphipathic helical region of the human thyroid Ht31 AKAP (10), to compete with AKAPs for binding to PKA RII subunits (69), thus competing off RII-AKAPs. cAMP was used to compete off R subunits and remaining RI AKAPs bound to R subunits. Results showed that a portion of the MAP2D in DEAE peaks 1 and 2 was eluted with the RII AKAP Ht31 (Fig. 6*D*, *lane 2*), and as expected, none of the R subunits were eluted. cAMP effectively eluted RI and RII as well as a significant fraction of the MAP2D, possibly bound to RI. MAP2D was not detected in DEAE peak 3 cAMP-agarose eluates (Fig. 6*D*, *lanes 4–6*), where the majority of RII protein was present. These results confirm that MAP2D is bound to R subunits in DEAE fractions that contain RI and RII (pooled from DEAE peak 1 and 2 fractions) but is not bound to R subunits in fractions that contain predominately RII (pooled peak 3 fractions). Moreover, these results showing differential elution of MAP2D with the RII AKAP Ht31 *versus* cAMP suggest that MAP2D is dual AKAP.

To explore more directly the association of MAP2D with RI and RII, we performed coimmunoprecipitation experiments from DEAE column fractions containing MAP2D, RI, and RII. Fractions were incubated with the cross-linking reagent DSP and then subjected to immunoprecipitation with antibodies to MAP2, RI, RII, or NI controls. An aliquot of the starting material representing 10% of the total volume was stopped in SDS-PAGE sample buffer and loaded onto the gel (Fig. 6*E*, *lanes 1* and *5*). Bound proteins were eluted with an acidic elution buffer (and are labeled *IP*). Immunoprecipitation from DEAE peak 1 fractions (region *a* in Fig. 6*C*) with either MAP2 or RI antibody pulled down MAP2D protein (Fig. 6*E*, *lanes 2* and *3*). However, when immunoprecipitations were conducted with DEAE peak 2 fractions (region *b* in Fig. 6*C*), MAP2 antibody and to a much lesser extent RII antibody pulled down MAP2D, whereas MAP2D was undetectable in anti-RI antibody immunoprecipitations (Fig. 6*E*, *lanes 5–9*).

These results suggest that MAP2D may preferentially associate with RI over RII but that not all of the RI is bound to MAP2D. Indeed, upon sucrose density gradient centrifugation (52) of DEAE peak 2, the majority of MAP2D and catalytic subunit-free RIα co-sediment with hemoglobin at 4.6 S (not shown), consistent with both RI and MAP2D existing in an unbound state. However, MAP2D also co-sediments with both PKA I and II from DEAE peaks 1 and 2, respectively (not shown), consistent with the formation of a larger complex.

We also evaluated the associations of MAP2D and R subunits by coimmunoprecipitation from DEAE-cellulose fractions corresponding to peaks 1 and 2 that were batch-eluted and then concentrated. Consistent with results shown in Fig. 6*E*, immunoprecipitation with MAP2D but not with NI antibodies depleted the extract of RI (Fig. 6*F*, *lanes 1* and *2*). RII was obscured by the prominent immunoglobulin band in MAP2 immunoprecipitation. Immunoprecipitation with RII but not with NI antibodies diminished RII from sucrose density gradient fractions containing PKA IIβ peak (not shown) and immunoprecipitated MAP2 (Fig. 6*F*, *lanes 3* and *4*). These results show that whereas MAP2D appears to strongly associate with RI (see Fig. 6, *E* and *F*), it also binds RIIβ in ovarian extracts. We conclude that MAP2D is a dual RI/RII AKAP.

RI and RII Colocalize with MAP2D in the Golgi Apparatus of PO Granulosa Cells—We next sought to determine whether or not an association between MAP2D and RI and RII was evident in PO granulosa cells as detected by immunofluorescence. Granulosa cells from PA follicles were plated on glass coverslips and treated for 72 h with either vehicle or FSH. The coverslips were fixed, blocked, and incubated with the MAP2D antibody overnight and subsequently with a secondary antibody conjugated to rhodamine or fluorescein labels, as indicated, and then visualized using confocal microscopy. The induction of MAP2D in FSH-treated granulosa cells is readily detected (Fig. 7*A*, compare *a* and *c*). The *arrows* (Fig. 7*A*, *c* and *d*) mark the location of concentrated amounts of MAP2D in a prominent, phase-dense circular structure of the cell located adjacent to the nucleus, which is not detected in vehicle-treated cells (Fig. 7*A*, *b*). Both RI and RII co-localized to this phase-dense structure in PO granulosa cells (Fig. 7*B*, *e–h* and *i–l*), although both RI and RII are also detected throughout the cytoplasm of PO cells.

In order to identify this phase-dense structure in PO granulosa cells that appears to concentrate MAP2D, we determined whether this structure reacted with antibodies that mark the centrosome, the Golgi apparatus, or the actin cytoskeleton. Results show that this circular structure does not correspond to the actin cytoskeleton (Fig. 7*C*, *m–p*) or the centrosome (Fig. 7*C*, *q–t*), based on the inability of actin phalloidin or an antibody to γ-tubulin, respectively, to localize at this spot. However, incubation of coverslips with an antibody to the Golgi matrix protein Gm 130 conjugated to fluorescein together with the MAP2 antibody shows that both MAP2D and Gm 130 localized to this phase-dense, circular structure (Fig. 7*D*, *u–x*). Treatment of granulosa cells, cultured on glass coverslips with FSH for 72 h, with 10 μg/ml brefeldin A for 1 h, which has been shown to disrupt the Golgi apparatus as well as to disrupt the Golgi localization of anchor proteins such as AKAP 350 (70), caused a redistribution of MAP2D and Gm 130 out of the

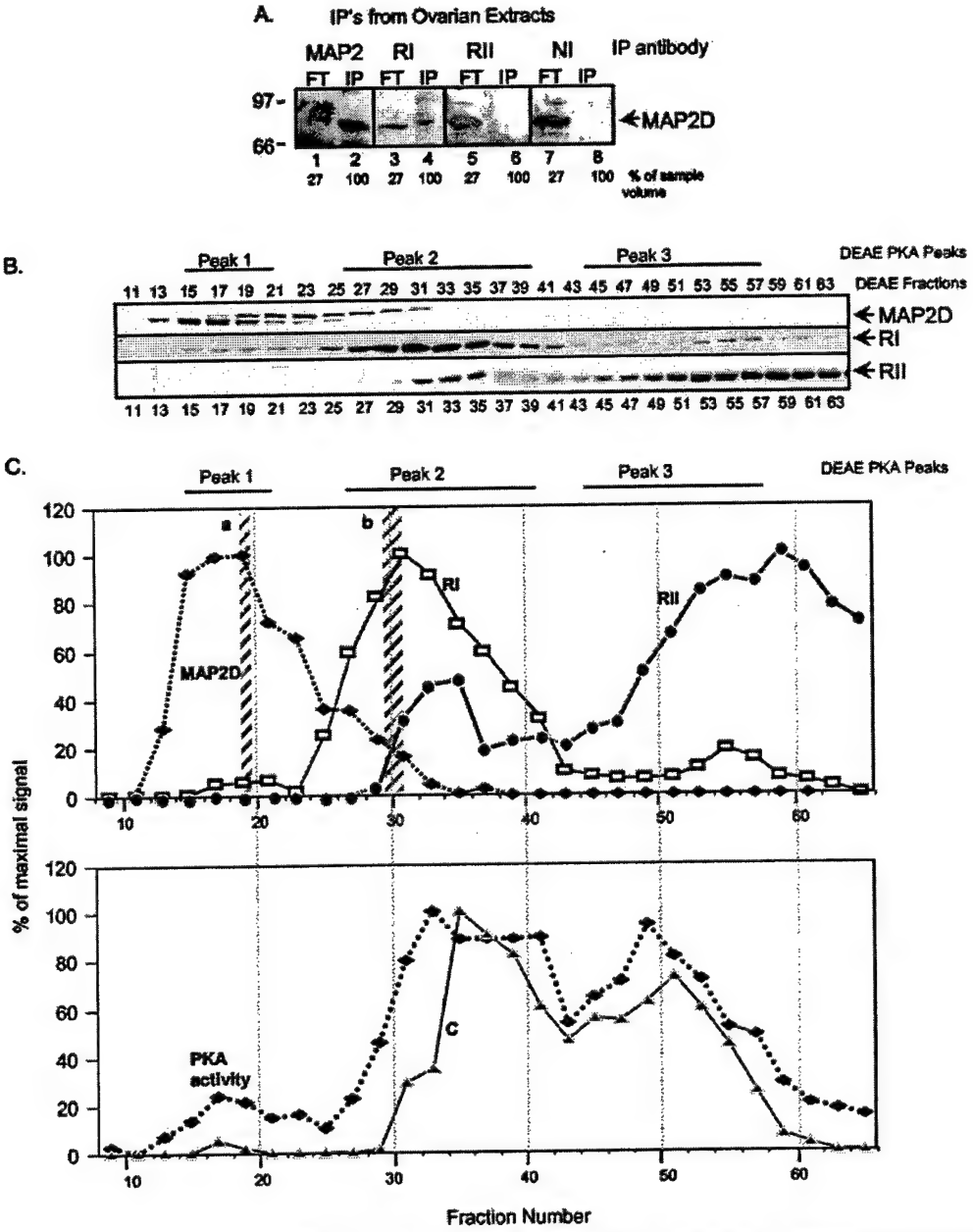

FIG. 6. **DEAE-cellulose and cAMP-agarose affinity chromatography of PO ovarian extracts.** *A*, detergent-soluble ovarian extracts (800 μg of protein in 300 μl) were prepared (without DTT), subjected to cross-linking by incubating with 1 mM DSP for 15 min at room temperature, and then subjected to immunoprecipitation using the indicated antibodies (anti-MAP2 (Sigma), anti-RI (BD Biosciences), and anti-RII (Upstate Biotechnology)). Flow-through (*FT*) represents 27% of the extract that was not pulled down by the antibody-agarose complex. *IP*, immunoprecipitated complex. Samples were subjected to SDS-PAGE and blotted with anti-MAP2 antibody. Results for RII and NI immunoprecipitations are overexposed to confirm the absence of signal in the immunoprecipitation complex lanes. Results are representative of three separate experiments. *B*, ovaries from 15 rats were harvested 48 h post-PMSG injection and homogenized in buffer E, and a soluble extract was prepared by centrifuging at 105,000 × *g* for 15 min and loading onto a DEAE-cellulose column. Proteins were eluted with a linear salt gradient, collecting fractions in buffer B but without DTT. Aliquots of odd-numbered fractions were mixed with SDS-PAGE sample buffer, boiled, and subjected to SDS-PAGE and Western blotting with the indicated antibodies. Results are representative of four separate experiments. *C*, a graphic representation of the Western data presented in *B* but now normalized to percentage of maximal signal. Also shown is the cAMP-stimulated PKA activity, also normalized to percentage of maximal signal (*lower portion* of *C*). In *D*, fractions from the indicated DEAE-cellulose peak fractions (shown in *C*) were pooled, concentrated, and incubated with cAMP agarose. The agarose was washed with low and high salt buffers to remove nonspecifically bound proteins, and the final wash (*FW*) was collected. Specifically bound AKAPs were eluted first with 5 μM Ht31 (*Ht31*) and then with 75 mM cAMP. The samples were mixed with SDS-PAGE sample buffer and boiled, and aliquots were then subjected to SDS-PAGE and Western blotting using the antibodies indicated. Results are representative of four separate experiments. *E*, fractions from indicated regions of the DEAE-cellulose column (shown in *C*) were pooled, 1-ml aliquots were incubated with the protein cross-linker (DSP; 1 μM) for 15 min at room temperature, and samples were subjected to immunoprecipitation with the indicated antibodies (see *A*). A 100-μl aliquot of the 1-ml starting material was boiled and applied to the gel (*Load*). Agarose pellets were washed with buffer D, and proteins were eluted from the protein A+G-agarose with 150 μl of Immunopure® elution buffer, pH 2.8, mixed with SDS-PAGE sample buffer, and boiled. 67% of the total eluate (*IP*) was loaded onto the gel for SDS-PAGE. Results are representative of two separate experiments. *F*, immunoprecipitations from pooled and concentrated DEAE peak 1 and 2 fractions (*lanes 1* and *2*) or from PKA IIβ holoenzyme in these fractions that was sedimented by sucrose density gradient centrifugation (*lanes 3* and *4*) were conducted with Sigma anti-MAP2 antibody, anti-HA (NI), or BD Biosciences anti-RIIβ antibodies. *Lanes 1* and *2*, immunodepletion results for proteins that were not imunoprecipitated. *Lanes 3* and *4*, immunoprecipitation results. Results are representative of two independent experiments.

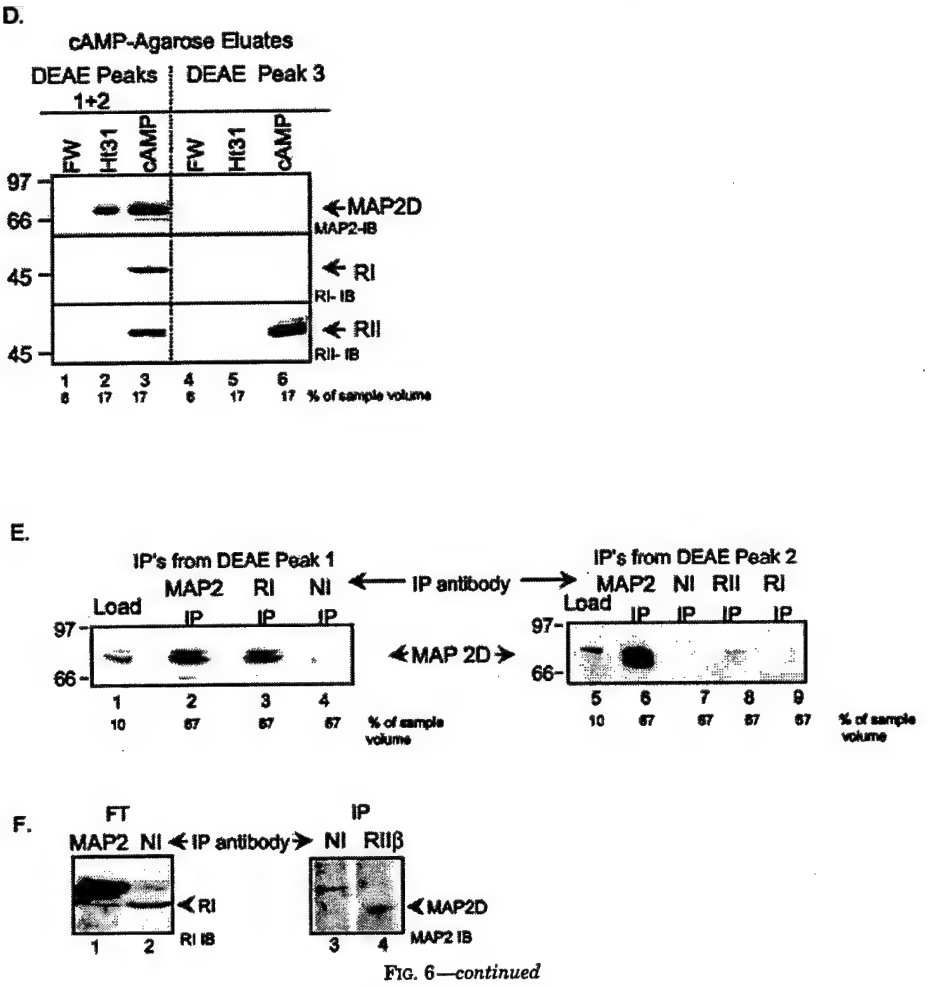

FIG. 6—*continued*

circular structure and into the cytosol (Fig. 7*D*, *y–b'*). This result provides evidence that MAP2D localizes to the Golgi apparatus in PO granulosa cells. Taken together, these results indicate that MAP2D is localized in granulosa cells at a large circular structure of the Golgi apparatus and suggest that this MAP2D may anchor a portion of the cellular PKA RI and perhaps RII in granulosa cells of PO follicles through its association with the Golgi apparatus.

MAP2D Plays a Functional Role in LH Receptor Signaling Events—To begin to ascertain the physiological role of MAP2D in granulosa cells of PO follicles, we explored the effect of antisense oligonucleotides against MAP2D on LH receptor signaling responses. Granulosa cells from estrogen-primed rats were treated with vehicle or FSH for 72 h and treated with either scrambled or antisense MAP2 oligonucleotides that have been shown to inhibit MAP2 expression in neuronal cells (41). In the presence of the scrambled, control MAP2 oligonucleotide, FSH induced MAP2D expression over vehicle (Fig. 8, compare *lanes 1* and *2*). In the presence of the antisense MAP2 oligonucleotide, FSH-induced MAP2D expression is decreased by 35 ± 5% (mean ± range, $n = 2$) relative to total ERK protein compared with MAP2D protein expression in control FSH-treated cells (Fig. 8, compare *lanes 2* and *5*). The effect of decreased MAP2D expression on CREB phosphorylation stimulated by the LH receptor agonist hCG was examined by treating the cells for 72 h with FSH and subsequently treating with hCG for 10 min in the presence of either the scrambled or the antisense MAP2 oligonucleotide. Under control conditions, hCG stimulated CREB phosphorylation (Fig. 8, compare *lanes 2* and *3*). When MAP2D expression was decreased by MAP2D antisense oligonucleotides, hCG-stimulated CREB phosphorylation was inhibited 62 ± 12% (mean ± range, $n = 2$) relative to total ERK protein (Fig. 8, compare *lanes 3* and *6*). However, hCG-stimulated histone H3 phosphorylation was not reduced when MAP2D protein levels were reduced (not shown). These results suggest that MAP2D may play a crucial role in acute select PKA-mediated hCG-stimulated signaling events in granulosa cells.

DISCUSSION

Our results demonstrate that the 80-kDa AKAP induced by FSH as ovarian granulosa cells mature from a PA to a PO phenotype corresponds to the neuronal protein MAP2D. MAP2 has been extensively studied in brain tissue not only as a microtubule-binding protein necessary for neurite outgrowth (38) but also as an RII-binding protein (47, 48). MAP2D is a low molecular weight splice variant of the MAP2 protein that is expressed predominately in adult brain (44) and functions to stabilize microtubules and especially microfilaments (42). Our results show that only the MAP2D isoform, and not the other MAP2 family members, is expressed in the ovary and that its expression is induced by FSH and restricted to PO granulosa cells. Moreover, whereas MAP2D is distributed throughout the granulosa cell, it is concentrated at a distinct, phase-dense circular region of the Golgi apparatus, as evidenced by its ability to co-localize with the Golgi marker Gm 130 and the ability of brefeldin A to redistribute MAP2D out of this circular structure. MAP2D does not localize to the actin cytoskeleton or

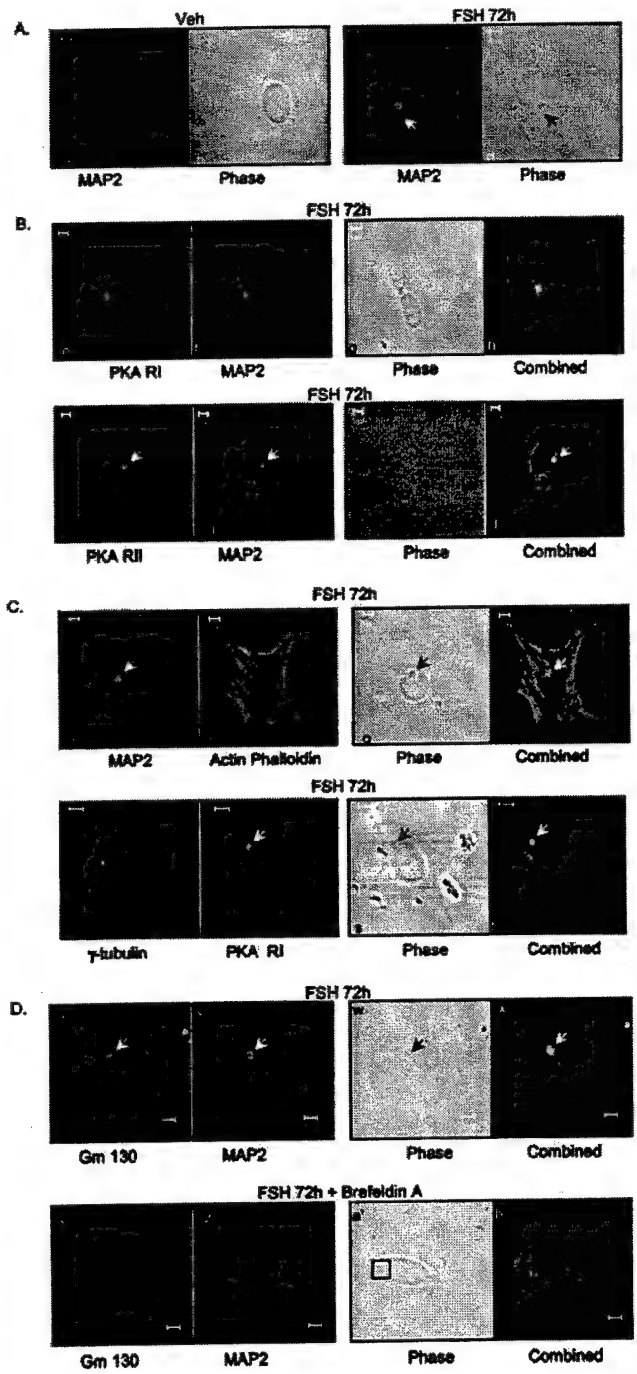

FIG. 7. **Cellular location of MAP2D.** Cells were plated on glass coverslips coated with fibronectin and treated for 72 h with vehicle (*Veh*) or 50 ng/ml FSH, as indicated. The cells were fixed in 4% paraformaldehyde plus Triton X-100, blocked in 1% bovine serum albumin, and incubated with the indicated primary antibodies overnight at 4 °C at a dilution of 1:200, with the exception of anti-PKA RII and MAP2 in *B*, in which primary antibodies were at a 1:1000 dilution. Secondary antibodies were added at a dilution of 1:100, with the exception of those for anti-PKA RII and MAP2 in *B*, in which secondary antibodies were at a 1:200 dilution. Slides were analyzed by confocal microscopy using a Zeiss LSM510 laser-scanning microscope. A phase-contrast image of the cells is also shown. No fluorescent signal was detected in the presence of primary or secondary antibodies alone. Primary and corresponding secondary antibodies used were as follows. *A*, mouse anti-MAP2 (Sigma) and goat anti-mouse rhodamine; *B*, *e–h*, rabbit anti-RI (82) and goat anti-rabbit fluorescein, mouse anti-MAP2, and goat anti-mouse rhodamine; *i–l*, goat anti-RII (Upstate Biotechnology) and donkey anti-goat rhodamine, mouse anti-MAP2 (Sigma), and donkey anti-mouse fluorescein; *C*, *m–p*, mouse anti-MAP2, goat anti-mouse fluorescein, and actin phalloidin; *q–t*, mouse anti-γ-tubulin (Sigma) and goat anti-mouse fluorescein, rabbit anti-RI, and goat anti-rabbit rhodamine; *D*, mouse anti-Gm 130 conjugated to fluorescein, mouse anti-MAP2, and goat anti-mouse rhodamine. *D*, cells were treated for 72 h with FSH and then for 1 h with 10 μM brefeldin A and fixed as described above. Results are representative of at least three separate experiments.

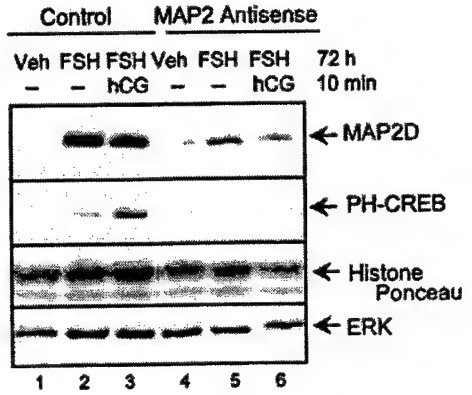

FIG. 8. **Effect of reduced MAP2D expression on LH receptor signaling to CREB.** Granulosa cells from estrogen-primed rats were plated on tissue culture plates coated with 100 ng/ml poly-L-lysine and treated with vehicle (*Veh*) or FSH for 72 h or with FSH for 72 h followed by 1 IU/ml hCG (*hCG*) for 10 min in the presence of either scrambled (*Control*) or antisense (*Antisense*) oligonucleotides against MAP2 as described under "Experimental Procedures." Oligonucleotides were added at a concentration of 10 μg/ml every 12 h during the 72-h incubation period. Cells were harvested in SDS-PAGE sample buffer and subjected to Western blotting with antibodies against MAP2 (*A*, *top*) or phospho-CREB (*PH-CREB*) (*middle*). Protein load was determined using an antibody that detects total ERK and by Ponceau S staining (*bottom*). Results are representative of two independent experiments.

the centrosome (the microtubule-organizing center), as evidenced by its inability to co-localize with actin phalloidin or γ-tubulin. These results suggest that, in contrast to its localization in neurons, the portion of MAP2D that is concentrated at the Golgi in PO granulosa cells does not appear to be associated with the microfilament or microtubular networks present in granulosa cells (71, 72). However, since microtubules are important for the cellular position and organization of the Golgi (73, 74), additional studies are required to determine whether the MAP2D in granulosa cells is associated with the microtubules that are specifically associated with the Golgi apparatus. Additional studies are also required to determine whether the remaining MAP2D not associated with the Golgi is associated with the microtubule network in granulosa cells.

Neuronal MAP2 contains a large number of phosphorylation sites that can be phosphorylated by a variety of kinases including PKA, ERK, glycogen synthase kinase 3β, casein kinase II, cyclin-dependent kinases, and protein kinase C (43). It is generally believed that the phosphorylation of MAP2 reduces its association with microtubules (43). At least 15 of the 46 phosphorylation sites present in MAP2A/2B are conserved in MAP2D (43). MAP2C, which is identical to MAP2D except that it is missing the fourth microtubule binding domain present in MAP2D (45), is phosphorylated by glycogen synthase kinase 3β in the proline-rich domain, resulting in an inhibition of microtubule bundling (64), and by PKA at KXGS motifs, resulting in a disruption of MAP2C-microtubule interaction and increased localization of MAP2C with actin at membrane ruffles (63). In granulosa cells from PO follicles, we have shown, upon labeling of intracellular ATP pools with $^{32}P_i$, that MAP2D is phosphorylated in the absence of acute hormone stimulation. Acute LH receptor signaling in response to the LH receptor agonist hCG has no detectable effect on the amount of phosphorylated MAP2D protein; how-

ever, it is possible that hCG stimulates a rearrangement of phosphorylated sites on MAP2D to modulate its association with cellular organelles or other proteins. MAP2D phosphorylation on Thr^{256}/Thr^{259} in the proline-rich domain, which immediately precedes the four microtubule binding domains, appears to be coincident with MAP2D expression in response to FSH treatment; however, the consequence of this phosphorylation has not yet been determined. Since it is well documented that MAP2 phosphorylation reduces its affinity for microtubules (43, 63), our results suggest that the majority of MAP2D in PO granulosa cells might not be associated with the microtubule network that extends from the centrosome to the cells' periphery. It is possible, however, that the phosphorylation of MAP2D on Thr^{256}/Thr^{259} or on other sites regulates its association with the microtubule network selectively associated with the Golgi apparatus in PO granulosa cells.

Most of the AKAPs identified have been shown to bind RII subunits with at least a 100-fold higher affinity than RI (9). Even the dual specificity AKAPs, such as sAKAP-84 and DAKAP 1 and 2, bind RII with as much as a 25-fold higher affinity over RI (65) and appear to contain overlapping RI/RII binding domains (76). The sperm fibrous sheath protein FSC1 contains two separate RI binding domains, one of which also binds RII, and this protein preferentially pulls down RI from testis extracts (18). Similarly, the neurofibromatosis 2 tumor suppressor protein merlin (16) as well as the peripheral type benzodiazepine receptor-associated protein PAP7 (19) preferentially binds RI. MAP2 contains a well characterized RII binding domain in its N-terminal region (48) that *in vitro* preferentially binds RIIα over RIIβ (78). Using a solid phase *in vitro* RII overlay binding assay, we showed that MAP2D also preferentially binds RIIα over RIIβ (37). These results establish that MAP2D is an RII AKAP. Although Therakauf *et al.* (47) showed that purified brain microtubules bound equal amounts of RIIα and RIIβ but did not bind RI, using a cAMP photoaffinity ligand to identify RI and RII subunits, fractionation and immunoprecipitation data from granulosa cells suggest that MAP2D is a dual AKAP that appears to preferentially associate with RI. This result suggests a unique role for MAP2D as a selective RI-binding AKAP in granulosa cells of the PO follicle. However, the PKA I holoenzyme comprises a very small fraction (~5%) of the PKA holoenzyme activity in PO granulosa cells (8) (see Fig. 6*C*). Although the predominant PKA holoenzyme contains RIIβ subunits, the RIIβ knock-out mouse is fertile (79), and RIIβ is compensated for by an increase in RI, at least in adipose tissue (80). Our results show that whereas MAP2D and RI coelute upon ion exchange chromatography of PO ovarian extracts (see Fig. 6*C*) and coimmunoprecipitate (see Fig. 6*E*), MAP2D also coelutes and coimmunoprecipitates with RII. However, not all of the MAP2D in granulosa cells is bound to R subunits. Likewise, most of the RIIβ and RIα do not appear to be associated with MAP2D, based on their distinct elution positions from DEAE-cellulose (see Fig. 6*C*). Both RI and RII colocalize with MAP2D in the Golgi matrix, as evidenced by confocal microscopy. However, there are other AKAPs associated with the Golgi apparatus that appear to preferentially bind either RII, such as MTG (81), an unidentified 85-kDa AKAP (57), and AKAP 350 (70) or RI, such as PAP7 (19). Thus, RI and RII localized to the Golgi are not exclusively bound to MAP2D. Taken together, these results suggest that MAP2D binds RI and RII; that the association of MAP2D with RI and RII is tightly regulated, since significant fractions of MAP2D, RI, and RII are not associated; and that the binding of RI and RII to MAP2D probably reflects distinct cellular localizations of these proteins.

Inhibition of MAP2 expression using antisense oligonucleotides in cultured rat cortical neurons inhibits elongation of neurites as well as causing destabilization of microtubules (41). Inhibition of MAP2D expression in PO granulosa cells inhibited the ability of hCG to effectively stimulate the PKA-mediated phosphorylation of the signaling intermediate CREB. This result suggests that MAP2D may play a functional role in acute LH receptor signaling events, possibly by acting as a molecular scaffold that coordinates the actions of PKA to phosphorylate select substrates. Perhaps MAP2D is a key component of the mechanism that distinguishes PKA signaling in granulosa cells of PA follicles compared with that of PO follicles.

In summary, we have shown that the neuronal protein MAP2D is also expressed in ovarian granulosa cells in response to the hormone FSH. We identify MAP2D as an apparent dual RI/RII AKAP based on its ability to coimmunoprecipitate with RI and RII. MAP2D in granulosa cells is predominately localized to the Golgi and not to the microtubule-organizing center and appears to be important for LH receptor signaling. Thus, the function of MAP2D in granulosa cells is expected to be quite novel and distinct from its established neuronal roles.

REFERENCES

1. McGee, E. A., and Hsueh, A. J. (2000) *Endocr. Rev.* **21,** 200–214
2. Richards, J. S. (1980) *Physiol. Rev.* **60,** 51–89
3. Robinson-White, A., and Stratakis, C. A. (2002) *Ann. N. Y. Acad. Sci.* **968,** 256–270
4. Taylor, S. S. (1989) *J. Biol. Chem.* **264,** 8443–8446
5. Dell'Acqua, M. L., and Scott, J. D. (1997) *J. Biol. Chem.* **272,** 12881–12884
6. Hunzicker-Dunn, M., Lorenzini, N. A., Lynch, L. L., and West, D. E. (1985) *J. Biol. Chem.* **260,** 13360–13369
7. Hunzicker-Dunn, M., Maizels, E. T., Kern, L. C., Ekstrom, R. C., and Constantinou, A. I. (1989) *Mol. Endocrinol.* **3,** 780–789
8. Carr, D. W., Cutler Jr., R. E., Cottom, J. E., Salvador, L. M., Fraser, I. D. C., Scott, J. D., and Hunzicker-Dunn, M. (1999) *Biochem. J.* **344,** 613–623
9. Michel, J. J., and Scott, J. D. (2002) *Annu. Rev. Pharmacol. Toxicol.* **42,** 235–257
10. Carr, D. W., Hausken, Z. E., Fraser, I. D. C., Stofko-Hahn, R. E., and Scott, J. D. (1992) *J. Biol. Chem.* **267,** 13376–13382
11. Carr, D. W., Stofko-Hahn, R. E., Fraser, I. D. C., Bishop, S. M., Acott, T. S., Brennan, R. G., and Scott, J. D. (1991) *J. Biol. Chem.* **266,** 14188–14192
12. Reinton, N., Collas, P., Haugen, T. B., Skalhegg, B. S., Hansson, V., Jahnsen, T., and Tasken, K. (2000) *Dev. Biol.* **223,** 194–204
13. Li, H., Adamik, R., Pacheco-Rodriguez, G., Moss, J., and Vaughan, M. (2003) *Proc. Natl. Acad. Sci. U. S. A.* **100,** 1627–1632
14. Huang, L. J., Wang, L., Ma, Y., Durick, K., Perkins, G., Deerinck, T. J., Ellisman, M. H., and Taylor, S. S. (1999) *J. Cell Biol.* **145,** 951–959
15. Huang, L. J., Durick, K., Weiner, J. A., Chun, J., and Taylor, S. S. (1997) *Proc. Natl. Acad. Sci. U. S. A.* **94,** 11184–11189
16. Gronholm, M., Vossebein, L., Carlson, C. R., Kuja-Panula, J., Teesalu, T., Alfthan, K., Vaheri, A., Rauvala, H., Herberg, F. W., Tasken, K., and Carpen, O. (2003) *J. Biol. Chem.* **278,** 41167–41172
17. Angelo, R., and Rubin, C. S. (1998) *J. Biol. Chem.* **273,** 14633–14643
18. Miki, K., and Eddy, E. M. (1998) *J. Biol. Chem.* **273,** 34384–34390
19. Li, H., Degenhardt, B., Tobin, D., Yao, Z. X., Tasken, K., and Papadopoulos, V. (2001) *Mol. Endocrinol.* **15,** 2211–2228
20. Li, Y., Ndubuka, C., and Rubin, C. S. (1996) *J. Biol. Chem.* **271,** 16862–16869
21. Dong, F., Feldmesser, M., Casadevall, A., and Rubin, C. S. (1998) *J. Biol. Chem.* **273,** 6533–6541
22. Dodge, K., and Scott, J. D. (2000) *FEBS Lett.* **476,** 58–61
23. Lin, R.-Y., Moss, S. R., and Rubin, C. S. (1995) *J. Biol. Chem.* **270,** 27804–27811
24. Ginsberg, M. D., Feliciello, A., Jones, J. K., Avvedimento, E. V., and Gottesman, M. E. (2003) *J. Mol. Biol.* **327,** 885–897
25. Keryer, G., Rios, R. M., Landmark, B. F., Skalhegg, B., Lohmann, S. M., and Bornens, M. (1993) *Exp. Cell Res.* **204,** 230–240
26. Diviani, D., Langeberg, L. K., Doxsey, S. J., and Scott, J. D. (2000) *Curr. Biol.* **10,** 417–420
27. Steen, R. L., Beullens, M., Landsverk, H. B., Bollen, M., and Collas, P. (2003) *J. Cell Sci.* **116,** 2237–2246
28. Pawson, T., and Scott, J. D. (1997) *Science* **278,** 2075–2080
29. DeManno, D. A., Cottom, J. E., Kline, M. P., Peters, C. A., Maizels, E. T., and Hunzicker-Dunn, M. (1999) *Mol. Endocr.* **13,** 91–105
30. Mukherjee, A., Park-Sarge, O. K., and Mayo, K. E. (1996) *Endocrinology* **137,** 3234–3245
31. Pei, L., Dodson, R., Schoderbek, W. E., Maurer, R. A., and Mayo, K. E. (1991) *Mol. Endocr.* **5,** 521–534
32. Cottom, J., Salvador, L. M., Maizels, E. T., Reierstad, S., Park, Y., Carr, D. W., Davare, M. A., Hell, J. W., Palmer, S. S., Dent, P., Kawakatsu, H., Ogata, M., and Hunzicker-Dunn, M. (2003) *J. Biol. Chem.* **278,** 7167–7179
33. Richards, J. S. (1994) *Endocr. Rev.* **15,** 725–751
34. Hsueh, A. J. W., Adashi, E. Y., Jones, P. B. C., and Welsh, T. H., Jr. (1984) *Endocr. Rev.* **5,** 76–110
35. Richards, J. S., Fitzpatrick, S. L., Clemens, J. W., Morris, J. K., Alliston, T., and Sirois, J. (1995) *Rec. Prog. Horm. Res.* **50,** 223–254
36. Salvador, L. M., Maizels, E., Hales, D. B., Miyamoto, E., Yamamoto, H., and

Hunzicker-Dunn, M. (2002) *Endocrinol* **143,** 2986–2994
37. Carr, D. W., DeManno, D. A., Atwood, A., Hunzicker-Dunn, M., and Scott, J. D. (1993) *J. Biol. Chem.* **268,** 20729–20732
38. Matus, A. (1991) *J. Cell Sci. (Suppl.)* **15,** 61–67
39. Doll, T., Meichsner, M., Riederer, B. M., Honegger, P., and Matus, A. (1993) *J. Cell Sci.* **106,** 633–639
40. Lim, R. W., and Halpain, S. (2000) *J. Biol. Chem.* **275,** 20578–20587
41. Sharma, N., Kress, Y., and Shafit-Zagardo, B. (1994) *Cell Motil. Cytoskeleton* **27,** 234–247
42. Ferhat, L., Represa, A., Bernard, A., Ben-Ari, Y., and Khrestchatisky, M. (1996) *J. Cell Sci.* **109,** 1095–1103
43. Sanchez, C., Diaz-Nido, J., and Avila, J. (2000) *Prog. Neurobiol.* **61,** 133–168
44. Ferhat, L., Represa, A., Ferhat, W., Ben-Ari, Y., and Khrestchatisky, M. (1998) *Eur. J. Neurosci.* **10,** 161–171
45. Ferhat, L., Bernard, A., Ribas, d. P., Ben-Ari, Y., and Khrestchatisky, M. (1994) *Neurochem. Int.* **25,** 327–338
46. Ferhat, L., Ben-Ari, Y., and Khrestchatisky, M. (1994) *Comptes Rendus l'Academie Sciences Ser. 3 Sci. Vie* **317,** 304–309
47. Theurkauf, W. E., and Vallee, R. B. (1982) *J. Biol. Chem.* **257,** 3284–3290
48. Rubino, H. M., Dammerman, M., Shafit-Zagardo, B., and Erlichman, J. (1989) *Neuron* **3,** 631–638
49. Lowry, O. W., Rosebrough, N. J., Farr, A. L., and Randall, R. J. (1951) *J. Biol. Chem.* **193,** 265–275
50. Hunzicker-Dunn, M. (1981) *J. Biol. Chem.* **256,** 12185–12193
51. Rudolph, S. A., and Krueger, B. K. (1979) *Adv. Cyclic Nucleotide Res.* **10,** 107–133
52. Hunzicker-Dunn, M., Cutler, R. E., Jr., Maizels, E. T., DeManno, D. A., Lamm, M. L. G., Erlichman, J., Sanwal, B. D., and LaBarbera, A. R. (1991) *J. Biol. Chem.* **266,** 7166–7175
53. Scott, J. D., Stofko, R. E., McDonald, J. R., Comer, J. D., Vitalis, E. A., and Mangili, J. A. (1990) *J. Biol. Chem.* **265,** 21561–21566
54. Coghlan, V. M., Langeberg, L. K., Fernandex, A., Lamb, N. J. C., and Scott, J. D. (1994) *J. Biol. Chem.* **269,** 7658–7665
55. Park, Y., Freedman, B. F., Lee, E. J., and Jameson, L. J. (2003) *Diabetologia* **46,** 365–377
56. Yu, R. N., Ito, M., and Jameson, J. L. (1998) *Mol. Endocrinol.* **12,** 1010–1022
57. Rios, R. M., Celati, C., Lohmann, S. M., Borens, M., and Keryer, G. (1992) *EMBO J.* **11,** 1723–1731
58. Hunzicker-Dunn, M., Scott, J. D., and Carr, D. W. (1998) *Biol. Repro.* **58,** 1496–1502
59. Hernandez, M. A., Avila, J., and Andreu, J. M. (1986) *Eur. J. Biochem.* **154,** 41–48
60. Matsunaga, W., Miyata, S., Itoh, M., Kiyohara, T., and Maekawa, S. (2002) *Neuroscience* **111,** 151–162
61. Tucker, R. P. (1990) *Brain Res. Brain Res. Rev.* **15,** 101–120
62. Woodruff, T. K., D'Agostino, J. B., Schwartz, N. B., and Mayo, K. E. (1989) *Endocrinology* **124,** 2193–2199
63. Ozer, R. S., and Halpain, S. (2000) *Mol. Biol. Cell* **11,** 3573–3587
64. Sanchez, C., Perez, M., and Avila, J. (2000) *Eur. J. Cel. Biol.* **79,** 252–260
65. Diviani, D., and Scott, J. D. (2001) *J. Cell Sci.* **114,** 1431–1437
66. Malkinson, A. M., and Butley, M. S. (1981) *Cancer Res.* **41,** 1334–1341
67. Corbin, J. D., Keely, S. L., and Park, C. R. (1975) *J. Biol. Chem.* **250,** 218–225
68. Deleted in proof
69. Herberg, F. W., Maleszka, A., Eide, T., Vossebein, L., and Tasken, K. (2000) *J. Mol. Biol.* **298,** 329–339
70. Shanks, R. A., Steadman, B. T., Schmidt, P. H., and Goldenring, J. R. (2002) *J. Biol. Chem.* **277,** 40967–40972
71. Herman, B., and Albertini, D. F. (1982) *Cell Motil.* **2,** 583–597
72. Albertini, D. F., and Clark, J. I. (1981) *Cell Biol. Int. Rep.* **5,** 387–397
73. Allan, V. J., Thompson, H. M., and McNiven, M. A. (2002) *Nat. Cell Biol.* **4,** E236–E242
74. Thyberg, J., and Moskalewski, S. (1999) *Exp. Cell Res.* **246,** 263–279
75. Deleted in proof
76. Huang, L. J., Durick, K., Weiner, J. A., Chun, J., and Taylor, S. S. (1997) *J. Biol. Chem.* **272,** 8057–8064
77. Deleted in proof
78. Valle, R. B., DiBartolomeis, M. J., and Theurkauf, W. E. (1981) *J. Cell Biol.* **90,** 568–576
79. Cummings, D. E., Brandon, E. P., Planas, J. V., Motamed, K., Idzerda, R. L., and McKnight, G. S. (1996) *Nature* **382,** 622–626
80. Planas, J. V., Cummings, D. E., Idzerda, R. L., and Knight, G. S. (1999) *J. Biol. Chem.* **274,** 36281–36287
81. Schillace, R. V., Andrews, S. F., Liberty, G. A., Davey, M. P., and Carr, D. W. (2002) *J. Immunol.* **168,** 1590–1599
82. Vijayaraghavan, S., Olson, G. E., Nag Das, S., Winfrey, V. P., and Carr, D. W. (1997) *Biol. Reprod.* **57,** 1517–1523

THE JOURNAL OF BIOLOGICAL CHEMISTRY

Vol. 278, No. 9, Issue of February 28, pp. 7167–7179, 2003
Printed in U.S.A.

Follicle-stimulating Hormone Activates Extracellular Signal-regulated Kinase but Not Extracellular Signal-regulated Kinase Kinase through a 100-kDa Phosphotyrosine Phosphatase*

Received for publication, April 22, 2002, and in revised form, November 25, 2002
Published, JBC Papers in Press, December 18, 2002, DOI 10.1074/jbc.M203901200

Joshua Cottom,[a,b,c] Lisa M. Salvador,[a,b] Evelyn T. Maizels,[a,b] Scott Reierstad,[a] Youngkyu Park,[a] Daniel W. Carr,[d] Monika A. Davare,[e,f] Johannes W. Hell,[e,g] Stephen S. Palmer,[h] Paul Dent,[i] Hisaaki Kawakatsu,[j] Masato Ogata,[k] and Mary Hunzicker-Dunn[a,l]

From the Departments of [a]Cell and Molecular Biology, Northwestern University Medical School, Chicago, Illinois 60611, [d]Veterans Affairs Medical Center and Oregon Health Sciences University, Portland, Oregon 97201, [e]Department of Pharmacology, University of Wisconsin, Madison, Wisconsin 53706, [h]Serono Reproductive Biology Institute, Rockland, Massachusetts 02370, [i]Radiation Oncology, Virginia Commonwealth University, Richmond, Virginia 23298, [j]Lung Biology Center, University of California, San Francisco, California 94110, and [k]Biomedial Research Center, Osaka University Medical School, Osaka 565, Japan

In this report we sought to elucidate the mechanism by which the follicle-stimulating hormone (FSH) receptor signals to promote activation of the p42/p44 extracellular signal-regulated protein kinases (ERKs) in granulosa cells. Results show that the ERK kinase MEK and upstream intermediates Raf-1, Ras, Src, and L-type Ca^{2+} channels are already partially activated in vehicle-treated cells and that FSH does not further activate them. This tonic stimulatory pathway appears to be restrained at the level of ERK by a 100-kDa phosphotyrosine phosphatase that associates with ERK in vehicle-treated cells and promotes dephosphorylation of its regulatory Tyr residue, resulting in ERK inactivation. FSH promotes the phosphorylation of this phosphotyrosine phosphatase and its dissociation from ERK, relieving ERK from inhibition and resulting in its activation by the tonic stimulatory pathway and consequent translocation to the nucleus. Consistent with this premise, FSH-stimulated ERK activation is inhibited by the cell-permeable protein kinase A-specific inhibitor peptide Myr-PKI as well as by inhibitors of MEK, Src, a Ca^{2+} channel blocker, and chelation of extracellular Ca^{2+}. These results suggest that FSH stimulates ERK activity in immature granulosa cells by relieving an inhibition imposed by a 100-kDa phosphotyrosine phosphatase.

The cytoplasmic p42/p44 mitogen-activated protein kinase (MAPK)[1]/extracellular signal-regulated kinases (ERKs) comprise a critical convergence point in the signaling pathways initiated by a variety of receptor agonists that promote cellular differentiation or proliferation. For the classic receptor tyrosine kinase-initiated pathway, growth factors like epidermal growth factor (EGF) induce the autophosphorylation of their receptors and create specific binding sites for Src homology 2-containing proteins such as Grb2 (1). Grb2 complexed to Sos associates with the receptor tyrosine kinase, and Sos stimulates GDP release from Ras, leading to Ras activation. Active Ras then binds to Raf-1, leading to its activation, and Raf-1 in turn catalyzes the serine phosphorylation and activation of the MAPK/ERK kinase MEK. MEK then catalyzes the phosphorylation of ERK on regulatory Thr and Tyr residues, resulting in ERK activation.

Guanine nucleotide-binding protein-coupled receptors (GPCRs) are also well known activators of ERK; however, there are a variety of pathways by which GPCRs promote ERK activation. Often, GPCRs such as those activated by lysophosphatidic acid or angiotensin II promote the transactivation of a receptor tyrosine kinase as evidenced by its increased tyrosine phosphorylation (2). Receptor tyrosine kinase transactivation directs the tyrosine phosphorylation of adaptor proteins such as Shc, recruitment of the Grb2-Sos complex, and subsequent Ras activation. It is less clear how GPCRs promote the tyrosine phosphorylation of the receptor tyrosine kinase, although Src activation downstream of the $G\beta\gamma$ has been implicated in some cells (3, 4). For those GPCRs whose activated $G\alpha$ subunits promote increased intracellular Ca^{2+} and consequent activation of Pyk and Src leading to EGF receptor (EGFR) transactivation, Src appears to catalyze the tyrosine phosphorylation

* This work was funded by National Institutes of Health Grants P01 HD21921 (to M. H.-D.), R01 HD36408 (to D. W. C.), and R01 DK52825 (to P. D.), United States Army U. S. Army Medical Research and Materiel Command Grant DAMD 17-00-1-0386 and Northwestern University Program in Endocrinology, Diabetes, and Hormone Action T32 DK07169 (to L. M. S.). Preliminary results were presented at the 83rd Annual Endocrine Society Meeting, June 20–23, 2001, Denver, CO. The costs of publication of this article were defrayed in part by the payment of page charges. This article must therefore be hereby marked "*advertisement*" in accordance with 18 U.S.C. Section 1734 solely to indicate this fact.

[b] These authors contributed equally to this work.

[c] Present address: Wyeth Ayerst Women's Health Research Institute, 145 King of Prussia Rd., Radnor, PA 19087.

[f] Present address: Vollum Institute, 3181 S. W. Sam Jackson Park Rd., Portland, OR 97291.

[g] Present address: Dept. of Pharmacology, University of Iowa College of Medicine, 51 Newton Rd., Iowa City, IA 55242.

[l] To whom correspondence should be addressed: Dept. of Cell and Molecular Biology, Northwestern University Medical School, 303 East Chicago Ave., Chicago, IL 60611. Tel.: 312-503-7459; Fax: 312-503-0566; E-mail: mhd@northwestern.edu.

[1] The abbreviations used are: MAPK, mitogen-activated protein kinase; ERK, extracellular signal-regulated kinase; PKA, protein kinase A; PKI, heat-stable PKA inhibitor; FSH, follicle-stimulating hormone; MEK, MAPK/ERK kinase; StAR, steroidogenic acute regulatory protein; EGFR, epidermal growth factor (EGF) receptor; CREB, cAMP-response element-binding protein; CPT-cAMP, 8-(4-chlorophenylthio)-cAMP; PMA, phorbol myristic acid; AKAP, A-kinase anchoring protein; RIPA, radioimmune precipitation assay buffer; GPCR, G protein-coupled receptor; PTP, protein-tyrosine phosphatase; R, regulatory subunit of PKA; PMSF, phenylmethylsulfonyl fluoride; BD, binding domain; PBS, phosphate-buffered saline; TRITC, tetramethylrhodamine isothiocyanate; GST, glutathione *S*-transferase; MOPS, 4-morpholinepropanesulfonic acid; GDS, guanine nucleotide dissociation stimulator; Akt, also known as protein kinase B.

of this receptor tyrosine kinase (5). GPCRs can also stimulate EGFR activation by stimulating the proteolytic cleavage and resulting release of the soluble EGFR ligand, heparin binding EGF (6).

The G protein-regulated second messenger cAMP has also been shown to both inhibit and activate ERKs, depending on the cell type. In cells where cAMP inhibits growth factor-stimulated cell proliferation and ERK activation, cAMP via PKA inhibits Raf-1 activity, although the relevant PKA substrate has been controversial (7, 8). A recent report shows that the elusive PKA substrate in this pathway appears to be Src (9). In fibroblasts, PKA-catalyzed Src phosphorylation directs the activation of Rap1, which binds and sequesters Raf-1, thereby preventing Ras activation of Raf-1 (9). Conversely, in PC12 cells, where cAMP stimulates differentiation, and in HEK293 cells transfected with the β_2-adrenergic receptor, cAMP via PKA promotes Rap1 phosphorylation and activation of B-Raf, leading to MEK and ERK activation (10, 11). cAMP can also bind to and directly activate the Rap1 guanine nucleotide exchange factor EPAC independent of PKA (12, 13), leading to B-Raf and ERK activation (14). In melanocytes, where cAMP leads to cell differentiation, cAMP independent of PKA promotes Ras and B-Raf activation, leading to ERK activation independent of Rap1 and EPAC (15). Thus, depending on the cell type, cAMP appears to utilize a variety of pathways to modulate ERK activity.

Ovarian granulosa cells comprise a unique cellular model in which the majority of both the differentiation and proliferation responses to the agonist follicle-stimulating hormone (FSH) are mediated by cAMP (16). The FSH receptor is a seven-transmembrane GPCR coupled to adenylyl cyclase (17) and is expressed exclusively on ovarian granulosa cells in female mammals (18). FSH stimulates both granulosa cell proliferation as well as differentiation to a preovulatory phenotype (16). Although the induction of cyclin D2 can be stimulated in primary granulosa cell cultures by cAMP (19), the proliferative response to FSH is poorly understood and likely includes a paracrine component from surrounding thecal cells since rat granulosa cells do not proliferate in serum-free media in the presence of FSH alone (16, 20). The differentiation response is readily induced in serum-free granulosa cells by FSH and is characterized by the induction of enzymes required for estrogen and progesterone biosynthesis, the luteinizing hormone receptor, the type II regulatory (RII) β subunit of PKA (16, 21), inhibin-α (22), and an A kinase-anchoring protein AKAP80 (23). We have shown that FSH-stimulated activation of the immediate early genes c-Fos and serum glucocorticoid kinase as well as inhibin-α are mediated in part via the apparently direct phosphorylation of histone H3 on Ser-10 by PKA (24). Additionally, FSH leads to ERK activation in target ovarian granulosa cells in an apparently PKA-dependent manner, based on the ability of the PKA inhibitor H89 to inhibit FSH-stimulated ERK activation (24, 25). Recent results using a transformed granulosa cell line support a role for PKA in FSH-stimulated ERK activation (26). However, the mechanism by which PKA leads to ERK activation in granulosa cells is not known.

In this investigation we sought to identify the cellular pathway by which FSH promotes ERK activation in primary granulosa cells. Results show that MEK, Raf-1, Ras, and L-type Ca^{2+} channels are already partially activated in vehicle-treated granulosa cells. This pathway appears to be restrained at the level of ERK by a 100-kDa phosphotyrosine phosphatase (PTP) that associates with ERK in vehicle-treated cells. FSH promotes the PKA-dependent phosphorylation of this PTP and its dissociation from ERK, leading to ERK activation and translocation to the nucleus. Consistent with this premise, FSH-stimulated ERK activation is inhibited by the cell-permeable PKA-specific inhibitor peptide PKI as well as by inhibitors of MEK, Src, EGFR tyrosine kinase activity, a Ca^{2+} channel blocker, and chelation of extracellular Ca^{2+}. These results suggest that FSH enhances ERK activity in immature granulosa cells by relieving an inhibition imposed by a 100-kDa PTP.

EXPERIMENTAL PROCEDURES

Materials—Ovine FSH (oFSH-19) was kindly provided by Dr. A. F. Parlow of the National Hormone and Pituitary Agency of the National Institute of Diabetes and Digestive and Kidney Diseases (Torrence, CA). The following were purchased. H89, AG1478, GF109203X, 8-(4-chlorophenylthio)-cAMP (CPT-cAMP), nifedipine, PP1 (4-amino-5-(4-methylphenyl)-7-(*t*-butyl)pyradzolol[3,4-d]pyrimidine), A23187, ionomycin, okadaic acid, and phorbol myristic acid (PMA) were from LC Laboratories (San Diego, CA); PD98059, BayK8644, myristoylated PKA inhibitor (PKI) 14–22 amide, farnesyltransferase inhibitor 1, and wortmannin were from Calbiochem; pertussis toxin was from List Biochemicals Inc. (Campbell, CA); anti-histone H3 phosphorylated on Ser-10, anti-CREB phosphorylated on Ser-133, anti-phospho-Tyr, Raf-1 Ras binding domain (BD) and Ral GDS-Rap BD glutathione-agarose conjugates, anti-Rap1, anti-human EGF receptor, and anti-CREB antibodies were from Upstate Biotechnology (Lake Placid, NY); anti-MAPK/ERK phosphorylated on Thr-202 and Tyr-204 was from Promega (Madison, WI); anti-MAPK/ERK antibody was from Zymed Laboratories Inc. (San Francisco, CA); anti-protein kinase C (PKC) ζ, anti-Raf-1 (C-12), anti-B-Raf (C-19), anti-ERK2-agarose conjugate, anti-AKT, and anti-Rap1 antibodies were from Santa Cruz Biotechnology (Santa Cruz, CA); anti-MEK phosphorylated on Ser-17 and Ser-221, total MEK, anti-AKT phosphorylated on Thr-308, and anti-histone H3 phosphorylated on Ser-10 antibodies were from New England Biolabs/Cell Signaling Technologies (Beverly, MA); anti-StAR antibody was kindly provided by Dr. Dale Buchanan Hales (27); anti-Ras and -PKCδ antibodies were from Transduction Laboratories (Lexington, KY); recombinant human EGF was from Intergen Co. (Purchase, NY); ADP-agarose was from Sigma; Trizol™ was from Invitrogen. All other chemicals were from sources previously described (28–30). The preimmune serum and polyclonal anti-PTP-SL antibody, directed to GST-mPTP-SL 147–549 (31), were kindly provided by Dr. Rafael Pulido. An affinity-purified monoclonal anti-PTPBR7 was generated by the Ogata laboratory by immunizing mice with a maltose binding fusion protein containing residues 289–656 in the cytoplasmic portion of murine PTPBR7. An antibody that recognizes active Src unphosphorylated on Tyr-532 was previously described (32).

Granulosa Cell Culture, Immunofluorescence, and Western Blotting—Granulosa cells were isolated from ovaries of 26-day-old Sprague-Dawley rats primed with subcutaneous injections of 1.5 mg of estradiol-17β on days 23–25 to promote growth of preantral follicles (23, 29). Cells were either plated on fibronectin-coated 33-mm plastic dishes (Falcon) at a density of ~5–10 × 10^6 cells/dish in serum-free medium (29), as indicated, or on coverslips (for immunofluorescence) and treated with indicated additions ~20 h after plating. Treatments were terminated by aspirating medium and rinsing cells once with PBS. Total cell extracts were collected by scraping cells in 0.5 ml of SDS sample buffer (33) followed by heat denaturation. Protein concentrations were controlled by plating identical cell numbers per plate in each experiment then loading equal volumes of total cell extract per gel lane. Equal protein loading was confirmed by total ERK, PKCδ, phosphatidylinositol 3-kinase, or Ponceau S staining as indicated. Collection of soluble cell extracts is described below. Granulosa cell proteins were separated by SDS-PAGE (10 or 12% acrylamide in running gel) (34) and transferred to Hybond C-extra nitrocellulose (Amersham Biosciences). Blots were incubated with primary antibody overnight at 4° C, and antigen-antibody complexes were detected by enhanced chemiluminescence (Amersham Biosciences). For immunofluorescence, cells were treated as indicated, fixed with 3.7% formaldehyde, permeabilized with 1% Triton X-100 in PBS, washed, blocked for 1 h in 1% bovine serum albumin in PBS, incubated overnight at 4° C with anti-histone H3 phosphorylated on Ser-10 (1:100 dilution, monoclonal antibody from New England Biolabs/Cell Signaling) and anti-ERK phosphorylated on Thr-202 and Tyr-204 (1:100 dilution, polyclonal antibody from Promega) in PBS containing 1% bovine serum albumin. Coverslips were washed and incubated for 1 h at 37° C with fluorescein isothiocyanate-conjugated goat anti-rabbit secondary antibody and TRITC-conjugated goat anti-mouse secondary antibody (Jackson ImmunoResearch, West Grove, PA). Cells on coverslips were washed and mounted on slides in Vecta-

shield™ mounting medium (Vector Laboratories, Burlingame, CA). Slides were analyzed by a Zeiss LFM 510 confocal microscope.

Rap Phosphorylation, Ras, Rap, and Raf Activation Assays, and Immunoprecipitations—Raf activity was measured by an immunocomplex kinase assay using purified His_6-MEK1 as substrate (35). After treatment of cells (6×10^6 cells/dish) with vehicle, FSH, or EGF for 2 min, cells were lysed in buffer A (10 mM potassium phosphate, pH 7.0, 1 mM EDTA, 5 mM EGTA, 10 mM $MgCl_2$, 50 mM β-glycerol phosphate, 1 mM sodium orthovanadate, 1 mM sodium pyrophosphate, 2 mM dithiothreitol, 0.23 mM phenylmethanesulfonyl fluoride (PMSF), 0.5% Nonidet P-40, and 0.1% deoxycholate), and insoluble cell debris was removed by centrifugation at 15,000 × *g* for 2 min. Raf-1 and B-Raf were immunoprecipitated overnight from the soluble cell extract as protein A + G-agarose complexes. Washed immunoprecipitates were then incubated for 20 min at 37° C in a 50-μl reaction mix containing 0.5 μg of His_6-MEK1, 0.1 mM [γ-^{32}P]ATP (10 μCi/tube), 15 mM $MgCl_2$, 1 mM $MnCl_2$, and 25 mM Tris-HCl, pH 7.4, followed by the addition of SDS sample buffer (33), heat denaturation, and SDS-PAGE.

To detect Rap1 phosphorylation, cells were incubated for 1 h in phosphate-free medium then overnight with 0.5 mCi of $^{32}P_i$/6 × 10^6 cells and treated as indicated. Cells were lysed in buffer B (10 mM Tris-HCl, pH 7.2, 150 mM NaCl, 50 mM β-glycerol phosphate, 1 mM sodium orthovanadate, 0.23 mM PMSF, 5 μg/ml aprotinin, 1% Nonidet P-40, and 0.5% deoxycholate, 0.1% SDS), insoluble cell debris was removed by centrifugation, and Rap1 was immunoprecipitated using anti-Rap1 antibody (Santa Cruz Biotechnology) as protein A + G-agarose complexes. Immunoprecipitates were washed, and immunoprecipitated Rap1 was mixed with SDS sample buffer and heat-denatured. After separation of proteins in the immunoprecipitated complex by SDS-PAGE, proteins were transferred to nitrocellulose and subjected to autoradiography and, after decay of radioactivity, to a Rap1 immunoblot.

To detect active Ras or Rap1, cells were treated as indicated, rinsed with phosphate-buffered saline, lysed in buffer C (25 mM Hepes, pH 7.5, 150 mM NaCl, 1% Nonidet P-40, 0.25% deoxycholate, 10% glycerol, 25 mM NaF, 10 mM $MgCl_2$, 1 mM EDTA, 1 mM sodium orthovanadate, 10 μg/ml aprotinin, and 10 μg/ml leupeptin) or buffer B containing protease inhibitors, respectively, and soluble extract was collected. The soluble extract was incubated with control GST plus glutathione-agarose, GST-tagged Raf-1 Ras BD, or Ral GDS-Rap BD glutathione-agarose conjugates for 3 h at 4 °C, and agarose pellets were collected and washed 4 times with radioimmune precipitation assay (RIPA) buffer (10 mM Tris-HCl, pH 7.2, 150 mM NaCl, 1% deoxycholate, 1% Triton X-100, 0.1% SDS, 1 mM sodium orthovanadate, 40 mM PMSF), mixed with SDS sample buffer, and heat-denatured. Active Ras bound to the Ras BD on Raf and active Rap1 bound to the Rap BD on Ral GDS were detected by Ras and Rap1 immunoblots, respectively (36, 37).

For anti-ERK-agarose pull-downs from total ovarian extracts, soluble ovarian extracts were prepared in buffer A and incubated (3 h at 4 °C) with anti-ERK-agarose or control ADP-agarose, and agarose pellets were collected, washed 4 times, mixed with SDS sample buffer, and heat-denatured. For anti-ERK-agarose pull-downs from soluble ovarian extracts enriched in PTP-SL, ovaries of 13 estrogen-treated rats (see above) were homogenized with 15 strokes using a ground glass homogenizer in buffer D (10 mM Tris-HCl, pH 7.0, 5 mM EDTA, 1 mM EGTA, 0.32 M sucrose, 5 μg/ml pepstatin, 5 μg/ml aprotinin, and 10 μg/ml leupeptin, 50 μg/ml soybean trypsin inhibitor, 10 mM benzamidine, and 10 μg/ml E-64). The homogenate was centrifuged at 105,000 × *g* for 15 min, supernatant was loaded onto a DEAE-cellulose column, the column was extensively washed with 10 mM potassium phosphate, pH 7.0, and PTP-SL was batch-eluted (along with RIIβ PKA holoenzyme (38)) with 0.15 M potassium phosphate, all at 4 °C. Eluate was concentrated to 1.15 ml, an aliquot was taken and mixed with SDS sample buffer and heat-denatured (designated "input"), and equal volumes of the eluate were mixed with 0.08 ml of ADP-agarose as a control or anti-ERK-agarose, respectively. After mixing overnight at 4 °C, the flow-through (designated "FT") was collected, mixed with SDS sample buffer, and heat-denatured, the agarose pellet was washed 4 times with RIPA buffer, 2 times with high salt RIPA buffer (containing 1 M NaCl), and 2 times with RIPA buffer, and bound proteins were eluted (designated "eluate") with 0.25 ml of SDS sample buffer and heat-denatured. For anti-ERK-agarose pull-downs, granulosa cells were sonicated for 1 min at 4° C in buffer D, extract was centrifuged at 15,000 × *g* for 5 min, and the supernatant was mixed with 0.06 ml of ADP-agarose or anti-ERK-agarose and rotated for 4 h at 4 °C. The rest of the details are as described above.

To detect active, Tyr-phosphorylated EGF receptor, 10×10^6 cells/dish were rinsed in phosphate-buffered saline and lysed by sonicating for 1 min at 4° C in buffer E (10 mM potassium phosphate, pH 7.0, 1 mM EDTA, 5 mM EGTA, 10 mM $MgCl_2$, 50 mM β-glycerol phosphate, 1 mM sodium orthovanadate, 1 mM sodium pyrophosphate, 2 mM dithiothreitol, 20 μM leupeptin, 100 μg/ml pepstatin). The membrane pellet was collected by centrifuging lysate at 15,000 × *g* for 10 min, and the resulting pellet was mixed with SDS sample buffer, heat-denatured, and probed with anti-phospho-Tyr antibody. Alternatively, granulosa cell extracts prepared by sonicating cells in buffer F (50 mM Tris-HCl, pH 7.5, 150 mM NaCl, 1% Nonidet P-40, 1 mM PMSF, 1 μg/ml aprotinin, 100 mM NaF, 2 mM sodium orthovanadate, and 20 mM sodium pyrophosphate) were subjected to immunoprecipitations with either anti-phospho-Tyr or anti-EGFR antibody; immunoprecipitates were washed with buffer G (20 mM Hepes, pH 7.0, 150 mM NaCl, 10% glycerol, 0.1% Triton X-100) and, after SDS-PAGE and transfer to nitrocellulose, probed with anti-EGFR or anti-phospho-Tyr antibodies, respectively.

For PTP-SL immunoprecipitations, cells were treated as indicated, rinsed, and lysed by sonicating for 1 min at 4° C in buffer F. Insoluble cell debris was removed by centrifugation. The soluble extract was first precleared with protein A+G-agarose and then incubated with anti-PTP-SL antibody plus protein A+G agarose for 4 h at 4° C (31). The agarose pellet was collected, washed with buffer G, and heat-denatured.

For Ca^{2+} channel immunoprecipitation, 24×10^6 cells were treated as indicated, rinsed with phosphate-buffered saline, and frozen at −70 °C. Using an antibody (anti-FP1) that recognizes the 210-kDa α subunit of class C L-type Ca^{2+} channel independent of its phosphorylation state, the α_{1C} subunit was immunoprecipitated from cell extracts solubilized in buffer H (1% Triton X-100, 10 mM EDTA, 10 mM EGTA, 25 mM sodium pyrophosphate, 25 mM sodium fluoride, 10 mM Tris-HCl, pH 7.4, 100 mM NaCl, 1 mM *p*-nitrophenyl phosphate, 1 μM microcystin, 1 μg/ml pepstatin, 10 μg/ml leupeptin, 20 μg/ml aprotinin, 200 nM PMSF, and 8 μg/ml each calpain inhibitors I and II). The precipitated proteins were washed and mixed with SDS sample buffer, subjected to SDS-PAGE, and transferred to nitrocellulose (39). Blots were first probed with affinity-purified anti-CH3P antibody to detect the relative level of phosphorylation at Ser-1928 on the α_{1C} subunit. Blots were then stripped and reprobed with anti-FP1 antibody to detect total α_{1C} subunit precipitated (39).

Northern Blot Analysis—Total RNA was isolated from rat tissues (brain, liver, and ovary) using Trizol™. RNA (5 μg each) was denatured in formamide and formaldehyde and electrophoresed through formaldehyde-containing 1% agarose gel in NorthernMax™ MOPS gel running buffer (Ambion Inc., Austin, TX). RNA was blotted to a nitrocellulose membrane (Schleicher & Schuell), and the membrane was cross-linked and hybridized with NorthernMax™ prehybridization/hybridization buffer using PTP-SL cDNA (3×10^6 cpm/ml) as a probe. PTP-SL cDNA (429 base pairs) corresponding to nucleotides 441–864 was labeled with [α-^{32}P]dCTP by Rediprime™ II DNA-labeling kit (Amersham Biosciences). The blot was washed 2 times with 2× SSC (1× SSC = 0.15 M NaCl and 0.015 M sodium citrate) and 0.1% SDS at room temperature and subjected to autoradiography.

In-gel PTP Assay—An in-gel PTP assay in which [^{32}P]poly(glutamic acid-tyrosine) was incorporated into the gel was performed (40). [^{32}P]Poly(glutamic acid-tyrosine) (1 mg) was phosphorylated with 50 units of active Src (Upstate Biotechnology), partially purified (40), and used at 1×10^6 cpm/ml in gel. After electrophoresis, SDS was removed, proteins were renatured, and the in-gel phosphatase reaction was performed by incubating the gel with 50 mM Tris-HCl, pH 8.0, 0.3% β-mercaptoethanol, 0.04% Tween 40, 1 mM EDTA, and 4 mM dithiothreitol for 6 h at room temperature. The gel was then stained, dried, and subjected to autoradiography. PTP activity was detected as regions on the autoradiogram from which ^{32}P was removed.

Other—Radioimmunoassays for progesterone and inhibin were conducted by the Hormone and Neurotransmitter Core Facility at Northwestern University (P01-HD21921). A commercially available kit (ICN Biochemicals, Carson, CA) was used for progesterone radioimmunoassay. Inhibin radioimmunoassay (41) used rat inhibin α (1–27) as the standard and for iodination and sheep anti-Tyr-27 rat inhibin α (antibody (Ab) 795). DEAE-cellulose chromatography, cAMP-agarose affinity chromatography, and RII overlay assays were performed as previously described (38). Results were analyzed using Student's *t* test ($p \leq 0.05$) (42) and are presented as the means ± S.E. ($n > 3$) or as the means ± range ($n = 2$).

RESULTS

FSH-stimulated ERK Activation Is PKA-dependent—We first investigated the time course of FSH-dependent ERK activation in serum-free cultures of primary rat granulosa cells.

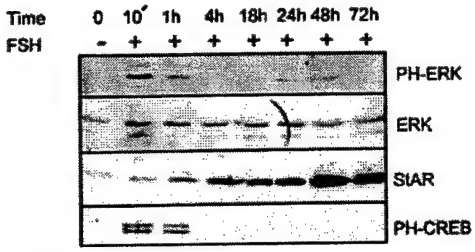

FIG. 1. **Time course of FSH-stimulated phosphorylation of ERK and CREB and expression of StAR.** Granulosa cells were treated for the indicated times with 50 ng/ml FSH followed by preparation of total cell extracts, as described under "Experimental Procedures." After SDS-PAGE and transfer of proteins to nitrocellulose, blots were probed with the indicated antibodies to phosphorylated (*PH*) and/or total p42/p44 MAPK/ERK (*ERK*), PH-CREB, and StAR. Results are representative of two independent experiments. Results for PH-ERK and -CREB at times 0, 10 min and 1 and 4 h were previously reported (24).

ERK activation, identified by the phospho-specific ERK antibodies, was readily detected by 10 min and was reduced by 1 h after FSH addition (Fig. 1). ERK activity remained low at 48 and 72 h after FSH addition, when granulosa cells had differentiated to the mature phenotype, as evidenced by the induction of StAR (Fig. 1), the protein responsible for mobilizing cholesterol substrate for steroidogenesis (43). Increased phosphorylation of CREB on Ser-133, an established PKA target (44), was detected by 10 min and undetectable by 4 h post-FSH. For subsequent studies, cells were treated for 10 min to detect maximal ERK activation unless otherwise indicated.

To determine whether or not FSH-stimulated ERK activation was cAMP- and PKA-dependent, cells were treated with FSH and forskolin (Fig. 2*A*) or the cell-permeable cAMP analog CPT-cAMP (Fig. 2*B*) or with FSH in the absence and presence of the cell-permeable-selective PKA inhibitor peptide, Myr-PKI (Fig. 2*C*). FSH stimulated ERK phosphorylation 4.1 ± 0.7-fold (n = 6) (Fig. 2*A*). Forskolin and CPT-cAMP mimicked FSH and activated ERK 3.1 ± 0.7 (n = 5)- and 5.7-fold, respectively. Myr-PKI reduced FSH-stimulated ERK activation by 53 ± 8% (n = 3). CREB phosphorylation in response to forskolin, CPT-cAMP, and the PKA inhibitor mirrored that of ERK. These results support our earlier studies (25) with the PKA inhibitor H89 (45, 46) and confirm that the majority of FSH-stimulated ERK activation in this granulosa cell model is PKA-dependent.

Treatment of granulosa cells with FSH for 30 min resulted in localization of the majority of phosphorylated/active ERK in the nucleus (Fig. 3*e*) in conjunction with phosphorylated histone H3 (Fig. 3*f*). Both ERK and histone H3 phosphorylations were abrogated by pretreatment of cells with Myr-PKI (Fig. 3, *m* and *n*). These results are consistent with the hypothesis that FSH stimulates ERK activation to promote changes in gene expression leading to granulosa cell differentiation.

Cell-permeable cAMP analogs are also known to mimic the long term responses to FSH, leading to granulosa cell differentiation (16). That PKA is also required for the differentiation of granulosa cells to a preovulatory phenotype is evidenced by the ability of the PKA inhibitor H89 (Fig. 4) and Myr-PKI (not shown) to block FSH-stimulated induction of AKAP80 (by 98 ± 1.5%, n = 2). H89 or Myr-PKI also inhibited the induction by FSH of StAR expression (not shown) and progesterone production (by 97.7 ± 2.3%, n = 2).

FSH-stimulated ERK phosphorylation as well as CREB phosphorylation was independent of the inhibitory G protein G_i, based on the inability of pertussis toxin, which inhibits receptor-stimulated G_i activation, to modulate FSH-stimulated ERK activation (not shown). These results are consistent with a direct action of PKA activated downstream of the FSH receptor to modulate ERK activity rather than the pathway reported for the β_2-adrenergic receptor in which the PKA-phosphorylated β_2-adrenergic receptor preferentially promotes activation of G_i and consequent ERK activation via $G\beta\gamma$ (47).

FSH-stimulated ERK Activation Is Dependent on MEK Activity, but FSH Does Not Stimulate MEK Activation—Because ERK activation requires the upstream kinase MEK, we utilized the MEK inhibitor PD98059 (48) to confirm that FSH-stimulated ERK activation also required MEK. Results showed that PD98059 fully blocked (by 100%, n = 2) acute FSH-stimulated ERK activation (Fig. 5*A*) but did not affect CREB phosphorylation (Fig. 5*B*), consistent with an earlier report (24). PD98059 also reduced the FSH-stimulated induction of AKAP80 with granulosa cell differentiation to a mature phenotype (Fig. 5*C*) by 90 ± 9% (n = 3) but did not consistently modulate progesterone (22 ± 12% inhibition, n = 5) or inhibin (3 ± 3% inhibition, n = 2) secretion or StAR expression (not shown) by these cells. However, when we evaluated the ability of FSH to stimulate MEK phosphorylation, results showed that MEK exhibited a detectable level of phosphorylation that was not enhanced by FSH or forskolin (10-min treatments) but was strongly increased by EGF (Fig. 5*D*) and the PKC activator PMA (Fig. 5*E*). Consistent with this result, a detailed time course of FSH treatment of granulosa cells confirmed equivalent MEK phosphorylation at time 0 (*i.e.* in the absence of FSH) and at 10–20 min post-FSH addition when FSH stimulated maximal ERK phosphorylation (Fig. 5*F*). These results show that FSH-stimulated ERK activation is dependent on MEK activation but that FSH does not stimulate MEK activation. However, mitogens like EGF or PMA that activate ERK through mechanisms independent of PKA promote strong MEK activation.

FSH Does Not Enhance B-Raf or Raf-1 Activities—The presence in granulosa cells of detectable MEK phosphorylation that was unaffected by FSH suggested that upstream enzymes in this pathway might also exhibit detectable activity in the absence of FSH. The activities of B-Raf and Raf-1 were evaluated in an immunocomplex kinase assay using recombinant His_6-MEK1 as substrate. Results in Fig. 6*A* showed that neither B-Raf nor Raf-1 activities was increased by FSH. Moreover, although the commonly high basal level of B-Raf activity (49) was readily detected and not affected by EGF (compare *lanes 1* and *3*), Raf-1 activity was detected in vehicle-treated cells and was strongly enhanced by EGF (compare *lanes 4* and *6*). These results indicate that FSH does not stimulate B-Raf or Raf-1 activation. Rather, a basal level of activity for both kinases was detected.

FSH actually stimulated the phosphorylation of Raf-1 on Ser-259 (Fig. 5*F*), an established inhibitory phosphorylation site (14, 50). Coincident with the inhibition of Raf-1 activity upon its phosphorylation on Ser-259, both MEK and ERK phosphorylations decreased beginning ~30 min post-FSH addition (see Fig. 5*F*). Based on evidence (*a*) that Raf-1 is phosphorylated on Ser-259 by AKT (50), (*b*) that FSH stimulates AKT phosphorylation/activation (Ref. 53 and Fig. 5*G*), and (*c*) that FSH-stimulated Raf-1 phosphorylation is inhibited by the phosphatidylinositol 3-kinase inhibitor wortmannin (not shown), we can conclude that FSH-stimulated Raf-1 phosphorylation is most likely downstream of FSH-stimulated AKT.

FSH Does Not Activate Ras or Rap1—We also evaluated the activation state of the upstream activators Ras and Rap1 in vehicle- and FSH-treated cells. Active Ras, indicated by Ras-GTP binding to the Ras BD on Raf-1 (14), was readily detected in vehicle-treated granulosa cells (Fig. 6*B*, *lane 1*). FSH did not increase the amount of Ras bound to the Ras BD of Raf-1 (Fig. 6*B*) (the reduced binding of Ras to the Ras BD of Raf-1 in

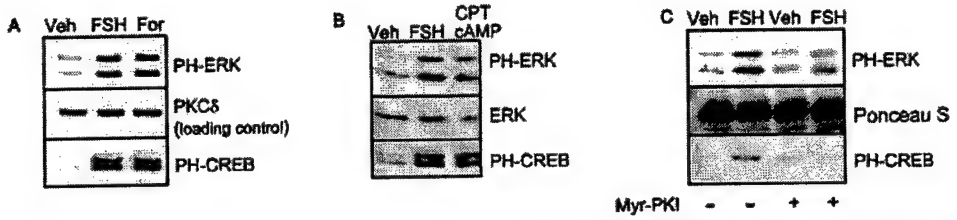

FIG. 2. **FSH-stimulated p42/44 MAPK/ERK activation is mimicked by forskolin and CPT-cAMP and inhibited by Myr-PKI.** In *panel A*, granulosa cells were treated for 10 min with 50 ng/ml FSH or 10 μM forskolin (*For*). After SDS-PAGE and transfer of proteins to nitrocellulose, total cell extracts were probed with the indicated antibodies. Results are representative of more than five experiments. *PH*, phosphorylated. In *panel B*, granulosa cells were treated for 10 min with 50 ng/ml FSH or 1 mM CPT-cAMP, and total cell extracts were analyzed as in *panel A*. In *panel C*, granulosa cells were pretreated for 60 min with vehicle (*Veh*) or 50 μM Myr-PKI amide followed by treatment with vehicle or 50 ng/ml FSH for 10 min. After SDS-PAGE and transfer of proteins to nitrocellulose, blots were first stained with Ponceau S to confirm equal protein loading per lane and then probed with the indicated antibodies. For the rest of the details see the legend to Fig. 1. Results are representative of three separate experiments.

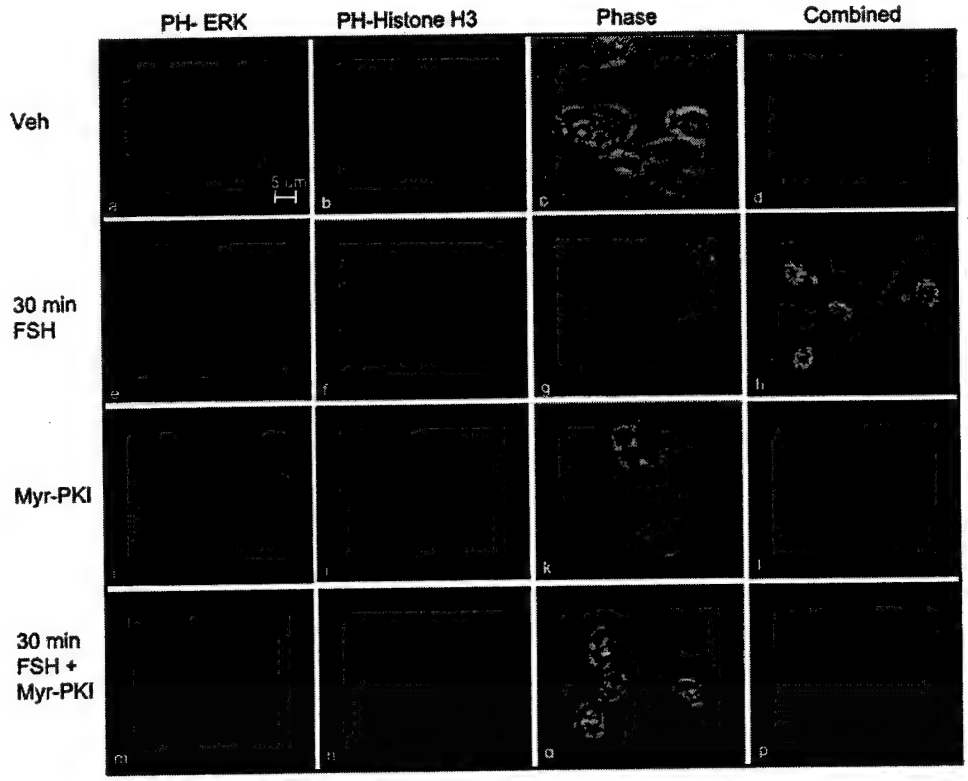

FIG. 3. **FSH-stimulated phospho-ERK is predominately localized to the nucleus of granulosa cells.** Granulosa cells on coverslips were pretreated 30 min with vehicle (*Veh*) or 50 μM Myr-PKI and then treated 30 min with vehicle or 50 ng/ml FSH. Cells were then subjected to immunofluorescence using anti-PH-ERK (polyclonal antibody, Promega) and anti-phosphorylated (*PH*)-histone H3 (monoclonal antibody, New England Biolabs/Cell Signaling), as detailed under "Experimental Procedures." Phase contrast image of cells is also shown. *Combined* shows the image of PH-ERK plus phosphorylated-histone H3. Results are representative of two separate experiments.

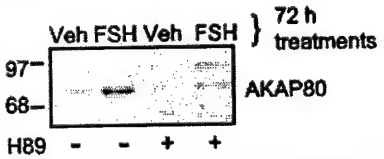

FIG. 4. **FSH-dependent induction of AKAP80 is prevented by H89.** Granulosa cells were pretreated 60 min with vehicle (*Veh*) or 10 μM H89 (in 50% Me_2SO) and then treated for 72 h in the absence and presence of 50 ng/ml FSH. Total cell extracts were subjected to SDS-PAGE, and proteins were transferred to Immobilon then subjected to an RII overlay assay to detect AKAPs, as detailed under "Experimental Procedures." Results are representative of two experiments.

response to FSH was not a consistent observation). Inhibition of the farnesylation of Ras by the cell-permeable farnesyltransferase inhibitor 1, resulting in reduced Ras but not Rap-1 function (54), also reduced FSH-dependent ERK activation by 66 ± 7% ($n = 2$) (Fig. 6*C*), consistent with an obligatory role for Ras in FSH-stimulated ERK activation. Although direct activation by cAMP of the guanine nucleotide exchange factors for Rap1 cannot explain PKA-dependent ERK activation in granulosa cells especially in the absence of detectable FSH-stimulated B-Raf activation (12, 13, 55), PKA is reported to phosphorylate Rap1 to promote its activation (57). To determine whether Rap1 was phosphorylated in response to FSH treatment granulosa cell ATP pools were labeled with $^{32}P_i$, and cells were pretreated with or without the PKA inhibitor H89 and then treated with vehicle or FSH for 10 min followed by a Rap1 immunoprecipitation. Results showed that although Rap1 was readily immunoprecipitated (Fig. 6*D*, *lower panel*), phosphorylated Rap1 was not detected in vehicle or FSH-treated granulosa cells (Fig. 6*D*, *upper panel*). Moreover, FSH did not stimulate the GTP loading (activation) of Rap1, as evidenced (Fig.

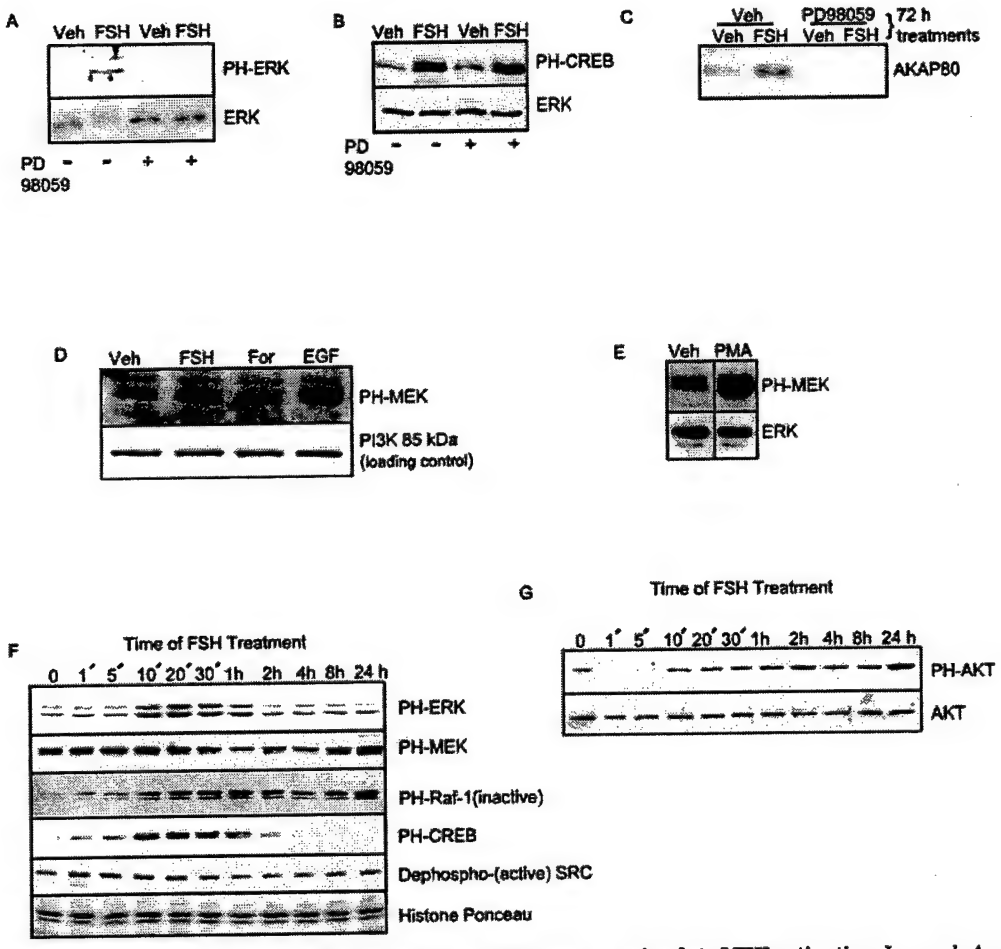

FIG. 5. **FSH-stimulated ERK activation is MEK-dependent, but FSH does not stimulate MEK activation.** In *panels A* and *B*, granulosa cells were pretreated for 90 min with 50 μM PD98059 or vehicle (*Veh*) followed by treatment for 10 min with vehicle or 50 ng/ml FSH and preparation of total cell extracts as in Fig. 1. Results in *panel A* are representative of two experiments. *PH*, phosphorylated. In *Panel C*, after pretreatments for 90 min with vehicle or 50 μM PD98059, cells were treated for 72 h with vehicle or 50 ng/ml FSH. For the rest of the details see the legend to Fig. 4. Results are representative of three separate experiments. In *panels D* and *E*, granulosa cells were treated for 10 min with vehicle, 50 ng/ml FSH, 10 μM forskolin, 25 ng/ml EGF, or 10 nM PMA as indicated. Total cell extracts were probed, as described in the legend to Fig. 1. Results for *panel C* are representative of four experiments. In *panels F* and *G*, granulosa cells were treated for the indicated times with 50 ng/ml FSH, and total cell extracts were probed with the indicated antibodies. Phosphorylated-Raf1 antibody is directed to Ser-259, an inhibitory phosphorylation site. Results are representative of two experiments. The data in *panel F* showing FSH-stimulated ERK and CREB phosphorylation have been previously reported (24).

6*E*) by the equivalent binding of GTP-Rap1 to the Ral GDS-Rap BD in vehicle and FSH-treated granulosa cells. Taken together, these results suggest the existence of a tonic stimulatory pathway leading to modest activation of Rap1, Ras, Raf-1, and MEK in vehicle-treated granulosa cells. In the following experiments, we seek to identify upstream components of this tonic pathway.

Upstream Components of the Tonic Pathway Leading to MEK Activation Include Src, the EGFR, and Extracellular Ca^{2+}—We initially determined whether Src activity contributed to FSH-stimulated ERK activation. Pretreatment of cells with the Src inhibitor PP1 completely blocked FSH-stimulated ERK activation but did not affect CREB phosphorylation (Fig. 7*A*). Blots probed with an antibody that detects active Src by recognizing unphosphorylated Tyr-532 (designated "dephospho-Src antibody") (32) showed that Src activity was readily detected in untreated granulosa cells (Fig. 7*B*, *lane 1*) and not further activated at 10-min post-FSH (Fig. 7*B*, *lane 2*) or at earlier or later FSH treatment times (Fig. 5*F*). Consistent with this result, the general tyrosine kinase inhibitor genistein completely blocked FSH-stimulated ERK phosphorylation (Fig. 8*A*). The EGFR-selective tyrosine kinase inhibitor AG1478 (58) also completely prevented FSH-, forskolin-, and EGF-stimulated ERK phosphorylation, whereas only EGF-stimulated CREB phosphorylation was blocked by AG1478 (Fig. 8*B*). The effectiveness of AG1478 to inhibit acute EGF-stimulated tyrosine phosphorylation of the EGFR is shown in Fig. 8*C* (compare *lanes 4* and *8*). Inhibition of the tyrosine kinase activity of nerve growth factor receptor by AG879 did not affect FSH-stimulated ERK activation (not shown). However, although a basal level of EGFR tyrosine phosphorylation was detected in vehicle-treated cells and EGF stimulated the tyrosine phosphorylation of the EGFR (Fig. 8*C*), as detected in a membrane pellet fraction obtained from $\sim 6 \times 10^6$ cells, we could not detect any transactivation of the EGFR by FSH or forskolin (Fig. 8*C*, compare *lanes 1–3*). Equivalent results were obtained when the EGFR was immunoprecipitated and probed with phospho-Tyr antibody and when tyrosine phosphorylated proteins were immunoprecipitated with phospho-Tyr antibody and probed with EGFR antibody (not shown). The EGFR inhibitor AG1478 also reduced the FSH-stimulated induction of AKAP80 by 90 ± 9% ($n = 2$) (not shown) but did not affect FSH-stimulated progesterone secretion (8 ± 8% inhibition, $n = 2$). These results suggest that EGFR activation is obligatory for FSH-stimulated ERK activation.

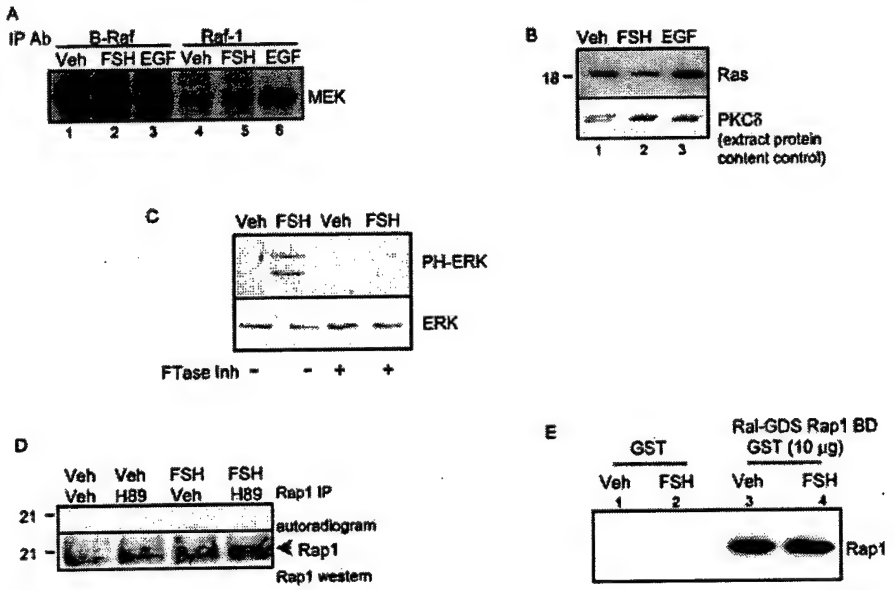

FIG. 6. **FSH does not stimulate Raf-1, B-Raf, Ras, or Rap1 activation.** In *panel A*, granulosa cells were treated for 10 min with 50 ng/ml FSH or 25 ng/ml EGF, B-Raf and Raf-1 were immunoprecipitated from soluble extracts of cells lysed in buffer A, and Raf activities were measured in an immunocomplex kinase assay using His_6-MEK1 as substrate, as detailed under "Experimental Procedures." *Veh*, vehicle; *IP*, immunoprecipitate. Results are representative of two separate experiments. In *panel B*, granulosa cells were treated for 2 min with vehicle, 50 ng/ml FSH, or 25 ng/ml EGF, cells were lysed in buffer C, and soluble cell extracts were mixed with GST-tagged Ras BD of Raf-1 conjugated to agarose as detailed under "Experimental Procedures." Washed agarose pellets were subjected to SDS-PAGE, and proteins were blotted to nitrocellulose; blots were probed with anti-Ras antibody. Total protein in cell extracts was assessed by anti-PKCδ antibody reactivity (*lower panel*). Results are representative of three separate experiments. In *panel C*, granulosa cells were preincubated for 60 min with vehicle or 10 μM farnesyltransferase inhibitor 1 (*FTase Inh*) then treated for 10 min with vehicle or 50 ng/ml FSH. Total cell extracts were probed with the indicated antibodies. Results are representative of two separate experiments. In *panel D*, granulosa cells were incubated overnight with 0.5 mCi of $^{32}P_i$ to label ATP pools, pretreated for 1 h with vehicle or 10 μM H89 (in 50% Me_2SO), then treated for 10 min with vehicle or 50 ng/ml FSH. Cells were then lysed in buffer B, Rap1 was immunoprecipitated, and proteins in the Rap1 immunoprecipitate were subjected to SDS-PAGE and transferred to nitrocellulose for subsequent autoradiography and, after ^{32}P decay, to Western blotting to detect immunoprecipitated Rap1. In *panel E*, granulosa cells were treated for 10 min with vehicle or 50 ng/ml FSH, cells were lysed in RIPA buffer, and soluble extracts were precleared with glutathione-agarose and then subjected to control GST or Ral-GDS-Rap1 BD GST pull downs, as described in *panel B*. Blots were probed with anti-Rap1 antibody. Results are representative of two separate experiments.

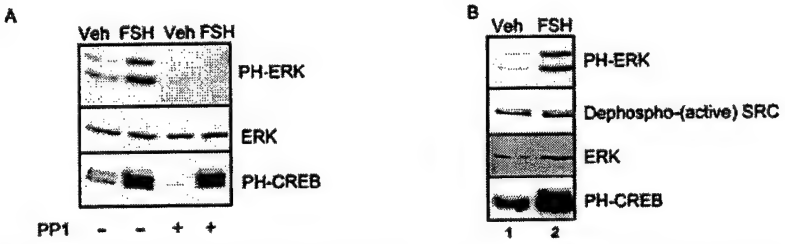

FIG. 7. **FSH does not activate Src but Src activity is required for FSH to activate ERK.** In *panel A*, granulosa cells were pretreated 30 min with vehicle (*Veh*) or 15 μM PP1 then treated for 10 min with vehicle or 50 ng/ml FSH. Total cell extracts were probed with the indicated antibodies. Results are representative of three independent experiments. In *panel B*, granulosa cells were treated with vehicle or FSH for 10 min, and total cell extracts were probed with the indicated antibodies. Results are representative of three experiments. *PH*, phosphorylated.

To ascertain whether Src was upstream or downstream of EGFR activity, we determined whether the EGFR inhibitor AG1478 inhibited Src activity using the dephospho-Src antibody (which detects active Src) to probe blots of cell extracts treated with vehicle or FSH (Fig. 8*D*). Results showed that the dephospho-Src signal was not reduced by AG1478, in contrast to FSH-stimulated ERK phosphorylation, which was reduced by 85 ± 12% (n = 3). Rather, levels of active Src were elevated in cells pretreated with AG1478. The basis for this elevation in the active Src signal is not known. This result suggests that Src activity lies upstream rather than downstream of the EGFR, leading to FSH-stimulated ERK activation.

We also determined whether extracellular Ca^{2+} contributed to the ability of FSH to stimulate ERK phosphorylation. Depletion of extracellular Ca^{2+} by EGTA strongly reduced FSH-stimulated ERK phosphorylation (by 86 ± 5%, n = 4), whereas the effect on CREB phosphorylation was variable (30 ± 20%, n = 2) (Fig. 9*A*). The Ca^{2+} ionophores A23187 (Fig. 8*D*) and ionomycin (Fig. 9*B*) also promoted ERK phosphorylation. To determine whether Ca^{2+} entry was mediated via Ca^{2+} channels, cells were pretreated with the Ca^{2+} channel inhibitor nifedipine. Results (Fig. 9*C*) showed that nifedipine reduced both basal and FSH-stimulated ERK phosphorylation (by 97 ± 2.5%, n = 2) but not affect CREB phosphorylation. Consistent with a role for Ca^{2+} entry into granulosa cells via a Ca^{2+} channel, we determined whether FSH stimulated the phosphorylation on Ser-1928 and the resulting activation of the α subunit of class C L-type Ca^{2+} channel (39). To this end, cells were treated for 10 min with vehicle or FSH, and the α_{1C} subunit of the L-type Ca^{2+} channel was immunoprecipitated from cell extracts using an antibody (anti-FP1) that recognizes total α_{1C} subunit L-type Ca^{2+} channel independent of its phos-

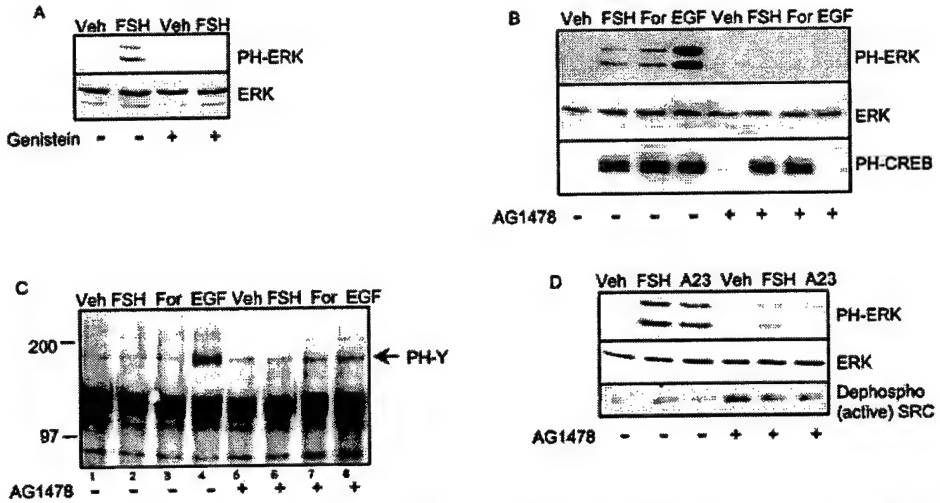

FIG. 8. **FSH-stimulated ERK activation is dependent on EGFR activity.** In *panel A*, granulosa cells were preincubated for 30 min with vehicle (*Veh*) or 30 μg/ml genistein then treated for 10 min with vehicle or 50 ng/ml FSH. Total cell extracts were probed with the indicated antibodies. Results are representative of two experiments. *PH*, phosphorylated. In *panel B*, granulosa cells were preincubated for 15 min with vehicle or 250 nM AG1478 then treated for 10 min with vehicle, 50 ng/ml FSH, 10 μM forskolin, or 25 ng/ml EGF. Total cell extracts were probed with the indicated antibodies. Results are representative of more than five experiments. In *panel C*, granulosa cells were preincubated 15 min without or with 250 nM AG1478 and then treated for 5 min with 50 ng/ml FSH, 10 μM forskolin, or 25 ng/ml EGF. Cells were sonicated in (detergent-free) buffer E, and a membrane pellet was collected, as detailed under "Experimental Procedures." Proteins in the total pellet fraction were separated by SDS-PAGE, blotted to nitrocellulose, and probed with phospho-Tyr (*PH-Y*) antibody. Results are representative of three experiments. In *panel D*, granulosa cells were pretreated 15 min with vehicle or 250 nM AG1478 then treated for 10 min with vehicle, 50 ng/ml FSH, or 125 μM A23187 (A23). Blots were probed with the indicated antibodies. Results are representative of three experiments.

phorylation state. The resulting blots were probed first with an affinity-purified antibody that detects α_{1C} subunit phosphorylated at Ser-1928 (anti-CH3P), stripped, and reprobed with an antibody that detects total α_{1C} subunit protein at 210 kDa (anti-FP1) (39). Results showed that the α_{1C} subunit L-type Ca^{2+} channel was already phosphorylated in vehicle-treated granulosa cells and that FSH did not enhance its phosphorylation (Fig. 9*D*). Consistent with results that suggest that L-type Ca^{2+} channels are phosphorylated and open in vehicle-treated cells, the L-type Ca^{2+} channel agonist BayK8644 did not enhance ERK phosphorylation over levels in vehicle-treated cells (Fig. 9*E*).

The requirement for Ca^{2+} in the pathway by which FSH stimulates ERK phosphorylation was shown to be independent of PKC based on the inability of the PKC inhibitor GF109203X to inhibit FSH-stimulated ERK phosphorylation (Fig. 9*F*). The effectiveness of this inhibitor is evidenced by its ability to prevent PMA-stimulated ERK phosphorylation.

We next determined whether the effect of Ca^{2+} on FSH-stimulated ERK activation was upstream or downstream of EGFR activity. As shown in Fig. 8*D*, pretreatment of cells with the EGFR inhibitor AG1478 blocked the ability of the Ca^{2+} ionophore A23187 to stimulate ERK phosphorylation (by 86 ± 6%, $n = 4$), suggesting that Ca^{2+} is upstream of the EGFR. We also determined whether the Ca^{2+} effect was upstream or downstream of Src. Pretreatment of cells with the Src inhibitor PP1 reduced the ability of the Ca^{2+} ionophore A23187 to stimulate ERK phosphorylation (by 75%, Fig. 9*G*), suggesting that the Ca^{2+} signal is also upstream of Src. CREB phosphorylation, however, was not affected by PP1.

Taken together, these results suggest the existence of a tonic stimulatory pathway leading to MEK activation in (serum-free) vehicle-treated granulosa cells. That FSH can stimulate ERK phosphorylation suggests that MEK-stimulated ERK activation must be suppressed in granulosa cells and that FSH must in some manner overcome this inhibition. In the following experiments, we investigated the phosphotyrosine phosphatase PTP-SL (60). This phosphatase has been shown to bind to and inactivate ERK by stimulating the dephosphorylation of the regulatory Tyr residue (Tyr-204 in ERK1; Tyr-185 in ERK2) (31, 61). Phosphorylation of PTP-SL by PKA on Ser-231 in the kinase interaction motif inhibits its ability to bind to and consequently catalyze the dephosphorylation of ERK (61, 62).

A 100-kDa PTPIs Associated with ERK and FSH Stimulates Its Phosphorylation—We first determined whether or not PTP-SL was expressed in rat ovaries. Proteins reactive with anti-PTP-SL antibody were readily detected at ~220, 180, 100, and 66 kDa in total granulosa cell extracts (Fig. 10*A*, *lane 1*). Detergent-soluble rat brain (Fig. 10*A*, *lane 2*) and ovarian (Fig. 10*B*, *lane 2*) extracts exhibited prominent anti-PTP-SL-reactive bands at 100 and 66 kDa that were absent when the blot was probed with preimmune serum (Fig. 10*B*, *lane 1*). The 100-kDa anti-PTP-SL-reactive band was retained in a soluble ovarian extract eluted from DEAE-cellulose with ~0.1–0.15 M salt (Fig. 10*C*, *lane 1*) but was undetectable in the 0.18–0.25 M salt DEAE eluate (*lane 2*). This result suggests that the 100-kDa anti-PTP-SL-reactive band is localized to the cytosolic fraction of granulosa cells.[2]

We determined whether the soluble 100-kDa anti-PTP-SL-reactive band exhibited PTP activity. Using the same DEAE

[2] The 100-kDa PTP was selectively detected in DEAE-cellulose eluates that corresponded to the elution position (~0.1–0.15 M salt) of the RIIβ PKA holoenzyme (38). We therefore determined whether this PTP or ERK was complexed with PKA R subunits or associated AKAPs. Upon cAMP-agarose affinity purification of R subunits from this PKA peak, the 100-kDa PTP eluted exclusively in the flow-through fraction and did not bind to the cAMP-agarose, as evidenced by the absence of detectable PTP-SL signal in the fractions eluted from cAMP-agarose by 75 mM cAMP or by SDS (not shown). Similarly, ERK protein was also detected only in the flow-through fraction and did not bind to cAMP-agarose (not shown). We also determined whether any AKAPs as identified by an RII overlay assay were detected in anti-ERK-agarose eluates. Results showed that characteristic ovarian AKAPs (38) were readily detected in ADP-agarose and anti-ERK-agarose flow-through fractions and none were detected in anti-ERK-agarose eluates (not shown). These results suggest that the 100-kDa PTP and ERK are not associated directly with the PKA R subunit or with an associated AKAP.

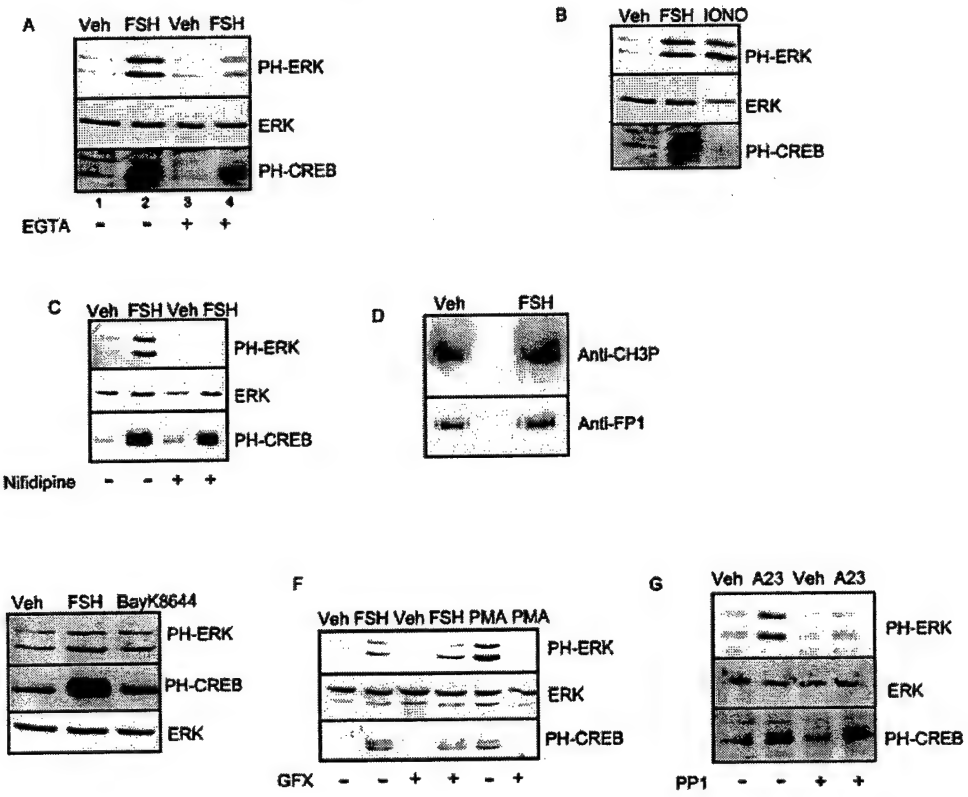

FIG. 9. **FSH-stimulated ERK activation is dependent on extracellular Ca^{2+}.** In *panel A*, granulosa cells were pretreated 60 min with vehicle (*Veh*) or 3 mM EGTA then treated 10 min with vehicle or 50 ng/ml FSH. Total cell extracts were probed with the indicated antibodies. Results are representative of four experiments. *PH*, phosphorylated. In *panel B*, cells were treated for 10 min with vehicle, 50 ng/ml FSH, or 4 μM ionomycin (*IONO*). Total cell extracts were probed with the indicated antibodies. Results are representative of three experiments. In *panel C*, cells were pretreated for 30 min with vehicle or 10 μM nifedipine then treated for 10 min with vehicle or 50 ng/ml FSH. Total cell extracts were probed with indicated antibodies. Results are representative of two experiments. In *panel D*, cells were treated with vehicle or 50 ng/ml FSH for 10 min, membrane proteins were extracted in buffer H, and the α_{1C} subunit of the L-type Ca^{2+} channel at 210 kDa was immunoprecipitated with an antibody (anti-FP1) that recognizes α_{1C} subunit independent of its phosphorylation state, as detailed under "Experimental Procedures." The resulting blot was probed with anti-CH3P antibody, which detects phosphorylation at Ser-1928 on the α_{1C} subunit, stripped, and reprobed for total α_{1C} subunit with anti-FP1 antibody. In *panel E*, granulosa cells were treated for 10 min with vehicle, 50 ng/ml FSH, or 1 μM BayK8644. Total cell extracts were probed with the indicated antibodies. In *panel F*, granulosa cells were pretreated for 30 min with vehicle or 5 μM GF109203X (*GFX*) then treated 10 min with vehicle, 50 ng/ml FSH, and 10 nM PMA. Blots of total cell extracts were probed with the indicated antibodies. Results are representative of three experiments. In *panel G*, cells were pretreated for 30 min with 15 μM PP1 then 10 min with vehicle or 125 μM A23187. Total cell extracts were probed with the indicated antibodies. Results are representative of two experiments.

extracts as those blotted in Fig. 10*C*, *lanes 1* and *2*, we performed an in-gel PTP assay in which a ^{32}P-labeled tyrosine-phosphorylated substrate was incorporated into the gel. Results confirmed the presence of PTP activity specifically at 100 kDa only in the samples containing anti-PTP-SL reactivity (Fig. 10*C*, *lanes 3* and *4*).

PTP-SL along with striatal-enriched protein-tyrosine phosphatase and hematopoietic-PTP belong to a subfamily of PTPs grouped on the basis of sequence conservation and regulation of ERK activity (31, 60, 63–65). PTP-SL and striatal-enriched protein-tyrosine phosphatase exist as both membrane and cytosolic forms that are produced by alternative splicing of the two precursor genes (60, 65). PTP-SL, brain-enriched PTPBR7, and the PC12-enriched PC12-PTP are all isoforms of the PTP-SL gene produced by alternative splicing (60, 64, 66). However, the molecular masses for all the identified family members are <80 kDa. For example, reported sizes for these proteins are~39 kDa for cytosolic PC12-PTP (66), ~45 kDa for cytosolic PTP-SL, and ~65–80 kDa for membrane-bound PTP-SL and PTPBR7, respectively (31, 67). Although the ~66-kDa band detected by anti-PTP-SL antibody (Fig. 10, *A* and *B*) might correspond to the membrane-bound isoform of PTP-SL, the abundant signal at 100 kDa in rat ovarian and brain extracts is either a new PTP-SL isoform or the product of a closely related but distinct gene.[3] We therefore determined by Northern blot whether a larger PTP-SL transcript was detected in rat ovarian and brain extracts. The largest mRNA reported for PTP-SL is ~4 kilobases (60). Using a cDNA corresponding to amino acid residues 147–288 of PTP-SL, we detected a weak signal of ~8.6 kilobases in rat brain and ovarian extracts under low stringency washing conditions (Fig. 10*D*). This result is consistent with the likely presence of a larger PTP-SL-like transcript in rat ovaries and brain. Taken together, these results show that a 100-kDa PTP-SL-like PTP is present in soluble ovarian extracts.

In the following experiments we determined whether one of the anti-PTP-SL-reactive proteins in ovarian extracts was complexed with ERK. We first evaluated whether ovarian PTP-SL-reactive proteins were pulled down by anti-ERK-agarose. Using a detergent-solubilized ovarian extract (with anti-PTP-SL reactivity at 66 and 100 kDa), the 100-kDa PTP was selectively immunoprecipitated by anti-ERK agarose and did not bind to control ADP-agarose conjugates (Fig. 11*A*). Most of the 100-

[3] Neither the 66- nor the 100-kDa proteins in total granulosa cell extracts is recognized by anti-PTPBR7, whereas this antibody detected a predominant ~70-kDa band in rat brain likely corresponding to PTPBR7.

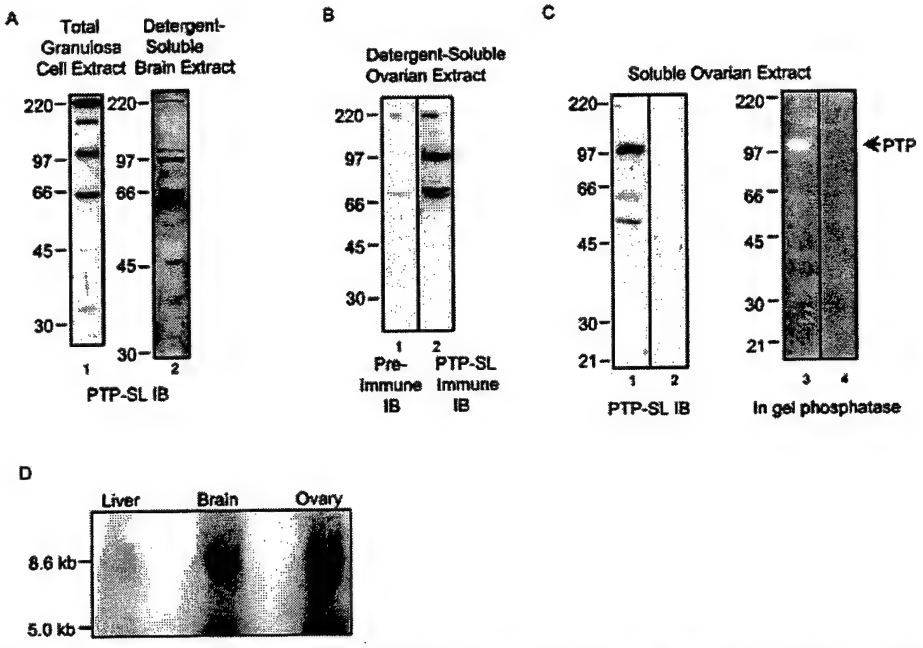

FIG. 10. **A 100-kDa PTP reactive with anti-PTP-SL antibody is present in a cytosol fraction of ovarian extracts.** In *panel A*, total granulosa cell extract (see legend to Fig. 1) and detergent-soluble rat brain extracts (prepared in buffer A) from ~24-day-old rats were probed with anti-PTP-SL antibody. Results are representative of three experiments. *IB*, immunoblot. In *panel B*, detergent-soluble ovarian extracts (prepared in buffer A) from ~24-day-old rats were probed with preimmune serum or anti-PTP-SL antibody. In *panel C*, partially purified soluble ovarian extracts were probed for PTP-SL immunoreactivity (*lanes 1* and *2*) and for PTP activity (*lanes 3* and *4*). To obtain the partially purified extracts, ovaries of 28 estrogen-treated rats were homogenized in (detergent-free) buffer D. A high speed supernatant was obtained by centrifugation of the homogenate at 105,000 × *g* and loaded onto a DEAE-cellulose column. Fractions eluting with ~0.1–0.15 M potassium phosphate (peak 2, representing the major peak of PKA activity (38)) or ~0.18–0.25 M salt (peak 3) were separately pooled, concentrated to 1 ml, and then incubated overnight with cAMP-agarose. For *lanes 1* and *2*, an aliquot (50 μl) of the flow-through that did not bind to cAMP-agarose was mixed with SDS sample buffer, heat-denatured, subjected to SDS-PAGE, blotted to nitrocellulose, and probed with anti-PTP-SL antibody. *Lane 1* is from DEAE peak 2, and *lane 2* from DEAE peak 3. For the rest of details, see "Experimental Procedures." For *lanes 3* and *4*, the same samples were subjected to an in-gel PTP assay. Results are representative of three separate experiments. In *panel D*, RNA in the indicated rat tissues was subjected to a Northern blot probed with PTP-SL cDNA corresponding to amino acid residues 147–288.

kDa PTP contained in soluble ovarian extracts (which exhibited anti-PTP-SL reactivity only at 100 kDa) bound to anti-ERK-agarose (Fig. 11*B*, *lane 5*); the 100-kDa PTP was only minimally detected in the anti-ERK-agarose flow-through fraction (*lane 3*). In contrast, all of the 100-kDa PTP was present in the ADP-agarose flow-through (Fig. 11*B*, *lane 2*), and none was detected in the ADP-agarose eluate (*lane 4*). Consistent with these results, total ERK protein was readily detected in the flow-through fraction from ADP-agarose (*lane 2*), and total ERK protein was only detected in anti-ERK-agarose eluate (*lane 5*) and not in ADP-agarose eluate (*lane 4*). Thus, the majority of the ovarian 100-kDa PTP appears to be complexed with ERK.

We next determined whether the 100-kDa PTP was phosphorylated in response to FSH. Granulosa cells in which the cellular ATP pools with labeled $^{32}P_i$ were treated with vehicle or FSH for 15 min then subjected to immunoprecipitation with anti-PTP-SL or control antibody. Results in Fig. 11*C* demonstrated increased phosphorylation of a band at 100 kDa in PTP-SL immunoprecipitates from FSH-treated cells. Increased phosphorylation of the 100-kDa band was not detected in control anti-PKCζ immunoprecipitations (Fig. 11*C*). Phosphorylation of the 100-kDa band in PTP-SL immunoprecipitates was stimulated by forskolin and blocked by pretreatment of cells with the PKA inhibitor H89 (Fig. 11*D*). These results suggest that FSH via PKA promotes the phosphorylation of the 100-kDa PTP in granulosa cells.

Finally we determined whether FSH stimulated the dissociation of the 100-kDa PTP from ERK. Granulosa cells were treated for 10 min with vehicle or FSH. Detergent-enriched cell extracts were then subjected to anti-ERK-agarose pull-downs followed by a PTP-SL Western blot. Results showed that the PTP signal at 100 kDa was reduced by 57% in FSH compared with vehicle-treated cells (Fig. 11*E*). These results show that FSH promotes the release of a portion of the ERK from the 100-kDa PTP.

DISCUSSION

FSH is obligatory for follicular development beyond the preantral stage (68). It is well established that cAMP mediates FSH-dependent induction of granulosa cell differentiation to a preovulatory phenotype (16). Among the genes induced include those for increased steroidogenesis including $P450_{aromatase}$ and $P450_{side\ chain\ cleavage}$, membrane receptors including those for luteinizing hormone and prolactin (16), signaling and anchoring proteins such as RIIβ and AKAP80 (23), and hormones such as inhibin-α (22). As depicted in Fig. 12, FSH via cAMP promotes activation of PKA (29), leading to the translocation of the PKA catalytic subunit to the nucleus (29, 69), and phosphorylation of CREB (24, 70). FSH via PKA also promotes phosphorylation of histone H3 (24, 29) and induction of the immediate early genes serum glucocorticoid kinase (71) and c-Fos (72). Because the majority of the actions of cAMP are mediated by PKA, it has been assumed that the actions of FSH to induce genes leading to the preovulatory phenotype are dependent on PKA. In support of this hypothesis, we previously reported that the association of phosphorylated histone H3 with promoters of serum glucocorticoid kinase, inhibin-α, and c-Fos was blocked by the PKA inhibitor H89 (24). Induction of AKAP80 as well as StAR expression and inhibin-α and progesterone secretion are also inhibited by the PKA inhibitor H89 (see "Results").

FSH also promotes the activation of ERK (24–26) and down-

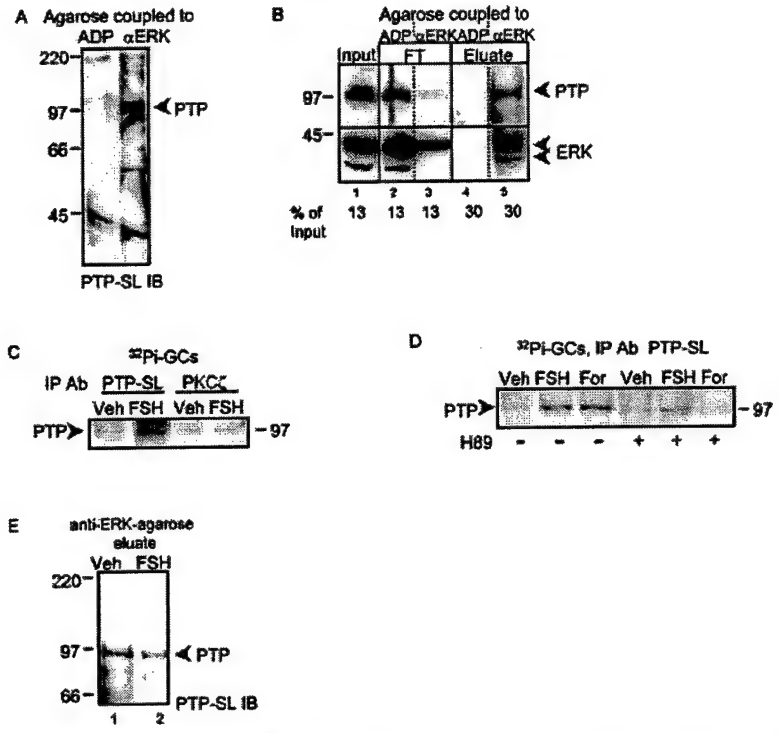

FIG. 11. **FSH stimulates the phosphorylation of the 100-kDa PTP in granulosa cells.** In *panel A*, ovarian extracts (1.36 mg protein) in (detergent-enriched) buffer A were incubated with control ADP-agarose or anti-ERK agarose. Agarose pellets were washed, heat-denatured, and subjected to SDS-PAGE, blotted to nitrocellulose, and probed with anti-PTP-SL antibody. Results are representative of two experiments. *IB*, immunoblot. In *panel B*, soluble ovarian extracts were prepared as described in the legend to Fig. 10*C* in detergent-free buffer D, loaded onto a DEAE-cellulose column, and batch-eluted with 0.15 M potassium phosphate; the eluate was concentrated to 1.15 ml. After removing an aliquot (*Input*), equal volumes of concentrated eluate were mixed overnight with control ADP-agarose and anti-ERK agarose. The flow-through (*FT*) that did not bind to agarose was collected, agarose was washed, and bound proteins eluted with SDS-sample buffer, as detailed under "Experimental Procedures." After SDS-PAGE and blotting to nitrocellulose, blots were probed with the indicated antibodies. The percentage of original input volume mixed with agarose conjugates that was loaded onto SDS-PAGE is indicated. Results are representative of two experiments. In *panels C* and *D*, cellular ATP pools were prelabeled with $^{32}P_i$, and granulosa cells were pretreated (*panel D*) for 60 min with vehicle (*Veh*) or 10 μM H89 and then treated for 15 min with vehicle or 50 ng/ml FSH. Cell extracts were prepared in detergent-enriched buffer F and then subjected to immunoprecipitation (*IP*) with the indicated antibodies (*Ab*), as detailed under "Experimental Procedures". After SDS-PAGE, gels were dried and exposed to film. Results in each panel are representative of at least two separate experiments. In *panel E*, granulosa cells were pretreated for 15 min with 1 μM okadaic acid, a Ser/Thr protein phosphatase 2A preferential inhibitor (56), then treated for 10 min with vehicle or FSH, sonicated for 1 min in (detergent-enriched) buffer F, and sonicate was centrifuged at 15,000 × *g* for 5 min, and the supernatant was mixed with 0.06 ml of anti-ERK-agarose for 4 h at 4° C. *IB*, immunoblot. For the rest of details see the *panel A* legend. Results are representative of two separate experiments.

stream RSK2 (24, 25). The PKA dependence of ERK activation in response to FSH in primary granulosa cells was conclusively established in this report. The goal of these studies was to identify the cellular mechanism by which PKA, activated downstream of the FSH receptor, promoted ERK activation. For these studies we used a serum-free primary granulosa cell culture model to identify the signaling pathway by which FSH activates ERK. Utilizing this model, our results show that ERK activation appears to be obligatory for the induction of AKAP80, based on the ability of the MEK inhibitor PD98059 to block this response to FSH. ERK activation, however, does not appear to be necessary for other PKA-mediated responses of granulosa cells to FSH, such as progesterone and inhibin secretion. PKA-dependent histone H3 phosphorylation is also independent of ERK activation (24).

Our results support the existence of a tonic stimulatory pathway leading to partial MEK but not ERK activation in (serum-free) vehicle-treated granulosa cells. This conclusion is based on evidence that FSH does not promote the activation of MEK, yet MEK inhibition with PD98059 blocks the ability of FSH to activate ERK (shown herein) as well as downstream RSK2 (24). We ruled out the well described pathways by which cAMP/PKA stimulates Rap1 activation leading to activation of B-Raf, MEK, and ERK (10, 11, 55) based on the inability of FSH to activate Rap1, B-Raf, or MEK (Fig. 12). Rather, MEK as well as the upstream activator Raf-1 exhibit detectable activity in the absence of FSH, and inhibition of Ras actions inhibits FSH-stimulated ERK activation. This tonic pathway leading to Ras activation appears to include Ca^{2+} entry, at least in part, through phosphorylated and activated L-type Ca^{2+} channels, leading to the activation of Src, the EGFR, and Ras followed by activation of Raf-1 and MEK (Fig. 12). However, we do not know what stimulates phosphorylation of the Ca^{2+} channel and consequent Ca^{2+} entry into granulosa cells. Notably, mitogens like EGF and PMA that activate ERK independent of PKA promote strong activation of MEK.

We have shown that granulosa cell extracts express a soluble 100-kDa PTP that is recognized by an antibody developed against PTP-SL. Moreover, a portion of the ovarian ERK is complexed with the 100-kDa PTP, based on the ability of anti-ERK-agarose to selectively pull-down ERK complexed to this PTP. PTP-SL has been shown to complex with ERK in other cell types, resulting in ERK dephosphorylation on the regulatory Tyr residue (Tyr-204 in ERK1) and consequent ERK inactivation (31, 61). It has also been established that PTP-SL is a PKA substrate, phosphorylated on Ser-231 (62). Similarly, striatal-enriched protein-tyrosine phosphatase and hematopoietic-PTP, two other members of this subfamily of PTPs, are both

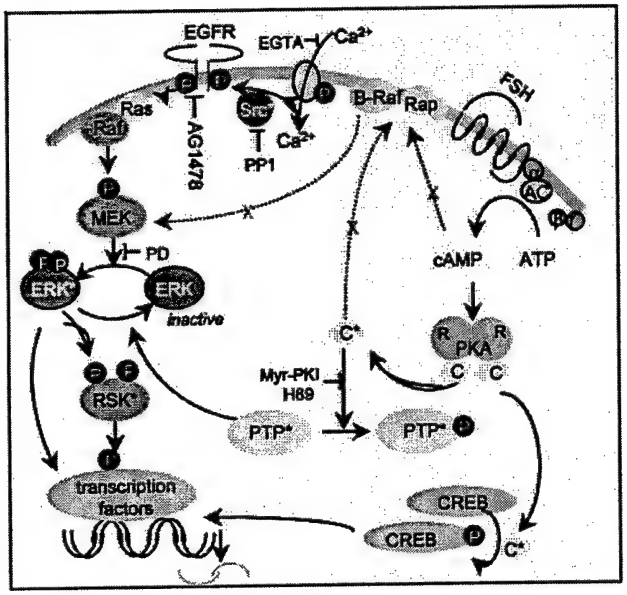

FIG. 12. **Schematic model of FSH-stimulated, PKA-dependent activation of ERK in granulosa cells.** Results support the existence of a tonic pathway leading from Ca^{2+} entry through activated L-type Ca^{2+} channels to Src, the EGFR, Ras, Raf-1, and MEK in granulosa cells. ERK activity is limited by its association with a PTP, and this inhibition is relieved upon PKA-dependent phosphorylation (*P*) of a PTP, resulting in FSH-stimulated ERK phosphorylation. FSH via cAMP/PKA does not appear to modulate Rap or B-Raf activation, as indicated by the × and *dotted lines*. *Asterisks* mark active enzymes; *C* is the catalytic subunit of PKA.

phosphorylated on the equivalent Ser by PKA (62, 73, 74). PKA-catalyzed phosphorylation of these PTPs results in release of ERK from the PTP and consequent ERK activation (62, 73, 74). Our results show that FSH as well as the adenylyl cyclase activator forskolin stimulates the phosphorylation of the 100-kDa PTP in granulosa cell extracts and that this phosphorylation is inhibited by pretreatment of cells with the PKA inhibitor H89. We also demonstrate in anti-ERK pull-down assays that FSH treatment of granulosa cells stimulates the release of the 100-kDa PTP from ERK. Thus, these functional characteristics of the 100-kDa PTP suggest that this protein belongs to the PTP-SL subfamily of PTPs that regulate ERK activities. However, there are no reports of a 100-kDa isoform of PTP-SL. The 100-kDa PTP most likely represents either a new PTP-SL isoform or the product of a closely related gene.

Taken together, our results support the hypothesis that PKA acts to stimulate ERK activity in granulosa cells by relieving the inhibition of ERK imposed by the 100-kDa PTP. With PKA-dependent phosphorylation of this PTP, ERK is released from its complex with the PTP in granulosa cell cytosol, becomes phosphorylated/activated as a consequence of a tonic pathway, and translocates to the nucleus (see Fig. 3). That granulosa cell ERK in its active conformation phosphorylates substrate proteins ultimately to alter gene expression is suggested by our data showing that the MEK inhibitor PD98059 reduces the ability of FSH to enhance expression of AKAP80.

We hypothesized the existence of a tonic stimulatory pathway leading to MEK activation based not only on inhibitor data but also on activity assays and/or epitope-specific antibodies that detect the active conformation of proteins for Src, Raf-1, MEK, and the α_{1C} subunit of the L-type Ca^{2+} channel. The tonic pathway leading to MEK activation appears to be initiated by the entry of extracellular Ca^{2+}. Because FSH has been shown to increase the entry of Ca^{2+} into granulosa cells (52), one would predict that ERK would remain active as a result of the positive feedback actions of Ca^{2+} coupled with actions of PKA to maintain the 100-kDa PTP in a phosphorylated conformation. However, FSH-stimulated ERK activation is transient (see Fig. 5*F*). This is in part attributable to the phosphorylation of Raf-1 on Ser-259 most likely by AKT (50) activated in response to FSH, resulting in the inactivation of Raf-1 (14, 50) and consequent reduction in the phosphorylation of MEK.

The ability of EGTA, the L-type Ca^{2+} channel blocker nifedipine, the Src inhibitor PP1, the EGFR tyrosine kinase inhibitor AG1478, and the Ras inhibitor to completely prevent FSH-stimulated ERK activation indicates that the tonic pathway involving extracellular Ca^{2+}, Src, the EGFR, and Ras is the predominant route to the ERK regulated by FSH in granulosa cells rather than an alternative pathway such as one involving Rap1. This conclusion is substantiated by our inability to detect enhanced MEK phosphorylation in response to FSH.

This is the first report demonstrating agonist-stimulated modulation of ERK activity in conjunction with agonist-stimulated PKA-dependent phosphorylation of a PTP in a physiological cell model. Thus, these studies support a physiological role for this PTP in regulating ERK activity in an intact cellular model in response to an extracellular ligand.

Acknowledgments—We gratefully acknowledge the gift of anti-PTP-SL polyclonal antibody and critical advice from Dr. Rafael Pulido, Instituto de Investigaciones Citologicas, 46010 Valencia, Spain.

REFERENCES

1. Cobb, M. H., and Goldsmith, E. J. (1995) *J. Biol. Chem.* **270,** 14843–14846
2. Luttrell, L. M., Daaka, Y., and Lefkowitz, R. J. (1999) *Curr. Opin. Cell Biol.* **11,** 177–183
3. Herrlich, A., Daub, H., Knebel, A., Herrlich, P., Ullrich, A., Schultz, G., and Gudermann, T. (1998) *Proc. Natl. Acad. Sci. U. S. A.* **95,** 8985–8990
4. Della Rocca, G. J., van Biesen, T., Daaka, Y., Luttrell, D. K., Luttrell, L. M., and Lefkowitz, R. J. (1997) *J. Biol. Chem.* **272,** 19125–19132
5. Andreev, J., Galisteo, M. L., Kranenburg, O., Logan, S. K., Chiu, E. S., Okigaki, M., Cary, L. A., Moolenaar, W. H., and Schlessinger, J. (2001) *J. Biol. Chem.* **276,** 20130–20135
6. Prenzel, N., Zwick, E., Daub, H., Leserer, M., Abraham, R., Wallasch, C., and Ullrich, A. (1999) *Nature* **402,** 884–888
7. Wu, J., Dent, P., Jelinek, T., Wolfman, A., Weber, M. J., and Sturgill, T. W. (1993) *Science* **262,** 1065–1069
8. Hafner, S., Adler, H. S., Mischak, H., Janosch, P., Heidecker, G., Wolfman, A., Pippig, S., Lohse, M., Ueffing, M., and Kolch, W. (1994) *Mol. Cell. Biol.* **14,** 6696–6703
9. Schmitt, J. M., and Stork, P. J. (2002) *Mol. Cell* **9,** 85–94
10. Grewal, S. S., Fass, D. M., Yao, H., Ellig, C. L., Goodman, R. H., and Stork, P. J. (2000) *J. Biol. Chem.* **275,** 34433–34441
11. Schmitt, J. M., and Stork, P. J. S. (2000) *J. Biol. Chem.* **275,** 25342–25350
12. deRooij, J., Zwartkruis, F. J. T., Verheijen, M. H. G., Cool, R. H., Nijman, S. M. B., Wittinghofer, A., and Bos, J. L. (2000) *Nature* **396,** 474–477
13. Kawasaki, H., Springett, G. M., Mochizuki, N., Toki, S., Nakaya, M., Matsuda, M., Housman, D. E., and Graybiel, A. M. (1998) *Science* **282,** 2275–2279
14. Kolch, W. (2000) *Biochem. J.* **351,** 289–305
15. Busca, R., Abbe, P., Mantoux, F., Aberdam, E., Peyssonnaux, C., Eychene, A., Ortone, J.-P., and Ballotti, R. (2000) *EMBO J.* **19,** 2900–2910
16. Hsueh, A. J. W., Adashi, E. Y., Jones, P. B. C., and Welsh, T. H., Jr. (1984) *Endocr. Rev.* **5,** 76–110
17. Sprengel, R., Braun, T., Nikolics, K., Segaloff, D. L., and Seeburg, P. H. (2000) *Mol. Endocrinol.* **4,** 525–530
18. Simoni, M., Gromoll, J., and Nieschlag, E. (1997) *Endocr. Rev.* **18,** 739–773
19. Robker, R. L., and Richards, J. S. (1998) *Mol. Endocrinol.* **12,** 924–940
20. Dorrington, J., Chuma, A. V., and Bendell, J. (1988) *Endocrinology* **123,** 353–359
21. Richards, J. S. (1994) *Endocr. Rev.* **15,** 725–751
22. Woodruff, T. K., Meunier, H., Jones, P. B., Hsueh, A. J., and Mayo, K. E. (1987) *Mol. Endocrinol.* **1,** 561–568
23. Carr, D. W., DeManno, D. A., Atwood, A., Hunzicker-Dunn, M., and Scott, J. D. (1993) *J. Biol. Chem.* **268,** 20729–20732
24. Salvador, L. M., Park, Y., Cottom, J., Maizels, E. T., Jones, J. C. R., Schillace, R. V., Carr. D. W., Cheung, P., Allis, C. D., Jameson, J. L., and Hunzicker-Dunn, M. (2001) *J. Biol. Chem.* **276,** 40146–40155
25. Das, S., Maizels, E. T., DeManno, D., St. Clair, E., Adam, S. A., and Hunzicker-Dunn, M. (1996) *Endocrinology* **137,** 967–974
26. Seger, R., Hanoch, T., Rosenberg, R., Dantes, A., Merz, W. E., Strauss, J. F., III, and Amsterdam, A. (2001) *J. Biol. Chem.* **276,** 13957–13964
27. Hales K. H., Diemer, T., Ginde, S., Shankar, B. K., Roberts, M., Bosmann, H. B., and Hales, D. B. (2000) *Endocrinology* **141,** 4000–4012
28. Mukherjee, S., Gurevich, V. V., Jones, J. C. R., Casanova, J. E., Frank, S. R., Maizels, E. T., Bader, M.-F., Kahn, R. A., Palczewski, K., Aktories, K., and Hunzicker-Dunn, M. (2000) *Proc. Natl. Acad. Sci. U. S. A.* **97,** 5901–5906
29. DeManno, D. A., Cottom, J. E., Kline, M. P., Peters, C. A., Maizels, E. T., and Hunzicker-Dunn, M. (1999) *Mol. Endocrinol.* **13,** 91–105
30. Ito, M., Park, Y., Weck, J., Mayo, K. E., and Jameson, L. J. (2000) *Mol.*

Endocrinol. **14,** 66–81
31. Pulido, R., Zúniga, A., and Ullrich, A. (1998) *EMBO J.* **17,** 7337–7350
32. Kawakatsu, H., Sakai, T., Takagaki, Y., Shinoda, Y., Saito, M., Owada, M. K., and Yano, J. (1996) *J. Biol. Chem.* **271,** 5680–5685
33. Hunzicker-Dunn, M. (1981) *J. Biol. Chem.* **256,** 12185–12193
34. Hunzicker-Dunn, M., Cutler, R. E., Jr., Maizels, E. T., DeManno, D. A., Lamm, M. L. G., Erlichman, J., Sanwal, B. D., and LaBarbera, A. R. (1991) *J. Biol. Chem.* **266,** 7166–7175
35. Dent, P., Chow, Y. H., Wu, J., Morrison, D. K., Jove, R., and Sturgill, T. W. (1994) *Biochem. J.* **303,** 105–112
36. Taylor, S. J., and Shalloway, D. (1996) *Curr. Biol.* **6,** 1621–1627
37. Franke, B., Akkerman, J.-W. N., and Bos, J. L. (2000) *EMBO J.* **16,** 252–259
38. Carr, D. W., Cutler, R. E., Jr., Cottom, J. E., Salvador, L. M., Fraser, I. D. C., Scott, J. D., and Hunzicker-Dunn, M. (1999) *Biochem. J.* **344,** 613–623
39. Davare, M. A., Dong, F., Rubin, C. S., and Hell, J. W. (1999) *J. Biol. Chem.* **274,** 30280–30287
40. Burridge, K., and Nelson, A. (1995) *Anal. Biochem.* **232,** 56–64
41. Vaughan, J. M., Rivier, J., Corrigan, A. Z., McClintock, R., Campen, C. A., Jolley, D., Voglmayr, J. K., Bardin, C. W., Rivier, C., and Vale, W. (1989) *Methods Enzymol.* **168,** 588–617
42. Bender, F. E., Douglass, L. W., and Kramer, A. (1982) *Statistical Methods for Food and Agriculture*, AVI Publishing Co., Inc., Westport, CT
43. Stocco, D. M. (2001) *Mol. Endocrinol.* **15,** 1245–1254
44. Montminy, M. (2000) *Annu. Rev. Biochem.* **66,** 807–822
45. Hidaka, H., Watanabe, M., and Kobayashi, R. (1991) *Methods Enzymol.* **201,** 328–339
46. Engh, R. A., Girod, A., Kinzel, V., Huber, R., and Bossemeyer, D. (1996) *J. Biol. Chem.* **271,** 26157–26164
47. Daaka, Y., Luttrell, L. M., and Lefkowitz, R. J. (1997) *Nature* **390,** 88–91
48. Alessi, D., Cuenda, A., Cohen, P., Dudley, D. T., and Saltiel, A. A. (2000) *J. Biol. Chem.* **270,** 27489–27494
49. Qiu, W., Zhuang, S., von Lintig, F. C., Boss, G. R., and Pilz, R. B. (2000) *J. Biol. Chem.* **275,** 31921–31929
50. Zimmerman, S., and Moelling, K. (1999) *Science* **286,** 1741–1744
51. Taylor, S. S. (1989) *J. Biol. Chem.* **264,** 8443–8446
52. Flores, J. A., Veldhuis, J. D., and Leong, D. A. (1990) *Endocrinology* **127,** 3172–3179
53. Gonzalez-Robayna, I. J., Falender, A. E., Ochsner, S., Firestone, G. L., and Richards, J. S. (2000) *Mol. Endocrinol.* **14,** 1283–1300
54. Garcia, A. M., Rowell, C., Ackermann, K., Kowalczyk, J. J., and Lewis, M. D. (1993) *J. Biol. Chem.* **268,** 18415–18418
55. Vossler, M. R., Yao, H., York, R. D., Pan, M. G., Rim, C. S., and Stork, P. J. S. (1997) *Cell* **89,** 73–82
56. Cohen, P., Klumpp, S., and Schelling, D. L. (1989) *FEBS Lett.* **250,** 596–600
57. Altschuler, D. L., Peterson, S. N., Ostrowski, M. C., and Lapetina, E. G. (1995) *J. Biol. Chem.* **270,** 10373–10376
58. Levitzki, A., and Gazit, A. (1995) *Science* **267,** 1782–1788
59. Deleted in proof
60. Hendriks, W., Schepens, J., Brugman, C., Zeeuwen, P., and Wieringa, B. (1995) *Biochem. J.* **305,** 499–504
61. Zúniga, A., Torres, J., Úbeda, J., and Pulido R. (1999) *J. Biol. Chem.* **274,** 21900–21907
62. Blanco-Aparicio, C., Torres, J., and Pulido, R. (1999) *J. Cell Biol.* **147,** 1129–1135
63. Zanke, B., Suzuki, H., Kishihara, K., Mizzen, L., Minden, M., Pawson, A., and Mak, T. W. (1992) *Eur. J. Immunol.* **22,** 235–239
64. Ogata, M., Sawada, M., Fujino, Y., and Hamaoka, T. (1995) *J. Biol. Chem.* **270,** 2337–2343
65. Lombroso, P. J., Murdoch, G., and Lerner, M. (1991) *Proc. Natl. Acad. Sci. U. S. A.* **88,** 7242–7246
66. Sharma, E., and Lombroso, P. J. (1995) *J. Biol. Chem.* **270,** 49–53
67. Ogata, M., Oh-hora, M., Kosugi, A., and Hamaoka, T. (1999) *Biochem. Biophys. Res. Commun.* **256,** 52–56
68. Burns, K. H., Yan, C., Kumar, T. R., and Matzuk, M. M. (2001) *Endo.* **142,** 2742–2751
69. Gonzalez-Robayna, I., Alliston, T. N., Buse, P., Firestone, G. L., and Richards, J. S. (1999) *Mol. Endocrinol.* **13,** 1318–1337
70. Mukherjee, A., Park-Sarge, O. K., and Mayo, K. E. (1996) *Endocrinology* **137,** 3234–3245
71. Alliston, T. N., Maiyar, A. C., Buse, P., Firestone, G. L., and Richards, J. S. (1997) *Mol. Endocrinol.* **11,** 1934–1949
72. Sharma, S. C., and Richards, J. S. (2000) *J. Biol. Chem.* **275,** 33718–33728
73. Paul, S., Snyder, G. L., Yokakura, H., Picciotto, M. R., Nairn, A. C., and Lombroso, P. J. (2000) *J. Neurosci.* **20,** 5630–5638
74. Saxena, M., Williams, S., Tasken, K., and Mustelin, T. (1999) *Nat. Cell Biol.* **1,** 305–311

Repression of *c-Myc* and inhibition of G_1 exit in cells conditionally overexpressing *p300* that is not dependent on its histone acetyltransferase activity

Sudhakar Baluchamy, Hasan N. Rajabi*, Rama Thimmapaya†, Arunasalam Navaraj‡, and Bayar Thimmapaya§

Department of Microbiology–Immunology, Feinberg School of Medicine, Northwestern University, 303 East Chicago Avenue, Chicago, IL 60611

Communicated by Irving M. Klotz, Northwestern University, Evanston, IL, June 16, 2003 (received for review May 23, 2002)

p300 and cAMP response element binding protein (CREB)-binding protein (CBP) are two highly homologous, conserved transcriptional coactivators, and histone acetyltransferases (HATs) that link chromatin remodeling with transcription. Cell transformation by viral oncogene products such as adenovirus E1A and SV40 large T antigen depends on their ability to inactivate p300 and CBP. To investigate the role of p300 in cell-cycle progression, we constructed stable rat cell lines, which conditionally overexpress *p300* from a tetracycline-responsive promoter. When *p300* was induced in these cells, serum-stimulated S-phase entry was significantly inhibited. The inhibition of S-phase induction was associated with down-regulation of *c-Myc*, but not of *c-Fos* or *c-Jun*. Simultaneous overexpression of *c-Myc* and *p300* before serum stimulation reversed the inhibition of S-phase induction to a significant level, indicating that the inhibition of *c-Myc* to a large extent is responsible for the p300 inhibition of G_1 exit. Similar studies with stable rat cell lines that overexpress a mutant p300, which lacks the HAT activity, showed that the intrinsic HAT activity of p300 is not required for the negative regulation of *c-Myc* or G_1. These findings, and our previously published results (Kolli, S., Buchmann, A. M., Williams, J., Weitzman, S. & Thimmapaya, B. (2001) *Proc. Natl. Acad. Sci. USA* 98, 4646–4651), establish an important negative regulatory role for p300 in *c-Myc* expression that may be important in maintaining the cells in the G_0/G_1 phase of the cell cycle.

Transcriptional coactivators p300 and the cAMP response element binding protein (CREB)-binding protein (CBP) are two highly conserved large nuclear phosphoproteins that contain histone acetyl transferase (HAT) activity. These proteins coactivate a large number of DNA-bound sequence specific transcription factors and remodel chromatin by acetylating nucleosomal histones (reviewed in refs. 1 and 2). p300 and CBP have also been shown to acetylate certain transcription factors, thereby affecting their DNA binding and/or transcriptional activation activities (3–6). Targeted gene disruption studies have shown that p300 is essential for normal cell proliferation and development (7), and haploinsufficiency of CBP in humans gives rise to severe abnormalities characteristic of Rubinstein–Taybi syndrome (8). Similar abnormalities are observed in mice lacking one allele of *CBP*, but not *p300*, suggesting that these two proteins may have certain nonoverlapping functions (9). *p300* and *CBP* are mutated in several cancers, suggesting a tumor suppressor function of these proteins (reviewed in refs. 1 and 10).

Growth factor-induced G_1-S transition in mammalian cells is negatively controlled by retinoblastoma tumor suppressor protein Rb that represses E2F-driven cell cycle-related genes by forming a complex with E2F and several cellular repressor complexes (reviewed in ref. 11). Earlier adenovirus E1A studies have indirectly suggested that p300 may also negatively regulate G_1 phase of the cell cycle. For example, E1A stimulates DNA synthesis in quiescent baby rat kidney cells (12–15), and also restimulates DNA replication in terminally differentiated cardiac myocytes through its p300/CBP-binding domain (16). Other studies have shown that p300 is involved in terminal differentiation in several cell types including muscles, neurons and enteroendocrine cells (reviewed in ref. 1). During terminal differentiation, p300 transactivates p21 in cooperation with Sp1, Sp3, or tissue-specific transcription factors, suggesting that p300 may play a role in keeping cells in G_0/G_1 (1, 17). To assess the role of p300 in cell-cycle control, we recently used an antisense approach, and showed that quiescent human cells depleted of p300 exit G_1 without serum. This premature G_1 exit was found to be the result of the up-regulation of *c-Myc* that occurs because of depletion of p300 (18). This result suggests that p300 negatively regulates *c-Myc* in quiescent cells, and provides an explanation, at least in part, for the effect of E1A on DNA synthesis in quiescent and terminally differentiated cells. However, some p300 functions may also be necessary for cell-cycle progression. For example, fibroblasts from p300 knockout mice are unable to replicate and appear to undergo a cell-cycle arrest (7). p300 acetylates both growth stimulatory transcription factors such as E2F (6), and growth inhibitory proteins such as p53 (3), and increases their DNA-binding activities. p300 is underphosphorylated in quiescent cells and hyperphosphorylated during S and G_2/M phases (19). Phosphorylation of CBP increases during G_1/S boundary with an associated increase in its HAT activity and entry of cells into S phase (20). Cyclin E/cyclin-dependent kinase (cdk2) binds to the C-terminal region of p300 *in vivo*, and this interaction results in the activation of NF-κB function, which is required for the coordinated cell-cycle progression (21). Therefore, the overall role of p300 in the cell cycle is unclear.

To directly assess the role of *p300* in G_1-S transition, we have constructed several stable Rat-1 cell lines capable of expressing *p300* from the tetracycline (tet)-responsive promoter. We demonstrate that when p300 is induced in these cells, the serum-stimulated induction of *c-Myc* and S phase are inhibited. We provide evidence that the repression of *c-Myc* by p300 contributes significantly to the inhibition of G_1-S transition. Furthermore, by constructing stable cell lines that conditionally overexpress a HAT-defective p300, we also show that the HAT activity of p300 that has been implicated in a number of p300 related functions is not required for this negative regulation. These findings and our published results (18) establish an important role for p300 in maintaining cells in G_1 phase of the cell cycle by preventing inappropriate expression of *c-Myc*. Thus, p300 may have a universal role as a checkpoint protein, preventing the untimely onset of DNA synthesis in senescent or differentiated cells.

Abbreviations: CBP, cAMP response element binding protein (CREB)-binding protein; HAT, histone acetyltransferase; tet, tetracycline; Ad, adenovirus; Adtet, Ad vector expressing the tet activator/repressor; Adβ-gal, Ad vector expressing β-gal; FACS, fluorescence-activated cell sorter; cdk, cyclin-dependent kinase.

*Present address: Dana–Farber Cancer Institute, Harvard Medical School, Boston, MA 02115.

†Pesent address: Abbott Laboratory, North Chicago, IL 60064.

‡Present address: Department of Medicine, University of Pennsylvania School of Medicine, Philadelphia, PA 19104.

§To whom correspondence should be addressed. E-mail: b-thimmapaya@northwestern.edu.

www.pnas.org/cgi/doi/10.1073/pnas.1633700100

Materials and Methods

Viral Vectors. Adenovirus (Ad) vectors expressing the tet activator/repressor (Adtet) (22), and β-gal (Adβ-gal) from the cytomegalovirus promoter were constructed as described (18). AdM4 is an Ad vector that contains a promoter-luciferase reporter cassette in which four copies of a c-Myc-binding site (E box element) are cloned upstream of the herpes simplex virus (HSV) *tk* minimal promoter (23). In AdM4mut the E box sequences are mutated so that c-Myc binds poorly to these sequences (23). Adc-Myc is an Ad vector that overexpresses *c-Myc* (24).

Construction of Rat Cell lines Overexpressing p300. The Rat-12 cell line, originally derived from Rat-1 cells (25), are indistinguishable from the Rat-1 cells with respect to their growth properties (unpublished results). Hemagglutinin epitope-tagged p300 cDNA (26) was cloned downstream of the tet-responsive promoter in a plasmid that also contains the hygromycin gene driven by the HSV *tk* promoter. Rat-12 cells were transfected with this plasmid, and selected for hygromycin resistance by using DMEM containing 150 μg of hygromycin per ml and 10% FBS. The drug-resistant colonies developed after 3 weeks were cloned and amplified by using standard procedures. Rat cell lines expressing a mutant p300 (p300mutAT2; ref 27), in which the HAT activity is abolished were constructed under identical conditions. The mutant p300AT2 contained a 6-aa substitution mutation (H1415A, E1423A, Y1423A, L1428S, Y1430A, and H1434A) in the HAT domain.

RNA, Protein, and Cell-Cycle Analysis. To analyze RNA, cells were seeded at a density of 1×10^6 cells per 100-mm dish and were serum starved for 32 h, infected at 25 pfu per cell with appropriate Ad vectors under continued serum-starvation condition. Sixteen h later, they were stimulated with DMEM containing 10% serum, and Poly(A)-containing RNA was isolated at indicated time points in the figure by using a Poly(A)-RNA isolation kit (Qiagen, Valencia, CA). The RNA was then analyzed on Northern blots by using probes specific for Rat *c-Myc* (a gift of L. Penn, University of Toronto, Toronto), *c-Jun*, and *c-Fos* (gifts of R. Tjian, University of California, Berkeley). The RNA bands in the autoradiograms were quantified by using a densitometer. To determine the induced expression of p300 in rat cell clones, cells were infected with Adβ-gal or Adtet and maintained in DMEM with hygromycin. Twelve hours after infection, they were labeled with 200 uCi (1 Ci = 37 GBq) of [^{35}S]methionine per ml (3,000 Ci/mmol; Amersham Pharmacia) for 10 h, lysed in radioimmunoprecipitation assay buffer (28), and equal quantities of protein were immunoprecipitated by using an anti-p300 mAb (sc-584; Santa Cruz Biotechnology), and analyzed on SDS/8% PAGE as described (13). For cell-cycle analysis, cells were serum starved, infected with appropriate Ad vectors, and serum stimulated as described above for RNA analysis. The distribution of cells in G_1, S, and G_2/M phases were quantified by fluorescence-activated cell sorter (FACS) analysis as described (18, 28).

Cdk Assays. Serum-stimulated cells were lysed at the time points shown in Fig. 3*C*, and 100 μg of protein from each cell lysate was immunoprecipitated with either an anti-cyclin E or cyclin A antibody (sc-751 and sc-481, respectively; Santa Cruz Biotechnology) and then assayed for kinase activity by using histones as substrates (18, 25).

Endogenous Myc Transcriptional Activation Activity Assays. Cells were serum starved and infected with either Adtet or Adβ-gal as above, and 2 h later, were superinfected with AdM4 or AdM4mut. Serum starvation was continued for another 16 h and cells were then stimulated with serum. Cells were lysed at the indicated times, and the luciferase activity in the lysates was determined by taking equal quantities of protein and by using a luciferase assay kit (Promega).

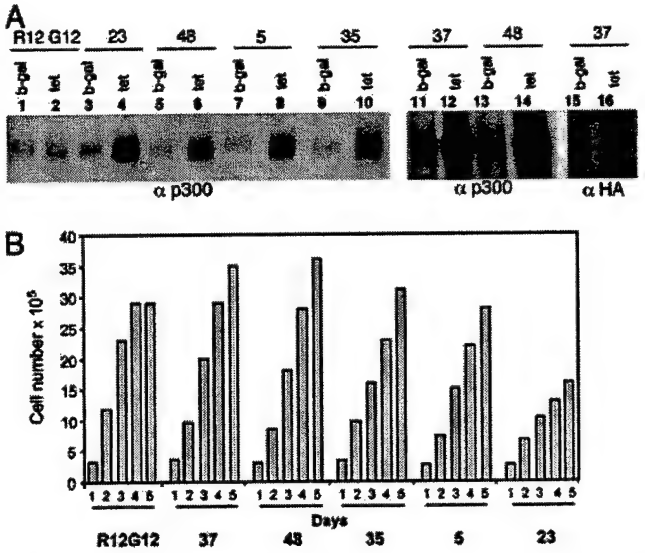

Fig. 1. Induction of p300 in rat cell clones and their growth properties. (*A*) Immunoprecipitation analysis of p300 (see *Materials and Methods* for details). Note that p300 levels for clones R12G12, 23, 48, 5, and 35 in lanes 1–10 and clones 37 and 48 cells in lanes 11–14 were assayed in separate experiments. For comparison of p300 between lanes, the levels of p300 in lanes 11–14 were normalized to clone 48 values in lanes 5–6. (*B*) Growth properties of rat cell clones.

HAT Assays. Proliferating cells from clones 37 and AT21 were infected with Adtet or Adβ-gal for 16 h and lysed, and p300 was immunoprecipitated exactly as described (29) by using a mixture of anti-p300 mAbs (catalog no. 05-267, Upstate Biotechnology). One mg of protein from each cell lysate were assayed for HAT activity by using histones H3 (3 μg) and H4 (5 μg; both from Upstate Biotechnology), 0.5 uCi of [^{3}H]acetyl CoA (catalog no. TRK688, Amersham Pharmacia) as described (29). Mouse IgG was as used a negative control.

Results

Conditional Overexpression of *p300* in Stable Rat Cell Lines. *p300* expressed from the tet-responsive promoter in stable rat cell lines (created as described in *Materials and Methods*) was induced by infecting them with Adtet. As a control, we used one of the Rat-12 clones (R12G12) that were selected for only the empty vector (25). In the initial screening, nearly half of the drug-resistant clones (5 of 11) were found to contain the inducible p300 gene. Immunoprecipitation analysis shows that the levels of p300 in cells derived from clones 5, 23, 35, 37, and 48, but not in R12G12 control cells infected with Adtet, increased by ≈8- to 10-fold when compared with those infected with control vector Adβ-gal (Fig. 1*A*). Immunoprecipitation of the cell extracts using the HA epitope-specific antibody confirmed that the large increase in p300 levels in clone 37 cells is solely because of the newly introduced p300 gene (Fig. 1*A*; data for other clones are not shown). The uninduced levels of p300 in these clones were similar, which were comparable to that of R12G12 cells (<2-fold difference), indicating that basal level expression of the tet-responsive promoter-driven *p300* is minimal (see legend to Fig. 1 for comparison of p300 levels between different lanes). These rat cells expressed normal levels of the endogenous p300 as

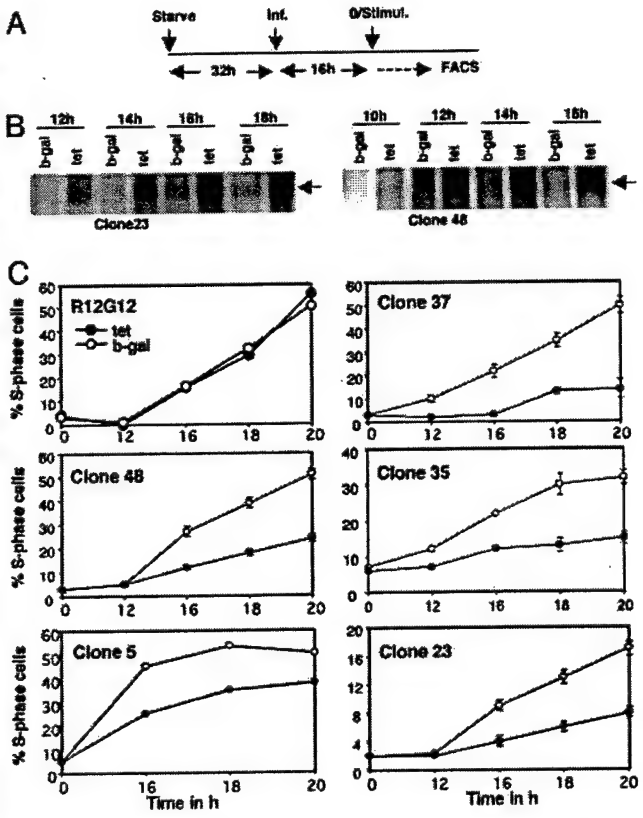

Fig. 2. Inhibition of the S-phase entry in p300-overexpressing cells. (*A*) Schematic representation of the time course of serum starvation, vector infection, and harvesting of cells for FACS analysis. (*B*) Induction of *p300* in serum-starved cells. Serum-starved cells were infected 16 h before serum stimulation with Ad vectors, labeled, and harvested at the indicated times, and p300 in the lysates was analyzed by immunoprecipitation. (*C*) Kinetics of S-phase entry of serum-stimulated cells. Cells were seeded, starved, and infected with Ad vectors as in *A*. The distribution of cells in G_1, S, and G_2/M phases after serum stimulation was determined by FACS analysis as described (18). The assays were done in triplicate, and the average number of cells in S phase with SD are shown.

judged by immunoprecipitation analysis (data not shown). p300 that is overexpressed in these cells coactivated cAMP response element binding protein in a reporter assay, indicating that we did not select cells that overexpress p300 with altered properties (data not shown). Growth rates of clones 5, 35, 37, and 48 were in general comparable to that of R12G12 (Fig. 1*B*). Even though p300 levels in clone 23 were comparable to that of other clones, the growth rate of these cells was significantly slower. Reasons for their poor growth rate are not clear at present; it could be due to integration of the exogenous p300 sequences in a locus whose function may be critical for the normal growth of the cell.

Overexpression of p300 in Growth-Arrested Cells Inhibits the G_1/S Transition. The effects of overexpression of *p300* on serum-stimulated S-phase induction were studied as described in *Materials and Methods* (shown schematically in Fig. 2*A*). High-level accumulation of p300 in clones 23 and 48 before serum stimulation was confirmed in a parallel time course experiment by inducing p300, followed by immunoprecipitation analysis as shown in Fig. 2*B* (a 7- to 8-fold increase by ≈16 h after Adtet infection in both cases; see Fig. 2 legend for details). Distribution of cells in G_1, S, and G_2/M fractions at various time points after serum stimulation were determined by FACS analysis. Each clone was analyzed in three independent experiments that yielded very similar results (except clone 5, which was analyzed only twice), and the representative data are shown in Fig. 2*C*. Control R12G12 cells emerged from quiescence at an identical rate when infected with either Adtet or Adβ-gal (Fig. 2*C*). Clones 35, 37, and 48 infected with control vector also exited G_1 at rates comparable to that of R12G12. For some unknown reasons, clone 5 cells emerged from G_1 slightly faster than from clone 37 or 48. Consistent with its poor proliferation rate, clone 23 infected with Adβ-gal exited G_1 significantly more slowly when compared with other clones (Fig. 2*C*). Induction of p300 in all p300-overexpressing clones, including clone 23, significantly inhibited the S-phase entry with the levels of inhibition ranging from 50 to 60% at the 18-h time point (for clone 5, 50% inhibition at 16 h after stimulation).

***c-Myc*, but Not *c-Fos* or *c-Jun*, Is Down-Regulated in Cells Overexpressing *p300*.** We showed (18) that when p300 is depleted in quiescent human cells, *c-Myc* is up-regulated, and such cells exited G_1 without serum. To examine whether *p300*-overexpressing cells contain reduced *Myc* expression, p300 was overexpressed in serum-starved cells, was serum stimulated as described for cell-cycle analysis, and then Poly(A)-containing RNA was isolated at 30-min intervals (for c-*Fos*, 15-min intervals) up to 3 h after serum stimulation, and analyzed on Northern blots by using rat cDNA probes. As shown in Fig. 3*A*, *c-Myc* RNA levels were barely detectable at the 0-h time point in clones 37 and 48 infected with Adβ-gal, appeared at significant levels at 1 h, peaked at ≈2 h, and declined thereafter. In cells overexpressing p300, *c-Myc* RNA levels were reduced by ≈4- to 5-fold, which was evident both at the 1- and 2-h time points (compare lanes Adβ-gal with Adtet in Fig. 3*A* for *c-Myc*). In contrast, *c-Fos* and *c-Jun* RNA levels were comparable in control and p300-overexpressing cells. Thus, we conclude that increased p300 levels in serum-starved cells led to reduced steady-state levels of *c-Myc* RNA, but not of *c-Fos* or *c-Jun* RNAs.

To determine whether the reduced *c-Myc* RNA levels correlate with the endogenous c-Myc transcriptional activation activity, p300 was induced in the cells as shown in Fig. 2*A*, infected with an Ad vector containing a promoter-reporter cassette in which four copies of the Myc-binding sites (23) were cloned upstream of a minimal promoter (AdM4; AdM4mut contained mutations in the Myc-binding sites; see *Materials and Methods*). Sixteen h later, they were stimulated with serum, harvested at 30-min to 1-h intervals, and then assayed for luciferase activity. The promoter-reporter activities in R12G12 cells infected with Adβ-gal or Adtet rose steadily with comparable increase, and peaked at ≈3 h (Fig. 3*B* and data not shown). As expected, the levels of the mutant promoter-reporter activities in cells infected with the β-gal vector was ≈4- to 5-fold lower than that of the WT promoter-reporter. In clone 37 and 48 cells infected with control vector, the WT promoter-reporter activity peaked at ≈3 h after serum stimulation (Fig. 3*B* and data not shown). In contrast, when p300 was induced in these cells, the reporter activity was significantly reduced. These experiments were repeated twice with reproducible values and data shown are of one such experiment. These results correlate well with the RNA data (Fig. 3*A*), and indicate that p300-overexpressing cells synthesize reduced amounts of Myc protein.

Cells Overexpressing *p300* Show Decreased Levels of Cdk Activities. Several S-phase-specific genes, including cyclin E and Cdk2, are direct targets of Myc (30). To determine whether the repression of *Myc* and S phase by p300 is associated with a decrease in the levels of Cdk activities, the levels of cyclins E- and A/Cdk2 activities in clone 37 cells were determined (see *Materials and Methods* for details). As shown in Fig. 3*C*, in control cells that transit from G_1 to S normally, induction of cyclin E/Cdk2 and cyclin A/Cdk2 activities was detected ≈9 h and 12 h after

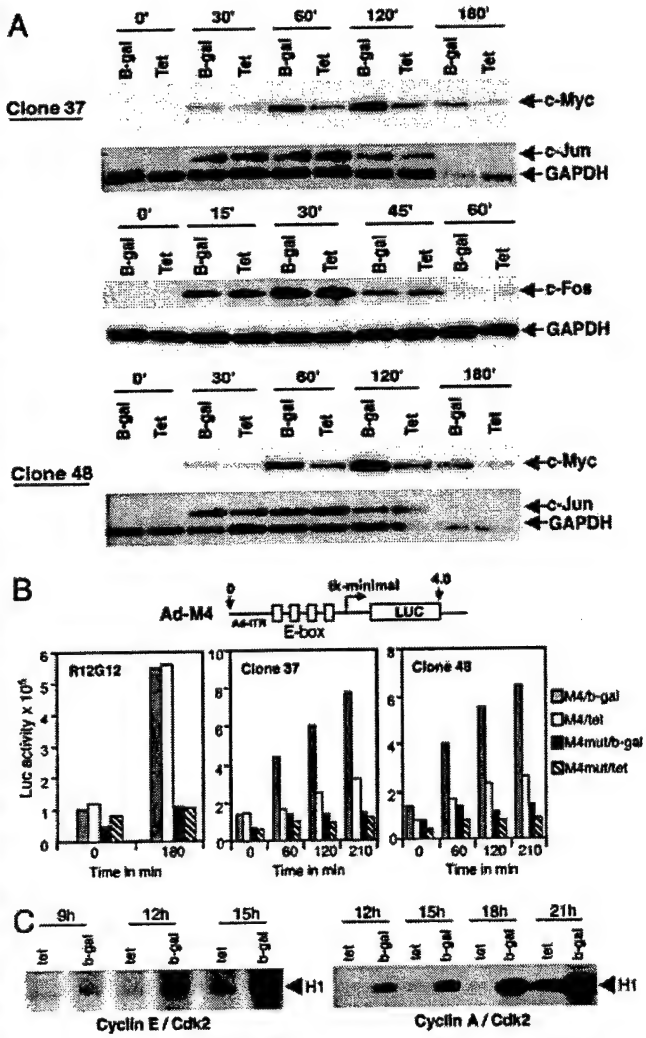

Fig. 3. (*A*) Northern blot showing the levels of *c-Myc*, *c-Fos*, and *c-Jun* RNAs in serum-stimulated clone 37 and 48 cells. Serum-starved clone 37 and 48 cells were infected with Ad vectors and stimulated with serum as shown in Fig. 2*A*. Poly(A)-containing RNA was isolated at different time points shown and was analyzed by using Northern blot hybridizations. *c-Jun* and *GAPDH* in each case were analyzed after reprobing the filters used for *c-Myc* analysis. One microgram of poly(A)-containing RNA was used in each case. (*B*) Transcriptional activation activity of *Myc* in serum-stimulated R12G12 (control) and clone 37 and 48 cells. (*Upper*) Structure of the Ad vector (AdM4) containing the Myc-responsive promoter-reporter cassette is shown. The inverted terminal repeat (ITR) and 0 and 4 map units of the Ad genome are shown. Serum-starved cells were infected with Ad vectors and were superinfected 2-h later with Ad-M4 or Ad-M4mut at 10 pfu per cell. Sixteen hours later, the cells were serum-stimulated, and at the indicated times the luciferase activity in the lysates was assayed by using 5 μg of protein. The experiments were repeated twice with reproducible values, and the data of one such experiment are shown. For R12G12 cells, only 0- and 3-h time points are shown. Luc, luciferase activity. (*C*) Determination of the levels of cyclin E/Cdk2 and cyclin A/Cdk2 activities in clone 37 cells. Assay details are as described in *Materials and Methods*. Phosphorylated histones were resolved on SDS/12% PAGE, dried, and autoradiographed.

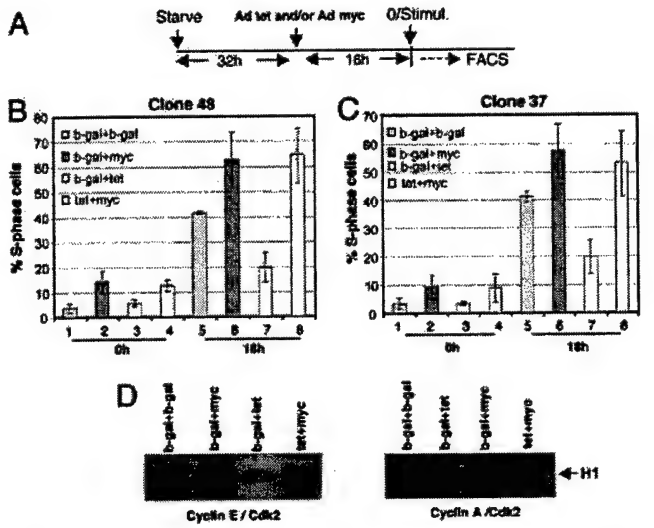

Fig. 4. Abrogation of p300-mediated S-phase inhibition by Myc. (*A*) Schematic representation of the time course of vector infection and harvesting of cells for FACS analysis. (*B*) Serum-starved cells were coinfected with Ad vectors as shown (all at 25 pfu per cell). Sixteen hours later, they were stimulated with serum and were harvested at indicated time points. Distribution of cells in G_1, S, and G_2/M phase were determined by FACS analysis as described (18). Adβ-gal was used where appropriate to keep the multiplicity of infection constant. Average values obtained in three independent experiments with SD are shown. For statistical validation, the mean cell numbers in lane 7 (cells infected with Adtet plus Adβ-gal) were compared with those of lane 8 (cells infected with Adtet plus Adc-Myc) by independent sample Student's two-tailed *t* test. *P* values for lane 7 vs. lane 8 for clone 48, 0.007; for clone 37, 0.011. (*C*) Determination of cyclin E/Cdk2 and cyclin A/Cdk2 activities in clone 37 cells at 15 h after infection with Ad vectors as shown in *B*.

stimulation, respectively (data for time points earlier than 9 h not shown), consistent with the normal coordinated S-phase progression. When p300 was induced in these cells, reduction of cyclin E/Cdk2 activity was observed as early as 9 h after serum stimulation when compared with that of control cells. Decrease in cyclin A/Cdk2 activity became evident at the 12-h time point, which is ≈3 h later than that observed for cyclin E/Cdk2 activity. These results are consistent with the reduced Cdk2 activities, contributing to the progression of S phase in p300 overexpressing cells. It is likely that the reduction of Myc protein in p300-overexpressing cells contributed to the reduction of Cdk2 activity, which could be rate limiting for the coordinated S-phase progression.

Overexpression of *c-Myc* Reverses the p300 Inhibition of S-Phase Induction. To determine whether overexpression of *Myc* would reverse p300-repression effects, *p300* and *Myc* were overexpressed in serum-starved clone 48 and 37 cells simultaneously by coinfecting cells with Adtet and an Ad vector overexpressing *c-Myc* (ref. 24 and Fig. 4*A*). We note here that these experiments work well only when cells from early passages are used. The serum-stimulated S-phase entry of cells was then determined by FACS analysis. The average number of cells obtained from three independent experiments with SD at 18 h after serum stimulation (a time point at which cells continue to accumulate in S phase, but do not yet move to G_2/M phase) are shown in Fig. 4 *B* and *C*. These data suggest that overexpression of *Myc* significantly abrogates the inhibition of S-phase induction caused by excess p300 in both cell clones. For example, in clone 48, when only *Myc* was overexpressed, 62 ± 11% (mean and SD, respectively) of the cells accumulated in S phase (Fig. 4*B*; lane 6). In contrast, only 19 ± 6% of the *p300*-overexpressing cells accumulated in S phase at this time point (lane 7). However, when *Myc* and p300 were overexpressed simultaneously, the number of S-phase-specific cells increased to 64 ± 9%, suggesting that overexpression of *Myc* in this clone completely abrogated the p300-inhibitory effects (lane 8). Overexpression of *Myc* in clone 37 also showed similar results, although the reversal effect was

slightly less efficient. For example, 57 ± 9% and 19 ± 6% of the *Myc*-, and *p300*-overexpressing cells, respectively, accumulated at 18 h after serum stimulation (Fig. 4*C*, lanes 6 and 7). When *Myc* and *p300* together were overexpressed, the number of cells accumulated in S phase increased to 52 ± 11% (lane 8). The differences between the mean cell numbers in lanes 7 and 8 for both clones are significant, as validated by statistical analysis (see legend to Fig. 4*B*). The Myc reversal effects were also evident at the 20-h time point (data not shown). Data presented in Fig. 4 *B* and *C* also show that the *Myc*-overexpressing cells move faster than the control cells, presumably because of the mitogenic effects of Myc.

CyclinA/Cdk2 and CyclinE/Cdk2 activities in clone 37 cells shown in Fig. 4*C* (lanes 5–8) were examined at 15 h after serum stimulation to determine whether overexpression of *Myc* reverses the inhibition of the Cdk2 activities. Data presented in Fig. 4*D* clearly show that the cyclin E/Cdk2 and cyclin A/Cdk2 activities in cells overexpressing *p300* plus *Myc* increased considerably when compared with cells overexpressing only *p300*, and they were comparable to that observed in cells expressing only *Myc*. These data support the FACS data discussed above, and suggest that overexpression of *Myc* was able to overcome the p300 repression of the S-phase entry.

Inhibition of Induction of *c-Myc* and S phase by p300 Is Independent of Its HAT Activity. The HAT activity of both p300 and CBP regulates gene expression by acetylating the transcription factors and the chromatin (1). To determine whether the HAT activity of p300 contributes to the inhibition of G_1 exit and *Myc* induction, we constructed rat cell lines as described above that conditionally overexpress a mutant p300 that lacks the HAT activity (ref. 27; see *Materials and Methods*). Two such clones were analyzed (AT21, AT41) in which p300 could be induced to levels comparable to that of clone 37 cells that expresses the WT p300 (Fig. 5*A*; ≈6- to 7-fold in this experiment), and these cells grew at rates similar to that of clone 37 (Fig. 5*B*). Data presented in Fig. 5*C* suggest that the inhibition of S-phase induction in cells overexpressing mutant p300 are comparable to that observed in cells overexpressing the WT p300 (clone 37; range of inhibition 50–70%). Thus, overexpression of the HAT-defective mutant p300 continues to inhibit the S-phase induction in two independently isolated clones to the same extent as the WT p300. Another clone overexpressing the HAT-defective p300 (AT10) also showed similar S-phase inhibition, although this clone grew more slowly compared with other clones (data not shown). The serum-stimulated Myc activity was also reduced in clone AT21 and AT41 cells to the same extent as that of clone 37 (≈60–65% reduction; Fig. 5D). To confirm that AT21 and AT41 cells overexpress the HAT-defective p300, p300 in proliferating cells was induced, immunoprecipitated, and assayed for HAT activity *in vitro* as described in *Materials and Methods*. Fig. 5*E* shows a 3.5-fold increase in radiolabeling of histones in p300-induced cells, as compared with uninduced cells for clone 37, but not for clone AT21 cells (induction of p300 in these clones was comparable as determined by immunoprecipitations, data not shown). Thus, we conclude that the HAT activity of p300 does not contribute to the inhibition of the serum-stimulated induction of *Myc* or S phase.

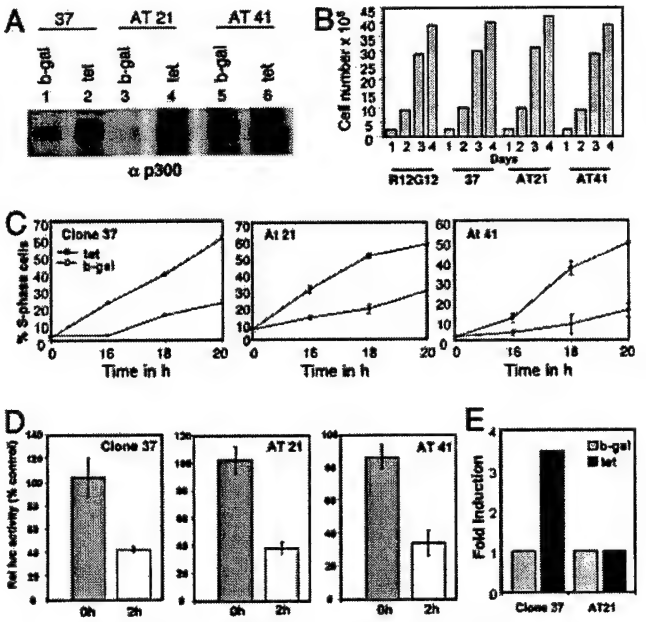

Fig. 5. HAT activity of p300 is not required for the inhibition of *Myc*- and S-phase induction. (*A*) Immunoprecipitation of p300 in cell clones AT21, AT41, and 37. (*B*) Comparison of growth properties of cell clones AT21 and AT41 with R12G12 and 37. (*C*) Induction of S phase in clones AT21 and AT41 with and without induction of *p300*. Details of this experiment were as in Fig. 2*C*. Assays for AT21 and AT41 were done in triplicate, for which the average values and SD are shown. (*D*) Determination of Myc activity in serum-stimulated clones 37, AT21, and AT41. Details are as in Fig. 3*B*. Values shown are luciferase activity expressed as percent of Adβ-gal controls. Averages values with SD obtained from three independent experiments are shown. (*E*) HAT activity of p300 in clone 37 and AT21 with induced and uninduced p300 levels. See *Materials and Methods* for details. Average values obtained from two experiments are shown. The radioactivity obtained from IgG incubations was subtracted from each matching sample. The values obtained for Adβ-gal infected cells were taken as 1 in calculating the fold induction.

Discussion

In this article, we showed that the down-regulation of *c-Myc* by p300 significantly contributes to the inhibition of G_1-S transition, because overexpression of *Myc* along with *p300* abrogates the p300 inhibitory effects in both clones 37 and 48 cells. These results are consistent with our recently published data (18), in which we showed that induction of *Myc* and S phase in cells because of depletion of p300 can be reversed by overexpressing antisense *c-Myc* in the cells. These results indicate that critical levels of p300 in G_1 phase of the cell cycle negatively regulate *c-Myc* and maintain cells in G_1. Our results also provide a molecular basis for the need for viral oncoproteins E1A and SV40 large T to inactivate p300 during cell transformation, and the p300-dependent effect of E1A on DNA synthesis in quiescent (15), and in terminally differentiated cells (reviewed in ref. 1). It is conceivable that p300 may contribute to cell differentiation by keeping *c-Myc* in a repressed state.

The HAT activity of p300 does not contribute to the negative regulation of G_1 or *Myc* expression, because overexpression of a HAT-defective mutant continues to inhibit *Myc* and G_1 to the same extent as the WT p300. p300 has been shown to down-regulate gene expression by acetylating transcription factors. For example, acetylation of HMG(I)Y by p300 shuts off IFN-β gene expression during the postinduction period (4). *Drosophila* dCBP acetylates dTCF [homolog of human T cell factor (TCF)], and down-regulates its activity as acetylation interferes in its interaction with armadillo (human homolog of β-catenin) that provides the transcription activation function (5); human *c-Myc* promoter is also activated by TCF4 (31). Thus, we considered it possible that p300 could acetylate and down-regulate the DNA binding and/or the transcriptional activation activity of the *Myc* promoter-specific transcription factors that could contribute to *Myc* repression. It is unlikely that repression of *Myc* and S-phase entry by the HAT-defective mutant is due to other p300-associated cellular HAT proteins such as PCAF, which are present at normal levels in these cells, because the induced p300 in AT21 did not show an increase in HAT activity (Fig. 5*E*).

However, we cannot completely rule out the possibility that other cellular acetylases associating with high levels of p300 may contribute to the effects reported here. Nonetheless, there are several examples in which specific requirement of the HAT activities of p300/CBP, but not that of PCAF (and vice versa), has been demonstrated (32–35). The HAT proteins such as PCAF and p300/CBP also exhibit differences in substrate specificities with respect to histones (36).

Our data showing only *c-Myc*, but not *c-Fos* or *c-Jun* transcription, is negatively regulated by p300 in G_0/G_1 (this article and ref. 18), suggests that the certain *Myc* promoter-specific transcription factors recruit p300 in G_0/G_1 and repress gene transcription. Studies have shown that in transient assays, *c-Myc* promoter is repressed by transcription factors including CTCF (37), E2F4 (38), Mxi (39), MBP-1 (40), MAZ (41), CDP/*cut* (42), and Blimp-1 (43, 44). E1A also can activate *Myc* promoter through the PRF element in a p300-dependent manner, suggesting that p300 may cooperate with factors binding to the PRF site and repress *Myc* promoter (45). Recent studies (46) suggest that E1A relieves YY1 repression by simultaneously interacting with p300 and YY1, raising the possibility that in serum-starved cells, p300 may cooperate with YY1 in keeping the *Myc* promoter in a repressed state. The majority of the transcriptional repressors mentioned above have been shown to interact with histone deacetylases (HDACs). p300 interacts with at least some of these transcription factors, although a functional link between p300 and HDAC by means of a transcription factor in repressing gene transcription not been established. One possibility is that in quiescent cells, p300 is recruited to the promoter by these transcriptional repressors that may then form an adapter to bridge the transcription factors and the chromatin remodeling complexes that function as repressors. Several such chromatin remodeling complexes that function as repressors have been described, including hBRM/BRG-1 (human homologs of yeast SWI/SNF), HDAC-containing Sin 3 complexes mSin3a and mSin3b, and the histone methylase complex SUV39H1/HP1 (reviewed in refs. 47 and 48). Repression of the *cyclin* E and A, and the *c-Fos* promoters are mediated by these repressors (49–51).

Finally, we are intrigued by our observations that we were unable to develop stable human cell lines conditionally overexpressing p300. For reasons that are not clear at present, Rat-1 cells could tolerate a newly introduced p300 gene, and could readily grow as stable cell lines. At present we do not know whether this difference is related to species difference or because of the embryonic origin of these cells.

We thank S. Reed for Rat 12 cells; R. Tjian, D. Engel, L. Penn, W. Lee Kraus, and J. Kadonaga for plasmids; members of Thimmapaya laboratory, including S. Balasubramanian, S. Kolli, R. Srinivas, and A. Buchmann, for the help received in early stages of this study; S. Reierstad and M. Rao for excellent technical assistance; and M. K. Rundell for critical reading of the manuscript. This work was supported by Public Health Service Grant CA74403, a pilot project through a Northwestern University Specialized Program of Research Excellence (SPORE) grant for breast cancer research, and by a U.S. Army training grant for breast cancer research (to S.B).

1. Goodman, R. H. & Smolik, S. (2000) *Genes Dev.* **14,** 1553–1577.
2. Man, H. M. & La Thangue, N. B. (2001) *J. Cell Sci.* **114,** 2363–2373.
3. Gu, W. & Roeder, R. G. (1997) *Cell* **90,** 230–236.
4. Munshi, N., Merika, M., Yie, J., Senger, K., Chen, G. & Thanos, D. (1998) *Cell* **2,** 457–467.
5. Waltzer, L. & Bienz, M. (1998) *Nature* **395,** 521–525.
6. Martinez-Balbas, M. A., Bauer, U. M., Nielsen, S. J., Brehm, A. & Kouzarides, T. (2000) *EMBO J.* **19,** 662–671.
7. Yao, T. P., Oh, S. P., Fuchs, M., Zhou, N. D., Ch'ng, L. E., Newsome, D., Bronson, R. T., Li, E., Livingston, D. M. & Eckner, R. (1998) *Cell* **93,** 361–372.
8. Petrij, F., Giles, R. H., Dauwerse, H. G., Saris, J. J., Hennekam, R. C., Masuno, M., Tommerup, N., van Ommen, G. J., Goodman, R. H., Peters, D. J., *et al.* (1995) *Nature* **376,** 348–351.
9. Kung, K. L., Bronson, R. T., Chang, L., Sieff, C. A., Livingston, D. M. & Yao, T. (2000) *Genes Dev.* **14,** 272–277.
10. Giles, R. H., Peters, D. J. & Breuning, M. H. (1998) *Trends Genet.* **14,** 178–183.
11. Harbour, J. W. & Dean, D. C. (2000) *Genes Dev.* **14,** 2393–2409.
12. Howe, J. A., Mymryk, J. S., Egan, C., Branton, P. E. & Bayley, S. T. (1990) *Proc. Natl. Acad. Sci. USA* **87,** 5883–5887.
13. Stein, R. W., Corrigan, M., Yaciuk, P., Whelan, J. & Moran, E. (1990) *J. Virol.* **64,** 4421–4427.
14. Subramanian, T., Kuppuswami, M., Nasr, R. J. & Chinnadurai, G. (1988) *Oncogene* **2,** 105–112.
15. Zerler, B., Roberts, R. J., Mathews, M. B. & Moran, E. (1987) *Mol. Cell. Biol.* **7,** 821–829.
16. Liu, Y. & Kitsis, R. N. (1996) *J. Cell Biol.* **133,** 325–334.
17. Billion, N., van Grunsven, L. A. & Rudkin, B. B. (1996) *Oncogene* **13,** 2047–2054.
18. Kolli, S., Buchmann, A. M., Williams, J. & Thimmapaya, B. (2001) *Proc. Natl. Acad. Sci. USA* **98,** 4646–4651.
19. Yaciuk, P. & Moran, E. (1991) *Mol. Cell. Biol.* **11,** 5389–5397.
20. Ait-Si-Ali, S., Ramirez, R., Barre, F. X., Skhissi, F., Magnaghi-Jaulin, L., Girault, J. A., Robin, J. A., Knibiehler, M., Pritchard, L. L., Ducommun, B., *et al.* (1998) *Nature* **396,** 184–186.
21. Perkins, N. D., Felzien, L. K., Betts, J. C., Leung, K., Beach, D. & Nabel, G. J. (1997) *Science* **275,** 523–527.
22. Gossen, M. & Bujard, H. (1992) *Proc. Natl. Acad. Sci. USA* **89,** 5547–5551.
23. Ayer, D. E., Kretzner, L. & Eisenman, R. N. (1995) *Cell* **72,** 211–222.
24. Mitchell, K. O. & El-Deiry, W. S. (1999) *Cell Growth Differ.* **10,** 223–230.
25. Resnitzky, D., Gossen, M., Bujard, H. & Reed, S. I. (1994) *Mol. Cell. Biol.* **14,** 1669–1679.
26. Eckner, R., Ewen, M. E., Newsome, D., Gerdes, M., DeCaprio, J. A., Lawrence, J. B. & Livingston, D. M. (1994) *Genes Dev.* **8,** 869–884.
27. Kraus, W. L., Manning, E. T. & Kadonaga, J. T. (1999) *Mol. Cell. Biol.* **19,** 8123–8135.
28. Buchmann, A. M., Swaminathan, S. & Thimmapaya, B. (1998) *Mol. Cell. Biol.* **18,** 4565–4576.
29. Fu, M., Wang, C., Reutens, A., Wang, J., Angeletti, R. H., Siconolfi-Baez, L., Ogryzko, V., Avantaggiati, M. L. & Pestell, R. G. (2000) *J. Biol. Chem.* **275,** 20853–20860.
30. Dang, C. V. (1999) *Mol. Cell. Biol.* **19,** 1–11.
31. He, T. C., Sparks, A. B., Rago, C., Hermeking, H., Zawel, L., daCosta, L. T., Morin, P. J., Vogelstein, B. & Kinzler, K. W. (1998) *Science* **281,** 1509–1512.
32. Korzus, E., Torchia, J., Rose, D. W., Xu, L., Kurokawa, R., Mclnerney, E. M., Mullen, T. M., Glass, C. K. & Rosenfield, M. G. (1998) *Science* **279,** 703–707.
33. Zhang, W. & Bieker, J. J. (1998) *Proc. Natl. Acad. Sci. USA* **95,** 9855–9860.
34. Munshi, N., Agalioti, T., Lomvaridas, S., Merika, M., Chen, G. & Thanos, D. (2001) *Science* **293,** 1133–1136.
35. Puri, P. L., Sartorelli, V., Yang, X. J., Hammamori, Y., Ogryzko, V. V., Howard, B. H., Kedes, L., Wang, J. Y., Graessmann, A., Nakatani, Y. & Leverero, M. (1997) *Mol. Cell* **1,** 35–45.
36. Roth, S. Y., Denu, J. M. & Allis, D. (2001) *Annu. Rev. Biochem.* **70,** 81–120.
37. Filippova, G. N., Fagerlie, S., Klenova, E. M., Myers, C., Dehner, Y., Goodwin, G., Neiman, P. E., Collins, S. J. & Lobanenkov, V. (1996) *Mol. Cell. Biol.* **16,** 2802–2813.
38. Albert, T., Wells, J., Funk, J., Pullner, A., Raschke, E., Stelzer, G., Meisterernst, M., Farnham, P. J. & Eick, D. (2001) *J. Biol. Chem.* **276,** 20482–20490.
39. Lee, T. C. & Ziff, E. (1999) *J. Biol. Chem.* **274,** 595–606.
40. Chaudhary, D. & Miller, D. M. (1995) *Biochemistry* **34,** 3438–3445.
41. Izzo, W. W., Strachan, G. D., Stubbs, M. C. & Hall, D. J. (1999) *J. Biol. Chem.* **274,** 19498–19506.
42. Li, S., Moy, L., Pittman, N., Shue, G., Aufiero, B., Neufeld, E. J., LeLeiko, N. S. & Walsh, M. J. (1999) *J. Biol. Chem.* **274,** 7803–7815.
43. Yu, J., Angelin-Duclos, C., Greenwood, J., Lio, J. & Calame, K. (2000) *Mol. Cell. Biol.* **20,** 2592–2603.
44. Lin, Y., Wong, K. & Calame, K. (1997) *Science* **276,** 569–599.
45. Jayachandra, S., Low, K. G., Thlick, A., Yu, J., Ling, P. D. & Chang, Y. (1999) *Proc. Natl. Acad. Sci. USA* **96,** 11566–11571.
46. Lee, J. S., Galvin, K. M., See, R. H., Eckner, R., Livingston, D., Moran, E. & Shi, Y. (1995) *Genes Dev.* **9,** 1188–1198.
47. Tyler, J. K. & Kadonaga, J. T. (1999) *Cell* **99,** 443–446.
48. Knoepfler, P. S. & Eisenman, R. N. (1999) *Cell* **99,** 447–450.
49. Zhang, H. S., Gavin, M., Dahiya, A., Postigo, A., Ma, D., Luo, R. X., Harbour, J. W. & Dean, D. C. (2000) *Cell* **101,** 79–89.
50. Nielsen, S., Schneider, R., Bauer, U., Bannister, A. J., Morrison, A., O'Carroll, D., Firestein, R., Cleary, M., Jenuwein, T., Herrera, R. & Kouzarides, T. (2001) *Nature* **412,** 561–565.
51. Murphy, D. J., Hardy, S. & Engel, D. A. (1999) *Mol. Cell. Biol.* **19,** 2724–2733.

British Journal of Cancer (2004) 90, 944–949

www.bjcancer.com

Minireview

Targeting oestrogen to kill the cancer but not the patient

JS Lewis[1], D Cheng[1] and VC Jordan[*,1]

[1]Robert H Lurie Comprehensive Cancer Center, Feinberg School of Medicine, Northwestern University, 303 East Chicago Avenue, Olson Pavilion, Room 8258, Chicago, IL, 60611, USA

The link between sex steroids and the development and growth of breast cancer has proved to be an invaluable clue for advances in the prevention and treatment of breast cancer. The identification of the oestrogen receptor (ER) not only allowed advances in the molecular endocrinology of oestrogen action, but also provided a target for antioestrogenic therapeutic agents. However, the application of long-term or indefinite treatment regimens has consequences for the breast cancer. New forms of resistance, based upon enhanced cellular survival networks independent of ER and the suppression of apoptotic mechanisms, develop and then evolve. Remarkably, low concentrations of oestrogen collapse survival pathways and induce apoptosis in completely antihormonally refractory breast cancer. However, recurrent oestrogen-stimulated disease is again sensitive to antihormonal therapy. The novel reapplication of the ER as a therapeutic target for apoptosis is emerging as a new strategy for the long-term targeted maintenance treatment of breast cancer, and in formulating a targeted strategy for endocrine independent cancer.
British Journal of Cancer (2004) **90,** 944–949. doi:10.1038/sj.bjc.6601627 www.bjcancer.com

Keywords: tamoxifen; raloxifene; aromatase inhibitor; estrogen receptor; apoptosis

There is an expanding clinical database that implicates oestrogen and progestins (hormone replacement therapy, HRT) in the development and growth of breast cancer. Evidence to support this conclusion comes from two major clinical sources: clinical studies of HRT, initially designed to determine the benefits of replacement approaches on postmenopausal women's health (Writing Group for the Women's Health Initiative Investigators, 2002; Million Women Study Collaborators, 2003) and the successful clinical strategy of treating breast cancer by blocking oestrogen action.

The Million Woman Study provides powerful (Million Women Study Collaborators, 2003) information about the actual impact of HRT on the incidence of breast cancer. A total of 1 084 110 UK women aged 50–64 years were recruited to determine the association of HRT use with breast cancer incidence and death. It is estimated that 10 years use of HRT produces 19 additional breast cancers per 1000 users. These data extrapolate to an estimated total of an excess of 15 000 breast cancers associated with HRT over the past decade in the UK.

In contrast to the effects of hormone replacement on the incidence of breast cancer, the use of either an antioestrogen, tamoxifen, to block the action of oestrogen in breast cancer (EBCTCG, 1998), or an aromatase inhibitor, to prevent oestrogen synthesis in postmenopausal patients (ATAC Trialist Group, 2002), is effective, and is considered to be the standard treatment strategy for breast cancer. Indeed, the concept of antioestrogenic interventions has been advanced with the reduction of risk from breast cancer by using tamoxifen (Cuzick *et al*, 2003) or raloxifene (Cummings *et al*, 1999), as well as suggestions for the evaluation of a number of aromatase inhibitors as chemopreventives in high-risk postmenopausal populations.

*Correspondence: Dr VC Jordan ; E-mail: vcjordan@northwestern.edu
Received 28 October 2003; revised 5 December 2003; accepted 5 December 2003

To the casual observer, the clinical evidence appears to demonstrate that oestrogen is detrimental to women's health and especially implicated in breast cancer development and growth. However, there have been consequences to current antihormonal strategies and we will propose new concepts about antihormonal drug resistance in breast cancer, which can be rapidly incorporated into the treatment plan. In otherwords, there are now opportunities to kill sensitised tumour cells with oestrogen and advance a new innovation in therapeutics.

CLASSICAL CONCEPT OF TUMOUR TARGETING

The discovery of the ER as a critical component of the oestrogen signal-transduction pathway in target tissues (Jensen and Jacobson, 1962) and the utilisation of this knowledge as a target for antihormonal therapy in breast cancer (Jensen and Jordan, 2003) improved the survival prospects for millions of breast cancer patients. However, the advance with antioestrogens occurred not only because of targeting the ER, to prevent oestrogen-stimulated tumour growth, but also because of the application of the appropriate duration of treatment. During the 1970s, when tamoxifen was initially being evaluated as an adjuvant therapy in patients, laboratory studies demonstrated that longer durations of complete antihormonal therapy were likely to provide more benefit for patients than shorter durations of therapy (Lerner and Jordan, 1990). At the time, the majority of clinical trials elected to use 1 year of therapy, because there was a sincere concern that longer durations would enhance the possibility of premature drug resistance. Following the methodical evaluation of randomised clinical trials, conducted over the past 20 years, it is now clear that 1 year of adjuvant tamoxifen is only minimally effective, but 5 years of tamoxifen produces an increase in disease-free and overall survival (EBCTCG, 1998). The use of long-term (5 years) adjuvant antihormone therapy is now standard for the treatment of breast cancer therapy.

Attempts to enhance the effectiveness of adjuvant tamoxifen by increasing the duration of treatment from 5 to 10 years have been disappointing (Fisher *et al*, 2001). It appears there is a reduced effectiveness of the antitumour actions of tamoxifen, possibly because of developing drug resistance, but also an increase in oestrogenic side effects such as endometrial cancer and blood clots. In contrast, the use of a non-crossresistant aromatase inhibitor as a continuing adjuvant after 5 years of adjuvant tamoxifen reduces the incidence of recurrence and contralateral breast cancer by nearly 50% compared to no treatment (Goss *et al*, 2003). Thus, the cycling of antihormonal strategies can maintain patients disease free for long periods.

Clinical trials of adjuvant tamoxifen therapy also provide an invaluable insight into the appropriate duration of treatment necessary for the evaluation of the prevention of primary breast cancer. The Oxford Overview of clinical trials (EBCTCG, 1998) demonstrated that 1 and 2 years of adjuvant tamoxifen produce only modest decreases in contralateral breast cancers, but 5 years of adjuvant tamoxifen reduce contralateral breast cancer by 50%. These data are consistent with the findings of the NSABP P-1 trial that 5 years of tamoxifen reduce the incidence of invasive and noninvasive breast cancer in high-risk pre- and postmenopausal women, by approximately 50% (Fisher *et al*, 1998). Currently, in the United States, appropriately selected high-risk women can use a course of 5 years of tamoxifen to reduce their risk of breast cancer.

The treatment of breast cancer has changed dramatically during the past 15 years, with all patients now receiving long-term antihormonal therapies, whether it is tamoxifen (EBCTCG, 1998), aromatase inhibitors (ATAC Trialists' Group, 2002), or LHRH superagonists plus tamoxifen (Emens and Davidson, 2003). However, the intense laboratory study of nonsteroidal antioestrogens led to the recognition of selective oestrogen receptor modulation (SERM) (Jordan, 2001), and the idea that SERMs could be used to treat and prevent osteoporosis but prevent breast cancer as a beneficial side effect (Lerner and Jordan, 1990). Raloxifene, a molecule related to tamoxifen, is used to treat and prevent osteoporosis with a reduction of breast cancer (Cummings *et al*, 1999). In the wake of the controversy surrounding the negative effects of HRT, there are new opportunities to develop novel SERMs to address the prevention of osteoporosis, coronary heart disease (CHD) and breast cancer. Raloxifene is currently being evaluated for the prevention of breast cancer and CHD in high-risk postmenopausal women, so it could become the first multifunctional medicine.

Despite the fact that SERMs introduce a new dimension into therapeutics for the prevention of osteoporosis and CHD, the question of unlimited treatment durations with SERMs will have consequences for the natural history of breast cancer. Early reductions in the incidence of ER-positive disease (Fisher *et al*, 1998; Cummings *et al*, 1999) will potentially result in SERM-resistant breast cancers, thereby confronting the oncologist with unanticipated and complex treatment decisions in an increasing proportion of women. However, laboratory studies have established a new understanding of SERM resistance that could potentially convert breast cancer from an acute to a chronic, controllable disease.

CHANGES IN THE UNDERSTANDING OF ANTIHORMONE RESISTANCE

During the past 20 years, there has been an important change in the understanding of drug resistance to the antioestrogen tamoxifen. In the early 1980s, tamoxifen was anticipated to be effective in ER-positive breast cancers, but ineffective in ER-negative disease. Resistance to tamoxifen would develop because the ER-positive tumour cells would be controlled, but eventually these would be overwhelmed by the outgrowth of ER-negative breast cancer cells (Figure 1A). However, this model was not consistent with the known clinical observation that select patients with metastatic breast cancer could be maintained on successive endocrine therapies for prolonged periods.

It is now clear that there are two types of drug resistance to tamoxifen: intrinsic resistance, where the tumour is either ER negative or ER positive with pre-existing enhanced survival pathways (HER2/neu plus a coactivator molecule AIB1) (Osborne *et al*, 2003), and acquired resistance where an ER-positive tumour that initially responds to treatment now becomes tamoxifen-stimulated and grows in response to either tamoxifen or oestrogen. An ER-positive breast tumour that initially responds to an SERM eventually develops acquired resistance by clonal selection for increased cell surface signalling that subverts the SERM ER complex through enhanced phosphorylation cascades. The laboratory description of acquired resistance forms the scientific basis for the understanding of current therapeutic interventions with aromatase inhibitors or fulvestrant as second-line agents, following the development of clinical resistance to tamoxifen. Aromatase inhibitors block oestrogen synthesis and fulvestrant destroys the ER to prevent the growth of breast cancers with acquired tamoxifen resistance. However, despite the remarkable investment in a broad range of antihormonal therapies, the actual advance in improved survival and reduced side effects has been modest.

The successful control of breast cancer with antihormonal therapy requires years of successive treatments. An obstacle to the progress in therapeutics is a clear understanding of the changes that occur in the breast cancer cell, as a consequence of exhaustive antihormonal therapies. It is presumed that the cancer cell must create a sophisticated survival network and suppress the natural process of apoptosis to subvert the continuous inhibitory signal through the ER. Until recently, no laboratory models replicated the former clinical scenario, but the deficiencies in our knowledge are being corrected.

Drug resistance to tamoxifen evolves through three phases: Phases I and II both require tamoxifen, or a related SERM

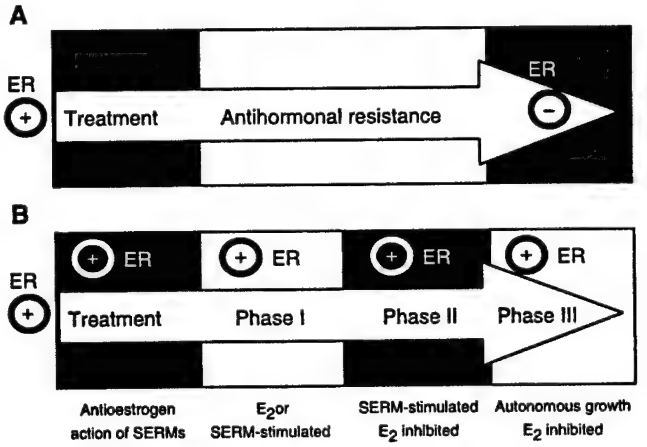

Figure 1 The evolution of antihormonal resistance. (**A**) About 20 years ago, it was believed that oestrogen receptor-positive (ER+) tumours would usually be expected to respond to oestrogen withdrawal or a selective oestrogen receptor modulator (SERM) such as tamoxifen, but eventually resistance would occur because ER− cells would overgrow the tumour. (**B**) Emerging laboratory and clinical evidence suggests that SERM resistance evolves from acquired resistance (Phase I) to Phase II, where any SERM will maintain growth, whereas, unliganded ER does not provoke growth. However, oestrogen at physiological levels causes rapid apoptosis. In Phase III, tumours are completely resistant to all antihormonal therapies and grow spontaneously. Nevertheless, physiological concentrations of oestrogen causes rapid apoptosis.

(O'Regan *et al*, 2002), to maintain growth, but in Phase III the ER-positive tumour is refractory to all antihormonal therapies and growth is SERM independent (Jordan *et al*, 2003) (Figure 1B).

Remarkably, the response of the breast tumour to oestrogen during the evolution of drug-resistance changes dramatically, from initially being growth stimulatory to becoming completely inhibitory after 5 years of antihormonal therapy. Apoptosis is initiated in response to minute concentrations of oestradiol, which results in dramatic tumour regression in heterotransplanted athymic mice. When this phenomenon was first noted and reported in the early 1990s (Wolf and Jordan, 1993), it was suggested that a woman's own oestrogen actually destroyed the micrometastases that were presensitised by 5 years of tamoxifen treatment. In otherwords, stopping tamoxifen at a critical time (5 years) was responsible for the long-term survival statistics. While the concept may have some veracity, the knowledge that minute concentrations of oestrogen can have a dramatic effect on tumour cell death could have important clinical implications for treatment. Indeed, a clear understanding of the mechanism of Phase II and III resistance is becoming increasingly important for the treatment of metastatic breast cancer.

The current focus on exhaustive antiendocrine therapy may in fact be disadvantageous for patients. The antitumour action of oestrogen in Phase II tamoxifen resistance can paradoxically be reversed by fulvestrant (Osipo *et al*, 2003). In otherwords, oestradiol causes rapid tumour regression, fulvestrant causes tumourstasis, but a combination of oestradiol and fulvestrant causes robust tumour growth. If Phase II or III drug resistance to tamoxifen can be shown to occur in patients, then an oestrogen-rich environment would subvert the actions of fulvestrant. Obviously, one could enhance the probability of a response to fulvestrant by administering an aromatase inhibitor, but perhaps oestrogen should be pursued as a targeted alternative. To advance this idea, it would be valuable to examine whether the observations in the laboratory with the evolution of tamoxifen drug resistance apply to other SERMs and to breast cancer cells that have adapted to oestrogen deprivation, that is, as an expression of resistance to aromatase inhibitors.

EXPANSION OF THE CONCEPT OF OESTROGEN-INDUCED APOPTOSIS

Song *et al* (2001) were the first to demonstrate that oestradiol causes apoptosis in breast cancer cells that have been adapted to grow in an oestrogen-free environment for prolonged periods. These investigators suggested that their data provided an explanation for the effectiveness of high-dose diethylstilboestrol formally used to treat breast cancer in elderly postmenopausal women, that is, women who were 10–25 years after menopause. Thus, a switch occurs in the cancer cell from oestrogen stimulating growth to oestrogen causing cell death after prolonged oestrogen deprivation. However, and perhaps more importantly, the apoptotic effect occurs with low concentrations of oestradiol. We illustrate the principle in Figure 2B by comparing and contrasting the action of oestradiol in wild-type breast cancer cells and an ER-positive progesterone receptor-negative, oestrogen-deprived clone referred to as MCF-7 5C (Jiang *et al*, 1992). Of interest is the observation that alterations in the media can enhance the actions of oestradiol as an apoptotic agent. Clearly, this is an area of research activity worthy of pursuit as the proposed therapeutic use of long-term aromatase inhibition can potentially reconfigure the cellular response to oestrogen.

The other relevant clinical scenario is the response of occult breast cancer cells to indefinite raloxifene administration for the treatment and prevention of osteoporosis. Long-term culture of breast cancer cells in 1 μM raloxifene results in adaptation of cell-survival mechanisms and raloxifene resistance. Transplantation of cells into athymic mice demonstrates Phase II SERM resistance; tamoxifen or raloxifene stimulates growth, no treatment (no ER binding ligand) results in no growth, but oestradiol causes apoptosis and rapid tumour regression (Liu *et al*, 2003). Thus, a

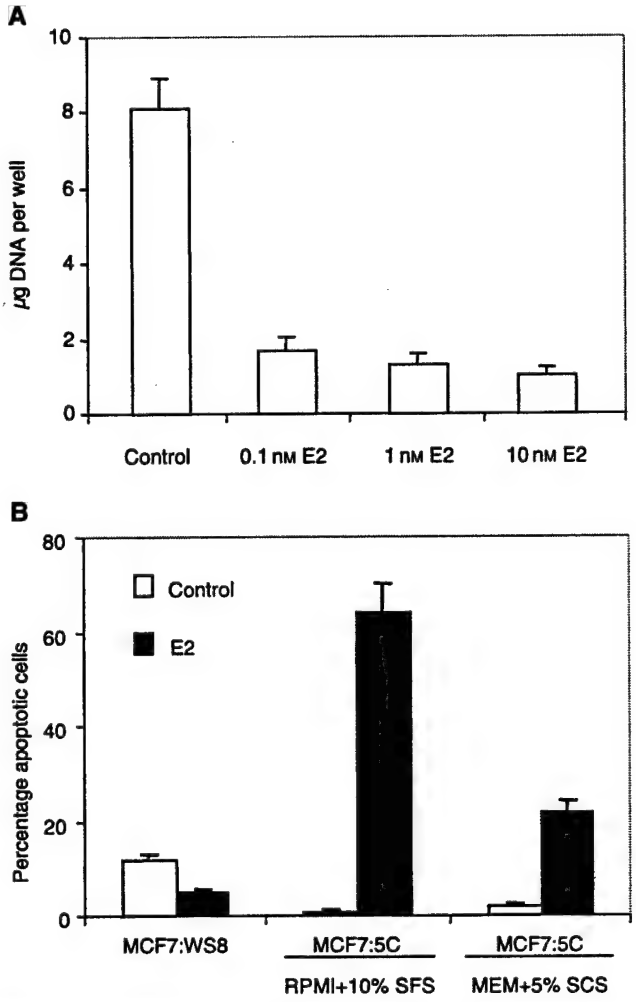

Figure 2 Oestradiol inhibits the growth of MCF-7:5C cells and induces apoptosis. MCF-7:5C cells were cloned from wild-type MCF-7:WS8 cells following long-term growth (~1 year) in oestrogen-free RPMI medium containing 10% (vv^{-1}) dextran charcoal-stripped (DCC) foetal bovine serum (FBS), 2 mM glutamine, 100 U ml^{-1} penicillin-streptomycin, 6 ng ml^{-1} bovine insulin, and 1 × nonessential amino acids. (**A**) For DNA assays, MCF-7:5C cells were seeded into 12-well plates at a density of ~20 000 cells per well in RPMI medium. The cells were left for 24 h to acclimatise, and then treated with 0.1, 1, or 10 nM oestradiol (E_2) for a total of 6 days, with the control cells receiving <0.1% ethanol vehicle. Cells were re-fed on days 3 and 5. Total DNA (μg) per well was used to measure cell growth. The data represent the average of five separate experiments. (**B**) Apoptotic cells were identified/quantified by double staining with recombinant FITC-conjugated annexin V and propidium iodide (PI), using the Annexin V-FITC kit (Immunotech, Beckman Coulter). For experiments, MCF-7:WS8 and MCF-7:5C cells were seeded in 100 mm plates at a density of 1×10^6 per plate in either oestrogen-free RPMI medium containing 10% DCC stripped fetal bovine serum (SFS) or MEM containing 5% DCC stripped calf serum (SCS). The cells were left for 24 h to acclimatise and then treated with either 1 nM E_2 or less than 0.1% ethanol vehicle (control) for 72 h. Data shown represent three separate experiments. It should be noted that oestradiol treatment of MCF-7:WS8 cells in oestrogen-free MEM media containing 5% SCS did not have any significant effect on apoptosis (data not shown).

general principle is emerging that merits investigation in the laboratory to discover mechanisms that could be targeted and amplified.

MOLECULAR MECHANISMS

The target site-specific actions of SERMs are not well understood, but there is an emerging understanding of the modulation of the SERM ER complex in breast cancer (Figure 3). Antioestrogenic action appears to be dominant in a cancer cell with no cell surface signalling, and the SERM ER complex binds preferentially to corepressor molecules to prevent gene activation and cell replication (Figure 3A). In contrast, the oestrogen-like actions of an SERM become dominant in acquired resistance when cells are selected with enhanced cell surface signalling, reduced corepressors but increased coactivator molecules (Figure 3B). This molecular mechanism could serve as a working model for Phase I drug resistance. It is plausible that the subsequent evolution of drug resistance into Phase II results from an enhanced sophistication in establishing survival pathways during continuing selection in an oestrogen-deprived environment. Ultimately, the ER appears to become redundant for growth in Phase III drug resistance (Jordan *et al*, 2003). However, it is the remarkable switch from oestrogen-stimulated growth in breast cancer to oestrogen-stimulated death that merits investigation. Song *et al* (2001) first focused attention on the fas, fas ligand pathway as a potential mechanism of oestrogen-induced apoptosis in oestrogen-deprived breast cancer cells. Study of molecular mechanisms for oestrogen-induced tumour regression have recently been extended with the demonstration that oestrogen simultaneously collapses survival mechanisms (HER2/neu NFκB) in the Phase II SERM-resistant tumour, and enhances the expression of the fas receptor (Liu *et al*, 2003; Osipo *et al*, 2003) (Figure 3C, D). Clearly, much needs to be done to understand the new molecular endocrinology of oestrogen action, but the knowledge now creates opportunities for novel applications in therapeutics.

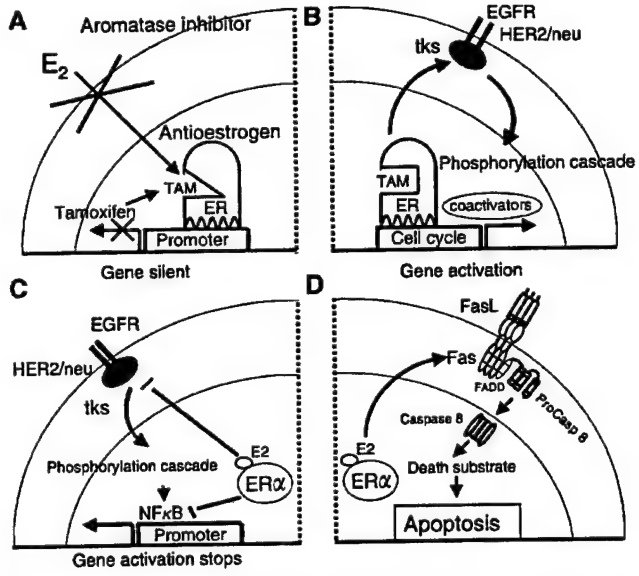

Figure 3 The development of tamoxifen (TAM)-resistant breast cancer and the changing role of oestradiol (E_2) in the life and death of ER-positive cancer cells. (**A**) E_2-stimulated growth is inhibited by the use of an aromatase inhibitor to block oestrogen synthesis or TAM to block the ER and prevent oestrogen-stimulated gene transcription. Optimal antioestrogenic effects occur in the absence of pre-existing cell surface signalling mechanisms. (**B**) Prolonged use of TAM promotes an increase in HER2/neu cell surface signalling that creates a survival pathway phosphorylating the TAM ER complex and coactivator proteins. The transcription complex becomes activated to enhance gene activation and TAM-stimulated growth. If this is Phase I resistance, then oestrogen will also promote growth; so an aromatase inhibitor is an appropriate second-line therapy. If it is Phase II resistance, E_2 causes apoptosis. (**C**) In Phase II tamoxifen resistance, the E_2 ER complex collapses the survival mechanisms by dramatically reducing the level of cell surface signalling by preventing HER2/neu mRNA transcription and the nuclear level of NFκB, a transcription factor. (**D**) In Phase II tamoxifen resistance, the E_2 ER complex also enhances the synthesis of Fas receptor mRNA and protein which, in the presence of Fas ligand (FasL) activates caspase 8 and a cascade of events resulting in apoptosis. These figures are summaries of the mechanisms described in Osipo *et al* (2003) and Liu *et al* (2003).

CLINICAL CORRELATIONS

Current clinical practice is focused on the premise that oestrogen is the principal growth stimulator in select ER-positive breast cancers. The application of this principle over the past 30 years has been at the forefront of targeted therapeutics, and has undoubtedly saved lives. However, clinical clues are emerging that the practice of exhaustive antihormonal therapy is not always appropriate, and useful palliation can occur with an application of the obsolete modality of pharmacological oestrogen treatment (diethylstilboestrol, 5 mg three times a day). Renewed interest in re-treating endocrine refractory disease with high-dose oestrogen has demonstrated improvement in the anecdotal patient (Ingle, 2002) and remarkable responses in metastatic breast cancer patients treated exhaustively with antihormonal therapies (Lonning *et al*, 2001). Out of 32 evaluable patients, four had complete response, six had partial response and two had stable disease. These encouraging data require confirmation, before any change in medical practice can be recommended, but for the individual patient with completely refractory disease the potential for palliation is clear. More importantly, there is now a renewed conversation between the laboratory and the clinic that offers opportunities not only to enhance the duration of responses based on retargeting the ER, but also to improve the proportion of response rates, based on an enhanced understanding of the survival and death pathways that could potentially be manipulated.

OPPORTUNITIES FOR TARGETING OESTROGEN TO THE TUMOUR

Professor Paul Erlich established the foundation for targeted therapeutics by describing the successful process for treating infectious disease. An effective treatment is based on selective toxicity to destroy the disease and not the patient. To achieve that goal, an appropriate laboratory model for the disease in question should be used to identify active synthetic molecules that will selectively destroy the disease *in vivo* under laboratory conditions. The successful chemotherapeutic candidate can subsequently be evaluated in clinical trials to establish 'real world' efficacy and selectivity. The process has been remarkably successful during the past Century, with the development of a diverse range of antibacterial agents and drugs to either prevent or palliate parasitic disorders. Unfortunately, the realisation of the goal of targeting cancer selectively has, until recent times, remained elusive. Not that there has not been a sincere attempt to achieve the goal. About 100 years ago, Professor Paul Erhlich was the first to apply the principles of chemotherapeutic drug discovery to cancer cures. His approach was not successful. He declared, 'I have wasted 15 years of my live in experimental cancer research', the year before he died on 20th August 1915.

What has become increasingly clear is that establishing target site specificity is not simple, especially in cancer, and that, for the

application of the Erhlich method in general, there are consequences of launching an attack that is not complete – drug resistance. The success in targeting breast cancer initially developed slowly by the reinvention and retargeting of existing molecules that had not succeeded in their primary applications. Tamoxifen, discovered in a fertility-control program, was reinvented as a breast cancer drug and subsequently targeted to the ER (Jordan, 2003). Raloxifene, discovered in a breast cancer program and targeted to the ER, was reinvented as a preventive for osteoporosis with breast and uterine safety. After 30 years of clinical usage, the ubiquitous application of SERMs has now provided clues to progress by retargeting the ER with oestrogen in SERM-resistant disease. However, rather than returning to the therapeutic modality of the 1960s by reintroducing high-dose oestrogen therapy for a few select patients, the new knowledge emerging from the laboratory now creates novel scientific and clinical opportunities to target the ER and extend response rates, cycle antihormonal therapies, enhance response rates and determine the precise molecular mechanism of ER-mediated apoptosis, so the knowledge could potentially be exported to kill ER-negative tumour cells.

There are at least two dimensions to consider when applying the targeted action of oestrogen to the tumour: the nature of the oestrogen ER complex and the length of time that oestrogen must be administered to initiate the apoptotic cascade. The ER can bind an enormous range of ligands with diverse shapes and structures. To date, laboratory and clinical studies of ER-mediated apoptosis have only used either oestradiol or DES. However, recent studies of the molecular biology of oestrogen action have defined two classes of ER complex. This is because the shape of the ligand preprograms the actual external shape of the ER complex (Bentrem *et al*, 2003). The planar oestrogens, oestradiol, DES and the phyto-oestrogens genistein and coumestrol are class I oestrogens that rely on helix 12 in the ligand-binding domain to seal the oestrogen molecule into the hydrophobic pocket (Bentrem *et al*, 2003). This causes activating function (AF) 2 to be triggered, and synergise with AF-1 at the other end of the complex during the formation of a gene transcription complex. In contrast, a nonplanar oestrogen binds in the ligand binding domain, but prevents activation of AF-2. Helix 12 cannot seal the ligand in the hydrophobic pocket, and the transcription complex occurs through the triple site interaction of AF-1, D351 and select acidic amino acids in helix 12 (Bentrem *et al*, 2003). The comparative testing of a range of phytoestrogens and the active constituents of conjugated equine oestrogens, equilin and equilenin, for their activity as apoptotic agents in Phase II and III antihormone drug resistance, will establish which types of low-dose oestrogen could be used in clinical studies.

An important laboratory observation is that the apoptotic response of SERM-resistant breast cancer occurs, not with pharmacologic doses of oestrogen but physiologic oestradiol in the postmenopausal range (Yao *et al*, 2000). The majority of SERM-resistant tumours regress completely, but the few that regress but regrow are again completely responsive to tamoxifen that prevents oestradiol-stimulated growth. Although the precise nature of switching mechanisms from tamoxifen stimulated and oestrogen killing to oestrogen stimulated and tamoxifen blocking has not been established, recent studies (Liu *et al*, 2003; Osipo *et al*, 2003) show that oestradiol rapidly collapses the survival mechanisms (HER2/neu and NFκB) that support tamoxifen-stimulated growth. It is therefore reasonable to speculate that surviving cells are selected to be exclusively oestrogen responsive but which do not possess the survival mechanisms to support tamoxifen-stimulated growth. Thus, tamoxifen would again express antitumour actions on oestradiol-stimulated tumour growth (Yao *et al*, 2000). Based on the laboratory findings (Yao *et al*, 2000), a clinical program should be initiated to determine the therapeutic value of short or extended conjugated equine oestrogen- or high phytoestrogen- containing diets. The results of the studies could establish new standards of clinical care initially to extend the effectiveness of antihormonal therapies for metastatic breast cancer and, subsequently, the consideration of rotating adjuvant antihormones with an 'oestrogen purge' to improve survival through extending the duration of disease-free survival.

The next two challenges have the potential to expand the value of the developing knowledge on ER-induced cellular apoptosis. Half of the ER-positive tumours do not respond to antihormonal therapy; therefore, any strategy to target the ER in endocrine refractory tumours would ultimately double response rates in breast cancer. Endocrine refractory disease appears to have developed survival pathways that are independent of regulation by ER. In otherwords, the pivotal role of the ER in growth has been subverted by alternate survival and growth pathways. One potential strategy could be to convert an endocrine nonresponsive tumour to become responsive to oestrogen-induced apoptosis by blocking the survival pathways with the expanding list of tyrosine kinase inhibitors and antibodies that block cell surface signalling. The goal would be to prevent cancer cell survival. This pharmacological strategy might enhance the possibility that the ER complex could initiate events which lead to apoptosis in the vulnerable cells. There would also be the possibility that the oestradiol ER complex could synergise with traditional inducers of apoptosis, for example, chemotherapy in cells paralysed with select cell survival inhibitors. All these options can be advanced in clinical trial.

The ultimate goal of the basic research will be to identify the molecular mechanism that permits the oestradiol ER complex to switch from being a survival mechanism through replication to a death signal. How does the ER complex know when it must induce the death of an aberrant cell? Clues are already available since the expression of ectopic ER in ER-negative cells prevents replication (Jiang and Jordan, 1992) so the next step will be to identify critical pathways in the ER-negative cell that can convert inhibition of replication to the induction of apoptosis.

CONCLUSIONS

New knowledge about the ability of low concentrations of oestrogens to cause apoptosis in exhaustively treated breast tumour has the potential to advance targeted therapeutics not only in breast cancer but also in other cancers. The remarkable ability of the oestradiol ER complex, a natural signal-transduction pathway, to discriminate between a growth and a death environment is unique. Application of the new knowledge has immediate relevance for the treatment of metastatic breast cancer and the eventual maintenance of breast cancer patients for decades using cycles of antihormones, but with regular 'oestrogen purges' to kill resistant cells, and subsequently reactivate antihormonal therapy. Most importantly, the new knowledge will establish a strategic plan to integrate novel survival blockers into a logical treatment strategy and simultaneously utilise the emerging power of the 'omics' technologies to identify specific targets for future apoptotic therapy.

ACKNOWLEDGEMENTS

This work was supported by DOD Training Grant in Breast Neoplasia DAMD17-00-1-0386, Training Program in Signal Transduction T32 CA70085-06, SPORE in Breast Cancer P50 CA89018-03, Lynn Sage Breast Cancer Research Foundation and the Avon Foundation.

REFERENCES

ATAC Trialists' Group (2002) Anastrozole alone or in combination with tamoxifen versus tamoxifen alone for adjuvant treatment of postmenopausal women with early breast cancer: first results of the ATAC randomized trial. *Lancet* **359**: 2131–2139

Bentrem D, Fox JE, Pearce ST, Liu H, Pappas S, Kupfer D, Zapf JW, Jordan VC (2003) Distinct moleular conformations of the estrogen receptor alpha complex exploited by environmental estrogens. *Cancer Res* **63**: 7490–7496

Cummings SR, Eckert S, Krueger KA, Grady D, Powles TJ, Cauley JA, Norton L, Nickelsen T, Bjarnason NH, Morrow M, Lippman ME, Black D, Glusman JE, Costa A, Jordan VC (1999) The effect of raloxifene on risk of breast cancer in postmenopausal women: results from the MORE randomized trial. Multiple Outcomes of Raloxifene Evaluation. *JAMA* **281**: 2189–2197

Cuzick J, Powles T, Veronesi U, Forbes J, Edwards R, Ashley S, Boyle P (2003) Overview of the main outcomes in breast-cancer prevention trials. *Lancet* **361**: 296–300

EBCTCG (1998) Tamoxifen for early breast cancer: an overview of the randomised trials. *Lancet* **351**: 1451–1467

Emens LA, Davidson NE (2003) Adjuvant hormonal therapy for premenopausal women with breast cancer. *Clin Cancer Res* **9**: 486s–489s

Fisher B, Costantino JP, Wickerham DL, Redmond CK, Kavanah M, Cronin WM, Vogel V, Robidoux A, Dimitrov N, Atkins J, Daly M, Wieand S, Tan-Chiu E, Ford L, Wolmark N (1998) Tamoxifen for prevention of breast cancer: report of the National Surgical Adjuvant Breast and Bowel Project P-1 Study. *J Natl Cancer Inst* **90**: 1371–1388

Fisher B, Dignam J, Bryant J, Wolmark N (2001) Five versus more than five years of tamoxifen for lymph node-negative breast cancer: updated findings from the National Surgical Adjuvant Breast and Bowel Project B-14 randomized trial. *J Natl Cancer Inst* **93**: 684–690

Goss PE, Ingle JN, Marino S, Robert NJ, Muss HB, Piccart MJ, Castiglione M, Tu D, Shepherd LE, Pritchard KI, Livingston RB, Davidson NE, Norton L, Perez EA, Abrams JS, Therasse P, Palmer MJ (2003) A randomized trial of letrozole in postmenopausal women after five years of tamoxifen therapy for early-stage breast cancer. *N Engl J Med* **349**: 1–10

Ingle JN (2002) Estrogen as therapy for breast cancer. *Breast Cancer Res* **4**: 133–136

Jensen EV, Jacobson HI (1962) Basic guides to the mechanism of estrogen action. *Recent Prog Horm Res* **18**: 387–414

Jensen EV, Jordan VC (2003) The estrogen receptor: a model for molecular medicine. The Dorothy P. Landon AACR Prize for Translational Research. *Clin Cancer Res* **9**: 1980–1989

Jiang SY, Jordan VC (1992) Growth regulation of estrogen receptor-negative breast cancer cells transfected with complementary DNAs for estrogen receptor (see comments). *J Natl Cancer Inst* **84**: 580–591

Jiang SY, Wolf DM, Yingling JM, Chang C, Jordan VC (1992) An estrogen receptor positive MCF-7 clone that is resistant to antiestrogens and estradiol. *Mol Cell Endocrinol* **90**: 77–86

Jordan VC (2001) Selective estrogen receptor modulation: a personal perspective. *Cancer Res* **61**: 5683–5687

Jordan VC (2003) Tamoxifen: a most unlikely pioneering medicine. *Nat Rev Drug Discov* **2**: 205–213

Jordan VC, Osipo C, MacGregor Schafer J, Cheng D, Liu H (2003) Changing role of the oestrogen receptor (ER) in the life and death of breast cancer. *The Breast* **12**: 432–441

Lerner LJ, Jordan VC (1990) The development of antiestrogens for the treatment of breast cancer: Eighth Cain Memorial Award Lecture. *Cancer Res* **50**: 4177–4189

Liu H, Lee E-S, Gajdos C, Pearce ST, Chen B, Osipo C, Loweth J, McKian K, De los Reyes A, Wing L, Jordan VC (2003) Apoptotic action of 17 beta-estradiol in raloxifene resistant MCF-7 cells *in vitro* and *in vivo*. *J Natl Cancer Inst* **95**: 1586–1596

Lonning PE, Taylor PD, Anker G, Iddon J, Wie L, Jorgensen LM, Mella O, Howell A (2001) High-dose estrogen treatment in postmenopausal breast cancer patients heavily exposed to endocrine therapy. *Breast Cancer Res Treat* **67**: 111–116

Million Women Study Collaborators (2003) Breast cancer and hormone-replacement therapy in the Million Women Study. *Lancet* **362**: 419–427

O'Regan RM, Gajdos C, Dardes RC, De Los Reyes A, Park W, Rademaker AW, Jordan VC (2002) Effects of raloxifene after tamoxifen on breast and endometrial tumor growth in athymic mice. *J Natl Cancer Inst* **94**: 274–283

Osborne CK, Bardou V, Hopp TA, Chamness GC, Hilsenbeck SG, Fuqua SA, Wong J, Allred DC, Clark G, Schiff R (2003) Role of the estrogen receptor coactivator AIB1 (SRC3) and HER2/neu in tamoxifen resistance in breast cancer. *J Natl Cancer Inst* **95**: 353–361

Osipo C, Gajdos C, Liu H, Chen B, Jordan VC (2003) Paradoxical action of fulvestrant on estradiol-induced regression of tamoxifen-stimulated breast cancer. *J Natl Cancer Inst* **95**: 1597–1607

Song RX, Mor G, Naftolin F, McPherson RA, Song J, Zhang Z, Yue W, Wang J, Santen RJ (2001) Effect of long-term estrogen deprivation on apoptotic responses of breast cancer cells to 17beta-estradiol. *J Natl Cancer Inst* **93**: 1714–1723

Wolf DM, Jordan VC (1993) A laboratory model to explain the survival advantage observed in patients taking adjuvant tamoxifen therapy. *Recent Results Cancer Res* **127**: 23–33

Writing Group for the Women's Health Initiative Investigators (2002) Risks and benefits of estrogen plus progestin in healthy postmenopausal women. *JAMA* **288**: 321–333

Yao K, Lee ES, Bentrem DJ, England G, Schafer JI, O'Regan RM, Jordan VC (2000) Antitumor action of physiological estradiol on tamoxifen-stimulated breast tumors grown in athymic mice (In Process Citation). *Clin Cancer Res* **6**: 2028–2036

JCB Article

Formation of filopodia-like bundles in vitro from a dendritic network

Danijela Vignjevic,[1] Defne Yarar,[2] Matthew D. Welch,[2] John Peloquin,[1] Tatyana Svitkina,[1] and Gary G. Borisy[1]

[1]Department of Cell and Molecular Biology, Northwestern University Medical School, Chicago, IL 60611
[2]Department of Molecular and Cell Biology, University of California, Berkeley, CA 94720

We report the development and characterization of an in vitro system for the formation of filopodia-like bundles. Beads coated with actin-related protein 2/3 (Arp2/3)–activating proteins can induce two distinct types of actin organization in cytoplasmic extracts: (1) comet tails or clouds displaying a dendritic array of actin filaments and (2) stars with filament bundles radiating from the bead. Actin filaments in these bundles, like those in filopodia, are long, unbranched, aligned, uniformly polar, and grow at the barbed end. Like filopodia, star bundles are enriched in fascin and lack Arp2/3 complex and capping protein. Transition from dendritic to bundled organization was induced by depletion of capping protein, and add-back of this protein restored the dendritic mode. Depletion experiments demonstrated that star formation is dependent on Arp2/3 complex. This poses the paradox of how Arp2/3 complex can be involved in the formation of both branched (lamellipodia-like) and unbranched (filopodia-like) actin structures. Using purified proteins, we showed that a small number of components are sufficient for the assembly of filopodia-like bundles: Wiskott-Aldrich syndrome protein (WASP)–coated beads, actin, Arp2/3 complex, and fascin. We propose a model for filopodial formation in which actin filaments of a preexisting dendritic network are elongated by inhibition of capping and subsequently cross-linked into bundles by fascin.

Introduction

Lamellipodia and filopodia are the two major types of protrusive organelles in crawling cells. Multiple lines of evidence indicate that lamellipodial protrusion occurs by a dendritic nucleation/array treadmilling model (Mullins et al., 1998; Borisy and Svitkina, 2000). In this model, members of the Wiskott-Aldrich syndrome protein (WASP)* family activate the actin-related protein 2/3 (Arp2/3) complex and nucleate the formation of actin filaments on preexisting filaments, which function as coactivators (Higgs and Pollard, 2001). Repeated dendritic nucleation generates a branched array of filaments, as found at the leading edge of cells (Svitkina et al., 1997; Svitkina and Borisy, 1999) or in comet tails (Cameron et al., 2001). Capping protein functions to cap excessive barbed ends (Cooper and Schafer, 2000), thus channeling actin polymerization close to the membrane.

Whereas lamellipodia seem designed for protrusion over a smooth surface, filopodia seem designed for exploring the extracellular matrix and surfaces of other cells. Filopodia, in contrast to the branched network of lamellipodia, contain an unbranched bundle of actin filaments that are aligned axially, packed tightly together, and of uniform polarity (Small et al., 1978; Lewis and Bridgman, 1992). Unlike lamellipodia, the Arp2/3 complex is excluded from filopodia (Svitkina and Borisy, 1999), and filaments in filopodia are relatively long and do not turn over rapidly (Mallavarapu and Mitchison, 1999). The roots of filopodia extend well into the cell lamellipodium. As proposed by the filament treadmilling model (Small et al., 1994), filaments elongate with their barbed ends oriented toward the leading edge, pushing the membrane and at the same time continuously depolymerizing from the pointed ends.

A major question in understanding filopodial formation is how they are initiated. One member of the WASP family, N-WASP, facilitates Cdc42-induced filopodia formation in cells (Miki et al., 1998), suggesting that Arp2/3-mediated nucleation of actin filaments plays a role in generating parallel bundles. How might Arp2/3 complex be involved in the formation of unbranched actin structures? One possibility is that the nucleation and branching activities of Arp2/3 complex can be separated, resulting in the production of dendritic

Address correspondence to Danijela Vignjevic, Northwestern University Medical School, Department of Cell and Molecular Biology, 303 E. Chicago Ave., Ward 8-063, Chicago, IL 60611. Tel.: (312) 503-2854. Fax: (312) 501-7912. E-mail: nele@northwestern.edu

*Abbreviations used in this paper: Arp2/3, actin-related protein 2/3; BB, brain buffer; Ena/VASP, enabled/vasodilator-stimulated phosphoprotein; REF, rat embryo fibroblast; VCA, verprolin-homology/connecting/acidic domain of WASP; WASP, Wiskott-Aldrich syndrome protein.

Key words: filopodia; actin; Arp2/3; capping protein; fascin

The Journal of Cell Biology, Volume 160, Number 6, March 17, 2003 951–962
http://www.jcb.org/cgi/doi/10.1083/jcb.200208059

or parallel actin structures, depending on the way in which it is activated. Another possibility is that the dendritic array initially produced by Arp2/3-mediated nucleation is subsequently transformed into parallel bundles of actin filaments.

Valuable insights into the mechanism of lamellipodial formation and protrusion have been obtained using bacterial- and bead-based in vitro motility systems (Theriot et al., 1994; Loisel et al., 1999; Cameron et al., 2000). Filopodial formation is less understood, one reason being that a similar in vitro approach is lacking. In this study, we report the development of in vitro systems for producing filopodia-like bundles, one of which employs cytoplasmic extracts and another that reconstitutes filopodia-like bundles from purified proteins. Using these systems, we provide evidence that filopodia-like bundles are formed by reorganization of the dendritic array.

Results

Formation of bead-associated actin bundles in extracts

Because filopodia are especially abundant in neuronal cell growth cones, we reasoned that brain cytoplasmic extracts might be a good source of filopodia-promoting factors, even though such extracts have previously been demonstrated to support comet tail motility (Laurent et al., 1999; Yarar et al., 1999). WASP-coated beads were introduced into rat brain extracts along with rhodamine–actin. Strikingly different structures were found associated with the beads depending on their position on the coverslip. In the center of the coverslip, beads were associated with a cloud of actin filaments or a typical comet tail (Fig. 1 A). In contrast, at the edge of the coverslip, straight actin bundles radiated from a bead in a star-like configuration (Fig. 1, A and B). These stars represented 84 ± 10% (n = 1,030) of all bead-associated actin structures at the edges of the coverslips (outermost third of the coverslip radius). No stars were found in the center of the coverslips (innermost third of the radius). In the transition zone between the center and edge of the coverslip, we observed large actin clouds and chimeras, structures intermediate between tails and stars (Fig. 1 A).

To determine whether star formation somehow resulted from special conditions at the coverslip edge, we altered the geometry of sample preparation. In the previous experiment, a 1-μl drop of assay mix was placed on a glass slide, and a coverslip was applied such that the drop spread outward from the coverslip's center. Here, the coverslip was applied such that one edge contacted the drop of assay mix, which was then forced to spread toward the coverslip's center. With this design, stars were not observed at the initial contacting edge of the coverslip (n = 527), whereas in the center of the coverslip, stars were abundant (83 ± 10%, n = 675), and in the transition zone, they represented 2 ± 2% (n = 745) of all structures. Thus, star formation was not a result of proximity to the coverslip edge. Rather, star formation correlated with distance of spreading across the glass surface.

One possible explanation for the formation of stars instead of comet tails was depletion of some protein(s) by adsorption to the glass during sample spreading. We tested this idea by blocking and preadsorption experiments. Pretreat-

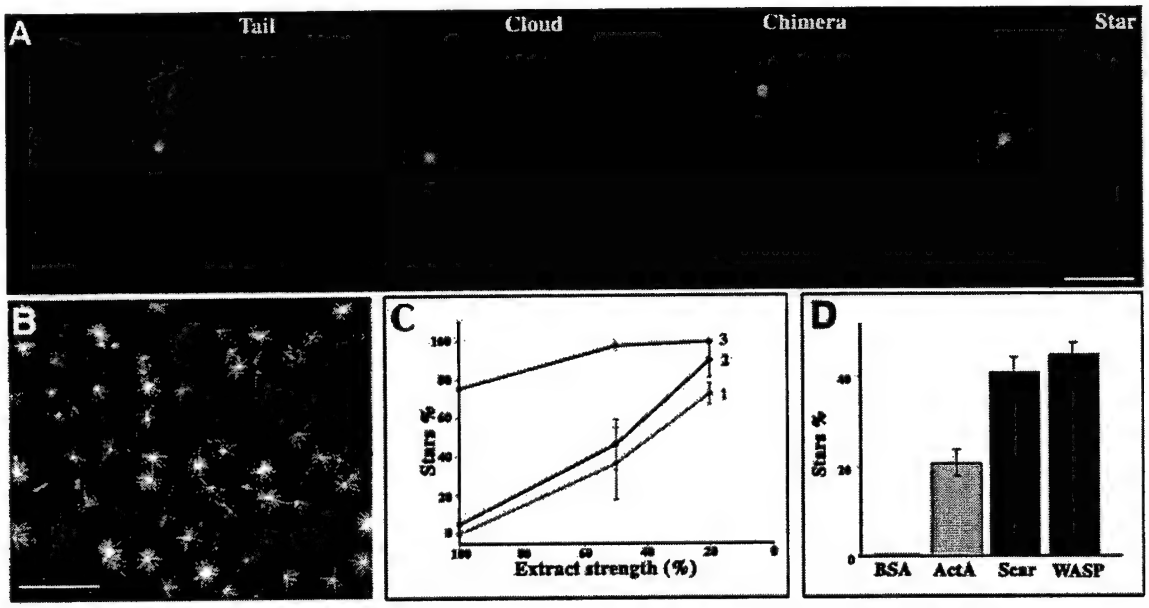

Figure 1. **Different actin structures are assembled on the beads.** Actin assembly was assayed on Arp2/3 activator-coated beads in brain extract supplemented with rhodamine-labeled actin. (A) The pattern of actin assembly depends on the location of the bead on the coverslip. In the center of the coverslip, beads induce the formation of tails. Halfway between the center and edge of the coverslip, actin clouds and chimeras are formed. At the edge of the coverslip, star-like structures are associated with the beads. Beads are shown in yellow. Bar, 5 μm. (B) Stars are the dominant actin structure at the edge of the sample. Low magnification view of a field at the edge of a coverslip. Bar, 50 μm. (C) Percentage of stars increases with extract dilution. 1, center of the coverslip; 2, transitional zone; 3, edge of the coverslip. (D) Percentage of stars produced at the edge of the coverslip in undiluted rat brain extract by beads coated with different Arp2/3-activating proteins.

ment of the coverslip with 1% BSA blocked star formation, whereas other actin structures (tails and clouds) did form (unpublished data), suggesting that protein adsorption to glass plays a critical role in star formation. Preadsorption was performed by mixing extract with ground glass to simulate protein depletion during sample spreading, followed by centrifugation to collect the unadsorbed fraction. Glass-depleted extracts supported star formation throughout the entire coverslip, not only at the edges. Further, glass-depleted extracts also supported the formation of stars on WASP-coated beads in plastic tubes. If absorption to glass reduced the concentration of some star-inhibiting factor(s), then simple dilution of the extract might be sufficient to induce stars. Indeed, as shown in Fig. 1 C, when extracts were diluted fivefold with buffer, stars formed across the entire coverslip. The percentage of stars at the center of the coverslip increased from 0% (n = 1603), for undiluted extracts, to 73 ± 6% (n = 542), for extracts diluted fivefold. Thus, the formation of stars could be induced by lowering the concentration of some factor(s) in the extract. Star formation was not limited to rat brain extracts. Extracts of *Xenopus* oocytes and rat embryo fibroblasts (REFs) also supported star formation (unpublished data), but required greater dilution than rat brain extracts. 10% *Xenopus* oocyte extracts and 50% REF extracts were comparable to full-strength brain extracts in their ability to produce stars.

Star formation in extracts is an Arp2/3-dependent process

The formation of bundles in association with WASP-coated beads suggested the involvement of the Arp2/3 complex. To investigate the role of Arp2/3 complex in star assembly, it was depleted from brain extracts by GST–verprolin-homology/connecting/acidic domain of WASP (VCA) sepharose beads. At least 90% depletion was achieved, as assayed by immunoblotting (Fig. 2 A). In control and mock-depleted extracts, stars were present throughout the entire coverslip, 96% (n = 126) and 90% (n = 138), respectively (Fig. 2, B and C). In Arp2/3-depleted extracts (Fig. 2 D), actin assembly around the beads was completely abolished (0%, n = 213). Only spontaneously polymerized filaments could be observed in the background. Add-back of pure Arp2/3 complex to the depleted brain extracts restored star formation (Fig. 2 E) (84%, n = 170), although stars were slightly smaller than in control samples. Based on our immunoblotting experiments, the concentration of Arp2/3 complex necessary to rescue star formation (0.5 μM) was similar to that calculated to be present in glass-depleted extracts (0.45 μM). Lower concentrations of added Arp2/3 complex induced the formation of branched filaments on the background or actin clouds on the beads. We conclude that star formation is mediated by the Arp2/3 complex.

We next assayed whether star formation would be supported by different Arp2/3 activators. Beads were coated with either the bacterial protein ActA or cellular proteins WASP or Scar1. All activator-coated beads induced star formation in rat brain extracts, whereas beads coated with BSA did not (Fig. 1 D). COOH-terminal domains of WASP and Scar (pVCA) proteins, which were sufficient for Arp2/3 activation (Higgs and Pollard, 2001), also induced stars in extracts. We also tested whether star formation depended on beads or could also occur on bacteria. Stars assembled on *Listeria* expressing ActA and on *Escherichia coli* expressing the *Shigella* protein IcsA (unpublished data), indicating that

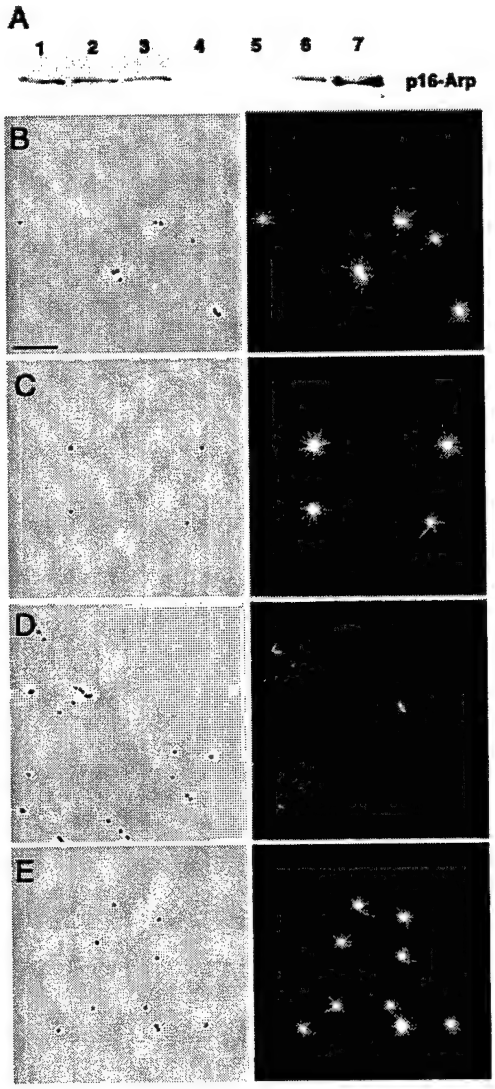

Figure 2. **Arp2/3 complex is essential for star formation.** (A) Arp2/3 complex depletion in brain extract. Glutathione-Sepharose or glutathione-Sepharose–coupled GST–VCA beads were incubated with 40 μl of brain extract. Arp2/3 depletion was monitored by immunoblotting using anti-p16 polyclonal antibody. Lane 1, 10 μl of untreated extract; lane 2, 10 μl of glass-depleted extract; lane 3, 10 μl of mock-depleted extract; lane 4, 10 μl of Arp2/3-depleted extract; lane 5, Arp2/3 associated with glutathione-Sepharose beads; lane 6, Arp2/3 associated with GST–VCA beads; lane 7, pure Arp2/3 from bovine brain, 4 μg. (B–E) Star assembly in Arp2/3-depleted brain extract. (B) Control, glass-depleted extract. (C) Mock-depleted extract. (D) Arp2/3-depleted extract; stars do not form. (E) Arp2/3-depleted extract rescued by add-back of 0.64 μM pure Arp2/3 complex; star formation is restored. Left panels, phase contrast. Individual 0.5-μm beads are visible. Right panels, fluorescence. Bright stars are evident on a background of faint individual filaments in B, C, and E. Only faint filaments are seen in D. Bar, 10 μm.

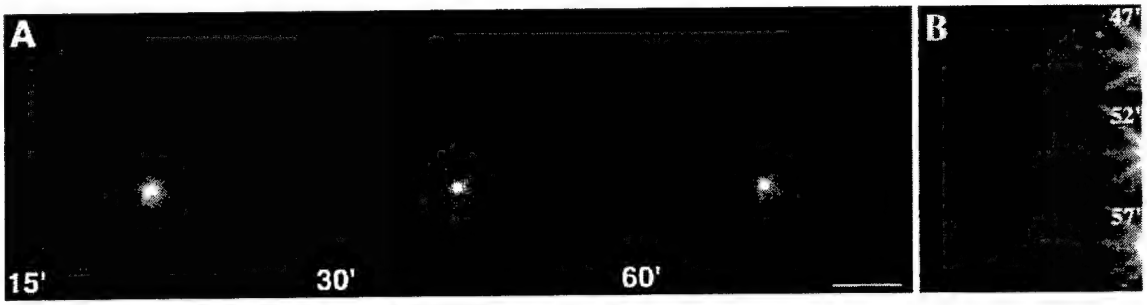

Figure 3. **Kinetics of star formation.** (A) Time-lapse sequence of star assembly in rat brain extract. Bar, 5 μm. (B) Actin bundle zippering. Two bundles zipper together in a centrifugal direction. Time shown in min.

the formation of stars was not restricted to coated synthetic beads. Because *Shigella* protein IcsA is known to recruit N-WASP from the extracts (Egile et al., 1999), this result also suggests that N-WASP supports star formation. Thus, star formation required active Arp2/3 complex but did not depend on a specific Arp2/3 activator.

Stars display both lamellipodial and filopodial types of actin organization

The radial bundles comprising stars bear a superficial similarity to filopodia in cells. To test whether these two kinds of structures have a deeper similarity, we analyzed the kinetics of star formation, their structural organization, sites of actin incorporation, and protein composition. Star development was observed by time-lapse microscopy. Initially, a diffuse actin cloud was formed around the bead (Fig. 3 A, 15 min). As time progressed, radial actin bundles appeared and began to elongate, with an average rate of 0.15 μm/min. Finally, we observed long stable actin bundles radiating from the bead-associated cloud. Some bundles in the course of star formation fused together by zippering in a proximal–distal direction, producing thicker bundles (Fig. 3 B). Zippering in a distal–proximal direction was also observed (unpublished data).

The structural organization of stars was examined by EM of platinum replicas (Fig. 4 A). Proximal to the bead, actin filaments formed a dendritic network, similar to that in lamellipodia. Many long unbranched filaments emanated from this network and, distal to the bead, gradually merged into bundles structurally similar to filopodia. Because one of the hallmarks of native filopodial bundles is uniform polarity of actin filaments, we performed myosin S1 decoration of actin filaments in stars to determine their polarity. The high density of filaments near the bead prevented determination of filament polarity in this region as well as in tight bundles. However, in the looser bundles distal to the bead (>1 μm), 93% ($n = 429$) of actin filaments had uniform polarity with their barbed ends pointing away from the bead (Fig. 4 B). Thus, stars display both lamellipodial (dendritic network) and filopodial (parallel bundle) types of actin organization, with the transition from one to the other occurring with distance away from the bead. The transition appeared as bundling of long filaments arising from the dendritic network.

Sites of actin polymerization in stars were analyzed by pulse-labeling experiments. After allowing stars to form, the distribution of newly incorporated rhodamine-labeled actin was determined relative to total actin, which was labeled with fluorescein-conjugated phalloidin (Fig. 4 C). Two major sites of actin incorporation were found: near the bead and at the tips of actin bundles. We interpret bead-associated sites to represent the growth of branches nucleated by WASP-activated Arp2/3 complex. In contrast, we interpret the incorporation at tips of radial bundles to represent elongation from preexisting, uncapped barbed ends, because no branched filaments were observed by EM at the tips of bundles. Actin incorporation was sometimes seen along the bundle, distant from its tip, consistent with EM data showing that some filaments in the bundle are shorter than others. This may result from unequal elongation of filaments or zippering of bundles of unequal length. Thus, stars display two modes of actin polymerization: Arp2/3-mediated nucleation at the bead, similar to that in lamellipodia, and barbed-end elongation at the tips of bundles, like that in filopodia.

Lamellipodia and comet tails, on the one hand, and filopodia in cells, on the other hand, have distinct protein composition (Goldberg, 2001; Small et al., 2002). For example, the Arp2/3 complex and capping protein are present in lamellipodia and comet tails but have not been found in filopodia (Svitkina and Borisy, 1999; Svitkina et al., 2003), whereas fascin is enriched in filopodia and less abundant in lamellipodia (Kureishy et al., 2002). α-Actinin has been found in lamellipodia (Langanger et al., 1984) but only in the roots of filopodia (Svitkina et al., 2003). We determined the localization of these proteins in stars by immunofluorescence staining or by incorporation of the labeled protein (Fig. 5). Arp2/3 complex and capping protein were found in the dendritic network proximal to the bead but not in actin bundles. α-Actinin was clearly enriched around the bead but could be faintly detected in bundles when a high amount of exogenous protein was added. In contrast, fascin was strongly localized to actin bundles but was diminished in the network surrounding the bead. Thus, by structural, kinetic, and biochemical criteria, our data demonstrate that the proximal dendritic network and radial bundles of stars are similar to the actin organization of lamellipodia and filopodia, respectively.

Parallel bundle formation can be shifted to dendritic network formation by capping protein

The absorption and dilution experiments indicated that reduced levels of factor(s) in the extract are critical in shifting

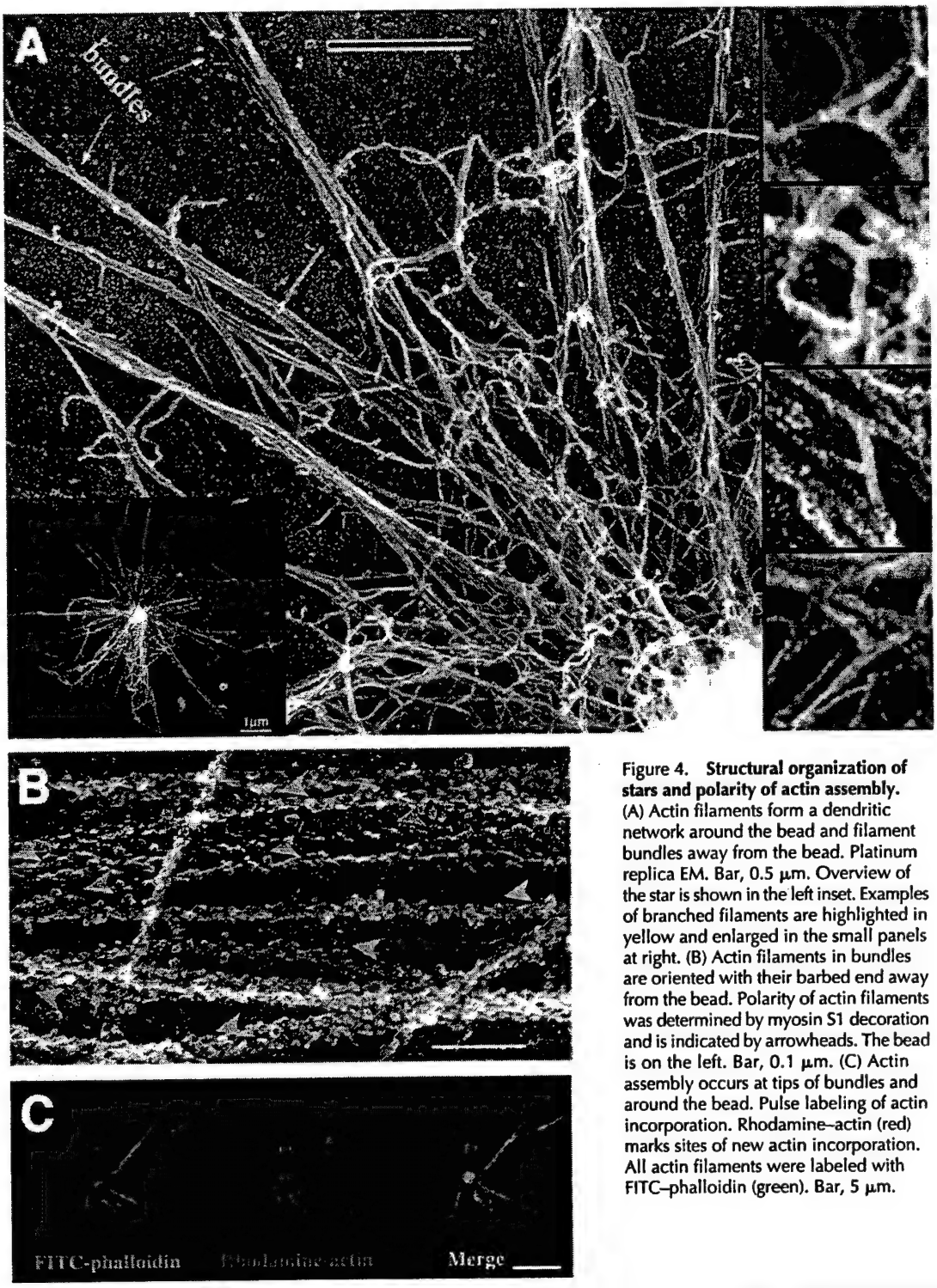

Figure 4. **Structural organization of stars and polarity of actin assembly.** (A) Actin filaments form a dendritic network around the bead and filament bundles away from the bead. Platinum replica EM. Bar, 0.5 μm. Overview of the star is shown in the left inset. Examples of branched filaments are highlighted in yellow and enlarged in the small panels at right. (B) Actin filaments in bundles are oriented with their barbed end away from the bead. Polarity of actin filaments was determined by myosin S1 decoration and is indicated by arrowheads. The bead is on the left. Bar, 0.1 μm. (C) Actin assembly occurs at tips of bundles and around the bead. Pulse labeling of actin incorporation. Rhodamine–actin (red) marks sites of new actin incorporation. All actin filaments were labeled with FITC–phalloidin (green). Bar, 5 μm.

the balance from a dendritic organization toward parallel bundles of actin. Several considerations suggest that one likely candidate for this role is capping protein. First, it has been shown (DiNubile et al., 1995) that increasing the concentration of neutrophil extract, and thus concentration of added capping protein, inhibited the extent and rate of polymerization of actin on spectrin–actin seeds. Conversely, we interpret that in our system, star formation after dilution or glass depletion might be due to decreased capping protein concentration. Second, when bacterial motility was reconstituted from purified proteins, suboptimal concentrations of capping protein (35 nM) produced comet tails with a fishbone appearance (Pantaloni et al., 2000), similar to chimeras observed in our samples in the transitional zone (Fig. 1 A).

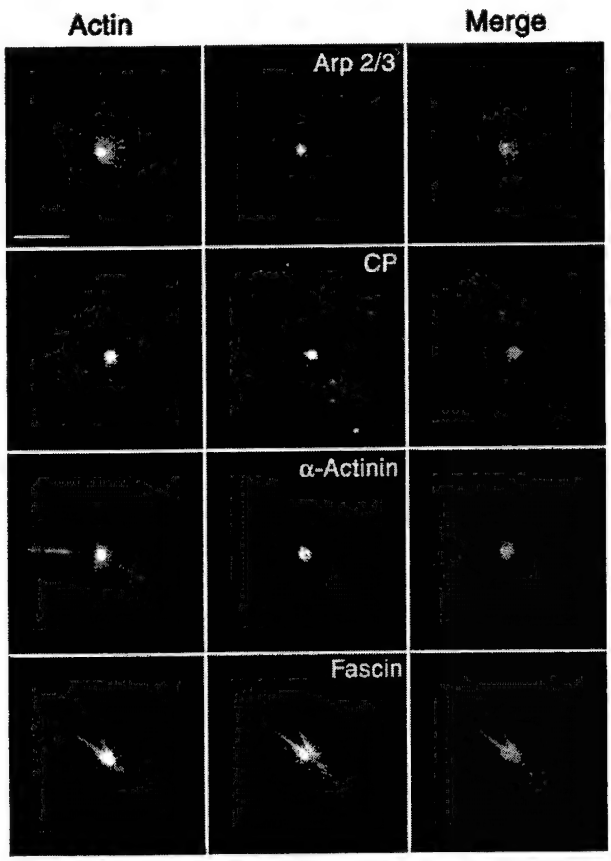

Figure 5. **Localization of actin binding proteins in stars.** Arp2/3 complex, capping protein, and α-actinin are enriched near the beads but not in bundles, whereas fascin is enriched in bundles but is not prominent at beads. Stars were labeled with rhodamine–actin (green) and FITC–α-actinin (red) during assembly. Immunostaining for Arp2/3 (p16 Arc), capping protein (β2), or fascin (red) was performed after fixation of stars. Bar, 5 μm.

Third, immunostaining for capping protein detected high levels of fluorescence on the coverslip (Fig. 3), suggesting that capping protein was adsorbed to the glass and thus depleted from the extract. Therefore, we investigated whether star formation was dependent on the concentration of capping protein in the extract.

Capping protein concentration was estimated in terms of a chicken capping protein standard by immunoblotting. Rat brain extracts contained 3.8 ng/μl (58 nM) and REF extracts contained 8 ng/μl (122 nM) capping protein (Fig. 6 A). The twofold higher concentration of capping protein in REF extracts was consistent with the twofold dilution of this extract required to produce stars. We were unable to estimate the concentration of capping protein in *Xenopus* oocyte extracts because of a lack of cross-reactivity of the antibodies used. The initial total protein concentration for all tested extracts was similar: brain extract, 16 mg/ml; REF, 21 mg/ml; and *Xenopus* oocyte, 24 mg/ml. Next, we examined how much capping protein was depleted from brain extract by its adsorption on ground glass. As assayed by immunoblotting, 35% of capping protein was depleted (Fig. 6 B), whereas actin was not depleted (0%) (Fig. 6 B), Arp2/3 was 18% depleted (Fig. 2 A), and fascin was only 8% depleted (unpublished data). These results demonstrate that glass absorbs motility proteins differentially and that capping protein is preferentially depleted.

Next, we supplemented 50% diluted brain extract with increasing amounts of exogenous capping protein. Capping protein inhibited star formation and facilitated cloud formation in a concentration-dependent manner (Fig. 6 C). In a kinetic analysis using time-lapse observation, addition of 50 nM capping protein to the extract (which normally produced mostly stars) blocked bundle formation around beads but allowed for continuous growth of actin clouds up to 20 times the bead diameter (Fig. 6 D). EM analysis of such clouds showed that actin filaments were organized into an extended dendritic network (Fig. 6 E). Higher concentrations of added capping protein, as expected, inhibited the extensive growth of clouds (unpublished data). At 400 nM capping protein, the diameter of the cloud was reduced to approximately twice the bead diameter. These results show that parallel bundle formation can be shifted to extended dendritic network formation by an optimal level of capping protein. As a specificity control, other proteins known to participate in actin dynamics were added to glass-depleted and diluted brain extracts. Addition of actin (7.5 μM), Arp2/3 complex (0.05, 0.1, and 0.6 μM), profilin (1.0, 2.5, and 10 μM), cofilin (2.5, 5.0, and 10 μM), and α-actinin (0.15, 0.25, 0.35, and 0.5 μM) did not affect star formation, whereas addition of 50 nM capping protein blocked star formation but allowed growth of actin clouds. These results show that capping protein was specific in antagonizing star formation.

Reconstitution of filopodia-like bundles using pure proteins

We tried to define a minimal set of components necessary for star assembly. Because data obtained with extracts indicated that Arp2/3 complex was necessary and capping protein had to be depleted, initial reconstitution experiments were performed with WASP-coated beads, actin, and Arp2/3 complex. Concentrations of proteins were based on published data for reconstitution of comet tails (Loisel et al., 1999). Beads coated with WASP were put into physiological ionic strength buffer solution, pH 7, containing rhodamine-labeled actin (6.9 μM) and increasing amounts of Arp2/3 complex over the range 0.1–0.9 μM. At 0.7 μM Arp2/3 complex and above, actin polymerization at the bead surface resulted in clouds within 15 min (Fig. 7 A). Clouds were ~3.2 mm in diameter (measured as full width at 1/e of maximum fluorescence) and were azimuthally homogeneous in intensity except for apparently stochastic fluctuations. Lower concentrations of Arp2/3 did not generate clouds or did so more slowly.

Because Arp2/3 alone was insufficient to induce stars, we then introduced a bundling protein. Fascin was selected to complement the reconstitution system because it is the major bundler in filopodia and in star bundles formed in extracts. Recombinant fascin was used in these experiments. Fascin was added to samples of WASP-coated beads preincubated with Arp2/3 complex (0.7 μM) and actin (6.9 μM)

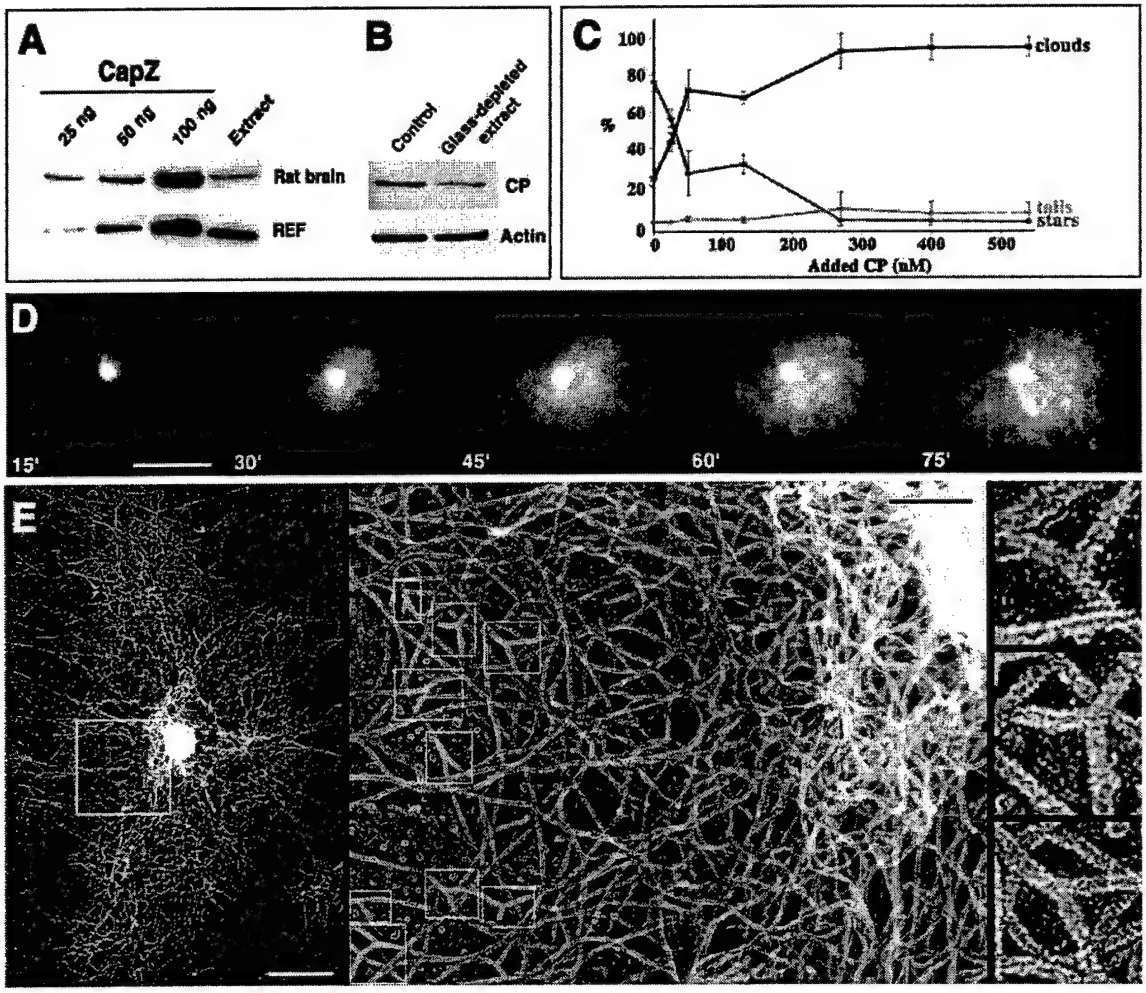

Figure 6. **Formation of stars depends on the concentration of capping protein.** (A) Capping protein concentration in rat brain and REF extracts (7.5 μl per lane) was determined by Western blotting. Purified CapZ was used as a standard at concentrations shown above the respective lanes. (B) Capping protein and actin concentration in control and glass-depleted brain extract. (C) Addition of capping protein inhibits star formation. Percentage of the indicated bead-associated structure (Y axis) is shown versus concentration of added capping protein (X axis) to the 50% diluted rat brain extract. (D) Addition of capping protein induces growth of clouds. Time-lapse sequence of actin assembly around a WASP-coated bead in 50% brain extract supplemented with 50 nM capping protein. Bar, 5 μm. (E) Dendritic organization of clouds formed after the addition of 50 nM capping protein to the 50% brain extract. Bar, 0.2 μm. Overview of the cloud is shown in the left panel. Bar, 1 μm. Examples of branched filaments are highlighted in boxes and enlarged in small right panels.

on ice for 20 min, and star formation was evaluated within 15 min incubation at RT. Increasing amounts of fascin promoted bundle formation both on beads and of filaments in the background. At 3.1 μM fascin, >95% of the beads showing actin polymerization displayed stars with straight, needle-like rays (Fig. 7 B). EM demonstrated that the star bundles formed in the presence of fascin were composed of long actin filaments that were packed tightly together (Fig. 7 C), similar to those of filopodia and bundles made in extracts. The actin cross-linking protein, α-actinin, also generated star-like structures, but they were qualitatively different from those induced by fascin. The bundles of α-actinin stars were wavy, not straight, and EM showed them to consist of loosely packed and cross-linked filaments (unpublished data), as previously reported for mixtures of α-actinin and actin (Jockusch and Isenberg, 1982). The reconstitution experiments demonstrate that in the absence of barbed-end capping, four components, WASP-coated beads, Arp2/3 complex, actin, and fascin, are sufficient for star formation.

Discussion

Formation of filopodia-like structures in vitro and initiation of filopodia in the cellular context (Svitkina et al., 2003) reveal remarkable similarities. A comparison of these two processes is presented in Fig. 8. The initial step, dendritic nucleation of actin filaments, is essentially the same in both cases. Nucleation is driven by activation of the Arp2/3 complex and results in the formation of new branches on preexisting filaments. Under conditions where capping activity is favored, filaments not specifically protected become terminated soon after nucleation, resulting in an overall dendritic organization, forming tails or clouds in the bead assay (Fig. 8, top left) and lamellipodia in cells

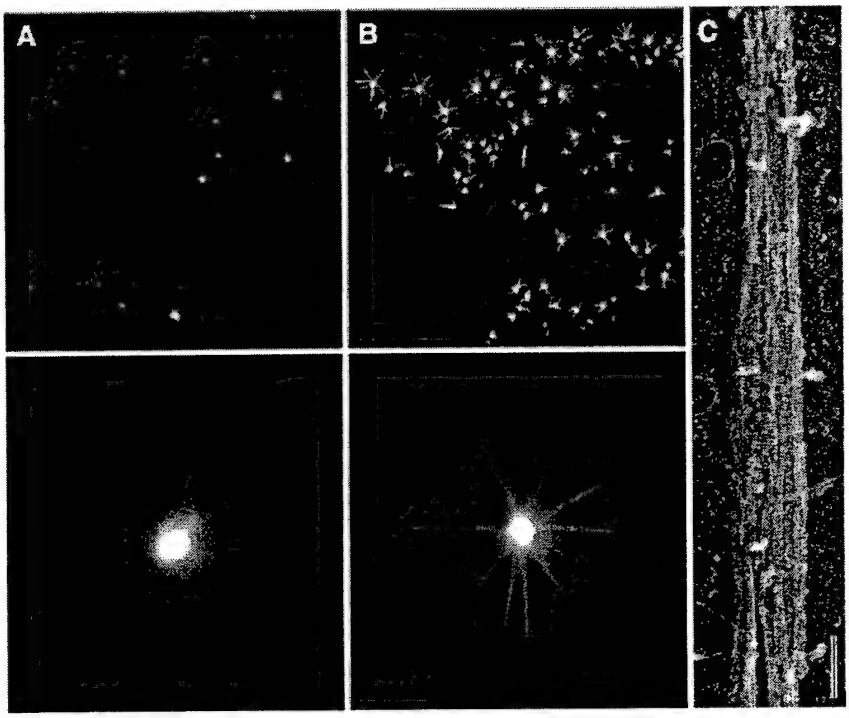

Figure 7. **Reconstitution of filopodia-like bundles from pure proteins.** Samples of WASP-coated beads preincubated on ice with 6.9 μM rhodamine-labeled actin and 0.7 μM Arp2/3 complex were brought to RT to allow for actin assembly. (A) Actin clouds formed in the absence of fascin. (B) Addition of 3.1 μM fascin to the sample before incubation at RT produced stars. Low magnification panels (top row) show distinctive pattern of actin assembly under each condition. (C) EM of star bundles formed in the presence of fascin as in B. Bars: (top row) 50 μM; (bottom row) 5 μm; (C) 100 nm.

(top right). In the in vitro system, using activator-coated beads, a reduced concentration of capping protein allows filaments to remain uncapped and continue elongation, followed by cross-linking into bundles to form stars (Fig. 8, bottom left). In the cellular context, where the cytoplasmic concentration of capping protein is presumably high, we postulate that filaments with barbed ends at the membrane are protected from capping, allowing them to elongate and be bundled to form filopodia (bottom right). Thus, we recognize three processes to be necessary for star or filopodia formation: nucleation, elongation, and bundling. These three processes and the molecules likely to be involved in them are discussed in turn.

Nucleation

The Arp2/3 complex is thought to play a role in filopodia formation because one of its activators, N-WASP, induces filopodia in cells (Miki et al., 1998). Because Arp2/3 is absent from established filopodia (Svitkina and Borisy, 1999; Svitkina et al., 2003), one may infer that it likely participates in initiation, not in steady-state elongation of filopodia. The question then becomes precisely how the Arp2/3 complex is involved in the initiation process. We suggest that our in vitro system for producing filopodia-like bundles reflects the situation in vivo and provides insights into the mechanism. First, formation of filopodia-like bundles, as well as dendritic clouds, depended on the presence and activity of the Arp2/3 complex. These findings agree with the observations in vivo, that perturbation of Arp2/3 complex function inhibits the formation of both lamellipodia and filopodia (Machesky and Insall, 1998; Li et al., 2002). Localization of Arp2/3 in stars was also analogous to the in vivo situation; it was present in dendritic arrays at the base of bundles, but not in bundles per se.

One possibility for how the action of the Arp2/3 complex can be explained is that it promotes dendritic or filopodial initiation depending upon the specific Arp activator. This

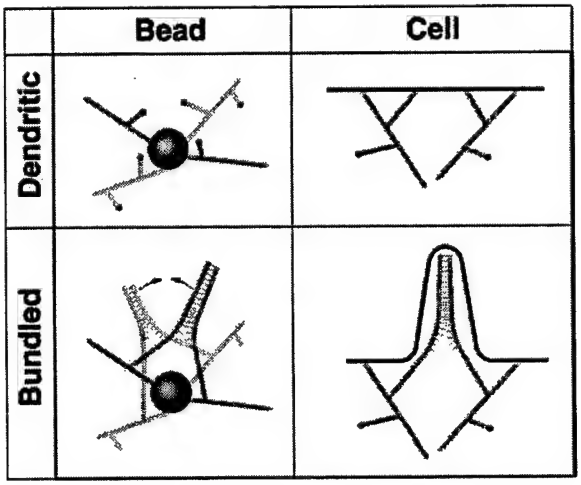

Figure 8. **Model for the formation of filopodial bundles.** We propose that filopodia are formed from a preexisting dendritic network by barbed-end elongation of actin filaments and their subsequent cross-linking into bundles. At normal levels of capping activity, clouds and tails are formed around the bead in the in vitro system (top left), and lamellipodia are formed in cells (top right). If the concentration of capping protein is lowered in the in vitro system, filaments elongate and become bundled by cross-linking proteins, e.g., fascin (bottom left). Two examples of cross-linking are presented. Thin bundles may further zipper into the thicker bundles (arrows). In the cell, some filament barbed ends at the membrane become protected from capping, perhaps by Ena/VASP proteins, so that they can elongate and be cross-linked to form bundles in filopodia (bottom right).

idea is consistent with findings that different members of the WASP family vary in their ability to activate the Arp2/3 complex (Zalevsky et al., 2001). However, we found no significant differences in the process of star formation when they were induced by a variety of Arp2/3 activators, including ActA, WASP, Scar, N-WASP, and the pVCA COOH-terminal domains of WASP and Scar. ActA was active both as endogenous bacterial protein and as a recombinant protein at the bead surface. Thus, our data do not support a model that Arp2/3 complex produces different arrays depending on the specific activator.

Our data are in agreement with a model in which the Arp2/3 complex, irrespective of its activator, produces a normal dendritic array, which subsequently becomes reorganized into bundles. Time-lapse observations showed that diffuse clouds with dendritic organization preceded the formation of bundles. Structural studies demonstrated a gradual transition from dendritic arrays around the bead to distal radial bundles. Both results suggest that a normal dendritic network serves as a precursor for bundles. These results are in close agreement with recent results elucidating the in vivo mechanism of filopodial initiation (Svitkina et al., 2003). We propose that the role of the Arp2/3 complex in the in vitro system is to supply barbed ends. The high local concentration of barbed ends created by activator-coated beads and the high concentration of Arp2/3 in solution were essential for bundle formation. A similar method may be used by cells if Arp2/3 activators (or molecules recruiting them) are not evenly distributed along the leading edge, but exist in clusters. A high local concentration of barbed ends could also be created by the clustering of some barbed end–binding molecules at the membrane. Possible candidates for such a role are members of the enabled/vasodilator-stimulated phosphoprotein (Ena/VASP) family (Bear et al., 2002; Svitkina et al., 2003) and formins (Pruyne et al., 2002), which have recently been shown to bind barbed ends but allow for filament elongation. Formins can also nucleate unbranched actin filaments (Pruyne et al., 2002; Sagot et al., 2002b) and thus are candidates for an alternative, Arp2/3-independent pathway of bundle initiation, similar to how actin cables in yeast are formed (Evangelista et al., 2002; Sagot et al., 2002a). However, this mechanism does not account for the N-WASP induction of filopodia.

Elongation

After filaments are nucleated, they have to elongate and encounter each other before they can form a bundle. A priori, elongation of filaments could be facilitated by increasing the concentration of an "elongation" factor or by decreasing the concentration of a "termination" factor. The main arguments in favor of the latter possibility are that star formation was induced in extracts by depletion of capping protein and was antagonized specifically by add-back of capping protein. A key point here is that add-back of capping protein to depleted extracts did not simply block all actin polymerization. Rather, it induced the formation of clouds as opposed to stars. Our interpretation is that cloud formation was the result of the termination of filament elongation shortly after branch nucleation under conditions when active Arp2/3 complex continuously nucleates new filaments. This process results in short filaments and a dense dendritic network. The fact that stars could be reconstituted in a pure protein system lacking barbed-end capping proteins but allowing for filament nucleation, elongation, and bundling is consistent with the interpretation that star formation was facilitated by decreasing a termination factor.

In the cellular context, the cytoplasmic concentration of capping protein is high (Huang et al., 1999). In lamellipodia where barbed ends are constantly being produced, the high concentration of capping protein can be understood as necessary to cap unproductive barbed ends. In filopodia where filaments elongate continuously, their barbed ends need to be protected from capping. Protection may be provided by Ena/VASP family proteins because they are present at the extreme leading edge, bind to barbed ends, and can antagonize capping in vitro and in vivo (Bear et al., 2002). Ena/VASP proteins are also enriched at the tips of filopodia (Lanier et al., 1999; Rottner et al., 1999) and become gradually accumulated at the tips of filopodial precursors during the filopodial initiation (Svitkina et al., 2003). It is attractive to speculate that the presence of Ena/VASP at the filopodial tips in the cellular context prevents filament termination and allows filopodial elongation. Consistent with this idea, our results showing that the level of capping protein controls the transition between two types of actin arrays in vitro match the observations that the level of Ena/VASP proteins performs analogous control in vivo, but in the opposite direction. That is, a low level of Ena/VASP induced short branched filaments, and an excess of Ena/VASP promoted the formation of long filaments (Bear et al., 2002).

In our in vitro system, the rates of bundle elongation in stars were ~0.15 μm/min, similar to the reported rates of comet tail motility in undiluted brain extracts (0.2–0.3 μm/min) (Laurent et al., 1999; Yarar et al., 1999). Whereas in *Xenopus* oocyte extract or during leading edge protrusion in cells, the rates of actin array assembly are at least an order of magnitude higher (Mallavarapu and Mitchison, 1999). These observations indicate that additional factors may contribute to the overall performance of actin machinery, but balance between nucleation and elongation seems to be critical for the determination of supramolecular organization of the actin array.

Bundling

Bundling is necessary to allow long filaments to push efficiently without buckling under the cell surface. The leading candidate for filament bundling in filopodia is fascin. It shows the greatest enrichment in filopodial bundles in cells (Kureishy et al., 2002), where it significantly prevails over α-actinin (Svitkina et al., 2003), and it is essential for the maintenance of filopodia (Yamashiro et al., 1998; Adams et al., 1999; Cohan et al., 2001).

Consistent with in vivo data, we found that fascin was the major bundling protein present in stars assembled in cytoplasmic extracts. Fascin was also sufficient to form filopodia-like bundles in a reconstitution system in which fascin represented the only bundling protein. The straightness of the fascin-induced star bundles suggests that they were quite rigid, similar to filopodia. In contrast to fascin, the other actin filament cross-linker, α-actinin, was more abundant in

the dendritic network surrounding beads and was absent from star bundles. Although α-actinin was also able to drive star assembly in a reconstitution system, the resulting star bundles had wavy rays and a dendritic, not parallel bundled, organization. Thus, α-actinin did not recapitulate filopodia formation in vitro. These results suggest that the two cross-linkers may be specialized with respect to the particular actin filament array that they stabilize. Segregation of fascin and α-actinin to bundles and the dendritic network, respectively, correlates with the biochemical properties of these two cross-linkers: fascin is a short cross-linker that makes tight parallel bundles (Yamashiro-Matsumura and Matsumura, 1985) and α-actinin is a longer molecule that, when combined with actin, makes loose bundles with both parallel and antiparallel filament orientation. The absence of α-actinin in filopodial bundles in more complex systems, such as extracts or cells, when both proteins are present may be explained as fascin outcompeting α-actinin because of a slightly higher affinity or, possibly, specific recruitment to areas of filopodial assembly.

In the course of star formation, we frequently observed zippering of radial bundles, an effect that superficially resembles fusion of filopodia during their normal dynamics in cells. However, distinctions between these two phenomena should be noted. In cells, the fusion site moves backward because of treadmilling and retrograde flow of the whole assembly, but no actual displacement of bundles, with respect to each other, occurs. In stars, we did not find independent indications of retrograde flow, suggesting that zippering in vitro actually brings distant bundles together. A likely reason for the difference between the two systems is that the movement of bundles in vivo is precluded by the more crowded conditions and cross-linking occurring in the cytoplasm, compared with extracts. Nevertheless, the similarity of the systems suggests that cross-linking molecules, presumably fascin, have a potential for zippering and may accomplish this function under permissive circumstances, for formation of bundles in vitro and for filopodia in vivo.

In summary, our results suggest that an Arp2/3-mediated pathway is compatible with filopodia formation, and that it is not necessary to postulate unusual properties of WASP family members to stimulate a nonbranching mode of actin filament formation. Filopodia-like structures can be accounted for as a transformation from a dendritic organization by a combination of elongation and bundling.

Materials and methods

Proteins

Actin was purified from rabbit muscle as previously described (Spudich and Watt, 1971). Rhodamine–actin was prepared by labeling actin with *N*-hydroxy succinimido-rhodamine (Molecular Probes) as previously described (Isambert et al., 1995) and stored at −80°C. Before use, labeled G-actin was recycled by polymerization for 2 h on ice in the presence of 50 mM KCl, 2 mM $MgCl_2$, and 1 mM ATP, sedimentation at 100,000 *g* for 1.5 h at 4°C, resuspension in cold G buffer (2 mM Tris-Cl, 0.2 mM $CaCl_2$, 0.2 mM ATP, and 0.5 mM DTT) to a final concentration of 2 mg/ml, and dialysis overnight against G buffer using microdialysis buttons (Hampton Research) and dialysis tubing (Pierce Chemical Co.).

DNA encoding WASP tagged at its NH_2 terminus with both Met, Arg, Gly, Ser (MRGS) 6xHis and FLAG epitopes was amplified by PCR from a human WASP cDNA (a gift of Arie Abo, PPD Discovery, Menlo Park, CA) and subcloned into pFastBac1 (Life Technologies; Amersham Biosciences). DNA encoding human Scar1 was amplified by PCR and subcloned into the WASP-pFastbac1 vector in the place of the WASP DNA. Recombinant WASP and Scar1 proteins were expressed in Sf9 cells using the baculovirus system. Baculovirus strains were generated and used for infections according to the Bac-to-Bac baculovirus expression system (Life Technologies). After 72 h of infection, cells were harvested by centrifugation at 500 *g* for 10 min at 25°C, resuspended in lysis buffer (50 mM NaH_2PO_4, pH 8.0, 300 mM KCl) with protease inhibitors (1 mM PMSF and 10 μg/ml leupeptin, pepstatin, and chymostatin [LPC]), and frozen in liquid N_2. To prepare the lysate, cells were thawed and centrifuged at 200,000 *g* for 15 min at 4°C.

To purify the recombinant proteins, Sf9 lysates were supplemented with 20 mM imidazole, incubated with Ni-NTA agarose (QIAGEN) resin for 45 min at 4°C, washed with 50 mM NaH_2PO_4, pH 8.0, 300 mM KCl, 20 mM imidazole, and eluted with 200 mM imidazole, 50 mM NaH_2PO_4, pH 8.0, 300 mM KCl, and protease inhibitors. Eluted proteins were further purified by gel filtration chromatography on a Superdex-200 column (Amersham Biosciences) equilibrated with 20 mM MOPS, pH 7.0, 100 mM KCl, 2 mM $MgCl_2$, 5 mM EGTA, 1 mM EDTA, 0.2 mM ATP, 0.5 mM DTT, 10% vol/vol glycerol. Full-length recombinant WASP has constitutive ability to activate Arp2/3 complex (Higgs and Pollard, 2001).

DNA encoding human fascin was amplified by PCR and subcloned into the pGEX-4T-3 vector (Amersham Biosciences) using BamH1/Xho I sites. Recombinant human fascin was prepared by a modification of the method of Ono et al. (1997). *E. coli* carrying the plasmid was grown at 37°C until the A600 reached 0.6. Protein expression was induced by adding 0.1 mM IPTG at 20°C for 4 h. Cells were harvested by centrifugation and extracted with B-PER in phosphate buffer (Pierce Chemical Co.) plus 1 mM PMSF and 1 mM DTT. The lysate was centrifuged at 20,000 *g* for 20 min, and the supernatant was mixed for 1 h at RT with 2 ml glutathione–Sepharose 4B (Amersham Biosciences) equilibrated with PBS plus 1 mM DTT. The glutathione-Sepharose was poured into a column and washed with 20 ml of PBS plus 1 mM DTT. 80 μl of thrombin (Amersham Biosciences) was added, and digestion was allowed to proceed overnight at 4°C. Flowthrough fractions were collected in 2 mM PMSF and concentrated by Centricon 10 (Amicon).

Arp2/3 was purified from bovine brain as described by Laurent et al. (1999). Recombinant chicken CapZ (Soeno et al., 1998; Palmgren et al., 2001) was provided by John Cooper (Washington University School of Medicine, St. Louis, MO). FITC-labeled α-actinin was provided by Marion Greaser (University of Wisconsin, Madison, WI). ActA protein (Cameron et al., 1999) was provided by Julie Theriot (Stanford University School of Medicine, Stanford, CA). Recombinant human cofilin and human profilin were purchased from Cytoskeleton, Inc.

Cytoplasmic extracts

Rat brain extract was prepared as previously described (Laurent et al., 1999). Metaphase *Xenopus* oocyte extract was prepared as previously described (Murray, 1991) and kept frozen at −80°C. Before use, it was centrifuged at 100,000 *g* for 1 h at 4°C, and the supernatant was used for experiments. Rat embryonic fibroblast extract was prepared as described by Saoudi et al. (1998).

Actin polymerization bead assay

Carboxylated polystyrene beads (Polysciences) were coated with ActA as previously described (Cameron et al., 1999). For coating beads with WASP/Scar proteins, we took 15 μl of 0.5 μM WASP or Scar proteins, mixed up with 15 μl of brain buffer (BB) (Laurent et al., 1999) or *Xenopus* buffer (Murray, 1991) and 0.5 μl of 0.5-μm carboxylated polystyrene beads. This mixture was incubated at RT for 1 h. Beads were washed twice with the appropriate buffer and resuspended in 10 μl of buffer. For longer storage, beads were supplemented with 50% glycerol and placed at −80°C.

Coated beads (0.5 μl) were introduced into 10 μl of cell extract supplemented with energy mix (15 mM creatine phosphate, 2 mM ATP, and 2 mM $MgCl_2$) and 1.25 μM rhodamine-labeled actin. In experiments to evaluate the effect of capping protein concentration, the assay mix was supplemented with increasing amounts of capping protein. The assay mix was incubated on ice for 1 h before preparation for observation.

For reconstitution system, 0.5 μl of coated beads was introduced in 1× KME buffer (50 mM KCl, 1 mM $MgCl_2$, 1 mM EGTA, 10 mM imidazole, pH 7) supplemented with Arp2/3 complex. After incubation for 5 min at RT, 6.9 μM actin was added, and the mixture was incubated on ice for 20 min before the addition of fascin and allowing for actin assembly at RT.

Microscopy

For light microscopy, a 1-μl sample was removed and pressed tightly between a microscope slide and a 22-mm square glass to create a chamber ~5

μm thick, which was then sealed with vaseline/lanolin/paraffin (at 1:1:1). Samples were incubated at RT for 15 min and then observed with a Nikon Eclipse inverted microscope equipped with phase contrast and epifluorescence optics. Time-lapse images were acquired with a back-thinned CCD camera (CH250; Photometrics) using METAMORPH (Universal Imaging Corp.) software. Fluorescence images were recorded every 5 min for 2 h.

For EM, samples were prepared as described by Cameron et al. (2001). After incubation for 2 h at RT in a humid environment, chambers were opened into solution containing 0.2% Triton X-100 and 2 μM phalloidin in BB. Although some stars were washed out during this procedure, some remained attached to the coverslip. Coverslips were washed with 2 μM phalloidin in BB, fixed with 2% glutaraldehyde, and processed for EM. Procedures for S1 decoration and EM were as previously described (Svitkina and Borisy, 1998). Polarity of filaments, determined in blind experiments by two independent observers, gave similar results.

Immunostaining

Rabbit polyclonal antibody to the Arc p16 subunit of the Arp2/3 complex was prepared against the RFRKVDVDEYDENKFVDEED peptide of the human sequence. By Western blotting, the affinity-purified antibody recognized in rat brain extract a doublet of closely spaced bands in the16-kD range, supposedly corresponding to two isoforms of Arc p16 (Millard et al., 2003). Polyclonal rabbit antibody against capping protein (R22) was provided by Dorothy A. Schafer (University of Virginia, Charlottesville, VA). Mouse monoclonal α-actinin antibody was from Sigma-Aldrich, and mouse monoclonal fascin antibody was from DakoCytomation. Immunostaining was performed in perfusion chambers. Solutions were applied on one side of the chamber with a pipet and withdrawn from the other side with filter paper. A 4-μl assay sample was sandwiched between a glass slide and a coverslip (22 × 22 mm) separated by two strips of teflon tape and sealed. Stars were allowed to form for 2 h at RT in humid conditions. 10 μl of BB containing 0.2% Triton X-100 and 2 μM phalloidin was perfused through the chamber, followed by 10 μl of 2 μM phalloidin in BB. For most immunostaining experiments, stars were fixed with 0.2% glutaraldehyde for 20 min at RT, washed with PBS, and quenched for 20 min with 2 mg/ml of $NaBH_4$ in PBS supplemented with 0.1% Tween 20. For fascin staining, samples were fixed with methanol for 10 min at −20°C.

Pulse-labeling assay

Stars were allowed to form for 1 h in a perfusion chamber containing 4 μl of assay sample without labeled actin. Then 1 μl of 1.8 μM rhodamine–actin was added by diffusion from the edge. After 10 min, FITC–phalloidin was added in the same way to label all actin filaments. The chamber was sealed, and observations were made after 10 min of incubation at RT.

Glass depletion experiment

30 μl of brain extract was applied to 70 mg of ground glass coverslip in a mini filtration tube (0.65 μm; UltraFree-MC; Millipore), and the filtrate was collected by centrifugation twice for 1 min at 11,000 *g*.

Depletion of Arp2/3 complex

Arp2/3 complex was depleted from glass-depleted brain extract using a variation of the method described by Egile et al. (1999). 15 μl of glutathione-Sepharose–coupled GST–VCA beads was incubated with 40 μl of brain extract for 30 min at 4°C on a rotating wheel. Beads were pelleted at 10,000 *g* for 2 min. Mock depletion is performed by the same amount of glutathione-Sepharose beads. Depletion of the Arp2/3 complex was monitored by Western blotting of aliquots of extracts and beads. The add-back experiment was performed using the Arp2/3 complex purified from bovine brain. For the microscopy assay, we scored the percentage of stars assembled on all beads.

Quantification of capping protein in cell extracts by Western blotting

Different amounts of rat brain and rat embryonic fibroblast extracts were subjected to SDS-PAGE (4–20% polyacrylamide) and immunoblotting with anti-CapZ. The amount of capping protein present was evaluated by comparing the intensity of the bands of each sample with the chicken CapZ standard by densitometry using NIH image software.

We thank Drs. Julie Theriot, Dorothy Schafer, John Cooper, Marie-France Carlier, Josephine Adams, Marion Greaser, and Elena S. Nadezhdina for generous gifts of reagents and bacterial strains. We also thank Dr. Tom Keating and members of the Borisy laboratory for constructive discussions.

This work was supported by United States Army USAMRMC grant DAMD 17-00-1-0386 (D. Vignjevic), National Institutes of Health (NIH) grant GM 62431 (G.G. Borisy), and NIH Glue Grant on Cell Migration IU 54 GM 63126.

Submitted: 12 August 2002
Revised: 24 January 2003
Accepted: 24 January 2003

References

Adams, J.C., J.D. Clelland, G.D. Collett, F. Matsumura, S. Yamashiro, and L. Zhang. 1999. Cell-matrix adhesions differentially regulate fascin phosphorylation. *Mol. Biol. Cell.* 10:4177–4190.

Bear, J.E., T.M. Svitkina, M. Krause, D.A. Schafer, J.J. Loureiro, G.A. Strasser, I.V. Maly, O.Y. Chaga, J.A. Cooper, G.G. Borisy, and F.B. Gertler. 2002. Antagonism between Ena/VASP proteins and actin filament capping regulates fibroblast motility. *Cell.* 109:509–521.

Borisy, G.G., and T.M. Svitkina. 2000. Actin machinery: pushing the envelope. *Curr. Opin. Cell Biol.* 12:104–112.

Cameron, L.A., M.J. Footer, A. van Oudenaarden, and J.A. Theriot. 1999. Motility of ActA protein-coated microspheres driven by actin polymerization. *Proc. Natl. Acad. Sci. USA.* 96:4908–4913.

Cameron, L.A., P.A. Giardini, F.S. Soo, and J.A. Theriot. 2000. Secrets of actin-based motility revealed by a bacterial pathogen. *Nat. Rev. Mol. Cell Biol.* 1:110–119.

Cameron, L.A., T.M. Svitkina, D. Vignjevic, J.A. Theriot, and G.G. Borisy. 2001. Dendritic organization of actin comet tails. *Curr. Biol.* 11:130–135.

Cohan, C.S., E.A. Welnhofer, L. Zhao, F. Matsumura, and S. Yamashiro. 2001. Role of the actin bundling protein fascin in growth cone morphogenesis: localization in filopodia and lamellipodia. *Cell Motil. Cytoskeleton.* 48:109–120.

Cooper, J.A., and D.A. Schafer. 2000. Control of actin assembly and disassembly at filament ends. *Curr. Opin. Cell Biol.* 12:97–103.

DiNubile, M.J., L. Cassimeris, M. Joyce, and S.H. Zigmond. 1995. Actin filament barbed-end capping activity in neutrophil lysates: the role of capping protein-β2. *Mol. Biol. Cell.* 6:1659–1671.

Egile, C., T.P. Loisel, V. Laurent, R. Li, D. Pantaloni, P.J. Sansonetti, and M.F. Carlier. 1999. Activation of the CDC42 effector N-WASP by the *Shigella flexneri* IcsA protein promotes actin nucleation by Arp2/3 complex and bacterial actin-based motility. *J. Cell Biol.* 146:1319–1332.

Evangelista, M., D. Pruyne, D.C. Amberg, C. Boone, and A. Bretscher. 2002. Formins direct Arp2/3-independent actin filament assembly to polarize cell growth in yeast. *Nat. Cell Biol.* 4:32–41.

Goldberg, M.B. 2001. Actin-based motility of intracellular microbial pathogens. *Microbiol. Mol. Biol. Rev.* 65:595–626 (table of contents).

Higgs, H.N., and T.D. Pollard. 2001. Regulation of actin filament network formation through ARP2/3 complex: activation by a diverse array of proteins. *Annu. Rev. Biochem.* 70:649–676.

Huang, M., C. Yang, D.A. Schafer, J.A. Cooper, H.N. Higgs, and S.H. Zigmond. 1999. Cdc42-induced actin filaments are protected from capping protein. *Curr. Biol.* 9:979–982.

Isambert, H., P. Venier, A.C. Maggs, A. Fattoum, R. Kassab, D. Pantaloni, and M.F. Carlier. 1995. Flexibility of actin filaments derived from thermal fluctuations. Effect of bound nucleotide, phalloidin, and muscle regulatory proteins. *J. Biol. Chem.* 270:11437–11444.

Jockusch, B.M., and G. Isenberg. 1982. Vinculin and α-actinin: interaction with actin and effect on microfilament network formation. *Cold Spring Harb. Symp. Quant. Biol.* 46:613–623.

Kureishy, N., V. Sapountzi, S. Prag, N. Anilkumar, and J.C. Adams. 2002. Fascins, and their roles in cell structure and function. *Bioessays.* 24:350–361.

Langanger, G., J. de Mey, M. Moeremans, G. Daneels, M. de Brabander, and J.V. Small. 1984. Ultrastructural localization of α-actinin and filamin in cultured cells with the immunogold staining (IGS) method. *J. Cell Biol.* 99:1324–1334.

Lanier, L.M., M.A. Gates, W. Witke, A.S. Menzies, A.M. Wehman, J.D. Macklis, D. Kwiatkowski, P. Soriano, and F.B. Gertler. 1999. Mena is required for neurulation and commissure formation. *Neuron.* 22:313–325.

Laurent, V., T.P. Loisel, B. Harbeck, A. Wehman, L. Grobe, B.M. Jockusch, J. Wehland, F.B. Gertler, and M.F. Carlier. 1999. Role of proteins of the Ena/VASP family in actin-based motility of *Listeria monocytogenes*. *J. Cell Biol.* 144:1245–1258.

Lewis, A.K., and P.C. Bridgman. 1992. Nerve growth cone lamellipodia contain

two populations of actin filaments that differ in organization and polarity. *J. Cell Biol.* 119:1219–1243.

Li, Z., E.S. Kim, and E.L. Bearer. 2002. Arp2/3 complex is required for actin polymerization during platelet shape change. *Blood.* 99:4466–4474.

Loisel, T.P., R. Boujemaa, D. Pantaloni, and M.F. Carlier. 1999. Reconstitution of actin-based motility of *Listeria* and *Shigella* using pure proteins. *Nature.* 401: 613–616 (see comments).

Machesky, L.M., and R.H. Insall. 1998. Scar1 and the related Wiskott-Aldrich syndrome protein, WASP, regulate the actin cytoskeleton through the Arp2/3 complex. *Curr. Biol.* 8:1347–1356.

Millard, T.H., B. Behrendt, S. Launay, K. Futterer, and L.M. Machesky. 2003. Identification and characterisation of a novel human isoform of Arp2/3 complex subunit p16-ARC/ARPC5. *Cell Motil. Cytoskeleton.* 54:81–90.

Mallavarapu, A., and T. Mitchison. 1999. Regulated actin cytoskeleton assembly at filopodium tips controls their extension and retraction. *J. Cell Biol.* 146: 1097–1106.

Miki, H., T. Sasaki, Y. Takai, and T. Takenawa. 1998. Induction of filopodium formation by a WASP-related actin-depolymerizing protein N-WASP. *Nature.* 391:93–96.

Mullins, R.D., J.A. Heuser, and T.D. Pollard. 1998. The interaction of Arp2/3 complex with actin: nucleation, high affinity pointed end capping, and formation of branching networks of filaments. *Proc. Natl. Acad. Sci. USA.* 95: 6181–6186.

Murray, A.W. 1991. Cell cycle extracts. *Methods Cell Biol.* 36:581–605.

Ono, S., Y. Yamakita, S. Yamashiro, P.T. Matsudaira, J.R. Gnarra, T. Obinata, and F. Matsumura. 1997. Identification of an actin binding region and a protein kinase C phosphorylation site on human fascin. *J. Biol. Chem.* 272: 2527–2533.

Palmgren, S., P.J. Ojala, M.A. Wear, J.A. Cooper, and P. Lappalainen. 2001. Interactions with PIP2, ADP-actin monomers, and capping protein regulate the activity and localization of yeast twinfilin. *J. Cell Biol.* 155:251–260.

Pantaloni, D., R. Boujemaa, D. Didry, P. Gounon, and M.F. Carlier. 2000. The Arp2/3 complex branches filament barbed ends: functional antagonism with capping proteins. *Nat. Cell Biol.* 2:385–391.

Pruyne, D., M. Evangelista, C. Yang, E. Bi, S. Zigmond, A. Bretscher, and C. Boone. 2002. Role of formins in actin assembly: nucleation and barbed-end association. *Science.* 297:612–615.

Rottner, K., B. Behrendt, J.V. Small, and J. Wehland. 1999. VASP dynamics during lamellipodia protrusion. *Nat. Cell Biol.* 1:321–322.

Sagot, I., S.K. Klee, and D. Pellman. 2002a. Yeast formins regulate cell polarity by controlling the assembly of actin cables. *Nat. Cell Biol.* 4:42–50.

Sagot, I., A.A. Rodal, J. Moseley, B.L. Goode, and D. Pellman. 2002b. An actin nucleation mechanism mediated by Bni1 and profilin. *Nat. Cell Biol.* 4:626–631.

Saoudi, Y., R. Fotedar, A. Abrieu, M. Doree, J. Wehland, R.L. Margolis, and D. Job. 1998. Stepwise reconstitution of interphase microtubule dynamics in permeabilized cells and comparison to dynamic mechanisms in intact cells. *J. Cell Biol.* 142:1519–1532.

Small, J.V., G. Isenberg, and J.E. Celis. 1978. Polarity of actin at the leading edge of cultured cells. *Nature.* 272:638–639.

Small, J.V., M. Herzog, M. Haner, and U. Abei. 1994. Visualization of actin filaments in keratocyte lamellipodia: negative staining compared with freeze-drying. *J. Struct. Biol.* 113:135–141.

Small, J.V., T. Stradal, E. Vignal, and K. Rottner. 2002. The lamellipodium: where motility begins. *Trends Cell Biol.* 12:112–120.

Soeno, Y., H. Abe, S. Kimura, K. Maruyama, and T. Obinata. 1998. Generation of functional β-actinin (CapZ) in an *E. coli* expression system. *J. Muscle Res. Cell Motil.* 19:639–646.

Spudich, J.A., and S. Watt. 1971. The regulation of rabbit skeletal muscle contraction. I. Biochemical studies of the interaction of the tropomyosin-troponin complex with actin and the proteolytic fragments of myosin. *J. Biol. Chem.* 246:4866–4871.

Svitkina, T.M., and G.G. Borisy. 1998. Correlative light and electron microscopy of the cytoskeleton of cultured cells. *Methods Enzymol.* 298:570–592.

Svitkina, T.M., and G.G. Borisy. 1999. Arp2/3 complex and actin depolymerizing factor/cofilin in dendritic organization and treadmilling of actin filament array in lamellipodia. *J. Cell Biol.* 145:1009–1026.

Svitkina, T.M., A.B. Verkhovsky, K.M. McQuade, and G.G. Borisy. 1997. Analysis of the actin-myosin II system in fish epidermal keratocytes: mechanism of cell body translocation. *J. Cell Biol.* 139:397–415.

Svitkina, T.M., Bulanova E.A., Chaga O.Y., Vignjevic D., Kojima S., Vasiliev J.M., and Borisy G.G. 2003. Mechanism of filopodia initiation by reorganization of a dendritic network. *J. Cell Biol.* 160:409–421.

Theriot, J.A., J. Rosenblatt, D.A. Portnoy, P.J. Goldschmidt-Clermont, and T.J. Mitchison. 1994. Involvement of profilin in the actin-based motility of *L. monocytogenes* in cells and in cell-free extracts. *Cell.* 76:505–517.

Yamashiro, S., Y. Yamakita, S. Ono, and F. Matsumura. 1998. Fascin, an actin-bundling protein, induces membrane protrusions and increases cell motility of epithelial cells. *Mol. Biol. Cell.* 9:993–1006.

Yamashiro-Matsumura, S., and F. Matsumura. 1985. Purification and characterization of an F-actin-bundling 55-kilodalton protein from HeLa cells. *J. Biol. Chem.* 260:5087–5097.

Yarar, D., W. To, A. Abo, and M.D. Welch. 1999. The Wiskott-Aldrich syndrome protein directs actin-based motility by stimulating actin nucleation with the Arp2/3 complex. *Curr. Biol.* 9:555–558.

Zalevsky, J., L. Lempert, H. Kranitz, and R.D. Mullins. 2001. Different WASP family proteins stimulate different Arp2/3 complex-dependent actin-nucleating activities. *Curr. Biol.* 11:1903–1913.

JCB Article

Mechanism of filopodia initiation by reorganization of a dendritic network

Tatyana M. Svitkina,[1] Elena A. Bulanova,[2] Oleg Y. Chaga,[1] Danijela M. Vignjevic,[1] Shin-ichiro Kojima,[1] Jury M. Vasiliev,[2] and Gary G. Borisy[1]

[1]Department of Cell and Molecular Biology, Northwestern University Medical School, Chicago, Illinois 60611
[2]Institute of Mechanisms of Carcinogenesis, Cancer Research Center of Russian Federation, 115478 Moscow, Russia

A filopodium protrudes by elongation of bundled actin filaments in its core. However, the mechanism of filopodia initiation remains unknown. Using live-cell imaging with GFP-tagged proteins and correlative electron microscopy, we performed a kinetic-structural analysis of filopodial initiation in B16F1 melanoma cells. Filopodial bundles arose not by a specific nucleation event, but by reorganization of the lamellipodial dendritic network analogous to fusion of established filopodia but occurring at the level of individual filaments. Subsets of independently nucleated lamellipodial filaments elongated and gradually associated with each other at their barbed ends, leading to formation of cone-shaped structures that we term Λ-precursors. An early marker of initiation was the gradual coalescence of GFP-vasodilator-stimulated phosphoprotein (GFP-VASP) fluorescence at the leading edge into discrete foci. The GFP-VASP foci were associated with Λ-precursors, whereas Arp2/3 was not. Subsequent recruitment of fascin to the clustered barbed ends of Λ-precursors initiated filament bundling and completed formation of the nascent filopodium. We propose a convergent elongation model of filopodia initiation, stipulating that filaments within the lamellipodial dendritic network acquire privileged status by binding a set of molecules (including VASP) to their barbed ends, which protect them from capping and mediate association of barbed ends with each other.

Introduction

The crawling movement of a cell involves protrusion of its leading edge coordinated with translocation of its cell body. Protrusion is driven by polymerization of actin within two organelles, lamellipodia and filopodia, which have strikingly different designs of the actin polymerization machinery and are regulated by different signaling pathways (Hall, 1998; Svitkina and Borisy, 1999b).

In lamellipodia, which are broad, flat protrusions, actin filaments form a branched network (Svitkina et al., 1997; Svitkina and Borisy, 1999a). The current model for lamellipodial dynamics (Borisy and Svitkina, 2000; Pollard et al., 2000) suggests that treadmilling of the branched actin filament array consists of repeated cycles of dendritic nucleation, elongation, capping, and depolymerization of filaments. Dendritic nucleation is mediated by the Arp2/3 complex, which is activated by members of WASP family (Higgs and Pollard, 2001). During a period of elongation after nucleation, the filament pushes the membrane. When a filament elongates beyond the efficient length for pushing, its growth is thought to be terminated by capping protein (Cooper and Schafer, 2000). Depolymerization is assisted by proteins of the ADF/cofilin family (Bamburg, 1999). Other proteins play supporting roles in this process. Profilin targets filament elongation to barbed ends (Carlier and Pantaloni, 1997), enabled/vasodilator-stimulated phosphoprotein (Ena/VASP)* family proteins protect elongating barbed ends from capping (Bear et al., 2002), cortactin stabilizes branches (Weaver et al., 2001), and filamin A (Flanagan et al., 2001) and α-actinin stabilize and consolidate the whole network.

In filopodia, which are thin cellular processes, actin filaments are long, parallel, and organized into tight bundles (Small, 1988; Lewis and Bridgman, 1992; Small et al., 2002). Other cellular structures, such as microspikes and retraction fibers, bear similarities to filopodia and may be related to them. Microspikes are parallel actin bundles within the lamellipodium. Retraction fibers are long, thin cellular processes that remain attached to the substratum after cell withdrawal.

Address correspondence to Tatyana M. Svitkina, Department of Cell and Molecular Biology, Northwestern University Medical School, 303 E. Chicago Ave., Ward 8-063, Chicago, IL 60611. Tel.: (312) 503-2854 Fax: (312) 501-7912. E-mail: t-svitkina@northwestern.edu

Key words: actin; Arp2/3; VASP; fascin; lamellipodia

*Abbreviations used in this paper: EM, electron microscopy; Ena/VASP, enabled/vasodilator-stimulated phosphoprotein.

The Journal of Cell Biology, Volume 160, Number 3, February 3, 2003 409–421
http://www.jcb.org/cgi/doi/10.1083/jcb.200210174

They also contain a parallel bundle of actin filaments (Small, 1988; Lewis and Bridgman, 1992; Svitkina et al., 1997). Filopodial protrusion is thought to occur by a filament treadmilling mechanism, which was originally proposed for both filopodia and lamellipodia (Small, 1994). According to this model, all actin filaments within a bundle elongate at their barbed ends and release subunits from their pointed ends. Existing experimental data support this model of filopodial elongation. Structurally, actin filaments in filopodia are long and unbranched (Svitkina and Borisy, 1999a), suggesting that assembly occurs by elongation, not by branched nucleation. Dynamic observations (Mallavarapu and Mitchison, 1999) revealed that labeled actin incorporated at the filopodial tips, moved backward, and dissipated at the rear (as predicted by a treadmilling mechanism), and that actin turnover in filopodia was slow; consistent with the idea of long filaments adding or losing subunits only at their ends. A frequent event in filopodial behavior is their fusion, which frequently occurs as elongating oblique bundles collide and subsequently grow as a single unit (Katoh et al., 1999b; Small et al., 2002).

A set of molecules essential for filopodial protrusion has not been explicitly determined. However, some proteins are enriched in filopodia, suggesting that they play important roles. One of them is a cross-linking protein (fascin) that mediates filament bundling (Bartles, 2000; Kureishy et al., 2002). Many different proteins are enriched at filopodial tips (Small et al., 2002), including Ena/VASP proteins (Lanier et al., 1999; Rottner et al., 1999), N-WASP and CR16 (Ho et al., 2001), myosin X (Berg and Cheney, 2002), talin (DePasquale and Izzard, 1991), syndapin I (Qualmann and Kelly, 2000), Abl interactor proteins (Stradal et al., 2001), and Vav (Kranewitter et al., 2001). Roles for these proteins remain largely unknown with the exception of Ena/VASP proteins. In lamellipodia, GFP-VASP forms a thin line along the extreme leading edge (Rottner et al., 1999), and in filopodia it appears as a bright dot at filopodial tips (Lanier et al., 1999; Rottner et al., 1999). Ena/VASP proteins bind barbed ends of actin filaments and protect them from capping at the leading edge of lamellipodia, which results in formation of longer filaments within the lamellipodial dendritic network (Bear et al., 2002). These data suggest that Ena/VASP proteins that are enriched at filopodial tips may mediate continuous elongation of filopodial actin filaments.

The major gap in our understanding of filopodia behavior is the mechanism of their initiation. The filament treadmilling model refers to the steady state of an established organelle, but does not explain how it arose in the first place. A small GTPase, Cdc42, is a well-known signaling molecule inducing filopodia in cells (Kozma et al., 1995; Nobes and Hall, 1995). One of its downstream effectors, N-WASP, is an ubiquitous activator of the Arp2/3 complex (Rohatgi et al., 1999, 2000), which significantly facilitates Cdc42-induced filopodial formation (Miki et al., 1998), suggesting that the Arp2/3 complex may be involved in filopodial protrusion. This suggestion has been supported experimentally by perturbing Arp2/3 function in permeabilized platelets with an inhibitory antibody (Li et al., 2002), and in HeLa cells by expressing VCA domain of N-WASP (Qualmann and Kelly, 2000). Because the Arp2/3 complex is absent from established filopodia (Svitkina and Borisy, 1999a), we hypothesized that it plays a role during filopodia initiation. One possibility for how the Arp2/3 complex induces filopodial bundles is that it forms a "nucleation center" which starts a bundle and subsequently dissociates. Another possibility is that the normal dendritic array produced by Arp2/3-mediated nucleation is rearranged into parallel bundles. In this work, we investigated the mechanism of filopodia initiation in B16F1 mouse melanoma cells and found that filopodial bundles were initiated by reorganization of the dendritic network in a process that involved elongation and convergence of subsets of privileged barbed ends.

Results

Filopodia, microspikes, and retraction fibers

Crawling cells elaborate filopodia, microspikes, and retraction fibers in the course of cycles of protrusion and withdrawal. These have been considered as distinct entities, but because of their structural similarities, we investigated whether they were truly distinct or interconvertible. Determining whether they were functionally related was important to define the scope of our study.

We followed the kinetics of peripheral actin bundles by phase contrast or fluorescence microscopy in untransfected or GFP-actin–expressing cells, respectively. We observed many examples of transition between filopodia, microspikes, and retraction fibers (Fig. 1). The predominant order of transitions was from microspike to filopodium to retraction fiber. Transitions in the opposite direction were also observed. For each type of structure, the filament bundle was able to protrude, suggesting that the actin polymerizing machinery was functional in each morphological state. The protrusive activity of the surrounding lamellipodium seemed to be an important factor determining the transitions between these organelles. Depending on whether the lamellipodium advanced as fast as or slower than an actin bundle elongated, the bundle appeared as a microspike or a filopodium. If the lamellipodium withdrew while the actin bundle remained stable or elongated, the bundle appeared as a retraction fiber. Increased net protrusion of an actin bundle also contributed to the transition from microspikes to filopodia, especially after fusion of two microspikes. Thus, filopodia, microspikes, and retraction fibers are interconvertible organelles, which may transform one into another because of a disparity in the protrusion velocity of the bundles themselves and of the surrounding lamellipodium. Therefore, in this paper, we will consider these types of peripheral actin bundles together and will refer to them collectively as "filopodia," because this is the most commonly used term.

Kinetics of filopodia initiation

To approach the central question of the mechanism of filopodia initiation, we first investigated the kinetics of spontaneous filopodia initiation using GFP-tagged structural proteins. If filopodia were initiated by an Arp2/3-containing nucleation center, one would expect a nascent filopodium to arise from a distinct fluorescent dot of actin or Arp2/3 complex, whereas the rearrangement model pre-

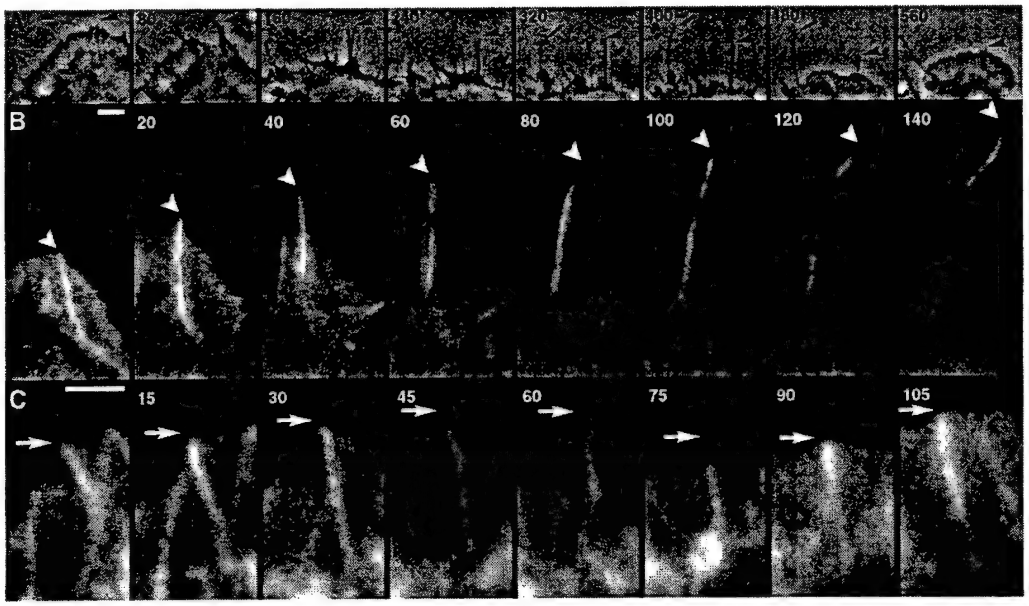

Figure 1. **Interconversion between microspikes, filopodia, and retraction fibers.** Time-lapse sequences of untransfected (A, phase contrast) or GFP-actin expressing (B and C, fluorescence) cells. Time in seconds. (A) Lamellipodium containing several microspikes (triple arrow and arrowhead in first frame) retracts leaving microspikes in the form of retraction fibers (240 s), some of which continue to protrude (240–400 s, arrow). At ~400 s, lamellipodium resumes protrusion and absorbs retraction fibers, some of which disappear, one becoming a filopodium (560 s, arrow), and another becoming a microspike (560 s, arrowhead). (B) Transition of a microspike (0 and 20 s) to filopodium (20–60 s) to retraction fiber (60–140 s). Actin bundle displayed continuous elongation, whereas surrounding lamellipodium initially kept up with the bundle (0–20 s), paused (40 s), and then withdrew (60–140 s). (C) Transition of microspike (0–30 s) to filopodium (45–75 s) and back to microspike (90–105 s) as a result of uncoordinated protrusive behavior of the bundle and the lamellipodium. Bars, 2 μm.

dicts a gradual condensation of actin fluorescence into a filopodial bundle.

Filopodia in GFP-actin–expressing cells displayed a broad range of lengths and fluorescence intensities. Histories of large filopodia revealed that they were formed by fusion of smaller filopodia, which in turn were the result of fusion at an even finer scale (Fig. 2 A). Events of true filopodia initiation were recognized as the appearance of thin, faint nascent filopodia contained within the lamellipodial network. In most cases (81%, $n = 124$), they arose from fishtail-shaped actin densities within the lamellipodium (Fig. 2, B and C). These densities, which we will call Λ-precursors because of their shape, were just slightly brighter than the surrounding lamellipodium at their vertices, but gradually diffused into a lamellipodial network at their bases (Fig. 2 D). Although hardly distinguishable from the rest of the lamellipodial network, Λ-precursors could be consistently recognized, after contrast enhancement, by tracing back in time the sequences of newly formed filopodia. In the remaining cases of filopodial initiation (19%), Λ-precursors were not visible, possibly because of insufficient temporal resolution or contrast. Nascent filopodia subsequently fused with each other (Fig. 2, B and C) or with other filopodia, and thus increased in size. Fusion produced Λ-configurations of filopodial bundles reminiscent of the shape of Λ-precursors, but with more distinct individual branches. Over time, these Λ-shaped bundles treadmilled backward at the root of the fused filopodium (Fig. 2 C) until they disappeared in the course of depolymerization. The observed actin kinetics appears more consistent with the idea of network reorganization as a mechanism of filopodia initiation.

The Arp2/3 complex is predicted to be enriched in the hypothetical filopodial nucleation center. Therefore, we performed kinetic analysis of GFP-Arp3–expressing cells (Fig. 3 A). Because filopodial bundles were invisible in GFP-Arp3 images, we acquired phase contrast images at the beginning and at the end of the sequence to detect nascent filopodia initiated during the sequence. Filopodia were observed to appear by phase microscopy and GFP-Arp3 was present throughout the lamellipodium, but no increase in GFP-Arp3 intensity was detected to spatially and temporally correlate with filopodial initiation. The essentially uniform distribution of the GFP-Arp3 signal does not support the hypothesis of an Arp2/3-based nucleation center for filopodial initiation.

To obtain insight into the actual mechanism of filopodia initiation, we next analyzed the kinetics of proteins enriched in filopodia, i.e., fascin and VASP. In GFP-fascin–expressing cells, a majority of nascent filopodia (66%, $n = 207$) first appeared as a bright dot or short rod on a dark background (Fig. 3, B and C). In other cases (34%), a bright dot of GFP-fascin rather suddenly appeared at the tip of a very faint Λ-shaped density in lamellipodia (Fig. 3 C, inset in 16 s frame). Both kinds of nascent fascin dots subsequently elongated to form a filopodium. Fusion of mature fascin-containing filopodia was also frequently seen (Fig. 3 C). Because fascin is present in lamellipodia, albeit at much lower concentration than in filopodia, the faint Λ-shaped fascin densities might correspond to Λ-precursors, suggesting that in the course of filopodia initiation, fascin initially appears at the tips of the Λ-precursors (see next section). In GFP-VASP sequences, we followed the formation of brighter dots corre-

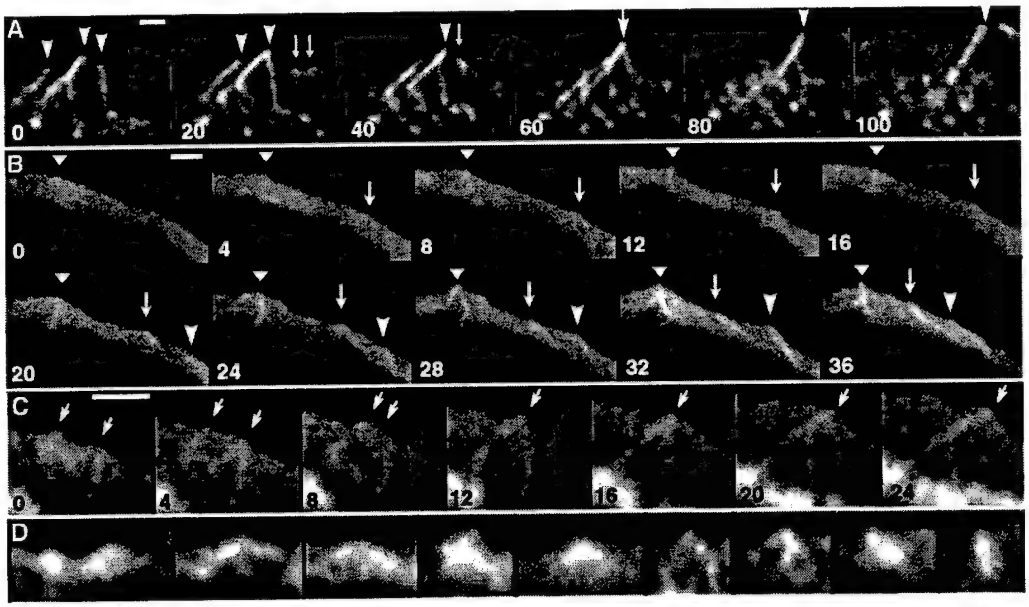

Figure 2. **Actin kinetics during filopodia initiation.** (A–C) Time-lapse sequences of GFP-actin–expressing B16F1 cells. Time in seconds; individual features marked by arrows and arrowheads. Nascent filopodia are marked starting from the frame preceding the appearance of the recognizable precursor. (A) Three established filopodia (0 s, arrowheads) fuse with each other (0–60 s). Two Λ-precursors (arrows) appear (20 s), and fuse with each other (40 s), forming a nascent filopodium that subsequently (60 s) joins the fusing older filopodia. (B) Several nascent filopodia form from Λ-precursors that appear within lamellipodium. (C) Two Λ-precursors existing at 0 s (arrows) fuse with each other (12 s), producing a nascent filopodium with a Λ-shaped root. The fusion point treadmills backward while the filopodium protrudes forward. (D) Gallery of Λ-precursors. First four examples represent enlarged and enhanced Λ-precursors from A (20 s), B (8 s), B (24 s), and C (0 s), respectively. Remaining examples are from other sequences. Bars, 2 μm.

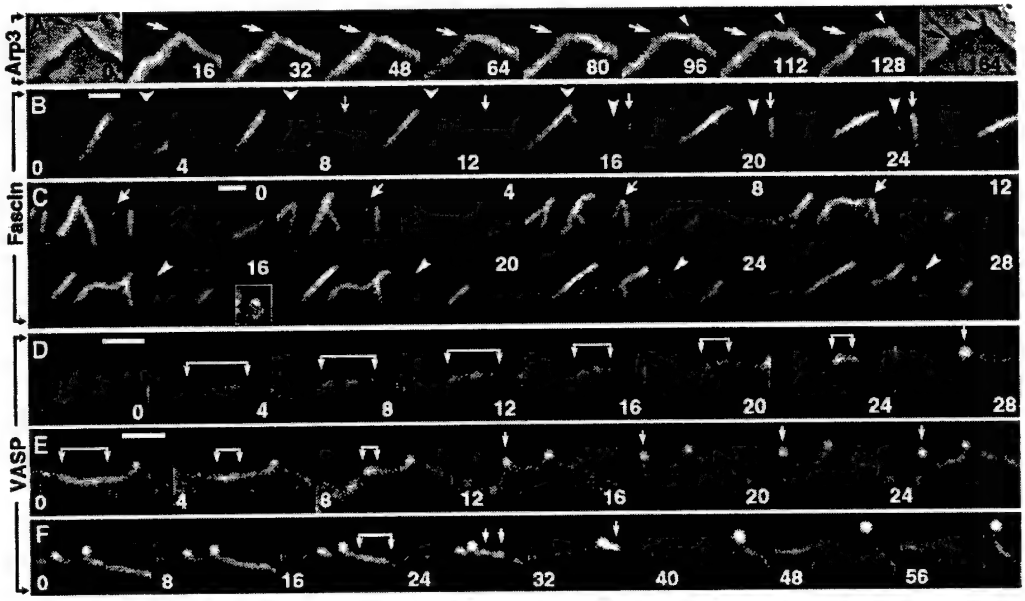

Figure 3. **Kinetics of marker proteins during filopodia initiation.** Time-lapse sequences of GFP-Arp3 (A), GFP-fascin (B and C), or GFP-VASP (D–F). (A) Two flanking phase contrast frames (0 and 164 s) demonstrate formation of a new filopodium during the sequence. Positions of preexisting (arrow) and nascent (arrowhead) filopodia are indicated. No focal enrichment of Arp3 was seen during formation of the nascent filopodium. (B and C) Most nascent filopodia arise from bright GFP-fascin dots without obvious Λ-precursors. In some cases, a bright dot localizes to the tip of a faint Λ-shaped density, as in the inset in 16 s frame in C, which shows the region indicated by arrowhead in this frame after enlargement and adjustment of contrast to reveal weak fluorescence. Filopodia fusion occurs in C (arrows). (D–F) Bright GFP-VASP dots corresponding to nascent filopodia arise by gradual coalescence of the initially even line of leading-edge fluorescence. Brackets indicate regions of brighter GFP-VASP fluorescence that shrink into dots over time. In F, two smaller dots (24 s) are formed during coalescence of the shrinking region, which subsequently fuse with each other (32 s) and with the adjacent preexisting dot (40 s). Bars, 2 μm.

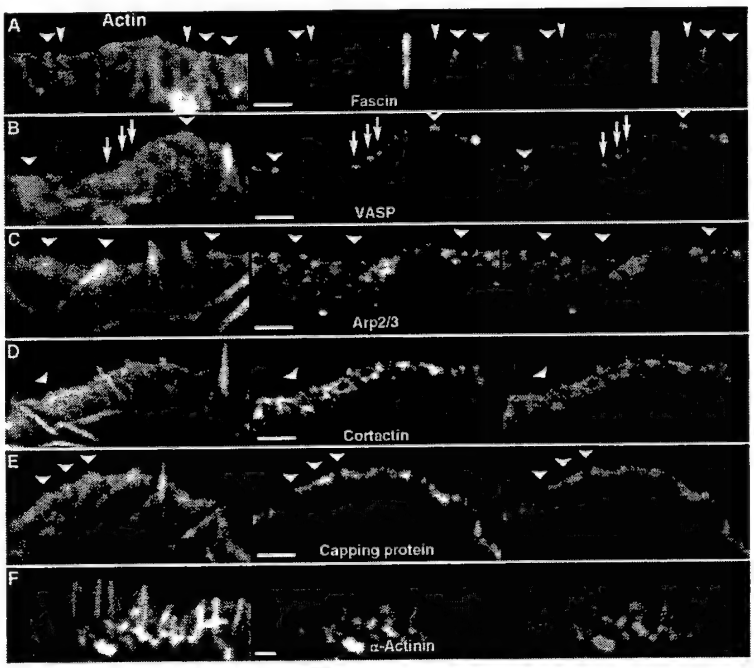

Figure 4. **Localization of filopodial and lamellipodial markers in Λ-precursors.** Left column; actin revealed by Texas Red-phalloidin (A, B, and F) or by GFP-actin expression (C–E). Central column; actin-binding proteins (as indicated) revealed by expression of GFP-fusion proteins (A, B, and F) or by immunostaining (C–E). Right column; merged images. Λ-precursors are indicated by arrowheads. (A) Fascin is strongly enriched in established filopodia and localizes to the distal section of some Λ-precursors (wide arrowheads), but not others (narrow arrowheads). (B) VASP forms bright dots at the tips of filopodia and Λ-precursors. Additional dots can be seen along the leading edge (arrows), which apparently do not correspond to Λ-precursors. (C–E) Lamellipodial markers, Arp2/3 complex (C), cortactin (D), and capping protein (E), are excluded from filopodia and are partially depleted from Λ-precursors. (F) α-Actinin localizes to proximal parts of lamellipodia and filopodia. Bars, 2 μm.

sponding to filopodial tips among the weaker fluorescence of the lamellipodial edge. The major pathway for filopodia initiation (Fig. 3, D–F) was a gradual coalescence of VASP to ultimately produce a bright dot. The first sign detected was a slight elevation of GFP-VASP fluorescence intensity within a small domain (2–4 μm) along the leading edge. Then, this region gradually shrank into a dot concurrently increasing its intensity. In some cases, the condensing region became discontinuous during shrinkage (Fig. 3 F), suggesting intermediate formation of smaller filopodia. Because Ena/VASP proteins bind barbed ends and protect them from capping (Bear et al., 2002), these data suggest that elongating barbed ends from the lamellipodial network gradually segregate into a small region, which becomes a filopodial tip.

Protein composition of Λ-precursors

Our kinetic analysis identified Λ-precursors as intermediates in filopodial initiation. Next, we examined whether molecular markers that discriminate between lamellipodia and filopodia are present in Λ-precursors (Fig. 4). Expression of GFP-actin or staining with labeled phalloidin was used to visualize actin. Putative Λ-precursors were identified in the actin channel based on their characteristic shape, and slightly increased actin density. Immunostaining or expression of GFP-tagged proteins was used to localize the second protein.

Fascin and VASP were used as filopodial markers. In GFP-fascin–expressing cells, putative Λ-precursors either did not contain significant amount of fascin (Fig. 4 A, arrows; also see Fig. 6), or they had fascin enriched only at the tip (Fig. 4 A, arrowheads), suggesting that fascin was recruited to the tips of the preformed Λ-precursors. In GFP-VASP–expressing cells (Fig. 4 B), VASP fluorescence at the leading edge became less uniform after extraction, perhaps revealing more strongly associated protein. The brightest VASP dots corresponded to established filopodia. The majority of Λ-precursors contained a distinct VASP dot at their vertex (Fig. 4 B, arrowheads). Weak VASP dots were also evident without recognizable Λ-precursors (Fig. 4 B, arrows). These may represent fluctuations in density of actin filament barbed ends within the lamellipodium or Λ-precursors not detected in the actin channel.

As lamellipodial markers, we used Arp2/3 complex, cortactin, and capping protein. Previously, we have shown that Arp2/3 complex is excluded from filopodial bundles (Svitkina and Borisy, 1999a). Here, we report that cortactin and capping protein are also excluded from filopodia (Fig. 4, D and E). In Λ-precursors, these proteins were partially depleted, especially close to the vertex, but not completely absent (Fig. 4, C–E), suggesting that gradual depletion of lamellipodial proteins occurs during formation of Λ-precursors and filopodia initiation. No enrichment of Arp2/3 complex was detected at filopodial roots.

We also investigated the ability of α-actinin to discriminate between filopodia and lamellipodia. Previously, α-actinin has been shown to localize to lamellipodia (Langanger et al., 1984), but its localization in filopodia is unclear. GFP-tagged α-actinin associated with both lamellipodia and filopodia (Fig. 4 F), but appeared in these organelles with delay and, consequently, localized to the base of the fast-protruding lamellipodia and filopodia. Thus, α-actinin is a late marker for actin bundling in filopodia and is apparently not involved in filopodia initiation.

Together, the molecular marker analysis suggests that Λ-precursors represent a transitional structure displaying enrichment of filopodial markers and partial depletion of lamellipodial proteins. Dual-channel correlation of actin distribution with that of filopodial markers suggested that VASP accumulation occurred early in the process of formation of Λ-precursors, and that fascin appeared at the tips of established Λ-precursors.

Structure of Λ-precursors

Light microscopic analysis suggested a gradual reorganization of the lamellipodial network into bundles through intermediate formation of Λ-precursors. This hypothesis was analyzed using a higher resolution technique; platinum replica electron microscopy (EM). Treadmilling behavior of filopodia has a remarkable consequence in that the history of the actin array is imprinted in its structure (Katoh et al., 1999a), so that moving from the leading edge in a proximal direction in space is analogous to traveling back in time. To understand the mechanism of filopodia initiation, we first focused on the analysis of filopodial roots. In this work, we were most interested in analyzing young filopodia, which are usually thin and short according to our kinetic study.

The majority of apparently young filopodial bundles were splayed apart at their roots into smaller bundles or individual filaments (Fig. 5), suggesting that the bundles were formed by convergence of the composing elements. Filopodial roots consisting of two or more smaller bundles are consistent with an event of filopodial fusion in the recent history of that filopodium (Fig. 5 B). More importantly, we observed many examples of filopodial bundles whose roots suggested the convergence of individual filaments originating from distant places in the surrounding lamellipodial network and entering the bundle at different levels. In some cases, it was possible to track filaments back from the bundle toward their origin as a branch on another filament in the surrounding network (Fig. 5 C). These findings suggest that filaments comprising filopodial bundles were asynchronously recruited from the dendritic network. Remarkably, filaments entering filopodial bundles were long compared with the branched network near the leading edge (Fig. 5, inset in A). Older filopodia, which could be recognized by their length and thickness, either had their actin bundles rooted deeply in the cytoplasm, which impeded visualization, or had tapered (not splayed) roots. This is consistent with depolymerization from the pointed ends of the composing filaments causing progressive elimination of the original splayed roots.

Splayed filopodial roots apparently corresponded to aged Λ-precursors that treadmilled backward during filopodium growth. To identify Λ-precursors at a stage when they had not yet produced a filopodium, we performed correlative light microscopy and EM (Fig. 6). Putative Λ-precursors were identified in cells by fluorescence microscopy and relocalized after EM processing of the same cells. For these experiments, we used cells expressing GFP-fascin, which allowed us to compare parts of the Λ-precursor containing and not containing fascin.

Λ-precursors lacking fascin clearly displayed features of dendritic organization, such as short filaments, branching filaments, and numerous free filament ends (Fig. 6). Also, consistent with the idea of the transitional character of Λ-precursors, we found many rather long filaments within Λ-precursors, whereas long filaments were not frequent in the dendritic network outside Λ-precursors (Fig. 6, A and C). These long filaments apparently became enriched during transition of Λ-precursors into splayed filopodial roots, perhaps because of faster depolymerization of short filaments. The actin array in fascin-positive parts (Fig. 6 B) had a clearly bundled organization with densely packed filaments.

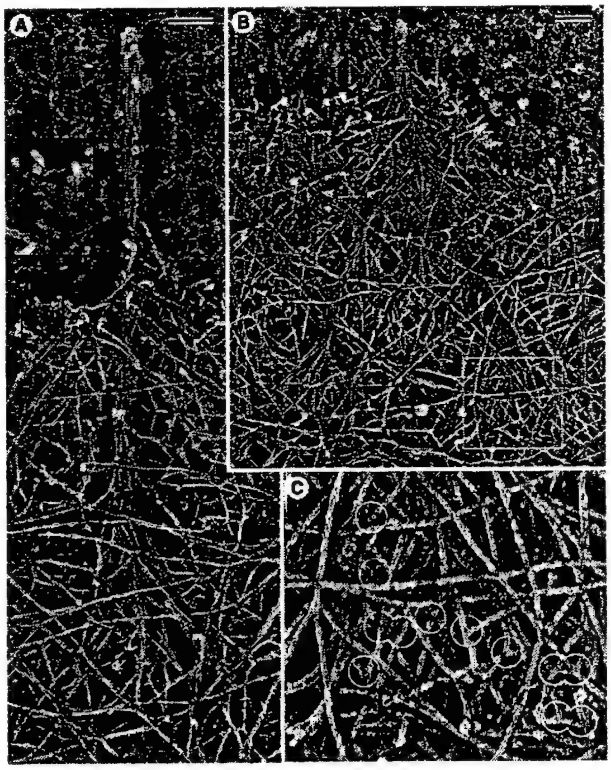

Figure 5. **Filopodial filaments originate from the surrounding dendritic network.** Platinum replica EM. (A) Filopodium contains a tight bundle of actin filaments that splays apart at its root and becomes an integral part of the surrounding network. Filaments in the roots are long compared with the branching network of the adjacent lamellipodium (inset). (B) Recently fused filopodium consists of two sub-bundles, each of which has a splayed root; the boxed region at the root of the right sub-bundle is enlarged in C and shows many branches (encircled) at which filopodial filaments originate. Rough background outside the cell edge is due to laminin coating of the glass coverslip. Bars, 0.2 μm.

The more proximal parts of actin bundles were not significantly enriched in fascin and displayed long, loosely aligned filaments (Fig. 6 B), suggesting that fascin-mediated bundling was delayed compared with accumulation of long filaments in the forming bundle. Thus, structural analysis of Λ-precursors and filopodial roots demonstrated enrichment of long filaments in these structures that apparently occurred before fascin-mediated bundling.

Structural organization of filopodia with known history

Because not every Λ-precursor produced a filopodium in kinetic studies, we performed correlative EM for cells with known history. For this purpose, we acquired time-lapse sequences of GFP-actin–expressing cells. After extraction and fixation, we prepared those cells for EM and analyzed filopodia formed in the course of the sequence (Fig. 7). Fig. 7 A illustrates the correlation between the last live image of one such cell, the image of the lysed cell, and the EM image of the same cell taken at low magnification comparable with that of light microscopy. During the 19-s interval between the last live image and the image of the lysed cell, the lamellipodium protruded ~0.9 μm, which is evident in the su-

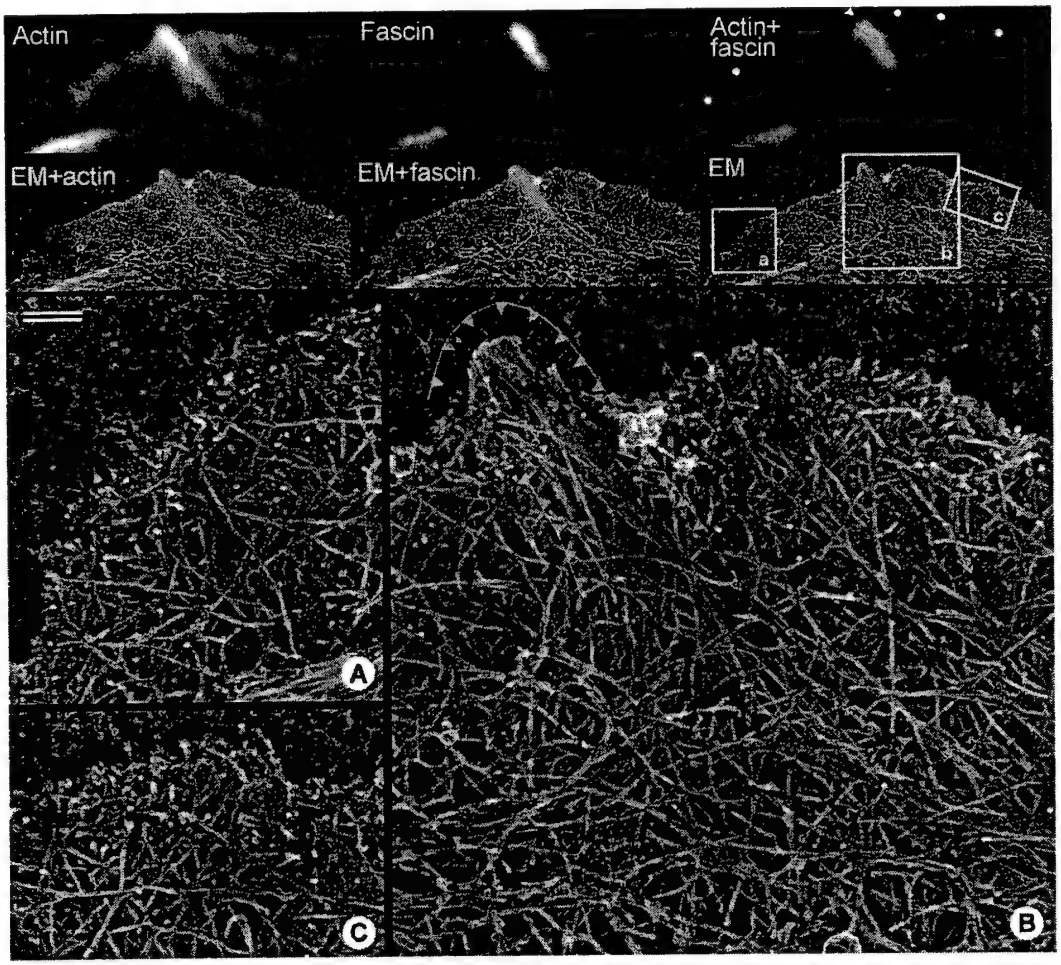

Figure 6. **Actin filament organization in Λ-precursors.** Correlative fluorescence and EM of the same cell. First row; fluorescence microscopy of the leading edge showing Texas Red-phalloidin labeled actin (left), GFP-fascin (middle), and merged image (right). White dots in the merged image mark putative Λ-precursors, and the arrowhead indicates a filopodium, which have been analyzed by EM. Second row; EM of the same region (right) overlaid with fluorescence images of actin in red (left) and fascin in green (middle). Boxed regions (a–c) are enlarged in the bottom panels, labeled respectively. Red outlines in enlarged panels denote areas of increased actin density in the fluorescence image that represent putative Λ-precursors or filopodia. Λ-precursors contain relatively long filaments, some of which are highlighted in cyan in A and C, along with short branching filaments highlighted in magenta; adjacent lamellipodium (C) contains mostly short branching filaments highlighted in magenta. Yellow outline denotes region enriched in fascin in the established filopodium. This region contains tightly bundled filaments. Bar, 0.2 μm.

perimposed image. The subsequent processing for EM did not introduce significant distortions into the structure of the lamellipodium because extracted light and low power EM images could be almost perfectly overlapped. Coincidence of light and EM features could also be seen at higher magnification, where brighter areas in fluorescence corresponded to denser actin arrays in EM (Fig. 7 B).

Several filopodia were spontaneously formed during the total period of 35 s of this sequence. Fig. 7 C illustrates the history of three nascent filopodia of different age, which are color coded in yellow, blue, and green for convenience of description. The filopodium marked with a yellow arrow was the oldest one. This filopodium was formed in the course of fusion of two faint, converging linear densities existing at the beginning of the sequence. A bright spot of actin fluorescence, which appeared in the filopodium shaft in the second frame, allows one to recognize treadmilling and retrograde flow in this filopodium. The filopodium marked with the blue arrow was not visible in the first frame; at 4 s, it appeared as a Λ-precursor, which at 8 s could be seen near the edge, and which produced a faint filopodium by 12 s. The filopodium marked with the green arrow is the youngest one. It was formed from a Λ-precursor first visible at 12 s. Tips of all three filopodia converged by the end of the sequence, suggesting that they began fusing at the moment of extraction.

The detailed structural organization of the region containing all three filopodia is shown in Fig. 7 D. The root of the "yellow" filopodium consisted of two thin, fusing bundles corresponding to two converging lines in the first frame of the sequence. Each of these sub-bundles, when followed backward, splayed into individual filaments originating from the surrounding dendritic network (not depicted). The Λ-precursor of the "blue" filopodium that

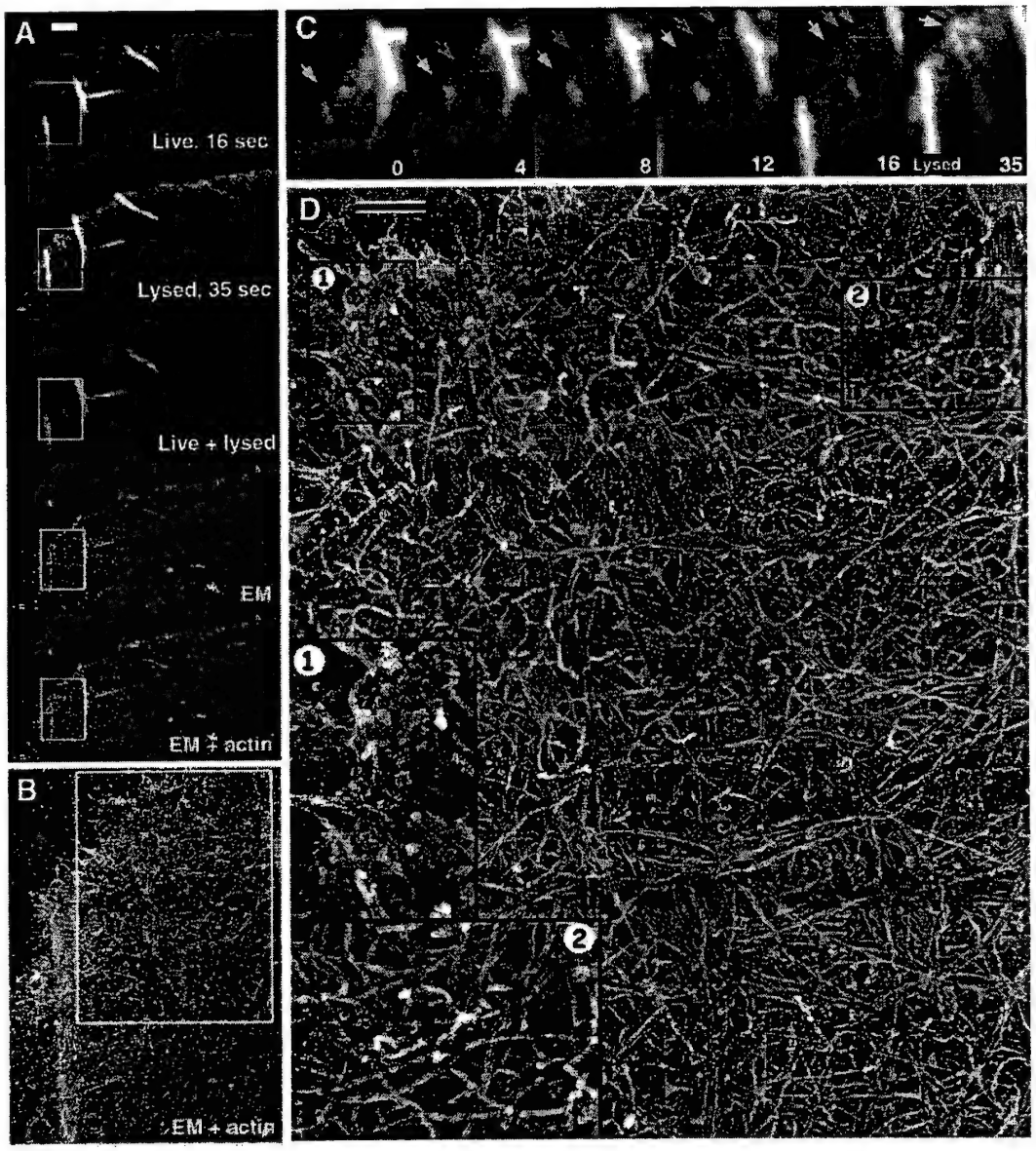

Figure 7. **Structural organization of filopodia with known history.** Correlative live imaging and EM. (A) Overview of the cell lamellipodium at different stages of sample processing. GFP-actin fluorescence images taken just before (live, 16 s) and immediately after (lysed, 35 s) cell lysis were merged (live + lysed) in green and red channels, respectively; cell advance during the 19 s between images appears as red strip at the leading edge. Low magnification EM image of the same region (EM) is overlaid with actin fluorescence image of the lysed cell (EM + actin). (B) Boxed region in A is enlarged in B to show correlation between light and EM in more detail. Brighter areas in fluorescence image correspond to denser actin arrays in EM. (C) Detailed history of the boxed region in A. Time in seconds. The 35 s frame is taken from the lysed cell. Arrows of different color indicate position of individual nascent filopodia. (D) Enlarged EM of the boxed region in B showing the structure of nascent filopodia, whose history is presented in C; individual nascent filopodia are outlined in colors corresponding to colors of arrows in C. Some filaments converging into the bundle of the "blue" filopodium are highlighted in shades of blue. Boxes 1 and 2 are further enlarged in corresponding insets and show organization of the filopodial tip (1) and of the root of "green" filopodium (2); branching filaments are highlighted in green in the inset (2). See detail in text. Bars, 2 μm (A) and 0.2 μm (D).

treadmilled backward during the sequence was identified with the splayed root of the blue filopodium in the EM image, indicating that splayed roots of filopodia indeed represent former Λ-precursors. Like in other EM images, filaments were collected into the bundle of the blue filopodium from the wide surrounding area (Fig. 7 D). In fluorescence images (Fig. 7 C), the splayed root became invisible already in 12 s frame, probably because of low fluorescence intensity. The root of the youngest "green" filopodium displayed many features of the dendritic organization of Λ-precursors. It had relatively high network density, many short filaments, frequent branching, and numerous free barbed ends (Fig. 7, inset 2 in D). Some filaments originating as a branch on another filament could be seen to enter the bundle of the green filopodium. These data support the idea that Λ-precursors initially represent a part of

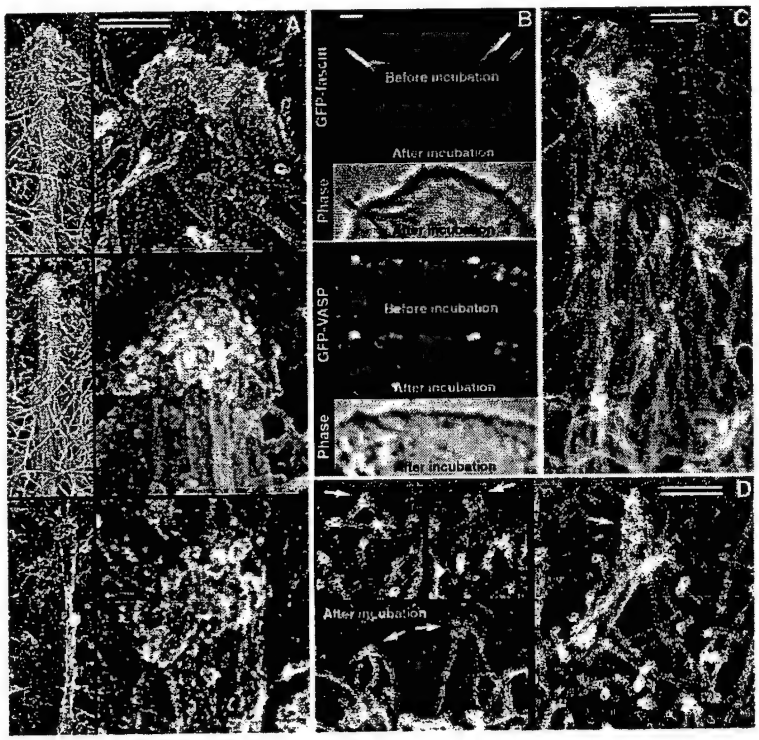

Figure 8. **Filopodial tip complex.** (A) Structure of tip complex in three filopodia seen by replica EM. Lower magnification, left; higher magnification, right. (B) Incubation of lysed cells in buffer causes dissociation of fascin (top) but not VASP (bottom) from filopodia. Phase contrast and GFP fluorescence images of cells transiently expressing indicated fusion proteins were taken immediately after cell lysis ("before incubation" phase images are not depicted) and after overnight incubation in phalloidin-containing buffer ("after incubation"). Acquisition and processing of fluorescence images was identical for each pair. (C) Filopodial bundle and tip complex after overnight incubation of the lysed cell in phalloidin-containing buffer. Replica EM. Filopodial tip complex keeps barbed ends of filopodial filaments together, whereas filaments within the bundle become loose. (D) Junctions between barbed ends of lamellipodial filaments (arrows) immediately after lysis or after incubation in buffer like in B or C ("after incubation"). Bars: 0.1 μm (A, C, and D), and 2 μm (B).

the dendritic network, but lose short filaments with age. An interesting feature of the green filopodium was that it was barely recognizable in the EM image because its filaments, although long, were not well-aligned, suggesting that filament cross-linking is not an early event during filopodial formation, in agreement with delayed recruitment of fascin to Λ-precursors.

In contrast to delayed bundling, the filament barbed ends at filopodial tips were in register, suggesting they were interacting with each other, even though they supposedly encountered each other just a few seconds before extraction. A substantial amount of granular material was associated with the tip of the fused filopodium (Fig. 7, inset 1 in D). The presence of tip-associated material may play an important role in filopodial formation, and we therefore investigated it in more detail.

Filopodial tip complex

In EM images, many filopodial tips were associated with a distinct structure, which had a rough granular surface and variable shape and size (Fig. 8 A). To test whether this tip complex was involved in physical association of filopodial barbed ends with each other, we incubated lysed cells overnight in phalloidin-containing buffer. Phalloidin prevented depolymerization of actin filaments during incubation, whereas dissociation of other proteins was allowed. We monitored dissociation of fascin or VASP using cells expressing GFP-fusion proteins. Although lysis removed soluble and weakly bound proteins, lysed cells initially retained most of filopodia-associated fascin and VASP. However, fascin was completely gone after incubation, whereas VASP remained (Fig. 8 B). EM of incubated cells revealed that filopodial bundles became loose, consistent with the loss of fascin, but the tip complexes were mostly preserved, consistent with retention of VASP, and filament barbed ends remained associated with each other and with the filopodial tip complex (Fig. 8 C). These results suggest that the tip complex physically links barbed ends in filopodia independently of fascin. Occasionally, the tip complex detached partially or completely during incubation. In such cases, released filopodial filaments completely splayed apart.

The next question we addressed was the origin of the tip complex. Because filopodia formation seemed to occur by gradual convergence of filaments from the dendritic network, we wondered whether smaller tip complexes existed in lamellipodia. Careful examination of the leading edge of lamellipodia indeed revealed junctions between barbed ends of two or more lamellipodial filaments (Fig. 8 D). Occasionally, additional material could be seen at the junction points, which may correspond to the tip complex of established filopodia. Association between filament-barbed ends was retained even after overnight incubation in the phalloidin-containing buffer (Fig. 8 D).

Discussion

Our kinetic and structural investigation of filopodial initiation in B16F1 melanoma cells demonstrated that filopodial bundles were formed by gradual reorganization of the lamellipodial dendritic network in a process that involved elongation of a subset of lamellipodial filaments, self-segregation of these filaments into filopodial precursors, and initiation of bundling at the tips of the precursors (Fig. 9). We propose that the mechanism of filopodia initiation is analogous to filopodial fusion, but that it begins at the level of individual filaments and gradually propagates to the fusion of thick bundles. We now discuss this hypothesis in detail.

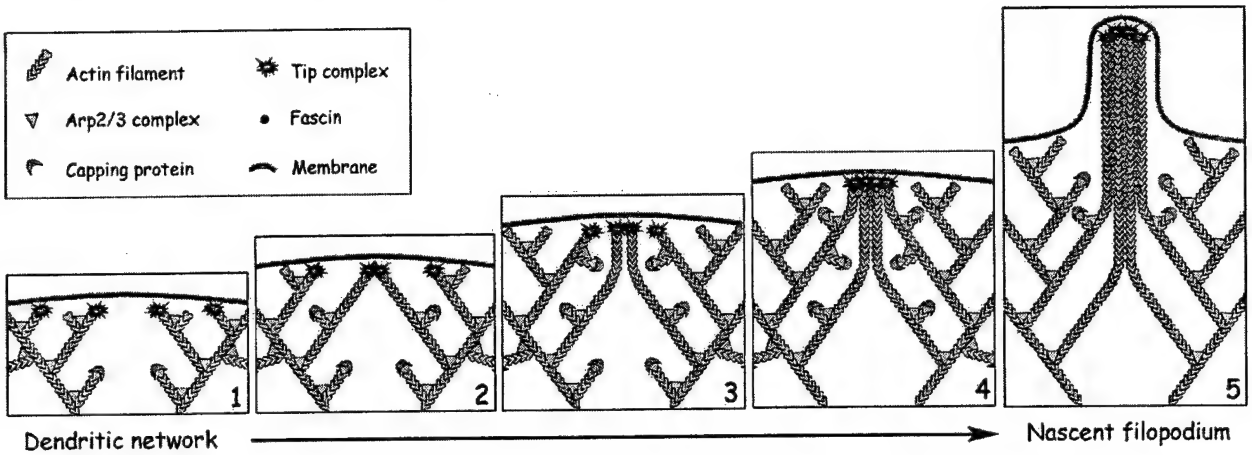

Figure 9. **Convergent elongation model for filopodia initiation.** (1) Lamellipodial network is formed by Arp2/3-mediated dendritic nucleation. Elongation of some barbed ends in the network is terminated by capping protein, but other barbed ends acquire a privileged status by binding a complex of molecules (tip complex) that allows them to elongate continuously. Ena/VASP proteins are likely members of the tip complex mediating protection from capping. (2) Privileged barbed ends drift laterally during elongation and collide with each other. Tip complex mediates clustering of privileged barbed ends upon collision. (3) Converged filaments with linked barbed ends continue to elongate together. Other laterally drifting barbed ends encounter and join the initial cluster of tip complexes. Multiple collisions of barbed ends during elongation lead to gradual clustering of their barbed ends, multimerization of associated tip complexes, and convergence of filaments. (4) The multimeric filopodial tip complex initiates filament cross-linking by recruiting and/or activating fascin, which allows the bundling process to keep up with the elongation and guarantee efficient pushing. (5) In the nascent filopodium, the filopodial tip complex retains its functions of promoting coordinated filament elongation and bundling, as well as fusion with other filopodia.

Dendritic network as a source of filopodial filaments

Arp2/3 complex has been suspected to play a role in filopodia initiation, but paradoxically, is not present in filopodial bundles. Our data do not support the idea of filopodial bundles arising from a nucleation center, but indicate that Arp2/3 complex produces a normal dendritic array which then becomes rearranged into parallel bundles through intermediate formation of Λ-precursors. Considering the ability to fuse displayed by filopodial bundles of all sizes, one can deduce that fusion may also occur below the resolution limit of the light microscope. Fusion of submicroscopic bundles or individual filaments may represent a mechanism of formation of Λ-precursors and explain their Λ-shape. The structure of Λ-precursors and filopodial roots was consistent with this idea, and showed that filaments composing bundles were collected from the surrounding area in an asynchronous manner, suggesting that Arp2/3-mediated actin filament nucleation provides a source of filaments to be rearranged into a bundle by gradual fusion.

Formation of long filaments as a prerequisite of filopodia initiation

The major difference between actin filament arrays in filopodia and lamellipodia is that filopodial filaments elongate continuously, reaching lengths of many micrometers, whereas lamellipodial filaments become capped after a brief period of elongation, and consequently, are relatively short (~100 nm). Extensive elongation of filopodial filaments would seem to require a way to antagonize or protect against capping activity in the cytoplasm. A mechanism for protection is likely to involve proteins of the Ena/VASP family because these proteins are enriched at filopodial tips (Lanier et al., 1999; Rottner et al., 1999), they antagonize the terminating activity of capping protein in vitro, and their depletion from or targeting to the membrane leads to shorter or longer filaments, respectively (Bear et al., 2002). Our data support an idea that distributed filaments with prebound Ena/VASP proteins are gradually brought together to form a filopodium. The kinetics of GFP-VASP demonstrated a correlation between coalescence of VASP and filopodia initiation. At present, it is not clear whether VASP remains associated with the same barbed end for a long time or frequently switches its protégé. The persistence of VASP at the leading edge and filopodial tips after overnight incubation in buffer is evidence that at least some actin filaments can remain tightly associated with VASP. However, in a living cell, the association of VASP with barbed ends may be subject to regulation that affects the degree of protection it confers against capping.

On the assumption that GFP-VASP reports on the behavior of the population of privileged barbed ends, the gradual coalescence of VASP to the tips of Λ-precursors reflects the gradual segregation of longer filaments into Λ-precursors. Consistent with this coalescence process, actin arrays within Λ-precursors were enriched in long filaments and depleted in the lamellipodial markers, Arp2/3 complex, cortactin, and capping protein. Long filaments became more clearly visible when Λ-precursors treadmilled away from the leading edge and became filopodial roots. Long filaments in lamellipodia have been also observed by other EM techniques (Small, 1988; Lewis and Bridgman, 1992; Resch et al., 2002), although no distinction has been made between Λ-precursors and other parts of lamellipodia.

Other studies have indicated that Ena/VASP family members contribute to the formation of filopodia, but the mechanism of their involvement has not been elucidated. In *Dictyostelium*, the VASP family homologue (DdVASP) is essential for filopodia formation (Han et al., 2002). Induction

of filopodia by Irs53 involved recruitment of a member of the Ena/VASP family, Mena (Krugmann et al., 2001). Our data suggest that the mechanism of action of Ena/VASP proteins is through the formation of privileged filaments that can elongate persistently.

Clustering of barbed ends as a mechanism of segregation of filopodial filaments

The persistent elongation of filaments by itself would not result in their local accumulation unless they were able to associate with each other. Consistent with this idea, we found structural interaction between filament barbed ends that was mediated by the filopodial tip complex in a fascin-independent manner. This result suggests that bundling and barbed-end interaction are mediated by different molecules. In addition, we detected formation of junctions between filament barbed ends at the extreme leading edge. Similar to filopodial tips, these junctions were stable even after overnight incubation in buffer and were frequently associated with additional material. The filopodial tip complexes described here may be similar to the material associated with distal filament ends in filopodia and lamellipodia of fibroblasts (Small et al., 1982) and neuronal growth cones (Lewis and Bridgman, 1992). Interaction between barbed ends appears to be responsible for the Λ-configuration of actin arrays at different scales from junctions between individual filaments to Λ-precursors to fusing bundles.

Privileged barbed ends seem to combine the ability for continuous elongation with multimerization potential. The cross-linking molecules mediating junction formation between barbed ends remain unclear, but they are likely to be components of the filopodial tip complex. The molecular composition of the filopodial tip complex remains to be established. However, proteins previously found to localize specifically to filopodial tips (see Introduction), including Ena/VASP proteins, are predicted to be members of this complex. One possibility is that Ena/VASP proteins, which mediate protection of barbed ends from capping, may also work as barbed end "glue" because of their ability to oligomerize (Bachmann et al., 1999). In support of this idea, a domain mediating oligomerization of Mena has been shown to be required for full function of Mena in cell motility (Loureiro et al., 2002). Another possibility is that additional (yet unidentified) molecules within the filopodial tip complex mediate interaction between barbed ends. These possibilities are not mutually exclusive, and the hypothetical barbed end linking molecules may act indirectly through Ena/VASP proteins, which would have the benefit of rendering the anti-capping and clustering capabilities to the same subset of filaments.

The combination of continuous elongation and self-association properties of privileged barbed ends allows one to explain how the privileged filaments in the dendritic network become gradually self-segregated during filopodia initiation. The lamellipodial filaments, on average, have a diagonal orientation of about ±35 degrees with respect to the leading edge (Maly and Borisy, 2001). During elongation, the barbed ends of diagonally oriented filaments drift laterally along the edge, which increases chances of their collision. Such lateral drift of lamellipodial filaments was proposed to mediate formation of filopodia due to activity of bundling proteins (Small et al., 1982, 1998). We propose that the cross-linking molecules at the barbed ends of colliding privileged filaments cause them to associate with each other and travel together. Multiple collisions lead to clustering of barbed ends of filaments and multimerization of individual barbed-end–associated molecular complexes, producing a filopodial tip complex.

Filament bundling as a mechanism of stabilization

Individual long actin filaments are not efficient at pushing. Because of their low persistence length, they bend rather than push. Filament cross-linking along the length is thought to be a solution for this problem (Mogilner and Oster, 1996). The existing evidence suggests that fascin is the major actin cross-linking protein in filopodia (Bartles, 2000; Kureishy et al., 2002) that is required for filopodia maintenance. In support of this idea, we found that fascin enrichment in actin arrays correlated with tight bundling of actin filaments, and fascin dissociation from filopodial bundles resulted in filament unbundling. To allow for efficient pushing, cross-linking of growing filaments is predicted to occur soon in the course of actin polymerization so that the effective length of the filament after the last cross-link remains short. Indeed, fascin is enriched in the distal section of filopodia (Cohan et al., 2001, and this paper) suggesting that its association with the growing actin bundles occurs in parallel with actin assembly. In contrast, association of α-actinin with fast-protruding filopodia and lamellipodia is detected toward their rear, indicating that the role of α-actinin is not to provide the pushing efficiency to growing filaments.

Fascin recruitment during filopodia initiation was not the earliest event. Instead, GFP-fascin rather abruptly appeared at the vertex of a preformed Λ-precursor. We suggest that recruitment and/or activation of fascin to tips of Λ-precursors cross-links the long filaments accumulated there, thus completing the initiation of filopodial bundle formation.

Convergent elongation mechanism of filopodium initiation

Based on our findings, we propose a convergent elongation model for filopodial initiation (Fig. 9), which stipulates that filopodia are formed by reorganization of the dendritic network formed in an Arp2/3-dependent manner. The key assumption of this model is that some filaments within the lamellipodial dendritic network acquire privileged status by binding a set of molecules to their barbed ends, which protect them from capping, and mediate association of barbed ends with each other on collision. Ena/VASP proteins are likely candidates for the role of protection from capping. The glue molecule remains to be established. Multiple collisions of privileged filaments during elongation lead to gradual clustering of their barbed ends and multimerization of associated barbed-end complexes. A set of privileged filaments originating from distant sites of the dendritic network and converging to the same spot forms a Λ-precursor, and aggregated barbed-end complexes form the tip complex of the future filopodium. The filopodial tip complex initiates filament cross-linking by recruiting and/or activating fascin, which allows the bundling process to keep up with elongation and

guarantee efficient pushing. Initiated filopodia elongate and attain steady-state by the filament treadmilling mechanism. The filopodial tip complex remains associated with the growing tip, allowing for continuous elongation of filopodial filaments and mediating filopodia fusion on collision.

Initiation of filopodial bundles within the lamellipodial network necessarily leads to their birth in the form of microspikes. They die either during ruffling or in the form of retraction fibers, when a cell decides to move in a different direction. In between, the microspikes may at some point elongate faster than lamellipodial advance to form a conventional filopodium. Additional evidence for the relatedness of these structures comes from the fact that Cdc42 induces cell retraction and formation of retraction fibers along with formation of genuine filopodia (Kozma et al., 1995). Consequently, the three morphological types of peripheral actin bundle, microspikes, filopodia, and retraction fibers, may be considered as transient states of the same core structure differing primarily in their relationship to the membrane and in the state of their cycle. Also, they may differ in protein composition and dynamics. Filopodia and retraction fibers are predicted to contain actin–membrane linkers, like ERM proteins, which are unnecessary for microspikes. The remote position of barbed ends in filopodia and retraction fibers may require a myosin motor, for example, myosin X (Berg and Cheney, 2002), to deliver building components to the tip.

The pathway of filopodia initiation established in this paper has a remarkable similarity to the mechanism of formation of filopodial-like bundles in vitro (unpublished data). In that work, we found that beads coated with Arp2/3-activating proteins induced formation of radial actin bundles when capping activity in cytoplasmic extracts was decreased. In vitro bundles displayed many filopodial characteristics; they had uniform polarity, grew at the barbed end, were enriched in fascin, and lacked Arp2/3 complex, capping protein, and α-actinin. As in the present paper, individual filaments in bundles in vitro originated from the dendritic network near the bead, and a decreased rate of capping in the extracts allowed them to elongate and be bundled by fascin.

A tightly packed parallel actin bundle, which is a hallmark of filopodia, can also be found in other organelles across tissues and organisms (Bartles, 2000; DeRosier and Tilney, 2000). Our findings that filopodia in B16F1 cells during normal locomotion were formed by reorganization of the dendritic network raises the possibility of a similar pathway for initiation of other parallel bundles, but does not exclude other mechanisms of bundle formation in other cells types or under other circumstances. For example, proteins of the formin family have recently been shown to nucleate actin filaments in vitro (Pruyne et al., 2002; Sagot et al., 2002b) and induce actin cables in yeast in vivo in the absence of the Arp2/3 complex (Evangelista et al., 2002; Sagot et al., 2002a). Thus, it remains an open question whether Arp2/3- or formin-dependent mechanisms operate in other cases, and whether they are exclusive or can cooperate.

In conclusion, we investigated the pathway of filopodia initiation in B16F1 cells and formulated the convergent elongation model for filopodia formation. Although many assumptions of this model remain to be tested, it provides a conceptual framework for further studies aimed at explicitly identifying participating molecules and their precise roles.

Materials and methods

Cells and reagents

Mouse melanoma B16F1 cell line stably expressing EGFP-β-actin, as well as untransfected B16F1 cells, were provided by Dr. C. Ballestrem (Weizmann Institute of Science, Rehovot, Israel) and were cultured as described previously (Ballestrem et al., 1998). For experiments, cells were plated onto coverslips coated with 10–25 μg/ml laminin (Invitrogen) and blocked with 0.1 μg/ml heat-inactivated BSA. For live imaging, cells were transferred from DME into L-15 medium at least 2 h before observation.

EGFP-VASP–expressing construct was obtained from Drs. J. Bear and F. Gertler (Massachusetts Institute of Technology, Cambridge, MA). EGFP-fascin (Adams and Schwartz, 2000) was provided by Dr. J. Adams (Cleveland Clinic Foundation, Cleveland, OH). EGFP-α-actinin (Edlund et al., 2001) was obtained from Dr. C. Otey (University of North Carolina, Chapel Hill, NC). For transient protein expression, cells were transfected with FuGENE™ 6 (Roche) according to the manufacturer's recommendation.

The following primary antibodies were used for immunostaining: affinity-purified rabbit antibody to ARPC5 subunit of Arp2/3 (unpublished data), capping protein antibody (Schafer et al., 1994; provided by Dr. D.A. Schafer, University of Virginia, Charlottesville, VA), and mouse monoclonal cortactin antibody, clone 4F11 (Upstate Biotechnology). Secondary TRITC-conjugated antibodies were purchased from Sigma-Aldrich.

Microscopy

Light microscopy was performed using an inverted microscope (Eclipse or Diaphot 300; Nikon) equipped with a Plan 100×, 1.3 NA objective and a back-illuminated cooled CCD camera (model CH250; Roper Scientific) or a slow-scan cooled CCD camera (model CH350; Photometrics), respectively, driven by MetaMorph® imaging software (Universal Imaging Corp.). FITC filter set was used for GFP-fusion protein observations, and Cy3 and Texas Red filter sets were used for rhodamine and Texas Red imaging, respectively. For live imaging, cells were kept on the microscope stage at 36–37°C during observation.

Immunostaining was performed after cell extraction for 3–10 min with 1% Triton X-100 in PEM buffer (100 mM Pipes, pH 6.9, 1 mM $MgCl_2$, and 1 mM EGTA), containing 4% polyethylene glycol, mol wt 40,000 (SERVA), and 2 μM phalloidin (Sigma-Aldrich), followed by fixation with 0.2% glutaraldehyde and quenching with $NaBH_4$. For phalloidin staining, 0.033 μM Texas Red phalloidin (Molecular Probes, Inc.) was added to the extraction solution instead of unlabeled phalloidin. GFP-fascin–expressing cells were stained with Texas Red phalloidin after fixation of unextracted cells, followed by permeabilization with 1% Triton X-100 in PBS.

For determination of protein dissociation from the cytoskeletons, GFP-fascin or GFP-VASP cells were grown on locator coverslips, extracted as for immunostaining, and images of cells expressing fusion proteins were acquired within 20 min after extraction. Then cells were washed twice with PEM containing 2 μM phalloidin and left in this buffer overnight at RT. After incubation, another set of images of the same cells was acquired. Platinum replica EM and correlative light EM were performed as described previously (Svitkina and Borisy, 1998).

We thank Drs. C. Ballestrem, J. Bear, F. Gertler, J. Adams, C. Otey, and D.A. Schafer for gifts of reagents and Dr. M. Mejillano, Dr. A. Biyasheva, and I. Maly for critical reading of the manuscript.

Supported by NIH Grants GM 62431 and IU 54 GM 63126 to G.G. Borisy.

Submitted: 31 October 2002
Revised: 23 December 2002
Accepted: 23 December 2002

References

Adams, J.C., and M.A. Schwartz. 2000. Stimulation of fascin spikes by thrombospondin-1 is mediated by the GTPases Rac and Cdc42. *J. Cell Biol.* 150: 807–822.

Bachmann, C., L. Fischer, U. Walter, and M. Reinhard. 1999. The EVH2 domain of the vasodilator-stimulated phosphoprotein mediates tetramerization, F-actin binding, and actin bundle formation. *J. Biol. Chem.* 274:23549–23557.

Ballestrem, C., B. Wehrle-Haller, and B.A. Imhof. 1998. Actin dynamics in living

mammalian cells. *J. Cell Sci.* 111:1649–1658.

Bamburg, J.R. 1999. Proteins of the ADF/cofilin family: essential regulators of actin dynamics. *Annu. Rev. Cell Dev. Biol.* 15:185–230.

Bartles, J.R. 2000. Parallel actin bundles and their multiple actin-bundling proteins. *Curr. Opin. Cell Biol.* 12:72–78.

Bear, J.E., T.M. Svitkina, M. Krause, D.A. Schafer, J.J. Loureiro, G.A. Strasser, I.V. Maly, O.Y. Chaga, J.A. Cooper, G.G. Borisy, and F.B. Gertler. 2002. Antagonism between Ena/VASP proteins and actin filament capping regulates fibroblast motility. *Cell.* 109:509–521.

Berg, J.S., and R.E. Cheney. 2002. Myosin-X is an unconventional myosin that undergoes intrafilopodial motility. *Nat. Cell Biol.* 4:246–250.

Borisy, G.G., and T.M. Svitkina. 2000. Actin machinery: pushing the envelope. *Curr. Opin. Cell Biol.* 12:104–112.

Carlier, M.F., and D. Pantaloni. 1997. Control of actin dynamics in cell motility. *J. Mol. Biol.* 269:459–467.

Cohan, C.S., E.A. Welnhofer, L. Zhao, F. Matsumura, and S. Yamashiro. 2001. Role of the actin bundling protein fascin in growth cone morphogenesis: localization in filopodia and lamellipodia. *Cell Motil. Cytoskeleton.* 48:109–120.

Cooper, J.A., and D.A. Schafer. 2000. Control of actin assembly and disassembly at filament ends. *Curr. Opin. Cell Biol.* 12:97–103.

DePasquale, J.A., and C.S. Izzard. 1991. Accumulation of talin in nodes at the edge of the lamellipodium and separate incorporation into adhesion plaques at focal contacts in fibroblasts. *J. Cell Biol.* 113:1351–1359.

DeRosier, D.J., and L.G. Tilney. 2000. F-actin bundles are derivatives of microvilli: What does this tell us about how bundles might form? *J. Cell Biol.* 148:1–6.

Edlund, M., M.A. Lotano, and C.A. Otey. 2001. Dynamics of alpha-actinin in focal adhesions and stress fibers visualized with alpha-actinin-green fluorescent protein. *Cell Motil. Cytoskeleton.* 48:190–200.

Evangelista, M., D. Pruyne, D.C. Amberg, C. Boone, and A. Bretscher. 2002. Formins direct Arp2/3-independent actin filament assembly to polarize cell growth in yeast. *Nat. Cell Biol.* 4:32–41.

Flanagan, L.A., J. Chou, H. Falet, R. Neujahr, J.H. Hartwig, and T.P. Stossel. 2001. Filamin A, the Arp2/3 complex, and the morphology and function of cortical actin filaments in human melanoma cells. *J. Cell Biol.* 155:511–517.

Hall, A. 1998. Rho GTPases and the actin cytoskeleton. *Science.* 279:509–514.

Han, Y.H., C.Y. Chung, D. Wessels, S. Stephens, M.A. Titus, D.R. Soll, and R.A. Firtel. 2002. Requirement of a vasodilator-stimulated phosphoprotein family member for cell adhesion, the formation of filopodia, and chemotaxis in *Dictyostelium*. *J. Biol. Chem.* 277:49877–49887.

Higgs, H.N., and T.D. Pollard. 2001. Regulation of actin filament network formation through ARP2/3 complex: activation by a diverse array of proteins. *Annu. Rev. Biochem.* 70:649–676.

Ho, H.Y., R. Rohatgi, L. Ma, and M.W. Kirschner. 2001. CR16 forms a complex with N-WASP in brain and is a novel member of a conserved proline-rich actin-binding protein family. *Proc. Natl. Acad. Sci. USA.* 98:11306–11311.

Katoh, K., K. Hammar, P.J. Smith, and R. Oldenbourg. 1999a. Arrangement of radial actin bundles in the growth cone of *Aplysia* bag cell neurons shows the immediate past history of filopodial behavior. *Proc. Natl. Acad. Sci. USA.* 96: 7928–7931.

Katoh, K., K. Hammar, P.J. Smith, and R. Oldenbourg. 1999b. Birefringence imaging directly reveals architectural dynamics of filamentous actin in living growth cones. *Mol. Biol. Cell.* 10:197–210.

Kozma, R., S. Ahmed, A. Best, and L. Lim. 1995. The Ras-related protein Cdc42Hs and bradykinin promote formation of peripheral actin microspikes and filopodia in Swiss 3T3 fibroblasts. *Mol. Cell. Biol.* 15:1942–1952.

Kranewitter, W.J., C. Danninger, and M. Gimona. 2001. GEF at work: Vav in protruding filopodia. *Cell Motil. Cytoskeleton.* 49:154–160.

Krugmann, S., I. Jordens, K. Gevaert, M. Driessens, J. Vandekerckhove, and A. Hall. 2001. Cdc42 induces filopodia by promoting the formation of an IRSp53:Mena complex. *Curr. Biol.* 11:1645–1655.

Kureishy, N., V. Sapountzi, S. Prag, N. Anilkumar, and J.C. Adams. 2002. Fascins, and their roles in cell structure and function. *Bioessays.* 24:350–361.

Langanger, G., J. de Mey, M. Moeremans, G. Daneels, M. de Brabander, and J.V. Small. 1984. Ultrastructural localization of alpha-actinin and filamin in cultured cells with the immunogold staining (IGS) method. *J. Cell Biol.* 99:1324–1334.

Lanier, L.M., M.A. Gates, W. Witke, A.S. Menzies, A.M. Wehman, J.D. Macklis, D. Kwiatkowski, P. Soriano, and F.B. Gertler. 1999. Mena is required for neurulation and commissure formation. *Neuron.* 22:313–325.

Lewis, A.K., and P.C. Bridgman. 1992. Nerve growth cone lamellipodia contain two populations of actin filaments that differ in organization and polarity. *J. Cell Biol.* 119:1219–1243.

Li, Z., E.S. Kim, and E.L. Bearer. 2002. Arp2/3 complex is required for actin polymerization during platelet shape change. *Blood.* 99:4466–4474.

Loureiro, J.J., D.A. Rubinson, J.E. Bear, G.A. Baltus, A.V. Kwiatkowski, and F.B. Gertler. 2002. Critical roles of phosphorylation and actin binding motifs, but not the central proline-rich region, for Ena/vasodilator-stimulated phosphoprotein (VASP) function during cell migration. *Mol. Biol. Cell.* 13: 2533–2546.

Mallavarapu, A., and T. Mitchison. 1999. Regulated actin cytoskeleton assembly at filopodium tips controls their extension and retraction. *J. Cell Biol.* 146: 1097–1106.

Maly, I.V., and G.G. Borisy. 2001. Self-organization of a propulsive actin network as an evolutionary process. *Proc. Natl. Acad. Sci. USA.* 98:11324–11329.

Miki, H., T. Sasaki, Y. Takai, and T. Takenawa. 1998. Induction of filopodium formation by a WASP-related actin-depolymerizing protein N-WASP. *Nature.* 391:93–96.

Mogilner, A., and G. Oster. 1996. Cell motility driven by actin polymerization. *Biophys. J.* 71:3030–3045.

Nobes, C.D., and A. Hall. 1995. Rho, rac, and cdc42 GTPases regulate the assembly of multimolecular focal complexes associated with actin stress fibers, lamellipodia, and filopodia. *Cell.* 81:53–62.

Pollard, T.D., L. Blanchoin, and R.D. Mullins. 2000. Molecular mechanisms controlling actin filament dynamics in nonmuscle cells. *Annu. Rev. Biophys. Biomol. Struct.* 29:545–576.

Pruyne, D., M. Evangelista, C. Yang, E. Bi, S. Zigmond, A. Bretscher, and C. Boone. 2002. Role of formins in actin assembly: nucleation and barbed-end association. *Science.* 297:612–615.

Qualmann, B., and R.B. Kelly. 2000. Syndapin isoforms participate in receptor-mediated endocytosis and actin organization. *J. Cell Biol.* 148:1047–1062.

Resch, G.P., K.N. Goldie, A. Krebs, A. Hoenger, and J.V. Small. 2002. Visualisation of the actin cytoskeleton by cryo-electron microscopy. *J. Cell Sci.* 115: 1877–1882.

Rohatgi, R., L. Ma, H. Miki, M. Lopez, T. Kirchhausen, T. Takenawa, and M.W. Kirschner. 1999. The interaction between N-WASP and the Arp2/3 complex links Cdc42-dependent signals to actin assembly. *Cell.* 97:221–231.

Rohatgi, R., H.Y. Ho, and M.W. Kirschner. 2000. Mechanism of N-WASP activation by CDC42 and phosphatidylinositol 4, 5-bisphosphate. *J. Cell Biol.* 150:1299–1310.

Rottner, K., B. Behrendt, J.V. Small, and J. Wehland. 1999. VASP dynamics during lamellipodia protrusion. *Nat. Cell Biol.* 1:321–322.

Sagot, I., S.K. Klee, and D. Pellman. 2002a. Yeast formins regulate cell polarity by controlling the assembly of actin cables. *Nat. Cell Biol.* 4:42–50.

Sagot, I., A.A. Rodal, J. Moseley, B.L. Goode, and D. Pellman. 2002b. An actin nucleation mechanism mediated by Bni1 and profilin. *Nat. Cell Biol.* 4:626–631.

Schafer, D.A., Y.O. Korshunova, T.A. Schroer, and J.A. Cooper. 1994. Differential localization and sequence analysis of capping protein beta-subunit isoforms of vertebrates. *J. Cell Biol.* 127:453–465.

Small, J.V. 1994. Lamellipodia architecture: actin filament turnover and the lateral flow of actin filaments during motility. *Semin. Cell Biol.* 5:157–163.

Small, J.V. 1988. The actin cytoskeleton. *Electron Microsc. Rev.* 1:155–174.

Small, J.V., G. Rinnerthaler, and H. Hinssen. 1982. Organization of actin meshworks in cultured cells: the leading edge. *Cold Spring Harb. Symp. Quant. Biol.* 46:599–611.

Small, J.V., K. Rottner, I. Kaverina, and K.I. Anderson. 1998. Assembling an actin cytoskeleton for cell attachment and movement. *Biochim. Biophys. Acta.* 1404:271–281.

Small, J.V., T. Stradal, E. Vignal, and K. Rottner. 2002. The lamellipodium: where motility begins. *Trends Cell Biol.* 12:112–120.

Stradal, T., K.D. Courtney, K. Rottner, P. Hahne, J.V. Small, and A.M. Pendergast. 2001. The Abl interactor proteins localize to sites of actin polymerization at the tips of lamellipodia and filopodia. *Curr. Biol.* 11:891–895.

Svitkina, T.M., and G.G. Borisy. 1998. Correlative light and electron microscopy of the cytoskeleton of cultured cells. *Methods Enzymol.* 298:570–592.

Svitkina, T.M., and G.G. Borisy. 1999a. Arp2/3 complex and actin depolymerizing factor/cofilin in dendritic organization and treadmilling of actin filament array in lamellipodia. *J. Cell Biol.* 145:1009–1026.

Svitkina, T.M., and G.G. Borisy. 1999b. Progress in protrusion: the tell-tale scar. *Trends Biochem. Sci.* 24:432–436.

Svitkina, T.M., A.B. Verkhovsky, K.M. McQuade, and G.G. Borisy. 1997. Analysis of the actin-myosin II system in fish epidermal keratocytes: mechanism of cell body translocation. *J. Cell Biol.* 139:397–415.

Weaver, A.M., A.V. Karginov, A.W. Kinley, S.A. Weed, Y. Li, J.T. Parsons, and J.A. Cooper. 2001. Cortactin promotes and stabilizes Arp2/3-induced actin filament network formation. *Curr. Biol.* 11:370–374.

1: Biotechniques. 2004 Jan;36(1):74-9.

Improved silencing vector co-expressing GFP and small hairpin RNA.

Kojima S, Vignjevic D, Borisy GG.

Department of Cell and Molecular Biology, Feinberg School of Medicine, Northwestern University, 303 E. Chicago Ave., Chicago, IL 60611, USA. s-kojima@northwestern.edu

Small interfering RNA (siRNA) is a powerful tool for the specific silencing of gene expression. We developed an improved vector, pG-SUPER, that co-expresses green fluorescent protein (GFP) and small hairpin RNA simultaneously to facilitate analysis of silencing at the level of individual cells. As a test system, we analyzed lamin A/C knockdow in HeLa cells. The GFP signal was a reliable reporter (93%-98%) of strong knockdown (approximately 90%) over a wide range of GFP intensities. The GFP reporter made possible the application of fluorescent-activated cell sorting (FACS) to purify the knockdown cell population. Such populations facilitated Western blotting analysis to determine depletion of the target protein. pG-SUPER was also applied to evaluate gene replacement by exogenous genes rendered refractory to siRNA by introducing silent mutations. Recovery of lamin A was linearly correlated to the expression level of the rescue gene. pG-SUPER will expand plasmid-based siRNA applications through the easy and reliable detection of knockdown an rescued cells.

Publication Types:
- Technical Report

PMID: 14740488 [PubMed - indexed for MEDLINE]

[CANCER RESEARCH 64, 162–168, January 1, 2004]

Cell Surface-Dependent Generation of Angiostatin4.5

Hao Wang, Ryan Schultz, Jerome Hong, Deborah L. Cundiff, Keyi Jiang, and Gerald A. Soff

Northwestern University Feinberg School of Medicine, Department of Medicine, Division of Hematology/Oncology, Chicago, Illinois

ABSTRACT

Angiostatin4.5 (AS4.5) is a naturally occurring human angiostatin isoform, consisting of plasminogen kringles 1–4 plus 85% of kringle 5 (amino acids Lys78 to Arg529). Prior studies indicate that plasminogen is converted to AS4.5 in a two-step reaction. First, plasminogen is activated to plasmin. Then plasmin undergoes autoproteolysis within the inner loop of kringle 5, which can be induced by a free sulfhydryl donor or an alkaline pH. We now demonstrate that plasminogen can be converted to AS4.5 in a cell membrane-dependent reaction. Actin was shown previously to be a surface receptor for plasmin(ogen). We now show that β-actin is present on the extracellular membranes of cancer cells (PC-3, HT1080, and MDA-MB231), and β-actin can mediate plasmin binding to the cell surface and autoproteolysis to AS4.5. In the presence of β-actin, no small molecule-free sulfhydryl donor is needed for generation of AS4.5. Antibodies to actin reduced membrane-dependent generation of AS4.5 by 70%. In a cell-free system, addition of actin to *in vitro*-generated plasmin resulted in stoichiometric conversion to AS4.5. Annexin II and α-enolase have been reported to be plasminogen receptors, but we did not demonstrate a role for these proteins in conversion of plasminogen to AS4.5. Our data indicate that membrane-associated β-actin, documented previously as a plasminogen receptor, is a key cell membrane receptor capable of mediating conversion of plasmin to AS4.5. This conversion may serve an important role in regulating tumor angiogenesis, invasion, and metastasis, and surface β-actin may also serve as a prognostic marker to predict tumor behavior.

INTRODUCTION

Tumor growth and development consists of two stages: a prevascular stage and a vascular or angiogenic stage (1–7). In the prevascular phase, tumors are noninvasive and typically not clinically detectable (1, 8, 9). Tumor growth is restricted by the absence of neovascularization, resulting in a balance of cancer cell proliferation and apoptosis (10). Angiogenesis, the process of generation of new microvessels from existing vasculature, is necessary for the vascular phase, which is characterized by rapid tumor growth and metastatic possibility. In tumor development, a nonmetastatic lesion can progress to an aggressive metastatic cancer, in which the switch of tumor cells from a nonangiogenic phenotype to an angiogenic phenotype plays an essential role (9, 11). Angiogenesis is controlled by a balance of angiogenesis promoters, such as vascular endothelial cell growth factor and basic fibroblast growth factor, and angiogenesis inhibitors, such as thrombospondin-1 (9, 12, 13). In invasive cancers, an increase in expression of an angiogenesis promoter, such as vascular endothelial cell growth factor expression, or loss of an antiangiogenic factor, such as thrombospondin-1, initiates an angiogenic cascade (13–15).

O'Reilly *et al.* (16) described angiostatin, an internal fragment of plasminogen, which is a potent inhibitor of angiogenesis. Plasminogen is the zymogen form of the serine proteinase plasmin and contains five consecutive kringle domains (17). Plasminogen is cleaved by a plasminogen activator through the hydrolysis of the Arg561-Val562 peptide bond to yield the two-chain serine proteinase, plasmin, which is the primary fibrinolytic enzyme. As originally described, angiostatin possesses the first three or four of the five kringle domains of plasminogen (16). A variety of proteinases may cleave plasminogen to form angiostatin-related proteins, with a range of NH_2 and COOH termini, and varied degrees of antiangiogenic activity (16, 18–23). We and others showed previously that in a human system, plasminogen is converted to angiostatin via plasmin autoproteolysis, which may be mediated by a free sulfhydryl donor (22, 24–26). This reaction results in an intra-kringle 5 cleavage after amino acids Arg530 or Lys531. The resulting angiostatin isoform is referred to as Angiostatin4.5 (AS4.5), because it includes kringles 1–4 plus 85% of kringle 5 (Lys78-Arg529; Ref. 24). An angiostatin isoform with identical amino acid sequence has been generated by Cao *et al.* (27, 28), using plasmin autoproteolysis in an alkaline pH, and Stathakis *et al.* (25, 26), also by plasmin autoproteolysis.

AS4.5 has been shown to be a potent angiogenesis inhibitor, inhibiting Lewis lung carcinoma and hemangioendothelioma (EOMA) tumors in mice (22, 29). In addition, with Mauceri *et al.* (30), we have shown that AS4.5 may potentiate the cytotoxic effect of ionizing radiation in murine tumor models. In our studies, as well as those of Cao *et al.* (27, 28), AS4.5 has been shown to be significantly more potent than angiostatinK1–3 and angiostatinK1–4 (24), suggesting the functional importance of the amino acid sequences/structures within kringle 5.

We now show that plasminogen can be converted to AS4.5 on the surface of human cancer cell lines, including PC-3 prostate, HT1080 fibrosarcoma, and MDA-MB231 breast cancer, in the absence of a small molecule-free sulfhydryl donor. Annexin II (and annexin II tetramer), α-enolase, and actin, have all been shown previously to be on the extracellular surface of cells and have been reported to be plasmin(ogen) receptors (31–37). In the following studies we demonstrate that β-actin is present on the extracellular surface on all three of the cell lines tested and that it serves a key role in conversion of human plasminogen to AS4.5.

MATERIALS AND METHODS

Materials

Plasminogen purification was described previously (22–24). Inhibitors of plasmin formation/action were as follows: Pefabloc (Roche, Indianapolis, IN), α2-antiplasmin (Sigma, St. Louis, MO), plasminogen-activator inhibitor-1 (American Diagnostica Inc., Greenwich, CT), and ε-aminocaproic acid (Acros Organics, Morris Plains, NJ).

Cell Culture

PC-3 (Human Prostate adenocarcinoma cells), HT1080 (Human fibrosarcoma cells), and MDA-MB231 (human breast adenocarcinoma cells) were from American Type Culture Collection (Manassas, VA). PC-3 cells were cultured in DMEM with 10% (v/v) fetal bovine serum, 100 units/ml penicillin G, 100 units/ml streptomycin, and 2.5 μg/ml amphotericin B (Invitrogen, Carlsbad, CA). HT1080 cells (fibrosarcoma) were cultured in DMEM with 10% heat-inactivated FCS. MDA-MB231 cells (breast cancer) were cultured in RPMI 1640 with 10% heat-inactivated FCS. HMVEC (human neonatal dermal microvascular endothelial cells; Passage 6) and NHDF (human neonatal dermal fibroblasts; Passage 8) were from BioWhittaker, Inc. (Walkersville, MD).

Received 6/24/03; revised 10/17/03; accepted 10/28/03.

Grant Support: National Cancer Institute (P50 CA90386), P50 CA89018-02), and (R21 CA89886-01).

The costs of publication of this article were defrayed in part by the payment of page charges. This article must therefore be hereby marked *advertisement* in accordance with 18 U.S.C. Section 1734 solely to indicate this fact.

Requests for reprints: Gerald Soff, Northwestern University Feinberg School of Medicine, Department of Medicine, Division of Hematology/Oncology, Chicago, Illinois. Phone: (312) 695-4442; Fax: (312) 695-6189; E-mail: g-soff@northwestern.edu.

HMVEC were cultured in EGM-MV Bulletkit (BioWhittaker, Inc.). NHDF were cultured in FGM-2 Bulletkit (BioWhittaker, Inc.).

Plasminogen to AS4.5 Conversion on Fixed Cells

Confluent PC-3 cells in 24-well-plates were fixed with 0.5% glutaraldehyde in PBS for 10 min. Cells were then washed with PBS and used for analysis of plasminogen conversion to AS4.5. Forty μg/ml (440 nM) of human plasminogen in 300 μl of HEPES-buffered saline (pH 7.5; HBS) was added to the wells. At various time points, aliquots of the supernatant were removed and assayed by Western blot or ELISA for AS4.5 and plasminogen.

PC-3 Membrane Fractions

Confluent PC-3 cells were scraped from plates, washed three times with PBS, and lysed by three freeze-thaw cycles. After each freeze-thaw cycle, the membrane fraction was pelleted by centrifugation (1500 × *g*), and the pellet was washed with PBS. The membrane pellet was resuspended in HBS.

Annexin II (p36) was removed from the cell membrane as described (38). Membrane aliquots were suspended in HBS with 30 mM CHAPS {3-[(3-cholamidopropyl)dimethylammonio]-1 -propanesulfonic acid; Bio-Rad, Hercules, CA} and 5 mM EGTA (Sigma) at 4°C for 1 h. Control aliquots were processed using HBS alone. Membranes were pelleted at 15,000 rpm for 5 min in an Eppendorf microcentrifuge to separate supernatant and pellet. Pellets were washed and resuspended in HBS. Plasminogen was incubated at 37°C with the control PC-3 membrane fraction or CHAPS:EGTA-treated PC-3 membrane fraction from which annexin II was removed. At various time points, aliquots of the supernatant were removed and assayed for AS4.5 content.

AS4.5 Generation in Fluid Phase

AS4.5 was generated by plasminogen, urokinase and *N*-acetyl-L-cysteine (Sigma) as described previously (22).

Western Blot Assay

The Western blot assay was performed as described previously (22, 23), using anti-kringle 1–3 monoclonal antibodies (VAP, a gift from V. Ploplis and F. Castellino, Notre Dame University, Notre Dame, IN, and GMA086 from Green Mt. Antibodies, Burlington, VT).

AS4.5 ELISA

COOH-Terminal Peptide Antisera. An 18 amino acid peptide of the COOH terminus of AS4.5 was generated with the sequence NH2-RNPDGD-VGGPWCYTTNPR-COOH, and was purified by reversed-phased high-performance liquid chromatography to >95% purity (Multiple Peptide Systems, San Diego, CA). The peptide was conjugated 1:1 (w/w) through the α-amino group to keyhole limpet hemocyanin using glutaraldehyde as the cross-linking agent. Polyclonal antiserum was generated in New Zealand White rabbits.

Preparation of AS4.5-Specific Antibody. AS4.5-Sepharose was used to affinity purify the antibodies to the COOH-terminal peptide. This antibody bound both AS4.5 and plasminogen. To remove the subpopulations of the antibodies that reacted with plasminogen (but presumably not with AS4.5), 20-fold mass excess of plasminogen was added to the antibody and incubated overnight at 4°C. The plasminogen:antibody complex as well as the excess plasminogen were removed with lysine-Sepharose chromatography. The COOH-terminal-specific antibodies in the flow-through from the lysine-Sepharose were collected and concentrated. Approximately 70% of the antibody was removed by this procedure, but the remaining anti-AS4.5 antibody did not cross-react with human plasminogen by Western blot and subsequent ELISA.

ELISA Assay. Microtiter plates (Fisher Scientific, Hanover Park, IL) were coated with AS4.5 (10 μg/ml) in binding buffer (0.2 M $NaHCO_3$; pH 9.2) for 1 h and washed three times with TBT (10 mM Tris, 150 mM NaCl, 0.2% BSA, and 0.1% Tween 20). Samples or standard AS4.5 sources were incubated with AS4.5-specific antibody at room temperature for 1 h and then mixtures added to the AS4.5-coated wells. After incubation for 1 h, the wells were washed with TBT. Goat-antirabbit IgG-conjugated with alkaline phosphatase (0.002 mg/ml; Kirkegaard & Perry Laboratories, Gaithersburg, MD) was added and incubated for 1 h. After washing three times with TBT, 200 μl/well of phosphatase substrate solution [1 mg/ml *p*-nitrophenyl phosphate (Sigma), in 0.05 M $NaHCO_3$ and 1 mM $MgCl_2$] was added to the wells and incubated for 6 h and A_{405} measured.

Endothelial Cell Proliferation Assay

Bovine aortic endothelial cells were plated in 24-well culture dishes at 3.3×10^3 cells/well in DMEM supplemented with 2.5% heat-inactivated calf serum, 1% penicillin-streptomycin, and 1% amphotericin B. The following day, fresh medium supplemented with 3 ng/ml human basic fibroblast growth factor (Becton Dickinson, Bedford, MA) alone or basic fibroblast growth factor supplemented with 200 nM of PC-3 cell-generated AS4.5 was added. For positive control, 200 nM affinity purified cell-free produced AS4.5 was used. After 72 h of treatment, the cell number was determined by counting from duplicate wells, using an automated cell counter (Beckman Coulter Corp., Miami, FL).

Plasmin Activity on Fixed Cell Surface

Glutaraldehyde-fixed PC-3 cells in 24-well plates were incubated with 5 μg/ml (55 nM) plasminogen in HBS at 37°C. At 1, 3, 7, and 20 h, aliquots of cells were washed with PBS twice and chromogenic plasmin substrate [0.33 μg/μl D-Val-Leu-Lys *p*-nitroanilide (Sigma) in HBS] added at 37°C. A_{405} was read for these solutions at the end of 1 h.

Generation of AS4.5 by Actin. Fifty μM human nonmuscle actin (Cytoskeleton, Inc., Denver, CO) was incubated with 440 nM plasminogen with and without urokinase. The AS4.5 generated was measured by ELISA.

Inhibition of AS4.5 Generation by Antiactin Antibody

Plasminogen (440 nM) was incubated with PC-3 cell membrane fraction or glutaraldehyde-fixed PC-3 cells in the presence or absence of an antibody to the COOH terminus of actin (Sigma). AS4.5 generation was measured by ELISA.

Detection of Actin on Cell Membrane

Membrane lysates from PC-3 cells, HT1080 cells, and MDA-MB231 cells were prepared by freeze-thaw lysis (see above). Membranes from $\sim 10^5$ cells were loaded onto SDS-PAGE gels and transferred to polyvinylidene difluoride paper. These Westerns were developed with monoclonal antibodies to α-actin, β-actin, or the COOH terminus of actin (common to all isoforms; Sigma). Parallel experiments were performed with PC-3 cells grown for 72 h in serum-free medium to eliminate possible sources of exogenous actin.

Immunofluorescence Staining

The surface and intracellular immunofluorescence staining was done using a similar protocol to that described previously (39). For surface proteins on nonpermeabilized cells, PC-3 cells grown on gelatin-coated coverslips were washed three times in PBS and then incubated for 3 h at 4°C with FITC-conjugated monoclonal antibody to the COOH terminus of actin (Sigma) or with FITC-conjugated monoclonal anticytokeratin 7 antibody (Sigma). Cells were washed three times with PBS and fixed in 3.7% formaldehyde for 5 min. Coverslips were washed in PBS and mounted in Vectashield mounting medium (Vector Laboratories, Inc., Burlingame, CA). For intracellular staining, PC-3 cells grown on gelatin-coated coverslips were washed with PBS and fixed in 3.7% formaldehyde for 5 min. The fixed PC-3 cells were permeabilized in −20°C acetone for 3 min, and then incubated for 3 h at 4°C with FITC-conjugated monoclonal antibody to the COOH terminus of actin or with FITC-conjugated monoclonal anticytokeratin 7 antibody. Coverslips were washed in PBS and mounted in Vectashield mounting medium.

Urokinase (uPA) Activity Measurement on Cell Membrane Fractions

Cell membrane fractions were collected from 5×10^6 cells after three freeze-thaw cycles. Cell membrane fractions were incubated with 30 μl of 3 mM S2444 (Chromogenix, Franklin, OH) and 270 μl of PBS at room temperature for 1 h. Two hundred μl of liquid was removed to measure A_{405}. uPA from Abbott Laboratories (Abbott Park, IL) was used to make the standard curve.

RESULTS

To determine whether the factors necessary and sufficient to convert plasminogen to AS4.5 are present on the surface of PC-3 cells, plasminogen was incubated with glutaraldehyde-fixed PC-3 cells at 37°C and aliquots were tested for conversion to AS4.5 by Western blot, and there was a complete conversion of plasminogen to AS4.5. When plasminogen was added to a suspension of the PC-3 plasma membranes from which all of the cytoplasmic and nonmembrane bound proteins and solutes had been removed, plasminogen was again completely converted to AS4.5 (Fig. 1*A*). The protein product was confirmed to be angiostatin based on binding to two different monoclonal antibodies to the kringle domains of human plasminogen (VAP and GMA086), by binding to lysine-Sepharose, and ability to inhibit proliferation of vascular endothelial cells (Fig. 1*B*). The angiostatin isoform was determined to be AS4.5 based on the molecular size (M_r 55,000) as well as the Western blot analysis and ELISA (see below) with a polyclonal antibody directed to the COOH-terminal 18 amino acids of AS4.5. No angiostatin isoforms other than AS4.5 were observed by Western blot. These data indicate that constituents necessary and sufficient to convert plasminogen to AS4.5 are on the cell membrane, and that nonmembrane-associated, small molecule-free sulfhydryl donors are not necessary for the plasmin autoproteolysis.

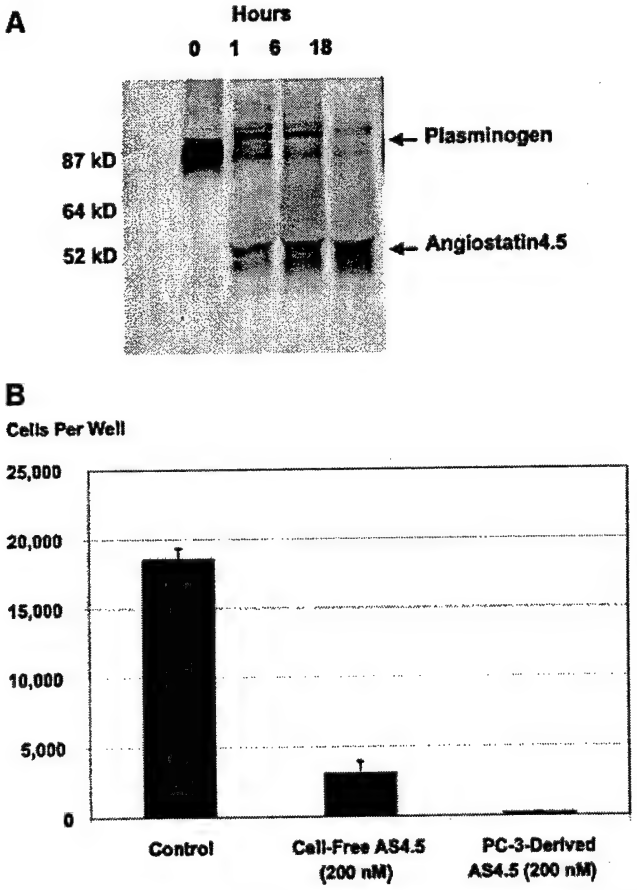

Fig. 1. *A*, plasminogen conversion to angiostatin4.5 (AS4.5) by suspension of PC-3 cell membrane fraction. Plasminogen (440 nM) was added to the PC-3 membranes and incubated at 37°C. Aliquots were taken out at 0, 1, 6, and 18 h. for Western blot analysis with GMA086, an antikringle 1–3 monoclonal antibody. There was efficient conversion of plasminogen to AS4.5, with the majority of plasminogen consumed and AS4.5 generated by 1 h. The observed AS4.5 runs as a doublet on the Western blot, reflecting glycosylation isoforms, as described previously (22). *B*, cell proliferation assay. Early passage bovine aortic endothelial cells were stimulated with 3 ng/ml basic fibroblast growth factor. AS4.5 (200 nM), generated from human plasminogen in a cell-free system of urokinase and *N*-acetyl-L-cysteine (22), or from the PC-3 membrane lysates, was added to aliquots of the cells. Control cells received basic fibroblast growth factor alone. The cell-free AS4.5 reduced the cell number by 84%, and the PC-3 membrane-derived AS4.5 reduced the cell number by >98%. Data are mean of duplicate wells; *bars*, ±SD. Similar results were obtained from three independent experiments.

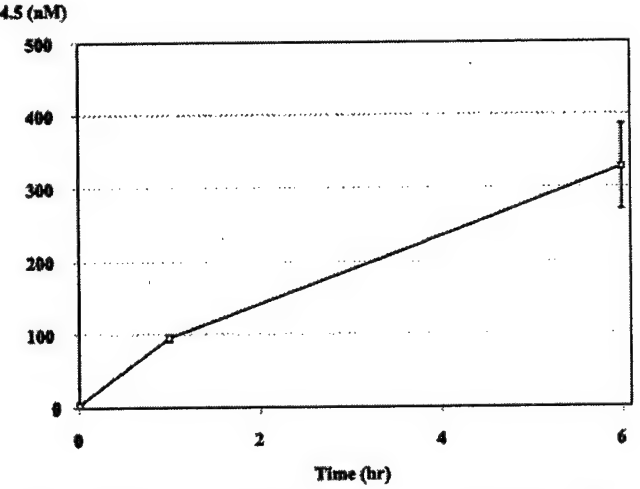

Fig. 2. Quantitation of generation of AS4.5 from plasminogen by PC-3 cell membrane lysates by ELISA. Human plasminogen (440 nM) was added to the PC-3 membrane preparations and aliquots removed at designated times for quantitation of AS4.5 levels. Membranes from ~107 of PC-3 cells were used per 1 mg plasminogen. As indicated above, the ELISA did not register the plasminogen substrate, but did show progressive generation of AS4.5. This is a representative experiment of numerous similar experiments. Membrane lysates from PC-3, HT1080, and MDA-MB231 cells all showed comparable, stoichiometric conversion of human plasminogen to AS4.5.

An ELISA specific for AS4.5 was developed using an affinity-purified polyclonal rabbit antiserum to an 18 amino acid peptide from the COOH terminus of AS4.5. The COOH terminus of AS4.5 is within the inner loop of kringle 5 (24, 25), and the specificity of the ELISA derived from the fact that the antibody does not bind to the peptide sequence within the intact kringle 5 of plasminogen, but does bind to the cleaved kringle 5 of AS4.5 (24). The assay was sensitive to AS4.5 from 0.5 to 50 μg/ml (10–1000 nM) and insensitive to plasminogen at up to 50 μg/ml. The ELISA was used to measure AS4.5 generated from plasminogen by cancer cell membranes as well as in cell-free, fluid-phase reactions (Fig. 2). Note that at the 0-h starting time point, in the presence of 40 μg/ml (440 nM) plasminogen, the ELISA result was 0 nM. This confirmed that the human plasminogen substrate did not cross-react and interfere with the assay. By 6 h, 330 nM of AS4.5 was detected of the theoretical maximum of 440 nM, based on amount of plasminogen added. By 20 h, the reaction reached stoichiometric conversion of plasminogen to AS4.5. This ELISA, based on the specific antibody for AS4.5, also confirmed that the AS isoform being generated was AS4.5 and not the kringle 1–3 or 1–4 isoforms observed in murine models (16).

Whereas we and others have published previously that plasminogen may be converted to AS4.5 by plasmin autoproteolysis mediated by disulfide reduction (22, 24, 26–28), other groups have reported that plasminogen may be converted to other angiostatin isoforms (*i.e.*, K1–3 and K1–4) by other proteolytic mechanisms (16, 18–23). If plasmin autoproteolysis is occurring on the cell surface, a plasminogen activator must be present to generate the plasmin intermediate. Western blots of PC-3, MDA-MB231, and HT1080 cell-conditioned media, as well as washed cell membranes all demonstrated the presence of uPA. In contrast, tissue plasminogen activator antigen was not detected in the conditioned media or washed cell membranes (data not shown). Plasminogen activation to plasmin by fixed PC-3 cell membrane preparations was demonstrated (Fig. 3). Within 1 h, PC-3 surface-bound plasmin reached a maximum. A gradual decline in

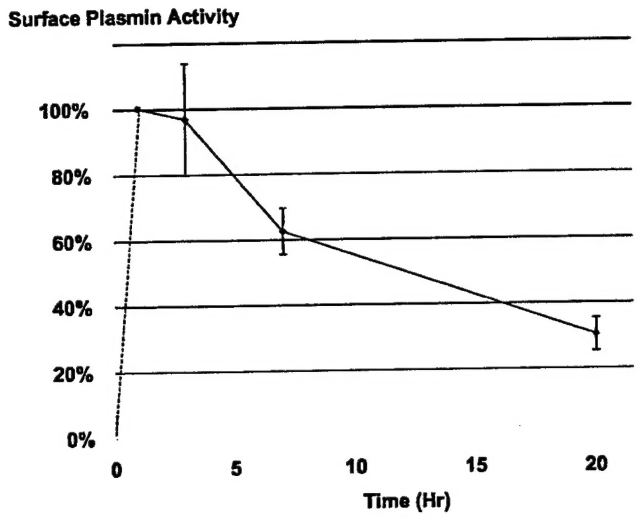

Fig. 3. Plasmin activity on glutaraldehyde-fixed PC-3 cells. Fixed PC-3 cells were incubated with plasminogen and at 1, 3, 7, and 20 h, and supernatants were removed from the wells. The cells were washed with PBS twice. D-Val-Leu-Lys *p*-Nitroanilide was incubated in the wells and change of A_{405} per hour was measured. Plasmin activity was normalized to the peak at 1 h (100%).

Table 1 *Influence of inhibitors of plasminogen activators and plasmin on Angiostatin 4.5 (AS4.5) generation*

Conversion of plasminogen to AS4.5 was performed on fixed PC-3 cells or in fluid phase. To evaluate the influence of different inhibitors on AS4.5 generation, Pefabloc, α-2-antiplasmin (A2AP), plasminogen-activator inhibitor, or ε-aminocaproic acid was added to the plasminogen-AS4.5 reaction samples, and AS4.5 generated was measured by ELISA.

	PC-3 cell surface	Fluid phase
εACA (10 mM)	93%	45%
Pefabloc (3 mM)	94%	99%
A2AP (1:1 molar ratio to Plasminogen	87%	30%
A2AP (10:1 molar ratio to Plasminogen)	97%	97%
PAI-1 (150 nM)	94%	99%

surface plasmin was observed over the subsequent 24 h, which was associated with an increase in AS4.5 levels, as shown in Fig. 2.

Specific inhibitors of plasminogen activators and/or plasmin were shown to inhibit AS4.5 generation by the PC-3 membranes indicating that plasmin generation and activity is necessary for the membrane-dependent conversion of plasminogen to AS4.5 (Table 1). Pefabloc, a broad-spectrum serine proteinase inhibitor, reduced PC-3 membrane-dependent conversion of plasminogen to AS4.5 by 94%. Plasminogen-activator inhibitor-1, at 150 nM, reduced AS4.5 generation by 94%, confirming the essential intermediate role of plasmin generation. α-2-Antiplasmin inhibited AS4.5 generation by 87% when in equal molar concentration to plasminogen and by 97% when in molar excess to plasminogen. The lysine analogue, ϵ-aminocaproic acid, reduced the PC-3 membrane generation of AS4.5 by 93% suggesting that kringle binding plays a key role in the plasminogen conversion to AS4.5, possibly by disrupting plasminogen/plasmin binding to a membrane receptor.

Cell surface actin has been shown previously to be a plasminogen binding site (34, 39, 40). Actin was associated with the cell membrane fractions of PC-3, MDA-MB231, and HT1080 cells as determined by Western blot (Fig. 4). Various actin isoforms exist, each differing in NH_2-terminal sequence (41), which allows identification of the isoforms. Cell surface actin can be recognized by specific antibodies to the NH_2-terminus of β-actin (Fig. 4), but not by specific antibodies to α-actin (Fig. 4) or γ-actin (data not shown). Whereas Fig. 4 showed the presence of membrane-associated β-actin, direct immunofluorescent staining showed that the β-actin was present on the extracellular surface of PC-3 cells (Fig. 5). Cytokeratin 7 staining was abundant in the cytoplasm in permeabilized cells and absent on the nonpermeabilized cells, serving as a control. Furthermore, the β-actin signal on the nonpermeabilized cells was punctate, distinct from the cytoplasmic signal in permeabilized cells.

An antibody to the COOH terminus of actin decreased the generation of AS4.5 by ~70%, both on the fixed cell surface and on cell

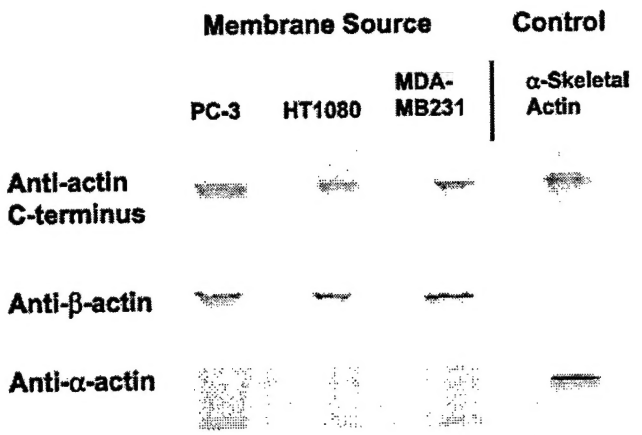

Fig. 4. Detection of actin on PC-3, HT1080, and MDA-MB231 cell membranes. Washed cell membranes from PC-3 cells, HT1080 cells, and MDA-MB231 cells were assayed by Western blot for the presence of actin using specific antibodies to α-skeletal actin, β-actin, and an antibody to the COOH terminus of actin, which reacts with all of the isoforms. Pure α-skeletal actin as control. All three of the cancer cell lines demonstrated membrane-associated β-actin.

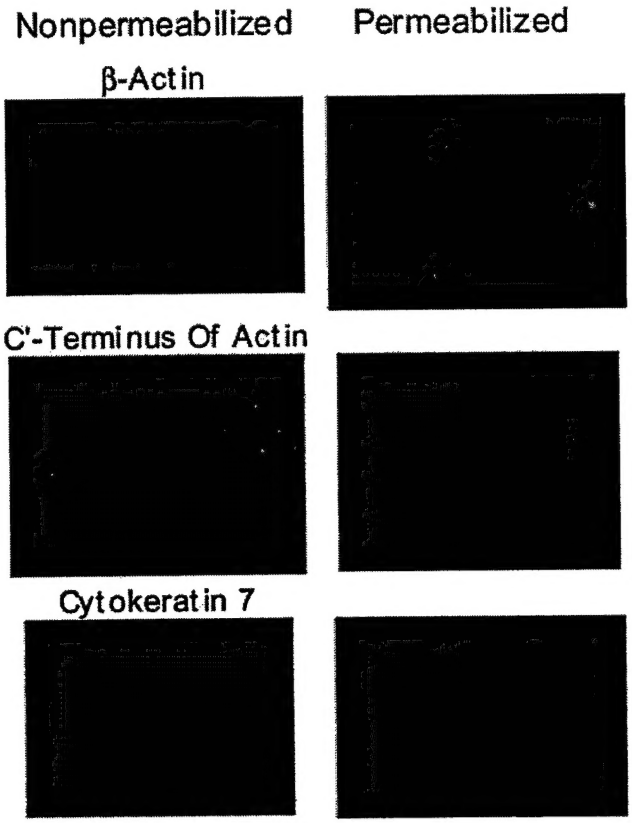

Fig. 5. Direct immunofluorescence staining for actin and cytokeratin 7. For surface protein staining, nonpermeabilized PC-3 cells were incubated with FITC-conjugated monoclonal antibodies to the COOH terminus of actin, β-actin, or cytokeratin 7. For intracellular protein staining, PC-3 cells were permeabilized in −20°C acetone before staining with the same antibodies. Cytokeratin 7 served as a negative control for surface protein staining. β-Actin was shown both on the PC-3 cell surface and in cytoplasm, whereas cytokeratin 7 was only present in the cytoplasm.

membrane fractions (Fig. 6, *A* and *B*). Nonspecific antibodies, such as a monoclonal antibody to α-2-antiplasmin, did not show significant influence on AS4.5 generation (Fig. 6*B*). This supports the hypothesis that the β-actin on the outer surface of the cell membrane serves as the receptor for plasminogen conversion to AS4.5.

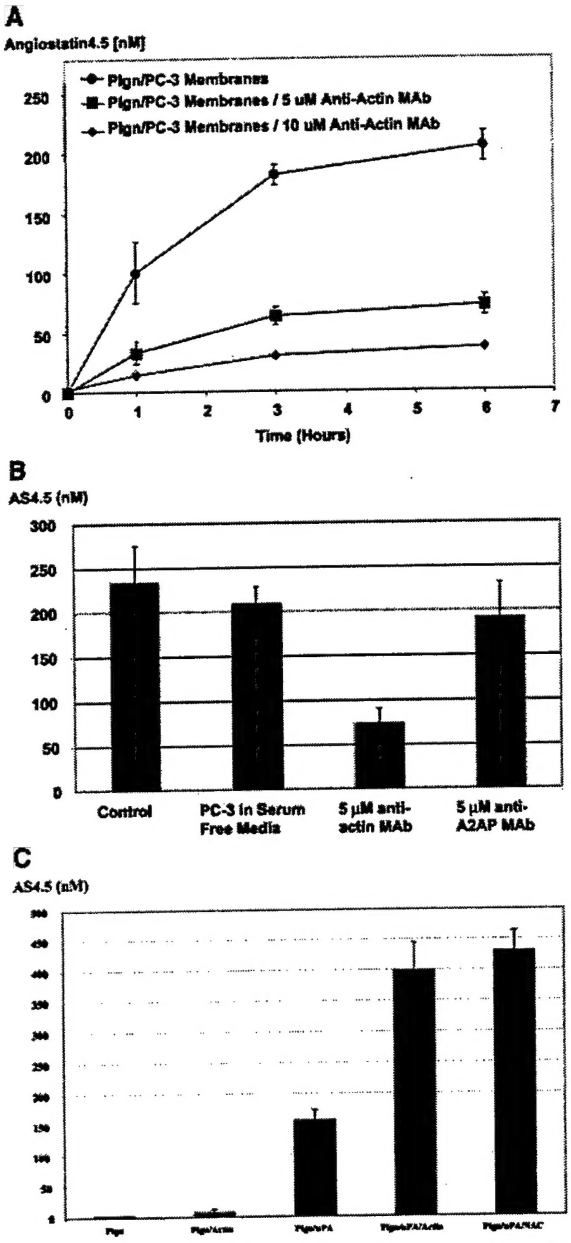

Fig. 6. *A*, inhibition of AS4.5 generation by antiactin antibody. Plasminogen (*Plgn;* 440 nM) was incubated with PC-3 cell membrane preparations, in the presence of 5 μM or 10 μM of an antibody to the COOH terminus of actin or no antibody as control. Aliquots were taken at different time points. The AS4.5 generated was measured by ELISA. *B*, conversion of plasminogen to AS4.5 is not dependent on serum-derived actin and is inhibited by antibodies to the COOH terminus of actin. Plasminogen was incubated with glutaraldehyde-fixed PC-3 cells cultured in serum-free or serum-containing medium. The withholding of serum, and possible serum-derived actin, did not affect the generation of AS4.5 indicating the actin was from the cells themselves. Antibodies to the COOH terminus of actin reduced the generation of AS4.5 by ~70%, whereas the nonspecific antibody (to α-2-antiplasmin) did not have an effect on AS4.5 generation. The AS4.5 generated was measured by ELISA. Data points are mean of mean of duplicate; *bars,* ±SE. *C,* role of actin in a cell-free system of conversion of plasminogen to AS4.5. AS4.5 generation was compared under the following conditions: 440 nM plasminogen incubated alone, 440 nM plasminogen with 50 μM actin, 440 nM plasminogen with 75 nM urokinase-type plasminogen activator (uPA), 440 nM plasminogen with 50 μM actin and 75 nM uPA, and 440 nM plasminogen with 75 nM uPA and 50 μM *N*-acetyl-L-cysteine. The AS4.5 generated was measured by ELISA. Data points are mean of mean of duplicate experiments; *bars,* ±SE.

Table 2 *Relationship between urokinase (uPA) activity and angiostatin4.5 (AS4.5) generation*

Surface uPA activity and the rate of conversion of plasminogen to AS4.5 (at 6 h) was measured on membrane fractions from normal cells (HMVEC and NHDF) and PC-3 cells. Results are expressed as mean and SD of triplicate measurements. Compared with PC-3 cells, HMVEC membranes had 38% of the uPA activity and generated 41% of the AS4.5. Compared with PC-3 cells, NHDF had 61% of the uPA activity and generated 39% of the AS4.5.

	uPA activity (U/ml)	AS4.5 Generation (nM)
PC-3	43.8 ± 0.3	64.5 ± 4.2
HMVEC	16.8 ± 0.8	26.3 ± 2.3
NHDF	26.5 ± 2	25.4 ± 3.8

Whereas actin alone had no discernable effect on plasminogen in a cell-free system, when added to uPA/plasminogen (a source of plasmin), actin caused complete conversion of plasminogen to AS4.5, comparable with the effect of a free sulfhydryl donor (Fig. 6*C*). This indicates that actin mediates plasmin autoproteolysis within kringle 5, yielding AS4.5. Furthermore, AS4.5 generation from plasmin by actin does not need a free sulfhydryl donor.

Annexin II has been reported to be a plasminogen and plasmin receptor (32, 33), and the annexin II tetramer was shown to be a reductase, mediating plasmin conversion to an angiostatin-like molecule, designated A61 in the HT1080 system (31, 35, 36). By Western blot, annexin II protein (p36) was detected on the membranes of the PC-3, MDA231, and HT1080 cells, and all of the detectable membrane-bound annexin II was removed by treatment with the detergent CHAPS and EGTA (data not shown). There was an ~50% reduction in surface-bound plasmin by the CHAPS:EGTA treatment (data not shown), but an insignificant reduction (<20%) in plasminogen conversion to AS4.5. The resistance of the AS4.5 generation to CHAPS:EGTA treatment (*i.e.,* annexin II removal), in the three cancer cell lines tested, indicates that annexin II is not an essential receptor for AS4.5 generation. Similarly, no evidence of a role for α-enolase, another reported plasminogen receptor, was observed for generation of AS4.5. Treatment with carboxypeptidase B was used to remove COOH-terminal lysine residues from surface proteins, including any α-enolase present. The AS4.5 generation was reduced by ~10% (data not shown) by carboxypeptidase B. However, carboxypeptidase B did reduce cell surface plasmin activity, consistent with the role of α-enolase as a plasmin receptor. These data suggest that α-enolase is not the plasminogen conversion receptor.

To determine whether the conversion of plasminogen to AS4.5 could also occur on primary, normal cell surfaces, HMVECs and NHDFs were tested for cell surface actin, plasminogen activator, and AS4.5 generation. On the basis of Western blot and immunofluorescent staining, HMVEC and NHDF cells express cell surface β-actin comparable with PC-3 cells both (data not shown). However, Western blot of HMVEC and NHDF cell membrane lysates revealed much less urokinase receptor (uPAR) on their surfaces than PC-3 cells (data not shown). Furthermore, HMVEC and NHDF cells had less uPA activity on the surface than PC-3 cells (Table 2). The two primary cell types did convert plasminogen to AS4.5, but at a reduced rate compared with the PC-3 cells (40%), approximately proportional with the uPA levels on the cell surfaces (Table 2). These data suggest that at least in tissue culture and among the cell types studied, normal cells have surface β-actin and uPA-type plasminogen activator, and the ability to convert plasminogen to AS4.5. However, the conversion by the normal cells is at a reduced rate compared with PC-3 and other cancer cell lines.

DISCUSSION

We and others have shown previously that human plasminogen may be converted to an angiostatin isoform in a two-step reaction, with plasmin

formation and activity as an essential intermediate (22, 25, 26). Furthermore, this process yields an isoform of angiostatin consisting of kringles 1–4 plus 85% of kringle 5 (amino acids Lys78 to Arg529), which has been designated AS4.5 (24, 25). In prior studies, the conversion of plasminogen to angiostatin was characterized in the soluble protein fractions. In this article, we now demonstrate that the conversion of plasminogen to angiostatin can be potentiated by a cell surface receptor for plasmin, supplanting the need for a free sulfhydryl donor to allow for cleavage within kringle 5. Furthermore, the plasmin receptor has been identified as β-actin. The three cancer lines tested all expressed β-actin on the cell membrane, and antibody blockade of the actin with a COOH-terminus antibody inhibited the conversion to AS4.5. Furthermore, in a cell-free system, purified actin was able to efficiently mediate conversion of plasmin to AS4.5.

Phosphoglycerate kinase has been reported to serve as a disulfide reductase for plasmin, which may mediate cleavage to an angiostatin isoform (42, 43). However, phosphoglycerate kinase is distinct from the cell surface reaction mediated by β-actin, because phosphoglycerate kinase is a secreted protein and would not be present at significant levels in the washed cell membranes.

Whereas many proteinases have been reported to cleave plasminogen to an angiostatin isoform, our model is an extension of the initial observation that cancer cells themselves can efficiently convert plasminogen to angiostatin (22, 23). Serine proteinase activity is essential for AS4.5 generation, as the AS4.5 generation can be completely blocked by the broad serine proteinase inhibitor, Pefabloc. More specifically, plasmin formation and activity are both required for AS4.5 generation. Plasminogen-activator inhibitor-1 inhibition of AS4.5 generation showed that uPA activity and plasmin formation is required for AS4.5 generation. As in fluid phase, α-2-antiplasmin, a specific inhibitor to plasmin activity, also can inhibit AS4.5 generation on cell surface, suggesting that plasmin autoproteolysis played a critical role in AS4.5 generation on cell surface. ϵ-Aminocaproic acid, which is an analogue of lysine, is used to disrupt the kringle-lysine interaction between plasminogen or plasmin and their receptors/substrates (17). The fact that ϵ-aminocaproic acid can reduce AS4.5 generation on the cell surface suggests that the plasmin receptor can provide lysine residues or analogues, and the interaction between the plasmin receptor and plasmin is dependent on lysine and the kringles of plasmin.

There have been a number of prior article describing putative plasmin or plasminogen receptors on cell surfaces. These receptors include annexin II (35, 36), α-enolase (37), and actin (5). Annexin II is a plasminogen/plasmin receptor and was reported to act as a reductase for generation of an angiostatin-like-molecule (31). Kassam *et al.* (35) also showed that the annexin II tetramer on HT1080 cells could mediate conversion of human plasminogen to an angiostatin-like isoform, consisting of amino acids Lys78-Lys468 and designated A61. Therefore, we considered whether one or more of these receptors contributed to the plasmin(ogen) binding and autoproteolysis to yield AS4.5. We showed that the angiostatin isoform being generated is indeed AS4.5 based on its molecular weight, binding to multiple antibodies to plasminogen kringle domains, and most specifically, binding to an antibody to the COOH terminus of the AS4.5 generated in a cell-free system (24). Our results demonstrate that annexin II is present on the surface of cancer cells and is an effective plasmin receptor, as removal of annexin II reduced plasmin binding to the membranes by ~50%. However, removal of annexin II from all three of the cancer cell lines tested resulted in only a modest reduction in plasminogen conversion to AS4.5.

Similarly, α-enolase has been reported to be a plasminogen receptor, although there has been no evidence that it contributes to generation of angiostatin or an angiostatin-like isoform (34, 37). The COOH-terminal lysine residue plays a critical role in the interaction of α-enolase and plasminogen (37). We treated PC-3 cells with carboxypeptidase B, which proteolytically removes the COOH-terminal lysine on cell surface proteins. Again, whereas the carboxypeptidase B treatment reduced plasmin binding to the cell surface, there was no significant affect on generation of AS4.5.

Whereas we saw evidence that the three cancer lines expressed the three putative plasmin(ogen) receptors on their cell surface, it was only the surface β-actin that was shown to have a functional role in the conversion of plasmin to an angiostatin isoform, specifically AS4.5. There have been a series of studies demonstrating the presence of one or more actin isoforms on the external cell surface. One or more actin isoform was found by several independent groups of researchers on the surface of lymphocytes (44, 45), brain capillary endothelial cells (46), and bovine pulmonary endothelial cells (47–50). Actin was also discovered as a cell surface binding site for plasminogen on endothelial cells (39), monocytoid cells, blood monocytes (34), and breast cancer cells (40). The mechanism of actin trafficking and binding to the cell surface is not well understood. However, actin can bind to membrane lipids such as phospholipids (51–55), and direct interactions between actin and cell membranes are possible *in vivo* although actin does not have a transmembrane domain. Furthermore, studies by Hu *et al.* (50) also showed that cell-surface actin was not derived from the serum in tissue culture experiments.

Two nontransformed cell lines, HMVEC and NHDF, were tested for surface expression of β-actin, uPA, and uPAR, as well as the ability to convert plasminogen to AS4.5. Surface β-actin was present on the normal cell surface in culture comparable with the cancer lines. However, uPAR antigen, and uPA antigen and activity were present in the primary cell lines, but at lower levels than in the PC-3 and other cancer lines, and this correlated with a reduced rate of conversion of plasminogen to AS4.5. These data suggest that the level of uPA and uPAR may be the rate-limiting factor in the cell surface conversion of plasminogen to AS4.5. If and how this represents the *in vivo* process in normal tissues remains to be determined.

Tumor angiogenesis is a significant prognostic factor (8, 56). The ability of tumors to convert plasminogen to AS4.5 influences the balance of tumor angiogenesis and may be a key prognostic factor. Recognition of the cell surface receptor for conversion of plasminogen to AS4.5 may contribute to the ability to predict the clinical course of cancers. Because cancer cell surface β-actin can serve as a receptor for plasminogen conversion to AS4.5, the generation and activity of AS4.5 may influence tumor angiogenic capability and tumor aggression. Cell surface β-actin may be an important prognostic indicator for human cancer and may correlate with patient survival. Greater levels of β-actin on the cancer cell surface may contribute to the rate of AS4.5 generation and the angiogenic capacity of the tumors. Additional studies, including studies of clinical specimens, may serve to clarify the actual prognostic power of the expression of cell surface β-actin.

Expression of uPA and its receptor uPAR have also been reported to have an important role in cellular invasion and cancer metastasis (57, 58). Interesting, numerous studies have suggested that increased levels of uPA and uPAR expression on cancer cell membranes serves as a negative prognostic parameter for the cancer (57, 58). Whereas our data do not address the *in vivo* generation of AS4.5 by normal or cancer cells, they do suggest that the role of the plasminogen system may be more complex than previously thought. Plasmin is known to promote angiogenesis and invasion, by cleaving matrix proteins, such as laminin, and activation of matrix metalloproteinases (57, 58). However, plasmin activity is also essential for the generation of human AS4.5, which inhibits angiogenesis (22, 23).

In discussions on angiostatin, it is often asked why cancer cells would mediate the generation of angiostatin, which would inhibit angiogenesis and cancer growth. Our data, characterizing the related processes of plasmin and AS4.5 formation, which result in opposing effects on an-

giogenesis, suggests the question is far more complex then at first appearance.

REFERENCES

1. Weidner, N., Semple, J. P., Welch, W. R., and Folkman, J. Tumor angiogenesis and metastasis–correlation in invasive breast carcinoma. N. Engl. J. Med., *324:* 1–8, 1991.
2. Folkman, J., and Klagsbrun, M. Angiogenic factors. Science (Wash. DC), *235:* 442–447, 1987.
3. Burke, T. W., Hoskins, W. J., Heller, P. B., Bibro, M. C., Weiser, E. B., and Park, R. C. Prognostic factors associated with radical hysterectomy failure. Gynecol. Oncol., *26:* 153–159, 1987.
4. Brem, S. S., Gullino, P. M., and Medina, D. Angiogenesis: a marker for neoplastic transformation of mammary papillary hyperplasia. Science (Wash. DC), *195:* 880–882, 1977.
5. Adcock, L. L., Julian, T. M., Okagaki, T., Jones, T. K., Prem, K. A., Twiggs, L. B., Potish, R. A., and Phillips, G. L. Carcinoma of the uterine cervix FIGO Stage I-B. Gynecol. Oncol., *14:* 199–208, 1982.
6. Blood, C. H., and Zetter, B. R. Tumor interactions with the vasculature: angiogenesis and tumor metastasis. Biochim. Biophys. Acta, *1032:* 89–118, 1990.
7. Folkman, J. What is the evidence that tumors are angiogenesis dependent? J. Natl. Cancer Inst., *82:* 4–6, 1990.
8. Weidner, N., Folkman, J., Pozza, F., Bevilacqua, P., Allred, E. N., Moore, D. H., Meli, S., and Gasparini, G. Tumor angiogenesis: a new significant and independent prognostic indicator in early-stage breast carcinoma. J. Natl. Cancer Inst., *84:* 1875–1887, 1992.
9. Folkman, J. Angiogenesis in cancer, vascular, rheumatoid and other disease. Nat. Med., *1:* 27–31, 1995.
10. O'Reilly, M. S., Holmgren, L., Chen, C., and Folkman, J. Angiostatin induces and sustains dormancy of human primary tumors in mice. Nat. Med., *2:* 689–692, 1996.
11. Bergers, G., Javaherian, K., Lo, K. M., Folkman, J., and Hanahan, D. Effects of angiogenesis inhibitors on multistage carcinogenesis in mice. Science (Wash. DC), *284:* 808–812, 1999.
12. Yancopoulos, G. D., Klagsbrun, M., and Folkman, J. Vasculogenesis, angiogenesis, and growth factors: ephrins enter the fray at the border. Cell, *93:* 661–664, 1998.
13. Good, D. J., Polverini, P. J., Rastinejad, F., Le Beau, M. M., Lemons, R. S., Frazier, W. A., and Bouck, N. P. A tumor suppressor-dependent inhibitor of angiogenesis is immunologically and functionally indistinguishable from a fragment of thrombospondin. Proc. Natl. Acad. Sci. USA., *87:* 6624–6628, 1990.
14. Volpert, O. V., Stellmach, V., and Bouck, N. The modulation of thrombospondin and other naturally occurring inhibitors of angiogenesis during tumor progression. Breast Cancer Res. Treat, *36:* 119–126, 1995.
15. Torimura, T., Sata, M., Ueno, T., Kin, M., Tsuji, R., Suzaku, K., Hashimoto, O., Sugawara, H., and Tanikawa, K. Increased expression of vascular endothelial growth factor is associated with tumor progression in hepatocellular carcinoma. Hum. Pathol., *29:* 986–991, 1998.
16. O'Reilly, M. S., Holmgren, L., Shing, Y., Chen, C., Rosenthal, R. A., Moses, M., Lane, W. S., Cao, Y., Sage, E. H., and Folkman, J. Angiostatin: a novel angiogenesis inhibitor that mediates the suppression of metastases by a Lewis lung carcinoma. Cell, *79:* 315–328, 1994.
17. Castellino, F. J. Plasminogen. *In:* H. R. Roberts (ed.), Molecular Basis of Thrombosis and Hemostasis, pp. 495–515. New York: Marcel Dekker, 1995.
18. Dong, Z., Kumar, R., Yang, X., and Fidler, I. J. Macrophage-derived metalloelastase is responsible for the generation of angiostatin in Lewis lung carcinoma. Cell, *88:* 801–810, 1997.
19. Lijnen, H. R., Ugwu, F., Bini, A., and Collen, D. Generation of an angiostatin-like fragment from plasminogen by stromelysin-1 (MMP-3). Biochemistry, *37:* 4699–4702, 1998.
20. Patterson, B. C., and Sang, Q. A. Angiostatin-converting enzyme activities of human matrilysin (MMP-7) and gelatinase B/type IV collagenase (MMP-9). J. Biol. Chem., *272:* 28823–28825, 1997.
21. O'Reilly, M. S., Wiederschain, D., Stetler-Stevenson, W. G., Folkman, J., and Moses, M. A. Regulation of angiostatin production by matrix metalloproteinase-2 in a model of concomitant resistance. J. Biol. Chem., *274:* 29568–29571, 1999.
22. Gately, S., Twardowski, P., Stack, M. S., Cundiff, D. L., Grella, D., Castellino, F. J., Enghild, J., Kwaan, H. C., Lee, F., Kramer, R. A., Volpert, O., Bouck, N., and Soff, G. A. The mechanism of cancer-mediated conversion of plasminogen to the angiogenesis inhibitor angiostatin. Proc. Natl. Acad. Sci. USA, *94:* 10868–10872, 1997.
23. Gately, S., Twardowski, P., Stack, M. S., Patrick, M., Boggio, L., Cundiff, D. L., Schnaper, H. W., Madison, L., Volpert, O., Bouck, N., Enghild, J., Kwaan, H. C., and Soff, G. A. Human prostate carcinoma cells express enzymatic activity that converts human plasminogen to the angiogenesis inhibitor, angiostatin. Cancer Res., *56:* 4887–4890, 1996.
24. Soff, G. A. Angiostatin and angiostatin-related proteins. Cancer Metastasis Rev., *19:* 97–107, 2000.
25. Stathakis, P., Lay, A. J., Fitzgerald, M., Schlieker, C., Matthias, L. J., and Hogg, P. J. Angiostatin formation involves disulfide bond reduction and proteolysis in kringle 5 of plasmin. J. Biol. Chem., *274:* 8910–8916, 1999.
26. Stathakis, P., Fitzgerald, M., Matthias, L. J., Chesterman, C. N., and Hogg, P. J. Generation of angiostatin by reduction and proteolysis of plasmin. Catalysis by a plasmin reductase secreted by cultured cells. J. Biol. Chem., *272:* 20641–20645, 1997.
27. Cao, R., Wu, H. L., Veitonmaki, N., Linden, P., Farnebo, J., Shi, G. Y., and Cao, Y. Suppression of angiogenesis and tumor growth by the inhibitor K1–5 generated by plasmin-mediated proteolysis. Proc. Natl. Acad. Sci. USA, *96:* 5728–5733, 1999.
28. Cao, Y., Veitonmaki, N., Keough, K., Cheng, H., Lee, L. S., and Zurakowski, D. Elevated levels of urine angiostatin and plasminogen/plasmin in cancer patients. Int. J. Mol. Med., *5:* 547–551, 2000.
29. Lannutti, B. J., Gately, S. T., Quevedo, M. E., Soff, G. A., and Paller, A. S. Human angiostatin inhibits murine hemangioendothelioma tumor growth *in vivo*. Cancer Res., *57:* 5277–5280, 1997.
30. Mauceri, H. J., Hanna, N. N., Beckett, M. A., Gorski, D. H., Staba, M. J., Stellato, K. A., Bigelow, K., Heimann, R., Gately, S., Dhanabal, M., Soff, G. A., Sukhatme, V. P., Kufe, D. W., and Weichselbaum, R. R. Combined effects of angiostatin and ionizing radiation in antitumour therapy. Nature (Lond.), *394:* 287–291, 1998.
31. Waisman, D. M. Annexin II tetramer: structure and function. Mol. Cell Biochem, *149–150:* 301–322, 1995.
32. Cesarman, G. M., Guevara, C. A., and Hajjar, K. A. An endothelial cell receptor for plasminogen/tissue plasminogen activator (t-PA). II. Annexin II-mediated enhancement of t-PA-dependent plasminogen activation. J. Biol. Chem., *269:* 21198–21203, 1994.
33. Hajjar, K. A., Jacovina, A. T., and Chacko, J. An endothelial cell receptor for plasminogen/tissue plasminogen activator. I. Identity with annexin II. J. Biol. Chem., *269:* 21191–21197, 1994.
34. Hawley, S. B., Green, M. A., and Miles, L. A. Discriminating between cell surface and intracellular plasminogen-binding proteins: heterogeneity in profibrinolytic plasminogen-binding proteins on monocytoid cells. Thromb. Haemost., *84:* 882–890, 2000.
35. Kassam, G., Kwon, M., Yoon, C. S., Graham, K. S., Young, M. K., Gluck, S., and Waisman, D. M. Purification and characterization of A61. An angiostatin-like plasminogen fragment produced by plasmin autodigestion in the absence of sulfhydryl donors. J. Biol. Chem., *276:* 8924–8933, 2001.
36. Kwon, M., Caplan, J. F., Filipenko, N. R., Choi, K. S., Fitzpatrick, S. L., Zhang, L., and Waisman, D. M. Identification of annexin II heterotetramer as a plasmin reductase. J. Biol. Chem., *277:* 10903–10911, 2002.
37. Redlitz, A., Fowler, B. J., Plow, E. F., and Miles, L. A. The role of an enolase-related molecule in plasminogen binding to cells. Eur. J. Biochem., *227:* 407–415, 1995.
38. Liu, L., Tao, J. Q., and Zimmerman, U. J. Annexin II binds to the membrane of A549 cells in a calcium-dependent and calcium-independent manner. Cell Signalling, *9:* 299–304, 1997.
39. Dudani, A. K., and Ganz, P. R. Endothelial cell surface actin serves as a binding site for plasminogen, tissue plasminogen activator and lipoprotein(a). Br. J. Haematol., *95:* 168–178, 1996.
40. Andronicos, N. M., and Ranson, M. The topology of plasminogen binding and activation on the surface of human breast cancer cells. Br. J. Cancer, *85:* 909–916, 2001.
41. Herman, I. M. Actin isoforms. Curr. Opin. Cell Biol., *5:* 48–55, 1993.
42. Lay, A. J., and Hogg, P. J. Measurement of reduction of disulfide bonds in plasmin by phosphoglycerate kinase. Methods Enzymol., *348:* 87–92, 2002.
43. Lay, A. J., Jiang, X. M., Kisker, O., Flynn, E., Underwood, A., Condron, R., and Hogg, P. J. Phosphoglycerate kinase acts in tumour angiogenesis as a disulphide reductase. Nature (Lond.), *408:* 869–873, 2000.
44. Owen, M. J., Auger, J., Barber, B. H., Edwards, A. J., Walsh, F. S., and Crumpton, M. J. Actin may be present on the lymphocyte surface. Proc. Natl. Acad. Sci. USA, *75:* 4484–4488, 1978.
45. Sanders, S. K., and Craig, S. W. A lymphocyte cell surface molecule that is antigenically related to actin. J. Immunol., *131:* 370–377, 1983.
46. Pardridge, W. M., Nowlin, D. M., Choi, T. B., Yang, J., Calaycay, J., and Shively, J. E. Brain capillary 46, 000 dalton protein is cytoplasmic actin and is localized to endothelial plasma membrane. J. Cereb. Blood Flow Metab., *9:* 675–680, 1989.
47. Moroianu, J., Fett, J. W., Riordan, J. F., and Vallee, B. L. Actin is a surface component of calf pulmonary artery endothelial cells in culture. Proc. Natl. Acad. Sci. USA, *90:* 3815–3819, 1993.
48. Hu, G. F., Chang, S. L, Riordan, J. F., and Vallee, B. L. An angiogenin-binding protein from endothelial cells. Proc. Natl. Acad. Sci. USA, *88:* 2227–2231, 1991.
49. Hu, G. F., and Riordan, J. F. Angiogenin enhances actin acceleration of plasminogen activation. Biochem. Biophys. Res. Commun., *197:* 682–687, 1993.
50. Hu, G. F., Strydom, D. J., Fett, J. W., Riordan, J. F., and Vallee, B. L. Actin is a binding protein for angiogenin. Proc. Natl. Acad. Sci. USA, *90:* 1217–1221, 1993.
51. St-Onge, D., and Gicquaud, C. Research on the mechanism of interaction between actin and membrane lipids. Biochem. Biophys. Res. Commun., *167:* 40–47, 1990.
52. St-Onge, D., and Gicquaud, C. Evidence of direct interaction between actin and membrane lipids. Biochem. Cell Biol., *67:* 297–300, 1989.
53. Gicquaud, C. Actin conformation is drastically altered by direct interaction with membrane lipids: a differential scanning calorimetry study. Biochemistry, *32:* 11873–11877, 1993.
54. Gicquaud, C. Does actin bind to membrane lipids under conditions compatible with those existing *in vivo*? Biochem. Biophys. Res. Commun., *208:* 1154–1158, 1995.
55. Gicquaud, C., and Wong, P. Mechanism of interaction between actin and membrane lipids: a pressure-tuning infrared spectroscopy study. Biochem. J., *303 (Pt 3):* 769–774, 1994.
56. Wiggins, D. L., Granai, C. O., Steinhoff, M. M., and Calabresi, P. Tumor angiogenesis as a prognostic factor in cervical carcinoma. Gynecol Oncol, *56:* 353–356, 1995.
57. Sidenius, N., and Blasi, F. The urokinase plasminogen activator system in cancer: recent advances and implication for prognosis and therapy. Cancer Metastasis Rev., *22:* 205–222, 2003.
58. Mazar, A. P., Henkin, J., and Goldfarb, R. H. The urokinase plasminogen activator system in cancer: implications for tumor angiogenesis and metastasis. Angiogenesis, *3:* 15–32, 1999.